

# Identification of Interacting Protein Partners of TOPORS in the Retina

A Thesis Submitted to the University College London for  
the Degree of Doctor in Philosophy

Barbara Czub  
BSc

Department of Molecular Genetics  
Institute of Ophthalmology  
University College London  
2015

## DECLARATION

I, Barbara Czub, confirm that the work presented in this thesis is my own.

Where information has been derived from other sources, I confirm that this has been indicated in the thesis.

Signature: 

Date: 15<sup>th</sup> May 2015

## **ABSTRACT**

Retinitis pigmentosa (RP, MIM#268000) is a heterogeneous disease characterised by loss of rod photoreceptors and pigment deposits in the retina. Historically, genes linked to RP were associated with rod-specific functions. Recently, a novel class of ubiquitously expressed causative genes has emerged including splicing factor genes and TOPORS (NM\_005802). To date, studies show *TOPORS* is expressed in all tested human tissues, including the retina. However, mutations in this ubiquitously expressed gene only cause RP without any systemic symptoms.

The purpose of this work was to understand why mutations in *TOPORS*, which encodes a multifunctional protein, cause a retina-only disease by identifying protein interacting partner(s) of TOPORS, using a yeast-two hybrid (Y2H) screen. In case the interacting partner(s) turn out to be retina specific, it may explain the retina-only phenotype.

Human retinal cDNA library was constructed from total retinal cDNA directly in the Y187 *Saccharomyces cerevisiae* yeast strain. Retina-specificity of the cDNA library was validated by sequencing, leading to identification of several retina-specific genes, including rhodopsin (*RHO*; NM\_000539). The library was screened for protein interacting partners of TOPORS, using Matchmaker™ Gold Yeast Two-Hybrid System (Clontech, CA, USA).

Over  $10^7$  cDNA clones were screened, leading to isolation of 53 potential interactions. The identified interacting partners were prioritised for further evaluation, based on literature and database searches, and re-tested in yeast leading to identification of three candidates for further functional studies: a soluble fragment of integral membrane protein 2B (*ITM2B*; NM\_0219999), previously linked to neurodegenerative disorders, and more recently associated with an inherited retinal dystrophy; a brain prostaglandin D2 synthase (*PTGDS*; NM\_000954), highly expressed in the retina, previously suggested to play a role in retinal homeostasis; a regulatory subunit 4 of the 26 S protease (*PSMC1*; NM\_002802), conferring substrate specificity to the proteasome complex during degradation of ubiquitinated proteins.

The outcomes suggest several scenarios for why mutations in *TOPORS* result only in RP; however, further studies are essential to elucidate the role of TOPORS and its interacting partners in the aetiology of this debilitating disease.

## **PUBLICATIONS**

Barbara Czub, Amna Z Shah, Giovanna Alfano, Lourdes Valdes Sanchez, Christina Chakarova and Shomi S Bhattacharya (2013). Identification of Interacting Protein Partners of TOPORS in the Retina. Poster presentation at ARVO 2013 Annual Meeting, Seattle, WA, USA

Barbara Czub, Amna Z Shah, Giovanna Alfano, Lourdes Valdes Sanchez, Berta De La Cerda Haynes, Christina Chakarova and Shomi S Bhattacharya (2013). Characterisation of associations between TOPORS and selected interacting protein partners. Poster presentation at ARVO and ISOCB Conference 2013, Oxford, UK

Barbara Czub, Amna Shah, Przemysław Kruczek, Giovanna Alfano, Christina Chakarova and Shomi S. Bhattacharya (2014). ITM2B, implicated in familial dementias and retinal dystrophy, associates with ciliary-centrosomal protein, TOPORS. Poster presentation at ASHG 2014 Annual Meeting, San Diego, CA, USA

Barbara Czub, Amna Shah, Przemysław Kruczek, Giovanna Alfano, Christina Chakarova and Shomi S. Bhattacharya (2014). Prostaglandin-D2 synthase localises to centrioles and primary cilium, and interacts with TOPORS, implicated in retinal ciliopathy. Poster presentation at Cilia 2014 Conference, Paris, France

Manuscript in preparation, working title: TOPORS, involved in retinal degeneration, associates with ITM2B, implicated in familial dementias with ataxia and a dominant retinal dystrophy.

## **DEDICATION**

*I dedicate this PhD thesis to my Family.*

*Firstly to Jerzy, my Dear Sweetheart, to whom I am forever indebted for the support he has given me, especially for his reassuring rational judgement in times of crises (which happen a lot in science!). He not only had the patience and understanding to endure my daily (nightly!) PhD routine during the last four years, but has even decided to transition from being a 'boyfriend' to a 'fiancé' during the stormy course of my studies.*

*I dedicate the thesis to my Parents, who made it possible for me to attend my undergraduate degree, and took care of my prior education, without which I would not have even considered a PhD.*

*Furthermore, I dedicate this work to my Sister, who motivated me to complete the project on the one hand, and jetted over here to bake my birthday cakes and ensure I go out and party, on the other hand.*

*Special dedication and gratitude go to my Grandparents, who were all always very supportive of my PhD, even though it meant I had less time for them, especially during the final year, whilst working on the thesis.*

*I would also like to dedicate the thesis to Uncle Janusz for never failing to remind me about the awaiting Nobel Prize! This was always a great encouragement.*

*And last, but not least, I dedicate this PhD thesis to all my Cousins, Friends, Aunts and Uncles, to whom I am very grateful for popping round to London and bringing a little bit of home to me with them at times, when I could not abandon the laboratory bench!*

## **DEDYKACJA**

*Dedykuję tę rozprawę doktorską mojej Rodzinie.*

*Jurkowi, mojemu Ukochanemu Skarbowi, któremu jestem niezwykle wdzięczna za wsparcie; jego racjonalne spojrzenie na moje sytuacje kryzysowe (które w świecie nauki niestety zdarzają się często!) działało szczególnie uspokajająco. Miał on nie tylko dość cierpliwości oraz wyrozumiałości, żeby przetrwać moją dzienną (nocną!) doktorską rutynę przez cztery ostatnie lata, ale nawet postanowił przeistoczyć się z 'chłopaka' w 'narzeczonego' w czasie moich burzliwych studiów.*

*Dedykuję tę pracę Rodzicom, którzy umożliwili mi ukończenie studiów licencjackich, jak również zadbali o moją wcześniejszą edukację, bez czego prawdopodobnie nie brałabym pod uwagę studiów doktorskich.*

*Ponadto dedykuję ten doktorat mojej Siostrze, która z jednej strony motywowała mnie do ukończenia projektu, a z drugiej potrafiła przyfrunąć tu, żeby upiec mi torcik urodzinowy i wyciągnąć na imprezę.*

*Specjalną dedykację oraz wyrazy wdzięczności kieruję też w stronę Babć i Dziadków, którzy okazywali mi wiele wsparcia podczas studiów doktorskich, nawet gdy oznaczało to, że miałam mniej czasu dla Nich, szczególnie podczas ostatniego roku, gdy pochłaniało mnie pisanie rozprawy doktorskiej.*

*Chciałabym zadedykować tę pracę również Wujowi Januszowi za nieustanne przypominanie mi o oczekującej Nagrodzie Nobla! Była to zawsze wspaniała zachęta.*

*Na zakończenie, dedykuję mój doktorat także Kuzynom, Przyjaciołom, Ciociom i Wujkom za to, że udawało im się od czasu do czasu wpaść do Londynu i przywieźć ze sobą choć trochę domowej atmosfery w okresach, kiedy nie mogłam sobie pozwolić na oddalenie się od laboratorium, żeby samej polecieć do domu!*

## **ACKNOWLEDGEMENTS**

*First and foremost, I wish to express my deepest gratitude to Professor Shomi S. Bhattacharya, without whom this project would not have been possible. His support throughout my studies was essential for achieving the goals of this doctorate.*

*Great thanks to Doctor Amna Z. Shah, my daily supervisor, a brilliant scientist and a great friend, without whom, I would not have been able to take this project so far. Her guidance and advice often helped me overcome unforeseen obstacles and 'see the greater picture.' Besides, Amna is the best thesis editor you could wish for!*

*I am particularly grateful to Professor Michel Michaelides for giving me the opportunity to be present during his consultations with patients at the Moorfields Eye Hospital Retina Clinic. This was a highly motivational experience, which emphasised to me the importance of the basic molecular research for developing treatments for the presently incurable retinal diseases.*

*I also wish to thank all my examiners. During my MPhil-PhD transfer examination Professor Michael E. Cheetham as well as Doctor Jacqui van der Spuy shared their invaluable knowledge about the yeast two-hybrid system and protein biochemistry techniques; their recommendations were very helpful to me especially in the initial stages of my PhD project. Similarly, I received insightful questions and suggestions from Professors Susan Lindsay and Glen Jeffery during my final viva examination; they helped me see my findings in the broader context of retinal and neurodegenerative disorders.*

*My great appreciation also goes to colleagues for their kind words (and actions!) as well as criticisms. Firstly, I would like to thank Peter Marshal for his very warm welcome, when I joined UCL. I also wish to thank all members of the Bhattacharya Lab. I am especially grateful to Giovanna for sharing her scrupulous analytical powers as well as her knowledge of numerous laboratory techniques. Many thanks to Bev for always working hard to get the sequencing results ready for analysis asap; to Christina for arranging the Retina Clinic visits, precluded by the morning coffees; to Naushin for sharing her super new SDS-PAGE tank; to Vinny for always emphasising the positives; to Przemek and Anna for setting the highly motivating good examples; to Prianka for relieving the laboratory workload during the summers when she was here; to Riddhi for giving me the opportunity to approach science as a teacher rather than as a student; to Heather for always being able to help; to Quincy and Tabitha for dealing with orders, and to the Porters for always taking great care of various deliveries and parcels (even those which were obviously not work-related!).*

*I also wish to thank Fight for Sight and the Rosetrees Trust for providing the funding for this PhD project, as well as many scientists who provided some of the plasmids, primers, cell lines, mouse eyes, or primate retinal sections, used in this project, as is indicated throughout the thesis.*

*Thank You!*

## PODZIĘKOWANIA

*Przede wszystkim, chciałabym wyrazić najgłębsze wyrazy wdzięczności profesorowi Shomi'emu S. Bhattacharya, bez którego ten projekt nie byłby możliwy. Jego wsparcie podczas moich studiów było niezbędne dla zrealizowania celów tego doktoratu.*

*Specjalne podziękowania dla doktor Amny Z. Shah, nieustannie trzymającej pieczę nad moją pracą, wspierającej badaczki oraz przyjaciółki, bez której nie byłabym w stanie doprowadzić tego projektu tak daleko. Jej porady często pomagały mi pokonać nieprzewidziane przeszkody, jak również zachować szerszy kontekst mojej pracy. Ponadto, Amna jest niezastąpiona w edytowaniu prac doktorskich!*

*Jestem szczególnie wdzięczna profesorowi Michael'owi Michaelides za możliwość uczestniczenia w jego konsultacjach z pacjentami przyjmowanymi w klinice chorób siatkówki w placówce Moorfields Eye Hospital. Było to bardzo motywujące doświadczenie, które uwydatniło mi znaczenie podstawowych badań molekularnych dla rozwoju terapii obecnie nieuleczalnych chorób siatkówki.*

*Dziękuję również moim egzaminatorom. Podczas egzaminu wstępnego Profesor Michael E. Cheetham i doktor Jacqueline van der Spuy udzielili cennych porad dotyczących systemów dwu-hybrydowych w drożdżach oraz technik badawczych biochemii białek; ich zalecenia były niezwykle pomocne w początkowych etapach mojej pracy. Podobnie, otrzymałam wnikliwe pytania i sugestie od profesorów Susan Lindsay oraz Glen'a Jeffery podczas egzaminu końcowego; pomogli mi oni dostrzec moje wyniki w szerszym kontekście schorzeń siatkówki oraz układu nerwowego.*

*Wyrazy uznania posyłam też koleżankom i kolegom z pracy, za życzliwe słowa (i czyny!), jak również i krytykę. Najpierw chciałabym podziękować Peter'owi Marshall za ciepłe powitanie, kiedy rozpoczęłam pracę w instytucie. Ponadto, jestem szczególnie wdzięczna doktor Giovannie Alfano za udzielanie swojej skrupulatnej 'mocy analitycznej' oraz wiedzy technicznej. Szczególne podziękowania dla Beverly, nieustannie ciężko pracującej, żeby wyniki sekwencjonowania DNA były jak najszybciej gotowe do analizy; dla Christiny za organizowanie wizyt w klinice siatkówki, poprzedzanych wspólną kawką; dla Naushin za udostępnianie swojego super sprzętu do elektroforezy; dla Vinny za optymistyczne akcenty; dla Przemka i Anny za szerzenie bardzo motywujących dobrych przykładów; dla Prianki za pomoc w laboratorium podczas jej letnich wakacji; dla Riddhi, dzięki której miałam możliwość doświadczenia pracy naukowej nie tylko, jako studentka, ale także jako nauczycielka; dla Heather za niesienie pomocy w każdych okolicznościach; dla Quincy'ego i Tabs za zamawianie odczynników, a także dla Portierów za trzymanie pieczy nad przesyłkami (nawet tymi nie mającymi nic wspólnego z pracą!).*

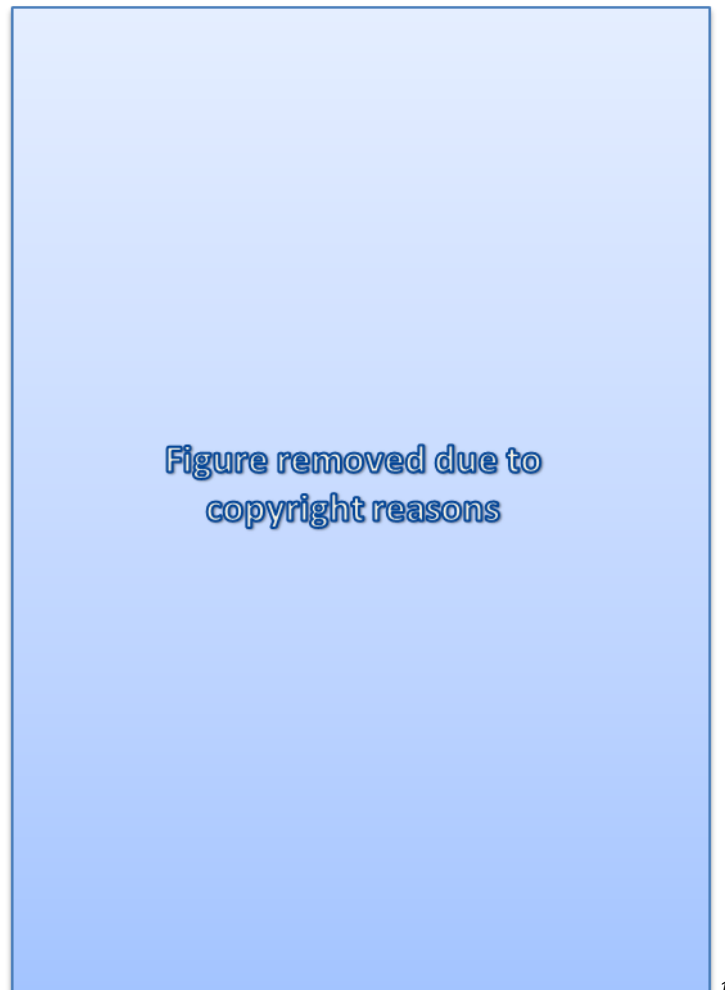
*Dziękuję też fundacjom Fight for Sight oraz Rosetrees Trust za udostępnienie funduszy na realizację tego doktoratu, a także wielu naukowcom, którzy dostarczyli fragmenty DNA, linie komórkowe, mysie oczy, czy też sekcje siatkówki ssaka naczelnego, wykorzystane w tym projekcie, jak jest sprecyzowane w metodach oraz rozdziałach eksperymentalnych rozprawy.*

*Wszystkim Wam serdecznie dziękuję!*



*"In the study of this membrane [the retina] I for the first time felt my faith in Darwinism (hypothesis of natural selection) weakened, being amazed and confounded by the supreme constructive ingenuity revealed not only in the retina and in the dioptric apparatus of the vertebrates but even in the meanest insect eye."*

- Santiago Ramón y Cajal



---

<sup>1</sup> Image modified from Wade (2007).

## **TABLE OF CONTENTS**

<b><u>DECLARATION</u></b> .....	<b>2</b>
<b><u>ABSTRACT</u></b> .....	<b>3</b>
<b><u>PUBLICATIONS</u></b> .....	<b>4</b>
<b><u>DEDICATION</u></b> .....	<b>5</b>
<b><u>DEDYKACJA</u></b> .....	<b>6</b>
<b><u>ACKNOWLEDGEMENTS</u></b> .....	<b>7</b>
<b><u>PODZIĘKOWANIA</u></b> .....	<b>8</b>
<b><u>CONTEXT</u></b> .....	<b>9</b>
<b><u>TABLE OF CONTENTS</u></b> .....	<b>10</b>
<b><u>LIST OF FIGURES</u></b> .....	<b>16</b>
<b><u>LIST OF TABLES</u></b> .....	<b>23</b>
<b><u>LIST OF EQUATIONS</u></b> .....	<b>27</b>
<b><u>ABBREVIATIONS</u></b> .....	<b>28</b>
<b><u>1 INTRODUCTION</u></b> .....	<b>33</b>
<b>1.1 THE SENSE OF VISION</b> .....	<b>33</b>
<b>1.2 THE RETINA: ANATOMY AND PHYSIOLOGY</b> .....	<b>35</b>
1.2.1 PHOTORECEPTORS OF THE RETINA.....	36
1.2.2 THE RETINAL PIGMENTED EPITHELIUM.....	40
1.2.3 PHOTOTRANSDUCTION .....	41
1.2.4 THE VISUAL CYCLE.....	42
<b>1.3 RETINITIS PIGMENTOSA</b> .....	<b>44</b>
1.3.1 RETINA-LIMITED DISORDERS .....	46
1.3.2 SYSTEMIC DISEASES.....	47
<b>1.4 TOPORS MUTATIONS ASSOCIATED WITH RETINAL DYSTROPHIES</b> .....	<b>48</b>
1.4.1 THE <i>RP31</i> PHENOTYPE.....	53
1.4.2 DISSIMILAR PHENOTYPES OF UTAD102 AND RFS169 PROBANDS .....	56
1.4.3 THE SCANDINAVIAN PERICENTRAL RETINAL DYSTROPHY.....	58
<b>1.5 TOPORS: NUCLEAR AND CELL CYCLE CONTEXTS</b> .....	<b>59</b>
<b>1.6 TOPORS: PROTEIN STRUCTURE AND FUNCTION</b> .....	<b>60</b>
<b>1.7 UBIQUITIN-LIKE PROTEIN MODIFICATIONS</b> .....	<b>62</b>
1.7.1 UBIQUITINATION .....	63
1.7.2 SUMOYLATION.....	66
<b>1.8 THE CENTROSOME CYCLE</b> .....	<b>68</b>
<b>1.9 VERTEBRATE CILIA</b> .....	<b>71</b>
1.9.1 THE PRIMARY CILIUM.....	71

1.9.2	THE CONNECTING CILIUM OF THE PHOTORECEPTOR CELL.....	72
1.9.3	CILIA AND CILIOPATHIES.....	74
<b>1.10</b>	<b>HYPOTHESES AND AIMS .....</b>	<b>75</b>
1.10.1	RETINAL LIBRARY CONSTRUCTION AND VALIDATION .....	75
1.10.2	BAIT CONSTRUCTION AND Y2H CONTROL EXPERIMENTS .....	76
1.10.3	VALIDATION OF INTERACTIONS AND mRNA EXPRESSION .....	76
1.10.4	CONFIRMATION OF PPI(S) IN HUMAN CELL LINES.....	77
1.10.5	CO-LOCALISATION STUDIES TO VALIDATE PPI(S) .....	77
1.10.6	FUTURE CONTEXT.....	78
<b>2</b>	<b><u>METHODS AND MATERIALS.....</u></b>	<b>79</b>
<b>2.1</b>	<b>YEAST TWO-HYBRID SYSTEM .....</b>	<b>79</b>
2.1.1	Y2H: AN OVERVIEW .....	80
2.1.2	YEAST CELL STOCK MAINTENANCE .....	83
2.1.3	TRANSFORMATION OF COMPETENT YEAST CELLS .....	84
2.1.4	AUTO-ACTIVATION AND TOXICITY TESTING .....	88
2.1.5	YEAST MATING .....	89
2.1.6	PLASMID ISOLATION FROM YEAST .....	94
2.1.7	PROTEIN ISOLATION FROM YEAST .....	96
2.1.8	GENERATION OF HUMAN RETINAL CDNA LIBRARY .....	99
2.1.9	MACROSCOPIC IMAGING .....	107
2.1.10	Y2H PROCEDURES SUMMARY.....	107
<b>2.2</b>	<b>DNA TECHNIQUES.....</b>	<b>113</b>
2.2.1	DNA AMPLIFICATION BY POLYMERASE CHAIN REACTION.....	113
2.2.2	AGAROSE GEL ELECTROPHORESIS.....	114
2.2.3	BACTERIAL TRANSFORMATION.....	115
2.2.4	DNA ISOLATION AND PURIFICATION.....	116
2.2.5	CLONING.....	117
2.2.6	SITE-DIRECTED MUTAGENESIS.....	126
2.2.7	DNA SEQUENCING .....	130
2.2.8	DNA PROCEDURES SUMMARY .....	133
<b>2.3</b>	<b>CELL CULTURE .....</b>	<b>134</b>
2.3.1	HUMAN CELL LINES MAINTENANCE .....	134
2.3.2	TRANSFECTION .....	134
2.3.3	SERUM STARVATION STUDIES.....	135
2.3.4	CELL PROCEDURES SUMMARY.....	135
<b>2.4</b>	<b>RNA TECHNIQUES .....</b>	<b>135</b>

2.4.1	RNA EXTRACTION.....	136
2.4.2	CDNA SYNTHESIS.....	138
2.4.3	PRIMERS FOR AMPLIFICATION OF TRANSCRIPTS OF INTEREST .....	141
2.4.4	PRIMERS FOR AMPLIFICATION OF ALTERNATIVE TRANSCRIPTS .....	141
2.4.5	RNA PROCEDURES SUMMARY .....	146
<b>2.5</b>	<b>PROTEIN TECHNIQUES .....</b>	<b>148</b>
2.5.1	PREPARATION OF PROTEIN SAMPLES.....	148
2.5.2	SDS-POLYACRYLAMIDE GEL ELECTROPHORESIS .....	148
2.5.3	WESTERN BLOTTING .....	149
2.5.4	CO-IMMUNO-PRECIPIATION.....	150
2.5.5	PROTEIN METHODS SUMMARY .....	151
<b>2.6</b>	<b>IMMUNOCYTOCHEMISTRY .....</b>	<b>151</b>
2.6.1	METHODS OF FIXATION: ADHERENT CELLS .....	151
2.6.2	IMMUNOFLUORESCENT STAINING OF CELLS.....	152
2.6.3	IMMUNOCYTOCHEMISTRY SUMMARY.....	152
<b>2.7</b>	<b>IMMUNOHISTOCHEMISTRY.....</b>	<b>153</b>
2.7.1	MOUSE EYE TREATMENT FOLLOWING ENUCLEATING .....	153
2.7.2	FIXATION AND CRYO-SECTIONING .....	153
2.7.3	IMMUNOFLUORESCENT STAINING OF TISSUE CRYO-SECTIONS.....	154
2.7.4	ANTIGEN RETRIEVAL .....	155
2.7.5	IMMUNOHISTOCHEMISTRY SUMMARY .....	156
<b>2.8</b>	<b>SUMMARY OF ANTIBODIES.....</b>	<b>156</b>
<b>2.9</b>	<b>MICROSCOPIC IMAGING.....</b>	<b>162</b>
<b>2.10</b>	<b>SUMMARY.....</b>	<b>162</b>
<b>3</b>	<b><u>CONSTRUCTION OF RETINAL LIBRARIES AND TOPORS BAITS.....</u></b>	<b>163</b>
<b>3.1</b>	<b>HUMAN RETINAL CDNA LIBRARY CONSTRUCTION AND CHARACTERISATION .....</b>	<b>164</b>
3.1.1	CDNA SYNTHESIS.....	164
3.1.2	YEAST TRANSFORMATION WITH CDNA FRAGMENTS.....	165
3.1.3	RETINAL CDNA LIBRARY CHARACTERISATION AND VALIDATION .....	166
<b>3.2</b>	<b>BAIT CONSTRUCTION AND CHARACTERISATION.....</b>	<b>174</b>
3.2.1	GENERATION OF FULL-LENGTH <i>TOPORS</i> BAIT AND DELETION CONSTRUCTS .....	175
3.2.2	CHARACTERISATION OF <i>TOPORS</i> BAIT AND DELETION CONSTRUCTS IN YEASTS .....	176
<b>3.3</b>	<b>DISCUSSION .....</b>	<b>185</b>
3.3.1	CONSTRUCTION AND VALIDATION OF CDNA LIBRARIES.....	185
3.3.2	BAIT CONSTRUCTION AND VALIDATION OF EXPRESSION.....	189
3.3.3	CONCLUSIONS.....	190

<b>4</b>	<b><u>LIBRARY SCREENING AND IDENTIFICATION OF POSITIVE INTERACTIONS</u></b>	<b>191</b>
4.1	YEAST MATING CONTROL EXPERIMENTS	193
4.2	IDENTIFICATION OF POSITIVE INTERACTIONS BY Y2H SCREENS	195
4.3	DISCUSSION	206
4.3.1	Y2H SCREENS AND PREY IDENTIFICATION	207
4.3.2	INTEGRAL MEMBRANE PROTEIN 2B	208
4.3.3	PROSTAGLANDIN D2 SYNTHASE	211
4.3.4	26 S PROTEASE REGULATORY SUBUNIT 4	215
4.3.5	CONCLUSIONS	219
<b>5</b>	<b><u>VERIFICATION OF EXPRESSION AND INTERACTIONS</u></b>	<b>220</b>
5.1	SPLICE VARIANTS OF <i>ITM2B</i> , <i>PTGDS</i> AND <i>PSMC1</i> EXPRESSED IN THE RETINA	221
5.1.1	<i>ITM2B</i> ISOFORM EXPRESSION STUDY	221
5.1.2	<i>PTGDS</i> ISOFORM EXPRESSION STUDY	224
5.1.3	<i>PSMC1</i> ISOFORM EXPRESSION STUDY	227
5.2	Y2H PPI VALIDATION EXPERIMENTS	230
5.2.1	CONTROL INTERACTION TESTING WITH GAL4 DNA-BD	230
5.2.2	DIRECT PROTEIN-PROTEIN INTERACTIONS (PPIs) IN YEAST	233
5.3	DISCUSSION	239
5.3.1	ISOFORM EXPRESSION EXPERIMENTS	240
5.3.2	Y2H DIRECT PPI VALIDATION EXPERIMENTS	244
5.3.3	CONCLUSIONS	251
<b>6</b>	<b><u>PROTEIN EXPRESSION AND INTERACTION ANALYSIS IN CELLS</u></b>	<b>252</b>
6.1	TOPORS PROTEIN EXPRESSION ANALYSIS	254
6.1.1	TOPORS WESTERN BLOT EXPERIMENTS	254
6.1.2	CONTROL COIP EXPERIMENT	255
6.2	<i>ITM2B</i> PROTEIN EXPRESSION ANALYSIS	257
6.2.1	<i>ITM2B</i> WESTERN BLOT EXPERIMENTS	257
6.2.2	<i>ITM2B</i> IS FOUND IN PROTEIN COMPLEXES WITH TOPORS	260
6.3	<i>PTGDS</i> PROTEIN EXPRESSION ANALYSIS	262
6.3.1	<i>PTGDS</i> WESTERN BLOT EXPERIMENTS	262
6.3.2	<i>PTGDS</i> IS FOUND IN PROTEIN COMPLEXES WITH TOPORS	264
6.4	<i>PSMC1</i> PROTEIN EXPRESSION ANALYSIS	266
6.4.1	<i>PSMC1</i> WESTERN BLOT EXPERIMENTS	267
6.4.2	<i>PSMC1</i> IS FOUND IN PROTEIN COMPLEXES WITH TOPORS	267
6.5	DISCUSSION	269
6.5.1	<i>ITM2B</i> PROTEIN EXPRESSION	269

6.5.2	PTGDS PROTEIN EXPRESSION .....	273
6.5.3	PSMC1 PROTEIN EXPRESSION .....	279
6.5.4	CONCLUSIONS.....	280
<b>7</b>	<b><u>CELLULAR LOCALISATION STUDIES.....</u></b>	<b>282</b>
7.1	CELLULAR LOCALISATION OF TOPORS .....	283
7.2	CELLULAR LOCALISATION OF ITM2B.....	287
7.3	CELLULAR LOCALISATION OF PTGDS.....	296
7.4	CELLULAR LOCALISATION OF PSMC1 .....	303
7.5	IDENTIFICATION OF CILIARY TARGETING SEQUENCES .....	308
7.6	DISCUSSION .....	310
7.6.1	EVALUATION OF LOCALISATION.....	310
7.6.2	CONCLUSIONS.....	315
<b>8</b>	<b><u>RETINAL TISSUE LOCALISATION STUDIES .....</u></b>	<b>316</b>
8.1	RETINAL LOCALISATION OF ITM2B .....	319
8.2	RETINAL LOCALISATION OF PTGDS.....	325
8.3	RETINAL LOCALISATION OF PSMC1.....	330
8.4	DISCUSSION .....	333
8.4.1	EVALUATION OF ITM2B LOCALISATION.....	337
8.4.2	EVALUATION OF PTGDS LOCALISATION.....	340
8.4.3	EVALUATION OF PSMC1 LOCALISATION .....	344
8.4.4	CONCLUSIONS.....	349
<b>9</b>	<b><u>DISCUSSION.....</u></b>	<b>350</b>
9.1	ITM2B COULD HAVE MULTIPLE ROLES IN THE RETINA.....	352
9.2	PTGDS COULD BE REQUIRED FOR INTRA-RETINAL SIGNALLING.....	360
9.3	PSMC1 COULD HAVE PROTECTIVE FUNCTIONS IN THE RETINA .....	366
9.4	FUTURE PERSPECTIVES .....	370
9.5	ALTERNATIVE APPROACHES.....	374
9.6	CONCLUSIONS.....	378
<b>10</b>	<b><u>BIBLIOGRAPHY.....</u></b>	<b>380</b>
<b>11</b>	<b><u>APPENDIX.....</u></b>	<b>403</b>
11.1	RETINAL CDNA LIBRARY CHARACTERISATION .....	403
11.2	SUMMARY OF INITIAL ATTEMPTS TO CLONE <i>TOPORS</i> .....	429
11.2.1	IN-FUSION CLONING.....	429
11.2.2	<i>EcoRI</i> & <i>SAL1</i> RESTRICTION DIGEST AND LIGATION.....	431
11.2.3	<i>NdeI</i> & <i>PstI</i> RESTRICTION DIGEST AND LIGATION .....	437
11.2.4	GATEWAY CLONING .....	445

<b>11.3</b>	<b>Y2H GOLD YEAST TRANSFORMATION RESULTS .....</b>	<b>446</b>
<b>11.4</b>	<b>SUMMARY OF INITIAL ATTEMPTS TO CONFIRM BAIT AND DELETION CONSTRUCT PROTEIN EXPRESSION IN TRANSFORMED YEAST CELLS.....</b>	<b>448</b>
<b>11.5</b>	<b><i>P53</i> CLONING USING GATEWAY SYSTEM.....</b>	<b>450</b>
<b>11.6</b>	<b>CANDIDATE INTERACTING PARTNERS OF TOPORS .....</b>	<b>451</b>
<b>11.7</b>	<b>DETERMINATION OF RETINAL EXPRESSION .....</b>	<b>470</b>
<b>11.8</b>	<b>CLONING OF <i>ITM2B</i>, <i>PTGDS</i> AND <i>PSMC1</i> .....</b>	<b>475</b>
11.8.1	RNA EXTRACTION AND CHARACTERISATION .....	475
11.8.2	COMPLEMENTARY DNA GENERATION AND CHARACTERISATION.....	476
11.8.3	AMPLIFICATION OF <i>ITM2B</i> AND ITS FRAGMENTS.....	476
11.8.4	<i>PTGDS</i> AMPLIFICATION .....	480
11.8.5	<i>PSMC1</i> AMPLIFICATION .....	481
<b>11.9</b>	<b>FULL-LENGTH TOPORS AND DOMAIN FRAGMENTS (N, M AND C) INTERACTIONS IN YEAST - RAW RESULTS.....</b>	<b>482</b>
<b>11.10</b>	<b>ALIGNMENT OF PROTEIN-CODING <i>PTGDS</i> ISOFORMS.....</b>	<b>486</b>
<b>11.11</b>	<b>POSTERS PRESENTED AT SCIENCE CONFERENCES .....</b>	<b>487</b>

## **LIST OF FIGURES**

FIGURE 1-1. STRUCTURE OF THE EYE .....	34
FIGURE 1-2. STRUCTURE OF THE RETINA .....	36
FIGURE 1-3. STRUCTURE OF THE PHOTORECEPTOR CELLS.....	39
FIGURE 1-4. THE RETINAL PIGMENTED EPITHELIUM, ITS COMPONENTS AND FUNCTIONS.....	40
FIGURE 1-5. THE VISUAL CYCLE .....	43
FIGURE 1-6. FUNCTIONAL CATEGORISATION OF GENES THAT INFLUENCE PHOTORECEPTOR DEGENERATION.....	45
FIGURE 1-7. FREQUENCY OF ADRP MUTATIONS FOUND IN ADRP COHORTS BY GENE.....	46
FIGURE 1-8. PEDIGREES AND SEQUENCE ANALYSES OF <i>TOPORS</i> MUTATIONS IN FRENCH-CANADIAN AND GERMAN PEDIGREES.....	49
FIGURE 1-9. PEDIGREES OF ADRP FAMILIES UTAD102 AND RFS169 AFFECTED BY <i>TOPORS</i> MUTATIONS.....	50
FIGURE 1-10. PEDIGREE OF THE ADPRD NORWEGIAN FAMILY CARRYING A MISSENSE <i>TOPORS</i> MUTATION.....	52
FIGURE 1-11. COLOUR PHOTOGRAPH OF THE RIGHT EYE OF A 10-YEAR-OLD AFFECTED CHILD (IV:3 IN FIGURE 1-8 A).....	54
FIGURE 1-12. RT-PCR ANALYSIS OF <i>TOPORS</i> TRANSCRIPT IN HUMAN TISSUES. ....	55
FIGURE 1-13. <i>TOPORS</i> EXPRESSION IN PATIENT LYMPHOBLASTOID CELL LINES. ....	55
FIGURE 1-14. FUNDUS PHOTOGRAPHS FROM A MEMBER OF FAMILY RFS169 (A AND B) AND A PATIENT WITH A PERICENTRAL RETINAL DYSTROPHY (C).....	57
FIGURE 1-15. FUNDUS PHOTOGRAPHS FROM A MEMBER OF THE NORWEGIAN FAMILY. ....	58
FIGURE 1-16. <i>TOPORS</i> PROTEIN STRUCTURE.....	61
FIGURE 1-17. THE UBIQUITINATION PATHWAY LEADING TO PROTEASOMAL DEGRADATION. ....	63
FIGURE 1-18. THE SUMOYLATION PATHWAY.....	66
FIGURE 1-19. MODEL OF THE REGULATION OF CILIA FORMATION BY CP110 IN CYCLING AND QUIESCENT CELLS.....	70
FIGURE 1-20. CILIARY STRUCTURE IN VERTEBRATES. ....	72
FIGURE 1-21. FIGURE 1 21. THE CONNECTING CILIUM OF PHOTORECEPTOR CELLS. ....	73
FIGURE 2-1. BASIS OF THE Y2H ASSAY.....	79
FIGURE 2-2. SMART cDNA SYNTHESIS. ....	100
FIGURE 2-3. <i>TOPORS</i> EXPRESSION AT mRNA LEVEL. IMAGE FROM GENE CARDS DATABASE. ....	108
FIGURE 2-4. <i>RHO</i> EXPRESSION AT mRNA LEVEL. IMAGE FROM GENE CARDS DATABASE.....	109
FIGURE 2-5. COMPARISON OF <i>TOPORS</i> AND <i>RHO</i> EXPRESSION IN HUMAN RETINA. ....	110
FIGURE 2-6. <i>TOPORS</i> EXPRESSION AT PROTEIN LEVEL. IMAGE FROM GENE CARDS DATABASE.....	112
FIGURE 2-7. IN-FUSION CLONING METHOD. ....	119
FIGURE 2-8. THE GATEWAY BP AND LR REACTIONS.....	123
FIGURE 2-9. A FRAGMENT OF A MUTATED SEQUENCE OF pDONR- <i>PSMC1</i> ENTRY CLONE.....	127
FIGURE 2-10. GENEART SDM WORKFLOW.....	129
FIGURE 2-11. OUTLINE OF PRIMER SETS FOR AMPLIFICATION OF <i>ITM2B</i> EXONS TO DETECT SPECIFIC ISOFORMS..	143
FIGURE 2-12. OUTLINE OF PRIMER SETS FOR AMPLIFICATION OF <i>PTGDS</i> EXONS TO DETECT SPECIFIC ISOFORMS.	145
FIGURE 2-13. OUTLINE OF PRIMER SETS FOR AMPLIFICATION OF <i>PSMC1</i> EXONS TO DETECT SPECIFIC ISOFORMS.	147
FIGURE 3-1. SMART cDNA SYNTHESIS RESULTS.....	164



FIGURE 3-2. HUMAN RETINAL CDNA LIBRARY CONSTRUCTION IN THE Y187 YEAST STRAIN.....	165
FIGURE 3-3. SELECTION OF THE HUMAN RETINAL CDNA LIBRARY AMPLICONS. ....	167
FIGURE 3-4. DEMONSTRATION OF A PPI BETWEEN TOPORS AND P53. ....	179
FIGURE 3-5. TOPORS PROTEIN DIAGRAM.....	181
FIGURE 3-6. BAIT AUTO-ACTIVATION TESTING. ....	182
FIGURE 3-7. COMPARISON OF COLONY SIZES TRANSFORMED WITH PGBKT7 VS. PGBKT7-N-TERM. ....	183
FIGURE 3-8. COMPARISON OF COLONY SIZES TRANSFORMED WITH PGBKT7 VS. PGBKT7-MID- <i>TOPORS</i> .....	183
FIGURE 3-9. COMPARISON OF COLONY SIZES TRANSFORMED WITH PGBKT7 VS. PGBKT7-C-TERM.....	184
FIGURE 3-10 COMPARISON OF COLONY SIZES TRANSFORMED WITH PGBKT7 VS. PBD- <i>TOPORS</i> .....	184
FIGURE 4-1. OVERVIEW OF THE Y2H LIBRARY SCREEN WORKFLOW. ....	192
FIGURE 4-2. Y2H CONTROL P53 X SV40 T AG PPI: A COMPARISON OF <i>P53</i> CONSTRUCTS (PBD-P53 VS. PGBKT7-53).....	195
FIGURE 4-3. A, EXAMPLE OF SINGLE PLATE FROM Y2H O-dT LIBRARY SCREEN. ....	196
FIGURE 4-4. A, EXAMPLE OF SINGLE PLATE FROM Y2H R&O-dT LIBRARY SCREEN.....	196
FIGURE 4-5. PCR AMPLIFICATION OF PREY INSERTS, PULLED OUT FROM THE R&O-dT CDNA Y2H LIBRARY SCREEN (MANGO <i>TAQ</i> POLYMERASE). ....	197
FIGURE 4-6. <i>PTGDS</i> ALIGNMENTS.....	203
FIGURE 4-7. MULTIPLE CLONING SITE (MCS) OF THE PGADT7-REC VECTOR, IN WHICH THE HUMAN RETINAL CDNA LIBRARY WAS CONSTRUCTED. ....	204
FIGURE 4-8. ONE OF <i>PTGDS</i> LIBRARY CLONES: SEQUENCE SNAPSHOT.....	204
FIGURE 4-9. <i>ITM2B</i> ALIGNMENTS. SNAPSHOT OF RESULTS OBTAINED FROM BLAT (UCSC) GENOME SEARCH.....	205
FIGURE 4-10. ONE OF <i>ITM2B</i> LIBRARY CLONES: SEQUENCE SNAPSHOT. ....	205
FIGURE 4-11. <i>PSMC1</i> CLONE R&O-dT 2.2 ALIGNMENT.....	205
FIGURE 4-12. <i>PSMC1</i> LIBRARY CLONE: SEQUENCE SNAPSHOT. ....	205
FIGURE 4-13. PROSTAGLANDIN D2 (PGD) SYNTHASE AS A COMPONENT OF ARACHIDONIC ACID METABOLISM.....	212
FIGURE 4-14. PSMC1 FORMS A KEY COMPONENT OF THE REGULATORY ATPASE RING OF THE 26 S PROTEASE...	216
FIGURE 4-15. <i>PSMC1</i> MUTATION EFFECTS ON THE MORPHOLOGY OF <i>ARABIDOPSIS THALIANA</i> SEEDLINGS.....	217
FIGURE 5-1. <i>ITM2B</i> ISOFORM 001. ....	222
FIGURE 5-2. RESULTS OF <i>ITM2B</i> ISOFORM EXPRESSION STUDY. ....	223
FIGURE 5-3. RESULTS OF <i>PTGDS</i> ISOFORM EXPRESSION STUDY.....	225
FIGURE 5-4. RESULTS OF <i>PSMC1</i> ISOFORM EXPRESSION STUDY.....	227
FIGURE 5-5. PSMC1 ISOFORM 001.....	228
FIGURE 5-6. PTGDS-001 PROTEIN CRYSTAL STRUCTURE. ....	242
FIGURE 5-7. <i>PTGDS</i> -004 ALIGNMENT WITH THE SEQUENCE OF THE IMMUNOGEN, USED TO GENERATE THE ANTIBODY AGAINST PTGDS-001 (SC-30067, SANTA CRUZ BIOTECHNOLOGY). ....	243
FIGURE 5-8. <i>PTGDS</i> -005 ALIGNMENT WITH THE SEQUENCE OF THE IMMUNOGEN, USED TO GENERATE THE ANTIBODY AGAINST PTGDS-001 (SC-30067, SANTA CRUZ BIOTECHNOLOGY). ....	243
FIGURE 5-9. AMINO-TERMINUS (N) TOPORS BAIT (RESIDUES 1-380).....	244
FIGURE 5-10. MID-TOPORS (M) BAIT (RESIDUES 373-781). ....	245

FIGURE 5-11. CARBOXY-TERMINUS (N) TOPORS BAIT (RESIDUES 705-1045).....	245
FIGURE 5-12. ITM2B PROTEIN STRUCTURE AND PROCESSING DETAILS.....	247
FIGURE 6-1. WESTERN BLOTS AGAINST TOPORS.....	255
FIGURE 6-2. GAMMA TUBULIN IS DETECTED IN COMPLEXES PRECIPITATED FROM HE <sup>L</sup> A CELL EXTRACT WITH ANTIBODY AGAINST TOPORS, RAISED IN MOUSE.....	255
FIGURE 6-3. TOPORS PROTEIN DOMAIN STRUCTURE.....	256
FIGURE 6-4. WESTERN BLOT AGAINST ENDOGENOUS ITM2B C-TERM (AB DILUTED 1/250).....	257
FIGURE 6-5. ITM2B PROTEIN DOMAIN STRUCTURE.....	258
FIGURE 6-6. WESTERN BLOT AGAINST OVER-EXPRESSED ITM2B.....	259
FIGURE 6-7. ITM2B C-TERM (ABGENT) IS DETECTED IN COMPLEXES PRECIPITATED FROM HE <sup>L</sup> A CELL EXTRACTS WITH ANTIBODY AGAINST TOPORS, RAISED IN MOUSE.....	260
FIGURE 6-8. PTGDS PROTEIN DOMAIN STRUCTURE.....	263
FIGURE 6-9. WESTERN BLOT AGAINST PTGDS (AB DILUTED 1/500).....	264
FIGURE 6-10. PTGDS IS DETECTED IN COMPLEXES PRECIPITATED FROM HE <sup>L</sup> A CELL EXTRACT WITH ANTIBODY AGAINST TOPORS, RAISED IN MOUSE.....	265
FIGURE 6-11. PSMC1 PROTEIN DOMAIN STRUCTURE.....	266
FIGURE 6-12. WESTERN BLOT AGAINST ENDOGENOUS PSMC1 (AB DILUTED 1/250).....	268
FIGURE 6-13. PSMC1 IS DETECTED IN COMPLEXES PRECIPITATED FROM HE <sup>L</sup> A CELL EXTRACT WITH ANTIBODY AGAINST TOPORS.....	268
FIGURE 6-14. VISUAL REPRESENTATION OF PUTATIVE CARBOHYDRATE MODIFICATIONS.....	274
FIGURE 7-1. CYTOPLASMIC TOPORS SIGNAL APPEARS PARTLY FILAMENTOUS AND PARTLY GRANULAR IN BOTH RETINAL EPITHELIAL AND NEUROBLASTOMA CELL TYPES.....	284
FIGURE 7-2. TOPORS SIGNAL IN BOTH RETINAL EPITHELIAL AND NEUROBLASTOMA CELL TYPES APPEARS MOSTLY CYTOPLASMIC: PARTLY FILAMENTOUS AND PARTLY GRANULAR; WHEREAS THE LOCALISATION IS MOSTLY NUCLEAR IN EMBRYONIC CELLS.....	286
FIGURE 7-3. ITM2B C-TERM LOCALISES THROUGHOUT THE CYTOPLASM IN RETINAL EPITHELIAL AND NEUROBLASTOMA CELL TYPES.....	289
FIGURE 7-4. ITM2B C-TERM LOCALISES THROUGHOUT THE CYTOPLASM IN RETINAL EPITHELIAL AND NEUROBLASTOMA CELL TYPES; HOWEVER, THE SIGNAL APPEARS MORE POLARISED IN THE LATTER.....	289
FIGURE 7-5. ITM2B LOCALISES THROUGHOUT THE CYTOPLASM IN A GRANULAR PATTERN IN RETINAL EPITHELIAL CELLS.....	290
FIGURE 7-6. ITM2B C-TERM AND TOPORS CO-LOCALISE IN RETINAL EPITHELIAL CELLS IN A CENTRIOLE-LIKE PATTERN.....	291
FIGURE 7-7. ITM2B C-TERM CO-LOCALISES WITH TOPORS AND FORMS AN ADDITIONAL CLOUD-LIKE SIGNAL AROUND THE REGION OF CO-LOCALISATION.....	291
FIGURE 7-8. ITM2B C-TERM CO-LOCALISES WITH THE PERI-CENTRIOLAR MARKER: PCM1.....	292
FIGURE 7-9. ITM2B C-TERM CO-LOCALISES WITH THE CENTRIOLAR AND DEUTEROSOMAL MARKER: PLK4.....	293
FIGURE 7-10. ITM2B C-TERM CO-LOCALISES WITH THE CENTRIOLAR MARKER: CENTRIN-2.....	294
FIGURE 7-11. ITM2B C-TERM DOES NOT LOCALISE TO THE CILIARY BASAL BODY.....	295

FIGURE 7-12. PTGDS LOCALISES THROUGHOUT THE CYTOPLASM OF RETINAL EPITHELIAL (hTERT-RPE1) CELLS IN A GRANULAR PATTERN, BUT APPEARS ABSENT FROM THE NEUROBLASTOMA (SK-N-SH) CELLS..... 297

FIGURE 7-13. PTGDS LOCALISES THROUGHOUT THE CYTOPLASM OF RETINAL EPITHELIAL (hTERT-RPE1) AND NEUROBLASTOMA (SK-N-SH) CELLS, INCLUDING MORE INTENSELY-STAINED CENTRIOLE-LIKE PUNCTA. .... 297

FIGURE 7-14. PTGDS CO-LOCALISES WITH TOPORS IN RETINAL EPITHELIAL CELLS IN A CENTRIOLE-LIKE PATTERN. .... 298

FIGURE 7-15. PTGDS CO-LOCALISES WITH TOPORS IN RETINAL EPITHELIAL CELLS IN A CENTRIOLE-LIKE PATTERN. .... 298

FIGURE 7-16. PTGDS CO-LOCALISES WITH THE PERI-CENTRIOLAR MARKER: PCM1. .... 300

FIGURE 7-17. PTGDS CO-LOCALISES WITH THE CENTRIOLAR AND DEUTEROSOMAL MARKER: PLK4..... 300

FIGURE 7-18. PTGDS CO-LOCALISES WITH THE CENTRIOLAR MARKER: CENTRIN-2..... 301

FIGURE 7-19. PTGDS LOCALISES TO BOTH CENTRIOLES OF THE CILIARY BASAL BODY..... 302

FIGURE 7-20. PTGDS LOCALISES TO THE CILIARY BASAL BODY AND ALONG THE CILIARY AXONEME..... 302

FIGURE 7-21. PSMC1 LOCALISES THROUGHOUT THE CYTOPLASM OF RETINAL EPITHELIAL (hTERT-RPE1) AND NEUROBLASTOMA (SK-N-SH) CELLS WITH A DISTINCT REGION OF HIGHER INTENSITY IN THE LATTER. .... 303

FIGURE 7-22. PSMC1 LOCALISES THROUGHOUT THE CYTOPLASM OF RETINAL EPITHELIAL (hTERT-RPE1) CELLS WITH DISTINCT REGIONS OF HIGHER INTENSITY. .... 304

FIGURE 7-23. PSMC1 LOCALISES THROUGHOUT THE CYTOPLASM IN A DOTTED PATTERN, SOME OF WHICH IS REMINISCENT OF CENTRIOLES (ARROWS). .... 305

FIGURE 7-24. PSMC1 CO-LOCALISES WITH TOPORS IN A CENTRIOLE-LIKE PATTERN. .... 305

FIGURE 7-25. IN THE SELECTED CELLS PSMC1 CO-LOCALISES WITH THE PERI-CENTRIOLAR MARKER: PCM1. .... 305

FIGURE 7-26. IN THE SELECTED CELLS PSMC1 DOES NOT CO-LOCALISE WITH THE PERI-CENTRIOLAR MARKER: PCM1..... 306

FIGURE 7-27. PSMC1 CO-LOCALISES WITH THE CENTRIOLAR AND DEUTEROSOMAL MARKER: PLK4. .... 306

FIGURE 7-28. IN SELECTED CELLS PSMC1 CO-LOCALISES WITH THE CENTRIOLAR MARKER: CENTRIN-2..... 306

FIGURE 7-29. PSMC1 DOES NOT LOCALISE TO THE CILIARY BASAL BODY..... 307

FIGURE 8-1. TOPORS AND PNA STAINING: C57 BLACK 6 MOUSE RETINA SECTION (2 WEEKS OLD AT TIME OF TISSUE COLLECTION)..... 318

FIGURE 8-2. ITM2B AND PNA (MARKING CONE PHOTORECEPTORS) STAINING: C57 BLACK 6 MOUSE RETINA SECTION (2 WEEKS OLD AT TIME OF TISSUE COLLECTION)..... 321

FIGURE 8-3. ITM2B STAINING: C57 BLACK 6 MOUSE RETINA SECTION (6.5 WEEKS OLD AT TIME OF TISSUE COLLECTION) SUBJECT TO HEAT-INDUCED EPITOPE RETRIEVAL (HIER)..... 322

FIGURE 8-4. TOPORS AND ITM2B STAINING: C57 BLACK 6 MOUSE RETINA SECTIONS (2 WEEKS OLD AT TIME OF TISSUE COLLECTION)..... 323

FIGURE 8-5. ITM2B & TOPORS CO-STAINING IN PRIMATE (MACACA FASCICULARIS) RETINA SECTION – KINDLY PROVIDED BY PROF. GLEN JEFFERY (SECTION DETAILS: #2, 992G, YOUNG, 6 & 7, 10 µM, PERIPHERAL RETINA)..... 324

FIGURE 8-6. PTGDS AND PNA STAINING: C57 BLACK 6 MOUSE RETINA SECTION (2 WEEKS OLD AT TIME OF TISSUE COLLECTION).....	326
FIGURE 8-7. TOPORS AND PTGDS STAINING: C57 BLACK 6 MOUSE RETINA SECTIONS (2 WEEKS OLD AT TIME OF TISSUE COLLECTION).....	327
FIGURE 8-8. PTGDS AND TOPORS STAINING IN C57 BLACK 6 MOUSE RETINA SECTIONS (6.5 MONTHS OLD AT TIME OF TISSUE COLLECTION).....	328
FIGURE 8-9. PTGDS & TOPORS STAINING IN PRIMATE (MACACA FASCICULARIS) RETINA SECTIONS (SLIDE DETAILS: #2, 992G, YOUNG, 6 & 7, 10 μM, PERIPHERY – KINDLY PROVIDED BY PROF. GLEN JEFFERY).....	329
FIGURE 8-10. PSMC1 AND TOPORS CO-STAINING: C57 BLACK 6 MOUSE RETINA SECTIONS (6.5 MONTHS OLD AT TIME OF TISSUE COLLECTION).....	331
FIGURE 8-11. PSMC1 AND TOPORS CO-STAINING: C57 BLACK 6 MOUSE RETINA SECTION (6.5 MONTHS OLD AT TIME OF TISSUE COLLECTION) SUBJECT TO HEAT-INDUCED EPITOPE RETRIEVAL (HIER).....	332
FIGURE 8-12. ITM2B CTS#1: AA44 – AA46. SPECIES AND CTS ARE BOXED INSIDE PURPLE RECTANGLES.....	338
FIGURE 8-13. ITM2B CTS#2 AND #3. SPECIES AND CTS ARE BOXED INSIDE PURPLE RECTANGLES.....	338
FIGURE 8-14. PTGDS CTS#1. SPECIES AND CTS ARE BOXED INSIDE PURPLE RECTANGLES.....	343
FIGURE 8-15. PTGDS CTS#2. SPECIES AND CTS ARE BOXED INSIDE PURPLE RECTANGLES.....	343
FIGURE 8-16. PSMC1 CTS#1.....	346
FIGURE 8-17. PSMC1 CTS#2.....	346
FIGURE 11-1. PCR AMPLIFICATION OF FULL-LENGTH TOPORS, USING KOD POLYMERASE.....	430
FIGURE 11-2. PCR AMPLIFICATION OF THE N-TERMINAL TOPORS FRAGMENT, USING KOD POLYMERASE.....	430
FIGURE 11-3. PCR AMPLIFICATION OF THE MID-TOPORS FRAGMENT, USING KOD POLYMERASE.....	430
FIGURE 11-4. PCR AMPLIFICATION OF THE C-TERMINAL TOPORS FRAGMENT, USING KOD POLYMERASE.....	430
FIGURE 11-5. GEL ELECTROPHORESIS OF UNDIGESTED AND DIGESTED PGBKT7 VECTORS.....	433
FIGURE 11-6. GEL ELECTROPHORESIS OF UNDIGESTED AND DIGESTED PGBKT7 VECTOR.....	433
FIGURE 11-7. SCHEMATIC REPRESENTATION OF THE REGION OF THE VECTOR-INSERT CONSTRUCT, WHICH WOULD BE AMPLIFIED USING THE T7 AND S8 PRIMERS.....	433
FIGURE 11-8. PCR AMPLIFICATION USING THE LIGATION REACTION AS TEMPLATE (VECTOR AND INSERT DIGESTION WITH <i>EcoRI</i> AND <i>SAL1</i> ), USING VECTOR-SPECIFIC PRIMER T7 (TABLE 2-50), AND <i>TOPORS</i> -SPECIFIC PRIMER S8 (TABLE 2-51).....	434
FIGURE 11-9. COLONY PCR SCREENING OF DH5A BACTERIAL CELLS TRANSFORMED WITH THE LIGATION REACTION (FOLLOWING VECTOR AND INSERT DIGESTION WITH <i>EcoRI</i> AND <i>SAL1</i> ).....	435
FIGURE 11-10. RESULT OBTAINED FROM SEQUENCING OF PLASMIDS, ISOLATED FROM COLONIES, WHICH APPEARED TO CONTAIN THE <i>TOPORS</i> INSERT, BASED ON THE COLONY PCR RESULTS (FIGURE 11-9).....	436
FIGURE 11-11. CONTROL EXPERIMENT TO CLARIFY THE INCONSISTENCY OF RESULTS (OBTAINED AMPLICON SIZES) BETWEEN THE LIGATION REACTION PCR (FIGURE 11-8) AND THE COLONY PCR (FIGURE 11-9).....	437
FIGURE 11-12. PCR AMPLIFICATION OF TOPORS USING THE FL F AND FL R PRIMERS (TABLE 2-36).....	438
FIGURE 11-13. PCR AMPLIFICATION OF TOPORS USING THE FL F AND FL R PRIMERS.....	439
FIGURE 11-14. GEL ELECTROPHORESIS OF DIGESTED AND UNDIGESTED PGBKT7 VECTOR.....	440

FIGURE 11-15. SCHEMATIC REPRESENTATION OF THE REGION OF THE VECTOR-INSERT CONSTRUCT, WHICH WOULD BE AMPLIFIED USING THE S9 AND PGBKT7 R1 PRIMERS. ....	440
FIGURE 11-16. PCR AMPLIFICATION USING THE LIGATION REACTION AS TEMPLATE, (VECTOR AND INSERT DIGESTION WITH ECORI AND SALI AS WELL AS NDEI AND PSTI).....	441
FIGURE 11-17. YEAST COLONY PCR SCREENING FOR <i>TOPORS</i> (THE LIGATION REACTION PRODUCTS WERE USED FOR A PILOT TRANSFORMATION OF THE YEAST, FOLLOWING UNSUCCESSFUL ATTEMPTS TO TRANSFORM BACTERIA). ....	443
FIGURE 11-18. PCR AMPLIFICATION OF PLASMIDS ISOLATED FROM THE YEAST COLONY PCR POSITIVE CLONE (SEE FIGURE 11-17). ....	444
FIGURE 11-19. COLONY PCR SCREENING FOR <i>TOPORS</i> IN THE PLASMIDS ISOLATED FROM BACTERIA, PREVIOUSLY TRANSFORMED WITH PLASMID ISOLATED FROM POSITIVE YEAST CLONE (SEE FIGURE 11-17).....	444
FIGURE 11-20. FULL-LENGTH <i>TOPORS</i> PCR PRODUCT AMPLIFIED USING GATEWAY-SPECIFIC PRIMERS.....	445
FIGURE 11-21. COMPLETE FULL-LENGTH <i>TOPORS</i> SEQUENCE CLONED INTO THE PBD VECTOR.....	446
FIGURE 11-22. PCR AMPLIFICATION PRODUCT OF <i>TOPORS</i> FROM PBD- <i>TOPORS</i> VECTORS ISOLATED FROM YEAST (CLONES A-D).....	446
FIGURE 11-23. PCR AMPLIFICATION PRODUCT OF N-TERM AND C-TERM <i>TOPORS</i> FRAGMENTS FROM THE PGBKT7- <i>TOPORS</i> VECTORS ISOLATED FROM YEAST.....	447
FIGURE 11-24. PCR AMPLIFICATION PRODUCTS OF THE SHORT <i>TOPORS</i> FRAGMENTS CLONED INTO PGBKT7 CONSTRUCTS ISOLATED FROM YEAST. ....	447
FIGURE 11-25. ANTI GAL4 BD AB.....	449
FIGURE 11-26. ANTI <i>TOPORS</i> AB.....	449
FIGURE 11-27. ANTI GAL4 BD AB.....	449
FIGURE 11-28. FULL-LENGTH <i>p53</i> PCR PRODUCT AMPLIFIED USING GATEWAY-SPECIFIC PRIMERS. ....	450
FIGURE 11-29. SNAPSHOT OF <i>ITM2B</i> TRANSCRIPT DETAILS AND THE RESULTING SPLICE VARIANTS FROM THE ENSEMBL DATABASE.....	470
FIGURE 11-30. SNAPSHOT OF <i>ITM2B</i> TRANSCRIPT DETAILS FROM THE EYEBROWSE GATEWAY, POWERED BY THE UCSC DATABASE.....	470
FIGURE 11-31. SNAPSHOT OF <i>PTGDS</i> TRANSCRIPT DETAILS AND THE RESULTING SPLICE VARIANTS FROM THE ENSEMBL DATABASE.....	471
FIGURE 11-32. SNAPSHOT OF <i>PTGDS</i> TRANSCRIPT DETAILS FROM THE EYEBROWSE GATEWAY, POWERED BY THE UCSC DATABASE. THE IMAGE WAS TRIMMED: NOT ALL OF THE RPE ESTS ARE DISPLAYED. ....	472
FIGURE 11-33. SNAPSHOT OF <i>PSMC1</i> TRANSCRIPT DETAILS AND THE RESULTING SPLICE VARIANTS FROM THE ENSEMBL DATABASE.....	473
FIGURE 11-34. SNAPSHOT OF <i>PSMC1</i> TRANSCRIPT DETAILS FROM THE EYEBROWSE GATEWAY, POWERED BY THE UCSC DATABASE.....	474
FIGURE 11-35. GENOMIC ALIGNMENTS OF PCR PRODUCTS AMPLIFIED FROM GDNA, USING <i>PSMC1</i> EXON-SPECIFIC PRIMERS. ....	474
FIGURE 11-36. EXTRACTED RNA SAMPLES A-C.....	476

FIGURE 11-37. HPRT AND VAX2 AMPLICONS, GENERATED TO TEST THE QUALITY OF THE NEWLY SYNTHESISED CDNA. ....	476
FIGURE 11-38. <i>ITM2B</i> AMPLICON FROM RPE1 CDNA.....	477
FIGURE 11-39. <i>ATTB-ITM2B-ATTB</i> AMPLICONS.....	477
FIGURE 11-40. PUTATIVE <i>ATTB-ITM2B90-ATTB</i> AMPLICONS.....	477
FIGURE 11-41. MUTANT <i>ITM2B</i> GATEWAY AMPLICONS.....	478
FIGURE 11-42. CONFIRMED SEQUENCE OF THE <i>ATTB-ITM2B_RET</i> MU- <i>ATTB</i> AMPLICON ( <i>ITM2B</i> RETINAL DYSTROPHY MUTANT).....	478
FIGURE 11-43. CONFIRMED SEQUENCE OF THE <i>ATTB-ITM2B_FBD-ATTB</i> AMPLICON ( <i>ITM2B</i> FAMILIAL BRITISH DEMENTIA MUTANT). ....	479
FIGURE 11-44. CONFIRMED SEQUENCE OF THE <i>ATTB-ITM2B_FDD_MU-ATTB</i> AMPLICON ( <i>ITM2B</i> FAMILIAL DANISH DEMENTIA MUTANT). ....	479
FIGURE 11-45. <i>PTGDS</i> AMPLICONS FROM RPE1 CDNA.....	480
FIGURE 11-46. <i>ATTB-PTGDS-ATTB</i> AMPLICONS.....	480
FIGURE 11-47. <i>ATTB-PSMC1-ATTB</i> AMPLICONS.....	481
FIGURE 11-48. MISSENSE MUTATION (c.55A>G → p.Lys19Glu) WAS IDENTIFIED IN THE <i>PSMC1</i> AMPLICON OF THE EXPECTED SIZE, AS WELL AS THE CONSTRUCT. ....	481
FIGURE 11-49. <i>pDONR_PSMC1</i> AMPLICON (LINEAR VECTOR).....	482
FIGURE 11-50. THE SEQUENCE OF THE IMMUNOGEN, USED TO GENERATE THE ANTIBODY AGAINST <i>PTGDS</i> (sc-30067, SANTA CRUZ BIOTECHNOLOGY), CORRESPONDS TO THE <i>PTGDS</i> ISOFORM 001. ....	486
FIGURE 11-51. THE SEQUENCE OF THE IMMUNOGEN, USED TO GENERATE THE ANTIBODY AGAINST <i>PTGDS</i> (sc-30067, SANTA CRUZ BIOTECHNOLOGY), ALIGNS APPROXIMATELY WITH THE N-TERMINAL HALF OF <i>PTGDS</i> ISOFORM 003. ....	487
FIGURE 11-52. THE SEQUENCE OF THE IMMUNOGEN, USED TO GENERATE THE ANTIBODY AGAINST <i>PTGDS</i> (sc-30067, SANTA CRUZ BIOTECHNOLOGY), SHOWS VIRTUALLY NO ALIGNMENT WITH <i>PTGDS</i> ISOFORM 008. ....	487

## **LIST OF TABLES**

TABLE 1-1. MUTATIONS IDENTIFIED IN <i>TOPORS</i> TO DATE.....	52
TABLE 1-2. CLINICAL PHENOTYPES ASSOCIATED WITH CILIARY DYSFUNCTION SYNDROMES.....	74
TABLE 2-1. IN-FUSION CLONING (CLONTECH, CA, USA) VECTORS.....	81
TABLE 2-2. GATEWAY CLONING (LIFETECHNOLOGIES, CA, USA) VECTORS.....	81
TABLE 2-3. Y2H GOLD (THE BAIT HOST STRAIN) REPORTER GENE CONSTRUCTS.....	82
TABLE 2-4. Y187 (THE PREY HOST STRAIN) REPORTER GENE CONSTRUCTS. ....	82
TABLE 2-5. YEAST PEPTONE DEXTROSE ADENINE (YPDA) MEDIA FOR YEAST CULTURE.....	84
TABLE 2-6. 1.1X TRIS-EDTA/LITHIUM ACETATE (TE/LiAc) SOLUTION. ....	85
TABLE 2-7. SYNTHETIC MINIMAL MEDIA FOR YEAST CULTURE.....	85
TABLE 2-8. DETAILS OF YEAST MEDIA SELECTING FOR BAIT OR PREY CONSTRUCTS.....	85
TABLE 2-9. SUMMARY OF YEAST STRAINS AND MAIN ASSOCIATED PLASMIDS. ....	86
TABLE 2-10. POLYETHYLENE GLYCOL/LITHIUM ACETATE (PEG/LiAc) SOLUTION.....	87
TABLE 2-11. 0.9 % SODIUM CHLORIDE (NaCl) SOLUTION.....	87
TABLE 2-12. DETAILS OF YEAST MEDIA USED FOR AUTO-ACTIVATION AND TOXICITY TESTING.....	89
TABLE 2-13. EXPECTED BAIT AUTO-ACTIVATION TEST RESULTS.....	89
TABLE 2-14. DETAILS OF YEAST MEDIA USED FOR MATING.....	90
TABLE 2-15. Y2H VECTORS FOR CONTROL MATING PROCEDURES.....	91
TABLE 2-16. CONTROL MATING TO CHECK FOR Y2H SYSTEM PERFORMANCE AND VECTOR COMPATIBILITY.....	91
TABLE 2-17. DETAILS OF YEAST MEDIA USED FOR Y2H PPI STUDIES.....	92
TABLE 2-18. Y2H CONTROL PLASMIDS.....	93
TABLE 2-19. EASY YEAST PLASMID ISOLATION KIT BUFFERS.....	95
TABLE 2-20. YEAST 'SMASH & GRAB DNA' BUFFERS.....	96
TABLE 2-21. CRACKING BUFFER. RECIPE FOR ONE PROTEIN EXTRACT.....	98
TABLE 2-22. PROTEASE INHIBITORS.....	98
TABLE 2-23. PRIMERS FOR CDNA LIBRARY GENERATION.....	100
TABLE 2-24. RNA DENATURATION AND PRIMING REACTION MIXTURE.....	101
TABLE 2-25. SINGLE-STRANDED cDNA GENERATION REACTION MIXTURE.....	101
TABLE 2-26. PRIMERS FOR LD-PCR.....	102
TABLE 2-27. LD PCR COMPONENTS.....	102
TABLE 2-28. MATE & PLATE™ LIBRARY – HUMAN BRAIN (NORMALISED). QUALITY CONTROL DATA.....	106
TABLE 2-29. DESCRIPTION OF COLUMN HEADINGS AND SAGE TAGS FROM FIGURE 2-5.....	111
TABLE 2-30. DNA POLYMERASES USED AND GENERAL PCR CONDITIONS.....	113
TABLE 2-31. TAE BUFFER.....	115
TABLE 2-32. 1 % AGAROSE GEL.....	115
TABLE 2-33. LURIA-BERTANI (LB) MEDIA FOR BACTERIAL CULTURE.....	116
TABLE 2-34. PRIMER PAIRS USED FOR PCR AMPLIFICATION OF FULL-LENGTH, AND SHORTER, <i>TOPORS</i> FRAGMENTS FOR IN-FUSION CLONING.....	118
TABLE 2-35. IN-FUSION REACTION COMPONENTS.....	119

TABLE 2-36. PRIMER PAIR USED FOR PCR AMPLIFICATION OF FULL-LENGTH <i>TOPORS</i> FOR CLONING, USING RESTRICTION ENZYMES AND LIGASE.....	120
TABLE 2-37. COMPONENTS OF RESTRICTION DIGEST REACTION.....	120
TABLE 2-38. DEPHOSPHORYLATION REACTION ACCORDING TO THE PROMEGA (WI, USA) PROTOCOL.....	121
TABLE 2-39. DEPHOSPHORYLATION REACTION ACCORDING TO THE SIMPLIFIED PROTOCOL.....	121
TABLE 2-40. PRIMER PAIR USED FOR PCR AMPLIFICATION OF FULL-LENGTH <i>TOPORS</i> FOR CLONING, USING THE GATEWAY SYSTEM.....	124
TABLE 2-41. PRIMER PAIR USED FOR PCR AMPLIFICATION OF FULL-LENGTH <i>P53</i> FOR CLONING, USING THE GATEWAY SYSTEM.....	124
TABLE 2-42. PRIMER PAIR USED FOR PCR AMPLIFICATION OF <i>ITM2B</i> , ITS FRAGMENT, AND DISEASE-CAUSING MUTANTS FOR CLONING, USING THE GATEWAY SYSTEM.....	125
TABLE 2-43. PRIMER PAIR USED FOR PCR AMPLIFICATION OF FULL-LENGTH <i>PTGDS</i> FOR CLONING, USING THE GATEWAY SYSTEM.....	126
TABLE 2-44. PRIMER PAIR USED FOR PCR AMPLIFICATION OF FULL-LENGTH <i>PSMC1</i> FOR CLONING, USING THE GATEWAY SYSTEM.....	126
TABLE 2-45. PRIMER PAIR FOR GENEART SDM OF pDONR- <i>PSMC1</i> ENTRY CLONE.....	127
TABLE 2-46. METHYLATION AND SDM REACTION MIXTURE. SAM = S-ADENOSINE METHIONINE.....	128
TABLE 2-47. METHYLATION AND SDM REACTION CYCLING CONDITIONS.....	128
TABLE 2-48. <i>IN VITRO</i> RECOMBINATION REACTION.....	129
TABLE 2-49. TRANSFORMATION REACTION DILUTIONS PRIOR TO PLATING.....	130
TABLE 2-50. VECTOR-SPECIFIC SEQUENCING PRIMERS.....	131
TABLE 2-51. SEQUENCING PRIMERS USED FOR <i>TOPORS</i> .....	132
TABLE 2-52. SEQUENCING PRIMERS USED FOR <i>P53</i> .....	132
TABLE 2-53. SEQUENCING PRIMERS FOR <i>ITM2B</i> .....	133
TABLE 2-54. SEQUENCING PRIMERS FOR <i>PTGDS</i> .....	133
TABLE 2-55. SEQUENCING PRIMERS FOR <i>PSMC1</i> .....	133
TABLE 2-56. CELL LINES USED FOR TOPORS CHARACTERISATION AND VALIDATION OF INTERACTIONS.....	134
TABLE 2-57. RQ1 DNASE (PROMEGA, WI, USA) MIX.....	137
TABLE 2-58. DNASE TREATMENT REACTION COMPONENTS' LIST.....	138
TABLE 2-59. GENOMIC DNA ELIMINATION REACTION COMPONENTS.....	139
TABLE 2-60. REVERSE-TRANSCRIPTION MIX.....	139
TABLE 2-61. <i>HPRT1</i> AMPLIFICATION REACTION MIX.....	140
TABLE 2-62. <i>HPRT1</i> AMPLIFICATION PCR CYCLING CONDITIONS.....	140
TABLE 2-63. <i>VAX2</i> AMPLIFICATION REACTION MIX.....	140
TABLE 2-64. <i>VAX2</i> AMPLIFICATION PCR CYCLING CONDITIONS.....	141
TABLE 2-65. <i>ITM2B</i> PRIMER DETAILS FOR ISOFORM AMPLIFICATION TO DETERMINE RETINAL EXPRESSION.....	142
TABLE 2-66. <i>PTGDS</i> PRIMER DETAILS FOR ISOFORM AMPLIFICATION TO DETERMINE RETINAL EXPRESSION.....	144
TABLE 2-67. <i>PSMC1</i> PRIMER DETAILS FOR ISOFORM AMPLIFICATION TO DETERMINE RETINAL EXPRESSION.....	146
TABLE 2-68. LYSIS BUFFER FOR PROTEIN EXTRACTION FROM HUMAN CELL LINES.....	149



TABLE 2-69. SDS-PAGE GEL COMPOSITION.....	149
TABLE 2-70. TRANSFER BUFFER. ....	149
TABLE 2-71. WESTERN BLOTTING (WB) BLOCKING BUFFER. ....	150
TABLE 2-72. TBS-T SOLUTION.....	150
TABLE 2-73. ICC BLOCKING BUFFER.....	151
TABLE 2-74. IHC BLOCKING BUFFERS. ....	154
TABLE 2-75. PRIMARY ANTIBODIES. ....	156
TABLE 2-76. REPORTED IMMUNOCYTOCHEMICAL LOCALISATION OF INVESTIGATED PROTEINS AND MARKERS. ....	159
TABLE 2-77. SECONDARY ANTIBODIES. ....	162
TABLE 3-1. RETINAL cDNA LIBRARY QUANTITATIVE RESULTS.....	166
TABLE 3-2. OLIGO-dT-PRIMED LIBRARY (O-dT) FRAGMENTS.....	168
TABLE 3-3. RANDOM-&-OLIGO-dT-PRIMED LIBRARY (R&O-dT) FRAGMENTS.....	168
TABLE 3-4. GENES FROM THE R&O-dT HUMAN cDNA LIBRARY ASSOCIATED WITH THE RETINA. ....	171
TABLE 3-5. SUMMARY OF COMPOSITION OF THE R&O-dT LIBRARY.....	173
TABLE 3-6. CONTROL TOPORS (Y2H GOLD) X P53 (Y187) INTERACTION: MATING OUTLINE. ....	178
TABLE 3-7. RESULTS EXPECTED FROM THE BAIT AUTO-ACTIVATION TESTING.....	182
TABLE 4-1. CONTROL MATING TO CHECK FOR Y2H SYSTEM PERFORMANCE.....	194
TABLE 4-2. EXPECTED CONTROL Y2H PPI RESULTS. ....	194
TABLE 4-3. QUANTITATIVE RESULTS OF Y2H SCREENS. ....	197
TABLE 4-4. QUANTITATIVE RESULTS FROM PREY SELECTION PROCESS. ....	197
TABLE 4-5. RETINA-ASSOCIATED Y2H PREYS. FUNCTIONAL DATA FROM UNIPROTKB AND REFSEQ (NCBI). ....	198
TABLE 4-6. A SUMMARY OF GENES ENCODING POTENTIAL INTERACTING PARTNERS OF TOPORS, AS IDENTIFIED BY PREY SEQUENCING. ....	201
TABLE 4-7. SUMMARY OF MUTATIONS IDENTIFIED IN <i>ITM2B</i> TO DATE.....	210
TABLE 4-8. PROSTAGLANDIN D2 SYNTHASE TYPES. ....	214
TABLE 5-1. <i>ITM2B</i> PRIMER DETAILS FOR ISOFORM AMPLIFICATION.....	223
TABLE 5-2. <i>PTGDS</i> PRIMER DETAILS FOR ISOFORM AMPLIFICATION.....	226
TABLE 5-3. <i>PSMC1</i> PRIMER DETAILS FOR ISOFORM AMPLIFICATION.....	229
TABLE 5-4. EXPECTED CONTROL Y2H PPI RESULTS. ....	230
TABLE 5-5. CONTROL YEAST MATING TO CONFIRM PUTATIVE INTERACTING PARTNERS (PREYS) OF TOPORS DO NOT BIND THE GAL4 DNA-BD. PART I.....	231
TABLE 5-6. CONTROL YEAST MATING TO CONFIRM PUTATIVE INTERACTING PARTNERS (PREYS) OF TOPORS DO NOT BIND THE GAL4 DNA-BD. PART II. ....	232
TABLE 5-7. AN OVERVIEW OF EXPECTED RESULTS IN Y2H PPI TESTING. ....	234
TABLE 5-8. CONTROL YEAST MATING TO TEST DIRECT TOPORS-P53 PPI (PUBLISHED INTERACTION USED AS AN OVERALL POSITIVE CONTROL).....	234
TABLE 5-9. CONTROL YEAST MATING TO TEST DIRECT TOPORS-ITM2B PPI.....	235
TABLE 5-10. CONTROL YEAST MATING TO TEST DIRECT TOPORS-ITM2B90 PPI.....	235
TABLE 5-11. CONTROL YEAST MATING TO TEST DIRECT TOPORS-ITM2B-RETMu PPI. ....	236

TABLE 5-12. CONTROL YEAST MATING TO TEST DIRECT TOPORS-ITM2B-FBD PPI .....	236
TABLE 5-13. CONTROL YEAST MATING TO TEST DIRECT TOPORS-ITM2B-FDD PPI .....	237
TABLE 5-14. CONTROL YEAST MATING TO TEST DIRECT TOPORS-PTGDS PPI.....	237
TABLE 5-15. CONTROL YEAST MATING TO TEST DIRECT TOPORS-PSMC1 PPI. ....	238
TABLE 5-16. PPIs SUMMARY. ....	238
TABLE 6-1. EXPECTED FRAGMENT SIZES OF ITM2B MONOMERS DETECTED BY ANTI-ITM2B ANTIBODIES.....	270
TABLE 6-2. SUMMARY OF REPORTED POST-TRANSLATIONAL MODIFICATIONS OF PTGDS.....	277
TABLE 7-1. COMPARISON OF ITM2B ANTIBODIES.....	288
TABLE 7-2. CTS DOMAINS IDENTIFIED IN TOPORS AND ITS INTERACTING PARTNERS.....	309
TABLE 7-3. SUMMARY OF LOCALISATION STUDY WITH CENTRIOLAR MARKERS. ....	311
TABLE 8-1. SUMMARY OF INTERACTORS' LOCALISATION IN RETINAL TISSUES. ....	334
TABLE 9-1. TOPORS AND ITM2B INTERACTIONS IN YEAST.....	353
TABLE 9-2. ITM2B LOCALISATION SUMMARY. ....	355
TABLE 9-3. TOPORS AND PTGDS INTERACTIONS IN YEAST.....	361
TABLE 9-4. PTGDS LOCALISATION SUMMARY.....	363
TABLE 9-5. TOPORS AND PSMC1 INTERACTIONS IN YEAST. ....	367
TABLE 9-6. PSMC1 LOCALISATION SUMMARY.....	368
TABLE 11-1. GENES IDENTIFIED IN THE R&O-DT HUMAN CDNA LIBRARY.....	403
TABLE 11-2. RESTRICTION ENZYMES WHICH HAVE BEEN SHOWN NOT TO CUT TOPORS (DNASTAR SEQBUILDER, LASERGENE 8) .....	432
TABLE 11-3. IDENTITIES OF PREY CLONES FROM THE O-DT LIBRARY SCREEN, AS IDENTIFIED BY BLAT (UCSC) GENOME SEARCH.....	451
TABLE 11-4. IDENTITIES OF PREY CLONES FROM THE R&O-DT LIBRARY SCREEN, AS IDENTIFIED BY BLAT (UCSC) GENOME SEARCH.....	453
TABLE 11-5. Y2H PREYS ASSOCIATED WITH CYTOSKELETON AND TRAFFICKING. FUNCTIONAL DATA FROM UNIProtKB AND RefSeq (NCBI). ....	455
TABLE 11-6. Y2H PREYS ASSOCIATED WITH PROTEIN TURNOVER AND MODIFICATION.....	456
TABLE 11-7. Y2H PREYS ASSOCIATED WITH MITOCHONDRIAL FUNCTION. ....	462
TABLE 11-8. Y2H PREYS ASSOCIATED WITH CELL NUCLEUS. ....	464
TABLE 11-9. Y2H PREYS – NOT CATEGORISED. ....	466
TABLE 11-10. YIELDS AND PURITY RATIOS OF THE EXTRACTED RNA SAMPLES. ....	475
TABLE 11-11. TOPORS x P53 INTERACTIONS. ....	482
TABLE 11-12. TOPORS x ITM2B INTERACTIONS.....	483
TABLE 11-13. TOPORS x ITM2B90 INTERACTIONS. ....	483
TABLE 11-14. TOPORS x ITM2B_RET INTERACTIONS. ....	484
TABLE 11-15. TOPORS x ITM2B_FBDINTERACTIONS.....	484
TABLE 11-16. TOPORS x ITM2B_FDD INTERACTIONS.....	485
TABLE 11-17. TOPORS x PTGDS INTERACTIONS. ....	485
TABLE 11-18. TOPORS x PSMC1 INTERACTIONS. ....	486

**LIST OF EQUATIONS**

EQUATION 2.1. MATING EFFICIENCY. .... 90  
EQUATION 2.2. OD<sub>600</sub> U CALCULATION..... 97  
EQUATION 2.3. TRANSFORMATION EFFICIENCY CALCULATION. KEY: CFU, COLONY-FORMING UNIT. .... 104  
EQUATION 2.4. NUMBER OF INDEPENDENT CLONES CALCULATION..... 104  
EQUATION 2.5. TITRE DETERMINATION. .... 105  
EQUATION 2.6. CELL DENSITY CALCULATION. .... 105

**ABBREVIATIONS**

<b>Ψ</b>	Hydrophobic amino acid
<b>A</b>	AbA aka Aureobasidin A
<b>aa</b>	Amino acid(s)
<b>AAA-ATPase</b>	ATPase Associated with diverse cellular Activities
<b>Ab(s)</b>	Antibody (-ies)
<b>Aβ</b>	Beta amyloid
<b>AbA</b>	Aureobasidin A
<b>ABCR</b>	ATP-binding cassette transporter, retina specific
<b>ABri</b>	FBD ITM2B C-terminal amyloid peptide
<b>AD</b>	Activation domain
<b>ad</b>	autosomal dominant
<b>ADAM10</b>	A Disintegrin and metalloproteinase domain-containing protein 10
<b>ADan</b>	FDD ITM2B C-terminal amyloid peptide
<b>adPRD</b>	autosomal dominant pericentral retinal dystrophy
<b>adRD</b>	autosomal dominant retinal dystrophy
<b>adRP</b>	Autosomal dominant retinitis pigmentosa
<b>aka</b>	also known as
<b>APP</b>	Amyloid Precursor Protein
<b>arRP</b>	Autosomal recessive retinitis pigmentosa
<b>Asn</b>	Asparagine
<b>ATP</b>	Adenosine triphosphate
<b>att</b>	attachment site (on Gateway cloning vectors)
<b>b/bp</b>	Base/base pair
<b>BBS</b>	Bardet-Biedl Syndrome
<b>BD</b>	Binding domain
<b>BH3</b>	Bcl 2 homology 3 (domain)
<b>BSA</b>	Bovine Serum Albumin
<b>C</b>	C-terminal TOPORS fragment
<b>CC</b>	Connecting cilium
<b>cdNA</b>	Complementary deoxyribonucleic acid
<b>cGMP</b>	cyclic guanosine monophosphate
<b>CIAP</b>	Calf Intestinal Alkaline Phosphatase
<b>CNS</b>	Central Nervous System
<b>coIP</b>	co-immuno-precipitation
<b>CP</b>	Core catalytic particle of the proteasome (20 S)
<b>CRABP</b>	Cellular retinoic acid-binding protein
<b>CRALBP</b>	Cellular retinal-binding protein
<b>CRBP</b>	Cellular retinol-binding protein
<b>CSF</b>	cerebrospinal fluid
<b>CTPP</b>	C-terminal pro-peptide (of ITM2B)
<b>CTS</b>	Ciliary Targeting Sequence
<b>Cys</b>	Cysteine

<b>Da</b>	Daltons
<b>DAPI</b>	4', 6-diamidino-2-phenylindole
<b>ddNTP</b>	Dideoxynucleotide
<b>DDO</b>	Double Dropout
<b>dH<sub>2</sub>O</b>	Distilled water
<b>DIC</b>	differential interference contrast
<b>DMEM</b>	Dulbecco's modified Eagle's medium
<b>DNA</b>	Deoxyribonucleic acid
<b>dNTP</b>	Deoxynucleotide
<b>EST</b>	Expressed Sequence Tag
<b>F</b>	forward primer
<b>FBD</b>	Familial British Dementia
<b>FCS</b>	Foetal Calf Serum
<b>FDD</b>	Familial Danish Dementia
<b>FL</b>	full-length
<b>Gal</b>	galactose
<b>GalNAc</b>	acetyl galactoseamine
<b>GCL</b>	Ganglion cell layer
<b>gDNA</b>	Genomic DNA
<b>GDP</b>	Guanosine diphosphate
<b>Glc</b>	glucose
<b>GlcNAc</b>	acetyl glucosamine
<b>Gly</b>	Glycine
<b>GTP</b>	Guanosine triphosphate
<b>h</b>	hours
<b>HEK293</b>	Human embryonic kidney cell line
<b>HeLa</b>	Human adenocarcinoma cell line
<b>Hex</b>	hexose
<b>HexNAc</b>	acetyl hexosamine
<b>His</b>	Histidine
<b>hTop1</b>	Human topoisomerase I
<b>ICD</b>	intracellular domain (of ITM2B)
<b>INL</b>	Inner nuclear layer
<b>IP</b>	Immuno-precipitation
<b>IPL</b>	Inner plexiform layer
<b>IPM</b>	Inter-photoreceptor matrix
<b>IRBP</b>	Interphotoreceptor retinoid-binding protein
<b>IS</b>	Inner segment
<b>ITM2B</b>	Integral Membrane Protein 2B
<b>ITM2B<sub>L</sub></b>	Integral Membrane Protein 2B long
<b>ITM2B<sub>S</sub></b>	Integral Membrane Protein 2B short
<b>JS</b>	Joubert syndrome
<b>KD</b>	knock-down

<b>LRAT</b>	Lecithin:retinol acyl transferase
<b>Lys</b>	Lysine
<b>Lys/His</b>	Lysine-Histidine-rich motif
<b>M</b>	Mid-TOPORS fragment
<b>M Ab</b>	Antibody raised in mouse
<b>Man</b>	mannose
<b><i>Mata</i></b>	Mating type a
<b><i>Mata</i></b>	Mating type alpha
<b>MDCK</b>	Madin Darby canine kidney cell line
<b>mRNA</b>	Messenger ribonucleic acid
<b>N</b>	N-terminal TOPORS fragment
<b>NAD<sup>+</sup>/H</b>	Nicotinamide adenine dinucleotide
<b>NADP<sup>+</sup>/H</b>	Nicotinamide adenine dinucleotide phosphate
<b>NDS</b>	Normal Donkey Serum
<b>NEDD8</b>	Neural precursor cell Expressed Developmentally Down-regulated protein 8
<b>Neu5Ac</b>	neuraminic acid aka sialic acid
<b>NGS</b>	Normal Goat Serum
<b>NLS</b>	Nuclear localisation signal
<b>nt</b>	nucleotide
<b>NTF</b>	N-terminal fragment (of ITM2B)
<b>OCT</b>	Optimal Cutting Temperature
<b>OD</b>	Optical density
<b>O-dT</b>	Oligo-dT-primed (cDNA library)
<b>ONL</b>	Outer nuclear layer
<b>OPL</b>	Outer plexiform layer
<b>OS</b>	Outer segment
<b>PAGE</b>	Polyacrylamide gel electrophoresis
<b>PBS</b>	Phosphate-buffered saline
<b>PCM1</b>	Pericentriolar material 1
<b>PCR</b>	Polymerase chain reaction
<b>PD</b>	Parkinson's disease
<b>PEST</b>	Proline, Glutamate, Serine, and Threonine-rich domain
<b>PFA</b>	Paraformaldehyde
<b>PG</b>	Prostaglandin
<b>PLK4</b>	polo-like kinase 4, centriolar-centrosomal
<b>PNA</b>	Peanut agglutinin
<b>PPI</b>	Protein-Protein Interaction
<b>PMSF</b>	Phenylmethylsulfonyl fluoride
<b>PRPF</b>	Pre-mRNA processing factor
<b>P/S</b>	Penicillin/Streptomycin
<b>PSMC1</b>	Regulatory subunit 4 of the 26 S protease
<b>PTGDS</b>	Prostaglandin D2 synthase aka Prostaglandin-H2 D-isomerase
<b>QDO</b>	Quadruple Dropout

<b>R</b>	Reverse primer
<b>RARRES3/RIG1</b>	Retinoic acid receptor responder protein 3 aka Retinoic acid-inducible gene 1
<b>Rb Ab</b>	Antibody raised in rabbit
<b>RBP</b>	Retinol-binding protein
<b>R&amp;O-dT</b>	Random- & Oligo-dT-primed (cDNA library)
<b>RegP</b>	Regulatory particle of the proteasome (19 S)
<b>RDH</b>	Retinol dehydrogenase
<b>RHO</b>	Rhodopsin
<b>RK</b>	Rhodopsin kinase
<b>RNA</b>	Ribonucleic acid
<b>RP</b>	Retinitis pigmentosa
<b>RPE</b>	Retinal pigment epithelium
<b>RPE1</b>	Human hTERT-immortalised retinal pigment epithelial (hTERT-RPE1) cell line
<b>RPGR</b>	Retinitis Pigmentosa GTPase regulator
<b>rpm</b>	Revolutions per minute
<b>RT-PCR</b>	Reverse transcription polymerase chain reaction
<b>S</b>	Svedberg unit
<b>SAM</b>	S-adenosine methionine
<b>SCD</b>	secreted C-term domain (of ITM2B)
<b>SD</b>	Synthetic Dropout
<b>SDM</b>	Site-Directed Mutagenesis
<b>SDO</b>	Single Dropout
<b>SDS</b>	Sodium dodecyl sulphate
<b>Ser</b>	Serine
<b>SK-N-SH</b>	Human neuroblastoma cell line
<b>SLS</b>	Senior-Løken syndrome
<b>SR</b>	Serine-Arginine-rich domain
<b>SPPL</b>	signal peptide peptidase-like
<b>SUMO1</b>	Small ubiquitin-related modifier 1
<b>SV40 T Ag</b>	Large T antigen of the tumour-inducing Simian virus 40
<b>TBS</b>	Tris-buffered saline
<b>TF</b>	Transcription factor
<b>Thr</b>	Threonine
<b>TM</b>	Transmembrane (domain)
<b>TOPORS</b>	Topoisomerase I binding RS domain protein
<b>Tx100</b>	Triton X-100
<b>Tyr</b>	Tyrosine
<b>U</b>	unit(s)
<b>UAS</b>	Upstream activation sequence
<b>Ub</b>	ubiquitin
<b>UPS</b>	ubiquitin-proteasome system
<b>USH</b>	Usher Syndrome
<b>UTR</b>	Untranslated region

<b>UV</b>	Ultra violet
<b>WB</b>	Western Blot
<b>X</b>	X- $\alpha$ -Gal aka 5-bromo-4-chloro-3-indolyl $\alpha$ -D-galactopyranoside
<b>xLRP</b>	X-linked retinitis pigmentosa
<b>X-<math>\alpha</math>-Gal</b>	5-bromo-4-chloro-3-indolyl $\alpha$ -D-galactopyranoside
<b>X-<math>\beta</math>-Gal</b>	5-bromo-4-chloro-3-indolyl- $\beta$ -D-galactoside
<b>Y2H</b>	Yeast two-hybrid



## **1 INTRODUCTION**

For most diurnal vertebrates vision dominates over their other senses. It is required for finding and gathering food, or hunting, as well as for avoiding predators and other potential dangers. Humans are no exception: the responsibilities of daily life, both at home and at work, are often hard, if not impossible, to fulfil without being able to see.

Despite the superiority of vision over other senses, and our strong dependence on it for completing everyday tasks, incurable eye disorders continue to exist. Retinitis pigmentosa (RP) is an example of such a disease (Hartong, Berson e Dryja, 2006); it results in degeneration of photoreceptor cells, which are highly specialised first order neurons, absolutely essential for eyesight to persist. A Scandinavian study demonstrated that RP is one of two leading causes of blindness in working age (20-64) adults (Buch *et al.*, 2004).

RP is a term referring to a broad group of retinal dystrophies, which can be caused by mutations in various genes, of which over fifty are known (Retnet, 1996-2010), yet many remain to be identified. *TOPORS* (MIM 609507; locus *RP31*) is one of the causative genes (Chakarova *et al.*, 2007); its expression in human is not restricted to the retina, and it has no known retina-specific functions. Hence this thesis aims to evaluate the role of TOPORS protein in the retina by characterising its interactions with three proteins from the human retina, identified as its interacting partners via a yeast two-hybrid (Y2H) screen (Fields e Song, 1989).

### **1.1 THE SENSE OF VISION**

Vision is the principal sense, which humans rely on to perceive external signals. It is conveyed by a highly specialised organ: the eye. Several types of eyes have evolved in the animal kingdom, which can be divided into two distinct categories: the camera eye and the compound eye.

The camera eye (Figure 1-1), specifically a cup eye with a lens and pupil is found in vertebrates. Its less evolutionarily advanced variants exist in some invertebrates, such as worms or molluscs, which possess simple cup eyes without a lens, but sometimes with a pinhole, serving to restrict light entry as in case of the pupil.

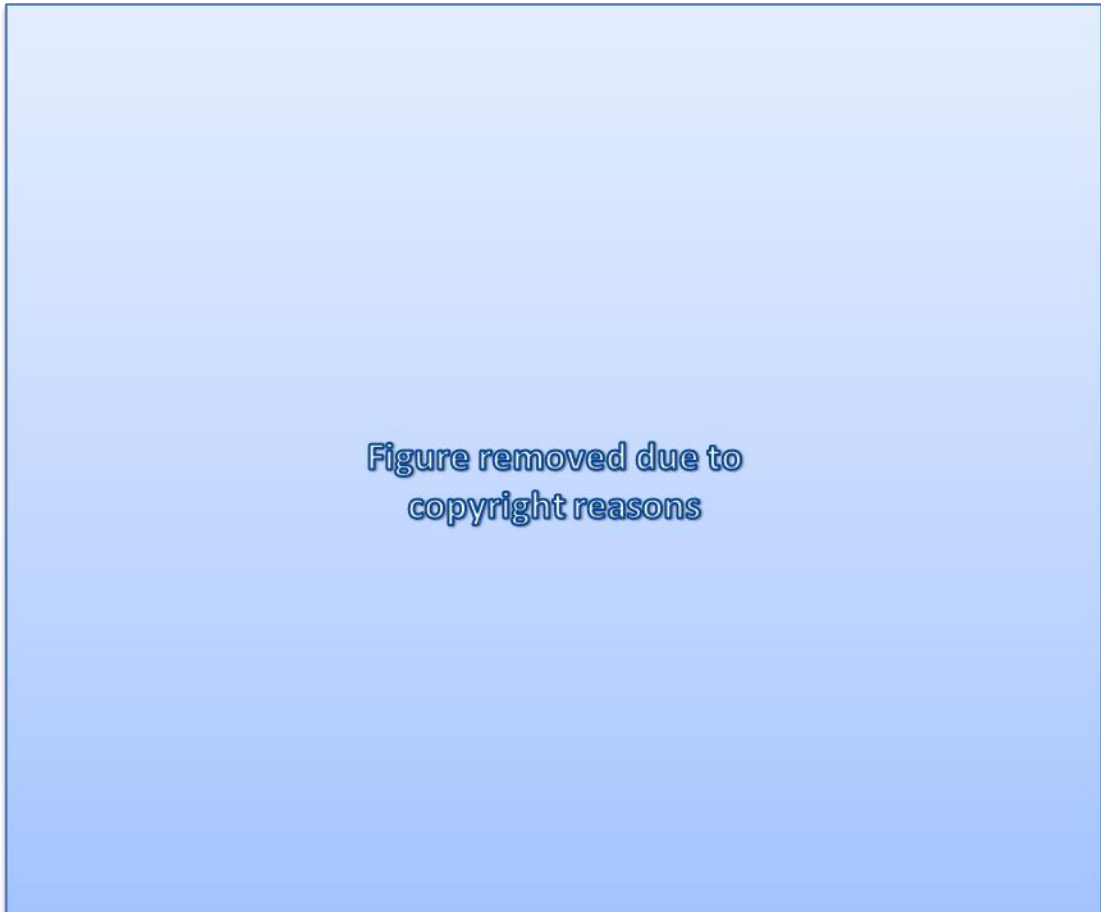


Figure 1-1. Structure of the Eye.

The eyeball is enclosed into three layers. The outermost fibrous layer consists of connective tissue, comprising the transparent cornea at the front of the eye, and tendon-like sclera, enclosing most of the eyeball in regions not exposed to the outside environment. This outermost layer of the eye has structural and protective functions. Below lays a layer of vasculature (the uvea), which comprises the choroid at the posterior eye regions underneath the sclera, as well as the iris and ciliary body at the anterior region of the eyeball. The vascular choroid nourishes the outer layers of the eye and its dark colouration prevents the scattering of light inside the eye. The ciliary body forms a ring of smooth muscle tissue around the lens and controls its shape. The iris is the coloured front part of the eye, which regulates the size of the pupil, and thus the amount of light that enters the eye. It consists of a smooth muscle tissue, shaped similarly to a flattened doughnut; it is continuous with the ciliary body. The retina forms the innermost, sensory layer of the eye. Several types of neurons are arranged into further sub-layers within the retina; axons of the innermost ganglion cell layer (GCL) collectively form the optic nerve, accompanied by the neighbouring central artery and central vein of the retina (these vessels serve the inner retinal layers of ganglion and bipolar cells). The outer retina (the photoreceptor cells) is supported by the retinal pigmented epithelial (RPE) cells, and nourished by blood from the choroidal capillaries. The primate retina is additionally characterised by the presence of a fovea, a region greatly enriched in cone photoreceptors, responsible for acuity and colour vision. The lens, which refracts light waves, separates the anterior and posterior eye cavities. The anterior cavity is filled with a constantly circulating aqueous humour, whereas the second one is filled with a gelatinous vitreous humour, which remains unchanged since completion of eye development (reviewed in: Martini e Nath, 2006; Marieb e Hoehn, 2007; Barrett *et al.*, 2010). Image from the Webvision electronic book (Kolb *et al.*, 1995).

The compound eye is common in arthropods, for example, insects, such as the fruit fly *Drosophila melanogaster*. This category can be further subdivided into apposition and superposition eyes. In apposition eyes each ommatidium detects a different signal; these signals are then combined into an image in the brain. The photons detected by ommatidia of superposition eyes all reach a shared retina before conducting the signal to the brain.

Despite these clear architectural differences, the key component of every type of eye is the photoreceptor cell, without which eyesight would have never developed.

In the camera eye, which evolved in vertebrates, the photoreceptor cells are located at the back of the eye in the retina (Figure 1-1). In order to reach the retina, specifically a photoreceptor cell, a photon of light enters the eye through the pupil, it is then focused by the lens (both structures are found within the anterior part of the eyeball), and it subsequently reaches the retina in the posterior fragment of the eye.

## **1.2 THE RETINA: ANATOMY AND PHYSIOLOGY**

The retina forms the innermost of the three layers of the eye. It is a sensory tissue, consisting primarily of nerve cells, supported by glial cells, which are collectively referred to as the neural retina (Figure 1-1). It is itself sub-divided into several distinct layers and it comprises the outermost projection of the central nervous system (CNS).

Just below the choroid lays the non-neural portion of the retina, the retinal pigment epithelium (RPE), a monolayer of epithelial cells, indispensable for correct functioning of the photoreceptor rod and cone cells. The photoreceptors are highly specialised nerve cells, which form the outermost layer of the neural retina, nourished and supported by the RPE (Figure 1-2).

The retina converts the light energy captured by the photoreceptors into graded electrical activity, and, subsequently, into action potentials along the optic nerve, formed from axons of ganglion cells. The structure of the retina is astonishingly well adapted to its function; however, this is also the reason why it is especially vulnerable to dysfunction (reviewed in: Martini e Nath, 2006; Marieb e Hoehn, 2007; Barrett *et al.*, 2010).

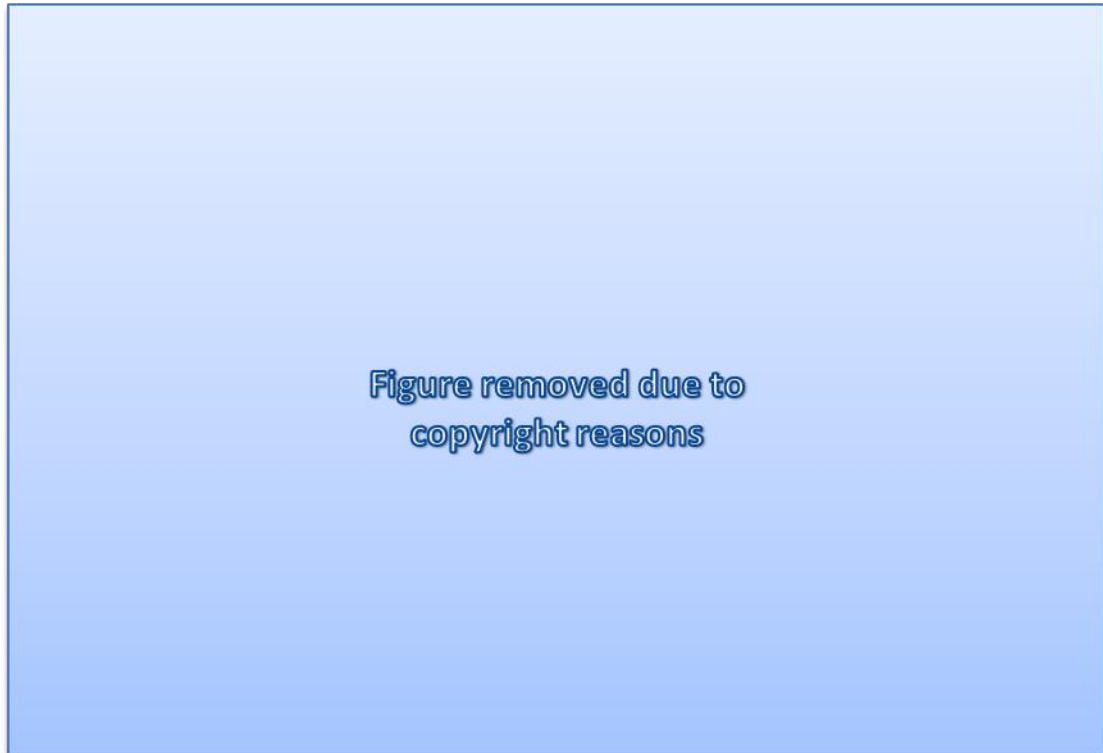


Figure 1-2. Structure of the Retina.

Left: Histological appearance of healthy human retina. Right: Diagram of the types of neurons found within specific layers of the retina. In order to reach the photoreceptor cells, light that enters the eye must first travel through the inner and outer retinal layers. Namely, first the light waves pass in between axons of the ganglion cells and the ganglion cell layer (GCL), which consists of the cell bodies of these neurons. The light then passes the inner plexiform layer (IPL), where the dendrites of the ganglions receive signal from the axons of bipolar and amacrine cells. The IPL is followed by the inner nuclear layer (INL), which comprises the nuclei, and thus the cell bodies, of the bipolar, horizontal and amacrine cells. The outer plexiform layer (OPL), located behind the INL, constitutes dendrites of the bipolar and horizontal cells as well as axons of the photoreceptor cells. The nuclei of the rod and cone photoreceptors are found within the next layer, known as the outer nuclear layer (ONL). Finally, the light reaches and activates the visual opsins in the photoreceptor outer segments (OS), supported by cells of the RPE. Image modified from Hartong *et al.* (2006).

### **1.2.1 PHOTORECEPTORS OF THE RETINA**

Photoreceptor cells are neurons modified to transduce light into graded electrical energy. Rods and cones (Figure 1-3), which comprise the two major classes of these nerve cells, have their nuclei, and thus the cell bodies, located within the outer nuclear layer (ONL), whereas their axons extend into the outer plexiform layer (OPL), where their synapses make connections with dendrites of the bipolar as well as the horizontal cells (Figure 1-2).

Whereas the bipolar and ganglion cells are served by the central artery and the central vein of the retina, which runs through the centre of the optic nerve, the photoreceptor layer is supplied by blood from vessels found in the choroid.

Rods are the predominant photoreceptors found in the human retina, where they reach numbers of 120 million. The rod cells generate responses to dim light (scotopic vision) and are involved in peripheral vision. The cone photoreceptors function most efficiently in bright light (photopic vision), and are required for high acuity and colour vision. They are about 20-fold less numerous than rods, reaching numbers of six to seven million (reviewed in: Masland, 2001; Sung e Chuang, 2010).

Due to the fact that rods are involved in peripheral vision, their density is greatest in the lateral peripheral side of the retina and it decreases towards the macula lutea, i. e. the 'yellow spot'. The latter is an oval spot at the posterior pole of the eye, which contains predominantly cones. It is a region located laterally to the blind spot and includes the fovea centralis, a pit approximately 600  $\mu\text{m}$  in diameter, which, in humans, comprises cones only.

Before light excites the photoreceptors, it must first pass through the cornea, aqueous humour, lens, vitreous humour and most of the neural layers of the retina. Consequently, in order to enhance the acuity of vision, retinal structures, such as axons and cell bodies are mainly displaced at the macula lutea to allow direct passage of light to the sensory area rich in cones. Furthermore, each cone (or a maximum of a few) is connected to one bipolar cell, which then transmits the signal onto one ganglion cell, enhancing the signal acuity further. On the contrary, as many as a hundred rods can ultimately feed into one ganglion cell, resulting in a less precise signal (refer to section 1.2.3 for an overview of phototransduction).

The photoreceptor cells (Figure 1-3) are highly specialised neurons, which comprise a cell body, continuous with inner and outer segments adjacent to the RPE, and, at the opposite end, with a synapse involved in transmitting the signal to the bipolar cells. In both types of photoreceptors the inner segment is continuous with the cell body, whereas the outer segment is joined to the inner segment via a connecting cilium; the connecting cilium and the outer segment jointly form a modified primary cilium (section 1.9).

The connecting cilium is a bridge-like structure connecting the inner and outer segment, which allows movement of cargo via the kinesin II-powered anterograde transport, and, subsequently, through the dynein 2 (DHC1b/2)-maintained retrograde transport (Sung e Chuang, 2010).

The shape of the outer segment, embedded within the RPE, is conical in cones and cylindrical or rod-shaped in rods. The human cone outer segments are normally between 40  $\mu\text{m}$  and 50  $\mu\text{m}$  long, and their diameter can be within the range of 0.5 – 4.0  $\mu\text{m}$ , depending on how

tightly they are packed (reviewed in: Marieb e Hoehn, 2007), whereas the rod outer segment can have a diameter within the range of 1.4–10  $\mu\text{m}$ , and can reach the length of 30–60  $\mu\text{m}$  (reviewed in: Sung e Chuang, 2010).

The key elements of the outer segments are the discs of cellular membrane, containing the photo-pigments, which are embedded within them. In cones the ‘discs’ are continuous with the plasma membrane of the cell, and (in human) can contain one of three types of opsins:

- Long wavelength-detecting opsin: red;
- Middle wavelength-detecting opsin: green;
- Short wavelength-detecting opsin: blue.

In rods the discs are discontinuous separate fragments of membrane, stacked onto each other within the outer segment. They contain only one type of opsin, rhodopsin, therefore, cannot generate colour vision.

These four opsins are G-protein coupled receptors, which covalently bind retinaldehyde chromophores derived from vitamin A. Light-sensitive rhodopsin binds, specifically, 11-*cis* retinal, which becomes isomerised to all-*trans* retinal, when a photon hits rhodopsin, initiating phototransduction (section 1.2.3). This occurs due to a conformational change in the photo-pigment (section 1.2.3).

The photo-pigment-containing discs are regenerated daily. The discs’ precursors are synthesised in the inner segment and they are assembled at the proximal end of the outer segment; as a result the old discs become pushed towards the RPE, where they are phagocytised (shown in Figure 1-3). In rods the regeneration occurs at the end of each night, whereas in cones it happens at the end of each day (reviewed in: Martini e Nath, 2006; Marieb e Hoehn, 2007; Barrett *et al.*, 2010).

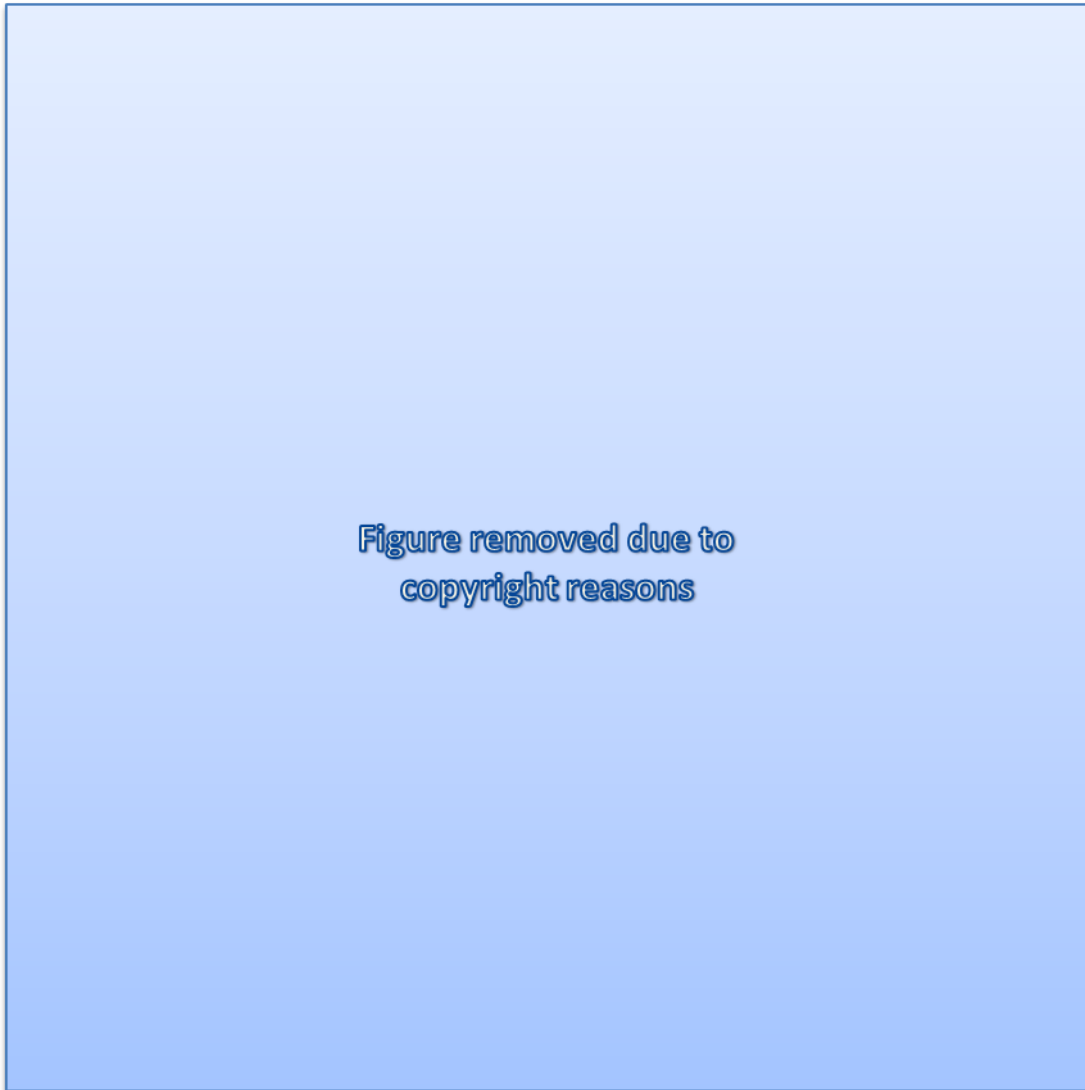


Figure 1-3. Structure of the photoreceptor cells.

Rods and cones are nerve cells modified to convert light impulses into electrical graded potentials. The two cell types have an analogous structure with the exception of the outer segments (OS), their strategic elements. The OS of a rod is cylindrical in shape and its membrane discs are individual structures, not continuous with the plasma membrane. On the contrary, the membranous structures of cone OS, within which opsin molecules reside, are continuous with the plasma membrane; they do not form individual 'discs.' As the OS of both photoreceptor (PR) types get turned over, they become phagocytised by the retinal pigment epithelium (RPE; depicted with fragments of discs and pigment vesicles inside the cell); at their proximal ends they are joined to the inner segments (IS) via connecting cilia (CC). The OS and CC together form a highly specialised primary cilium (section 1.9). The IS of rods and cones contain the 'house-keeping' organelles; at their distal regions they are especially rich in the energy-generating mitochondria. The IS are continuous with the cell bodies, where the nuclei are found. The synaptic endings of rods and cones contain vesicles enclosing the inhibitory neurotransmitter glutamate, which is constantly released when the PRs receive no light stimulation. When a photon of light reaches a PR cell and hits an opsin molecule (e.g. rhodopsin: magnified fragment of the rod disc membrane), its conformation changes, triggering a cascade of intracellular reactions, leading to inhibition of glutamate release, and, consequently, phototransduction initiation (section 1.2.3). Rhodopsin and cone opsins are membrane-spanning proteins, residing within the phospholipid bilayer (phospholipid molecules with the fatty acid chains: magnified fragment of the rod disc membrane) of discs. Figure from Neuringer (2000).

## 1.2.2 THE RETINAL PIGMENTED EPITHELIUM

The retinal pigment epithelium (RPE; Figure 1-4) is a monolayer of cells forming the blood-retina barrier.

In addition to absorbing light scattered within the eye, like the choroid does, the RPE serves a number of other functions. The primary role of the RPE is to phagocytise dead and damaged photoreceptor cells; about 10 % of photoreceptor outer segments are shed every day and then phagocytised by the RPE (Young, 1967). Furthermore, this single-celled layer is also involved in recycling of retinal; this is essential for the photoreceptors to be able to retain their phototransduction activity, as all-*trans* retinal cannot be re-isomerised to the 11-*cis* form within photoreceptor cells.



Figure 1-4. The Retinal Pigmented Epithelium, its components and functions.

The basolateral surface of the RPE lays adjacent to fenestrated blood capillaries, whereas the apical membrane contacts the outer segments (OS) of photoreceptor (PR) cells; it forms microvilli (MV) extending towards the OS and surrounding them. Light Absorption: the pigments of the RPE absorb light, preventing its scattering. Epithelial Transport: the RPE is involved in transport of nutrients (e.g. glucose, vitamin A) from blood to PRs and in ion exchange important for maintaining correct pH in the sub-retinal space; the latter is also a major function of Müller (glia) cells. Furthermore, a constant circulation of retinal (visual cycle: section 1.2.4) keeps occurring between the RPE and rods, as all-*trans* retinal can only be isomerised back to 11-*cis* retinal in the RPE. Phagocytosis of shed fragments of OS and secretion of growth factors (PEDF, pigment epithelium-derived growth factor; VEGF, vascular epithelium growth factor) important for maintenance of neighbouring cells are also performed by the RPE. Figure from Strauss (2005).

The RPE forms a part of the blood-retina barrier; it captures nutrients from the blood and displaces waste metabolites from the sub-retinal space into the blood. Nutrients taken up by the RPE include vitamin A, i.e. retinol, glucose and fatty acids. This layer also releases growth factors involved in sustaining the retina as well as the endothelium of the choroid capillaries.



The RPE is additionally involved in spatial buffering of ions in the interphotoreceptor (IPR) matrix; this function is performed with the assistance of the Müller glia cells (reviewed in: Strauss, 2005; Martini e Nath, 2006; Marieb e Hoehn, 2007; Barrett *et al.*, 2010).

### 1.2.3 PHOTOTRANSDUCTION

Phototransduction is a term used to describe a process by which light energy is converted into a graded action potential.

Retinal is the key molecule involved in phototransduction. It combines with different opsin proteins to form four different types of photo-pigments, each of which preferentially absorbs light of different wavelengths. Vitamin A is the dietary precursor for retinal in the human body. Overall, many isomers of this molecule exist; when bound to an opsin the retinal is present as the 11-*cis* isomer.

In the dark, the cation channels in the photoreceptor (PR) outer segments (OS) are held open by cyclic GMP (cGMP), allowing a continuous inflow of sodium and calcium cations, which results in a 'dark membrane potential' of  $-40$  mV. Consequently, the PR cells remain depolarised, and thus the voltage-gated calcium channels at the synaptic terminals of the PR cells remain open, resulting in a continuous release of glutamate. This neurotransmitter triggers the inhibitory postsynaptic potentials (IPSPs) in the bipolar cells, leading to their hyperpolarisation. The IPSPs inhibit neurotransmitter release from the synapses of the cells, and signal transmission stops. When a photon of light is absorbed by the 11-*cis* retinal, its conformation changes to all-*trans* and it subsequently detaches from the opsin, triggering the cascade of phototransduction reactions. This bleaching of the pigment is very rapid, taking a few milliseconds and is the only light-dependent stage of the visual perception process.

The activated, retinal-free form of rhodopsin is referred to as metarhodopsin II; it activates a G-protein, called transducin, which in turn activates a phosphodiesterase (PDE). This last enzyme breaks down cGMP into GMP, which results in closure of the cGMP-gated calcium and sodium channels in the PR OS, subsequently leading to hyperpolarisation of the PR cells. This hyperpolarising membrane potential, i.e.  $-70$  mV, causes closure of the voltage-gated cation channels at the synaptic terminals of the PRs. When the concentration of calcium and other cations falls within the synapses, no glutamate neurotransmitter is released.

The absence of glutamate at the bipolar cell receptors results in no IPSPs forming; therefore, the cells depolarise, the voltage-gated cation channels open, allowing inflow of calcium ions. In

consequence, the bipolar cells release their neurotransmitter molecules, which bind to receptors on the ganglion cells' synapses. Binding of the neurotransmitter triggers excitatory postsynaptic potentials (EPSPs) in the ganglion cells, resulting in generation of action potentials, which are then propagated along the optic nerve (reviewed in: Thompson e Gal, 2003; Martini e Nath, 2006; Marieb e Hoehn, 2007; Barrett *et al.*, 2010)

#### 1.2.4 THE VISUAL CYCLE

Photo-pigments bleached in the first step of the phototransduction need to be regenerated in order for vision to continue. In contrast to the rapid breakdown of the photo-pigments, their replenishment is a slow, energy-requiring process. It involves re-isomerisation of the all-*trans* retinal to its 11-*cis* form. In the meanwhile, more 11-*cis* retinal is being synthesised by oxidation of vitamin A acquired from diet.

The process of regeneration of the rhodopsin and cone opsins is referred to as the visual cycle (Figure 1-5). When a photon of light hits rhodopsin, it triggers a conformational change of retinal from 11-*cis* retinal to all-*trans* retinal. As a consequence, the latter isomer is released from the pigment opsin, which it was bound to via a protonated Schiff base linkage, into the space inside the disc. The retinal then reacts with phosphatidylethanolamine to form *N*-retinylidene-phosphatidylethanolamine, which becomes bound by the retina-specific ATP-binding cassette transporter (ABCR), and is transferred to the cytoplasmic surface of the disc. The all-*trans* retinal is released into the cytoplasm, where it is reduced to vitamin A, i.e. all-*trans* retinol, by the all-*trans* retinol dehydrogenase (RDH). The vitamin A is transported across the sub-retinal space into the RPE; it is additionally supplied to this cell layer by vessels in the choroid (from dietary intake). In the RPE the all-*trans* retinol becomes bound by the cellular retinol-binding protein (RBP), and is esterified to all-*trans* retinyl esters by the lecithin retinol acyltransferase (LRAT). These esters are subsequently isomerised to 11-*cis* retinol; this step also involves the action of retinyl ester hydrolase (REH) and the RPE65 protein. At last, the 11-*cis* retinol dehydrogenase isomerises 11-*cis* retinol to 11-*cis* retinal in a process accelerated by the presence of the cellular retinaldehyde-binding protein (CRALBP). The product is then transported into the rod outer segments; the interphotoreceptor retinoid-binding protein (IRBP) is present throughout the transfer of the 11-*cis* retinal to the rod (OS), however, its role is not understood. Alternatively, 11-*cis* retinol can be esterified and stored in the RPE (reviewed in: Thompson e Gal, 2003).

In addition to the cycle summarised in Figure 1-5, another pathway for 11-*cis* retinal production has been shown to exist in the RPE and the Müller glia cells. The reaction involves the RPE-retinal G-protein coupled receptor (RGR), and it is light-dependent. Specifically, the all-*trans* retinal, bound to the RGR via a Schiff base linkage, is converted to 11-*cis* retinal, as a result of illumination of the RGR (reviewed in: Thompson e Gal, 2003).

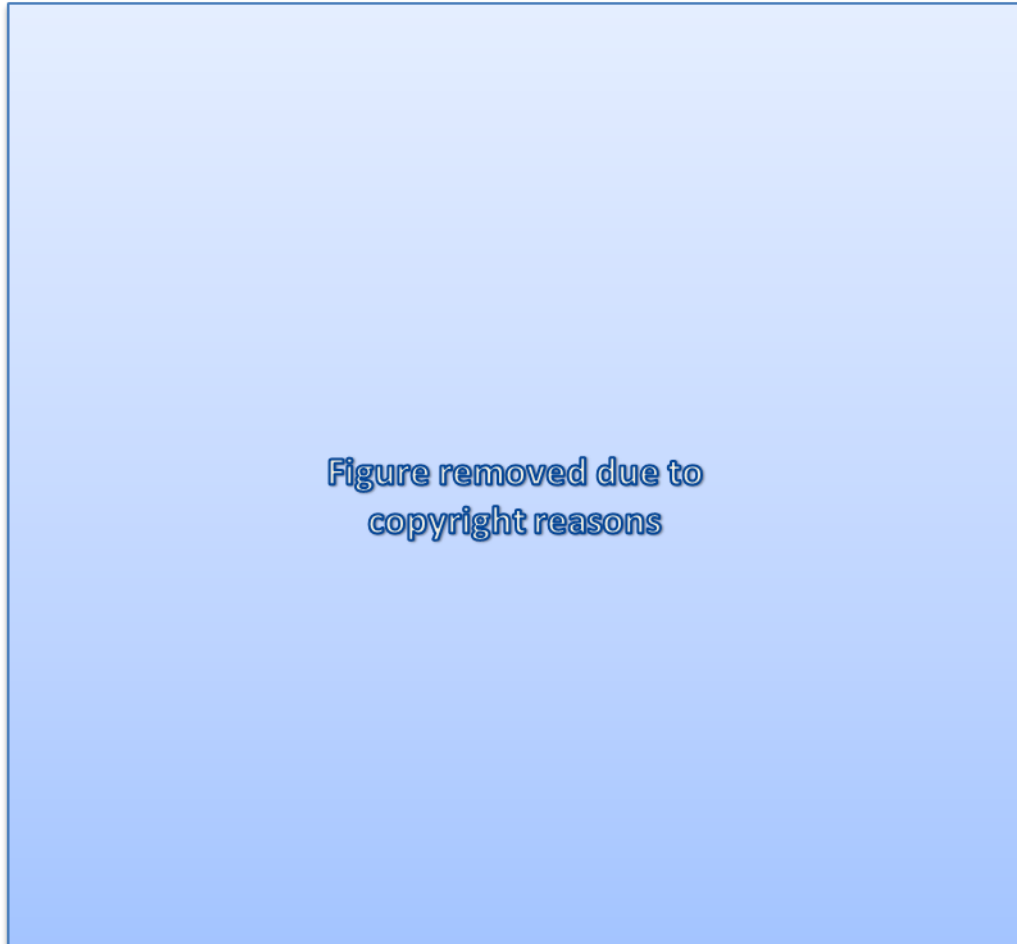


Figure 1-5. The Visual Cycle.

Schematic representation of retinal regeneration with the major intermediate analogues is illustrated. When a photon of light ( $h\nu$ ) hits rhodopsin in the rod OS, the conformation of its chromophore 11-*cis* retinal changes to all-*trans* retinal, and is released from the covalent bond holding it with the opsin. Whilst still in the OS, all-*trans* retinal is reduced to all-*trans* retinol, and in this form it is transported across the sub-retinal space to the retinal pigment epithelium (RPE); there it is, firstly, esterified and then further isomerised to 11-*cis* retinol. At last, 11-*cis* retinol is oxidised to 11-*cis* retinal and transported back across the sub-retinal space to the rod OS to form a light-sensitive rhodopsin. Image from Arshavsky (2010).

### 1.3 RETINITIS PIGMENTOSA

Retinitis pigmentosa (RP) is an inherited, heterogeneous retinal dystrophy, characterised by the loss of photoreceptors and pigment deposits on the fundus of the eye (reviewed in the seminar by: Hartong, Berson e Dryja, 2006). RP is the most common type of inherited photoreceptor (PR) degeneration (Wright *et al.*, 2010). The disorder may occur as a component of a broader syndrome characterised by other non-ocular features, or it can be non-syndromic.

It has been estimated, based on population studies, that non-syndromic RP has a prevalence of approximately 1 in 4 000, whereas Usher syndrome and Bardet-Biedl syndrome (BBS), the two most commonly diagnosed forms of syndromic RP, have a prevalence of approximately 1 in 20 000 and between 1 in 13 500 and 1 in 175 000, respectively (Hamel, 2006; Kremer *et al.*, 2006; Rooryck e Lacombe, 2008; Zaghoul e Katsanis, 2009). Overall, approximately 1.8 million people are affected by RP worldwide. Furthermore, a Scandinavian study conducted by Buch *et al.* (2004) has demonstrated that RP is one of the two major causes of blindness in people aged 20-64.

More than fifty different genetic subtypes of RP have been identified (Retnet, 1996-2010; Fahim, Daiger e Weleber, 2000 Aug 4 [Updated 2013 Mar 21]). The disease is usually inherited in a monogenic mode; however, a case of digenic inheritance has also been demonstrated (Kajiwara, Berson e Dryja, 1994). It has been estimated that autosomal dominant (adRP) traits comprise 15 – 25 % of all RP cases, the autosomal recessive (arRP) disease contributes 5 – 20 % of cases, and 5 -15 % are due to the X chromosome-linked (xlRP) inheritance. Mutations responsible for the cases as yet unaccounted for, comprising the remaining 40 – 50 %, remain to be identified. The functions of known genes involved in photoreceptor degeneration (inclusive of, but not limited to RP), and their approximate contribution to the known causes of retinal dystrophies are summarised in Figure 1-6.

It must also be highlighted that most causative genes contribute only a very small proportion of cases (less than 1 % per causative gene). Exceptions include mutations in the retinitis pigmentosa GTPase regulator (*RPGR*), which, being the predominant cause of xlRP (up to 90 % incidence), is responsible for up to 13.5 % of all RP cases. Up to 8 % of total RP can be attributed to mutations in rhodopsin (*RHO*; both dominant and recessive); whereas, usherin (*USH2A*) and *PRPF31* have been associated with up to 3 % and 2.5 % of all RP cases, respectively.



Figure 1-6. Functional categorisation of genes that influence photoreceptor degeneration. Pie chart showing the functional categorization of 146 genes implicated in PR degeneration. ECM, extracellular matrix; pre-mRNA, precursor mRNA; unknown, function undetermined; VRD, vitreo-retinal degeneration. Some of the categories include genes specific to retinal structure and function, such as 'Outer segment structure,' 'Phototransduction' and 'Visual cycle.' However, others, such as 'Lipid metabolism,' 'Protein degradation,' or 'Ciliary trafficking' comprise ubiquitously expressed genes. Figure from Wright *et al.* (2010).

Furthermore, mutations in certain genes, although not known to be prevalent worldwide, have extremely high incidence within smaller social groups. For instance, mutations in the *EYS* gene are estimated to cause up to 30 % of all recessive RP cases reported in Spain (Fahim, Daiger e Weleber, 2000 Aug 4 [Updated 2013 Mar 21].).

Bowne *et al.* (2008) and Sullivan *et al.* (2013) characterised the contributions of causative adRP genes (Figure 1-7), using a panel comprising samples of predominantly (but not exclusively) Western European origin, and the eyeGENE resource, respectively.

Most of the causative genes have numerous disease alleles. There are cases where a specific allele predominates; for instance, the 2299delG allele of the *USH2A* gene causes a substantial proportion of the Usher syndrome cases (Dreyer *et al.*, 2001; Aller *et al.*, 2004; Aller *et al.*, 2010).

The RP phenotype can also be influenced by modifying or low penetrance genes, which are difficult to identify, but which significantly contribute to the variability of RP. The already-mentioned processing factor 31 of the precursor mRNA, *PRPF31* (Vithana *et al.*, 2003), as well

as the A229T allele of the RPGR-interacting protein 1-like (*RPGRIP1L*) (Khanna *et al.*, 2009), are two examples of such modifiers.



Figure 1-7. Frequency of adRP mutations found in adRP cohorts by gene.

A, The cohort was mostly, but not exclusively, of Western European origin (Bowne *et al.*, 2008); testing identified mutations in 60% of 215 families.

B, The cohort comprised adRP eyeGENE probands (Sullivan *et al.*, 2013); testing identified mutations in 52% of 170 families. Figures and legends modified from Bowne *et al.* (2008) and Sullivan *et al.* (2013).

### 1.3.1 RETINA-LIMITED DISORDERS

In its most typical course, the non-syndromic RP first manifests itself in early mid-life, as night blindness. This is followed by a progressive loss of vision in the peripheral field, and, in some patients, by the subsequent loss of central vision. Many patients are often left with a residual field of central vision due to the remaining functional macular cones (reviewed in: Hartong, Berson e Dryja, 2006). Physiologically this is reflected as degeneration and loss of, firstly rod, then cone, photoreceptors (PRs). Nonetheless, cone-rod degenerations, where the primary defects occur in cones, have also been observed, and they have a prevalence of approximately 1 in 40 000. The progression of degeneration varies between patients, even within the same

family carrying the same mutation; in some cases PR death occurs very rapidly, whereas in others it can be slow and never lead to complete blindness (reviewed in: Hamel, 2006).

Typically, autosomal-dominant (ad) RP cases manifest as the mildest RP forms, and they can sometimes be mistaken for sporadic RP, if earlier generations experienced milder symptoms. This may happen due to partial or variable penetrance of the causative mutations, not unusual in dominantly inherited RP, and quite frequently associated with some genes, such as, *PRPF31* (*RP11*; MIM 600138) (Vithana *et al.*, 2003). Moreover, the onset of disease may occur quite late, sometimes even in the fifth decade of life (reviewed in: Hamel, 2006).

On the contrary, autosomal recessive (ar) RP forms are usually diagnosed much earlier, often already within the first decade of life, and the disease progression tends to proceed faster, causing the recessive form to manifest as more aggressive. The same is often also true for the X-linked (xl) RP, where transmission is usually (but not always) recessive (reviewed in: Hamel, 2006).

Although these are the overall trends of RP manifestations depending on a specific mode of transmission, it must be highlighted, that exceptions from these assumed patterns exist. Dominantly-inherited aggressive early-onset RP cases have been recorded for some *rhodopsin* mutations (Keen *et al.*, 1991). The opposite is also true: apparently milder, adRP-resembling forms of arRP have also been recorded (Kaplan *et al.*, 1990).

### **1.3.2 SYSTEMIC DISEASES**

Numerous syndromic forms of RP have been identified, overall 20-30 % of RP patients suffer also from non-ocular disease. Of these Usher Syndrome (USH) and Bardet-Biedl Syndrome (BBS), inherited via the autosomal recessive mode, are the most common, contributing to approximately 19 % (Boughman, Vernon e Shaver, 1983) and 5 % (Haim, 1992) of all RP cases, respectively. They are both ciliopathies (section 1.9.3).

Besides photoreceptor degeneration, Usher Syndrome is characterised by defects of the inner ear, which lead to a hearing impairment, and which sometimes also result in vestibular malfunction. Three subtypes of Usher Syndrome (USH 1-3) have been identified based on the clinical features, and genetic heterogeneity is characteristic of all three forms. Twelve USH loci have been identified to date (reviewed in: Petit, 2001).

The BBS phenotype is variable, and can be divided into numerous subtypes, based on clinical features, which include cognitive impairment, obesity, renal disease, hypogonadism and

polydactyly. Fourteen BBS loci with variable occurrence frequencies have been identified to date (reviewed in: Zaghoul e Katsanis, 2009).

Numerous other forms of syndromic RP have been identified, many of which may result from mutations in one gene. For instance, the above-mentioned BBS can be caused by a mutation in a gene encoding a centrosomal protein NPHP6 (*CEP290*). A mutation in this gene can also lead to Senior-Løken Syndrome (SLS) encompassing the renal cystic disease, Joubert Syndrome (JS) where cerebral malformation is a common clinical feature, or Meckel Syndrome (MS), which encompasses developmental abnormalities of the renal, the biliary, and/or the central nervous system. Similarly, mutations in the *RPGRIP1L* gene, encoding the RPGR interacting protein-1-like NPHP8, may be a cause of either JS, or MS; furthermore, these genes may also act as modifiers in ciliopathic RP (reviewed in: Retnet, 1996-2010; Wright *et al.*, 2010).

#### **1.4 TOPORS MUTATIONS ASSOCIATED WITH RETINAL DYSTROPHIES**

*TOPORS* is located on the short arm of chromosome 9, within the 9p21 region; the gene spans approximately 13 kb of genomic DNA, and encodes a 3135-nucleotide long transcript, comprising three exons. The largest portion of the gene is encoded within the third exon. Exon 1 encodes just the start codon; exon 2 is 195 bases long. An isoform of *TOPORS* has also been detected, in which the whole exon 2 is spliced out (Chakarova *et al.*, 2011).

In year 2007 a role for *TOPORS* has been demonstrated in inherited eye diseases, specifically autosomal dominant retinitis pigmentosa (adRP; RP31 phenotype MIM: 609923). Chakarova *et al.* (2007) identified two mutations in *TOPORS* in families of French-Canadian and German origins (Figure 1-8). The large French Canadian family had eighteen affected members and harboured a heterozygous 1-bp insertion (c.2474\_2475insA) in exon 3, which resulted in a frameshift (p.Tyr825\*) leading to a premature stop codon. The small German family (four affected members) carried a 2-bp deletion in a proximate region (c.2552\_2553delGA) in the same exon, which also lead to shifting of the reading frame (p.Arg851fs). The observed phenotype was intriguing as it was limited to retinal degeneration despite the ubiquitous expression of *TOPORS* (refer to section 1.4.1 for an overview of the pedigrees and phenotype). No mutant protein was detected in the affected individuals, and consequently, the authors suggested haplo-insufficiency as a likely disease mechanism.



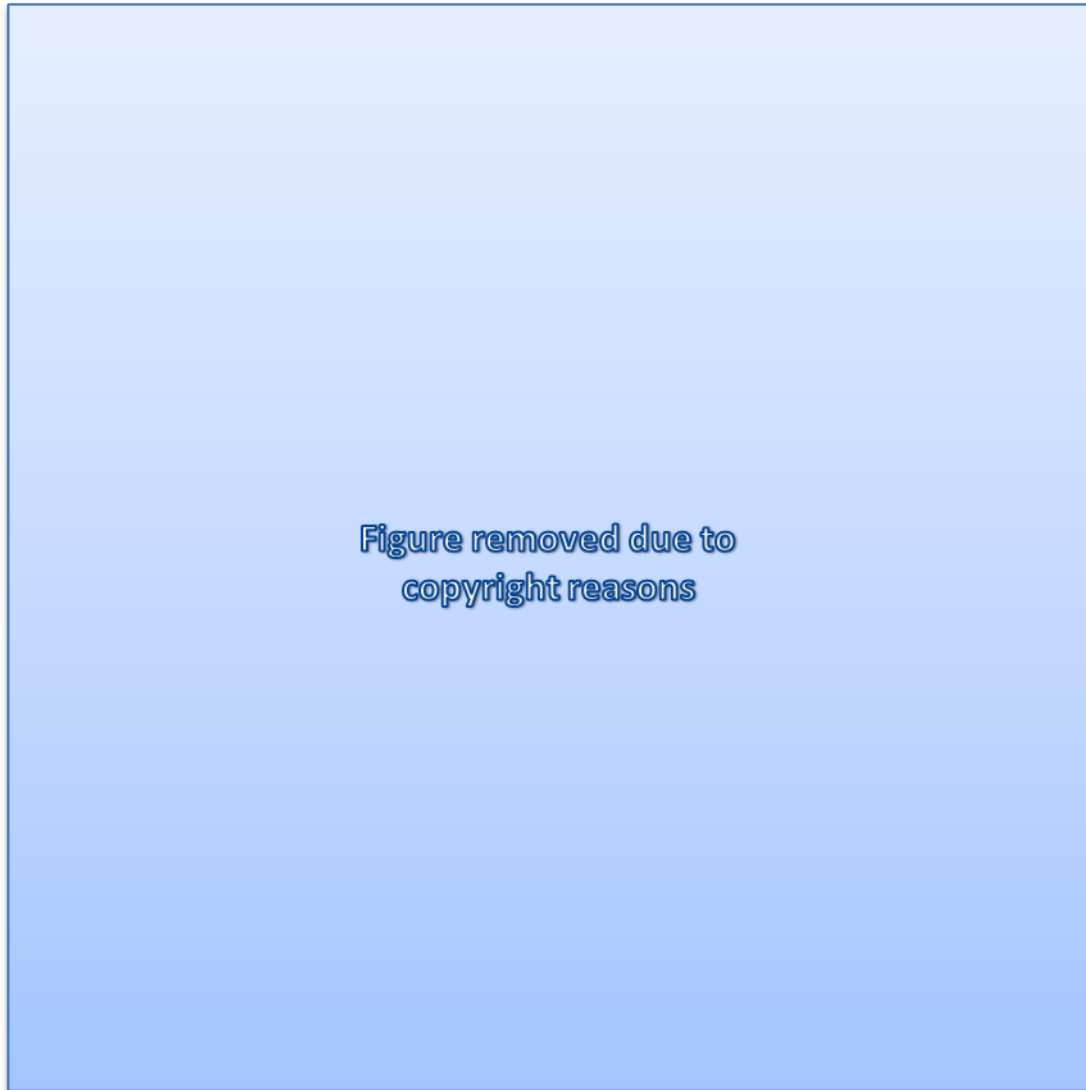


Figure 1-8. Pedigrees and sequence analyses of *TOPORS* mutations in French-Canadian and German pedigrees.

A and C, Canadian and German adRP-affected pedigrees, respectively. Circles indicate females; squares indicate males. Black filled symbols are affected individuals, open symbols are unaffected individuals, and deceased individuals are indicated by a slash (/). Asymptomatic individuals are marked by an asterisk (\*). Mutation segregation is shown on the pedigree as (homozygous/normal) or +/- (heterozygous/affected). Roman numbers indicate the generation and Arabic numbers indicate pedigree position. B and D, Electropherograms of the hetero-zygous mutations in exon 3 of the *TOPORS* gene. B, Mutation found in the French-Canadian family (c.2474\_2475insA/p.Tyr825\*). D, Mutation found in the German family (c.2552\_2553delGA/p.Glu852Aspfs\*20). Both mutations were identified after cloning of the amplified PCR product into pGEMT-Easy vector (Promega, WI, USA). Figure and legend modified from Chakarova *et al.* (2007).

A year later Bowne *et al.* (Bowne *et al.*, 2008) attempted to determine the frequency of *TOPORS* mutations in a cohort of 215 adRP families. The group demonstrated that small insertion/deletion (indel) mutations in *TOPORS* contribute approximately 1% to all adRP mutations. In the same study, the researchers identified two novel *TOPORS* mutations (Figure 1-9), which also led to premature stop codons, and were found in a proximal location to the previous two mutations, suggesting this region is a mutational hotspot. The first identified proband harboured a 1-bp deletion: c.2569delA (p.Arg857Glyfs\*9), whereas the second proband, which came from a different family, carried a nonsense point mutation: c.2422G>T (p.Glu808\*).



Figure 1-9. Pedigrees of adRP families UTAD102 and RFS169 affected by *TOPORS* mutations. A, UTAD102 family carrying the c.2569delA/p.Arg857GlyfsX9 mutation. B, RFS169 family carrying the c.2422C>T/p.Glu808X mutation. Circles indicate females; squares indicate males. Black filled symbols are affected individuals, open symbols are unaffected individuals, and deceased individuals are indicated by a slash (/). The “Q” indicates an individual in New York who reports being asymptomatic. “E”s indicate individuals who had eye examination at either the Retina Foundation of the Southwest or the Jules Stein Eye Institute. “M”s indicate individuals for whom ophthalmic medical records were reviewed. Plus signs show individuals whose DNA tested positive for the family's mutation; minus signs are individuals whose DNA tested negative for the family's mutations. Figure and legend modified from Bowne *et al.* (2008).

Another two heterozygous novel missense mutations were found in a panel of adRP patients, mostly of German origin, but including a smaller proportion of probands from other regions within continental Europe. Nonetheless, it could not be confirmed then that these mutations were causative of the observed retinal phenotypes, as relatives of the probands were not available for examination. The changes included c.1205A>C (p.Gln402Pro) and c.1818T>G (p.Ser606Arg) (Schob *et al.*, 2009), neither one of which is located in the previously established mutational hotspot region. The former change was later shown to segregate in a Norwegian pedigree, dating back to the eighteenth century (Selmer *et al.*, 2010).

The Scandinavian study identified the above-mentioned missense *TOPORS* mutation (c.1205A>C/p.Gln402Pro) in a large Norwegian family (Figure 1-10), in which 35 members were known to be affected by autosomal dominant pericentral retinal dystrophy (adPRD) (Selmer *et al.*, 2010); this phenotype is milder and has a more favourable prognosis than canonical adRP (refer to section 1.4.3 for an overview of the pedigree and phenotype).

Selmer *et al.* (2010) elegantly linked the p.Gln402Pro change to the Norwegian retinal dystrophy, which provided indirect support that the aetiology of disease in the proband from the German/European panel (Schob *et al.*, 2009) was very probably the same, even though pedigree data were not available<sup>2</sup>.

Finally, a recent cohort study by Sullivan *et al.* (2013) identified two novel *TOPORS* mutations in a panel of 'presumed adRP' patients (c.2264A>G/p.Asn755Ser; c.2554\_2557delGAGA/p.Glu85Glnfs\*13) from the National Ophthalmic Disease Genotyping and Phenotyping Network (eyeGENE) (Goetz *et al.*, 2012; Blain *et al.*, 2013).

However, for the substitution mutation, it could not be confirmed whether it segregates with the disease, and thus is responsible for the observed phenotype, as only one family member was available for examinations. The novel deletion/frameshift mutation occurs in the previously delineated mutational hotspot region (Sullivan *et al.*, 2013).

This study additionally found another patient, affected by the mutation initially identified by Chakarova *et al.* (2007) in the small German family (c.2552\_2553delGA/p.Arg851fs<sup>3</sup>).

---

<sup>2</sup> Phenotype details were not provided by Schob *et al.* (2009).

<sup>3</sup> This notation was later corrected by Sullivan *et al.* (2008) to c.2556\_2557delGA (p.Glu852Aspfs\*20). Three GA di-nucleotides are found in tandem at this region (c.2552\_2557), overlapping with codons for Arg and Glu.

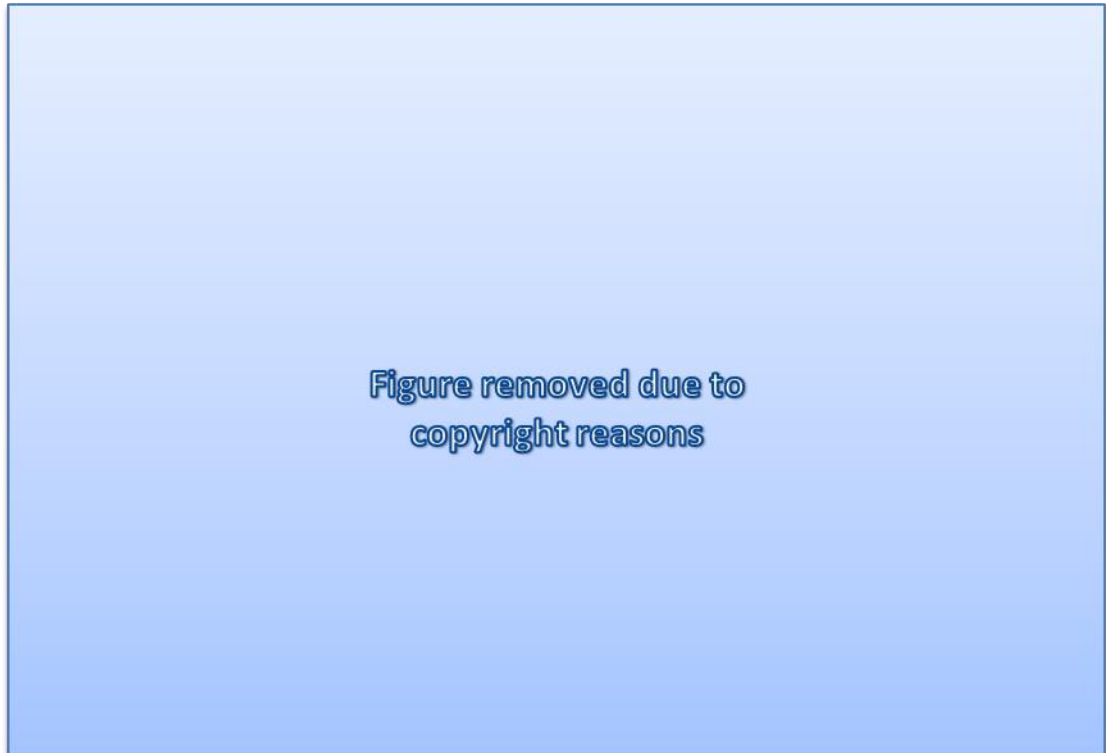


Figure 1-10. Pedigree of the adPRD Norwegian family carrying a missense *TOPORS* mutation. Circles indicate females; squares indicate males. Black filled symbols are affected individuals, open symbols are unaffected individuals, half-filled symbols are individuals affected by history, and deceased individuals are indicated by a slash (/). Examined individuals are marked by an asterisk (\*). Mutation segregation is shown on the pedigree as +/+ (homozygous/normal) or +/- (heterozygous/affected). Roman numbers indicate the generation and Arabic numbers indicate pedigree position. Figure and legend modified from Selmer *et al.* (2010).

Table 1-1. Mutations identified in *TOPORS* to date.

DNA mutation	Protein mutation	Phenotype	Reference
<b>c.2474_2475 insA</b>	p.Tyr825*	adRP with perivascular RPE atrophy (the latter observed in affected children, but not adults)	(Chakarova <i>et al.</i> , 2007)
<b>c.2556_2557 delGA</b>	p.Glu852Aspfs*20	adRP with perivascular RPE atrophy (the latter observed in affected children, but not adults)	(Chakarova <i>et al.</i> , 2007; Sullivan <i>et al.</i> , 2013)
<b>c.2569delA</b>	p.Arg857Glyfs*9	adRP	(Bowne <i>et al.</i> , 2008)
<b>c.2422G&gt;T</b>	p.Glu808*	adRP	(Schob <i>et al.</i> , 2009; Selmer <i>et al.</i> , 2010)
<b>c.1205A&gt;C</b>	p.Gln402Pro	adPRD	(Schob <i>et al.</i> , 2009; Selmer <i>et al.</i> , 2010)
<b>c.1818T&gt;G</b>	p.Ser606Arg	N/A → Uncertain pathogenicity or variable expressivity/partial penetrance	(Schob <i>et al.</i> , 2009)
<b>c.2264A&gt;G</b>	p.Asn755Ser	N/A → Uncertain pathogenicity	(Sullivan <i>et al.</i> , 2013)
<b>c.2554_2557 del</b>	p.Glu852Glnfs*13	adRP	(Sullivan <i>et al.</i> , 2013)

### 1.4.1 THE *RP31* PHENOTYPE

The *RP31* phenotype was firstly described by Papaioannou *et al.* (2005) when the new adRP locus was shown to segregate with retinal disease in a French-Canadian family (before it was known that *TOPORS* was the causative gene).

Fourteen members of the pedigree (Figure 1-8 A) were phenotyped (age range: 8 – 64 years); they had an early disease onset at 10-50 years of age, which differed between generations. Their visual acuity was good: better than 20/40 in 13/14 individuals among whom nine had 20/20 vision, and all were able to count fingers (for explanation of visual acuity tests and definitions refer to: Schulze-Bonsel *et al.*, 2006). The visual fields of the affected individuals ranged from 10° to 80°, and their ERG abnormalities were also very variable. Typically, rod defects were followed by cone defects. Interestingly, the earliest disease sign, found in three children from the youngest generation, was an ‘unusual perivascular cuff of RPE atrophy (...) surrounding the superior and inferior arcades.’ The disease in these children subsequently progressed to a diffuse pigmentary retinopathy with choroidal sclerosis. Furthermore, one of the affected patients was found to be asymptomatic and had a completely normal retinal appearance; the only phenotype results suggestive of disease were ERG abnormalities similar to those observed in symptomatic family members (Papaioannou *et al.*, 2005).

When *TOPORS* was identified as the adRP-causative gene within the *RP31* locus (Chakarova *et al.*, 2007), the French-Canadian family members were re-examined. This time 17 family members (rather than 14 as previously) were available for phenotyping. All had good visual acuity: 16/17 patients had better than 20/40 vision, among whom eleven had 20/20 vision; all were able to count fingers. The results of visual fields and ERG testing were still variable between individuals, and rod defects were still followed by cone dysfunction.

The ‘perivascular cuff of RPE atrophy (...)’ followed by the diffused pigmentary retinopathy with choroidal sclerosis remained as the earliest disease signs in this *RP31* pedigree. In fact, a fourth child was diagnosed with these characteristic clinical features (Figure 1-11).

Interestingly, three of the affected patients were asymptomatic and had a normal retinal appearance, but ERG abnormalities were analogous to those observed in symptomatic patients. During the previous phenotyping by Papaioannou *et al.* (2005) only one of the asymptomatic affected patients was examined and identified. No phenotype details of the small German family (Figure 1-8 C) were provided.



Figure 1-11. Colour photograph of the right eye of a 10-year-old affected child (IV:3 in Figure 1-8 A). At this age, a very obvious and unusual perivascular “cuff” of atrophy (arrows) around the superior and inferior vascular arcades is visible. The optic disc appears normal in colour, although the retinal arterioles are narrow, and there was no pigmentary degeneration at this stage. The cuff of RPE atrophy was found in three other children in this family as well but was not found in the adults of this pedigree. At a later age, this feature apparently disappears. Figure and legend modified from Chakarova *et al.* (2007).

*TOPORS* expression analysis, performed by Chakarova *et al.* (2007), demonstrated that *TOPORS* transcript was found in all tested tissues; however, the expression levels appeared much higher in the retina than in the other tested tissues (with the exception of liver and pancreas; Figure 1-12). Subsequently, the researchers also extracted lymphoblastoid cell lysates from affected and unaffected individuals in order to determine whether the truncated mutant *TOPORS* proteins are expressed. Only wild-type *TOPORS* protein was detected (Figure 1-13), leading the scientists to conclude that the mutants were rather unstable and quickly degraded; hence, haploinsufficiency was proposed as the disease mechanism.



Figure 1-12. RT-PCR analysis of *TOPORS* transcript in human tissues. PCR was performed with primers selected from exon 3 (with 28 cycles). A band of 2.69 kb was observed in all the tested QUICK-Clone cDNAs (Clontech) from retina, brain, kidney, liver, heart, skeletal muscle, pancreas, lung, and placenta. A ubiquitously expressed gene, *PGM1*, was used as a control. Figure and legend modified from Chakarova *et al.* (2007).



Figure 1-13. *TOPORS* expression in patient lymphoblastoid cell lines. Protein extracts from cell lines from one unaffected and two affected individuals from the Canadian and German families with p.Tyr825\* and p.Glu852Aspfs\*20 mutations, respectively, were analysed by SDS-PAGE and immunoblotting, with the use of anti-*TOPORS* antibody (Abnova, Taiwan).  $\alpha$ -tubulin was used as a control. WT = wild type. Figure and legend modified from Chakarova *et al.* (2007).

### **1.4.2 DISSIMILAR PHENOTYPES OF UTAD102 AND RFS169 PROBANDS**

The cohort study performed by Bowne *et al.* (2008) on a panel of adRP patients, who were mostly (but not only) of Western European origin, led to identification of two novel *TOPORS* mutations. The mutations were found in a member of Hispanic family UTAD102 (c.2569delA/p.Arg857Glyfs\*9) as well as a member of a Caucasian family RFS169 (c.2422G>T/p.Glu808\*), both males (Figure 1-9).

The 52 year old UTAD102 proband had severely impaired eyesight with only hand motion acuity of vision in both eyes (for explanation of visual acuity tests and definitions refer to: Schulze-Bonsel *et al.*, 2006). The patient's fundus examination revealed features of end-stage RP; specifically, he had extensive bone-spicule-like pigment deposits and severely attenuated blood vessels. Optic disc pallor and macular RPE atrophy were also present. The proband's two brothers and three children also had RP.

On the contrary, the phenotype of the RFS169 family was considerably milder. The 31 year old proband was fully aware of his poor peripheral vision, and his main complaint was 'difficulty going down steps and curbs in dim light or at night.' He reported that his mother was affected by severe night blindness at the age of thirty, and at present at the age of 60 years she has very poor vision. In addition to his mother, his sister, maternal aunt, grandfather, great grandfather and great uncle all had RP (Figure 1-9 B).

Except for the above-mentioned signs of early-stage RP, the proband had good eyesight with visual acuity of 20/20-2. Fundus examination showed abundant bone-spicule-like deposits in mid-periphery (but not far periphery) and his optic discs and maculae appeared normal. The proband's visual sensitivity was slightly impaired in the fovea and central 15° (based on static perimetry using a Humphrey Field Analyser (Humphrey Instruments, CA, USA), and was equal to zero at most regions beyond 7° eccentricity. On the contrary, the patient's 60-2 field, corresponding to peripheral retina, showed an area of preserved function in lower temporal field. ERG recordings showed no detectable standard rod response, whereas the cone b-wave was decrease to less than a quarter of normal lower limit response.

A 41 year old sister of the proband displayed a similar phenotype (Figure 1-14 A and B). Remarkably, the fundus appearance resembles that described in the Norwegian family with autosomal dominant pericentral retinal dystrophy (adPRD) caused by a missense *TOPORS* mutation (section 1.4.3) as well as the fundus of a pericentral RP patient (Figure 1-14 C), from a retrospective study clearly demonstrating that the pathology began in mid-



periphery/pericentric retina rather than the further periphery as would happen in classical RP. Cousins of the proband were also affected by early-stage RP. Interestingly, the cousins' mother was an asymptomatic carrier of the c.2422G>T *TOPORS* mutation. According to a self-reported questionnaire (which she completed aged 66 years), she was not affected either by night blindness, or by peripheral vision problems. This is a fourth known case of an asymptomatic carrier of a *TOPORS* mutation, the previous three being members of the French-Canadian family, in which the *RP31* locus was first identified.

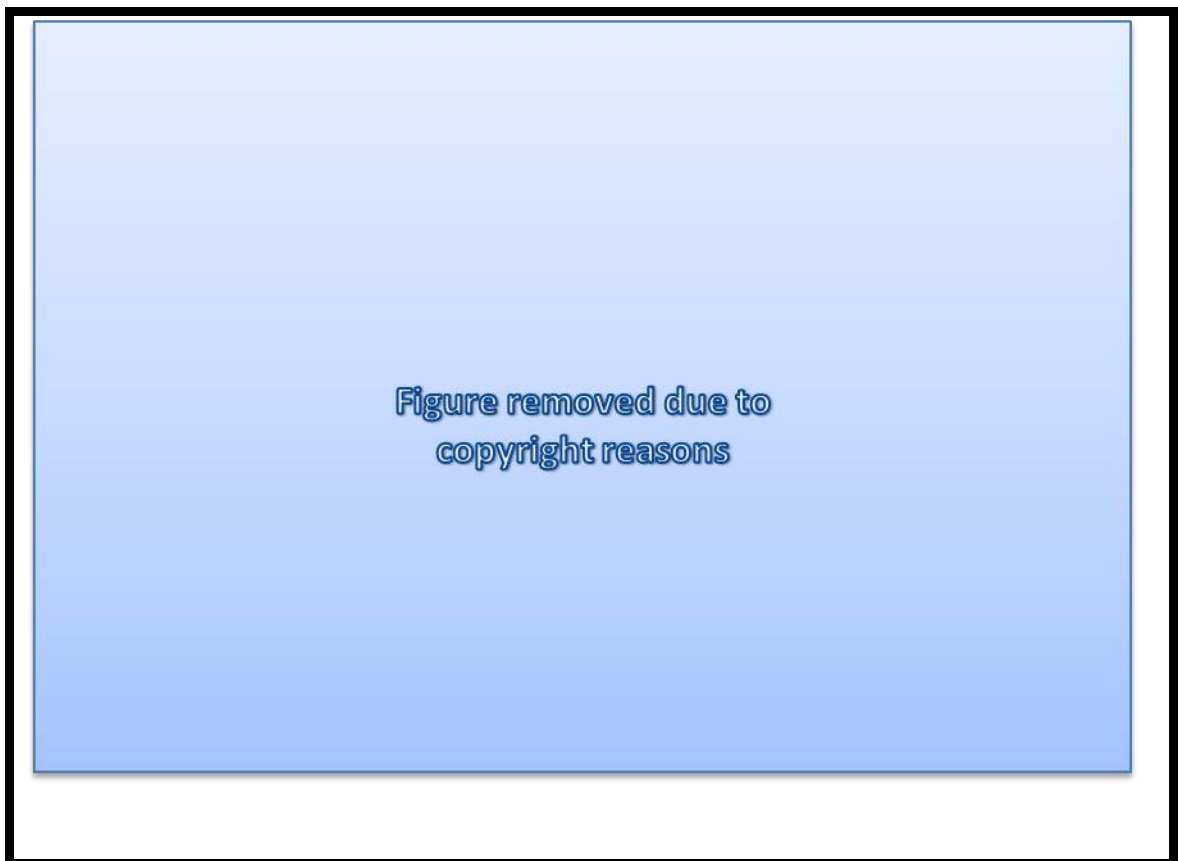


Figure 1-14. Fundus photographs from a member of family RFS169 (A and B) and a patient with a pericentral retinal dystrophy (C).

A and B, Right mid-peripheral fundus (A) and right peripheral fundus (B) photographs from the 41-year-old sister of the proband from family RFS169. The mid-periphery of both eyes contained numerous bone-spicule-like pigment deposits and the retinal arterioles were slightly narrowed by comparison to the veins. There was no evidence of a perivascular cuff of retinal pigment epithelium atrophy around the superior and inferior arcades in this family. Note the sharp border between the abnormal area and the normal appearance of the periphery. Figure and legend modified from Bowne *et al.* (2008).

C, Fundus photographs from Patient 5276 with pericentral retinitis pigmentosa/pericentral retinal dystrophy, taken in year 1982 and then in 2000, demonstrating an increase in pericentral bone-spicule pigmentation over an 18-year interval. Note the sharp border between the abnormal area and the normal appearance of the periphery. Figure and legend modified from Sandberg *et al.* (2005).

### 1.4.3 THE SCANDINAVIAN PERICENTRAL RETINAL DYSTROPHY

The large Norwegian pedigree (Figure 1-10) was affected by autosomal dominant pericentral retinal dystrophy (adPRD) caused by a missense *TOPORS* mutation: c.1205A>C/p.Gln403Pro (Selmer *et al.*, 2010). Comparing to classical RP, PRD is characterised by less severe night blindness, which typically appears later in life. As the authors described, the pathology begins ‘within 15° of fixation point, encircles, but spares, the macula, and comes close to the optic disc’ (Figure 1-14 and Figure 1-15). Fundus periphery looks essentially normal and ERG recordings also tend to be closer to the norm. Nonetheless, expressivity may be variable and, therefore, end-stage PRD may be apparently indistinguishable from end-stage classical RP.

Sixteen family members were examined (marked by an asterisk (\*) on the pedigree diagram in Figure 1-10), ten affected, and six unaffected by the adPRD. Among the unaffected ones three were older than sixty years of age, and they were fully examined, confirming that they had no signs of disease. All of the affected individuals presented with adPRD except for a 23 year old male (VII:4 in Figure 1-10), who was only affected by night blindness at the time of examination.

In contrary to the truncating *TOPORS* mutations, for which haploinsufficiency was proposed as disease mechanism, and which did not cause any symptoms in four of the affected patients (Chakarova *et al.*, 2007; Bowne *et al.*, 2008), suggesting incomplete penetrance, the missense *TOPORS* mutation appears to show complete penetrance in the Norwegian family. As a result, Selmer *et al.* (2010) speculated that a dominant-negative effect of the mutation *TOPORS* protein probably underlays the disease mechanism in this adPRD phenotype.



Figure 1-15. Fundus photographs from a member of the Norwegian family.

The right eye of person VI:28, a 64-year-old male. The pericentral localisation of an area of abnormal pigment deposits is apparent on the fundus. Note the sharp border between the abnormal area and the normal appearance of the periphery. Figure and legend modified from Selmer *et al.* (2010).

## 1.5 TOPORS: NUCLEAR AND CELL CYCLE CONTEXTS

A *Drosophila* study identified, using a Y2H screen, the Gypsy chromatin insulator complex as an interacting partner of dTopors. The Gypsy insulator has three known components: Su(Hw), Mod(mdg4)2.2, and CP190. Mod(mdg4)2.2 was used as bait in the protein-protein interaction (PPI) with dTopors, whereas subsequent studies in yeast showed that dTopors also directly associates with Su(Hw), but less strongly. All three Gypsy insulator components were found in immune complexes precipitated using antisera against dTopors. Further characterisation showed that dTopors is required for Gypsy insulator function, as its lack impairs the establishment of independent chromatin domains. On the other hand, dTopors over-expression rescues the Gypsy insulators activity, induced by Mod(mdg4)2.2 knock-down. Localisation of dTopors to the nuclear lamina was also demonstrated; this localisation was disrupted by mutations in lamin, which also negatively affect the Gypsy insulator activity and nuclear organisation.

This is in agreement with the fact that interactions between chromosomes and the nuclear membrane affect homologue pairing and fusion (synapsis) in the beginning of meiosis in many organisms; however, synapsis does not occur in *Drosophila* males. A study of *dTopors* showed that it corresponds to *nbl*, a gene involved in nuclear blebbing (Matsui *et al.*, 2011), and that it localised to nuclear lamina at prophase. Further characterisation demonstrated that dTopors was required for maintaining nuclear shape and lamin localisations in spermatocytes. During meiosis dTopors was needed chromosome transmission, prophase I chromatin condensation, and prevention of anaphase I bridges formation. The group also showed that dTopors is required for correct centriole separations, and, in contrast to previous findings, it is not essential for Gypsy insulator findings.

Outcomes of the *Drosophila* studies support conclusions from the functional experiments aiming to evaluate the role of TOPORS in the retina. Chakarova *et al.* (2011) confirmed the nuclear localisation of TOPORS in hTERT-RPE1 cell line; however, the group additionally showed that the protein also localises to centrosomes and mid-body (Flemming body) in a cell cycle-dependent manner. During stages G0, G1, S and G2 TOPORS was observed mostly in the nucleus in association with PML NBs as well as co-localising with  $\gamma$  tubulin in centrioles of centrosomes. During mitosis higher levels of TOPORS were observed in the centrioles of the spindle poles, and just prior to the completion of cytokinesis the protein was enriched in the mid-body.

The nuclear localisation of TOPORS was also demonstrated in MDCK cells, but only when they were dividing. In ciliated non-dividing MDCK cells TOPORS localised only to the basal body of primary cilium. The same localisation was observed in ciliated ARPE19 and IMCD3 cell lines. Due to its key localisation at the basal bodies, TOPORS may also mediate primary cilia signalling pathways, in addition to its role in the syndecan-based signalling (Braun *et al.*, 2012).

Cellular localisation of TOPORS at the base of primary cilium was in agreement with the protein's localisation in adult retinal sections of mouse, pig and human, where the protein was observed mostly at the basal body of the connecting cilium in rod photoreceptors, its daughter centriole as well as the pericentriolar region. TOPORS signal was also observed in the nuclei of retinal ganglion cells.

Furthermore, Chakarova *et al.* (2011) also showed that TOPORS co-immunoprecipitates with cilia-centrosomal proteins from bovine retinal extracts. Specifically, TOPORS was found in complexes with  $\gamma$  tubulin, and proteins involved in the retrograde transport, namely p150<sup>glued</sup>, p50-dynamitin and dynein intermediate chain (DIC). It should be emphasised that, in *Drosophila* spermatocytes, dTopors is required for centriole separations (Matsui *et al.*, 2011), which could suggest homologous functions for mammalian TOPORS proteins.

## **1.6 TOPORS: PROTEIN STRUCTURE AND FUNCTION**

TOPORS protein was first identified as a human topoisomerase I (hTop1)-binding partner in a Y2H screen (Haluska *et al.*, 1999). TOPORS bound to the first 250 amino acids (aa) of hTop1, a fragment, which also participates in interactions with helicases. The fragment of TOPORS pulled out from the cDNA library with the hTop1 bait, encompassed residues 456-882. The same group also showed that, in HeLa cells, TOPORS localised in a punctate pattern in the nucleus, and was precipitated in complexes with hTop1. Furthermore, it was emphasised that TOPORS possesses a RING finger domain homologous to a domain in a family of ICP0 viral proteins, which regulate viral transcription. Hence, it was suggested that TOPORS may be involved in recruiting hTop1 to RNA polymerase II transcriptional assemblies. Later Hammer *et al.* (2007) showed that TOPORS acts as a SUMO1 E3 ligase for hTop1.

Approximately a month after identifying the hTop1-TOPORS PPI, an independent paper was published, in which Zhou *et al.* (1999) performed a Y2H screen and identified a novel p53-binding protein, which was later confirmed as TOPORS. The researchers showed that TOPORS was ubiquitously expressed at mRNA level, and had a mouse orthologue. Subsequent functional work by Rajendra *et al.* (2004) demonstrated that the E3 ubiquitin ligase activity of

TOPORS is dependent on its C3HC4 RING finger, specifically on a conserved tryptophan residue within this domain. It was also demonstrated that TOPORS ubiquitinates p53, leading to proteasome-mediated decrease in its levels, providing evidence that TOPORS serves as ubiquitin E3 ligase for transcription factors. An analogous proteasome degradation of p53 occurs during over-expression of MDM2. Association between TOPORS and E2 ubiquitin-conjugating enzymes: UbcH5a, UbcH5c, and UbcH6, was also documented (Rajendra *et al.*, 2004). An evolutionary study of RING finger domains additionally suggests that TOPORS (alongside Mul1 and Deltex) has the ability to bind a greater variety of E2 conjugating enzymes than other RING E3 ligases (Ying *et al.*, 2011)

Thus, TOPORS was the first protein shown to possess dual ubiquitin and SUMO1 E3 ligase activity. Since then three other such dual ligases have been identified, namely: TRAF7 (Morita *et al.*, 2005), TRIM27 (Chu e Yang, 2011), and UHRF2 (Oh e Chung, 2013).

TOPORS protein comprises several characteristic domains (Figure 1-16).

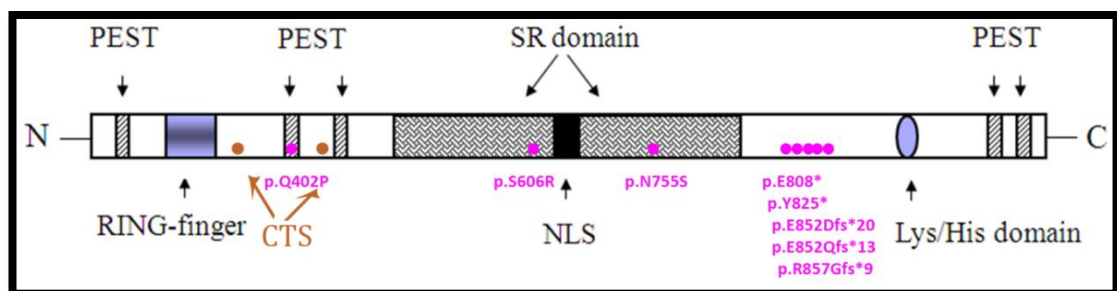


Figure 1-16. TOPORS protein structure.

Protein domains and known TOPORS mutations are indicated. PEST: proline-glutamate-serine-threonine domain associated with short protein half-life; RING finger: domain responsible for DNA-binding and for ubiquitin E3 ligase activity; SR domain: serine-arginine domain typical of proteins cycling between nucleus and cytoplasm depending on phosphorylation status (often found in splicing factors); Lys/His domain: lysine-histidine-rich region associated with punctate nuclear localisation of TOPORS; CTS: ciliary targeting sequence; NLS: nuclear localisation sequence.

The already-mentioned ring finger domain, located near the amino-terminus, is usually involved in modulation of chromatin structure, and regulates RNA polymerase II-mediated transcription. This structural motif strongly resembles a domain in the *infected-cell protein 0* (ICP0) family of viral proteins, which are implicated in regulation of viral transcription, as well as in reactivation of latent viruses, such as the *Herpes simplex virus* (Everett, 1984; Gelman e Silverstein, 1986; Boutell *et al.*, 2005). Regions rich in arginine (R) and serine (S) dipeptides are found in the centre of the protein; there are 33 of these RS/SR domains, which are separated in the middle by a nuclear localisation signal (NLS). TOPORS is unique in the respect that it is

the only known protein, which possesses both the RING finger domain and the RS/SR dipeptides domain; the latter is characteristic of proteins, which travel between the nucleus and cytoplasm depending on their phosphorylation status (Gui, Lane e Fu, 1994; Colwill *et al.*, 1996), and of some splicing proteins (Gross *et al.*, 1997; Siebel *et al.*, 1999; Cowper *et al.*, 2001). Amino acid sequences enriched in proline (P), glutamic acid (E), serine (S) and threonine (T) are also abundant in TOPORS, which possesses five of these PEST regions. These sequences are associated with targeting proteins for rapid degradation (reviewed in: Rechsteiner e Rogers, 1996). The protein also has a lysine/histidine (Lys/His) cluster, located towards the carboxyl-terminus. This fragment is thought to give TOPORS its distinct localisation pattern within the nucleus; it is punctuate and mostly excludes nucleoli. The speckled localisation is similar to patterns exhibited by RS/SR-rich splicing proteins as well as ring finger proteins; TOPORS associates, and thus co-localises with promyelocytic nuclear bodies (PML) (Rasheed *et al.*, 2002).

## **1.7 UBIQUITIN-LIKE PROTEIN MODIFICATIONS**

TOPORS is known to have a dual E3 ligase activity for ubiquitin as well as SUMO1 (Weger, Hammer e Heilbronn, 2005; Pungaliya *et al.*, 2007; Guan *et al.*, 2008; Miteva *et al.*, 2010), which, however, do not share a significant sequence homology. In both processes, ubiquitination and SUMOylation, a reaction cascade involving three types of enzymes: E1, E2 and E3, and analogous steps occur. TOPORS plays a role of the E3 enzyme.

Modifications by ubiquitin-like proteins result in covalent attachments of a single ubiquitin-like protein, or a chain of such proteins. Depending on whether a protein becomes modified by a mono- or a poly-ubiquitin-like protein, the cellular site at which this mutation occurs, as well as the specific site on the protein being modified, to which the ubiquitin-like protein (chain) attaches, the resulting modification will trigger variable consequences for cellular functions.

The canonical role of ubiquitination is marking proteins for degradation (Figure 1-17). SUMOylation on the other hand is associated with less clearly defined functions, and could influence DNA transcription, replication and repair, chromatin modifications, or cell cycle and apoptosis regulation (Perry, Tainer e Boddy, 2008; Wilson e Heaton, 2008).

### 1.7.1 UBIQUITINATION

Ubiquitination is initiated with the involvement of ATP by an E1 ubiquitin-activating enzyme, which binds a ubiquitin molecule. The ubiquitin monomer is subsequently transferred from E1 to an E2 ubiquitin-conjugating enzyme. The E2 enzyme and the substrate for ubiquitination are then bound by an E3 ubiquitin ligase (E3 enzymes are often specific for specific E2-substrate pairs), which catalyses the transfer of ubiquitin from the E2 onto a lysine residue of the substrate protein; an isopeptide bond is formed between ubiquitin and its substrate. At this point, depending on the purpose of the ubiquitination, the substrate may remain mono-ubiquitination, or poly-ubiquitin chain formation may occur (reviewed in: Welchman, Gordon e Mayer, 2005).

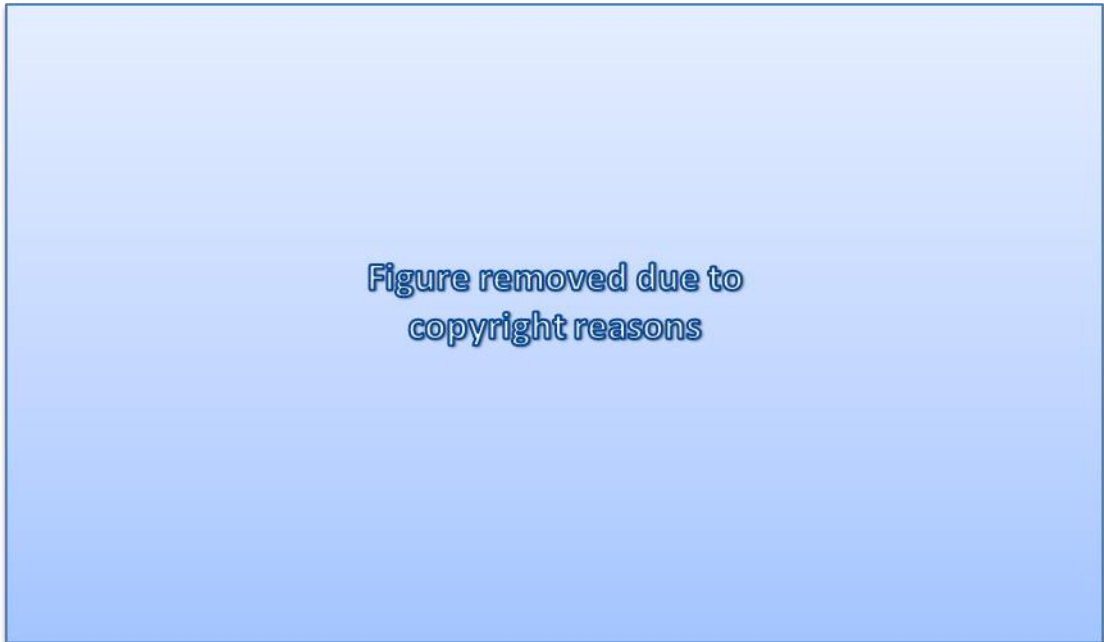


Figure 1-17. The ubiquitination pathway leading to proteasomal degradation.

Ubiquitin is activated by the ubiquitin-activating enzyme (E1) and then transferred to a ubiquitin-conjugating enzyme (E2), which transfers it to the protein substrate that is bound specifically to a particular ubiquitin ligase (E3; e.g. TOPORS). The transfer of ubiquitin takes place either directly (in the case of RING finger ligases, such as TOPORS) or via an additional thiol-ester intermediate on the ligase (in the case of HECT domain ligases). Repeated conjugation of ubiquitin units to each other generates a polyubiquitin chain that serves as the binding and degradation signal for the 26 S proteasome. The protein substrate is degraded, generating short peptides and free ubiquitin that can be further re-used. Ub, ubiquitin. Figure and legend modified from Rahimi (2012).

### 1.7.1.1 THE 26 S PROTEASE

As was mentioned in the introduction to this section, the classical purpose of ubiquitination is to mark proteins for degradation. Poly-ubiquitin-marked proteins can either be targeted for degradation either by the lysosomal degradation system, or by the 26 S proteasome. The latter is introduced here, as this project resulted in identification of a key regulatory protein of this multi-component protease (Chapter 4).

The 26 S proteasome is a multi-subunit protease system, which comprises two main components: a 20 S catalytic core particle (CP), and a 19 S regulatory particle (RegP). The CP is approximately barrel-shaped, and it comprises four stacked heptameric rings. The middle two rings are made from seven  $\beta$  subunits (*PSMB1-7*), of which  $\beta 1$ ,  $\beta 2$  and  $\beta 5$  confer the peptidase activity of the CP, i. e. the central proteasomal compartment contains a total of six catalytic sites, which are not substrate-specific. The outer two rings of CP consist of seven  $\alpha$  subunits each (*PSMA1-7*); these peripheral rings form narrow pores, which prevent entry of proteins, which have not yet been unfolded. Additionally, subunits  $\alpha 2-4$  have flexible extensions at their amino terminals, which enhance the proteasome gating. The CP is independent of ubiquitin and/or ATP binding (Voges, Zwickl e Baumeister, 1999; Lee *et al.*, 2011).

The 19 S RegP, of which at least twenty protein subunits have been identified to date, docks onto the  $\alpha$ -rings of the CP, and confers substrate specificity and ATP-dependence to the fully assembled 26 S proteasome. The RP can further subdivided into a base and cap. The base comprises a hexameric ring of AAA-ATPases (ATPases Associated with diverse cellular Activities), encoded by human genes *PSMC1-PSMC6* as well as three non-ATPase subunits, encoded by *PSMD1*, *PSMD2* and *PSMD4*. ATPases PSMC1-4 have  $\Psi Y X$  motifs at their carboxy-termini, which are used for docking of the RP onto the CP. The  $\Psi Y X$  fragments, comprising a hydrophobic residue ( $\Psi$ ), a tyrosine (Y) and any amino acid (X), become embedded in between the  $\alpha$  subunits of the CP, stabilising the assembled proteasome. The ATPase ring also regulates the gating of the 26 S proteasome, by moving the extended parts of  $\alpha 2-4$ . The AAA cassette domains of each of the six ATPases contain two Walker P-loop motifs. ATP binding to Walker A promotes CP-RP assembly, whereas ATP hydrolysis within Walker B is believed to promote unfolding and import of ubiquitinated proteins. The lid of the RP comprises regulatory non-ATPase particle and other accessory proteins; its main known function is to identify ubiquitin-tagged substrates, and remove the ubiquitin chains prior to import into the CP (Voges, Zwickl e Baumeister, 1999; Lee *et al.*, 2011).



### 1.7.1.2 ROLE OF TOPORS IN REGULATED PROTEOLYSIS

Park *et al.* (2008) demonstrated that the ubiquitin E3 ligase activity of TOPORS is modulation by phosphorylation of its serine 98 (Ser98) located just four amino acids upstream of the RING finger domain. The Ser98 phosphorylation enhanced the ubiquitin E3 ligase activity as well as binding of TOPORS to UbcH5a. The phosphorylation had no effect on the punctate nuclear localisation of TOPORS or its SUMO1 E3 ligase activity. In agreement with these findings, phosphorylation of TOPORS Ser718 by Polo-like kinase 1 (Plk1) leads to inhibition of p53 SUMOylation by TOPORS, and, simultaneously, to enhanced ubiquitination of p53 by TOPORS, and hence its degradation. Expression of phospho-deficient S718A TOPORS mutant leads to p53 accumulation due to inhibition of its degradation (Yang *et al.*, 2009).

This demonstrates that the ubiquitin and SUMO1 E3 ligase activities of TOPORS are mutually exclusive, and result in antagonistic outcomes. Furthermore, TOPORS Ser718 phosphorylation is essential for its degradation, which in turns delays the onset and progress of mitosis. In physiological conditions TOPORS is degraded in response to spindle checkpoint activation (Yang *et al.*, 2010).

Findings regarding the *Drosophila* orthologue of TOPORS, denoted as dTopors, provide additional valuable insight into this protein's functions. In this species, like in mammals, dTopors is also shown to localise to cell nucleus, where it binds to the basic region of Hairy, an orthologue of mammalian Hes1 (Secombe e Parkhurst, 2004). The relationship between dTopors and Hairy occurs at both: a genetic as well as proteomic level. Genetically, dTopors antagonises transcriptional repression by Hairy, however, it does not affect its ability to bind DNA. Furthermore, dTopors is involved in degrading the Hairy protein by ubiquitinating it, i.e. similarly to its mammalian orthologues, dTopors also possesses the ubiquitin E3 ligase activity; hence, the authors concluded that regulated proteolysis of Hairy is required for correct fruit fly segmentation.

It is noteworthy that Hes1, the mammalian homologue of *Drosophila* Hairy, the expression of which is regulated by Notch, in turn itself regulates the expression of PTGDS (Fujimori, Kadoyama e Urade, 2005), which has been identified as an interacting partner of TOPORS in this project. Furthermore, the proteolytic processing of Notch is homologous to the processing of ITM2B (Martin *et al.*, 2008), which has been identified here as yet another protein, associating with TOPORS.

Differential expression of *TOPORS* has also been documented in a muscle atrophy (Fujita *et al.*, 2010), characterised by a decrease in protein synthesis and/or an increase in protein degradation. This presents a possible involvement for TOPORS as a ubiquitin E3 ligase in muscle protein degradation. Hence, the summarised findings provide evidence that TOPORS-regulated proteolysis is important in developmental as well as degradation processes.

### 1.7.2 SUMOYLATION

Steps involved in SUMOylation are analogous to those described for ubiquitination (section 1.7.1); however, SUMOylation involves one additional step. Specifically, prior to SUMO activation, a specific proteolytic cleavage of its C-terminal tail must occur. A proteolytically processed SUMO molecule is then activated, with involvement of ATP, by an E1 enzyme, precisely the Uba2/Aos1 hetero-dimer. The activated SUMO molecule is subsequently transferred to the Ubc9 protein, which acts as an E2 SUMO-conjugating enzyme. At last, the E2 enzyme and a substrate become bound by an E3 SUMO ligase, which catalyses the attachment of the SUMO molecule to a lysine residue on the substrate. In most cases mono-SUMOylation occurs; however, formation of poly-SUMO chains has also been observed (reviewed in: Geiss-Friedlander e Melchior, 2007).

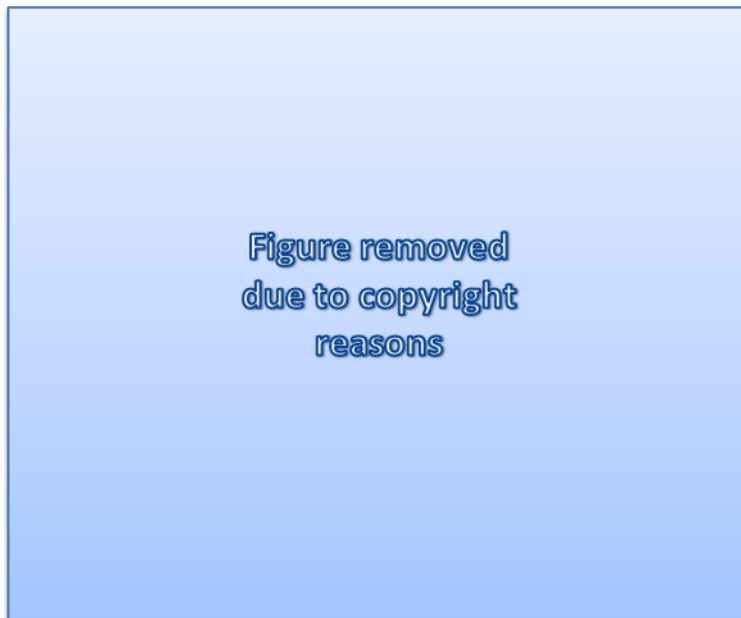


Figure 1-18. The SUMOylation pathway.

Pre-SUMO (small ubiquitin-related modifier) peptide needs to be proteolytically cleaved by SUMO-specific isopeptidases (sentrin-specific proteases; SENPs). These enzymes remove carboxy-terminal amino acids from pre-SUMO proteins to reveal their carboxy-terminal G-G motif (where G is glycine). Cleaved mature SUMO is activated by the E1 heterodimer AOS1–UBA2 in an ATP-dependent reaction, which results in a thioester bond between the carboxy-terminal glycine and cysteine 173 (C173) in UBA2 ubiquitin protein.

SUMO is then transferred to the catalytic cysteine residue of the E2 enzyme UBC9. Finally, an isopeptide bond is formed between the carboxy-terminal glycine residue of SUMO and a lysine residue in the substrate protein. This step is usually aided by an E3 ligase, for instance, TOPORS. SUMOylated targets serve as substrates for SENPs, which ensures the reversible and dynamic nature of this process. Figure and legend modified from Geiss-Friedlander and Melchior (2007).

### 1.7.2.1 TOPORS AS SUMO1 E3 LIGASE

Shortly after TOPORS was first described, it was shown, also via a Y2H method, that TOPORS associates with AAV2 proteins, involved in the virus's replication, specifically Rep68 and Rep78 (Weger, Hammer e Heilbronn, 2002). This interaction involved residues 871-917 of TOPORS – a region additionally shown to be required for interaction with p53, and later demonstrated to also mediate an interaction with Ubc9, and included within a basic C-term region mediating interactions of TOPORS with SUMO1 (Weger, Hammer e Engstler, 2003), and DEDa fragment of caspase 8 (Yao *et al.*, 2007). Overall, TOPORS enhanced AAV gene expression, and it was concluded that it has a role as a transcriptional regulator.

Rasheed *et al.* (2002) later showed that speckled localisation of TOPORS in the nucleus of exponentially growing HeLa cells was due to its association with promyelocytic leukaemia nuclear bodies (PML-NBs). The above-mentioned basic C-term region of TOPORS is required for this localisation. Importantly, the experiments established that the association of TOPORS with PML bodies was dynamic; if the cells were treated with transcription-inhibiting nucleoside analogues, or with hTop1 inhibitor, then TOPORS would re-located to nucleoplasm.

TOPORS was also shown to act as a SUMO1 E3 ligase towards mammalian Sin3A, which is a repressor of transcription (Pungaliya *et al.*, 2007).

Independent functional experiments demonstrated that TOPORS also SUMOylates p53 and DJ-1 (Shinbo *et al.*, 2005), involved in transcriptional regulation and anti-oxidative stress responses; its loss of functions is associated with early-onset Parkinson's disease. DJ-1 and p53 interact not only with TOPORS, but also with each other; moreover, in cells DJ-1 co-localised with both TOPORS and p53, however, its co-localisation with the latter needs to be stimulated by UV irradiation. Overall, in the described experimental settings, DJ-1 positively regulated p53, whose transcriptional activity was repressed by TOPORS SUMOylation. On the contrary, Weger *et al.* (2005) showed in an independent study that TOPORS acts as a SUMO1 E3 ligase for p53, which is associated with an increase in p53 protein levels as well as its transcriptional activity.

Detailed Y2H-based analysis showed that regions involved in PPIs with SUMO1 included residues 415-737 as well as 854-1045, whereas the fragment sufficient for interaction with UBC9 entailed amino acids 871-917 (Weger, Hammer e Engstler, 2003). The authors also showed that SUMO1-interaction motif (SIM) in TOPORS is homologous to the SIM of human PIASx, and that TOPORS itself is modified by SUMO1 on lysine 560. Residues 437-574 were

sufficient for SUMOylation of TOPORS as well as for its localisation to nuclear speckles in HeLa cells; it was shown that some, but not all, of these speckles co-localised with PML bodies, and that SUMOylation of TOPORS was not necessary for this localisation.

It should be noted that PIAS $\alpha$  and PIAS $\gamma$  also SUMOylate DJ-1 (Shinbo *et al.*, 2006); and the SIMs of TOPORS and PIAS $\alpha$  are homologous. In addition, PIAS $\gamma$  associates with CGI-55, which in turn is an interacting partner of TOPORS (Lemos e Kobarg, 2006). The interaction with CGI-55 was demonstrated by a Y2H as well as co-localisation in HeLa cells. It was also re-established that TOPORS localised to the PML bodies, however, CGI-55 associated with them only weakly, despite what its punctate localisation in the nucleus (and the cytoplasm) might have initially suggested. It is also worth highlighting that in another Y2H screen TOPORS interacted with Mx1, which is involved in cellular responses to viral stress (Engelhardt *et al.*, 2001). Mx1 also associates with Daxx, which was also shown to interact with CGI-55 (Lemos e Kobarg, 2006). Furthermore, it was also demonstrated that Mx1 localises to PML NBs and interacts with SUMO1 as well as with a subunit of its activating enzyme SAE2 (Engelhardt *et al.*, 2001).

## 1.8 THE CENTROSOME CYCLE

As was described in section 1.5, TOPORS protein is involved in cell cycle regulation and its fate and functions differ depending on the cell cycle stage. This is further reflected the close association of TOPORS with the centrosome, a unique organelle, which is also essential for development of the primary cilium, forming its basal body (section 1.9.1), where TOPORS was shown to localise.

The centrosome is a key organelle in animal cells, where it acts as the main microtubule-organising centre (MTOC), and is involved in maintaining the polarity, adhesion and motility of interphase cells, whereas in mitotic processes it mediates processes such as spindle formation, positioning and cell division. Moreover, it is also distinct in the sense that, like the DNA, it is doubled at every cell cycle in a semi-conservative manner – a process referred to as the centrosome cycle. Aberrations of centrosome functions and duplications often lead to malignant changes due to resulting chromosomal segregation and cytokinesis complications as well as enhanced motility.

The semi-conservative duplication of the centrosome is possible due to the fact that the organelle constitutes two centrioles: a mother centriole (which can form the basal body at G0) and a daughter centriole, both surrounded by peri-centriolar material (PCM).

During cell division (phase M in Figure 1-19) the two centrioles separate, moving off to opposite sides of the cell, where they facilitate the formation of spindle poles and, ultimately, cell division. Just following cytokinesis, i.e. at G1 stage of the cycle, a cell will only possess one centrosome. As the cell-centrosomal cycle progresses the centrosome will either start duplicating at the S phase (step E in Figure 1-19), whilst DNA synthesis is also occurring, or it will leave the cell division cycle and enter the quiescent G0 stage (step B in Figure 1-19).

The classic cell cycle comprises four major phases, specifically G1, S, G2, and mitosis (M), followed by cell division (Figure 1-19). G1 is characterised by overall growth and duplication of cellular contents other than DNA and centrosomes, which are duplicated at the S-phase. The G2 phase involves further cellular growth as well as activities, serving to verify that the processes, performed at G1 and S phases, were completed without errors, before the cell enters mitosis, and subsequently divides.

It should be noted that as the centrosome prepares for duplication at the G1 phase, its two centrioles become disengaged from each other, i.e. they are held together by a loose tether rather than being tightly combined and positioned at 90° to each other (compare centrosome appearance at stage M and G1 in Figure 1-19). The original two mother and daughter centrioles remain bound by this tether until late G2 phase. As duplication commences in the S phase, new pre-centrioles grow from both: the mother centriole and the daughter centriole; once the cycle is complete the 'old' daughter centriole acquires appendage proteins (not shown in Figure 1-19) and becomes the 'new' mother centriole. During the G2 phase the pro-centrioles are elongating and maturing. The elongated pro-centrioles become 'new' daughter centrioles closely engaged with their mother centrioles in each of the resulting centrosomes. Maturation is completed towards the end of the G2 phase, and the two centrosomes become separated during the G2/M transition. Centrosome disengagement additionally occurs approximately during the M/G1 transition, and is involved in preparation of the centrosome for the subsequent cell cycle (reviewed in: Meraldi e Nigg, 2002).

As was mentioned above, some cells, such as neurons, including the photoreceptors, become differentiated and exit the cell cycle in a transition from a G1 to G0 phase. It is at this quiescent stage that cells will undergo ciliogenesis and acquire a primary cilium, whilst the mother centriole will be acting as the basal body.

It is noteworthy that centriolar staining can be indicative of the cell cycle stage, at which an observed cell was fixed (Durcan *et al.*, 2008; Li, J. *et al.*, 2012; Li *et al.*, 2013).

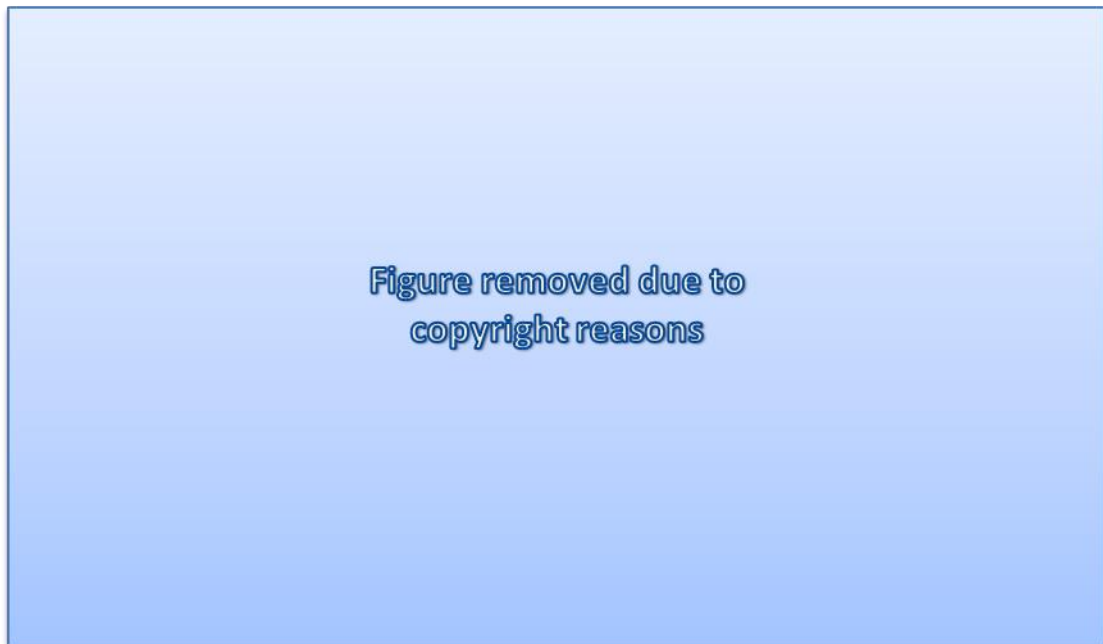


Figure 1-19. Model of the regulation of cilia formation by CP110 in cycling and quiescent cells.

A, When a cell enters a new cycle it only has one centrosome comprising a mother and a daughter centriole. The mother centriole matures on mitotic entry, recruiting molecules that enable it to form appendages, such as ODF2 (brown triangle). It is possible that upon mitotic exit, CEP97 (yellow circle) is degraded or removed from centrioles leading to destabilization of CP110 at the mother centriole (blue square). B, In G1, the absence of CP110 and presence of ODF2 specifically in the mother centriole enables it to become a basal body, tethering at the membrane, where it begins to form a ciliary axoneme. C, If nutrients are removed, cells can exit the cell cycle and become quiescent (G0). At this stage, the cilium can grow further. D, On serum stimulation, cells re-enter the cell cycle and the cilia are re-absorbed. E, The centrioles (or basal bodies) duplicate in S phase. CP110 is necessary in the daughter centrioles for their biogenesis. F, On centrosome maturation at the G2/M transition, the cilium is re-absorbed and centrioles move to the centre to participate in mitotic-spindle assembly. The mitotic kinase Aurora A (pink oval) activates tubulin deacetylase, hence promoting ciliary disassembly and internalization of the basal body. Figure and legend modified from Bettencourt-Dias and Carvalho-Santos (2008).

Specifically, two dots, shown by centrin-2 immuno-staining, represent G1-phase cells; three to four clustered dots of centrin-2 indicate the S-phase of the cell cycle; whereas G2-phase cells can be recognised by centrin-2 staining, which shows three to four dots, where pairs of dots are observed at least 3  $\mu\text{m}$  apart from each other (Li *et al.*, 2013).

Throughout the centrosomal cycle, tightly coupled to the cell division cycle, diverse groups of proteins are associated with this organelle, among which cyclins and cyclin-dependent kinases (CDKs) comprise the backbone for cell cycle progression (Meraldi e Nigg, 2002). However, the focus in Figure 1-19 is to depict proteins involved, specifically, in promotion or inhibition of entering the G0 stage and primary cilium formation (section 1.9.1).

It will be demonstrated in the experimental Chapter 7 that some of the novel interacting partners of TOPORS will associate with the centrosome throughout the cell cycle (like TOPORS

does), whereas others will be observed co-localising with this organelle only in dividing cells, and then sometimes with only one of its centrioles.

It is also noteworthy that the centrosome was revealed to function as a central hub for protein degradation machinery in dividing human embryonic kidney (HEK) 293 and HeLa cells (Wigley *et al.*, 1999), of which the key constituents are the 26 S protease/proteasome complexes (section 1.7.1.1). Additionally, the components of the ubiquitin-proteasome system (UPS) were shown to interact with centrosomes in primary neurons to regulate dendrite development, demonstrating that the centrosome-proteasome relationship is not limited solely to cycling cells, but also occur in cells at the G0 stage (Puram *et al.*, 2013). Furthermore, independent studies demonstrated that close cooperation between these two structures is critical for maintenance of cell signalling (Gerdes *et al.*, 2007; Liu *et al.*, 2014). Consequently, these findings allow for speculating that modulation of the UPS activity may serve as a potential therapeutic strategy for ciliopathies (section 1.9.3).

## **1.9 VERTEBRATE CILIA**

Eukaryotic cilia, often referred to as flagella, when they are involved in generating movement, are cellular organelles, which appeared early in evolution; they are remarkably well conserved from protozoa to humans (reviewed in: Singla e Reiter, 2006; Gerdes, Davis e Katsanis, 2009). In vertebrates, these organelles are found ubiquitously in polarised cells, where they serve a number of sensory and signalling functions; they are a characteristic of quiescent cells, most of which develop just one cilium per cell, a non-motile primary cilium. The proteome of these highly complex structures has been shown to comprise approximately a thousand various polypeptides (Gherman, Davis e Katsanis, 2006). Cilia are profoundly involved in development, as well as maintaining homeostasis of specific cell types, tissues and organs. Hence, a significant association between ciliary defects and numerous clinical phenotypes, including inherited retinal disorders, has been demonstrated (section 1.9.3).

### **1.9.1 THE PRIMARY CILIUM**

Cilia are polarised structures consisting of two major components: the basal body and the axoneme (Figure 1-20). The basal body is formed from a modified mother centriole, surrounded by a pericentriolar material, and it serves as an anchor for the whole organelle; this structure forms a hollow cylinder comprising nine evenly distributed microtubule triplets. The axoneme, which protrudes away from the cell, is connected to the basal body via a transition zone, and it can be of two main types.

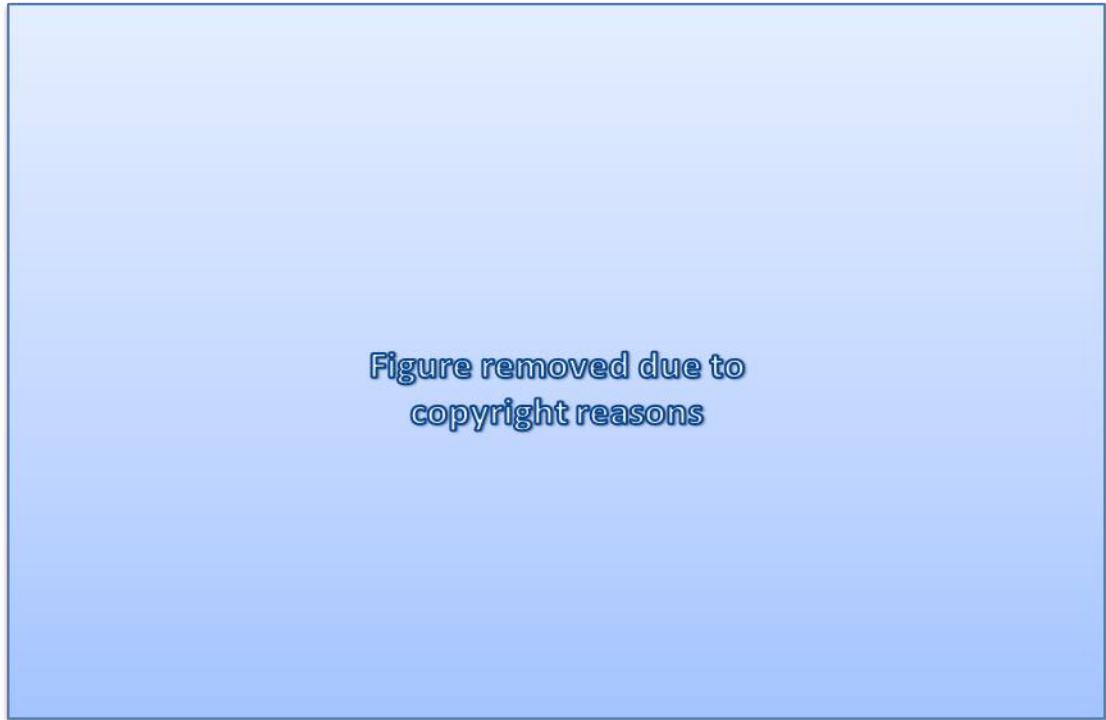


Figure 1-20. Ciliary structure in vertebrates.

A: Scanning electron micrograph of motile cilia; B: Scanning electron micrograph of a solitary primary cilium; C: Structural comparison of the motile and primary cilia. Figure from Davenport *et al.* (2005).

The axonemes of primary cilia comprise nine microtubule doublets continued from the microtubules of the basal body; this is known as the 9+0 microtubule configuration, and it is found predominantly in non-motile cilia (primary cilia). An additional doublet of microtubules, centrally located inside the axoneme and embedded within a sheath (9+2 configuration), is found in most motile cilia (flagella). The microtubules within both axoneme types are joined together by nexin links, and they are held in place by radial spokes, which extend from the outer microtubules towards the centre of the structure. Within each microtubule doublet, the 'A' tubule serves for binding dynein and retrograde intraflagellar transport (IFT) proteins, whereas the anterograde IFT proteins and kinesin-2 bind to the 'B' tubule (Fliegau, Benzing e Omran, 2007; Gerdes, Davis e Katsanis, 2009).

### **1.9.2 THE CONNECTING CILIUM OF THE PHOTORECEPTOR CELL**

The outer segment of the photoreceptor cell can be considered a specialised primary cilium. The sensory photoreceptor cells are unique in the fact that they comprise two segments physically joined together by a bridge-like structure, the photoreceptor connecting cilium (CC). Of all the cellular functions, performed by photoreceptors, impairment of the ciliary transport is the most frequent cause of photoreceptor degeneration (reviewed in: Wright *et al.*, 2010). As is depicted in Figure 1-21, the cellular organelles required for protein synthesis in the rod



cell are all located within the inner segment. The outer segment, responsible for light-sensing, is entirely dependent on the anterograde ciliary transport for receiving rhodopsin and the building blocks required for its daily renewal. Metabolised, turned-over protein products are transported back to the inner segment by the retrograde IFT proteins. Consequently, any defects in the structure of the connecting cilium or the components of the IFT system within this organelle result in photoreceptor malfunction and, eventually, cell death.



Figure 1-21. Figure 1 21. The connecting cilium of photoreceptor cells. Left: an electron micrograph of rod photoreceptors and a corresponding detailed diagram, depicting the inner and outer segments joined together by a connecting cilium (CC); structural components of the CC, and proteins known to be involved in its function are highlighted. Right: Schematic representation of rod and cone photoreceptor cells, demonstrating the distinct structure of their outer segments. Figure from Wright *et al.* (2010).

### 1.9.3 CILIA AND CILIOPATHIES

In addition to photoreceptors, cilia are found on almost all types of differentiated, mammalian cells, which have exited the cell cycle (i.e. which are at the quiescent phase, or G0).

It has been shown in recent years that defects in these organelles lead not only to retinal disorders due to impaired function of the photoreceptor connecting cilium, but they result in a much wider range of disease phenotypes (Table 1-2). The variable diseases resulting from malfunction of this cellular organelle are collectively referred to as ciliopathies.

Table 1-2. Clinical phenotypes associated with ciliary dysfunction syndromes.

BBS, Bardet-Biedl Syndrome; SLS, Senior-Løken Syndrome; MS, Meckel Syndrome; JS, Joubert Syndrome; USH, Usher Syndrome. Table modified from Badano *et al.* (2006).

Disease	BBS	SLS	MS	JS	USH
<b>Retinitis pigmentosa</b>	√	√	√	√	√
<b>Renal cystic disease</b>	√	√	√	√	
<b>Polydactyly</b>	√		√	√	
<b><i>Situs inversus/Isomerism</i></b>	√	√	√	√	
<b>Mental retardation/developmental delay</b>	√		√	√	
<b>Hypoplasia of corpus callosum</b>	√		√	√	
<b>Dandy-Walker malformation</b>	√	√	√	√	
<b>Posterior encephalocele</b>	√*		√	√	
<b>Hepatic disease</b>	√	√	√	√	
<b>Impaired vestibular function</b>					√
<b>Sperm abnormalities</b>					√
<b>Ataxia</b>					√
<b>Anosmia</b>	√				√
<b>Hearing impairment</b>	√				√

\*In mice.

Besides retinal dystrophies, clinical phenotypes associated with the ciliopathies include hearing impairment due to defects of the inner ear, cysts in the pancreas, liver and kidney, polydactyly, *situs inversus*, as well as developmental and nervous system abnormalities (reviewed in: Fliegauf, Benzing e Omran, 2007; Gerdes, Davis e Katsanis, 2009). The outlined phenotypic features have all been identified in different combinations in a number of ciliopathic syndromes, as summarised in Table 1-1. USH and BBS, which are the two most commonly diagnosed forms of syndromic RP (section 1.3.2), are also classified as ciliopathies, which further underlines the key role of the cilia and, in particular, the connecting cilium in maintaining the photoreceptor cell homeostasis.

## **1.10 HYPOTHESES AND AIMS**

To date, the studies of TOPORS have revealed that it is a protein of a multifunctional character with numerous important functions within a range of cellular processes, such as ubiquitination or SUMOylation (Weger, Hammer e Heilbronn, 2005; Guan *et al.*, 2008). It is ubiquitously expressed in human tissues, including the retina, and it has been shown to localise to the nucleus as well as to the centrosome and basal body of dividing and non-dividing cells, respectively (Chakarova *et al.*, 2011).

Interestingly, mutations in *TOPORS* are only known to cause retinal dystrophies with no other systemic symptoms. Hence, the aim of this project is to ascertain why mutations in a ubiquitously expressed, multifunctional gene like *TOPORS* only result in a retina-specific disease by identifying interacting protein partner(s) of TOPORS from the retina.

Since TOPORS does not appear to have a role in classical retinal pathways, such as phototransduction, or the visual cycle, it may be assumed that its retinal pathology is probably associated with the protein's localisation to the basal body of the photoreceptor connecting cilium.

The uniqueness of the photoreceptor cell structure and physiology, coupled to the localisation of TOPORS at the base of the cell's strategic organelle, may help explain the restricted disease phenotype caused by *TOPORS* mutations. If the identified interacting partner(s) are also found to localise to the basal body, this would reveal an additional valuable piece of the puzzle.

### **1.10.1 RETINAL LIBRARY CONSTRUCTION AND VALIDATION**

A human retinal cDNA library was generated (Chapter 3) and used for the yeast two-hybrid (Y2H) screening (Chapter 4), aiming to test the hypothesis that novel interacting partner(s) of TOPORS are proteins expressed specifically in the retina rather than ubiquitously, or that they perform a function specific to the retina.

The library was made in-house in the Y187 *Saccharomyces cerevisiae* yeast strain, using the 'Make Your Own "Mate & Plate" Library System' (Clontech, CA, USA). The library was cloned into the pGADT7-Rec vector in order to generate constructs coding for retina-expressed proteins fused to the GAL4 activation domain (GAL4 AD).

The generated library was characterised in order to determine its suitability for the Y2H screen. Transformation efficiencies, cell densities, titres and numbers of independent clones were calculated, and examples of the obtained retinal cDNA sequences were identified.

The approximate insert sizes were also determined for a proportion of library clones. It was critical that rhodopsin, or another retina-specific transcript, was isolated in order to validate the retinal cDNA library.

A ready-made human brain cDNA library (Clontech, CA, USA) was purchased for contingencies.

### **1.10.2 BAIT CONSTRUCTION AND Y2H CONTROL EXPERIMENTS**

Full-length *TOPORS* cDNA sequence, encoding the TOPORS bait, was cloned into a Y2H-compatible vector, in frame with the cDNA, encoding GAL4 DNA binding domain (GAL4 DNA-BD) (Chapter 3). The purpose for generating a TOPORS - GAL4 DNA-BD fusion-encoding construct, was to express a bait fusion protein in yeast, which would be compatible with the cDNA library clones fused to GAL4 AD. If TOPORS and its prey(s) from the retinal library interact, this will bring the two domains of GAL4 into sufficient proximity to activate the expression of reporter genes, demonstrating protein-protein interactions (PPIs).

The Y2H Gold *Saccharomyces cerevisiae* yeast strain (Clontech, CA, USA) was transformed with the resulting bait vector. Following yeast transformation with the bait plasmid, control experiments to check for expression, auto-activation, and potential toxicity to the host yeast cells, were completed in order to determine whether the bait construct was suitable for use in the Y2H (or whether an alternative method for detecting PPIs should be used).

Additional Y2H control PPI experiments were also performed prior to the screening to test the experimental set-up. Specifically, previously reported interactions between p53 and the SV40 T antigen (Ag) as well as p53 and TOPORS were tested.

Yeast-two hybrid (Y2H) screen (Chapter 4) was performed by mating the library yeast culture with the bait culture, and spreading the mated cultures on media selective for interactions. Identification of interacting partner(s) of TOPORS, which would have an obvious relation to the retina, was anticipated.

### **1.10.3 VALIDATION OF INTERACTIONS AND mRNA EXPRESSION**

The interacting partners of TOPORS identified through the Y2H screen (Chapter 4) were prioritised for downstream experiments based on their retinal status. Specifically, if a protein expressed only in the retina, or a more widely-expressed protein with a function exclusive to the retina, was found to interact with TOPORS, this protein would be prioritised for

downstream experiments (rather than a ubiquitously expressed protein with no known associations to the retina).

The selected interaction(s) were verified by additional studies in yeast (Chapter 5). The goal was to confirm that the PPI(s) occur, when they are repeated, using a full-length cDNA corresponding to the interacting partner(s), rather than just its/their fragment from the retinal library.

Furthermore, known protein-coding isoforms of the identified interacting partner(s) were searched for on the Ensembl genomic database to subsequently determine whether any of them was also expressed in the retina (Chapter 5).

Isoform-specific primers were designed and a reverse-transcriptase (RT) PCR study was performed to establish whether any of the known protein-coding transcripts of the identified interacting partner(s) could also be amplified from the human retinal RNA. If this was the case, they would also be included in the further validation and characterisation experiments.

#### **1.10.4 CONFIRMATION OF PPI(s) IN HUMAN CELL LINES**

Following the completion of validation experiments in yeast as well as the isoform expression study, the subsequent objective was to show that the PPI(s) also occur in human cell lines between endogenously-expressed TOPORS and its newly identified endogenously-expressed partner(s) (Chapter 6).

Firstly, Western blotting was performed to confirm that the interacting partner(s) were expressed in human cell lines at protein level. If their expression was not detected, then transfections of cells with constructs encoding the interacting protein(s) of interest would need to be performed prior to the co-immunoprecipitation (coIP) studies.

Following positive validation of expression of protein(s) of interest, coIP was performed on cultured cells to test the hypothesis that the PPI(s) identified via the Y2H do indeed occur in human cell lines.

#### **1.10.5 CO-LOCALISATION STUDIES TO VALIDATE PPI(s)**

In order to test the hypothesis that, like TOPORS, its newly-identified and validated interacting partner(s), also localise to the centrosome, and/or the basal body of primary cilia, immunofluorescence (IF) localisation studies with centriolar and ciliary markers were performed in human cell lines (Chapter 7). The localisation was subsequently studied in mouse

retinal sections to test the hypothesis that the identified PPI(s) could have occurred within the native retinal tissue (Chapter 8).

Ultimately, findings from the tissue localisation studies would allow for evaluating the argument that the retinal protein(s), shown to interact with TOPORS in two different systems (yeast and human cells), would also co-localise with TOPORS at the base of the connecting cilium in the mouse retinal sections.

Demonstration of interaction(s) and localisation at the expected retinal region would fulfil the overall aim of the thesis, which was to identify protein partner(s) of TOPORS from the retina and to characterise the interaction(s). Ultimately, this could help answer a major question of the thesis in RP context, i.e. why mutations in ubiquitously-expressed *TOPORS* result only in retinal disease by investigating the functional relationship(s) between TOPORS and its interacting partner(s).

#### **1.10.6**      **FUTURE CONTEXT**

The results of this research would ultimately help to elucidate the role of TOPORS in causing the retina-specific phenotype regardless of the ubiquitous expression of this protein. The work may help define the cellular pathways and/or networks that TOPORS is implicated in within the retina as well as this may help to understand the general intra- and intercellular protein interactions implicated in retinal degeneration. Finally, the knowledge gained throughout conducting this project could aid the development of future therapies, targeting, for instance, the identified cellular pathways, which TOPORS and its protein partner(s) are involved in.

## **2 METHODS AND MATERIALS**

This chapter provides a synthesis of techniques and materials required to fulfil the aims and objectives of this project. Firstly, an overview of the yeast two-hybrid (Y2H) system is provided. This is followed by basic molecular biology and genetics as well as immuno-chemical methods. The chapter ends with a summary of materials and recipes for buffers and other solutions used throughout the project.

### **2.1 YEAST TWO-HYBRID SYSTEM**

The yeast two-hybrid (Y2H) method (Figure 2-1) for detecting protein-protein interactions (PPIs) was used to fulfil the preliminary objective of this PhD thesis, specifically, to identify the interacting partners of TOPORS from the human retina.



Figure 2-1. Basis of the Y2H assay.

If GAL4 DNA-BD is fused with TOPORS, here called the bait protein, whereas GAL4 AD is fused with one of its interacting protein partners, denoted as the prey protein, and bait and prey interact, BD and AD are brought into sufficient proximity to activate transcription of the reporter genes (BD of the reconstituted transcription factor binds to the promoter region of a reporter gene, whereas AD activates transcription of the reporter gene by recruiting RNA polymerase (pol) II. Figure from the Matchmaker™ Gold Yeast Two-Hybrid System (Clontech, CA, USA) user manual.

### 2.1.1 Y2H: AN OVERVIEW

The method was pioneered by Fields and Song (1989), who demonstrated the advantageous properties of GAL4, a protein, which, in its endogenous environments, acts as a transcriptional activator of galactose utilisation genes in the yeast *Saccharomyces cerevisiae*.

Results presented in experimental Chapters 3, 4 and 5 are based on the Y2H system.

#### 2.1.1.1 Y2H: FUNCTIONAL BASIS

GAL4 comprises two strategic functional domains: a DNA-binding domain (BD) and a transcriptional activation domain (AD). The binding domain, located at the amino terminus of GAL4, binds to specific DNA sequences upstream of the gene to be transcribed, i.e. the GAL upstream activation sequences (UAS) or promoters. The carboxyl-terminus activation domain is essential for activating transcription via recruiting RNA polymerase II.

The GAL4 BD and AD domains can be physically separated and still retain their functions, as physical separation does not interfere with GAL4 protein folding. This quality of GAL4 is exploited in the Y2H system, where each one of the two GAL4 domains is fused to another protein (in context of this project: TOPORS and one of its interacting partners). If both hybrid proteins are brought into sufficient proximity due to an interaction between TOPORS and the interacting partner, they can act as a fully functional transcriptional activator (Navaratnam, 2009).

#### 2.1.1.2 Y2H: PLASMID CONSTRUCTS

In order to screen for the interactions, suitable DNA vectors must first be designed and constructed (Methods and Materials section 2.2.5 and experimental Chapter 3). For the purposes of the Y2H method the GAL4 BD and GAL4 AD are normally cloned into two different vectors. Each one of the vectors also carries a gene for antibiotic resistance for propagation in bacteria, as well as nutritional selection genes for use in the Y2H. A complementary DNA (cDNA) encoding the protein of interest, i.e. the bait is normally cloned into the GAL4 BD vector in frame with the *GAL4 BD* cDNA. The preys are cloned into the GAL4 AD vectors in frame with the cDNA encoding the activation domain. Plasmids manufactured by Clontech (CA, USA) as well as the Gateway cloning vectors (LifeTechnologies, CA, USA) were used (Table 2-1, Table 2-2).



Table 2-1. In-fusion cloning (Clontech, CA, USA) vectors.

Vector	Purpose	Features
pGBKT7 (Clontech, CA, USA)	In-fusion cloning (Clontech, CA, USA) vector containing the GAL 4 DNA BD. Genes encoding Y2H bait proteins can be cloned into this vector.	Contains the <i>TRP1</i> nutritional reporter gene for selection in yeast and a gene for kanamycin resistance for selection in bacteria.
pGADT7 (Clontech, CA, USA)	In-fusion cloning (Clontech, CA, USA) vector containing the GAL 4 AD. Genes encoding Y2H prey proteins can be cloned into this vector.	Contains the <i>LEU2</i> nutritional reporter gene for selection in yeast and a gene for ampicillin resistance for selection in bacteria.
pGADT7 –Rec (Clontech, CA, USA)	In-fusion cloning (Clontech, CA, USA) vector containing the GAL 4 AD. Recommended vector for cloning of a cDNA library.	Contains the <i>LEU2</i> nutritional reporter gene for selection in yeast and a gene for ampicillin resistance for selection in bacteria.

Table 2-2. Gateway cloning (LifeTechnologies, CA, USA) vectors.

Vector <sup>4</sup>	Purpose	Features
pDONR/Zeo (LifeTechnologies, CA, USA)	Donor vector used in the Gateway cloning BP reaction as shuttle vector (see section 2.2.5.3 Gateway cloning).	Contains <i>attP1</i> and <i>attP2</i> sequences and a gene for zeocin resistance.
pAD <sup>5</sup>	Destination vector, containing the GAL 4 AD, used in the Gateway cloning LR reaction (see section 2.2.5.3 Gateway cloning). Genes encoding Y2H prey proteins can be cloned into this vector.	Contains <i>attR1</i> and <i>attR2</i> sequences, the <i>LEU2</i> nutritional reporter gene for selection in yeast and a gene for ampicillin resistance for selection in bacteria.
pBD <sup>5</sup>	Destination vector, encoding the GAL 4 DNA BD, used in the Gateway cloning LR reaction (see section 2.2.5.3 Gateway cloning). Genes encoding Y2H bait proteins can be cloned into this vector.	Contains <i>attR1</i> and <i>attR2</i> sequences, the <i>TRP1</i> nutritional reporter gene for selection in yeast and a gene for chloramphenicol resistance for selection in bacteria.

<sup>4</sup> The *E. coli* DB3.1 cells were used for propagation of Gateway vectors in bacteria (see bacterial transformation section 2.2.3).

<sup>5</sup> These vectors were a gift from Dr Ronald Roepman. They had been modified from original Stratagene (CA, USA) vectors to contain the *att* sequences, i.e. to allow compatibility with Gateway cloning (LifeTechnologies, CA, USA; see section 2.2.5.3).

### 2.1.1.3 Y2H: PPI SCREENING

The process of screening for bait - prey interactions requires the expression of genes encoded on both plasmids within a single yeast cell. Yeast cells intended for use in Y2H screening can grow either as haploid, or as diploid mated cells; in natural conditions higher ploidy levels have also been recorded (Gunge e Nakatomi, 1972).

Traditionally, the standard Y2H PPI screening procedure involved co-transformation of baits and preys into haploid yeast cells. As an alternative, the bait and prey plasmids can be transformed into haploid yeast cells of different mating types. When the yeast cells mate to form diploids, both plasmids are then found within one cell, where the genes can be expressed and their products can interact.

The Matchmaker™ Gold Yeast Two-Hybrid System (Clontech, CA, USA), used for this project, is based on the yeast mating procedure. Two strains of the yeast *S. cerevisiae* are provided; the Y2H Gold, which serves as the bait reporter strain, is of the *MATa* mating type, whereas the Y187 prey reporter strain is of the *MATα* mating type.

The Y2H Gold strain and the Y187 strain possess four and two reporter genes, respectively, which are under control of GAL4-responsive promoters (Table 2-3, Table 2-4).

Table 2-3. Y2H Gold (the bait host strain) reporter gene constructs.

GAL4-responsive promoter	Reporter gene
<b>G1 Promoter</b>	<i>HIS3</i>
<b>G2 Promoter</b>	<i>ADE2</i>
<b>M1 Promoter</b>	<i>AUR1-C</i>
<b>M1 Promoter</b>	<i>MEL1</i>

Table 2-4. Y187 (the prey host strain) reporter gene constructs.

GAL4-responsive promoter	Reporter gene
<b>G1 Promoter</b>	<i>lacZ</i>
<b>M1 Promoter</b>	<i>MEL1</i>

The Y2H Gold strain is auxotrophic for histidine and adenine, encoded by the *HIS3* and the *ADE2* genes, respectively. However, both of these genes can be expressed under control of the GAL4-responsive promoters, therefore, when bait and prey proteins interact, this allows the yeast to synthesise both the essential amino acid as well as the purine base. Thus, strains, in which the protein interaction occurs, should be able to grow on media that lack both of these substrates.

The *AUR1-C* is a dominant mutant version of the *AUR1* gene, which codes for the inositol phosphoryl ceramide synthase. This enzyme, when expressed in yeast, confers resistance to the highly toxic antifungal agent, Aureobasidin A (AbA). According to the Matchmaker™ Gold Yeast Two-Hybrid System User Manual (Clontech, CA, USA) the use of AbA, as a drug reporter, leads to less background than, for instance, the use of histidine reporter, hence, using AbA is advantageous over using the nutritional reporters only.

*MEL1* codes for the enzyme  $\alpha$ -galactosidase, which allows the yeast to utilise the colourless 5-bromo-4-chloro-3-indolyl  $\alpha$ -D-galactopyranoside (X- $\alpha$ -Gal). The resulting product is blue, which is reflected in the appearance of yeast colonies, in which *MEL1* is expressed. Both the Y2H Gold and the Y187 strains can express *MEL1*, if protein interactions occur. The latter strain also expresses a component of the *lac* operon, the *lacZ* gene, if protein interactions occur. This gene encodes  $\beta$ -galactosidase; the expression of this enzyme also results in the yeast colonies producing a blue product, given that they are grown on media supplemented with the colourless 5-bromo-4-chloro-3-indolyl- $\beta$ -D-galactoside (X- $\beta$ -Gal).

The yeast methods described in subsequent sub-sections were used to generate results reported in experimental Chapters 3, 4 and 5.

### **2.1.2 YEAST CELL STOCK MAINTENANCE**

In order to prepare for the Y2H experiments the yeast cells need to be maintained in appropriate conditions throughout the course of the project.

Two strains of yeast cells were provided with the Matchmaker™ Gold Yeast Two-Hybrid System (Clontech, CA, USA) as frozen glycerol stocks: the *Saccharomyces cerevisiae* Y2H Gold strain (*MATa* mating type) and the *S. cerevisiae* Y187 strain (*MAT $\alpha$*  mating type).

In addition to maintaining a frozen glycerol stock, both strains were maintained on solid media by re-streaking on fresh YPDA agar (Table 2-5) plates every month. The untransformed yeast cells were spread on YPDA agar dishes, sealed with Parafilm (Pechiney Plastic Packaging, IL, USA), incubated at 30 °C for approximately 48-72 hours to allow for sufficient growth, and stored at 4 °C.

The Y2H Gold strain was used for transformation of plasmids encoding the bait, whereas the Y187 strains serves as a host for the prey fusion proteins.

Table 2-5. Yeast Peptone Dextrose Adenine (YPDA) media for yeast culture.

YPDA Agar Medium	YPDA Liquid Medium
25 g YPD	25 g YPD
0.02 g adenine hemisulphate salt	0.02 g Adenine hemisulphate salt
10 g agar	-
500 ml dH <sub>2</sub> O	500 ml dH <sub>2</sub> O

### 2.1.3 TRANSFORMATION OF COMPETENT YEAST CELLS

For the purpose of performing the Y2H PPI experiments, yeast cells needed to be transformed with constructs, encoding the human retinal proteins of interest. Specifically, these included TOPORS and clones of the human retinal cDNA library (section 2.1.8 and experimental Chapter 3).

Prior to yeast transformation the yeast cells must firstly be made competent. This is performed using the TrisEDTA/lithium acetate (TE/LiAc) methods (section 2.1.3.1). Yeast cells prepared in this way are subsequently ready for transformation using the TE/polyethylene glycol (TE/PEG) method (2.1.3.2).

Construction of the cDNA library in yeast and culture of TOPORS bait constructs as well as the control plasmids (Chapter 3) in yeast highly relied on the transformation procedure.

#### 2.1.3.1 PREPARATION OF COMPETENT YEAST CELLS

Preparation of competent yeast cells was performed under sterile conditions based on Section VI. A. of the Yeastmaker™ Yeast Transformation System 2 User Manual (Clontech, CA, USA); several changes were introduced.

A single yeast colony (either Y2H Gold, or Y187, depending on the plasmid to be transformed – see section 2.1.2) was inoculated into 3 ml YPDA medium in a sterile 50-ml tube; the culture was incubated with shaking (7-8 h, 30 °C, 250 rpm; Innova 4200 Incubator Shaker, New Brunswick Scientific, NJ, USA).

Fifty microlitres of this culture were then inoculated into 200 ml of fresh YPDA medium in a sterile 250 ml conical flask; the culture was incubated with shaking (16-20 h, 30 °C, 215 rpm; Innova 4200 Incubator Shaker, New Brunswick Scientific, NJ, USA) until it reached an optical density of 0.8 - 1.0, when measured at a 600 nm wavelength (OD<sub>600</sub> 0.8-1.0).

The culture was equally divided into two sterile conical-bottom 50 ml tubes and centrifuged at 1700 rpm for five minutes (RT) to pellet the cells (Megafuge 1.0 R, Heraeus, UK);

the supernatant was discarded and each pellet was re-suspended in 30 ml sterile, deionised water (dH<sub>2</sub>O).

The centrifugation was repeated, the supernatant was discarded, and each pellet was re-suspended in 6 ml of 1.1X TE/LiAc (Table 2-6).

Each cell suspension was transferred to 1.5 ml micro-

centrifuge tubes (1 ml per tube) and centrifuged at 14000 rpm for 20 seconds (Centrifuge 5417R,

Eppendorf, Germany). The supernatant was discarded and each pellet was re-suspended in a final volume of 600 µl 1.1X TE/LiAc. The competent cells were used for transformation with plasmid DNA (section 2.1.3)

Table 2-6. 1.1X Tris-EDTA/Lithium Acetate (TE/LiAc) Solution.

1.1X TE/LiAc Solution
1.1 ml 10X TE (supplied with the kit)
1.1 ml 1 M LiAc (10X) (supplied with the kit)
7.8 ml sterile dH <sub>2</sub> O

### 2.1.3.2 YEAST TRANSFORMATION

The freshly prepared competent yeast cells (section 2.1.3.1) were transformed with plasmid DNA, according to Section VI. B. of the Yeastmaker™ Yeast Transformation System 2 User Manual (Clontech, CA, USA) and were spread on appropriate agar media (Table 2-7, Table 2-8), using sterile glass beads (3 mm; Merck, Germany).

Table 2-7. Synthetic Minimal Media for yeast culture.

Synthetic Minimal Media
3.35 g Yeast nitrogen base
91.1 g D-sorbitol
0.37 g of relevant dropout solution
20 g agar
20 ml 50 % glucose
pH 5.8
500 ml dH <sub>2</sub> O

Table 2-8. Details of yeast media selecting for bait or prey constructs.

Media type	Selects for
<b>SD/-W (synthetic dropout lacking tryptophan)</b>	bait plasmids
<b>SD/-L (synthetic dropout lacking leucine)</b>	prey (library) plasmids

The Y2H Gold competent cells were transformed (Table 2-9) with either the pGBKT7 vector (Table 2-1), or the pBD vector (Table 2-2); both vectors carry the GAL4 binding domain (BD), and a selective nutritional marker, *TRP1*, encoding the amino acid tryptophan. Inserts encoding the bait proteins were cloned into these vectors.

The Y187 competent cells were transformed (Table 2-9) with the pGADT7 as well as the pGADT7-Rec vectors (Table 2-1), carrying the GAL4 activation domain (AD), and a selective nutritional marker, *LEU2*, encoding the amino acid leucine.

The human retinal cDNA library (Methods and Materials section 2.1.8 and experimental Chapter 3) was cloned directly into the pGADT7-Rec, and transformed into the Y187 competent yeast cells. The potential prey proteins were subsequently cloned into the pGADT7 vector for verification in yeast (direct interaction). Both plasmids are based on the same backbone sequence; however, the few differences between them are significant. The pGADT7-Rec vector comprises two short sequences; the SMART III Sequence and the CDS III Sequence, which enable *in vivo* cloning by homologous recombination, whereas the pGADT7 vector contains specific restriction sites, which are not found in the former vector.

Table 2-9. Summary of yeast strains and main associated plasmids.

Yeast strain	GAL4 Domain	Plasmid(s) used for strain transformation	Insert(s) carried in the plasmid	Function
<b>Y2H Gold</b>	BD	pGBKT7 (Clontech)	<i>TOPORS</i> fragments	Baits in Y2H direct PPIs
<b>Y2H Gold</b>	BD	pBD <sup>6</sup>	Full-length <i>TOPORS</i>	Bait in Y2H screen
<b>Y187</b>	AD	pGADT7-Rec (Clontech)	Fragments of clones amplified from human retinal cDNA library	Preys in the Y2H screen
<b>Y187</b>	AD	pGADT7 (Clontech)	Full-length and/or deletion constructs of interacting partners identified in the initial Y2H screen	Preys in Y2H direct PPIs

#### 2.1.3.2.1 SMALL SCALE TRANSFORMATION

The small scale transformation procedure was used for introducing bait plasmids into the Y2H Gold strain as well as relevant control plasmids into the corresponding strains (Chapter 3), or the newly-identified preys into the Y187 strain (Chapter 5).

---

<sup>6</sup> This vector was a gift from Dr Ronald Roepman. It had been modified from original pBD-GAL4 Cam (Stratagene, CA, USA) vector to contain the *att* sequences, i.e. to allow compatibility with Gateway cloning (LifeTechnologies, CA, USA; see section 2.2.5.3).

Before each transformation the Yeastmaker Carrier DNA (from herring testes cells; 10 µg/µl) was denatured by incubation at 95 °C for five minutes, and then immediately stored on ice; 5 µl of the denatured carrier DNA was then combined with 100 ng of the plasmid DNA in a sterile 1.5 ml tube.

The competent yeast cells (50 µl) and the PEG/LiAc solution (500 µl; Table 2-10) were subsequently added, and the suspensions were mixed gently; the cells were incubated at 30 °C for thirty minutes

Table 2-10. Polyethylene glycol/Lithium Acetate (PEG/LiAc) Solution.

PEG/LiAc Solution
8 ml 50 % PEG 3350 (supplied with the kit)
1 ml 10X TE Buffer (supplied with the kit)
1 ml 1 M LiAc (10X) (supplied with the kit)

with mixing by tapping or gentle vortexing (~800 rpm) every ten minutes. Twenty microlitres of DMSO were added to each tube, and the tubes were incubated in a 42 °C water bath for 15 minutes with gentle vortexing (~800 rpm) every five minutes; Vortex Genie 2 (Scientific Industries, NY, USA) was used. The cells were pelleted by centrifugation at 14000 rpm for 15 seconds (Centrifuge 5417R, Eppendorf, Germany).

The supernatant was removed and the pellet was re-suspended in 1 ml of YPD Plus Medium (Clontech, CA, USA). The cells were then incubated in Innova 4200 Incubator Shaker (New Brunswick Scientific, NJ, USA; 1 h, 30 °C, 215 rpm).

The cells were pelleted by centrifugation at 14000 rpm for 15 seconds (Centrifuge 5417R, Eppendorf, Germany); and the supernatant was discarded. The pellet was re-suspended in 500 µl of 0.9 % (w/v) NaCl Solution (Table 2-11).

Table 2-11. 0.9 % Sodium Chloride (NaCl) Solution.

0.9 % (w/v) NaCl Solution
0.9 g NaCl
100 ml dH <sub>2</sub> O
Dissolved and filter-sterilised

A hundred microlitres of each cell suspension (diluted 1:10 and/or 1:100) were spread on 100 mm agar plates with the appropriate SD selection media; i.e. SD/-W for pGBKT7, and SD/-L for pGADT7 (Table 2-8). The plates were incubated upside down at 30 °C for 72-120 hours or until colonies appeared.

#### 2.1.3.2.2 LIBRARY-SCALE TRANSFORMATION

This transformation procedure was used for construction of the human retinal cDNA library in the yeast Y187 stain (experimental Chapter 3).

Before each transformation the Yeastmaker Carrier DNA (from herring testes cells; 10 µg/µl) was denatured by incubation at 95 °C for five minutes, and then immediately cooled on ice;

20 µl of the denatured carrier DNA was then combined with 5-15 µg of the plasmid DNA and purified cDNA in a sterile 15 ml tube.

The competent yeast cells (600 µl) and the PEG/LiAc solution (2.5 ml) were subsequently added, and the suspensions were mixed gently; the cells were incubated at 30 °C for 45 minutes with mixing by tapping or gentle vortexing (~800 rpm) every 15 minutes (Vortex Genie 2, Scientific Industries, NY, USA).

One hundred and sixty microlitres of DMSO were added to each tube, and the tubes were incubated in a 42 °C water bath for twenty minutes with gentle vortexing (~800 rpm; Vortex Genie 2, Scientific Industries, NY, USA) every ten minutes. The cells were pelleted by centrifugation at 700 x *g* for five minutes.

The supernatant was removed and the pellet was re-suspended in 3 ml of YPD Plus Medium (Clontech, CA, USA). The cells were then incubated with shaking (1 h 30', 30 °C, 215 rpm; Innova 4200 Incubator Shaker, New Brunswick Scientific, NJ, USA). The cells were pelleted by centrifugation at 1700 rpm for five minutes; and the supernatant was discarded (Centrifuge 5417R, Eppendorf, Germany).

The pellet was then re-suspended in 15 ml of 0.9 % (w/v) NaCl Solution. A hundred microlitres of each cell suspension (diluted 1:10 and/or 1:100) were spread on 100 mm agar plates with the appropriate SD selection media; i.e. SD/-W for pGBKT7, and SD/-L for pGADT7. The remaining mixture was spread at a volume of 150 µl per 150 mm plates. The plates were incubated upside down at 30 °C for 72-120 hours or until colonies appeared.

#### **2.1.4 AUTO-ACTIVATION AND TOXICITY TESTING**

Baits constructed and transformed into yeast for the purposes of the Y2H PPI screening first had to be tested for potential auto-activation of PPI reporter genes and potential toxicity towards their yeast host cells. The former test was supposed to ensure that any reporter gene activation, observed as a result of the Y2H PPI screen, would be more likely to represent a genuine interaction, given that the reporter gene expression could not be triggered by the bait on its own.

Competent Y2H Gold cells were transformed according to the Clontech protocol (section 2.1.3). The cells were transformed with: 100 ng of the pGBKT7 vector without inserts, or the pBD-wt vector without inserts, and with 100 ng of the pGBKT7-bait(s) plasmids, or the pBD-bait plasmid (i.e. *TOPORS* fragments or its full-length cDNA).



Each transformation mixture was diluted 1:10 and 1:100, and spread onto selective agar plates (Table 2-12).

Table 2-12. Details of yeast media used for auto-activation and toxicity testing.

Media type	Selects for
SD/-W (=SDO)	bait plasmids
SD/-W/+X- $\alpha$ -Gal (=SDO/X)	bait plasmids activating the <i>Mel1</i> reporter
SD/-W/+X- $\alpha$ -Gal/+Aba (=SDO/X/A)	bait plasmids activating the <i>Mel1</i> and <i>Aur1-C</i> reporters

The expected results of the auto-activation test are summarised in Table 2-13. Diploid positive control mating plasmids (section 2.1.5.1) were re-streaked, as a control.

In order to evaluate the potential toxicity of the baits the SD/-W plates were to be examined. Colonies transformed with a vector-bait plasmid were expected to be smaller than the corresponding empty vector, if the bait was toxic.

Table 2-13. Expected bait auto-activation test results.

Sample	Selective agar medium	Colonies	Colour
Auto-activation test	SD/-W	Yes	White
Auto-activation test	SD/-W/+X- $\alpha$ -Gal	Yes	White or Very Pale Blue
Auto-activation test	SD/-W/+X- $\alpha$ -Gal/+Aba	No	n/a
Positive control	DD/-W/-L/+X- $\alpha$ -Gal/+Aba	Yes	Blue

The outcomes of the auto-activation and toxicity procedures are described in Chapter 3.

### 2.1.5 YEAST MATING

Yeast mating, rather than co-transformation, was the method of choice for the YH PPI screening (section 2.1.1.3). Additionally, prior to the Y2H PPI screen (experimental Chapter 4), control mating procedures were performed to validate the system (section 2.1.5.1 and experimental Chapter 3).

Plasmids carrying DNA sequences for the bait and prey proteins, fused with the GAL4 BD and AD, respectively, were transformed into different haploid strains of yeast (section 2.1.3.2.1).

They were grown on media selecting either for baits or for preys (Table 2-14). Vectors with inserts encoding the bait were transformed into the Y2H Gold *MAT $\alpha$*  strain, whereas the prey-encoding plasmids were transformed into the Y187 *MAT $\alpha$*  strain.

The two compatible yeast strains (mating types a and  $\alpha$ ) underwent a mating procedure, forming diploid yeast cells containing both of the previously transformed bait and prey plasmids, after being inoculated together into 500  $\mu$ l of 2X YPDA in a 15-ml tube.

The tubes were incubated with shaking (20-24 h, 30 °C, 200 rpm; Innova 4200 Incubator Shaker, New Brunswick Scientific, NJ, USA). Dilutions of the mated cultures were prepared (1/10, 1/100 and 1/1000), and 100  $\mu$ l of each dilution were spread on agar plates selective for mated diploid yeasts and on additional control media (Table 2-14). The plates were incubated upside down at 30 °C for up to 72-120 hours.

Table 2-14. Details of yeast media used for mating.

Media type	Selects for
SD/-W	bait plasmids
SD/-L	prey (library) plasmids
SD/-L/-W (=DDO)	both: bait and prey plasmids

Equation 2.1 was used to calculate the efficiency of yeast mating. According to the Matchmaker™ Gold Yeast Two-Hybrid System User Manual (Clontech, CA, USA) ‘mating efficiencies of 2-5 % are readily achieved’.

Equation 2.1. Mating Efficiency.

$$\text{MATING EFFICIENCY (\% OF DIPLOIDS)} = \frac{\text{\# OF CFU/ML OF DIPLOIDS}}{\text{\# OF CFU/ML OF LIMITING PARTNER}} \times 100 \%$$

#### 2.1.5.1 CONTROL MATING PRIOR TO Y2H PPI SCREENING

The Y2H PPI screen was carried out using the yeast mating strategy (section 2.1.1.3). Before this could be attempted, control mating experiments had to be completed in order to demonstrate the correct functionality of the system (Table 2-16) as well as compatibility of the Y2H vectors acquired from Clontech (CA, USA) and Life Technologies (CA, USA) (Table 2-1, Table 2-2, Table 2-18). Four control mating experiments were set up, using control vectors (Table 2-15): two for the positive controls and two for the corresponding negative controls (Table 2-16). The tubes were incubated with shaking (20-24 h, 30 °C, 200 rpm; Innova 4200

Incubator Shaker (New Brunswick Scientific, NJ, USA). Dilutions of the mated cultures were prepared (1:10, 1:100 and 1:1000), and 100 µl of each dilution were spread on agar plates selective for PPIs, and on additional control plates (Table 2-17).

Table 2-15. Y2H vectors for control mating procedures.

Strain	Transformation Plasmid	Plating Medium
Y2H Gold	pGBKT7-p53	SD/-W with Agar
Y2H Gold	pBD-p53	SD/-W with Agar
Y2H Gold	pGBKT7-Lam	SD/-W with Agar
Y2H Gold	pBD-pLC	SD/-W with Agar
Y187	pGADT7-T	SD/-L with Agar

Table 2-16. Control mating to check for Y2H system performance and vector compatibility.

Y187 [pGADT7-T] colony	
Y2H Gold [pGBKT7-p53] colony	Positive control mating (1)
Y2H Gold [pBD-p53] colony	Positive control mating (2)
Y2H Gold [pGBKT7-Lam] colony	Negative control mating (1)
Y2H Gold [pBD-pLC] colony	Negative control mating (2)

The positive control experiments involved mating the Y2H Gold strain, transformed with the GAL4 BD vectors, i.e. either the pGBKT7-53 or the pBD-p53, and the Y187 strain, transformed with pGADT7-T, the GAL4 AD vector (Table 2-18). The DNA binding domain vectors carried an insert, encoding the tumour suppressor p53 protein (bait), whereas the activation domain vector carried a gene for the large T antigen of the tumour-inducing Simian virus 40 (SV40; prey). These two proteins are known to interact (Carbone *et al.*, 1997); hence, they can be used as a reliable positive control interacting protein-protein pair.

The negative control experiment involved mating of the Y2H Gold strain, transformed with either pGBKT7-Lam or pBD-pLC (Table 2-18), both of which encode GAL4 BD fused with human lamin C (bait), and the Y187 strain, transformed with the pGADT7-T plasmid described in the previous paragraph. No interaction between these two proteins had ever been reported, therefore, the diploid yeast cells, resulting from the negative control mating, were not expected to grow on selective media enriched with AbA.

Prior to the mating procedure, competent yeast cells had to be transformed with relevant plasmids (section 2.1.3.2.1). The plates were incubated at 30 °C for approximately 72 hours; colonies used in each mating experiment were picked and inoculated into 500 µl of

2X YPDA in 50 ml conical-bottom tubes (Table 2-16). The plates were incubated upside down at 30 °C for up to 120 hours.

Table 2-17. Details of yeast media used for Y2H PPI studies.

Media type	Selects for
<b>SD/-W</b>	bait plasmids
<b>SD/-L</b>	prey (library) plasmids
<b>SD/-L/-W (=DDO)</b>	both: bait and prey plasmids
<b>SD/-L/-W/+X-<math>\alpha</math>-Gal/+AbA (=DDO/X/A)</b>	bait and prey plasmids and PPI interaction ( <i>Mel1</i> and <i>Aur1-C</i> PPI reporter genes)

Table 2-18. Y2H control plasmids.

Vector	Purpose	Features	Notes
pGBKT7 -53 (Clontech, CA, USA)	In-fusion cloning vector encoding GAL 4 BD fused to p53 protein.	Contains the <i>TRP1</i> nutritional reporter gene for selection in yeast and a gene for kanamycin resistance for selection in bacteria.	Positive control for PPI mating, when used with pGADT7-T.
pGBKT7 - Lam (Clontech, CA, USA)	In-fusion cloning vector encoding GAL 4 BD fused to human lamin C.	Contains the <i>TRP1</i> nutritional reporter gene for selection in yeast and a gene for kanamycin resistance for selection in bacteria.	Negative control for PPI mating, when used with pGADT7-T.
pGADT7 -T (Clontech, CA, USA)	In-fusion cloning vector encoding GAL 4 AD fused to SV40 large T antigen.	Contains the <i>LEU2</i> nutritional reporter gene for selection in yeast and a gene for ampicillin resistance for selection in bacteria.	Used in positive and negative PPI mating control experiments with pGBKT7-53 and pGBKT7- Lam. Control for Clontech-Life Technologies vectors compatibility (with pBD- p53 as positive PPI control and with pBD-pLC as negative PPI control).
pAD-p53 <sup>7</sup>	Vector encoding GAL 4 AD fused to p53 protein.	Contains the <i>LEU2</i> nutritional reporter gene for selection in yeast and a gene for ampicillin resistance for selection in bacteria.	Used with TOPORS fused to GAL4 DNA BD as a known PPI interaction control.
pBD-p53 <sup>7</sup>	Vector encoding GAL 4 BD fused to p53 protein.	Contains the <i>TRP1</i> nutritional reporter gene for selection in yeast and a gene for chloramphenicol resistance for selection in bacteria.	Used with pGADT7-T as control for Clontech-Life Technologies vectors compatibility (positive PPI control).
pBD-pLC <sup>7</sup>	Vector encoding GAL 4 BD fused to human lamin C.	Contains the <i>TRP1</i> nutritional reporter gene for selection in yeast and a gene for ampicillin resistance for selection in bacteria..	Used with pGADT7-T as control for Clontech-Life Technologies vectors compatibility (negative PPI control).

<sup>7</sup> These vectors were a gift from Dr Ronald Roepman. They had been modified from original Stratagene (CA, USA) vectors to contain the *att* sequences, i.e. to allow compatibility with Gateway cloning (LifeTechnologies, CA, USA; see section 2.2.5.3).

### **2.1.6 PLASMID ISOLATION FROM YEAST**

In order to verify the identity of interacting partners of TOPORS isolated via the Y2H PPI screen plasmids, carrying library clone inserts, must be isolated. Two different plasmid isolation methods were used depending on the intended destiny of the isolated constructs.

Plasmids needed to be isolated from yeast after to Y2H screen for protein interacting partners of TOPORS in order to determinat the identity of the latter. This was described in Chapter 4.

#### **2.1.6.1 EASY YEAST PLASMID ISOLATION**

In order to prepare a yeast plasmid for bacterial transformation and subsequent plasmid propagation the Easy Yeast Plasmid Isolation Kit (Clontech, CA, USA) was used. This procedure led to extraction of pure plasmid DNA without any contamination from the yeast genomic DNA.

Plasmids were isolated from yeast, using the Easy Yeast Plasmid Isolation Kit (Clontech, CA, USA); several changes were introduced to the Clontech protocol. All values are given per plasmid isolation, i.e. per a 1.5-ml tube, and all spins were performed in a micro-centrifuge. All buffers and solutions were provided with the kit, unless specified otherwise.

Up to 10 mg of yeast cells, taken either from an agar plate or a liquid culture, were used. The cells were re-suspended in 500 µl of 10 mM EDTA in a 1.5-ml tube. The cells were centrifuged at 13000 rpm for 2 minutes (Centrifuge 5417R, Eppendorf, Germany), and the supernatant was discarded.

The pellet was re-suspended in 200 µl of ZYM buffer until the suspension was homogenous. Twenty microlitres of a uniform zymolyase suspension were added, the tubes were vortexed gently (~1000 rpm; Vortex Genie 2, Scientific Industries, NY, USA), and incubated with shaking (1 h, 30 °C, 100 rpm; Innova 4200 Incubator Shaker, New Brunswick Scientific, NJ, USA). The enzyme dissolved the yeasts' cell walls, resulting in formation of spheroplasts, which were subsequently centrifuged at 5800 rpm for ten minutes (Centrifuge 5417R, Eppendorf, Germany) and the supernatant was discarded. The spheroplasts were re-suspended in 250 µl of Y1 Buffer/RNase A solution (see Table). Two hundred fifty microlitres of Y2 Lysis buffer were added, the tube was inverted ten times, and incubated at room temperature for up to five minutes; 300 µl of Y3 Neutralisation buffer were added and the tubes was inverted again ten times.

The lysate was clarified by centrifugation at 13000 rpm for six minutes (Centrifuge 5417R, Eppendorf, Germany); this step was performed twice. The supernatant was loaded into a Yeast

Plasmid Spin Column, placed in a 2 ml collection tube, and centrifuged at 13000 rpm for 2 minutes (Centrifuge 5417R, Eppendorf, Germany); the column flow-through was discarded. Y4 Wash buffer (supplied with the kit; previously diluted with ethanol: Table 2-19) was added to each column (450  $\mu$ l), and the tubes were centrifuged at 14000 rpm for five minutes (Centrifuge 5417R, Eppendorf, Germany). The spin column was transferred to a 1.5 ml tube, 30  $\mu$ l of deionised H<sub>2</sub>O (dH<sub>2</sub>O) were added, and the tubes were incubated at room temperature for three minutes before centrifugation to elute the DNA.

Table 2-19. Easy Yeast Plasmid Isolation Kit Buffers.

Table A. Y1 Re-suspension Buffer/RNase A Solution.

Y1 Buffer/RNase A solution
RNase A (supplied with the kit)
Y1 Resuspension Buffer (supplied with the kit)
Stored at 4 °C

Table B. Y4 Wash Buffer.

Y4 Wash Buffer
Y4 Wash Buffer (supplied with the kit)
24 ml 96-100 % ethanol

#### 2.1.6.2 YEAST 'SMASH & GRAB DNA' METHOD

For the purposes of library characterisation (Methods and Materials section 2.1.8.8 and experimental Chapter 3) and identification of clones pulled out from the Y2H PPI screen (Methods and Materials section 2.1.1.3 and experimental Chapter 4) the Yeast 'Smash & Grab DNA' technique was used.

As the name suggests, this is a rather crude, but less expensive procedure, thus allowing for higher throughput. It is based on phenol-chloroform separation and ethanol precipitation (Sambrook e Russell, 2001).

The disadvantage of this method is that yeast genomic DNA is isolated together with the plasmid DNA. In this form it is suitable for amplification of library clones by PCR (section 2.2.1), and the products can then be sequenced (section 2.2.7). However, such a preparation of plasmids together with genomic DNA is not suitable for subsequent bacterial transformation (section 2.2.3).

Plasmids were isolated from yeast, using the Yeast 'Smash & Grab DNA' method, based on a protocol by Rose *et al.* (1990). All values are given per plasmid isolation, i.e. per a 1.5-ml tube.

The procedure was performed in a fume extraction cupboard. Prior to plasmid extraction, glass beads (425-600  $\mu$ m; Sigma-Aldrich, MO, USA) were prepared. The beads were fully submerged in a beaker with 1 M HCl, and allowed to stand for 15 minutes. The beads were then washed

with large volumes of sterile dH<sub>2</sub>O until all HCl was removed (determined with a pH meter); they were dried in an oven cupboard for several days, and poured into a sterile bottle for storage.

Yeast cells (10 mg per sample), taken either from an agar plate or a liquid culture, were used. The acid-washed glass beads (425-600 µm; Sigma-Aldrich, MO, USA) were added (300 µl per tube), and the cells were re-suspended in 200 µl of yeast lysis buffer (Table) and 200 µl of a 25:24:1 Phenol:Chloroform:Isoamyl Alcohol mix (Sigma-Aldrich, MO, USA) per tube. Tubes were vortexed at maximum speed for 2 minutes, and 200 µl of TE (Table) were added per tube. The tubes were centrifuged for a further five minutes at 14000 rpm (Centrifuge 5417R, Eppendorf, Germany), and the upper, aqueous layer was transferred into a fresh 1.5-ml tube (300 µl). Two volumes (600 µl) of 100 %, room temperature ethanol were added to each tube, the tubes were vortexed, then micro-centrifuged at 14000 rpm for three minutes (Centrifuge 5417R, Eppendorf, Germany).

The supernatant was discarded, and the precipitate was rinsed with cold (4 °C) 70 % ethanol (500 µl per tube). The samples were centrifuged at a maximum speed for 30 seconds (Centrifuge 5417R, Eppendorf, Germany), supernatant was discarded, and the tubes were left open to air-dry. The DNA pellet was dissolved in 30 µl of dH<sub>2</sub>O.

Table 2-20. Yeast ‘Smash & Grab DNA’ Buffers.

Table A. Yeast ‘Smash & Grab DNA’ Lysis Buffer

Lysis Buffer
10 mM Tris, pH 8
1 mM EDTA
100 mM NaCl
1 % SDS
2 % Tx100

Table B. Tris-EDTA Solution.

TE, pH 8
10 mM Tris
1 mM EDTA
pH 8

### 2.1.7 PROTEIN ISOLATION FROM YEAST

In order to verify the expression of proteins encoded on the Y2H plasmids, they must firstly be isolated from the yeast cells, prior to their identification by biochemical methods.

The outcomes of these procedures are summarised in Chapter 3 (section 3.2.2.2) and Appendix 11.4.

For the purpose of protein extraction, the yeast clones to be tested were re-streaked on fresh nutritional selective agar media, and they were incubated for up to 96 hours at 30 °C. A single



colony of each clone was then picked and inoculated into 5 ml of relevant nutritional selective liquid media (in 50 ml sterile tubes).

An untransformed yeast colony was inoculated, in parallel, into 10 ml YPDA as a negative control (in a 50 ml sterile tube). The cultures were incubated overnight with shaking (16 h, 30 °C, 250 rpm; Innova 4200 Incubator Shaker, New Brunswick Scientific, NJ, USA).

The following morning all cultures were vortexed at maximum speed for one minute in order to disperse cell clumps. Each 5 ml culture of the transformed clones was then inoculated into 50 ml of YPDA (in 250 ml sterile flasks). One hundred microlitres of the 10 ml untransformed culture were inoculated into 50 ml of YPDA (in a 250 ml sterile flask). The cultures were incubated with shaking (5 h, 30 °C, 250 rpm; Innova 4200 Incubator Shaker, New Brunswick Scientific, NJ, USA).

One hour before the end of the 5 hour incubation period, pre-labelled 50 ml sterile tubes and dH<sub>2</sub>O were pre-chilled at -20 °C, and a centrifuge (for the 50 ml tubes) was pre-chilled to 4 °C.

After the 5 hour incubation period, the 600 nm wavelength optical density (OD<sub>600</sub>) of the incubated cultures was measured, using a spectrophotometer; the OD<sub>600</sub> was expected to be within the range of 0.4-0.6.

The 50 ml tubes were half-filled with ice; each yeast culture was poured into one of the tubes, and centrifuged at 2400 rpm for five minutes at 4 °C (Megafuge 1.0 R, Heraeus, UK). The supernatant and ice were removed, and the yeast cell pellets were re-suspended in 25 ml of ice-cold dH<sub>2</sub>O, previously pre-chilled at -20 °C.

The suspensions were centrifuged at 2400 rpm for five minutes at 4 °C, and the supernatants were removed (Megafuge 1.0 R, Heraeus, UK). The obtained cell pellets were frozen on dry ice, or liquid nitrogen, for five minutes, and stored at -80 °C. The OD<sub>600</sub> units (u) were calculated for each culture, as summarised in Equation 2.2.

Equation 2.2. OD<sub>600</sub> u calculation.

Key: u, unit.

$$\text{OD}_{600} \text{ u} = \text{obtained OD}_{600} \times \text{final culture volume}$$

Prior to protein extraction the required amount of complete cracking buffer (Table 2-21) was calculated (100 µl per 7.5 OD<sub>600</sub> u); the buffer was prepared and pre-heated to 60 °C. Protein extraction from the yeast cell pellets was performed in a fume cupboard, and tubes with all samples were kept on ice, unless stated otherwise.

Table 2-21. Cracking Buffer. Recipe for one protein extract.

Table A. Stock solution.

Cracking Buffer Stock Solution
8 M Urea
5 % (w/v) SDS
40 mM Tris-HCl, pH 6.8
0.1 mM EDTA
0.4 mg/ml bromophenol blue
dH <sub>2</sub> O

Table B. Complete Buffer.

Complete Cracking Buffer
1 ml of Cracking Buffer Stock Solution
10 µl of β-mercaptoethanol
70 µl of pre-chilled protease inhibitor solution (Table 2-22)
50 µl of 100X PMSF stock solution (Table 2-22)
Up to 1.13 ml total volume with dH <sub>2</sub> O

Table 2-22. Protease Inhibitors.

Table A. Phenylmethylsulphonyl fluoride (PMSF) stock solution [100X].

100X PMSF Stock Solution
0.1742 g PMSF
10 ml isopropanol

Table B. Protease Inhibitor Solution.

Protease Inhibitor Solution
0.1 mg/ml Pepstatin A
0.03 mM Leupeptin
145 mM Benzamidine
0.37 mg/ml Aprotinin

The pre-heated complete cracking buffer (Table 2-21) was added to the 50 ml tubes with cell pellets to thaw them quickly; the tubes were placed onto the 60 °C heat block to enhance thawing for a maximum of 2 minutes (to avoid proteolysis).

The thawed pellets were re-suspended, and each suspension was transferred to a corresponding micro-centrifuge tube, containing glass beads (425-600 µm; Sigma-Aldrich, MO, USA). The tubes were heated to 70 °C for ten minutes, and 50 µl of serine protease inhibitor, Phenylmethylsulfonyl fluoride (PMSF; Table 2-22), were added to each tube.

The tubes were vigorously for one minute, and centrifuged at 14000 rpm for five minutes at 4 °C (Centrifuge 5417R, Eppendorf, Germany). The supernatants were transferred to fresh, pre-chilled micro-centrifuge tubes ('first supernatants') and kept on ice. Fifty microlitres of PMSF were added to each tube (with pellets and with first supernatants).

The tubes with pellets were placed in a 100 °C water bath for 3-five minutes, vortexed (Vortex Genie 2, Scientific Industries, NY, USA) vigorously for one minute, and centrifuged at 14000 rpm for five minutes at 4 °C (Centrifuge 5417R, Eppendorf, Germany). The obtained supernatants ('second supernatants') were combined with their corresponding first

supernatants, and boiled briefly (100 °C). The tubes were then kept on dry ice, or stored at -80 °C until they were used for SDS-PAGE and Western blotting (sections 2.5.2 and 2.5.3).

If no 'second supernatant' was obtained, 50-100 µl more complete cracking buffer were added, the tubes were vortexed vigorously for one minute, and centrifuged at 14000 rpm for five minutes at 4 °C (Centrifuge 5417R, Eppendorf, Germany) prior to combining with the 'first supernatant'.

## **2.1.8 GENERATION OF HUMAN RETINAL CDNA LIBRARY**

Prior to the Y2H screening for novel interacting partners of TOPORS, the human retinal cDNA library had first to be created. The experimental outcomes of the library construction and characterisation procedures are summarised in Chapter 3.

The human retinal cDNA library was constructed directly in the Y187 yeast strain, using its endogenous homologous recombination machinery, using the 'Make Your Own "Mate & Plate™" Library System' (Clontech, CA, USA), which utilises the SMART™ technology (Zhu *et al.*, 2001). Library generation was performed according to the manufacturer's instructions.

### **2.1.8.1 COMPLEMENTARY DNA SYNTHESIS**

The complementary DNA (cDNA) was synthesised from human retinal total RNA purchased from Clontech (CA, USA). The procedure comprised three major steps:

- First-strand cDNA generation;
- Amplification of cDNA by long distance PCR (LD PCR);
- Column purification of double-stranded cDNA with a CHROMA SPIN TE-400 column.

The first cDNA strand was transcribed from the total retinal RNA using the Moloney Murine Leukaemia Virus Reverse Transcriptase (MMLV RT). In addition to catalysing the transcription of RNA into cDNA, MMLV RT also possesses terminal transferase and template switching activities.

Due to these characteristics, when MMLV RT encounters a 5' terminus of the RNA template, it not only transcribes this template into cDNA, but it also adds several extra nucleotides, specifically deoxycytidine, to the 3' end of the cDNA. This allows for hybridisation of the SMART III Oligonucleotide, which comprises an oligo-G tail. This annealing of the SMART III Oligo with the dCTPs leads to extension of the RNA template, and subsequently, it results in switching of the template by the MMLV RT, which then continues the transcription (Figure 2-2).

The generated single-stranded (ss) cDNA comprises the complete 5' end of the mRNA as well as a sequence complementary to the SMART III Oligo; the latter then serves as a universal priming site, the SMART anchor, and it is essential for amplification of the ss cDNA by LD PCR.

Two different primers were used for the retinal cDNA library construction: a modified oligo-dT primer, the CDS III Primer, and a random primer, the CDS III/6 Primer. The former oligonucleotide hybridises to the 3'-end of poly A+ RNA, which may result in sequences located towards the 5'-end being slightly under-represented.

The CDS III/6 Primer is able to hybridise to a variety of sequences on the RNA template, hence a library generated using this priming molecule should contain a wider array of sequences, all of which should be present in a similar proportion to each other.

Consequently, two retinal cDNA libraries were generated. One primed just by the oligo-dT CDS III Primer, and another one primed by both primers.

**2.1.8.1.1 FIRST STRAND cDNA GENERATION**

Total human retinal RNA (0.1-2.0 µg; Clontech, CA, USA) and a primer (1 µl; Clontech, CA, USA; Table 2-23) were combined in a sterile 1.5-ml tube in a total volume of 4.0 µl adjusted with sterile dH2O (Table 2-24).

Table 2-23. Primers for cDNA library generation.

Provided with the 'Make Your Own "Mate & Plate™" Library System (Clontech, CA, USA). NOTE: N = A, G, C, or T; V = A, G, or C.

Primer	Sequence
	ATTCTAGAGGCCGAGGCGGCCGACATG-d(T) <sub>30</sub> VN
CDS III/6	ATTCTAGAGGCCGAGGCGGCCGACATG-NNNNNN
SMART III Oligo	AAGCAGTGGTATCAACGCAGAGTGGCCATTATGGCCGGG



Figure 2-2. SMART cDNA synthesis. Figure from the 'Make Your Own "Mate & Plate™" Library System User Manual (Clontech, CA, USA).

Table 2-24. RNA denaturation and priming reaction mixture.

Components	Volume
0.1-2.0 µg	1 µl
CDS III or CDS III/6 primer	1 µl
dH <sub>2</sub> O	2 µl
Total volume	4 µl

A positive control reaction was set up in parallel, using 1 µl of Mouse Liver Poly A+ RNA. The reactions were denatured at 72 °C for 2 minutes, followed by cooling on ice for 2 minutes, and centrifugation at 14000 rpm for 10 seconds (Centrifuge 5417R, Eppendorf, Germany).

The following components were mixed in a total volume of 9.0 µl (Table 2-25): 2.0 µl of 5X First-Strand Buffer, 1.0 µl of DDT (100 mM), 1.0 µl of dNTP Mix (10 mM) and 1.0 µl of SMART MMLV RT.

Table 2-25. Single-stranded cDNA generation reaction mixture.

Components	Volume
5X First-Strand Buffer	2 µl
DTT (100 mM)	1 µl
dNTP Mix (10 mM)	1 µl
SMART MMLV RT	1 µl
Components from RNA denaturation and priming (see Table 2-22)	4 µl
Total volume	9 µl

This reaction mix was then combined with the previously denatured, primed RNA, and mixed by tapping; if the random primer (CDS III/6) was used, the reaction was additionally incubated at 25 °C for ten minutes.

The reactions were incubated at 42 °C for ten minutes in a heated lid thermal cycler in order to prevent evaporation. One microlitre of SMART III-modified Oligo (Table 2-23) was added; the reactions were mixed and incubated for one hour.

The first-strand synthesis was terminated by incubation at 75 °C for ten minutes. The reactions were allowed to cool down to room temperature, 1 µl of RNase H (2 units) was added to each reaction, and the reactions were incubated at 37 °C for twenty minutes.

The reaction products were either immediately used in the LD PCR amplification, or they were store at -20 °C for up to 3 months.

**2.1.8.1.2 *cDNA AMPLIFICATION BY LONG DISTANCE PCR***

First-strand cDNA was prepared and the thermal cycler was pre-heated (Table 2-25). Two PCR reactions were prepared for each experimental sample. Each reaction was prepared in a total of 100  $\mu$ l and contained the following components: 2  $\mu$ l of the first-strand cDNA, 10  $\mu$ l of 10X Advantage 2 PCR buffer, 2  $\mu$ l of 50X dNTP Mix, 2  $\mu$ l of 5' PCR primer, 2  $\mu$ l of 3' PCR primer (Table 2-26), 10  $\mu$ l of 10X Melting Solution, 2  $\mu$ l of 50X Advantage 2 Polymerase Mix and 70  $\mu$ l of dH<sub>2</sub>O (Table 2-27).

The thermal cycling conditions involved initial denaturation at 95 °C for 30 seconds, followed by 22 cycles of denaturation at 95 °C for 10 seconds and annealing/extension at 68 °C for initially 6 minutes, increasing by 5 seconds with each successive cycle; the reaction was completed by a final extension at 68 °C for five minutes.

Table 2-26. Primers for LD-PCR.

Provided with the 'Make Your Own "Mate & Plate"<sup>TM</sup>' Library System (Clontech, CA, USA).

Primer	Sequence
5' PCR primer	TTCCACCCAAGCAGTGGTATCAACGCAGAGTGG
3' PCR primer	GTATCGATGCCACCTCTAGAGGCCGAGGCCGCCGACA

Table 2-27. LD PCR components.

Components	Volume
First-strand cDNA	2 $\mu$ l
10X Advantage 2 PCR buffer	10 $\mu$ l
50X dNTP Mix	2 $\mu$ l
5' PCR primer	2 $\mu$ l
3' PCR primer	2 $\mu$ l
10X Melting Solution	10 $\mu$ l
50X Advantage 2 Polymerase Mix	2 $\mu$ l
dH <sub>2</sub> O	70 $\mu$ l
Total volume	100 $\mu$ l

The concentrations of the PCR products' were determined using the Nanodrop spectrophotometer, absorbing at 260 nm wave length; a minimum of 3  $\mu$ g of DNA was expected per PCR amplification.

The samples were also analysed by agarose gel electrophoresis; 7  $\mu$ l aliquots of each sample were subject to electrophoresis on 1.2 % agarose gels with ethidium bromide. The obtained PCR products were either immediately purified (next section) or stored at -20 °C.

#### 2.1.8.1.3 PURIFICATION OF DOUBLE-STRANDED cDNA

The amplified human retinal cDNA was purified using the CHROMA SPIN TE-400 Columns (Clontech, CA, USA). The columns contain resin, which serves to fractionate DNA molecules according to size; it selects for DNA molecules larger than 200 bp.

One CHROMA SPIN column was prepared per each double-stranded (ds) cDNA sample according to manufacturer's instructions: the column was inverted to re-suspend the gel matrix until homogenous, the top cap was removed, the break-away end was snapped off from the bottom of the column, and the column was placed in a collection tube.

The columns were centrifuged at 1700 rpm for five minutes (Centrifuge 5417R, Eppendorf, Germany) to purge the equilibration buffer, which was then discarded along with the collection tube. The spin column was placed in a second collection tube, and each ds cDNA sample (93 µl) was then loaded onto the centre of the semi-dry gel matrix (two samples were generated for each library, i.e. two columns were used for each library constructed); the tubes were centrifuged at 1700 rpm for five minutes (Centrifuge 5417R, Eppendorf, Germany). The two samples were then combined into a single 1.5-ml tube, and were subject to ethanol precipitation as described previously (Sambrook e Russell, 2001).

The cDNA was re-suspended in 20 µl dH<sub>2</sub>O per tube, and the cDNA concentration was determined using the Nanodrop spectrophotometer; the expected amount of DNA was within the range of 2-5 µg. The double-stranded (ds) cDNA was stored at -20 °C until being used for library construction by *in vivo* recombination in yeast.

#### 2.1.8.2 CONTROLLING FOR HOMOLOGOUS RECOMBINATION IN YEAST

Prior to construction of a cDNA library in yeast, it is essential to establish that the yeast endogenous homologous recombination machinery functions properly. A control experiment was performed, which involved a homologous recombination-mediated cloning of SV40 Large T antigen PCR fragment into the pGADT7-Rec Cloning Vector.

The Y187 yeast competent cells were prepared (section 2.1.3.1 in Methods and Materials). The SV40 Large T antigen PCR product fragment (25 ng/µl) and the pGADT7-Rec vector (500 ng/µl) were provided ready-linearised using the *Sma*I restriction enzyme. Two samples were prepared in sterile 1.5-ml tubes:

- 1 µl pGADT7-Rec only;
- 1 µl pGADT7-Rec + 3 µl SV40 Large T antigen PCR fragment.

Each sample was used to transform the Y187 yeast competent cells (section 2.1.3). One hundred microlitres of 1/10 and 1/100 dilutions were spread on SD/-L yeast media, which selects for the pGADT7-containing yeast colonies. The plates were incubated at 30 °C for 48-72 hours.

Given that the homologous recombination was successful, it was expected that approximately ten times more colonies would be observed on plates, where cells were co-transformed with both the linearised vector and the PCR product, than where cells were transformed with the vector only. Such a result would imply that over 90 % of colonies contain SV40 Large T antigen PCR fragment successfully cloned into the pGADT7-Rec plasmid, using the yeast homologous recombination system (see 'Make Your Own "Mate & Plate™" Library System User Manual, Clontech, CA, USA).

### 2.1.8.3 DETERMINATION OF TRANSFORMATION EFFICIENCY

Transformation efficiency was determined for the large-scale retinal cDNA library transformation. Colony-forming units (cfu) were counted, and the transformation efficiency was determined, using Equation 2.3.

Equation 2.3. Transformation efficiency calculation. Key: CFU, colony-forming unit.

$$\text{TRANSFORMATION EFFICIENCY (CFU/}\mu\text{L)} = \frac{\text{CFU X SUSPENSION VOLUME (ML)}}{\text{VOLUME PLATED (ML) X AMOUNT OF DNA (}\mu\text{G)}} \times \text{DILUTION FACTOR}$$

### 2.1.8.4 DETERMINATION OF NUMBER OF INDEPENDENT CLONES

Number of independent clones was determined following the large-scale retinal cDNA library transformation, as summarised in Equation 2.4. A viable cDNA library is expected to comprise at least a million independent clones.

Equation 2.4. Number of independent clones calculation.

Key: #, number; cfu, colony-forming unit; SD/-L, synthetic dropout media lacking leucine, thus selecting for prey plasmids.

$$\text{\# of independent clones} = \text{\# of cfu/ml on SD/-L} \times \text{re-suspension volume (15 ml)}$$



#### 2.1.8.5 *ETERMINATION OF cDNA LIBRARY TITRE*

The titre of the library is the number of colonies (colony-forming units, cfu) per 1 ml of diluted library spread on solid media. Colony-forming units were counted on plates having 30-300 colonies, and the titre was determined (Equation 2.5).

Equation 2.5. Titre determination.

Key: #, number; cfu, colony-forming unit.

$$\text{TITRE (CFU/ML)} = \frac{\text{\# OF COLONIES}}{\text{VOLUME PLATED (ML) X DILUTION FACTOR}}$$

#### 2.1.8.6 *HARVESTING OF THE cDNA LIBRARY*

Following confirmation of the number of independent clones, the human retinal cDNA library was harvested according to the manufacturer's instructions.

The agar plates were chilled to 4 °C for 3-4 hours, and 5 ml of freezing medium (YPDA & 25 % glycerol) were added per plate. Sterile glass beads (3 mm; Merck, Germany) were used to detach the colonies from the plates, and all liquids were combined into a sterile flask, yielding a combined total of approximately 0.5 L of library.

Cell density was determined using a haemocytometer, and it was adjusted to yield at least  $2 \times 10^7$  cells per 1 ml. The library was separated into 50-ml aliquots for long-term storage at -80 °C.

#### 2.1.8.7 *DETERMINATION OF CELL DENSITY*

The mean number of yeast cells in each library was counted using a haemocytometer; growth of new buds observed on a yeast cell was counted as one cell. The volume over the 1 mm<sup>2</sup> counting area of the haemocytometer is 0.1 µl. Cell density was calculated using Equation 2.6.

Equation 2.6. Cell density calculation.

$$\text{CELL DENSITY (CELLS/ML)} = \frac{\text{\# OF CELLS PER 1 MM2 COUNTING AREA X DILUTION FACTOR}}{\text{VOLUME OVER THE 1 MM2 COUNTING AREA (ML)}}$$

### 2.1.8.8 CHARACTERISATION OF THE cDNA LIBRARY

In order to characterise and validate the oligo-dT-primed and the oligo-dT- & random-primed human retinal cDNA libraries, an aliquot of each library was spread on SD/-L media and incubated at 30 °C until growth appeared.

Single colonies were subsequently picked, re-patched on fresh SD/-L media as 1 cm<sup>2</sup> squares, and incubated at 30 °C until growth appeared. Cells were then picked from each 'square', and plasmids were isolated from these cells (section 2.1.6).

Inserts contained within the isolated plasmids were amplified by PCR (section 2.2.1), sequenced (section 2.2.7), and identified using the BLAST and BLAT programs available on the NCBI and UCSC Genome Browser websites, respectively.

Thirty clones from each library were initially analysed. Firstly, numbers of library plasmids with inserts were determined. Next, the proportions of protein-coding and different types of non-coding sequences were determined. Following the outcomes of such preliminary analysis, only one library, richer in protein-coding sequences, was analysed in depth.

For comparison, the quality control data, provided with the ready-made brain cDNA library purchased from Clontech (CA, USA; Mate & Plate™ Library – Human Brain (Normalised)) for contingencies, were summarised (Table 2-28).

Table 2-28. Mate & Plate™ Library – Human Brain (Normalised). Quality control data.

Quality	Data
<b>Titre</b>	≥5 x10 <sup>7</sup> cfu/ml
<b>Number of independent clones</b>	3.2 x 10 <sup>6</sup>
<b>Average cDNA size</b>	1.56 kb
<b>cDNA size range</b>	0.7 – 3.0 kb

*TOPORS* expression levels in the library were expected to be within a comparable range to other tissues in the human body according to a graphical summary, provided by the Gene Cards (Figure 2-3). In contrast, Chakarova *et al.* (2007) showed by RT-PCR that although *TOPORS* is expressed ubiquitously, its levels in the retina appear strongly enhanced (Figure 1-12). The Serial Analysis of Gene Expression (SAGE) data, accessible on Gene Cards (Figure 2-3), also suggests that *TOPORS* levels are higher in the retina than in most other evaluated tissues.

According to the Swiss-Prot (UniProtKB) records at mRNA level *TOPORS* is most highly expressed in testis and at lower levels in adrenal gland, bone marrow, brain, colon, heart, kidney, liver, muscle, ovary, pancreas, placenta, prostate, skeletal muscle, skin, small intestine, spleen, stomach, testis, thymus, thyroid and uterus. It is also expressed in healthy lung, but at decreased levels in lung cancers (and colon adenocarcinomas).

This strongly contrasts with the mRNA expression of rhodopsin (*RHO*), specific to rod photoreceptor cells (Figure 2-4), as was also demonstrated by the EyeSAGE Project (Figure 2-5).

### **2.1.9 MACROSCOPIC IMAGING**

The yeast work was documented using one of the following cameras:

- Olympus  $\mu$ 780 All Weather Compact Digital Camera (Olympus Corporation, Japan);
- Olympus SP-590UZ (Olympus Corporation, Japan);
- Canon PowerShot A810 (Canon Corporation, Japan).

For imaging purposes the yeast plates were placed on a light box, and the camera was mounted on a tripod above the light box. All images were collected sequentially using the same settings.

### **2.1.10 Y2H PROCEDURES SUMMARY**

In summary, full-length *TOPORS* cDNA was used as bait in the Y2H PPI screen (Chapter 4). The cDNA was cloned into GAL4 BD Y2H vector, and it was transformed into the Y2H Gold yeast strain (Chapter 3). Auto-activation and toxicity testing was subsequently performed (Chapter 3). The preys comprised fragments of the human retinal cDNA library cloned into GAL4 AD Y2H vectors transformed into the Y187 yeast strain (Chapters 3 and 4). Relevant control plasmids were also transformed and used for control mating experiments (Chapters 3 and 5). The initial Y2H screen involved mating of both yeast strains, expressing the bait and the preys, and spreading the resulting diploid cultures on selective media (Chapter 4). Positive clones were then amplified by PCR and sequenced, and their functions were characterised to determine whether they showed a retina-specific expression pattern or a function exclusive to the retina (Chapters 4 and 5). On this basis, candidate interacting proteins were selected for further analyses (Chapters 6, 7 and 8).

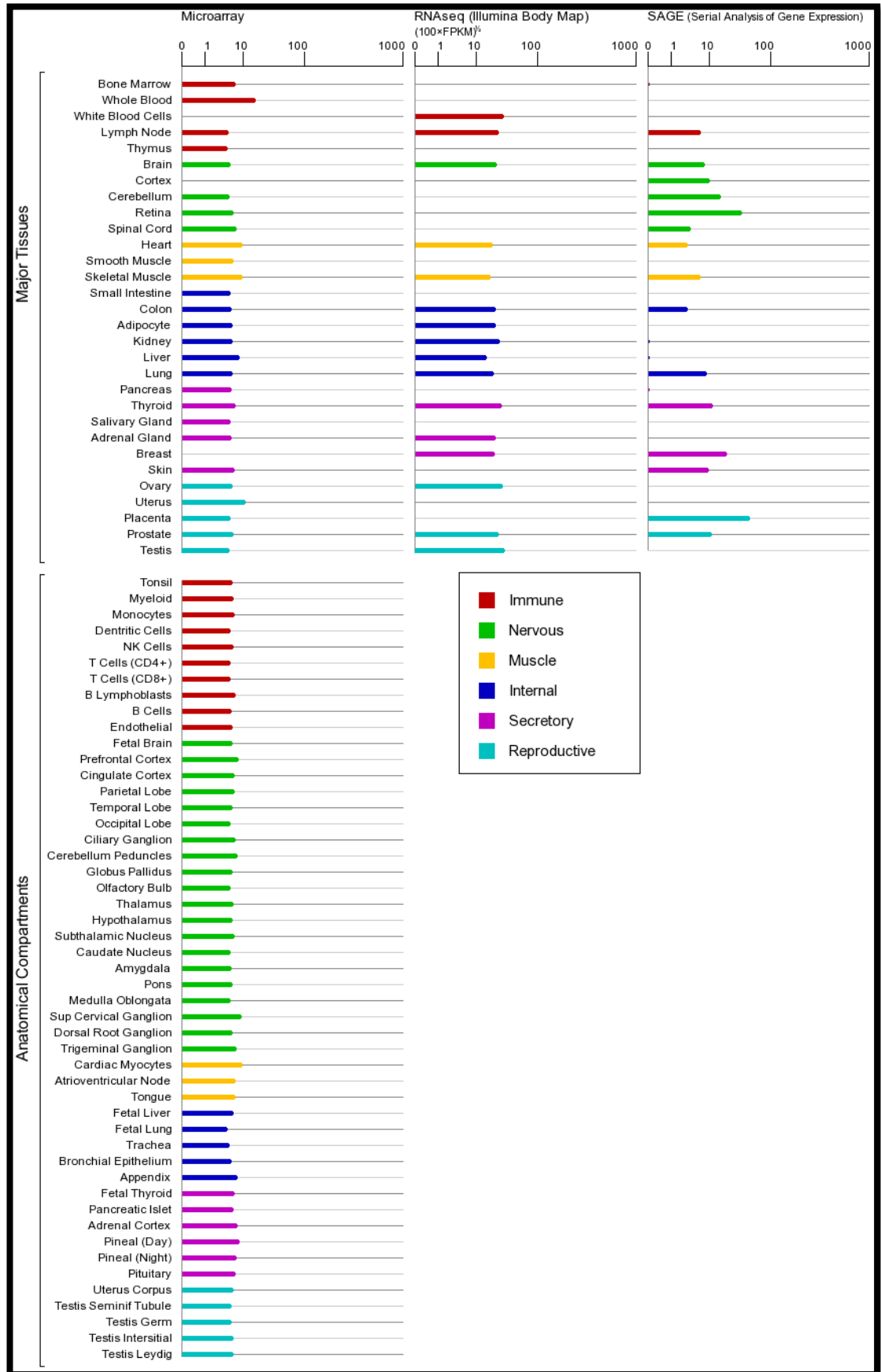


Figure 2-3. TOPORS expression at mRNA level. Image from GeneCards Database.

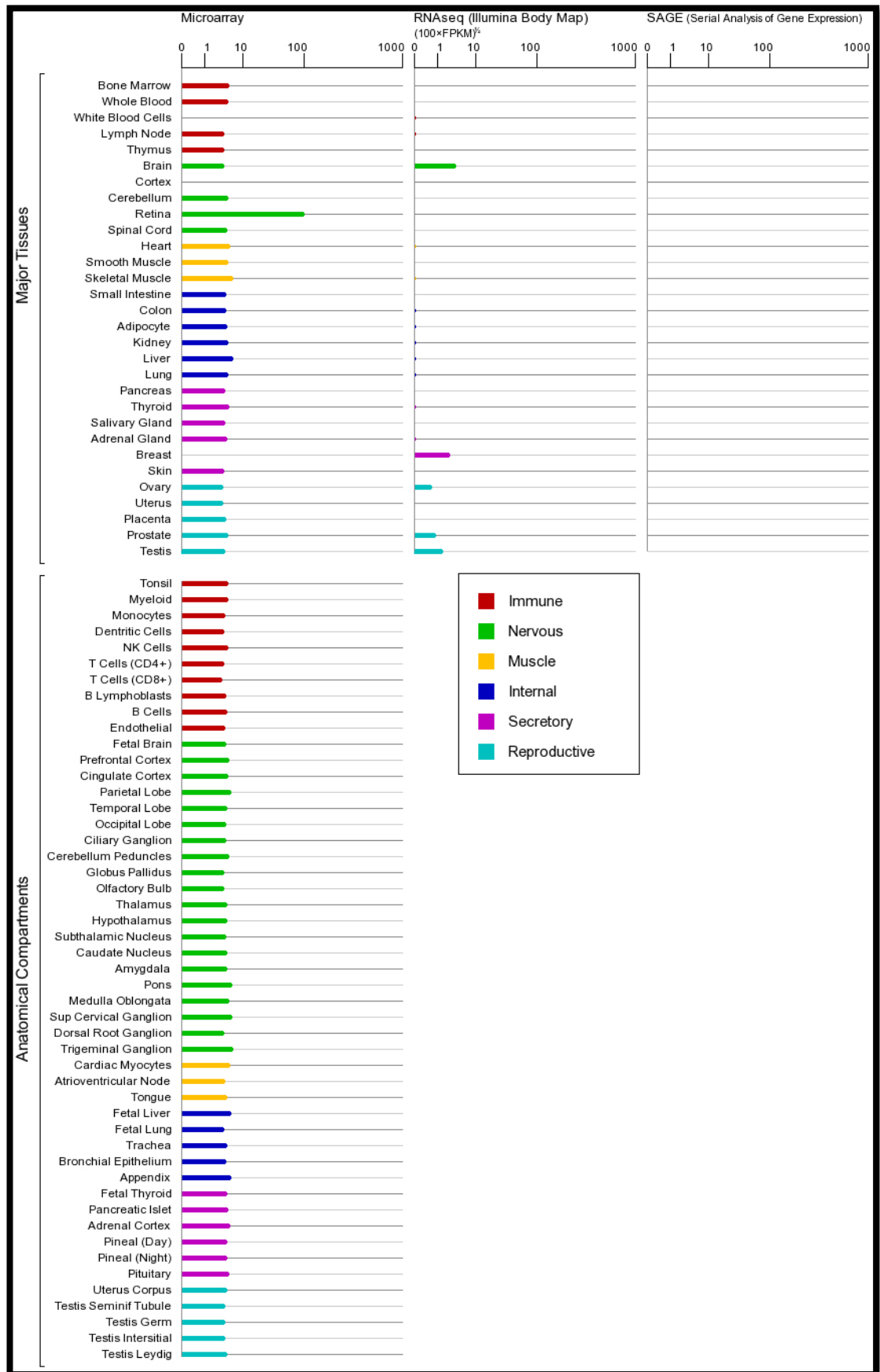


Figure 2-4. *RHO* expression at mRNA level. Image from GeneCards Database.

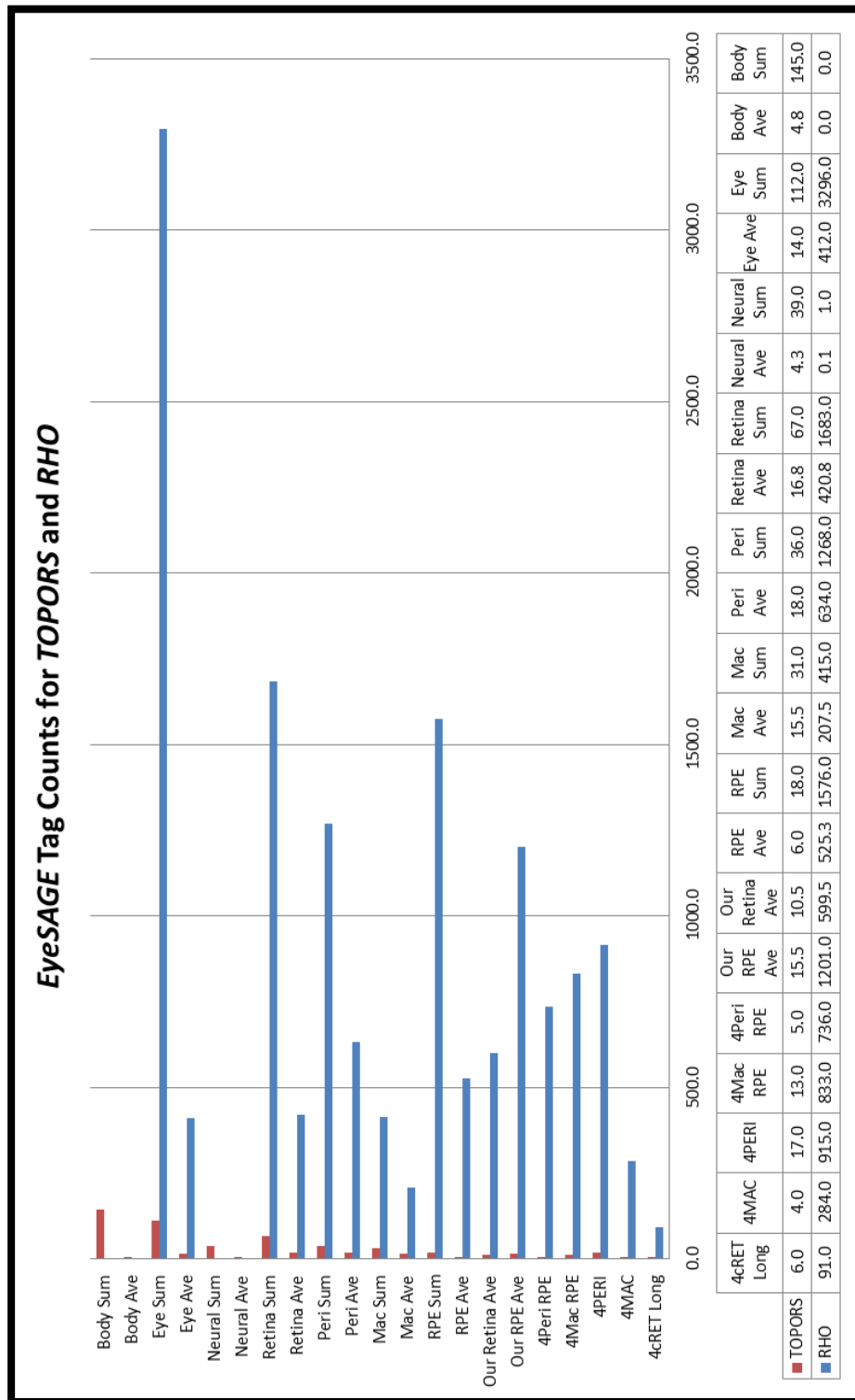


Figure 2-5. Comparison of TOPORS and RHO expression in human retina. The diagram was compiled based on EyeSAGE\_Dataset.xls file, generated by the Bowes Rickman and Hauser Laboratories, and available online (Wistow *et al.*, 2008; Eyesage, [Accessed 03/02/2015]). The TOPORS 'Tag sequence,' 'Best Tag for Gene,' and 'Long Tag' were: CTTATGTAGA, [none], and CTTATGTAGATATAAAA, respectively; whereas for RHO the respective sequences comprised: CTCACCCACCA, GCCCCAGTT, and CTCACCCACCATCTGCTG (key in

Table 2-29. Description of column headings and SAGE tags from Figure 2-5. Legend modified from the EyeSAGE\_Legend.xls file available online (Eyesage, [Accessed 03/02/2015]).

Column Heading	Description
<b>Tag Sequence</b>	sequence of the 10 bp short SAGE tag
<b>Best Tag For Gene</b>	sequence of the 10 bp short SAGE tag considered the most representative match for the given UniGene cluster. If this tag matches the tag in the adjacent 'Tag Sequence' column, then all the associated data to the right should be the most representative for that gene.
<b>Long Tag</b>	sequence of the 17 bp long SAGE tag that matches the short tag in 'Tag Sequence', if there was a match in '4cRET Long'. There may be several long SAGE matches for a given short SAGE tag.
<b>4cRET Long</b>	tag counts from "LSAGE_Retina_central_normal_B_4cRet"; long SAGE library prepared from pooled 4 mm punches of human macula and central peripheral retina from 7 morphologically normal donor eyes
<b>4MAC</b>	tag counts from "SAGE_Retina_Macula_normal_B_4Mac"; SAGE library prepared from 5 pooled 4 mm punches of human macula from morphologically normal donor eyes
<b>4PERI</b>	tag counts from "SAGE_Retina_Peripheral_normal_4Peri"; SAGE library prepared from 5 pooled 4 mm punches of human peripheral retina from the same donor eyes as '4Mac'
<b>4Mac RPE</b>	tag counts from "SAGE_Retina_Pigment_Epithelium_normal_B_4MacRPE"; SAGE library prepared from 10 pooled 4 mm punches of human RPE/choroid from morphologically normal donor eyes
<b>4Peri RPE</b>	tag counts from "SAGE_Retina_Pigment_Epithelium_normal_B_4PeriRPE"; SAGE library prepared from 10 pooled 4 mm punches of human RPE/choroid from the same donor eyes as '4MacRPE'
<b>Our RPE Ave</b>	average tag count per library for '4Mac RPE' and '4Peri RPE'
<b>Our Retina Ave</b>	average tag count per library for '4MAC' and '4PERI'
<b>RPE Ave</b>	average tag count per library for 3 RPE short SAGE libraries included in 'RPE Sum'
<b>RPE Sum</b>	summation of tag counts from RPE SAGE libraries ('4Mac RPE', '4Peri RPE', and 'RPEB1')
<b>Mac Ave</b>	average tag count per library for the two macular retina libraries
<b>Mac Sum</b>	summation of tag counts from macular retina libraries ('4MAC' and 'HMAC2')
<b>Peri Ave</b>	average tag count per library for the two peripheral retina libraries included in 'Peri Sum'
<b>Peri Sum</b>	summation of tag counts from peripheral retina libraries ('4PERI' and 'PeriB2')
<b>Retina Ave</b>	average tag count per library for 5 retina short SAGE libraries included in 'Retina Sum'
<b>Retina Sum</b>	summation of tag counts from retina short SAGE libraries ('4MAC', '4PERI', 'HMAC2', 'PeriB2', and 'PeriB1')
<b>Neural Ave</b>	average tag count per library for the 9 libraries included in 'Neural Sum'
<b>Neural Sum</b>	summation of tag counts from 9 publicly archived SAGE libraries prepared from the different regions of the brain designated in columns BC through BK (text in green)
<b>Eye Ave</b>	average tag count per library for all 8 eye short SAGE libraries
<b>Eye Sum</b>	summation of tag counts from all 8 eye short SAGE libraries
<b>Body Ave</b>	average tag count per library for the 30 libraries included in 'Body Sum'
<b>Body Sum</b>	summation of tag counts from 30 publicly archived SAGE libraries prepared from the various non-neural tissues designated in columns BL through CO

The scarce information demonstrating TOPORS protein expression (Figure 2-6), suggests that levels of this protein can be variable in healthy as well as malignant tissues.

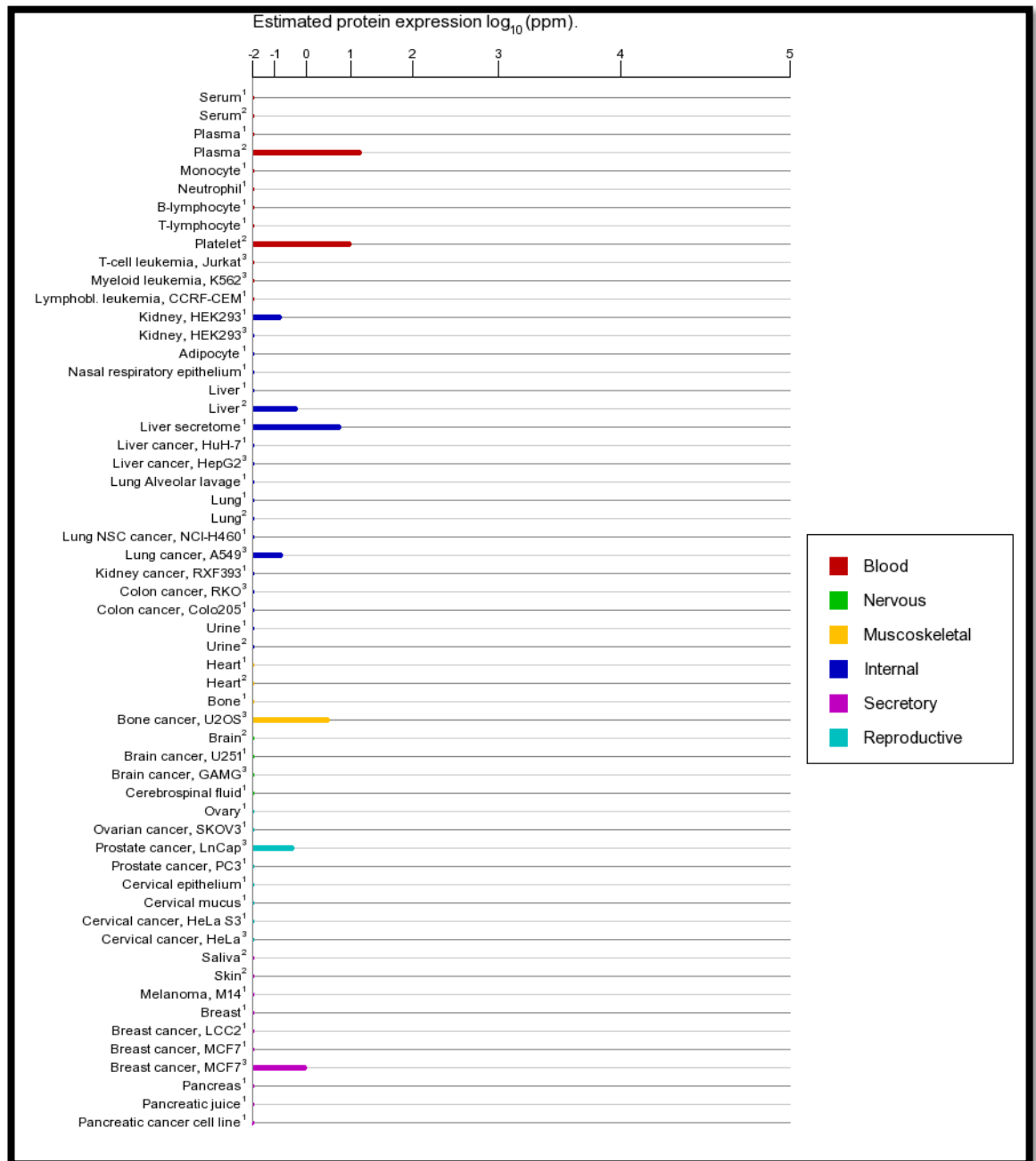


Figure 2-6. TOPORS expression at protein level. Image from GeneCards Database.



## 2.2 DNA TECHNIQUES

Standard DNA techniques have been used throughout the project, starting with PCR amplification of TOPORS cDNA and its fragments for construction of Y2H cDNA library and baits (Chapter 3 and Appendix 11.2), followed by amplification and cloning of its novel interacting partners (Chapters 4 and 5).

Plasmids propagation and isolation from bacterial cultures was frequently performed (Chapters 3, 4 and 5).

Di-deoxy chain-terminating sequencing was also used throughout the project to validate results of cloning, colony screening, and mutagenesis procedures (Chapters 3, 4 and 5).

### 2.2.1 DNA AMPLIFICATION BY POLYMERASE CHAIN REACTION

Polymerase chain reactions (PCRs) were carried out using KOD DNA polymerase (Novagen, Merck KGaA, Germany), BioTAQ DNA polymerase (Bioline, UK) and MangoTAQ DNA polymerase (Bioline, UK). *PFU* DNA polymerase (Promega, WI, USA) was added to the BioTAQ DNA polymerase (Bioline, UK) before first use (7 units of *PFU* per full tube of BioTAQ), in order to enhance the proof-reading activity of the enzymatic mixture.

The reactions were normally performed using approximately 1 µg of DNA in total volume of 25 µl (see Table 2-30) according to the respective manufacturer's specifications.

Table 2-30. DNA polymerases used and general PCR conditions

Components	BioTAQ polymerase (Bioline) with <i>PFU</i> polymerase (Promega)	MangoTAQ polymerase (Bioline)	KOD Hot Start DNA Polymerase (Novagen)
<b>Buffer</b>	1X NH <sub>4</sub> buffer	1X MangoTAQ reaction buffer	1X KOD polymerase buffer
<b>MgCl<sub>2</sub></b>	1.5 mM - 2.5 mM	1.5 mM – 4.0 mM	-
<b>MgSO<sub>4</sub></b>	-	-	1.0 mM – 2.0 mM
<b>dNTPs</b>	0.2 mM	0.2 mM	0.2 mM
<b>Primers</b>	25.0 pM	25.0 pM	25.0 pM
<b>Polymerase</b>	0.5 units	0.25 units	1.0 unit
<b>Total volume</b>	<b>25.0 µl</b>	<b>25.0 µl</b>	25.0 µl

The temperature cycling profile for products amplified using the BioTAQ (Bioline, UK)/*PFU* (Promega, WI, USA) polymerases comprised an initial denaturing step at 95 °C for three minutes for genomic- or cDNA, or five minutes for plasmid DNA; followed by 35 cycles of

denaturation at 94 °C for 30 seconds, annealing for 15 seconds (temperature set in accordance with primer pair used); and an extension step at 72 °C for which time was approximated using 1 minute per 1.0 kb of DNA. The reaction was completed by a final extension step at 72 °C for five minutes.

The temperature cycling profile for products amplified using the *MangoTAQ* (Bioline, UK) polymerases comprised an initial denaturing step at 95 °C for five minutes for plasmid DNA; followed by 35 cycles of denaturation at 95 °C for 15 seconds, annealing for 15 seconds (temperature set in accordance with primer pair used); and an extension step at 72 °C for which time was approximated using 1 minute per 1.0 kb of DNA. The reaction was completed by a final extension step at 72 °C for ten minutes. *MangoTAQ* was also the polymerase of choice for colony PCR screens (section 2.2.3.1).

The temperature cycling profile for products amplified using the *KOD* polymerase (Novagen, Merck KGaA, Germany) comprised an initial denaturing step at 95 °C for three minutes for genomic- or cDNA, or five minutes for plasmid DNA; followed by 30-35 cycles of denaturation at 94 °C for 30 seconds, annealing for 30 seconds (temperature set in accordance with primer pair used); and an extension step at 75 °C for which time was approximated using 20 seconds per 1.0 kb of DNA. The reaction was completed by a final extension step at 75 °C for 1 minute per 1.0 kb.

Annealing temperature was calculated prior to optimisation of PCR conditions using the following formula:  $T_m = 4(C + G) + 2(A + T)$ . Primers for PCR amplifications were all synthesised by Sigma-Aldrich, MO, USA.

Sequences and annealing temperatures of primers used for DNA amplification procedures are summarised in subsequent cloning sections (2.2.3, 2.2.5.1, 2.2.5.3).

The *BioTAQ* and *MangoTAQ* polymerase-based amplifications were used predominately for amplification of Y2H screen preys (Chapter 4) and identification of retinal isoforms of the identified preys (Chapter 5), whereas the *KOD* polymerase-based amplification, utilising its proof-reading activity, was used in construction of baits and control constructs (Chapters 3 and 5).

## **2.2.2 AGAROSE GEL ELECTROPHORESIS**

DNA fragments were separated on agarose (Bioline, UK) gels (0.8 % - 2.0 %), buffered with 1x TAE (Table 2-31) and supplemented with 0.01 µl/ml of ethidium bromide (Sigma-Aldrich, PhD Thesis 2015 || Methods and Materials - 114 -

MO, USA), or with 0.02  $\mu\text{l/ml}$  of Gel Red (Biotium, CA, USA). BioRad (CA, USA) power packs and tanks were used.

Table 2-31. TAE Buffer.

TAE
2.0 M TRIS-Acetate
0.05 M EDTA

Table 2-32. 1 % agarose gel.

0.8 % - 2.0 % agarose gel
2.4 g – 6.0 g of agarose
0.01 $\mu\text{l/ml}$ of ethidium bromide, or 0.02 $\mu\text{l/ml}$ of Gel Red
300 ml 1X TAE

Prior to electrophoresis the DNA samples were loaded using 1X bromophenol blue loading dye (Sigma-Aldrich, MO, USA); products of MangoTAQ PCR reactions, in which the coloured buffer was used, were loaded straight onto the gel without addition of bromophenol blue. Unless stated otherwise, Smart Ladder (Eurogentec, UK), Hyper Ladder I (Bioline, UK) and 1kb DNA Ladder (Promega, WI, USA) were used as markers to determine the size of the DNA fragments.

This methods was utilised whilst performing cloning, screening and mRNA expression studies (Chapters 3, 4 and 5).

### 2.2.3 BACTERIAL TRANSFORMATION

Transformation of competent bacterial cells was used frequently throughout the project, specifically, for construction of Y2H vectors (Chapters 3, 4 and 5). Firstly, whilst cloning (section 2.2.3) of the Y2H baits, and, subsequently, the preys into yeast as well as mammalian expression vectors.

DH5 $\alpha$  (Life Technologies, CA, USA) and XL1-Blue (Stratagene, CA, USA) strains of bacteria were used for cloning, unless stated otherwise. The cells were thawed on ice and aliquoted (50-150  $\mu\text{l}$  per transformation) into pre-chilled 1.5 ml tubes.

If XL1-Blue cells were used, then  $\beta$ -mercaptoethanol was added to the tubes (1.7  $\mu\text{l}$  1.4 M per 100  $\mu\text{l}$  bacteria), and the mixtures were incubated on ice for ten minutes.

Plasmid DNA (0.1-50.0 ng per transformation) was added to the competent bacteria, and gently mixed. The cells were incubated on ice for thirty minutes, heat-shocked (42  $^{\circ}\text{C}$  for 45 seconds) and placed immediately back on ice for further 2 minutes.

The bacteria were mixed with 100  $\mu\text{l}$  SOC media (LifeTechnologies, CA, USA) and incubated with shaking (1 h, 37  $^{\circ}\text{C}$ , 225 rpm; Innova 4200 Incubator Shaker, New Brunswick Scientific, NJ,

USA). Cells were centrifuged at 10000 rpm for three minutes (Centrifuge 5417R, Eppendorf, Germany) and excess media was removed; the cells were re-suspended in 100-200 µl of media.

The cells were spread onto LB agar plates supplemented with the relevant antibiotics (Table 2-33); the plates were incubated at 37 °C for 12-24 hours. Single colonies were inoculated into 1 ml LB-broth cultures with the relevant antibiotics (12-24 hours, 37 °C, 225 rpm; Innova 4200 Incubator Shaker, New Brunswick Scientific, NJ, USA) for further analyses.

Table 2-33. Luria-Bertani (LB) Media for bacterial culture.

LB Agar Medium	LB Liquid Medium
<b>4 g Tryptone</b>	<b>4 g Tryptone</b>
<b>2 g Yeast extract</b>	<b>2 g Yeast extract</b>
<b>3.2 g NaCl</b>	<b>4 g NaCl</b>
<b>6 g Agar</b>	-
<b>400 ml dH<sub>2</sub>O</b>	<b>400 ml dH<sub>2</sub>O</b>

### 2.2.3.1 COLONY PCR

Following a bacterial transformation, colonies can be screened for inserts prior to plasmid extraction. Each picked colony is first either: inoculated into liquid LB media, or: spotted on an LB agar plate (LB supplemented with relevant antibiotics), and then dipped in a corresponding well of a 96-well PCR plate, containing a vector- or insert-specific PCR mix. Inoculation into liquid media was used for lower throughput screening of up to fifty colonies; whereas spotting of colonies onto an agar plate, followed by subsequent inoculation of positive clones, was used for screening of fifty or more colonies.

The colony PCRs were performed using the MangoTAQ DNA polymerase (Bioline, UK), as specified in section 2.2.1, using coloured buffer (Table 2-30). The temperature cycling profile was extended relative to a standard PCR: the initial denaturation step at 95 °C lasted ten minutes; followed by 30 cycles of denaturation at 95 °C for 1 minute, annealing for 1 minute (temperature set in accordance with primer pair used); and an extension step at 72 °C for which time was approximated using 1-2 minutes per 1.0 kb of DNA. The reaction was completed by a final extension step at 72 °C for ten minutes.

### 2.2.4 DNA ISOLATION AND PURIFICATION

DNA was extracted from microorganisms and purified at various stages throughout the project. Phenol/chloroform extraction and ethanol precipitation were carried out as

described in Sambrook *et al.* (2001) to isolate total DNA from a bacterial or a yeast cells (Chapters 3 and 4). The PureYield™ Plasmid Miniprep System (Promega, WI, USA) and the Easy Yeast Plasmid Isolation Kit (Clontech, CA, USA; section 2.1.6.1) were used, according to the respective manufacturer's instructions, for isolation of sole plasmids from bacteria or yeasts, respectively (Chapters 3, 4 and 5).

A number of purification kits, such as Wizard® SV Gel and the PCR Clean-up System (Promega, WI, USA) and QIAQuick Gel Extraction Kit (Qiagen, Netherlands) were used for purification of PCR products, and/or of DNA fragments excised from agarose gel, following electrophoresis (section 2.2.2). Such purified DNA fragments were then used for downstream procedures, such as cloning (e.g. a ligation reaction) (Chapters 3 and 5 and Appendices).

Sequencing reaction products (section 2.2.7) were purified using either the MultiScreen HTS filter plates (Millipore, Merck KGaA, Germany) and the Sephadex® G-50 filtration gel (Sigma-Aldrich, MO, USA), or the Montage Sequencing Reaction Clean-Up Kit (Millipore, Merck KGaA, Germany). In the first case the PCR products were transferred to the pre-washed Sephadex® G-50 Plate and centrifuged at 910 x *g* for five minutes; the cleaned PCR product was pulled through the filtration gel and collected in a clean 96-well plate, leaving any impurities and sequencing primers within the gel. When using the Millipore method, 25 µl of Injection Solution (provided with kit) were added to each reaction before transferring the reactions to the Montage plate. The plate was then attached to a vacuum pump and the reaction mixture was aspirated through the base membrane leaving the sequencing products bound to the membrane. The membrane was washed twice with 25 µl Injection Solution; the sequencing reaction products were then re-suspended in 25 µl of Injection Solution by gentle shaking at 1000 rpm for ten minutes (Stuart Mini orbital shaker SSM1, Bibby Scientific Limited, UK).

## **2.2.5 CLONING**

Several cloning methods were used throughout the project, with different degrees of success, primarily due to challenges in sub-cloning *TOPORS* cDNA into a yeast vector.

### **2.2.5.1 IN-FUSION CLONING**

In-Fusion Cloning (Clontech, CA, USA) was the primary method of choice for cloning *TOPORS*, and its fragments, as it would generate PCR amplicons capable of recombining with the Clontech (CA, USA) Y2H vectors, without the need for restriction digestion and ligation.

*TOPORS* deletion constructs were cloned using this method (Appendix 11.2). Prior to the cloning procedure the pGBKT7 vector (Clontech, CA, USA; Table 2-1) was digested with *Bam*HI and *Eco*RI restriction enzymes (Promega, WI, USA) for 1 hour at 37 °C, using 1 unit (u) of nuclease per 1 µg of DNA. *TOPORS* and its fragments were amplified using primers (Table 2-34), which would generate amplicons, extended by tails, which would allow for recombination with the pGBKT7 plasmid.

Table 2-34. Primer pairs used for PCR amplification of full-length, and shorter, *TOPORS* fragments for In-fusion cloning.

The primers were designed to incorporate restriction sites into the amplicon (indicated in italics within the primer sequences); the *Eco*RI site is included within all of the forward primers; the *Sal*I site is found within the sequences of all of the reverse primers. F – forward primer, R – reverse primer. *KOD* polymerase was used for the amplification.

Fragment name	Amino acids	Size (Bp)	Primer name	Sequence (5' → 3')	Tm (°C)
<b>Full-length TOPORS</b>	1-1045	3135	TOP-in-fusion-1-pGBKT7-F	<b>CATGGAGGCCGAATTCATGG</b> GGTCGCAGCCCGCTGGGG	75 °C
			TOP-in-fusion-6-pGBKT7-R	<b>GCAGGTCGACGGATCCTTAA</b> GACATATCACAGTCTCTACC	
<b>N-term TOPORS</b>	1-380	1140	TOP-in-fusion-1-pGBKT7-F	<b>CATGGAGGCCGAATTCATGG</b> GGTCGCAGCCCGCTGGGG	70 °C
			TOP-in-fusion-2-pGBKT7-R	<b>GCAGGTCGACGGATCCTGAA</b> GGAGCAGGGCAATCATAATT	
<b>Middle-TOPORS</b>	373-781	1224	TOP-in-fusion-3-pGBKT7-F	<b>CATGGAGGCCGAATTC</b> AATT ATGATTGCCCTGCTCCTCA	70 °C
			TOP-in-fusion-5-pGBKT7-R	<b>GCAGGTCGACGGATCCGTTA</b> GTACCCTCAAATGCCGTGT	
<b>C-term TOPORS</b>	705-1045	1020	TOP-in-fusion-4-pGBKT7-F	<b>CATGGAGGCCGAATTC</b> ACTTA TTACAGTAGAAACAAGGAC	70 °C
			TOP-in-fusion-6-pGBKT7-R	<b>GCAGGTCGACGGATCCTTAA</b> GACATATCACAGTCTCTACC	

The amount of DNA to be used in the reaction was calculated, using the In-Fusion® Molar Ratio Calculator, available at the <http://bioinfo.clontech.com/infusion/> webpage.

The In-fusion reaction was set up in a total volume of 10 µl, containing 2 µl of the 5X In-fusion Reaction Buffer, 1 µl of the In-fusion enzyme, and the required amount of deionised water (Table 2-35). The reaction was incubated for 15 minutes, firstly, at 37 °C, and, subsequently, for 15 minutes at 50 °C to terminate the reaction. The reaction was cooled on ice and 40 µl of TE buffer (pH 8) were added. The reaction was either immediately used for transformation of competent *Escherichia coli* cells, or stored at -20 °C.

The amplified DNA fragments and the vector have 15 bp-long regions of homology at the insertion site, which are recognised by the In-fusion enzyme. The enzyme removes one

strand at the homology region in both the PCR product and the linearised vector, forming single-stranded overhangs; it then ligates the two DNA molecules together (Figure 2-7).

Table 2-35. In-fusion reaction components.

Insert and vector recommended ratio is 2:1. The exact DNA weight required for this reaction is calculated based on the number of base pairs of both insert and vector, using the In-Fusion® Molar Ratio Calculator, available online: <http://bioinfo.clontech.com/infusion/molarRatio.do>

Components	Amount
	[Calculated using the In-Fusion® Molar Ratio Calculator online]
<b>Linearised vector</b>	[Calculated using the In-Fusion® Molar Ratio Calculator online]
<b>5X In-fusion Reaction Buffer</b>	2 µl
<b>In-fusion enzyme</b>	1 µl
<b>dH<sub>2</sub>O</b>	Up to 10 µl
<b>Total volume</b>	10 µl

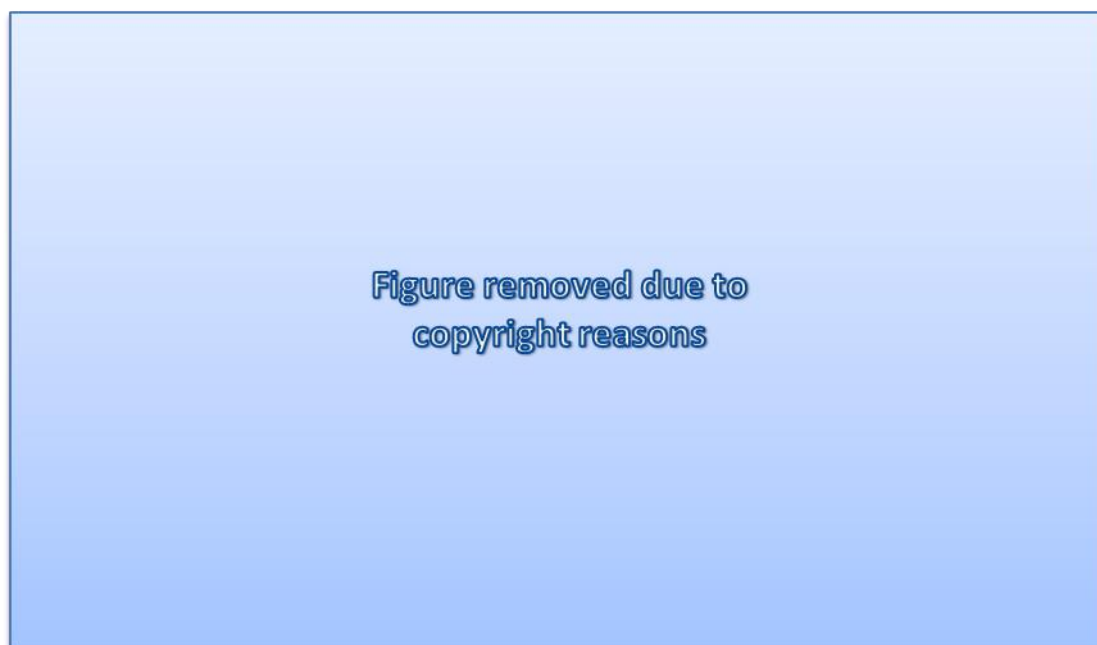


Figure 2-7. In-fusion cloning method.

Figure from the In-Fusion® Advantage PCR Cloning Kit User Manual (Clontech, CA, USA).

### 2.2.5.2 DIGESTION- AND LIGATION-BASED CLONING

The 'traditional' cloning techniques were attempted when In-Fusion Cloning was not successful for full-length *TOPORS* cDNA. Initially, digestion of the amplicons prepared for In-Fusion cloning (Table 2-34) was performed. Primers, incorporating alternative restriction sites, were also designed (Table 2-36).

This method was used in attempts to clone full-length *TOPORS* (Appendix 11.2).

Digestion by restriction endonucleases, vector dephosphorylation and ligation were subsequently performed.

Table 2-36. Primer pair used for PCR amplification of full-length *TOPORS* for cloning, using restriction enzymes and ligase.

The primers were designed to incorporate restriction sites into the amplicon (indicated in italics within the primer sequences); the *NdeI* site is included within the forward primer; the *PstI* site is found within the sequence of the reverse primer. F – forward primer, R – reverse primer. . *KOD* polymerase was used for the amplification.

Fragment name	Amino acids	Bp	Primer name	Primer components	Sequence (5' → 3')	T <sub>m</sub> (°C)
<b>Full-length TOPORS</b>	1-1045	3135	FL F	'GC F clamp', <i>NdeI</i> seq., first 20 nt of <i>TOPORS</i>	<b>GCCGCATATGATGGGGT</b> CGCA CC CCG	57 °C
			FL R	'GC R clamp', <i>PstI</i> seq., last 20 nt of <i>TOPORS</i> (reverse complemented)	<b>GCGCCTGCAGTTAAGACA</b> TATCACAGTCTC	

#### 2.2.5.2.1 RESTRICTION ENZYME DIGEST

Restriction enzyme digests were performed on both plasmid DNA and the PCR products, using 1 unit (u) of enzyme per 1 µg of DNA for 1 h at the optimal temperature for each specific enzyme, according to the manufacturer's instructions. The reactions were set up in a total volume of 10 µl containing the DNA, restriction enzyme(s), 1X corresponding restriction buffer(s) and sterile deionised water (Table 2-37). Restriction enzymes and their corresponding buffers, manufactured by Promega (WI, USA), were used. The reaction products were purified prior to further treatment.

Table 2-37. Components of restriction digest reaction.

Components	
<b>DNA</b>	1 µg
<b>Restriction endonuclease(s)</b>	1 u
<b>Restriction buffer</b>	1X
<b>dH<sub>2</sub>O</b>	Up to 10 µl
<b>Volume</b>	10 µl

#### 2.2.5.2.2 DEPHOSPHORYLATION OF VECTOR 5' ENDS

The digested plasmid molecules were dephosphorylated at their 5' ends, using a calf intestinal alkaline phosphatase (CIAP; Promega, WI, USA) in order to prevent the plasmid ends from self-ligating during the ligation reaction. The dephosphorylation was performed according to two different protocols.



The first dephosphorylation procedure was based on the Promega (WI, USA) protocol (Table 2-38). Ten microlitres of CIAP 10 X reaction buffer were diluted at a 1:10 ratio in deionised water (dH<sub>2</sub>O) to yield CIAP 1 X reaction buffer. CIAP (1 u/μl) was diluted in the CIAP 1 X reaction buffer at a 1:50 ratio to yield 0.02 u/μl CIAP.

According to the manufacturer 1 μg of 1 kb DNA is equal to 1.52 pmol of DNA, which is equal to 3.03 pmol of DNA ends. Ten picomoles of DNA ends were used per dephosphorylation reaction; the DNA was diluted up to 40 μl in Tris-HCl (pH 8).

Five microlitres of CIAP 10 X reaction buffer and 5 μl of the 0.02 u/μl CIAP were subsequently added and the reaction was incubated at 37 °C for thirty minutes. Another 5 μl of the 0.02 u/μl CIAP were added to the reaction mixture and the incubation was repeated.

An alternative simplified dephosphorylation method was used in parallel. Ten picomoles of DNA ends were incubated with 2 μl of CIAP 10 X reaction buffer and 1 μl of 1 u/μl CIAP in a total volume of 20 μl at 37 °C for 1 hour (Table 2-39). The reaction products were purified prior to further use.

Table 2-38. Dephosphorylation reaction according to the Promega (WI, USA) protocol

Components	Volume
<b>10 pmol of DNA ends diluted up to 40 μl in Tris-HCl (p</b>	40 μl
<b>CIAP 10 X reaction buffer</b>	5 μl
<b>0.02 u/μl CIAP</b>	5 μl (+5 μl)
<b>Total volume</b>	50 μl (+5 μl)

Table 2-39. Dephosphorylation reaction according to the simplified protocol

Components	Amount
<b>10 pmol of DNA ends</b>	10 pmol of DNA ends
<b>CIAP 10 X reaction buffer</b>	2 μl
<b>1 u/μl CIAP</b>	1 μl
<b>dH<sub>2</sub>O</b>	Up to 20 μl
<b>Total volume</b>	20 μl

#### 2.2.5.2.3 LIGATION

The PCR fragments were cloned into dephosphorylated vectors, using T4 DNA Ligase (Promega, WI, USA) according to the manufacturer's instructions. Reactions were prepared with vector:insert ratios of 1:1 to 1:3, and incubated at room temperature (RT) overnight, or at 4 °C overnight.

### 2.2.5.3 GATEWAY CLONING

The Gateway cloning technique (Life Technologies, CA, USA) was eventually utilised, when In-Fusion and 'traditional' cloning attempts did not yield the expected results for *TOPORS*.

Full-length *TOPORS* and its control protein interacting partner-encoding *p53* as well as the novel interacting partners of TOPORS were cloned using the Gateway method (Appendices 11.2, 11.5 and 11.8). *ITM2B* constructs, encoding the FBD, FDD and retinal dystrophy mutants, were kindly provided by Audo *et al.* (2013) in pBUD vectors and used for sub-cloning into yeast vectors.

The method relies on the bacteriophage lambda ( $\lambda$ ) site-specific recombination system, which in natural conditions facilitates the integration of the lambda virus into the *Escherichia coli* genome, and the switch between the lytic and lysogenic cycles.

Site-specific attachment (*att*) sites are required for the recombination event; they serve as recognition sites for the recombination proteins. The *att* sites used in the Gateway system are denoted as *attB* on the *E. coli* chromosome and *attP* on the lambda chromosome (Figure 2-8).

The crossing-over between two interacting DNA molecules occurs at the *att* sites, and it does not involve any loss or gain of nucleotides; i.e. the *attB* and *attP* sites are joined together to become a hybrid *attL* sequence.

The lambda recombination adapted for the Gateway method is catalysed by a number of enzymes, which bring the *att* sites together, cleave them and covalently bind the DNA molecules.

The actual crossing-over happens between 15-bp-long core DNA regions; however, a longer sequence is required for the recombination proteins to bind. In the endogenous lambda system the exact enzymes involved depend on whether the bacteriophage is undergoing the lytic or the lysogenic cycle.

The lambda Integrase (Int) and the *E. coli* Integration Host Factor (IHF) proteins catalyse the recombination during the lysogenic cycle; this corresponds to the BP clonase enzyme mix in the Life Technologies Gateway system.

During the lytic cycle, the recombination involves the above-mentioned lambda Int and *E. coli* IHF as well as a lambda Excisionase (Xis); in the Gateway system the equivalent proteins are known as the LR clonase enzyme mix.

PCRs were performed, using the *KOD* polymerase (section 2.2.1). Specific primers were designed encompassing the first 25 nucleotides near the 5' end, and last 25 nucleotides near the 3' end of the transcript for the forward and for the reverse primer, respectively; the *attB1* and *attB2* sites were incorporated into the forward and reverse primers respectively, allowing them to be amplified in-frame either side of the intended DNA sequence (termed *attb*-[PCR]-*attb*).

The *attB*-PCR products were purified and recombined with the pDONR/Zeo vector (with corresponding *attP1* and *attP2* sequences). The resulting entry vector was then used as a shuttle vector for sub-cloning into various destination vectors.

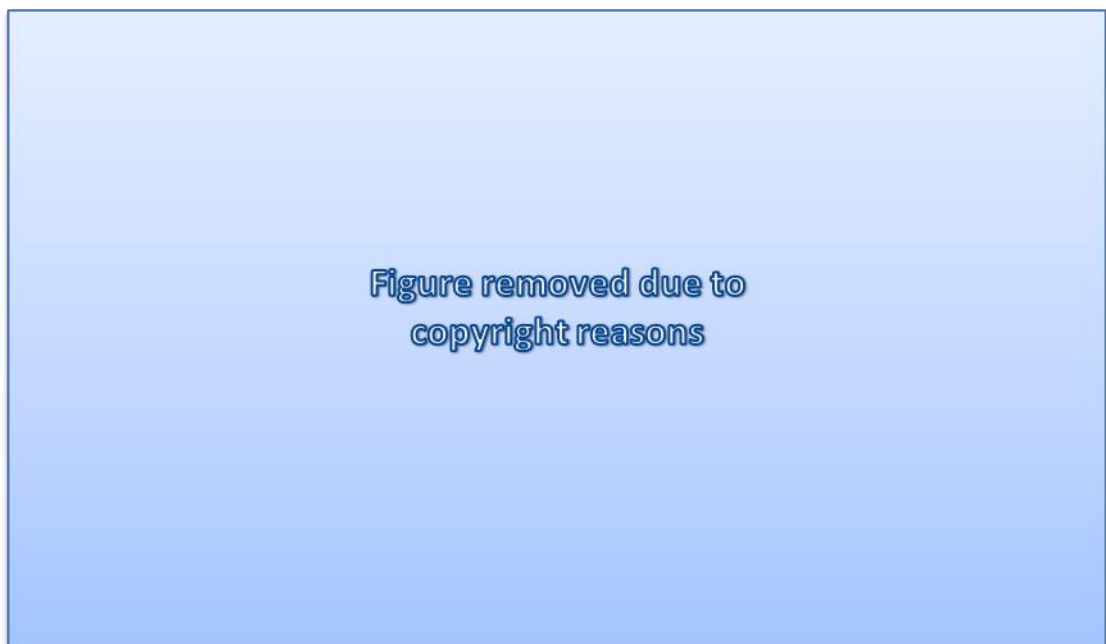


Figure 2-8. The Gateway BP and LR reactions.

The Gateway system comprises two recombination events based on the lambda integration cycles. The BP reaction facilitates recombination between the *attB* substrate, i.e. the *attB*-PCR product, and the *attP* substrate, i.e. the donor vector (pDONR/Zeo; Table 2-2). These two *att* sites become joined together to form a hybrid *attL* site; hence, the key product obtained during the BP reaction is an entry clone containing the DNA sequence of interest, flanked by the *attL* sites. This entry clone is used as the *attL* substrate in the LR reaction, during which it is recombined with an *attR* substrate (destination vector; Table 2-2); the LR reaction results in a formation of the expression clone and the *attB* site. Figure from GibcoBRL Life Technologies Gateway cloning manual.

The BP recombination involved combining the *attB*-PCR product (150 ng) with 150 ng of the pDONR vector, and TE buffer (pH 8.0) up to a final volume of 4  $\mu$ l. The BP Clonase enzyme mix was thawed on ice for 2 minutes and vortexed briefly, before adding 2  $\mu$ l to the reaction. The reaction mixtures were centrifuged briefly and incubated at 25° C for 1 hour. Proteinase K (1  $\mu$ l) was added to terminate the reaction by incubating at 37° C for ten minutes.

The entry clones were transformed into the DH5 $\alpha$  competent *E. coli* bacterial strain and grown on selective media. Single colonies were picked and inoculated into overnight cultures of up to 5 ml; the entry clone plasmids were isolated from the liquid cultures.

Once verified by sequencing, the isolated entry clones were subject to the LR recombination with the relevant destination vectors. The reaction comprised the entry clone DNA (150 ng) and the destination vector (150 ng) in a total volume of 4  $\mu$ l made up to with TE buffer (pH 8.0). The LR Clonase enzyme mix was thawed on ice for 2 minutes and vortexed briefly, before adding 2  $\mu$ l to the reaction. The reaction mixtures were centrifuged briefly and incubated at 25° C for 1 hour. Proteinase K (1  $\mu$ l) was added to terminate the reaction by incubating at 37° C for ten minutes. The new clones were confirmed by sequencing and digestion with restriction enzymes. This methods was used for successfully cloning TOPORS (Table 2-40), *p53* (Table 2-41) for the control experiments, as well as the novel interacting partners of *TOPORS* (Tables 2-42, 2-43 and 2-44).

Table 2-40. Primer pair used for PCR amplification of full-length *TOPORS* for cloning, using the Gateway system.

The primers were designed to incorporate the *attB1* and *attB2* recombination sites into the amplicon (indicated in bold). F – forward primer, R – reverse primer.

Fragment name	Amino acids	Length (Bp)	Primer name	Primer components	Sequence (5' $\rightarrow$ 3')	Tm (°C)
Full-length TOPORS	1-1045	3135	Top-attb-F	<b><i>attB1</i> sequence,</b> first 25 nt of <i>TOPORS</i>	<b>GGGGACAAGTTTGTAC</b> <b>CAAAAAGCAGGCTT</b> CATGGGGTTCGAGCC GCCGCTGGGGT	60 °C
			Top-attb-R	<b><i>attB2</i> sequence,</b> last 25 nt of <i>TOPORS</i> (reverse complemented)	<b>GGGGACCACTTTGTAC</b> <b>AAGAAAGCTGGGTGT</b> TAAGACATATCACAGT CTTACCA	

Table 2-41. Primer pair used for PCR amplification of full-length *p53* for cloning, using the Gateway system.

The primers were designed to incorporate the *attB1* and *attB2* recombination sites into the amplicon (indicated in bold). F – forward primer, R – reverse primer.

Fragment name	Amino acids	Length (Bp)	Primer name	Primer components	Sequence (5' $\rightarrow$ 3')	Tm (°C)
Tumour protein 53 ( <i>p53</i> )	1-393	1182	p53-attb-F	<b><i>attB1</i> sequence,</b> first 25 nt of <i>p53</i>	<b>GGGGACAAGTTTGTAC</b> <b>AAAAAAGCAGGCTTCA</b> TGGAGGAGCCGCAGTC AGATCCTA	60 °C
			p53-attb-R	<b><i>attB2</i> sequence,</b> last 25 nt of <i>p53</i> (reverse complemented)	<b>GGGGACCACTTTGTAC</b> <b>AAGAAAGCTGGGTGT</b> CAGTCTGAGTCAGGCC CTTCTGTC	

Table 2-42. Primer pair used for PCR amplification of *ITM2B*, its fragment, and disease-causing mutants for cloning, using the Gateway system.

 The primers were designed to incorporate the *attB1* and *attB2* recombination sites into the amplicon (indicated in bold). F – forward primer, R – reverse primer.

Fragment name	Amino acids	Length (Bp)	Primer name	Primer components	Sequence (5' → 3')	T <sub>m</sub> (°C)
Full-length <i>ITM2B</i>	1-266	801	ITM2B-attb-F	<b><i>attB1</i> sequence,</b> first 25 nt of <i>ITM2B</i>	<b>GGGGACAAGTTTGTAC</b> <b>AAAAAAGCAGGCTTCA</b> TGGTGAAGGTGACGTT CAACTCCG	60 °C
			ITM2B-attb-R	<b><i>attB2</i> sequence,</b> last 25 nt of <i>ITM2B</i> (reverse complemented)	<b>GGGGACCACTTTGTAC</b> <b>AAGAAAGCTGGGTGT</b> CAAGAACAAATTAAG TTCCACG	
<i>ITM2B90</i>	90-266	534	<i>ITM2B90</i> -attb-F	<b><i>attB1</i> sequence,</b> first 25 nt of <i>ITM2B</i>	<b>GGGGACAAGTTTGTAC</b> <b>AAAAAAGCAGGCTTC</b> GGAATAAAGTACATCA AAGATGATG	60 °C
			Reverse as for full-length <i>ITM2B</i>			
Full-length <i>ITM2B</i> c.782A>C mutant (mu)	1-266	801	Forward as for full-length wild-type <i>ITM2B</i>			
			ITM2B-c.782A>C-attb-R	<b><i>attB2</i> sequence,</b> last 25 nt of <i>ITM2B</i> c.782A>C mu (reverse complemented)	<b>GGGGACCACTTTGTAC</b> <b>AAGAAAGCTGGGTGT</b> CAAGAACAAATTAAG TTGCCACG	60 °C
Full-length <i>ITM2B</i> c.799T>A mutant (mu)	1-266	801	Forward as for full-length wild-type <i>ITM2B</i>			
			ITM2B-c.799T>A-attb-R	<b><i>attB2</i> sequence,</b> last 25 nt of <i>ITM2B</i> c.799T>A mu (reverse complemented)	<b>GGGGACCACTTTGTAC</b> <b>AAGAAAGCTGGGTGT</b> TAATTTTCCTCAATAAT GTTTTTC	60 °C
Full-length <i>ITM2B</i> c.795-796ins TTTAATT TGT mutant (mu)	1-266	801	Forward as for full-length wild-type <i>ITM2B</i>			
			ITM2B-c.795-796ins TTTAATTT GT-attb-R	<b><i>attB2</i> sequence,</b> last 25 nt of <i>ITM2B</i> c.795-796ins TTTAATTTGT mu (reverse complemented)	<b>GGGGACCACTTTGTAC</b> <b>AAGAAAGCTGGGTGT</b> CAATAATGTTTTTCTTG ACTGTTC	60 °C

Table 2-43. Primer pair used for PCR amplification of full-length *PTGDS* for cloning, using the Gateway system.

The primers were designed to incorporate the *attB1* and *attB2* recombination sites into the amplicon (indicated in bold). F – forward primer, R – reverse primer.

Fragment name	Amino acids	Length (Bp)	Primer name	Primer components	Sequence (5' → 3')	T <sub>m</sub> (°C)
Full-length <i>PTGDS</i>	1-190	573	PTGDS -attb-F	<b><i>attB1</i>sequence,</b> first 25 nt of <i>PTGDS</i>	<b>GGGGACAAGTTTGTACA</b> <b>AAAAAGCAGGCTTCATGG</b> CTACTCATCACACTGTG GA	60 °C
			PTGDS -attb-R	<b><i>attB2</i>sequence,</b> last 25 nt of <i>PTGDS</i> (reverse complemented)	<b>GGGGACCACTTTGTACAA</b> <b>GAAAGCTGGGTGCTATTG</b> TTCCGTCATGCACTTATCG	

Table 2-44. Primer pair used for PCR amplification of full-length *PSMC1* for cloning, using the Gateway system.

The primers were designed to incorporate the *attB1* and *attB2* recombination sites into the amplicon (indicated in bold). F – forward primer, R – reverse primer.

Fragment name	Amino acids	Length (Bp)	Primer name	Primer components	Sequence (5' → 3')	T <sub>m</sub> (°C)
Full-length <i>PSMC1</i>	1-440	1323	PSMC1 -attb-F	<b><i>attB1</i>sequence,</b> first 25 nt of <i>PSMC1</i>	<b>GGGGACAAGTTTGTACA</b> <b>AAAAAGCAGGCTTCATGG</b> GTCAAAGTCAGAGTGGTG GTC	60 °C
			PSMC1 -attb-R	<b><i>attB2</i>sequence,</b> last 25 nt of <i>PSMC1</i> (reverse complemented)	<b>GGGGACCACTTTGTACAA</b> <b>GAAAGCTGGGTGTTAGA</b> GATACAGCCCCTCAGGGG TG	

## 2.2.6 SITE-DIRECTED MUTAGENESIS

Site-directed mutagenesis (SDM) was carried out using the GeneArt® Site-Directed Mutagenesis System (Life Technologies, CA, USA; Figure 2-10) to 'correct' errors introduced (most likely) by the polymerase during PCR amplification of *PSMC1* (Appendix 11.8.5). This SDM method comprises four major steps:

- Mutation-specific primer design and synthesis;
- Template plasmid methylation and PCR-based mutagenesis;
- *In vitro* recombination reaction to enhance mutagenesis efficiency;
- Transformation into One Shot® MAX Efficiency® DH5α™-T1<sup>R</sup> competent *E. coli* cells.

### 2.2.6.1 PRIMER DESIGN AND SYNTHESIS

The forward and reverse primers were designed to begin and end with either a cytosine or a guanine nitrogen base and to be 32-35 nucleotides in length each with a 10-12 nucleotides long complementary overlapping region. The change to be introduced, i.e. the mutation site, was incorporated into each primer in the middle of its complementary overlap region. The primer oligo-nucleotides were synthesised by Sigma-Aldrich (MO, USA) and purified by desalting. An example of an SDM primer pair is shown in Figure 2-9.

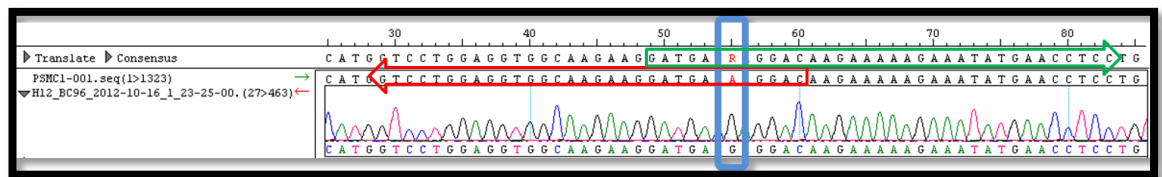


Figure 2-9. A fragment of a mutated sequence of pDONR-*PSMC1* entry clone. SDM forward and reverse primer regions are highlighted within green and red arrow shapes, respectively. The mutagenesis site is highlighted within a blue box: a c.55G>A change is required.

Table 2-45. Primer pair for GENEART SDM of pDONR-*PSMC1* entry clone.

Primer name	Primer components	Sequence (5' → 3')
<b>PSMC1 SDM F</b>	Nucleotides 49 – 83 of PSMC1-001 ENST00000261303 cDNA	GATGACAAGGACAAGAAAAAGAAATATGAACCTCC
<b>PSMC1 SDM R</b>	Nucleotides 29 – 60 of PSMC1-001 ENST00000261303 cDNA (reverse complemented)	GTCCTGTGCATCCTTCTTGCCACCTCCAGGAC

### 2.2.6.2 METHYLATION AND MUTAGENESIS

Methylation of the plasmid template and the SDM both occur during one reaction (Table 2-46). All except for two components listed in the table are products of Life Technologies (CA, USA). The SDM primers were provided by Sigma-Aldrich (MO, USA) and the plasmid DNA is the substrate of the reaction, i.e. the template. PCR cycling conditions for the methylation and SDM reactions are summarised in Table 2.-47.

Table 2-46. Methylation and SDM reaction mixture. SAM = S-adenosine methionine.

Components	Volume	Final concentration
<b>10X AccuPrime™ Reaction mix</b>	5.0 µl	1X
<b>10X Enhancer</b>	5.0 µl	1X
<b>SDM primer mix (10 µM each)</b>	X	0.3 µM each
<b>Plasmid DNA (40 ng/µl)</b>	X	40 ng in 50 µl
<b>DNA methylase (4 U/µl)</b>	1.0 µl	4 U in 50 µl
<b>25X SAM</b>	2.0 µl	1X
<b>AccuPrime™ Pfx (2.5 U/µl)</b>	0.4 µl	1 U in 50 µl
<b>PCR H<sub>2</sub>O</b>	Up to 50 µl	n/a
<b>Total volume</b>	50.0 µl	n/a

Table 2-47. Methylation and SDM reaction cycling conditions.

Temperature	Duration	Number of cycles
37 °C	12-20 minutes	1
94 °C	2 minutes	
94 °C	20 seconds	12-18
57 °C	30 seconds	
68 °C	30 seconds/kb of plasmid	
68 °C	five minutes	1
4 °C	Final hold	1

The first 37 °C incubation allows for the methylation reaction to occur. The manufacturer recommends 12 minutes incubation for 2.8 to 4.0 kb plasmids, and twenty minutes for 4.0 to 14.0 kb plasmids. Furthermore, for optimal mutagenesis efficiency it is recommended to perform 12-15 reaction cycles for 2.8 to 4.0 kb plasmids, and 18 cycles for 4.0 to 14.0 kb plasmids.



The extension time in each cycle should be 30 seconds per 1 kb of plasmid DNA. Products (5 µl) of the mutagenesis PCR were evaluated on 0.8 % agarose gel.



Figure 2-10. GENEART SDM workflow. The procedure relies on inherent DNA methylase properties, high fidelity Pfx DNA polymerase, recombination enzymes and MrcBC endonuclease. Figure from GENEART Site-Directed Mutagenesis System User Guide (LifeTechnologies, CA, USA).

### 2.2.6.3 RECOMBINATION REACTION

Given that a clear band of the expected size was observed following the agarose gel electrophoresis, the *in vitro* recombination reaction (Table 2-48) was set up in order to enhance the mutagenesis efficiency as well as to increase the colony yield following transformation of the competent cells.

Table 2-48. *In vitro* recombination reaction.

Components	Volume	Final concentration
5X Reaction buffer	4 µl	1X
PCR H <sub>2</sub> O	10 µl	n/a
SDM PCR Sample	4 µl	n/a
10X Enzyme mix	2 µl	1X
Total Volume	20 µl	n/a

The reaction was incubated for ten minutes at room temperature, and subsequently stopped by adding 1 µl of 0.5 M EDTA. The reaction products were stored on ice until transformation. All reagents used for the reaction and its termination are from Life Technologies (CA, USA).

#### 2.2.6.4 TRANSFORMATION OF ONE SHOT® MAX EFFICIENCY® DH5A™-T1<sup>R</sup> CELLS

The cells were thawed on ice for approximately 5-7 minutes; one 50-µl vial was used per transformation. Two microliters of the *in vitro* recombination reaction were transferred into the vial with cells and mixed by tapping. The vials were covered completely with ice and incubated for 12 minutes. The cells were heat-shocked at 42 °C for 30 seconds and placed immediately back in ice (covered completely) for further 2 minutes. The bacteria were mixed with 250 µl of SOC media per vial and incubated with shaking (1 37 °C, 225 rpm; Innova 4200 Incubator Shaker, New Brunswick Scientific, NJ, USA). Dilutions of the cell suspensions were made (Table 2-49) using SOC media in a total volume of 100 µl.

Table 2-49. Transformation reaction dilutions prior to plating.

Plasmid Size	Dilution
3 kb	5 µl reaction + 95 µl SOC
6 kb	10 µl reaction + 90 µl SOC
9 kb	20 µl reaction + 80 µl SOC
14 kb	50 µl reaction + 50 µl SOC

The cells were spread, using plastic sterile spreaders, on LB agar plates supplemented with the relevant antibiotics; the plates were incubated at 37 °C for 16-20 hours. Single colonies were inoculated into 1 ml LB-broth cultures with the relevant antibiotics (16-20 hours, 37 °C, 225 rpm; Innova 4200 Incubator Shaker, New Brunswick Scientific, NJ, USA) for further analyses.

#### 2.2.7 DNA SEQUENCING

DNA sequencing was used regularly throughout the project in order to validate the outcomes of cloning (Chapters 3 and 5) and library characterisation and screening for the interacting partners of TOPORS (Chapters 3 and 5). The BigDye™ Terminator v3.1 Cycle Sequencing Kit and the ABI PRISM® 3730 DNA Analyser (Applied Biosystems, Life Technologies, CA, USA) were used for DNA sequencing. The temperature cycling profile comprised an initial denaturing step at 94 °C for five minutes, followed by 25 cycles of denaturation at 96 °C for 10-15 seconds,

annealing at 50 °C for 5 seconds and an extension step at 60 °C for 4 minutes. The reaction was completed by a final hold step at 10 °C. The DNA (PCR product, 5-20 ng; plasmid, 100-150 ng) was sequenced using 1X BigDye™ v3.1 Cycle ready mix (containing ddNTPs, dNTPs, Amplitaq® DNA polymerase, pyrophosphate and MgCl<sub>2</sub>), 1X BigDye™ Sequencing Buffer, 1 µmol of primer and dH<sub>2</sub>O to a final volume of 20 µl. Sequencing electropherograms were analysed using the DNASTAR Software (DNASTAR Inc., WI, USA) and the Chromas™ program (Technylesium Pty Ltd., QLD, Australia).

### 2.2.7.1 SEQUENCING PRIMERS

Primers for sequencing of *TOPORS* cDNA and its control interacting partner *p53* cDNA as well as its novel interacting partners identified via the Y2H screen are detailed in this section (Tables 2-50, 2-51, 2-52, 2-53, 2-54 and 2-55).

Table 2-50. Vector-specific sequencing primers.

Forward primers (denoted with an 'F' in the primer name, or not defined) were designed to bind to the sense vector strand. Reverse primers (always denoted with an 'R' in the primer name) were designed to bind to the anti-sense strand (hence their sequences are reverse-complemented relative to the template sense strand). Primer sequences are given in the 5' to 3' direction.

Name	Sequence (5' → 3')	Vector	Complementary base pairs on vector
<b>T7</b>	TAATACGACTCACTATAGGG	pGBKT7 (Clontech)	1213-1233
<b>M13F</b>	GTAAACGACGGCCAG	pDONR/Zeo (Life Technologies)	537-552
<b>M13R</b>	CAGGAAACAGCTATGAC	pDONR/Zeo (Life Technologies)	3027-3043
<b>pGBKT7 F</b>	TCATCGGAAGAGAGTAGT	pGBKT7 (Clontech)	1155-1172
<b>pGBKT7 R1</b>	TTTTTCGTTTTAAACCTAAGAGTC	pGBKT7 (Clontech)	1487-1510
<b>pBD F</b>	GGAGACTGATATGCCTCTAACAT	pBD <sup>8</sup>	1922-1944
<b>pBD R</b>	GAATTAGCTTGGCTGCAGTAAT	pBD <sup>8</sup>	999-1020
<b>pAD_BRP 2F</b>	AAACCACTGTCACCTGGTTGG	pAD <sup>8</sup>	1962-1982
<b>pAD_BRP R</b>	GTGCACGATGCACAGTTGAAGT	pAD <sup>8</sup>	1043-1064

<sup>8</sup> These vectors were a gift from Dr Ronald Roepman. They had been modified from original pBD-GAL4 Cam and pAD-GAL4-2.1 (Stratagene, CA, USA) vectors to contain the *att* sequences, i.e. to allow compatibility with Gateway cloning (LifeTechnologies, CA, USA; see section 2.2.5.3).

Table 2-51. Sequencing primers used for *TOPORS*.

Forward primers (denoted with an 'F' in the primer name, or not defined) were designed to bind to the sense cDNA strand. Reverse primers (always denoted with an 'R' in the primer name) were designed to bind to the anti-sense strand (hence their sequences are reverse-complemented relative to the template sense strand). Primer sequences are given in the 5' to 3' direction.

Primer	Sequence (5' → 3')	Complementary base pairs on <i>TOPORS</i> cDNA
<b>F</b>	ATGGGGTCGCAGCCGCCGCTG	1-23
<b>S8 (R)</b>	CTCGGAGGATGCCGGCGCAG	179-198
<b>S1</b>	GACAACTTTTCACCTAAAG	232-250
<b>S2</b>	CGTACAACCTCTGACAAGG	451-468
<b>S3</b>	AACGTGAACTTACAGTTC	902-919
<b>S4</b>	GGACCATCTTACTCAAGCTC	1264-1283
<b>S5</b>	GTCATTGTGATTCTAGTAC	1643-1661
<b>S6</b>	TCTCTAAGTAGTGAAAGC	1981-1997
<b>S7</b>	TCTACCGGGACTGACCGG	2386-2403
<b>S9</b>	CACCATGGAGATAATGCTTC	2786-2705
<b>S10 (R)</b>	GAGCTTGAGTAAGATGGTCC	1264-1283
<b>S11 (R)</b>	AGCAGGGCAATCATAATT	937-1134
<b>S12 (R)</b>	CATTTTCTCATAAGAACC	1513-1530
<b>S13 (R)</b>	ATGATTCTTCTGATCATG	1828-1845
<b>S14 (R)</b>	ATACTCCCATTGTATCT	2095-2112
<b>S15 (R)</b>	CCGGTCAGTCCCGGTAGA	2386-2403
<b>R</b>	TTAAGACATATCACAGTC	3076-3138

 Table 2-52. Sequencing primers used for *p53*.

Forward primers designed to bind to the sense *p53* cDNA strand.

Primer	Sequence (5' → 3')	Complementary base pairs on <i>p53</i> cDNA
<b>p53-S1</b>	ATGGAGGAGCCGCAGTCA	1-18
<b>p53-S2</b>	CATCTTCTGTCCCTTCCC	281-298
<b>p53-S3</b>	CAGCATCTTATCCGAGTGGA	574-593
<b>p53-S4</b>	GCACTAAGCGAGCACTGCC	908-926

Table 2-53. Sequencing primers for *ITM2B*.

Forward primers (denoted with an 'F' in the primer name, or not defined) were designed to bind to the sense cDNA strand. Reverse primers (always denoted with an 'R' in the primer name) were designed to bind to the anti-sense strand (hence their sequences are reverse-complemented relative to the template sense strand). Primer sequences are given in the 5' to 3' direction. Primers with 'PCR' in the name were also optimised for cDNA amplification by PCR. 'ITM2B90' refers to cDNA, which encodes a peptide corresponding to ITM2B missing its first 90 amino acids, i.e. generating a non-membrane bound, soluble, form of ITM2B.

Primer	Sequence (5'→3')	Complementary base pairs on <i>ITM2B</i> cDNA
<b>ITM2B-PCR-F</b>	ATGGTGAAGGTGACGTTCAACTCCG	1-25
<b>ITM2B-PCR-R</b>	TCAAGAACAAATTAAGTTTCCACG	776-801
<b>ITM2B-S1</b>	ACATCAAAGATGATGTCA	278-295
<b>ITM2B-S2-R</b>	TCAATGCGATCAGTAATA	612-629
<b>ITM2B90-PCR-F</b>	GGAATAAAGTACATCAAAGATGATG	268-293

Table 2-54. Sequencing primers for *PTGDS*.

Forward primers (denoted with an 'F' in the primer name, or not defined) were designed to bind to the sense cDNA strand. Reverse primers (always denoted with an 'R' in the primer name) were designed to bind to the anti-sense strand (hence their sequences are reverse-complemented relative to the template sense strand). Primer sequences are given in the 5' to 3' direction. Primers with 'PCR' in the name were also optimised for cDNA amplification by PCR.

Primer	Sequence (5'→3')	Complementary base pairs on <i>PTGDS</i> cDNA
<b>PTGDS-PCR-F</b>	ATGGCTACTCATCACACTGTGGA	1-25
<b>PTGDS-PCR-R</b>	CTATTGTTCCGTCATGCACTTATCG	782-807
<b>PTGDS-S1-R</b>	TCTCACACTGGTTTTTCC	254-271
<b>PTGDS-S2</b>	GGAAAAACCAAGTGTGAGA	254-271

Table 2-55. Sequencing primers for *PSMC1*.

Primer	Sequence (5'→3')	Complementary base pairs on <i>PSMC1</i> cDNA
<b>PSMC1-SF</b>	ATGGGTCAAAGTCAGAGT	1-18
<b>PSMC1-S1</b>	GTGATAGGGGTGCTGATG	175-492
<b>PSMC1-S2-R</b>	CATCAGCACCCCTATCAC	175-492
<b>PSMC1-S3</b>	TGGATGGATTTGATTCTA	947-964
<b>PSMC1-SR</b>	TTAGAGATACAGCCCCTC	1306-1323

## 2.2.8 DNA PROCEDURES SUMMARY

In summary, the DNA methods were used for cloning and validation of Y2H baits and preys (Chapters 3 and 5), for library construction and characterisation (Chapter 3), for identification of interacting partners of TOPORS (Chapter 4), and for identification of retinal isoforms of the novel interacting partners of TOPORS (Chapter 5).

## 2.3 CELL CULTURE

Three major classes of cells were used in order to fulfil the goals of this project. Initially the eukaryotic yeast *Saccharomyces cerevisiae* cells were essential for constructing the cDNA library and completing the Y2H PPI studies (section 2.1 and experimental Chapters 3, 4 and 5).

For the purposes of cloning (section 2.2.3) and mutagenesis (section 2.2.6) several types of prokaryotic competent *Escherichia coli* cells were used.

Finally, for experiments requiring the use of RNA and protein of human origin, adherent human cell lines were maintained in culture in order to fulfil the objectives of characterising the newly-identified PPIs (experimental Chapters 6 and 7).

### 2.3.1 HUMAN CELL LINES MAINTENANCE

Several different adherent cell lines were used throughout this project; a summary of their growing conditions is shown in Table 2-56.

Table 2-56. Cell lines used for TOPORS characterisation and validation of interactions.

FCS – foetal calf serum; P/S – penicillin/streptomycin antibiotic mixture.

Name	Details	Media	Supplements	Source
<b>hTERT RPE1</b>	Human hTERT-immortalised retinal pigment epithelial cell line	DMEM/ F-12	10 % FCS, 1 % P/S	Kindly provided by Dr Rosa M. Rios from the Andalusian Molecular Biology and Regenerative Medicine Centre (CABIMER; Seville, Spain)
<b>SK-N-SH</b>	Human neuroblastoma cell line	DMEM/ F-12	10 % FCS, 1 % P/S	Kindly provided by Prof Mike Cheetham from the UCL Institute of Ophthalmology (London, UK)
<b>HeLa</b>	Human adenocarcinoma cell line	DMEM (4.5g/L glucose)	10 % FCS, 1 % P/S	Purchased from the American Type Culture Collection (ATCC; VA, USA)
<b>HEK293</b>	Human embryonic kidney epithelial cell line	DMEM (4.5g/L glucose)	10 % FCS, 1 % P/S	Kindly provided by Prof David Hunt from the UCL Institute of Ophthalmology (London, UK)

### 2.3.2 TRANSFECTION

Prior to transfection adherent cells were grown to approximately 90 % of confluence at 37 °C with 5 % CO<sub>2</sub> in a 24-well plate; the growth medium was removed and changed to serum-free media.

The prepared plasmid DNA was diluted in OptiMEM (Life Technologies, CA, USA) in a total volume of 50 µl per well. Simultaneously, Lipofectamine Reagent 2000 (Life Technologies, CA, USA) was diluted in OptiMEM (Life Technologies, CA, USA) in a total volume of 50 µl per well, and incubated at room temperature for five minutes.

The two mixtures were combined and incubated at room temperature for twenty minutes.

The total mixture was added directly into the wells (100 µl per well) containing 500 µl serum-free media. The cells were incubated for four hours at 37 °C with 5 % CO<sub>2</sub>, and the media were changed to the standard growth media supplemented with 10 % FCS and 1 % P/S. The cells were incubated for 24 to 48 hours at 37 °C with 5 % CO<sub>2</sub> prior to fixation.

### **2.3.3 SERUM STARVATION STUDIES**

Human TERT RPE1 cells were cultured on sterile glass coverslips, in 24 well plates, until approximately 50 % confluent (growing in islands). Medium supplemented with 10 % FCS was then replaced with medium containing only 0.25 % FCS, and incubated for 48 hours at 37 °C. The cells were subsequently washed with PBS, and fixed for analysis by immunofluorescence (IF; section 2.6).

### **2.3.4 CELL PROCEDURES SUMMARY**

In summary, the mammalian cell cultures were used for isolation of RNA to clone full-length fragments of the novel interacting partners of TOPORS (Appendix 11.8), for extraction of proteins for validation of expression and PPIs by Western blotting and coIP, respectively (Chapter 6) as well as for delineating the sub-cellular localisation of TOPORS and its novel interacting partners (Chapter 7).

## **2.4 RNA TECHNIQUES**

Following the identification of novel protein interacting partners of TOPORS (experimental Chapter 4), the next objective was to amplify full-length cDNA corresponding to each interacting partner of interest pulled out from the Y2H PPI screen.

For this purpose, RNA was extracted from the human telomerase reverse transcriptase-immortalised retinal pigment epithelial-1 (hTERT-RPE1/hRPE1; ATCC® CRL-4000™) cell line in order to preserve the precious human RNA, purchased from Clontech (CA, USA) for library generation.

The extracted RPE1 RNA was subsequently used for cDNA synthesis, and then for amplification of the preys of interest (Appendix 11.8).

The complementary DNA was also synthesised from the human retinal RNA purchased from Clontech (CA, USA) (originally for library generation) in order to identify potential protein-coding isoforms of the newly-identified protein interacting partners of TOPORS (Chapter 5).

Prior to RNA extraction, the required adherent mammalian cell line was grown in culture until it reached confluence.

#### **2.4.1 RNA EXTRACTION**

Pure Link RNA Mini Kit (LifeTechnologies, CA, USA) was used for RNA isolation from the hRPE1 cell line. Five million cells were used per one procedure of RNA extraction. The manufacturer's protocol was followed, except for minor changes.

The growth medium was removed from cells, and the cells were washed once with PBS. Six hundred microlitres of the Lysis Buffer (provided with the kit), supplemented with 1 %  $\beta$  mercaptoethanol, were added onto the cell monolayer, and the mixture was incubated for seven minutes at room temperature. The cells were subsequently transferred into a 1.5 ml tube, and homogenised by passing fifteen times through an 18-gauge needle attached to a syringe.

One volume of 70 % ethanol was added per one volume of cell homogenate. The homogenate suspension was mixed by vortexing, loaded into the Spin Cartridge with a Collection Tube (provided with the kit; 700  $\mu$ l of sample per tube), and vortexed at top speed for five minutes. Wash Buffer I (350  $\mu$ l per tube) was added to each Spin Cartridge with the bound RNA, and the tubes were centrifuged at top speed for five minutes; the flow-through was discarded, and the Spin Cartridge was transferred into a new Collection Tube.

The RQ1 DNase (Promega, WI, USA; 70  $\mu$ l per tube) mixture (Table 2-57) was added directly onto the Spin Cartridge membrane, and the tubes were incubated at 37 °C for twenty minutes. The samples were then washed with Wash Buffer I (350  $\mu$ l per tube); the tubes were centrifuged at top speed for one minute and the flow-through was discarded.

Alternatively, the RQ1 DNase treatment could have been omitted; a wash with 700  $\mu$ l per sample of Wash Buffer I could have been performed instead prior to the next step. Five hundred microlitres of Wash Buffer II (provided with the kit), supplemented with ethanol



according to instructions, were added per sample, and the tubes were centrifuged at top speed for one minute; this washing step with Wash Buffer II was performed twice.

The tubes were subsequently centrifuged at top speed for one minute to dry the membrane (with the bound DNA) of the Spin Cartridge; the Collection Tube was discarded and the Spin Cartridges were inserted into Recovery Tubes (provided with the kit).

RNAse-Free Water (provided with the kit) was used for elution of the extracted RNA; 30  $\mu$ l were added per sample, and incubated on the membrane for one minute at room temperature. The tubes were then centrifuged at top speed for one minute.

Table 2-57. RQ1 DNase (Promega, WI, USA) mix.

Component	Volume
1 $\mu$ l RQ1 DNase (Promega, WI, USA)	3 $\mu$ l
RQ1 DNase Buffer	7 $\mu$ l
RNAse-free dH <sub>2</sub> O	60 $\mu$ l
Total volume	70 $\mu$ l

#### 2.4.1.1 RNA YIELD EVALUATION

Firstly, the Nanodrop spectrophotometer was used to evaluate the yield of the extracted RNA as well as its purity from protein and organic solvents by measuring absorbance at 260 nm wave length. Subsequently, the RNA sample was analysed by gel electrophoresis.

Prior to the electrophoresis procedure the electrophoresis tank and equipment for agarose gel preparation were sterilised to remove RNAses by soaking them in either 0.4 M NaOH or RNAse Away Reagent (Life Technologies, CA, USA) and thoroughly rinsed with dH<sub>2</sub>O. The gel tray, comb and rubbers were additionally wiped with RNAseZap™ (Sigma-Aldrich, MO, USA) prior to making the agarose gel.

Fresh 1X TAE buffer was prepared using diethylpyrocarbonate (DEPC)-treated water, and it was used for making the 1.2 % agarose gel with ethidium bromide as well as for buffering the electrophoresis reaction; sterile bottles were used.

The RNA sample (400 ng) to be tested was mixed with 1  $\mu$ l of RNAse-free loading dye and with RNAse-free water up to 10  $\mu$ l. The mixture was incubated at 65 °C for five minutes and then it was placed on ice for two minutes. After the two incubation steps, the RNA was subject to electrophoresis at 80 V for approximately one hour. The gel was subsequently visualised and photographed, using a UV Illuminator. If ribosomal RNA bands, corresponding to 28 S, 18 S and

5.0-5.8 S rRNA molecules, were observed, the extracted RNA sample was considered pure and fit for further experiments. If a smear was observed on the agarose gel rather than distinct bands, the RNA was considered degraded and was discarded. The extracted RNA was stored at -80 °C.

#### 2.4.1.2 DNase TREATMENT FOLLOWING RNA EXTRACTION

If no DNase treatment was included during the RNA extraction procedure, the RQ1 DNase (Promega, WI, USA) was used to treat the extracted RNA samples for removal of any residual DNA. One unit of RQ1 DNase was used per 1 µg of treated RNA; the reaction components are summarised in Table 2-58.

Table 2-58. DNase treatment reaction components' list.

Component	Amount
RNA	1-8 µl
RQ1 DNase 10X Reaction Buffer	1 µl
RQ1 DNase	1 u/1 µg of RNA
Nuclease-free water	Up to 10 µl total volume

## 2.4.2 cDNA SYNTHESIS

Complementary DNA was synthesised, using the QuantiTect Reverse Transcription Kit (Qiagen, Netherlands), which involved two major stages:

- Genomic DNA elimination reaction;
- Reverse-transcription reaction.

The manufacturer's instructions were followed with several exceptions.

### 2.4.2.1 GENOMIC DNA ELIMINATION

The template RNA was thawed on ice, and approximately 1 µg was used for cDNA synthesis. The kit components, i.e. gDNA Wipeout Buffer, Quantiscript Reverse Transcriptase, Quantiscript RT Buffer, RT Primer Mix and RNase-free water, were thawed at room temperature. The genomic DNA elimination reaction was prepared on ice (Table 2-59). The reaction was incubated at 42 °C for eight minutes, and then immediately cooled on ice.

Table 2-59. Genomic DNA elimination reaction components.

Table modified from the QuantiTect Reverse Transcription Handbook 03/2009 (Qiagen, Netherlands).

Components	Volume	Final concentration
7X gDNA Wipeout Buffer	2 $\mu$ l	1X
Template RNA	Up to 1 $\mu$ g	n/a
RNAse-free dH <sub>2</sub> O	Up to 14 $\mu$ l	n/a
Total Volume	14 $\mu$ l	n/a

#### 2.4.2.2 *REVERSE-TRANSCRIPTION*

The reverse-transcription reaction was prepared on ice (Table 2-60); total reaction from Table 2-59 was added to the reverse-transcription master mix. The total reaction mixture was incubated for thirty minutes at 42 °C, and inactivated for three minutes at 95 °C. The reaction products were diluted in 20  $\mu$ l RNAse-free dH<sub>2</sub>O and stored at -20 °C prior to further use.

Table 2-60. Reverse-transcription mix.

Table modified from the QuantiTect Reverse Transcription Handbook 03/2009 (Qiagen, Netherlands).

Components	Volume	Final concentration
Quantiscript Reverse Transcriptase with RNAse inhibitor	1 $\mu$ l	n/a
5X Quantiscript RT Buffer with Mg <sup>2+</sup> and dNTPs	4 $\mu$ l	1X
RT Primer Mix	1 $\mu$ l	n/a
Total Volume	6 $\mu$ l	n/a

#### 2.4.2.2.1 *cDNA QUALITY CONTROL*

Control PCR amplifications were performed on the newly synthesised cDNA in order to evaluate its quality. The optimised protocols and reaction components, including the GoTaq Mix (Promega, WI, USA; includes the Taq polymerase, dNTPs, MgCl<sub>2</sub> and reaction buffer) as well as primers, were kindly provided by Dr Giovanna Alfano.

The quality of the synthesised cDNA was evaluated by amplifying a housekeeping gene, *HPRT1* (NM\_000194); expected amplicon: 150 bp. The control PCR for this gene had been optimised using GoTaq Mix (Promega, WI, USA) by Dr Alfano. The reaction components for this amplification are summarised in Table 2-61, and the PCR cycling conditions are given in Table 2-62. The obtained PCR products (10  $\mu$ l) were subject to agarose (1.5 %) gel electrophoresis for thirty minutes at 150 V.

Table 2-61. *HPRT1* amplification reaction mix.

Components	Volume
GoTaq Mix	12.5 µl
<i>HPRT1</i> forward primer	1.0 µl
<i>HPRT1</i> reverse primer	1.0 µl
cDNA	1.0 µl
dH <sub>2</sub> O	9.5 µl
Total volume	25.0 µl

Table 2-62. *HPRT1* amplification PCR cycling conditions.

Temperature	Duration	Number of cycles
95 °C	10 minutes	1
95 °C	30 seconds	33
60 °C	30 seconds	
72 °C	45 seconds	
72 °C	10 minutes	1
4 °C	Final hold	1

The cDNA was also tested for presence of larger genes, such as the homeobox gene *VAX2* (NM\_012476); expected amplicon: 952 bp. The control PCR for this gene had been optimised using GoTaq Mix (Promega, WI, USA) by Dr Giovanna Alfano.

The reaction components for this amplification are summarised in Table 2-63, and the PCR cycling conditions are given in Table 2-64. The obtained PCR products (10 µl) were subject to agarose (1.5 %) gel electrophoresis for thirty minutes at 150 V. The synthesised cDNA was stored at -20 °C.

Table 2-63. *VAX2* amplification reaction mix.

Components	Volume
GoTaq Mix	12.5 µl
<i>VAX2</i> forward primer #2	1.0 µl
<i>VAX2</i> reverse primer #1	1.0 µl
cDNA	1.0 µl
dH <sub>2</sub> O	9.5 µl
Total volume	25.0 µl

Table 2-64. VAX2 amplification PCR cycling conditions.

Temperature	Duration	Number of cycles
95 °C	10 minutes	1
95 °C	30 seconds	40
55 °C	30 seconds	
72 °C	1 minute	
72 °C	10 minutes	
4 °C	Final hold	1

### **2.4.3 PRIMERS FOR AMPLIFICATION OF TRANSCRIPTS OF INTEREST**

The hTERT-RPE1 cDNA was used for amplification of novel interacting partners of TOPORS using flanking PCR primers described in section 2.2.7.1 (these same primers were also used for sequencing). Primers details for *ITM2B*, *PTGDS* and *PSMC1* amplification are given in Tables 2-53, 2-54 and 2-55, respectively. The PCR products amplified from the cDNA using these primers were subsequently used as templates for Gateway cloning using the *attb* primers (section 2.2.5.3: Table 2-42, Table 2-43 and Table 2-44).

### **2.4.4 PRIMERS FOR AMPLIFICATION OF ALTERNATIVE TRANSCRIPTS**

Complementary DNA synthesised from human retinal RNA (Clontech, CA, USA) was used for determination of retinal expression of previously reported protein-coding isoforms of *ITM2B*, *PTGDS* and *PSMC1*.

The following tables and corresponding figures provide an overview of primer binding regions corresponding to specific protein-coding isoforms. The tables also contain primer sequences, the expected amplicon length as well as the PCR names corresponding to specific results in Chapter 5.

Table 2-65. *ITM2B* primer details for isoform amplification to determine retinal expression. Primer names correspond to names in Figure 2-11, and the primer sequences are given in the neighbouring column. Fragments of isoforms expected to be amplified by the designed primers are included; the sizes of fragments, amplified from the expected isoforms are given in brackets. The last column contains a reference to the corresponding PCR result image.

Primer name	Primer Sequence	Expected isoform fragments (size)	PCR name
Ex1F	CTGGGAGGCTGCGAGATCCC	Isoform 001 (918 bp)	ITM2B-1
Ex6R	CTGGCTTCACGTTTCTGAATAC		
Ex1Fb	ATGGTGAAGGTGACGTTCAACT	Isoforms 001 (737 bp) & 003 (419 bp)	ITM2B-2
Ex6R	CTGGCTTCACGTTTCTGAATAC		
Ex1F	CTGGGAGGCTGCGAGATCCC	Isoform 001 (530 bp)	ITM2B-3
Ex3R	CTTCAATTGTCTGGTAGAGAGCAGC		
Ex2F	GACTAGCATTATGCTTGCAGG	Isoform 001 (445 bp) & 003 (127 bp)	ITM2B-4
Ex5R	CGATCAGTAATAACCATGTGCTC		
Ex3F	CAGATGACGTGTACTACTGTGGAAT	Isoform 001 (490 bp)	ITM2B-5
Ex6R	CTGGCTTCACGTTTCTGAATAC		

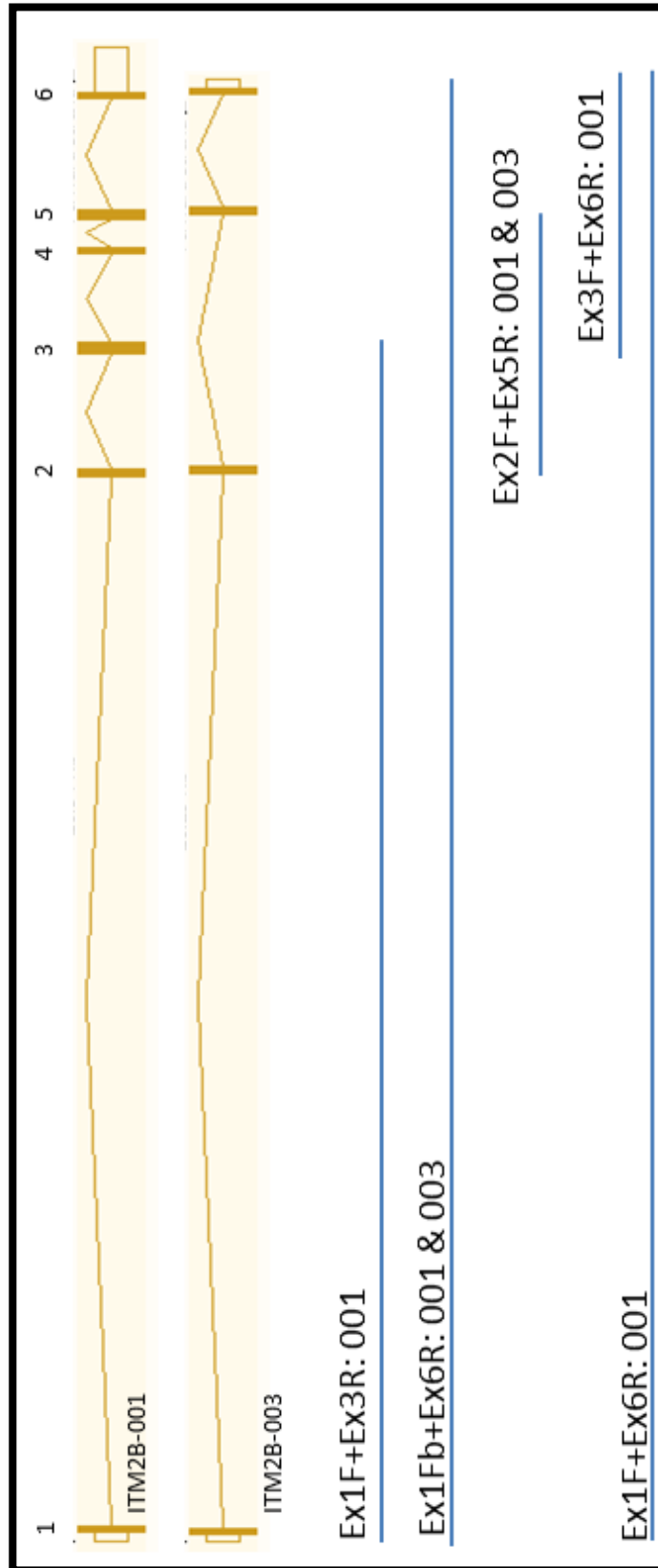


Figure 2-11. Outline of primer sets for amplification of *ITM2B* exons to detect specific isoforms. Isoforms are labelled just with their three-digit numbers. Exons are numbered at the top of each figure, sizes not to scale. See Table 5-1 for amplicon details.

Table 2-66. *PTGDS* primer details for isoform amplification to determine retinal expression. Primer names correspond to names in Figure 2-12, and the primer sequences are given in the neighbouring column. Fragments of isoforms expected to be amplified by the designed primers are included; the sizes of fragments, amplified from the expected isoforms are given in brackets. The last column contains a reference to the corresponding PCR result image (Figure 5-4).

Primer name	Primer Sequence	Expected isoform fragments (size)	PCR name
Ex1F	CTGCAGGAGAATGGCTACTCATC	Isoforms 201 (845 bp) & 001 (743 bp)	PTGDS-1
Ex7R	GACTTGCTTCCGGAGTTTATTG		
Ex1F	CTGCAGGAGAATGGCTACTCATC	Isoform 003, 004, 201 (443 bp)	PTGDS-2
Ex3RII	CTCCCACCCCATGGATCTCC		
Ex1F	CTGCAGGAGAATGGCTACTCATC	Isoform 004 (560 bp)	PTGDS-3
Ex3Rb	GGCTCCAGAGAGGATCCAACC		
Ex2F	GTTGTCCATGTGCAAGTCTGTGG	Isoforms 201 (462 bp), 001 (391 bp) & 005 (360 bp)	PTGDS-4
Ex5R	GGCAGGAAGACAATGGTATCCTCTG		
Ex2Fb	GGAGACCGGAGGAGTAGACG	Isoform 005 (624 bp)	PTGDS-5
Ex7Rb	GAGCAGAGACATCCAGAGCG		
Ex3F	CCAGTGTGAGACCCGAACC	Isoforms 201 (418 bp) 001 (316 bp) 005 (313 bp)	PTGDS-6
Ex6R	CTATTGTTCCGTCATGCACTTAT		
Ex3Fb	CACTTGCCGGGACGACTC	Isoforms 201 & 003 (213 bp)	PTGDS-7
Ex5Rb	TCTCCTTAACTCAGCCCTG		
Ex4F	GCAGCACCTACTCCGTGTCAG	Isoforms 201 (399 bp) & 001 (396 bp)	PTGDS-8
Ex7R	GACTTGCTTCCGGAGTTTATTG		
Ex5F	CCATTGTCTTCTGCCCC	Isoforms 201, 001 (207 bp) & 008 (363bp)	PTGDS-9
Ex7R	GACTTGCTTCCGGAGTTTATTG		



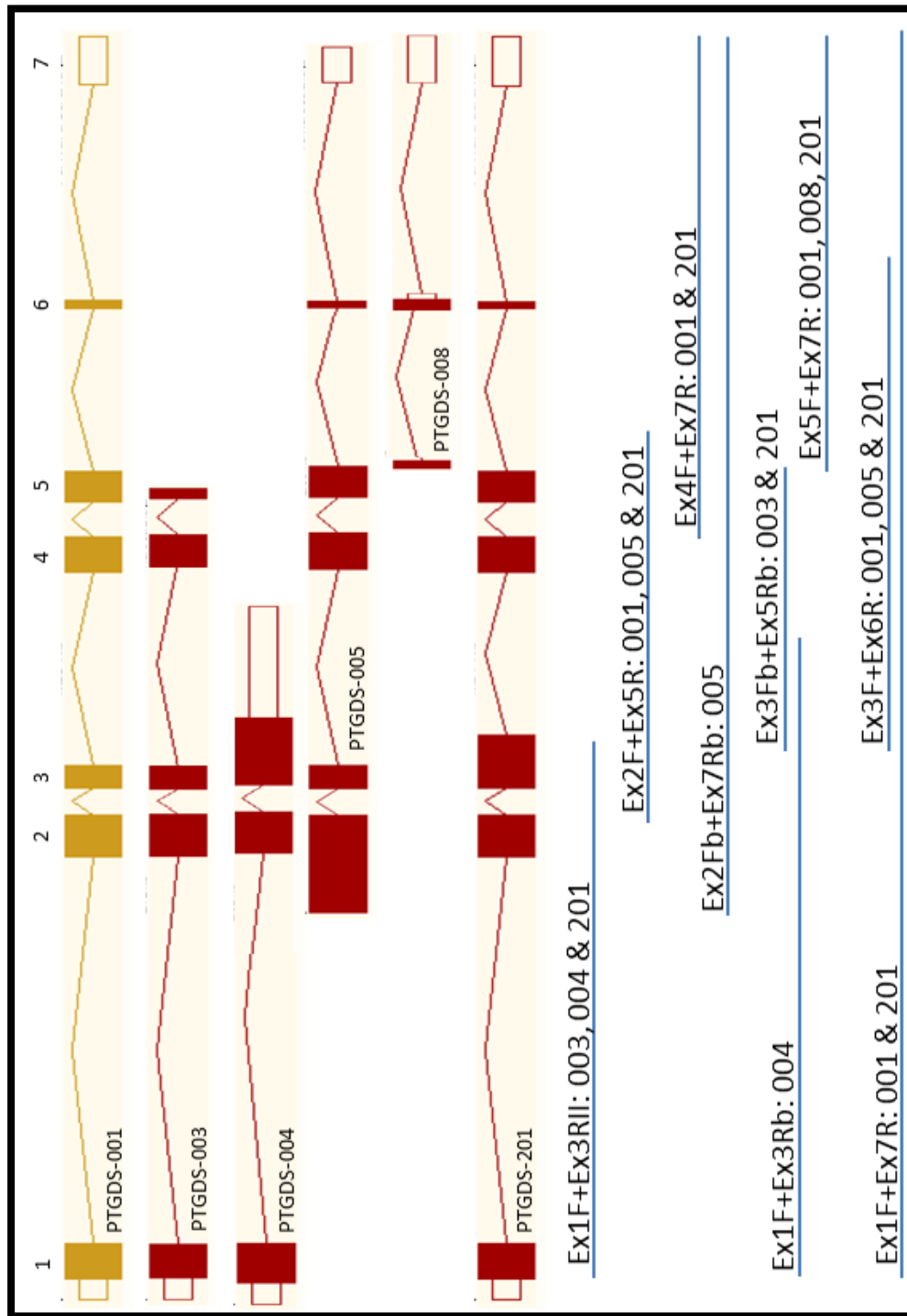


Figure 2-12. Outline of primer sets for amplification of *PTGDS* exons to detect specific isoforms. Isoforms are labelled just with their three-digit number. Exons are numbered at the top of each figure, sizes not to scale. See Table 5-2 for primer details.

Table 2-67. *PSMC1* primer details for isoform amplification to determine retinal expression. Primer names correspond to names in Figure 2-13, and the primer sequences are given in the neighbouring column. Fragments of isoforms expected to be amplified by the designed primers are included; the sizes of fragments, amplified from the expected isoforms are given in brackets. The last column contains a reference to the corresponding PCR result image.

Primer name	Primer Sequence	Expected fragments (size)	isoform	PCR name
Ex1F	GCTCAAGTGGCCAAGGCAAG	Isoform (1495 bp), (1237 bp)	001	PSMC1-1
Ex11R	GGCACTTACACATCGTACTCC		002	
Ex1F	GCTCAAGTGGCCAAGGCAAG	Isoform 001 (476 bp), 002 (379 bp) & 004 (67 bp)		PSMC1-2
Ex5R	GAGCAGGACCGAGCAGCCA			
Ex2F	CAGAGTGGTGGTCATGGTCC	Isoform 001 (520 bp), 002 (423 bp)		PSMC1-3
Ex6R	TTTCTACCTTCATCACTGTGACC			
Ex3F	GGGACCAGATGCTGCCAGC	Isoforms 001 (569 bp)		PSMC1-4
Ex7R	CTGTGCCAGGTGGACCATAGAGAA			
Ex5F	GATGTCAGTAGGAACCTTGG	Isoforms 001 & 002 (714 bp)		PSMC1-5
Ex9R	GGTCTGATAAGTGCTGGAT			
Ex8F	GAACTTATTCAGAAGTACCTAGGTG	Isoforms 001 & 002 (715 bp)		PSMC1-6
Ex11R	GGCACTTACACATCGTACTCC			

#### 2.4.5 RNA PROCEDURES SUMMARY

In summary, the RNA procedures were used, firstly, for amplification of cDNA corresponding to the novel protein interacting partners of TOPORS (Appendix 11.8), and subsequently for identification of their isoforms in the human retina (Chapter 5).

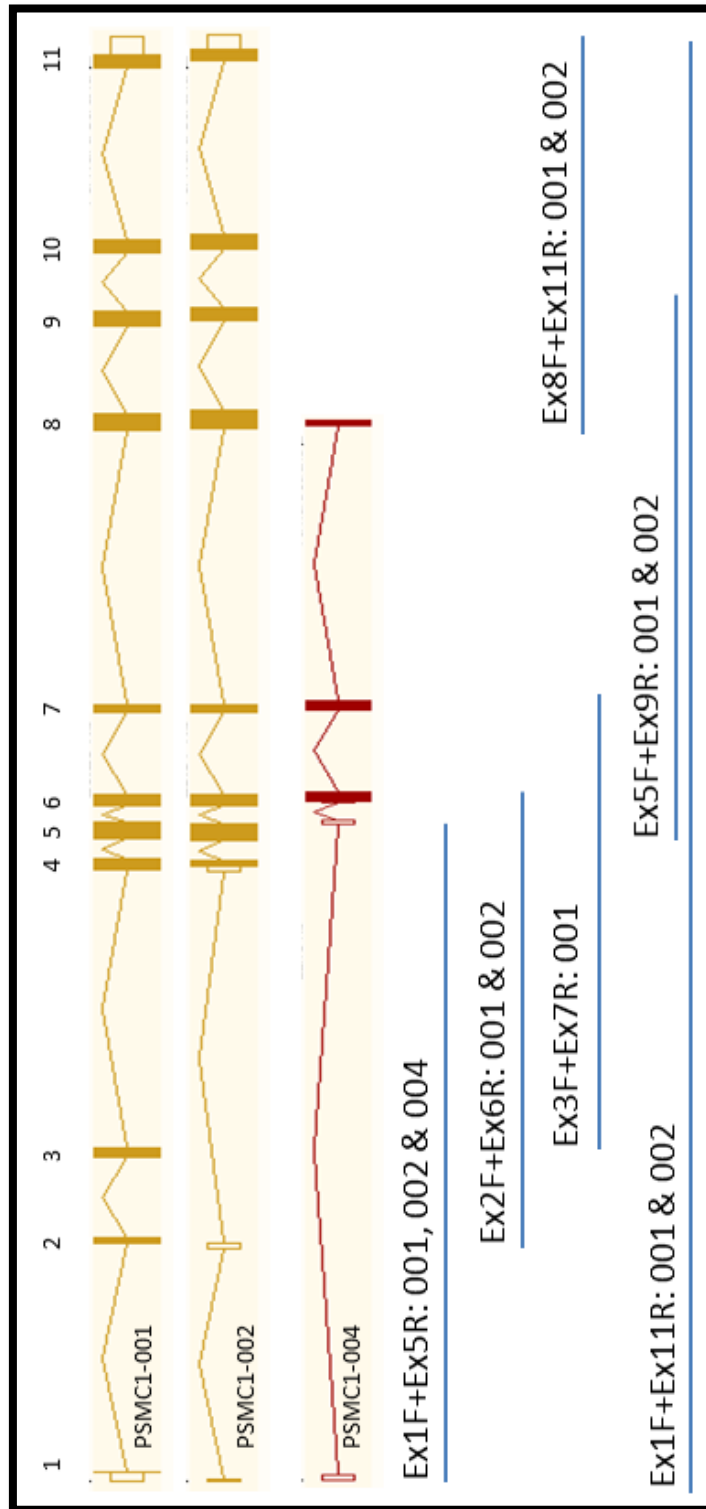


Figure 2-13. Outline of primer sets for amplification of *PSMC1* exons to detect specific isoforms. Isoforms are labelled just with their three-digit numbers. Exons are numbered at the top of each figure, sizes not to scale. See Table 5-3 for primer details.

## **2.5 PROTEIN TECHNIQUES**

Proteins evaluated throughout the project were extracted from mammalian as well as *Saccharomyces cerevisiae* yeast cells (section 2.1.7: details on preparation of protein samples from yeast cells. Analysis of mammalian protein lysates was described in Chapter 6.

### **2.5.1 PREPARATION OF PROTEIN SAMPLES**

Following the validation of PPIs in yeast, protein expression and PPI studies were performed using mammalian cell lines. The purpose of these experiments was to demonstrate that the human proteins, shown to interact when exogenously expressed in yeast, are also expressed and associate with each other in native conditions, i.e. human cells. The robust HeLa cell line, originating from a cervix adenocarcinoma, was used for these studies.

Total mammalian cell protein extracts were prepared using a Tx100-based buffer with an added mixture of protease and phosphatase inhibitors (Table 2-68); when available the ProteaseArrest™ (G Biosciences, MO, USA) reagent was used as an alternative to the individual protease inhibitors.

The cell culture dish with cells was placed on ice and the cells were washed with ice-cold PBS. The PBS was removed and the cells were then lysed, using 1 ml of the lysis buffer (Table 2-68) per 100-mm dish.

Cells were subsequently scraped off with a pre-cooled plastic cell scraper, and the resulting suspension was transferred into a pre-cooled micro-centrifuge tube. The suspension was incubated in the lysis buffer at 4°C for thirty minutes with gentle agitation. The suspension was then centrifuged at 4°C for ten minutes at the maximum speed.

The supernatant was divided into aliquots on ice, and stored at -80 °C. The pellet was discarded. Five microliters of each extract were kept for concentration determination, using the Novagen® BCA Assay (Merck Group, Darmstadt, Germany).

### **2.5.2 SDS-POLYACRYLAMIDE GEL ELECTROPHORESIS**

Proteins were separated using sodium dodecyl sulphate polyacrylamide gel electrophoresis (SDS-PAGE) with a discontinuous, 1X TRIS/glycine/SDS buffered system. For this purpose 10x Tris/Glycine/SDS #161-0772 (BioRad, CA, USA) was purchased and diluted with dH<sub>2</sub>O. For the purposes of this study, 7.5 % or 12 % gels were routinely used.

Table 2-68. Lysis buffer for protein extraction from human cell lines.

<b>Buffer basis</b>	150 mM NaCl
	1 % Triton X-100
	50 mM Tris
<b>Protease inhibitors</b>	10 µg/ml Aprotinin
	10 µg/ml Leupeptin hemisulphate
	10 µg/ml Pepstatin A
	50 µg/ml Benzamidine hydrochloride
	1 mM PMSF
<b>Phosphatase inhibitors</b>	50 mM NaF
	3 mM Na <sub>4</sub> P <sub>2</sub> O <sub>7</sub>
	1 mM Na <sub>3</sub> VO <sub>4</sub>
<b>Solvent</b>	Sterile dH <sub>2</sub> O

The resolving gel mixture was prepared in a fume cupboard with: 7.25 ml sterile, deionised water (dH<sub>2</sub>O) and 3.75 ml acrylamide for 7.5 % gels; or 6 ml sterile dH<sub>2</sub>O and 5 ml acrylamide for 12 % gels; followed by 3.75 ml TRIS (pH 8.8), 150 µl SDS, 100 µl 10 % (w/v) APS and 25 µl TEMED (Sigma-Aldrich, MO, USA) in that order and mixed thoroughly. The stacking gel comprised: 3 ml sterile water, 0.625 ml acrylamide, 1.25 ml TRIS (pH 6.8), 50 µl SDS, 30 µl 10 % (w/v) APS and 10 µl TEMED (Sigma-Aldrich, MO, USA) (Table 2-19). Protein samples were denatured at 95 °C for ten minutes prior to loading. Gels were subject to electrophoresis until suitable separation of the marker had been achieved, typically at 100 V, 3 A, 30 W for one hour. Precision Plus Protein Standards (BioRad, CA, USA) was used as a marker for protein band size estimation.

Table 2-69. SDS-PAGE gel composition.

	Resolving gel: 7.5 %	Resolving gel: 12 %	Stacking gel
<b>dH<sub>2</sub>O</b>	7.25 ml	5.00 ml	3.00 ml
<b>30% acrylamide</b>	3.75 ml	6.00 ml	625 µl
<b>1.5M Tris, pH 8.8</b>	3.75 ml	3.75 ml	-
<b>0.5 M Tris, pH 6.8</b>	-	-	1.25 ml
<b>10% (w/v) SDS</b>	150 µl	150 µl	50 µl
<b>10% (w/v) APS</b>	100 µl	100 µl	30 µl
<b>TEMED</b>	<b>25 µl</b>	<b>25 µl</b>	10 µl

### 2.5.3 WESTERN BLOTTING

Proteins were transferred onto a nitrocellulose membrane using a semi-dry transfer system; the transfer buffer was prepared using 20 % methanol in the SDS-

Table 2-70. Transfer buffer.

	Volume
<b>10x Tris/Glycine/SDS</b>	100 ml
<b>Methanol</b>	200 ml
<b>dH<sub>2</sub>O</b>	700 ml

PAGE running buffer (Table 2-70).

Transfer was carried out at 25 V, 3 A and 30 W for between thirty minutes and an hour depending on the size of protein of interest.

The membrane was then blocked overnight at 4 °C with agitation (60 rpm; Stuart Mini orbital shaker SSM1, Bibby Scientific Limited, UK), using 5 % milk (The Co-op, UK) in TBS–0.1 % (v/v) Tween-20 (Sigma-Aldrich, MO, USA) (Table 2-71).

Table 2-71. Western blotting (WB) blocking buffer.

	Volume
<b>10x Tris-buffered saline (TBS)</b>	10 ml
<b>Tween20</b>	0.1 ml
<b>Dried non-fat milk</b>	5 g
<b>dH<sub>2</sub>O</b>	89.9 ml

Membranes were incubated with the primary antibody at room temperature for two to four hours with agitation (60 rpm; Stuart Mini orbital shaker SSM1, Bibby Scientific Limited, UK); the antibody was diluted according to the manufacturer's instructions in blocking solution.

Membranes were washed in TBS-0.1 % Tween-20 (TBS-T; four times for ten minutes each time), and were then incubated for 45 minutes with the HRP (horse-radish peroxidase) conjugated secondary antibody (diluted 1/5000 in TBS-0.1 % Tween-20) at room temperature (Table 2-72).

Table 2-72. TBS-T solution.

	Volume
<b>10x TBS</b>	100 ml
<b>Tween20</b>	1.00 ml
<b>dH<sub>2</sub>O</b>	899 ml

Membranes were washed in TBS-0.1 % Tween-20 (five times for five minutes each time), and then in TBS only (twice for five minutes each time) prior to visualisation using the ECL development reagent (Amersham Bioscience, GE Healthcare, UK), according to the manufacturer's instructions.

Exposure time varied according to the strength of the signal; Super RX X-ray film (FujiFilm Europe GmbH, Germany) was used for imaging, using SRX-101A X-ray developer (Konica Minolta Medical Imaging U.S.A., Inc).

#### **2.5.4 CO-IMMUNO-PRECIPIATION**

Recombinant Protein G Agarose beads (Life Technologies, CA, USA) were washed with TBS, and 100 µl were added to a sample, containing the cellular lysate pre-incubated with the mouse monoclonal anti-TOPORS antibody (Abnova) for one hour at 4 °C; this was then incubated for 30' at 4 °C. The tube was centrifuged at 13000 rpm for ten minutes (Centrifuge 5417R, Eppendorf, Germany) and the supernatant was removed, and the beads were washed three times with 1 % Triton-X100 in phosphate-buffered saline (PBS).

Laemmli Sample buffer was added to the sample, and heated to 70 °C for ten minutes. The supernatant was then loaded on to SDS-PAGE gels for analysis.

## 2.5.5 PROTEIN METHODS SUMMARY

In summary, the protein methods, described in this section, were implemented in the experimental Chapter 6.

## 2.6 IMMUNOCYTOCHEMISTRY

Following the validation of PPIs between TOPORS and its novel interacting partners, identified using the Y2H system and confirmed by co-immuno-precipitation from human cell lines, the sub-cellular localisation of the novel proteins needed to be evaluated (Chapter 7).

Immunofluorescent (IF) staining studies of TOPORS, its identified interacting partners, and marker proteins were performed using human cell lines (section 2.3.1).

### 2.6.1 METHODS OF FIXATION: ADHERENT CELLS

Cells were cultured in 24-well plates on 12 mm sterilised cover slips until they reached 50-60 % confluence, unless stated otherwise. Prior to fixation the cells were washed with PBS, and fixed using paraformaldehyde (PFA)/Triton X-100 (Tx100) or methanol.

#### 2.6.1.1 PFA/Tx100 FIXATION

In order to preserve cellular morphology, the PFA/Tx100 method was used, as PFA acts by forming cross-links between proteins, thus maintaining the structure.

The cells were fixed for twenty minutes in 4 % PFA in 1x PBS at room temperature (500 µl per well). They were subsequently incubated in the permeabilisation solution (4 % Tx100 and 0.3 % BSA in 1x PBS) for five minutes at room temperature (300 µl per well).

The cells were washed twice in immunocytochemistry (ICC) blocking buffer (0.5 % bovine serum albumin (BSA) & 20 mM glycine in 1x PBS; Table 2-73), followed by incubation in the blocking buffer for fifteen minutes.

Table 2-73. ICC blocking buffer.

	Volume
<b>0.58 % BSA</b>	1.16 g
<b>33.3 mM glycine</b>	0.5 g
<b>1x PBS</b>	200 ml

The fixed cells were either immediately immuno-stained, or stored at 4 °C in an evaporation-proof container.

### 2.6.1.2 METHANOL FIXATION

Methanol fixation was used for preserving cytoskeletal proteins, rather than maintaining the overall morphology of the cells.

Ice-cold methanol (-20 °C) was added to each well (500 µl per well), and the 24-well plate was incubated at -20 °C for five minutes. The methanol was removed and the cells were washed with 1x PBS twice, and rehydrated with 1x PBS for five minutes at room temperature.

The fixed cells were then incubated in the blocking buffer (0.5 % BSA & 20 mM glycine in 1x PBS) for fifteen minutes prior to immuno-staining or storage at 4 °C.

### 2.6.2 IMMUNOFLUORESCENT STAINING OF CELLS

The primary antibodies (1 ° Ab) were diluted according to the manufacturer's instructions in blocking buffer (0.5 % BSA & 20 mM glycine in 1x PBS). Cover slips with the fixed cells were incubated with 1 ° Ab at room temperature for one hour; the cover slips were then washed three times for ten minutes in blocking buffer with gentle agitation.

The corresponding fluorescent secondary antibodies (2 ° Ab; diluted 1:300 in blocking solution unless stated otherwise) were added, and the cells were incubated for 45 minutes at room temperature protected from exposure to light; the cover-slips were subsequently washed three times for ten minutes in blocking buffer.

A nuclear stain (Hoechst or DAPI) was added onto the coverslips and the cells were incubated for ten minutes at room temperature protected from exposure to light; the cover-slips were subsequently washed twice for ten minutes in 0.1 % Tween20 in 1x PBS, and once for ten minutes in 1x PBS.

The cells were then briefly stored in 1x PBS before mounting onto slides using ProLong Gold Antifade Mounting Medium (Life Technologies, CA, USA), or DAKO Fluorescence Mounting Medium (Agilent Technologies, CA, USA).

### 2.6.3 IMMUNOCYTOCHEMISTRY SUMMARY

In summary, methods, described in this section, were implemented in the experimental Chapter 7, in order to determine the sub-cellular (co)localisation of TOPORS and its novel interacting partners identified via the Y2H screen.



## **2.7 IMMUNOHISTOCHEMISTRY**

The ultimate aim of this project was to determine why mutations in *TOPORS*, which is ubiquitously expressed, are known to cause disease only in the retina. Consequently, once it was confirmed that TOPORS and its novel interacting partners, associate and co-localise in cultured human cells, an attempt was made to investigate the localisation of these proteins in the retina, i.e. the only tissue known to be affected by *TOPORS* mutations (experimental Chapter 8).

Immunofluorescent staining studies were performed on mouse (*Mus musculus*) and macaque (*Macaca fascicularis*) retinal cryo-sections. Mouse eyes (strain C 57 Black 6 (C57Bl6) were kindly provided by Nozie (Dominic) Aghaizu (from a two-week-old mouse), Ewa Kubała (from mice aged 7-9 weeks) and Dr Kate Powell (from 6.5-month-old mouse). Primate (young adult macaque) retinal sections were kindly provided by Professor Glen Jeffery.

### **2.7.1 MOUSE EYE TREATMENT FOLLOWING ENUCLEATING**

For each animal the left eye was intended for future extraction (of either protein or RNA), and, therefore, was frozen down on dry ice in a 2 ml tube immediately after being enucleated, whereas the right eye was intended for cryo-sectioning, i.e. it was washed in and immersed in ice-cold 1x PBS in a 15 ml tube (kept on ice) prior to paraformaldehyde (PFA) fixation.

The eyes were stored in ice cold 1x PBS prior to fixation for ten to thirty minutes, depending on the number of animals and transfer time from the animal house to the laboratory.

Additionally, a fragment of tail was taken from each animal and placed in a 1.5 ml tube, kept on ice, for genotyping, or sequencing, if required.

The 2 ml tubes with eyes frozen for RNA or protein extraction and the 1.5 ml tubes with tail fragments were stored at -80 °C.

### **2.7.2 FIXATION AND CRYO-SECTIONING**

This procedure was performed in a fume extraction cupboard. The ice-cold 1x PBS was removed from the 15 ml tubes, and 5 ml of 4 % PFA in 1x PBS were added per tube. The eyes were fixed for 24 hours at 4 °C with gentle shaking.

The following day the 4 % PFA solution was discarded, and the eyes were subject to sucrose gradient using freshly prepared 20 % sucrose in 1x PBS (8 ml per tube) for 4-8 hours at

4 °C with gentle shaking. This solution was then discarded and followed by incubation overnight at 4 °C with gentle shaking in freshly prepared 30 % sucrose in 1x PBS (8 ml per tube).

The following day the 30 % sucrose solution was discarded. Freshly prepared 30 % sucrose in 1x PBS solution was mixed at 1:1 ratio with the Optimal Cutting Temperature (OCT) medium (VWR International, PA, USA). Each eye was then incubated in this mixture for two hours at room temperature. The eyes were subsequently positioned in embedding molds, filled with OCT, and frozen immediately on dry ice. The fixed, embedded eyes were permanently stored -80 °C.

Prior to cryo-sectioning, an embedded eye was transferred to -20 °C for an overnight incubation. The eyes were sectioned using a Leica CM1850 cryostat (Leica Biosystems, Germany) at a thickness of 10 µm, and collected on positively-charged Superfrost slides (VWR International, PA, USA). The slides were stored at -80 °C.

### 2.7.3 IMMUNOFLUORESCENT STAINING OF TISSUE CRYO-SECTIONS

Prior to immuno-staining, sections were thawed out and allow to dry in a fume extraction cupboard; they were subsequently washed with 1x PBS without shaking three times for ten minutes each time to remove excess OCT. Next, the sections were blocked for one hour at room temperature.

Depending on the origin of the secondary antibody (2° Ab) to be used two different immunohistochemistry (IHC) blocking buffers (Table 2-74) were used: either 6 % bovine serum albumin (BSA), 5 % normal goat serum (NGS) & 0.3 % Tween20 in 1x PBS (blocking buffer A); or 5 % normal donkey serum (NDS) & 0.3 % TritonX-100 (Tx100) in 1x PBS (blocking buffer B).

Table 2-74. IHC blocking buffers.

Table A. NGS-based IHC blocking buffer.

	Amount
6 % BSA	0.6 g
5 % NGS	500 µl
0.3 % Tween20	30 µl
1x PBS	9.47 ml

Table B. NDS-based IHC blocking buffer.

	Amount
5 % NDS	500 µl
0.3 % Tween20	30 µl
1x PBS	9.47 ml

After incubation in the blocking buffer, primary antibodies (1° Abs) were diluted in the blocking buffer according to manufacturers' instructions, the sections were encircled with

a hydrophobic pen (Dako Pen, Agilent Technologies, CA, USA), and the relevant 1° Ab dilutions were applied within the circled areas. The sections were incubated with the 1° Ab in a humidified chamber overnight at 4 °C, followed by one-hour incubation at room temperature.

The slides were then washed three times for ten minutes each with gentle shaking at room temperature. If blocking buffer A was used, the washes were performed with 0.1 % Tween20 in 1x PBS, whereas if blocking buffer B was used, the washes were performed with 0.3 % Tx100 in 1x PBS.

The fluorescent 2° Abs were diluted in the relevant blocking buffers according to manufacturers' instructions, and the sections were incubated with the 2° Abs in a dark humidified chamber for 45 minutes at room temperature.

If the sections were being stained with peanut agglutinin (PNA) to mark the cone photoreceptors, this dye was applied at the same time as the 2° Abs. These steps, and those following, were all performed in an environment protected from light.

The slides were then washed twice for ten minutes each time, with gentle agitation at room temperature, protected from light. As previously, if blocking buffer A was used, the washes were performed with 0.1 % Tween20 in 1x PBS; if blocking buffer B was used, the washes were performed with 0.3 % Tx100 in 1x PBS.

Next the slides were washed once for ten minutes in 1x PBS, gently shaking at room temperature, protected from light. Following this, the tissue sections were subject to nuclear staining using 4', 6-Diamidino-2-phenylindole dihydrochloride (DAPI; Sigma-Aldrich, MO, USA), diluted 1/10000 in 1x PBS, for ten minutes at room temperature.

Finally the slides were washed three times for ten minutes each time in 1x PBS with; the washes were performed with gentle shaking at room temperature.

The slides were then dried, and coverslips were mounted above the stained tissue sections using DAKO Fluorescence Mounting Medium (Agilent Technologies, CA, USA), and sealed with nail polish.

#### **2.7.4 ANTIGEN RETRIEVAL**

Sometimes the staining method, described in section 2.7.3, would yield no signal, suggesting that antigen epitopes were not available to the corresponding antibody. In order to expose

the antigens, the citrate-buffered Antigen Unmasking Solution (pH 6.0; Vector Laboratories, CA, USA) was used. After the first three 1x PBS washes (section 2.4.1.2), the slides were submerged in 1x Antigen Unmasking Solution (diluted in 1x PBS) in a 200 ml glass container with a lid. The container was then placed in a microwave oven (Model AM925EFP, Morphy Richards, UK) and boiled: at 80 % power (P80) for three minutes, at 50 % power (P50) for five minutes and at 10 % power (P10) for ten minutes. After the boiling steps the glass container was allowed to cool down for fifteen minutes at room temperature. The sections were then washed once for thirty minutes in 1x PBS at room temperature, following which they were blocked for one hour at room temperature, and the staining procedure was followed as described in section 2.7.3.

### 2.7.5 IMMUNOHISTOCHEMISTRY SUMMARY

In summary, the immunohistochemistry methods were implemented in the experimental Chapter 8. This allowed for defining the (co)localisation of TOPORS and its novel interacting partners in the retina, i.e. the tissue affected by retinitis pigmentosa.

### 2.8 SUMMARY OF ANTIBODIES

The antibodies were used for determining protein expression and interaction (Chapter 5) as well as localisation in cells (Chapter 7) and tissues (Chapter 8). All primary antibodies were purchased from commercial providers (Table 2-75). The Clontech antibody against GAL4 DNA-BD (630403) was validated by the manufacturer by SDS-PAGE and Western blotting.

Table 2-75. Primary Antibodies.

Cat. No.	Manufacturer	Raised in	Raised against
<b>630403</b>	Clontech	Mouse	Yeast GAL4 DNA-BD
<b>H00010210-M01</b>	Abnova	Mouse	Human TOPORS
<b>sc-292009</b>	Santa Cruz Biotechnology	Rabbit	Human TOPORS
<b>AP13163b</b>	Abgent	Rabbit	Human ITM2B C-term
<b>HPA029292</b>	Sigma-Aldrich	Rabbit	Human ITM2B
<b>sc-30067</b>	Santa Cruz Biotechnology	Rabbit	Human PTGDS
<b>HPA000872</b>	Sigma- Aldrich	Rabbit	Human PSMC1
<b>sc-27794</b>	Santa Cruz Biotechnology	Goat	Human Centrin-2
<b>sc-50164</b>	Santa Cruz Biotechnology	Goat	Human PCM1
<b>ab2642</b>	Abcam	Goat	Human PLK4
<b>sc-803</b>	Santa Cruz Biotechnology	Rabbit	6His Probe

The Abnova anti-TOPORS antibody (H00010210), used in this project, was previously validated by Chakarova *et al.* (2007; 2011), who showed the antibody detects no TOPORS signal following knock-down by siRNA. TOPORS was shown to localise, in hTERT-RPE1, MDCK, ARPE19 and IMCD3 cell lines, to centrosomes and basal bodies as well as the mid-body (Flemming body; in addition to the previously demonstrated nuclear localisation). In the retina of mouse, pig and human TOPORS was detected at the basal body of primary cilium and the nuclei of retinal ganglion cells. On immunoblots the antibody detected a band migrating at 150 kDa following separation of human lymphoblastoid lysates (Figure 1-13). The antibody was also used by Yang *et al.* (2010) for Western blotting.

The SCB anti-TOPORS antibody (sc-292009) was validated by the manufacturer by Western blotting on nuclear extracts from HeLa, Jurkat, K-562, HEL92.1.7 and IMR-32 cells as well as a whole cell lysate from NTERA-2 cl. D1 cells. The antibody detected a band migrating half-way between the 110 kDa and 222 kDa markers in all of the tested samples.

The Abgent anti-ITM2B C-term antibody (AP13163b) was validated by the manufacturer. Western blot analysis of mouse cerebellum and lung tissue lysates detected bands migrating half-way between 36 kDa and 55 kDa markers. In the lung lysate an extremely faint additional band was also observed half-way between the 55 kDa and 72 kDa markers.

The Sigma-Aldrich anti-ITM2B antibody (HPA029292) was used for protein characterisation for the Human Protein Atlas, demonstrating granular, perinuclear staining in human U-251MG cell line. Western blot analysis showed two bands migrating between the 36 kDa and 55 kDa markers (lysate from HEK293T cells over-expressing ITM2B). The antibody was also used by Audo *et al.* (2013) who demonstrated reactivity in the ganglion cell layer of mouse retina (in addition to less strong signal in inner nuclear layers). Cytoplasmic localisation was shown by immunocytochemistry. Baron *et al.* (2014) showed granular cytoplasmic staining and immunoreactive bands at 47 kDa and 50 kDa.

The SCB anti-PTGDS antibody (sc-00067) validation by the manufacturer demonstrated cytoplasmic staining in HeLa cells and a cryo-section of normal mouse intestine. Chatterjee *et al.* (2012) demonstrated, using the antibody of interest, that PTGDS is expressed in mast cells lining the mesenteric lymphatic vessels, whereas Lim *et al.* (2015) used it for immunohistochemical studies of female reproductive tract.

The Sigma-Aldrich anti-PSMC1 antibody (HPA000872) was used for protein characterisation for the Human Protein Atlas, demonstrating localisation in the nucleus (excluding the nucleoli) and

the cytoplasm in U-2 OS, U-251MG and A-431 cell lines. Western blotting on protein extracts from RT4, U-251MG and A-431 cells as well as liver and tonsil showed a band migrating about a quarter of the way from the 49 kDa marker to the 85 kDa marker (however the band was much fainter in the latter two lysate samples); an additional band was detected in the A-431 lysate at 85 kDa.

The SCB anti-Centrin2 antibody (sc-27794) was used by Cunningham *et al.* (2014) who demonstrated that just over a third of Centrin-2 signal in HeLa cells is centrosomal. Centrin-2 knock-down by siRNA additionally validated antibody specificity.

The SCB anti-PCM1 antibody (sc-50164) was validated by the manufacturer demonstrating by Western blotting a 228 kDa band in lysates from U-562 and Ramos cells.

The Abcam anti-PLK4 antibody (ab2642) was validated by the manufacturer who showed a band migrating at 110 kDa (lysate from normal human colon), which was also showed by Syed *et al.* (2006). Martindill *et al.* (2007) demonstrated localisation at nucleoli in Rcho-1 cells at the G2/M transition phase. On the other hand, Rosario *et al.* (2014) demonstrating, using this same antibody, localisation of PLK4 to tips of protrusions in motile and spreading mouse embryonic fibroblasts; whereas in spreading HeLa cells the protein was observed at cell boundaries/periphery.

The SCB anti-six histidines (6 His) tag antibody (sc-803) was validated by the manufacturer by Western blot. It was also used by Vulsteke *et al.* (2004), providing additional evidence for its specificity to this probe.

A summary of previously reported localisations of each protein, detected by the above-mentioned antibodies (other than against the six histidine tag), is given in Table 2-76). Secondary antibodies used for immunofluorescence (IF) and Western blotting (WB) studies are summarised in Table 2-77. The antibodies were employed in Section 3.2, Appendix 11.4 as well as Chapters 6, 7 and 8.

Table 2-76. Reported immunocytochemical localisation of investigated proteins and markers.

Protein localisation	Sub-cellular	Tissue
<b>TOPORS (topo-isomerase I-binding, serine- and arginine-rich, E3 ubiquitin and SUMO1 ligase; Q9NS56)</b>	Nucleus (excluding nucleoli; including PML bodies and nuclear speckles) (Haluska <i>et al.</i> , 1999; Rasheed <i>et al.</i> , 2002). Centrioles and centrosome; ciliary basal body; $\gamma$ tubulin complex; mid-body; spindle pole (Chakarova <i>et al.</i> , 2011). Ubiquitin ligase complex (Rajendra <i>et al.</i> , 2004; Capelson e Corces, 2005; Guan <i>et al.</i> , 2008); SUMO1 ligase complex (Boutell, Orr e Everett, 2003; Weger, Hammer e Heilbronn, 2005; Pungaliya <i>et al.</i> , 2007). Cell boundaries/periphery (in mouse) (Braun <i>et al.</i> , 2012). Nuclear lamina (in fruit fly) (Capelson e Corces, 2005; Matsui <i>et al.</i> , 2011).	Basal body of photoreceptor connecting cilium; nuclei of retinal ganglion cells (Chakarova <i>et al.</i> , 2011).
<b>ITM2B (integral membrane protein 2B; Q9Y287)</b>	Intracellular membranes; cell membrane (Choi <i>et al.</i> , 2001; Martin <i>et al.</i> , 2008; Fluhrer <i>et al.</i> , 2012). Golgi/TGN membranes; intracellular and secretory vesicles (Choi <i>et al.</i> , 2004). Mitochondrial membrane (Fleischer, Ayllon e Rebollo, 2002). Neuronal processes (Akiyama <i>et al.</i> , 2004). Pre-synaptic terminals (Saul <i>et al.</i> , 2013). Synaptic membranes (Matsuda, Tamayev e D'adamio, 2011; Tamayev <i>et al.</i> , 2011). Peri-nuclear (Berglund <i>et al.</i> , 2008). Extracellular space/secreted <sup>9</sup> (Martin <i>et al.</i> , 2008; Tsachaki <i>et al.</i> , 2011).	Retinal ganglion cell layer (GCL); retinal inner nuclear layer (Audo <i>et al.</i> , 2013). Blood vessels of nervous system; pancreas and myocardium (pathological ABri deposits) (Ghiso <i>et al.</i> , 2001; Holton <i>et al.</i> , 2001).

<sup>9</sup> The protein is cleaved at three sites by three proteases resulting in some of its fragments remaining membrane-bound, and others being targeted for secretion (and putatively other cellular locations).

Protein localisation	Sub-cellular	Tissue
<p><b>PTGDS</b> <b>(lipocalin-type, glutathione-independent, prostaglandin D2 synthase; P41222)</b></p>	<p>Peri-nuclear localisation (Berglund <i>et al.</i>, 2008). Cytoplasm; peri-nuclear cytoplasmic granules (Beuckmann <i>et al.</i>, 2000). Endoplasmic reticulum and nuclear envelope (Urade <i>et al.</i>, 1989). Golgi apparatus (Grabenhorst e Conradt, 1999). Ganglion cell membrane (ganglioside-associated) (Mohri <i>et al.</i>, 2006). Extracellular space/secreted: Cerebrospinal fluid (Harrington <i>et al.</i>, 1993; Hoffmann <i>et al.</i>, 1993; Tumani <i>et al.</i>, 1998; Sampaio <i>et al.</i>, 2009). Sub-retinal fluids (in detached retinae) (Jaggi <i>et al.</i>, 2008). Amniotic fluid (Melegos, Yu e Diamandis, 1996; Shiki <i>et al.</i>, 2004). Serum (Dorta-Contreras <i>et al.</i>, 1998; Cheung <i>et al.</i>, 2013). Urine (pathological) (Hoffmann, Nimtz e Conradt, 1997; Nagata <i>et al.</i>, 2009; Tin <i>et al.</i>, 2013).</p>	<p>Retina (chick) (Yamakawa e Ogino, 1986). Retinal pigment epithelium (chick and rat) (Beuckmann <i>et al.</i>, 1996; Shiroma <i>et al.</i>, 1996). Interphotoreceptor space; photoreceptor cells (rat) (Beuckmann <i>et al.</i>, 1996). Cerebral cortex (Mohri <i>et al.</i>, 2006). Leptomeninges; choroid plexus (Beuckmann <i>et al.</i>, 2000). Testis (Ujihara <i>et al.</i>, 1988; Fouchécourt, Dacheux e Dacheux, 1999; Wu <i>et al.</i>, 2012; Shyu <i>et al.</i>, 2013; Sreenivasulu <i>et al.</i>, 2013). Spleen (Urade, Fujimoto, Ujihara, <i>et al.</i>, 1987).</p>



Protein localisation	Sub-cellular	Tissue
<b>SMC1 (26 S protease regulatory subunit 4; P62191)</b>	Cytoplasm; nucleus (N-myristoylation-dependent (Kimura, Kato e Hirano, 2012)), but not nucleolus; cell junctions (Berglund <i>et al.</i> , 2008). Proteasome (ATPase hexa-ring of the regulatory subunit) (Müller <i>et al.</i> , 2006; Bedford <i>et al.</i> , 2008; Kim e Demartino, 2011; Lee <i>et al.</i> , 2011). Endoplasmic reticulum (ER)-associated degradation (ERAD) (Lipson <i>et al.</i> , 2008). Membrane/acrosome <sup>10</sup> (Yi <i>et al.</i> , 2009). Plant nucleosome assembly complex (Lee <i>et al.</i> , 2011; Lee, K. H. <i>et al.</i> , 2012).	n/a
<b>Centrin-2 (P41208)</b>	Centriole and centrosome cytoplasm; xeroderma pigmentosum group C complex (Araki <i>et al.</i> , 2001). Centriole (Salisbury <i>et al.</i> , 2002). Centrosome (Martinez-Sanz <i>et al.</i> , 2006; Cunningham <i>et al.</i> , 2014). Ciliary basal body (UniProtKB).	n/a
<b>PCM1 (peri-centriolar material 1; A2RUU9)</b>	Peri-centriolar (Kubo <i>et al.</i> , 1999). Centrosome; nuclear membrane; cytoplasm (Berglund <i>et al.</i> , 2008).	n/a
<b>PLK4 (polo-like kinase 4; O00444)</b>	Centrosome; nucleus; vesicles (Berglund <i>et al.</i> , 2008). Centriole (Habedanck <i>et al.</i> , 2005; Kuriyama, 2009). Deuterosome (Klos Dehring <i>et al.</i> , 2013; Zhao <i>et al.</i> , 2013). Acentriolar spindle poles and membrane (Coelho <i>et al.</i> , 2013). Nucleoli (Martindill <i>et al.</i> , 2007).	n/a

<sup>10</sup> The acrosome is cap-like structure over the anterior half of the sperm's head. As the sperm approaches the zona pellucida of the egg, which is necessary for initiating the acrosome reaction, the membrane surrounding the acrosome fuses with the plasma membrane of the oocyte, exposing the contents of the acrosome.

Table 2-77. Secondary Antibodies.

Key: Fitc, fluorescein; Cy3, Cyanine 3; A488, Alexa Fluor 488; A594, Alexa Fluor 594; HRP, horse-radish peroxidase; IF, immunofluorescence; WB, Western blotting. Specificity was verified during each individual experiment by control staining of fixed cells or tissue sections, which were not pre-stained with any primary antibody.

Cat. No.	Manufacturer	Raised in	Raised against	Tagged with	Application
<b>715-095-151</b>		Donkey	Mouse	Fitc	IF
<b>711-095-152</b>	Jackson Immuno	Donkey	Rabbit	Fitc	IF
<b>705-095-147</b>	Research	Donkey	Goat	Fitc	IF
<b>715-165-150</b>	Laboratories, Inc.	Donkey	Mouse	Cy3	IF
<b>711-165-152</b>	(PA, USA)	Donkey	Rabbit	Cy3	IF
<b>705-165-003</b>		Donkey	Goat	Cy3	IF
<b>A11001</b>		Goat	Mouse	A488	IF
<b>A11008</b>		Goat	Rabbit	A488	IF
<b>A11005</b>	Life Technologies	Goat	Mouse	A594	IF
<b>A11034</b>	(CA, USA)	Goat	Rabbit	A594	IF
<b>A11055</b>		Donkey	Goat	A488	IF
<b>A11058</b>		Donkey	Goat	A594	IF
<b>115-035-003</b>	Jackson Immuno	Goat	Mouse	HRP	WB
<b>111-035-003</b>	Research	Goat	Rabbit	HRP	WB
<b>305-035-003</b>	Laboratories, Inc. (PA, USA)	Donkey	Goat	HRP	WB

## 2.9 MICROSCOPIC IMAGING

Immunofluorescent samples were imaged using either fluorescent or confocal microscopy (experimental Chapters 7 and 8). Fluorescent microscopy imaging was performed using Zeiss Axiovert S100 inverted microscope (Carl Zeiss AG, Germany) and the corresponding software. All data were collected sequentially, using the same microscope settings. The resulting images were processed, using Adobe Photoshop CS4 (Adobe Systems, CA, USA). Confocal microscopy imaging was performed using the Zeiss laser scanning microscope (LSM) 700 and the LSM Software (Carl Zeiss AG, Germany). All data were collected sequentially, using the same microscope settings. The resulting images were processed, using ZEN 2012 (blue edition; Carl Zeiss AG, Germany). The microscopic imaging techniques were implemented in experimental Chapters 7 and 8.

## 2.10 SUMMARY

Chapter 2 provided details of all methods used in the project with references to specific experimental chapters given in individual methods sections. The subsequent Chapters 3-8 include empirical data generated throughout the time course of the project. Chapters 9, 10 and 11 comprise the final Discussion, Bibliography and the Appendix, respectively.

### **3 CONSTRUCTION OF RETINAL LIBRARIES AND TOPORS BAITs**

The primary aim of the project was to identify novel interacting protein partners of TOPORS from the human retina. *TOPORS* is ubiquitously expressed, yet its mutations are only known to cause disease in the retina. Hence it was hypothesised that TOPORS must have a retina-specific interacting partner, or it must participate in a retina-specific metabolic and/or signalling pathway, the impairment of which results in retinal degeneration.

In the retina TOPORS protein was shown to localise to the basal body of the rod photoreceptor connecting cilium (Chakarova *et al.*, 2011). The rod cells serve as photon receptors in dim light, in addition to mediating peripheral vision; along with cones they comprise the first order neurons involved in the transduction of visual signals (retina structure diagram: Figure 1-2). The signals then need to be conducted via the bipolar and the ganglion cells to the brain for processing, which, in addition to changes in membrane potentials, will also involve synaptic transmitter release and binding. This process will involve tightly controlled PPIs, demonstrating their importance of inter-cellular protein-protein interactions (PPIs) in signal transduction. For instance, following the release of glutamate by photoreceptor synapses, its binding to receptors on the post-synaptic bipolar cells is in itself an example of a PPI<sup>11</sup> essential to retinal physiology.

PPIs are equally important for intracellular signalling and metabolism, for which the photoreceptor cells provide perfect evidence. The cells comprise inner and outer segments (Figure 1-3), which results in the need for protein trafficking between these two compartments. TOPORS itself was shown to reside at the bottle-neck of this transport pathway at the base of the connecting cilium. Hence, it has been believed that *TOPORS* mutations lead to RP by impairing the entry and/or exit of proteins from the cilium. Furthermore, since TOPORS is known to possess E3 ubiquitin and SUMO1 ligase activities, this is very definite evidence for its central role in mediating protein interactions, and being directly involved in regulating the destiny of proteins modified by either ubiquitin or SUMO1.

Identification of protein(s) from the retina, which interact with TOPORS, may help elucidate the part *TOPORS* plays in retinal homeostasis, and thus the putative disease mechanism. This understanding may then have wider implications for developing future therapies for retinal degeneration triggered by *TOPORS* mutations.

---

<sup>11</sup> In this example, it needs to be assumed that 'amino acid' and 'protein' are synonymous.

In proteomics, identification of protein interactions is usually performed using one of two very distinct methods: either a mass spectrometry-based analysis of protein complexes, or a screen of a cDNA library to detect direct binary interactions (reviewed in: Brückner *et al.*, 2009). Performing yeast two-hybrid (Y2H) screens against human retina cDNA libraries, using TOPORS bait constructs, was the method selected for this project.

The yeast two-hybrid (Y2H) method for detecting protein-protein interactions was pioneered by Fields and Song (1989), who demonstrated the advantageous properties of GAL4, a protein, which, in its endogenous environments, acts as a transcriptional activator of galactose utilisation genes in the yeast *Saccharomyces cerevisiae* (section 2.1 in Methods and Materials).

### 3.1 HUMAN RETINAL cDNA LIBRARY CONSTRUCTION AND CHARACTERISATION

Two human retinal cDNA libraries were constructed in the Y187 *Saccharomyces cerevisiae* yeast strain of mating type alpha (*Mata*), using the ‘Make Your Own “Mate & Plate” Library System’ (Clontech, CA, USA), which utilises the SMART™ technology (Zhu *et al.*, 2001).

The cDNA library was generated from commercially available total human retina RNA (Clontech, CA, USA) according to the manufacturer’s instructions.

#### 3.1.1 cDNA SYNTHESIS

First strand cDNA was generated using the SMART technology. The cDNA was amplified by long distance PCR (LD PCR), and purified using CHROMA SPIN TE-400 columns (select for DNA molecules larger than 0.2 kb). Prior to the purification process products of the LD PCR were subject to agarose gel (1.2 %) electrophoresis. Inserts larger than 0.2 kb were expected, which was indicated by the smear observed on the agarose gel after the electrophoresis (Figure 3-1).

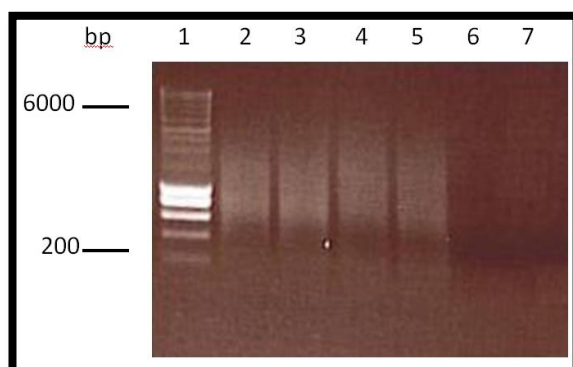


Figure 3-1. SMART cDNA synthesis results. 1.2 % agarose gel with ethidium bromide. Lane 1: marker: Hyper Ladder I. Lanes 2-3: oligo-dT-primed cDNA samples. Lanes 4-5: random-primed cDNA samples. Lane 6: Negative control for oligo-dT-primed PCR. Lane 7: Negative control for random-primed PCR. Expected sizes irrespective of primers: 0.2-6.0 kb.

### 3.1.2 YEAST TRANSFORMATION WITH cDNA FRAGMENTS

Two to five micrograms of cDNA were required for library transformation. Two cDNA libraries were constructed as described in section 2.1.8. The amount of cDNA used for construction of each one of the libraries was approximately 5 µg after the CHROMA-spin purification process:

- Oligo-dT-primed → 4.6 µg
- Oligo-dT-primed → 2.7 µg & random-primed → 2.8 µg (~1:1)

Purified double-stranded cDNA and linearised pGADT7-Rec vector were transformed into the Y187 yeast strain using the library-scale transformation procedure (section 2.1.3.2.2); the cultures were spread on approximately one hundred agar media plates (150 mm) per library. The cDNA amplicons were incorporated into the pGADT7-Rec plasmid *in vivo* using the endogenous homologous recombination machinery of the yeast. The cells were then harvested, and stored at -80 °C as 1 ml (short-term) and 50 ml (long-term) aliquots (summarised in Figure 3-2).

Transformation efficiency and number of independent clones were calculated according to Equation 2.3 and Equation 2.4, respectively. A library should only be harvested, if the number of independent clones is above  $1.0 \times 10^6$ . The obtained numbers of independent clones in both libraries are equal to or just above this threshold. The titre and cell density were calculated using Equation 2.5 and Equation 2.6, respectively; the obtained numbers represent the number of colonies and cells, respectively, per 1 ml of library (Table 3-1).



Figure 3-2. Human retinal cDNA library construction in the Y187 yeast strain.

Figure from Make Your Own "Mate & Plate™" Library System User Manual (PT4085-1; Clontech, CA, USA).

Table 3-1. Retinal cDNA library quantitative results.

	Oligo-dT library	Oligo-dT + random library
<b>Transformation efficiency</b>	1.8 X 10 <sup>5</sup> cfu/μg (of transformed DNA)	1.3 X 10 <sup>5</sup> cfu/μg (of transformed DNA)
<b>No. of Independent clones</b>	1.9 X 10 <sup>6</sup>	1.0 X 10 <sup>6</sup>
<b>Titre</b>	(6.6 X 10 <sup>6</sup> cfu/ml)	(6.1 X 10 <sup>6</sup> cfu/ml)
<b>Cell density</b>	43.8 X 10 <sup>7</sup> cells/ml	41.5 X 10 <sup>7</sup> cells/ml

### 3.1.3 RETINAL cDNA LIBRARY CHARACTERISATION AND VALIDATION

Single colonies were picked from the cDNA library transformation plates and re-patched on fresh media. During the initial evaluation of the cDNA libraries 42 plasmids were isolated from each one of the two libraries, using the Easy Yeast Plasmid Isolation Kit (Clontech, CA, USA; section 2.1.6.1 in Methods and Materials). These plasmids were then subject to PCR, resulting in generation of 23 amplicons (~55 %) from the oligo-dT-primed (O-dT) library and 35 amplicons (~83 %) from the random-&-oligo-dT-primed (R&O-dT) library (Figure 3-3). On average the insert size in O-dT library was 315 base pairs (bp), whereas in the R&O-dT library it was 444 bp. The isolated plasmids were subsequently sequenced, and the results submitted to genome browsers, such as BLAT (UCSC) and BLAST (NCBI); search results with the highest percentage identity were always selected for further analysis.

Outcomes varied slightly depending on the database used, and are summarised in Table 3-2 for the O-dT clones and in Table 3-3 for the R&O-dT clones.

Among the 23 O-dT clones 14 showed no matches in either of the databases. One had no matches in the UCSC database, but it aligned with a human transcript in the NCBI database (highlighted in blue in Table 3-2). The remaining sequences all aligned with various fragments of the human genome, however, according to the UCSC browser, only three of them were exonic protein-coding sequences (two highlighted in magenta in Table 3-3); only one of the three transcripts (green) was in frame with the GAL4 AD sequence.

Among the 35 R&O-dT clones seven showed no matches in the UCSC database; three of these seven sequences aligned with human DNA according to the NCBI database (highlighted in blue in Table 3-3). The remaining sequences aligned with fragments of the human genome, however, according to the UCSC browser, only three of them were protein-coding transcripts

(two are highlighted in magenta in Table 3-3); only one of these three transcripts (green) was in frame with the GAL4 AD sequence.

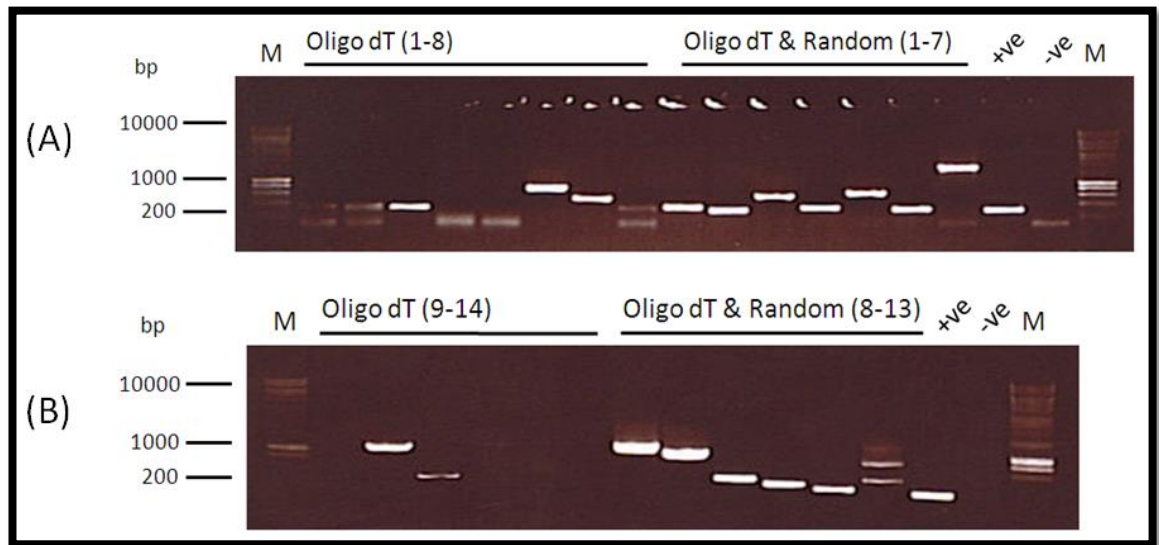


Figure 3-3. Selection of the human retinal cDNA library amplicons.

(A) Lanes 1 and 19: marker: Hyper Ladder I. Lanes 2-9: samples 1-8 isolated from the oligo-dT-primed cDNA library clones. Lanes 10-16: samples 1-7 isolated from the oligo-dT-&-random-primed cDNA library clones. Lane 17: positive control: empty pGADT7-Rec vector. Lane 18: negative control. (B) Lanes 1 and 16: marker: Hyper Ladder I. Lanes 2-7: samples 9-14 isolated from the oligo-dT-primed cDNA library clones. Lanes 8-13: samples 8-13 isolated from the oligo-dT-&-random-primed cDNA library clones. Lane 14: positive control: empty pGADT7-Rec vector. Lane 15: negative control.

Furthermore, the PCR and sequencing results collectively showed that the O-dT library contained a high proportion of sequences, which had no matches in either of the human genome databases, only 14/23 clones (61 %) were identifiable. The remaining nine aligned with protein-coding genes, but, except for three, which aligned with untranslated region (UTR) and/or intronic regions.

Sequencing of the R&O-dT library fragments showed that only four of the 35 clones (11 %) had no matches in either database. The remaining proportion of the tested sequences revealed fragments of protein-coding genes; however, they also comprised mostly UTR and intronic regions.

This preliminary evaluation of both libraries showed that clones of the R&O-dT library appear more likely to contain inserts. Based on this outcome, the R&O-dT library was subsequently characterised in more depth. In order to increase the throughput and lower the cost of library testing, the Yeast ‘Smash & Grab DNA’ method (section 2.1.6.2 in Methods and Materials), based on a protocol optimised by Rose *et al.* (1990), was used to extract total DNA from

the yeast clones. Vector-specific primers were then used to amplify inserts from the library plasmids, and the resulting PCR products were purified and sequenced. The UCSC genome browser was used to identify the cDNA fragments.

Table 3-2. Oligo-dT-primed library (O-dT) fragments.

Key to colour coding: blue, fragments aligning with annotated transcripts in the NCBI database, but not in the UCSC database; magenta, protein-coding fragments not in frame with GAL4 AD; green, protein-coding fragments in frame with GAL4 AD. In addition to inserts included in the table, 14 other clones were sequenced and showed no matches in either database.

BLAT (UCSC)	BLAST (NCBI)
No matches	Homo sapiens mRNA; cDNA DKFZp779E152 (from clone DKFZp779E152)
Chr. 15: Homo sapiens ribosomal protein, large, P1 (RPLP1), transcript variant 1, mRNA.	Homo sapiens ribosomal protein, large, P1, mRNA (cDNA clone IMAGE:3864103)
Chr. 9: 3' UTR of Homo sapiens endoglin (ENG), transcript variant 3, mRNA.	Homo sapiens endoglin (ENG), transcript variant 1, mRNA
Chr. 15: Homo sapiens ribosomal protein, large, P1 (RPLP1), transcript variant 1, mRNA.	Homo sapiens ribosomal protein, large, P1, mRNA (cDNA clone IMAGE:3864103)
Homo sapiens ribosomal protein S2 (RPS2), mRNA.	Homo sapiens mRNA similar to collagen, type XVII, alpha 1 (cDNA clone IMAGE:5431129)
Chr. 3: Intronic region of Homo sapiens PEST proteolytic signal containing nuclear protein (PCNP), mRNA.	Homo sapiens ribosomal protein S18 pseudogene 5 (RPS18P5) on chromosome 3
Chr. 12: Intronic region of Homo sapiens TAO kinase 3 (TAOK3), mRNA.	PREDICTED: Homo sapiens ribosomal protein S2 (RPS2), transcript variant X1, mRNA
Chr. 1: Intronic region of Homo sapiens HFM1, ATP-dependent DNA helicase homolog (S. cerevisiae) (HFM1), mRNA.	Chain 5, Structure Of The H. Sapiens 60s rRNA
Chr. 12: Intronic region of Homo sapiens chromobox homolog 5 (CBX5), transcript variant 3, mRNA.	Homo sapiens SH2B adaptor protein 3 (SH2B3), RefSeqGene on chromosome 12

Table 3-3. Random-&-oligo-dT-primed library (R&O-dT) fragments.

Key to colour coding: blue, fragments aligning with annotated transcripts in the NCBI database, but not in the UCSC database; magenta, protein-coding fragments not in frame with GAL4 AD; green, protein-coding fragments in frame with GAL4 AD. In addition to inserts included in the table, four other clones were sequenced and showed no matches in either database.

BLAT (UCSC)	BLAST (NCBI)
No matches	Homo sapiens mRNA; cDNA DKFZp686C06106 (from clone DKFZp686C06106)
Chr. 4: Intronic region of Homo sapiens UDP-N-acetyl-alpha-D-galactosamine:polypeptide N-acetylgalactosaminyltransferase-like 6 (GALNTL6), mRNA.	Homo sapiens FOSMID clone ABC8-40969800B21 from chromosome unknown, complete sequence
Chr. M: Homo sapiens mRNA expressed only in placental villi, clone SMAP47, encoding mitochondrial rRNA.	Homo sapiens haplogroup U4a3 mitochondrion, complete genome
Homo sapiens RNA, tRNaseZL-interacting RNA B1.	Homo sapiens RNA, 45S pre-ribosomal 5 (RNA45S5), ribosomal RNA
Chr. 11: 5'UTR Homo sapiens MT-RNR2-like 8 (MTRNR2L8), mRNA.	Homo sapiens mRNA; cDNA DKFZp686B0995 (from clone DKFZp686B0995)
Chr. 5: Intronic region of Homo sapiens SH3 and PX domains 2B (SH3PXD2B), mRNA.	Homo sapiens SH3 and PX domains 2B (SH3PXD2B), RefSeqGene on chromosome 5



BLAT (UCSC)	BLAST (NCBI)
Chr. 10: Intronic region of Homo sapiens La ribonucleoprotein domain family, member 4B (LARP4B), mRNA.	Human DNA sequence from clone RP11-363N22 on chromosome 10, complete sequence
Chr. 16: Intronic region of Homo sapiens LUC7-like (S. cerevisiae) (LUC7L), transcript variant 1, mRNA.	Homo sapiens interleukin 9 receptor (IL9Rps) pseudogene, complete sequence
Homo sapiens uncharacterized LOC100507412 (LOC100507412), non-coding RNA.	Homo sapiens RNA, 45S pre-ribosomal 5 (RNA45S5), ribosomal RNA
No matches	Human DNA sequence from clone RP11-142J11 on chromosome 6, complete sequence
Chr. 11: Intronic region of Homo sapiens zinc finger and BTB domain containing 16 (ZBTB16), transcript variant 1, mRNA.	Homo sapiens zinc finger and BTB domain containing 16 (ZBTB16), RefSeqGene on chromosome 11
Homo sapiens cDNA FLJ38039 fis, clone CTONG2013934. mRNA AK095358	PREDICTED: Homo sapiens WD repeat and FYVE domain containing 2 (WDFY2), transcript variant X1, mRNA
Chr. 1: Homo sapiens TSNAX-DISC1 read-through (TSNAX-DISC1), transcript variant 1, non-coding RNA.	Homo sapiens disrupted in schizophrenia 1 (DISC1), RefSeqGene on chromosome 1
Chr. 10: Intronic region of Homo sapiens inositol polyphosphate-5-phosphatase, 40kDa (INPP5A), mRNA.	Human DNA sequence from clone RP11-500B2 on chromosome 10, complete sequence
Homo sapiens uncharacterized LOC100507412 (LOC100507412), non-coding RNA.	Chain 5, Structure Of The H. Sapiens 60s rRNA
Chr. 2: 3' UTR of Homo sapiens endothelial PAS domain protein 1 (EPAS1), mRNA.	Homo sapiens endothelial PAS domain protein 1 (EPAS1), RefSeqGene on chromosome 2
Chr. 11: Intronic region of Homo sapiens pleckstrin homology domain containing, family A member 7 (PLEKHA7), mRNA.	Homo sapiens FOSMID clone ABC9-43939000016 from chromosome 11, complete sequence
Chr. 3: Intronic region of Homo sapiens microtubule-associated protein 4 (MAP4), transcript variant 4, mRNA.	Homo sapiens chromosome 3 clone RP11-1029M24, complete sequence
Homo sapiens uncharacterized LOC100507412 (LOC100507412), non-coding RNA.	Homo sapiens RNA, 45S pre-ribosomal 5 (RNA45S5), ribosomal RNA
Homo sapiens RNA, tRNaseZL-interacting RNA B1.	Homo sapiens mRNA; cDNA DKFZp686C06106 (from clone DKFZp686C06106)
Homo sapiens RNA, tRNaseZL-interacting	Homo sapiens isolate CEss737 18S ribosomal RNA gene, partial sequence
Homo sapiens RNA, tRNaseZL-interacting RNA B1.	Homo sapiens RNA, 45S pre-ribosomal 5 (RNA45S5), ribosomal RNA
Chr. 2: Homo sapiens chromosome 2 open reading frame 71 (C2orf71), mRNA.	Homo sapiens chromosome 2 open reading frame 71 (C2orf71), mRNA
No matches	Homo sapiens mRNA; cDNA DKFZp779E152 (from clone DKFZp779E152)
Chr. 8: Unannotated region	Homo sapiens chromosome 8, clone RP3-388N13, complete sequence
Chr. 11: Homo sapiens transgelin (TAGLN), transcript variant 2, mRNA.	Homo sapiens transgelin (TAGLN), transcript variant 1, mRNA
Homo sapiens uncharacterized LOC100507412 (LOC100507412), non-coding RNA.	Homo sapiens RNA, 45S pre-ribosomal 5 (RNA45S5), ribosomal RNA
Chr. 1: Intronic region of Homo sapiens HFM1, ATP-dependent DNA helicase homolog (S. cerevisiae) (HFM1), mRNA.	Homo sapiens RNA, 45S pre-ribosomal 5 (RNA45S5), ribosomal RNA
Chr. 12: Intronic region of Homo sapiens chromobox homolog 5 (CBX5), transcript variant 3, mRNA.	Homo sapiens 12 BAC RP11-968A15
Chr. 1: Unannotated region	Human DNA sequence from clone CH507-528H12 on chromosome 21, complete sequence
3'UTR of Homo sapiens kelch-like family member 21 (KLHL21), mRNA.	Homo sapiens kelch-like 21 (Drosophila), mRNA (cDNA clone IMAGE:6577755)

Plasmids were isolated from over six hundred clones (Appendix 11.1), leading to identification of several genes associated with retinal function and homeostasis (Table 3-4). The retina specificity of the R&O-dT human cDNA library was further validated by identification of the rhodopsin-encoding gene, *RHO* (MIM#180380; RefSeq: NM\_000539; UniProt: P08100).

Collectively, the results from Tables 3-3 and 3-5 show that 117 of the library inserts, found among the total 668 clones (i.e. 17.5 %), aligned with known protein-coding sequences. Retinal association could be found for eleven of these protein-coding inserts (Table 3-4); this is equivalent to 1.6 % (11/668) of total library inserts, and approximately 9.4 % (11/117) of all identified protein-coding sequences. Three (0.4 %) retinal sequences, which did not align with protein-coding exons, were also identified. Complementary DNA (cDNA) sequences of human mRNA molecules, described in published literature, made up 2.5 % (17 of 668) of the total library fragments, similarly to the expressed sequence tags (ESTs), which comprise 2.4 % (16 of 668) of the fragments. Unannotated chromosomal regions aligned with 41 of the 668 library clones (6.1 %). Intronic regions and 3' UTRs comprise 152 (22.8 %) and 67 (10.0 %) of the cDNA library fragments, respectively. *Homo sapiens* uncharacterized LOC100507412 (LOC100507412), non-coding RNA, was found in 16.8 % of clones (112 of 668). Nine inserts contained mitochondrial mRNA, encoding ribosomal RNA (rRNA), which, according to the UCSC search results, is expressed only in placental villi. Twenty nine sequences (4.3 %; other than LOC100507412 or the mitochondrial rRNA) aligned with annotated sequences, which did not code for proteins. Ninety five searches (14.2 %) generated no matches at all (Table 3-5 and Appendix 11.1).

Despite a high proportion of non-protein-coding inserts, the constructed human retina cDNA library was used for subsequent Y2H screens due to its content of retinal transcripts. Even though a human brain cDNA library was available for contingencies, it was crucial that retina-specific proteins are expressed for the purpose of testing the main hypothesis (section 1.10).

It was essential to analyse the content of the constructed retinal library thoroughly enough to allow for an objective subsequent interpretation of Y2H PPI screen results.

Table 3-4. Genes from the R&O-dT human cDNA library associated with the retina. Information regarding retinal relevance of the identified genes was obtained from the UCSC and/or UniProt databases, unless a reference is included. Protein-coding sequences are highlighted in green.

Clone no <sup>12</sup> .	BLAT (UCSC) highest score result	RefSeq & UniProt IDs	Relevance to retina
71	Chr. 1: Intronic region of Homo sapiens phosducin (PDC), transcript variant 1, mRNA.	NM_002597, P20941	Potential regulation of visual phototransduction, or photoreceptor metabolism; forms a complex with beta and gamma subunits of transducin. Preferentially expressed in retina.
83			
101	Chr. 9: Homo sapiens prostaglandin D2 synthase 21kDa (brain) (PTGDS), mRNA.	NM_000954, P41222	Catalyses the conversion of PGH2 to PGD2; binds small non-substrate lipophilic molecules, including retinal and retinoic acid; potential secretory retinoid and thyroid hormone transporter; possibly involved in development and maintenance of the blood-brain, blood-retina, blood-aqueous humour and blood-testis barrier; potentially important for maturation and maintenance of the CNS. Preferentially expressed in brain.
107			
144	Chr. 10: Intronic region of Homo sapiens retinal G protein coupled receptor (RGR), transcript variant 1, mRNA.	NM_002921, P47804	Receptor for all-trans- and 11-cis-retinal. Binds preferentially to the former and may catalyse the isomerization of the chromophore by a retinochrome-like mechanism.
182	Chr. 18: Last exon and 3'UTR of Homo sapiens transthyretin (TTR), mRNA.	NM_000371, P02766	Thyroid hormone-binding protein. Interacts with RBP4. About 40% of plasma transthyretin circulates in a tight protein-protein complex with the plasma retinol-binding protein (RBP).
199	Chr. 11: Bicistronic gene (two non-overlapping reading frames): Homo sapiens C1q and tumour necrosis factor related protein 5 (C1QTNF5), transcript variant 1, mRNA & Homo sapiens membrane frizzled-related protein (MFRP), mRNA.	NM_015645; Q9BXJ0, Q9BY79	C1QTNF5 – associated with autosomal dominant late-onset retinal degeneration. MFRP – associated with: Nanophthalmos 2: Rare autosomal recessive disorder of eye development; Microphthalmia, isolated, 5: A disorder characterized by posterior microphthalmia, retinitis pigmentosa, foveoschisis and optic disc drusen.
223	Chr. 19: Last exon and 3'UTR of Homo sapiens retinol dehydrogenase 8 (all-trans) (RDH8), mRNA.	NM_015725, Q9NYR8	A visual cycle enzyme located in the photoreceptor OS (aka photoreceptor retinol dehydrogenase): reduces all-trans-retinal to all-trans-retinol (requires NADPH) - a rate-limiting step in the rhodopsin regeneration pathway

<sup>12</sup> A full list of identified library clones is included in Appendix 11.6.

Clone no <sup>12</sup> .	BLAT (UCSC) highest score result	RefSeq & UniProt IDs	Relevance to retina
264	Chr. 1: 3' UTR of Homo sapiens opticin (OPTC), mRNA.	NM_014359.3, Q9UBM4	Opticin is present in significant quantities in the vitreous of the eye and also localizes to the cornea, iris, ciliary body, optic nerve, choroid, retina, and foetal liver. The opticin gene is mapped to a region of chromosome 1 that is associated with the inherited eye diseases age-related macular degeneration (AMD) and posterior column ataxia with retinosa pigmentosa (AXPC1).
269	Chr. 12: Homo sapiens premelanosome protein (PMEL), transcript variant 1, mRNA.	NM_001200054, P40967	Photobleaching of RPE melanosomes makes RPE more sensitive to light-induced cytotoxicity; possibly, aged melanosomes increase RPE cell photic stress, contributing to impaired tissue function and to degeneration of the adjacent retina (Zareba <i>et al.</i> , 2007)
331 342	Chr. 3: Homo sapiens rhodopsin (RHO), mRNA.	NM_000539, P08100	Rod photoreceptor-specific protein rhodopsin.
403	Chr. 2: Homo sapiens S-antigen; retina and pineal gland (arrestin) (SAG), mRNA.	NM_000541, P10523	One of major proteins of rod photoreceptor OS, which binds to photoactivated-phosphorylated rhodopsin; associated with night blindness and RP.
515	Chr. 11: Homo sapiens bestrophin 1 (BEST1), transcript variant 1, mRNA.	NM_004183, O76090	Predominantly expressed in the basolateral membrane of RPE; associated with retinal dystrophies

Table 3-5. Summary of composition of the R&amp;O-dT library.

Library feature	Number in library	Total library fragments evaluated	%
Known protein-coding sequences	117	668	17.5%
Retinal protein-coding sequences	11	668	1.6%
Retinal protein-non-coding sequences	3	668	0.4%
Published cDNA sequences	17	668	2.5%
Expressed sequence tags (ESTs)	16	668	2.4%
Unannotated chromosomal regions	41	668	6.1%
Intronic regions of genes	152	668	22.8%
3' untranslated regions (UTRs) of genes	67	668	10.0%
Non-protein-coding annotated sequences <sup>13</sup>	29	668	4.3%
<i>Homo sapiens</i> uncharacterized LOC100507412 (LOC100507412), non-coding RNA	112	668	16.8%
Chr. M: <i>Homo sapiens</i> mRNA expressed only in placental villi, clone SMAP47, encoding mitochondrial rRNA.	9	668	1.3%
No matches in UCSC database	95	668	14.2%

<sup>13</sup> Other than '*Homo sapiens* uncharacterized LOC100507412 (LOC100507412), non-coding RNA' and 'Chr. M: *Homo sapiens* mRNA expressed only in placental villi, clone SMAP47, encoding mitochondrial rRNA.'

### **3.2 BAIT CONSTRUCTION AND CHARACTERISATION**

Full-length *TOPORS* cDNA, cloned in frame downstream of the cDNA encoding the GAL4 BD, was used as bait in the Y2H screen. The bait was subsequently split into three fragments to generate *TOPORS* deletion constructs (Figure 3-5) for use in subsequent characterisation of interactions. *TOPORS* protein structure and function were reviewed in depth in section 1.6. The rationale for generating the constructs, highlighted in the figure, was to help determine, once *TOPORS*' interacting partners would be known, which of the domains of *TOPORS* may be involved in mediating these novel PPIs, and thus to help explain their nature.

The N-term *TOPORS* construct (red in Figure 3-5) comprises a PEST domain, the RING finger motif and a ciliary-targeting sequence (CTS), conserved among primate *TOPORS* orthologues. Hence, using this construct for PPI characterisation would help in establishing whether *TOPORS* acts as ubiquitin E3 ligase in a specific interaction.

The mid-*TOPORS* construct (blue in Figure 3-5) includes two PEST regions, a CTS widely conserved among metazoan orthologues of human *TOPORS*, a nuclear localisation signal (NLS) and the SR/RS dipeptide-rich region. The construct also covers the locations of mutations, two of uncertain origin and effect (identified within an adRP panel with no proband family data), and one causing a pericentral retinal dystrophy in a Norwegian family (and also found in a patient from the adRP panel). The SR/RS domain would be the key component of this construct as it would help determine whether a potential prey may, in concert with *TOPORS*, be involved in genome stabilisation, or transcription. This fragment is also associated with mediating the SUMO1 E3 ligase activity of *TOPORS*, and also comprises a SUMO1 acceptor site (*TOPORS* itself is subject to SUMOylation).

The C-term *TOPORS* construct (green in Figure 3-5) covers the mutational hotspot region of *TOPORS* as well as a small proportion of the SR/RS dipeptide region, the Lys/His domain and two PEST domains. The hotspot where adRP mutations occur is the strategic component of this construct. If a retina-specific protein would be among preys, identified by the Y2H screen, and it would then interact strongly with the C-term *TOPORS* construct, it could help elucidate the deleterious effects of *TOPORS* mutations on the retina.

### **3.2.1 GENERATION OF FULL-LENGTH *TOPORS* BAIT AND DELETION CONSTRUCTS**

Several attempts were made to sub-clone the full-length *TOPORS* gene into the pGBKT7 (Clontech, CA, USA) Y2H vector, as summarised in the Appendix 11.2. Traditional restriction enzyme digestion and ligation (methods section 2.2.3) initially appeared successful; however, sequencing showed that the use of *EcoRI* and *SalI* restriction enzyme pair resulted in cleavage of *TOPORS* (Figure 11-10 in Appendix 11.2), despite prior bioinformatics-based verification that no restriction sites specific for these enzymes existed within the *TOPORS* sequence (DNASTAR SeqBuilder, Lasergene 8; Table 11-2 in Appendix 11.2). The insert was amplified using the In-fusion primers that incorporated these restriction sites (Table 2-34 in Material and Methods). Another attempt was made with similar primers with the *NdeI* and *PstI* restriction sites (Table 2-36 in Material and Methods) and ligation (Figure 11-3 in Appendix 11.2) were successful; however, attempts to transform bacteria with the ligation reactions, resulted in identification of empty vectors only (108 clones screened by colony PCR). Yeast transformation was performed as an alternative method, which appeared to yield one positive clone (Figure 11-17 in Appendix 11.2). However after the corresponding plasmid was isolated and used for transformation of bacteria, it did not appear to contain an insert (Figure 11-18 in Appendix 11.2). The In-fusion method (Clontech, CA, USA; methods section 2.2.5.1) did not yield any positive results for full-length *TOPORS*. However, all three *TOPORS* deletion constructs were designed and sub-cloned in frame with the GAL4 BD using the In-fusion method (Appendix 11.2.1).

The full-length *TOPORS* cDNA was eventually successfully sub-cloned into the pBD Y2H vector (Table 2-2 in Methods and Materials) using the Gateway system (Life Technologies, CA, USA; methods section 2.2.5.3) (Appendix 11.2.4).

### 3.2.2 CHARACTERISATION OF *TOPORS* BAIT AND DELETION CONSTRUCTS IN YEASTS

Prior to library screening it was important to ascertain that TOPORS and its fragments are expressed in the yeast cells without affecting their physiology too adversely, and that they do not bind to the activation domain of GAL4.

#### 3.2.2.1 TRANSFORMATION OF Y2H GOLD STRAIN WITH THE BAIT AND DELETION CONSTRUCTS

The following plasmids, generated as summarised in sections 3.2.1 and 0, were transformed into the Y2H Gold yeast cells:

- pBD-*TOPORS*;
- pGBKT7-N-term;
- pGBKT7-mid-*TOPORS*;
- pGBKT7-C-term.

The identity of the yeast clones was confirmed by plasmid isolation, followed by insert amplification by PCR and sequencing using vector-specific primers (Table 2-50 in Methods and Materials). As the plasmids were previously fully sequenced, the purpose for sequencing the generated PCR products after yeast transformation was to confirm the identity of the inserts. The obtained results are summarised in Appendix 11.3.

#### 3.2.2.2 DETERMINATION OF BAIT EXPRESSION

Evaluation of the expression of the TOPORS proteins in the Y2H Gold strain was initially attempted by Western blotting. In preparation for the protein extraction process, the transformed yeast cells were cultured in selective, nutrient-limited media until the optimal OD<sub>600</sub> was reached (methods section 2.1.7). The proteins were extracted from the yeast cells using the Urea/SDS method; they were then separated by SDS-PAGE and transferred onto a nitrocellulose membrane by Western blotting (section 2.5.3 in Methods and Materials). Detection of the hybrid GAL4 BD-bait proteins was performed using two different antibodies; a GAL4 BD monoclonal antibody (mAb; Clontech, CA, USA), purified from a murine hybridoma culture, which binds specifically to the binding domain (amino acids 1-147) of the GAL4 protein, or a TOPORS monoclonal antibody, raised in mouse, which binds to amino acids 98-205 of TOPORS protein. Positive detection of the GAL4 BD (without a bait protein fused to it) would have served as a positive control of protein expression from the yeast bait constructs. A horseradish peroxidase (HRP) anti-mouse antibody was used as the secondary antibody



(Table 2-75 in Methods and Materials). Three attempts were made at evaluating TOPORS protein expression, using this procedure; however, they were not successful (Appendix 11.4).

As the expression of TOPORS could not be demonstrated by an immunochemical method; it was, therefore, shown indirectly by recreating the interaction between TOPORS and p53. These two proteins were first shown to interact in a Y2H assay (Zhou, Wen e Ao, 1999), and the interaction has since then been repeated by other research groups using alternative methods (Rajendra *et al.*, 2004; Lin *et al.*, 2005; Weger, Hammer e Heilbronn, 2005). Hence, a Y2H assay was performed to check for interaction between TOPORS and p53, in order to confirm TOPORS protein expression in yeast. Prior to the assay the cDNA encoding p53 had been cloned into a suitable Y2H vector in frame with GAL4 AD (Appendix 11.5).

#### 3.2.2.2.1 CONTROL INTERACTION: TOPORS X P53

A control interaction with a previously reported interacting partner tumour protein 53 (p53) (Zhou, Wen e Ao, 1999) was performed to determine TOPORS protein expression in the host yeast system. Prior to the expression assay (control interaction), the relevant cultures were prepared: cultures carrying the pAD-p53 (control prey plasmid) were mated with cultures carrying plasmids encoding full-length TOPORS and the deletion constructs, fused with GAL4 DNA-BD. The mated cultures were incubated with shaking (~20 h, 30 °C, 200 rpm; Innova 4200 Incubator Shaker, New Brunswick Scientific, NJ, USA) prior to spreading on selective agar plates, as shown in figures 3-5, 3-6, 3-7 and 3-8, along with a key in Table 3-7.

- SD/-W (lacks tryptophan) – selects for bait;
- SD/-L (lacks leucine) – selects for prey;
- DDO (lacks both: tryptophan and leucine) – selects for diploids;
- DDO/X/A (lacks tryptophan and leucine, but is supplemented with X- $\alpha$ -galactose and aureobasidin A) – selects for diploids in which the PPI of interest occurred.

SD/-W and SD/-L selected for bait and prey plasmids, respectively. Diploid cells were selected for on the double dropout (DDO) media, lacking both amino acids, therefore, the yeast needs both bait and prey plasmids in order to thrive on it. DDO media additionally supplemented with X- $\alpha$ -Gal (extra carbon source) and AbA (antifungal agent) selected for diploid cells (DDO/X/A media), in which protein interactions occurred; presence of the latter two ingredients in the media provides a readout, if reporter gene expression is triggered by interaction between the bait and prey. AbA is toxic to the yeast cells, they are not able to grow unless they express the resistance gene, *Aur-C*; the expression can only be triggered by

an interaction between the bait and the prey proteins, here: TOPORS (or its fragment) and p53. Consequently, any growth on DDO/X/A plates provides evidence for TOPORS-p53 interaction. If the observed colonies are blue, this further demonstrates that expression of the other reporter gene, *Mel1*, was also activated. Hence, the *Mel1* phenotype of colonies growing on the DDO/X/A plates can be indicative of the strength of the TOPORS-p53 interaction; i.e. growth of white colonies indicates that *Aur-C* has been expressed, but perhaps the interaction was either not strong enough, or did not last long enough to additionally trigger the expression of *Mel1*, which would be demonstrated by blue growth.

Overall, this control experiment has provided evidence for an interaction between TOPORS and p53 within the yeast two-hybrid (Y2H) system, supporting the previously published result (Zhou, Wen e Ao, 1999). More importantly, the demonstrated interaction verified the expression of TOPORS within the yeast host cell environment.

### 3.2.2.3 AUTO-ACTIVATION AND TOXICITY EVALUATION OF BAIT CONSTRUCTS

Prior to the auto-activation and toxicity experiments the GAL 4 BD vectors, all four TOPORS bait constructs and BD-only (empty pGBKT7 vector) were transformed into the Y2H Gold yeast strain; the yeast cells were transformed with the following plasmids (100 ng of DNA were used per transformation):

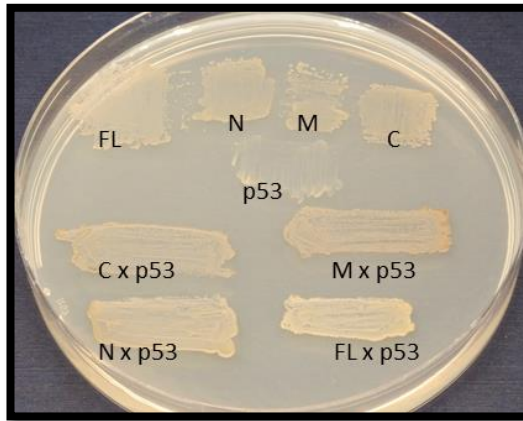
- pBD-*TOPORS*;
- pGBKT7-N-term;
- pGBKT7-mid-*TOPORS*;
- pGBKT7-C-term;
- pGBKT7 (see Table 2-32).

Following the transformation, each of the transformed yeast cultures were diluted 1:10 and 1:100, and 100 µl of each of the following diluted cell suspensions were spread on the following agar media:

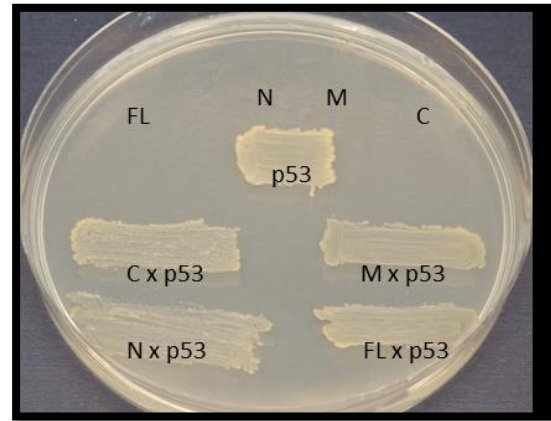
- SD/-W (=SDO; lacks tryptophan);
- SD/-W/+X-α-Gal (=SDO/X; lacks tryptophan, but is supplemented with X-α-galactose);SD/-W/+ X-α-Gal/+AbA (=SDO/X/A; lacks tryptophan, but is supplemented with X-α-galactose and aureobasidin A).

Table 3-6. Control TOPORS (Y2H Gold) x p53 (Y187) interaction: mating outline.

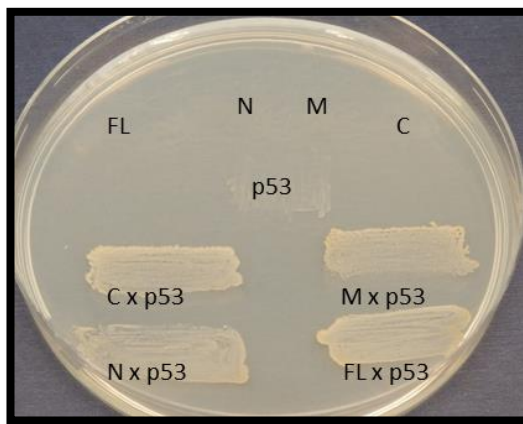
Host strain (vector-bait)		Host strain (vector-prey)	
Y2H Gold (pBD- <i>TOPORS</i> )	X	Y187 (pAD-p53)	
Y2H Gold (pGBKT7-N- <i>TOPORS</i> )			
Y2H Gold (pGBKT7-mid- <i>TOPORS</i> )			
Y2H Gold (pGBKT7-C- <i>TOPORS</i> )			



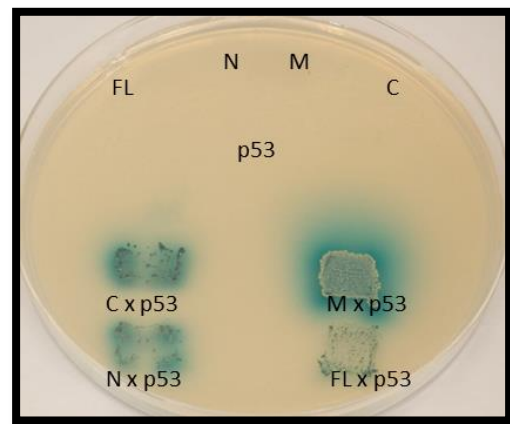
A. SD/-W medium, selecting for colonies expressing bait plasmids.



B. SD/-L medium, selecting for colonies expressing prey plasmids.



C. DDO medium, selecting for colonies expressing both: bait and prey plasmids.



D. DDO/X/A medium, selecting for colonies expressing both: bait and prey plasmids, and PPIs, as indicated by the reporter gene expression: *Mel1* (blue growth) and *Aur1-C* (growth on media supplemented with AbA lethal to yeasts, which do not express the *Aur1-C* resistance gene).

Key for labels in figures A-D: FL, Y2H Gold strain transformed with pBD-TOPORS (full-length); N, Y2H Gold strain transformed with pGBKT7-N (amino-terminal TOPORS fragment); M, Y2H Gold strain transformed with pGBKT7-M (mid-TOPORS fragment); C, Y2H Gold transformed with pGBKT7-C (carboxy-terminal TOPORS fragment); p53, Y187 strain transformed with pAD-p53; FL, N, M, C and p53: patches of haploid transformed yeasts. C x p53, Y2H Gold [pGBKT7-C] x Y187 [pAD-p53] mating; M x p53, Y2H Gold [pGBKT7-M] x Y187 [pAD-p53] mating; N x p53, Y2H Gold [pGBKT7-N] x Y187 [pAD-p53] mating; FL x p53, Y2H Gold [pBD-TOPORS] x Y187 [pAD-p53] mating; patches of the mated cultures all correspond to diploid yeasts, expressing both: a bait plasmid and a prey plasmid.

					+ve		-ve			
Bait	Prey	GAL4 BD	p53	Lamin C	GAL4 BD	p53	Lamin C	GAL4 BD	p53	Lamin C
	p53	SV40 T Ag	SV40 T Ag		p53	SV40 T Ag	SV40 T Ag	p53	SV40 T Ag	SV40 T Ag
10 <sup>0</sup>										
M.		SD/-W	SD/-L	DDO	DDO/X/A					

E. Negative control experiment demonstrating that p53 does not interact with GAL4 BD. Interaction positive (p53 x T Ag) and negative (Lamin C and T Ag) controls are shown. See labels for figure parts A-D for details of selection media ('M.').

Figure 3-4. Demonstration of a PPI between TOPORS and p53.

### 3.2.2.3.1 AUTO-ACTIVATION TESTING

Growth of white colonies was expected on the SDO as well as the SDO/X plates; in the latter case pale blue colonies could also be observed, as expression of the X- $\alpha$ -Gal reporter might not be stringent enough. No growth was expected on the SDO/X/A plates due to the toxic AbA. Diploid cultures expressing GAL 4 BD-p53 and GAL 4 AD-T Ag hybrid proteins, which have been shown to interact, were additionally spread on DDO/X/A plates as a positive control. The experiment was performed in triplicate.

Representative results from one of the three experiments are summarised in Figure 3-6. As demonstrated by growth on SDO/X media, the pGBKT7-N-TOPORS appears to activate the *MeI1* reporter to some extent (this was observed in two out of the three experiments); however, not as strongly as the positive control (interaction between p53 and SV40 large T antigen). This was deemed acceptable as per Clontech's instructions, stating that the *MeI1* reporter may be 'leaky'. The remaining constructs displayed growth without any hints of blue, providing evidence for there being no auto-activation. No growth, other than for the positive control, was observed on the SDO/X/A, validating the stringency of the AbA-based reporter gene.

### 3.2.2.3.2 EFFECT OF TOPORS EXPRESSION ON HOST YEAST CELLS

In order to determine how the expression of the bait constructs affected the host yeast cells, each bait construct and corresponding empty vector was transformed into the Y2H Gold strain, and incubated on SD/-W media to compare growth. If TOPORS and/or its fragments negatively affect the yeast cell, or are toxic, it is expected that the colonies containing these bait vectors will be significantly smaller than colonies carrying the empty vector encoding only the GAL4 DNA-BD.

A wide range of colony sizes (0.1 mm to 1.5 mm) was observed within as well as between all plates (Figure 3-7 - Figure 3-10). In general, colonies transformed with the *TOPORS* constructs appeared smaller, but more numerous.

This suggests that expression of TOPORS protein is exerting a negative effect on the host cells. However, they are still able to grow and mate (as was demonstrated in section 3.2.2.2.1).

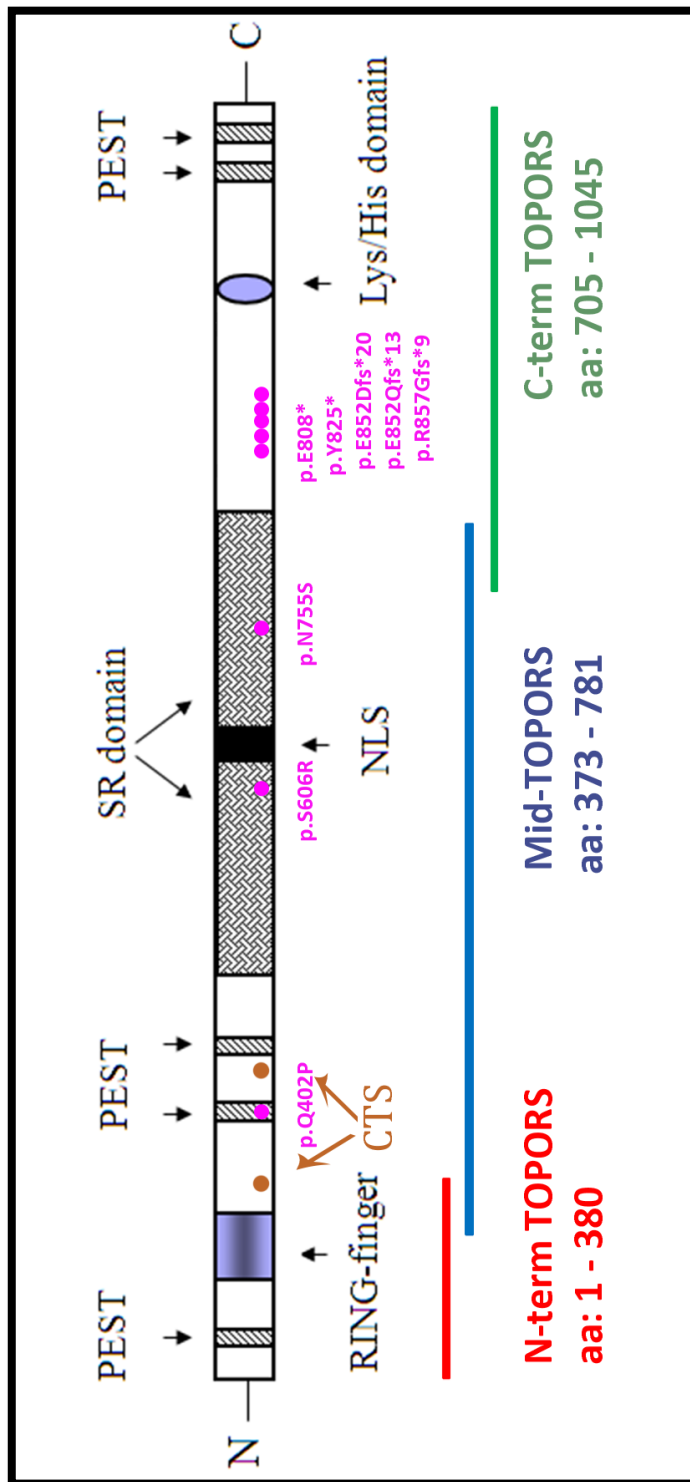


Figure 3-5. TOPORS protein diagram. Specific domains are indicated by arrows, and were described in Figure 1-16 (section 1.6). Mutations identified in TOPORS to date are highlighted as magenta dots. Deletion constructs are indicated by the red, blue and green bars underneath; aa: indicates the amino acid range that a specific construct spans. Figure modified from (Chakarova *et al.*, 2007); not to scale.

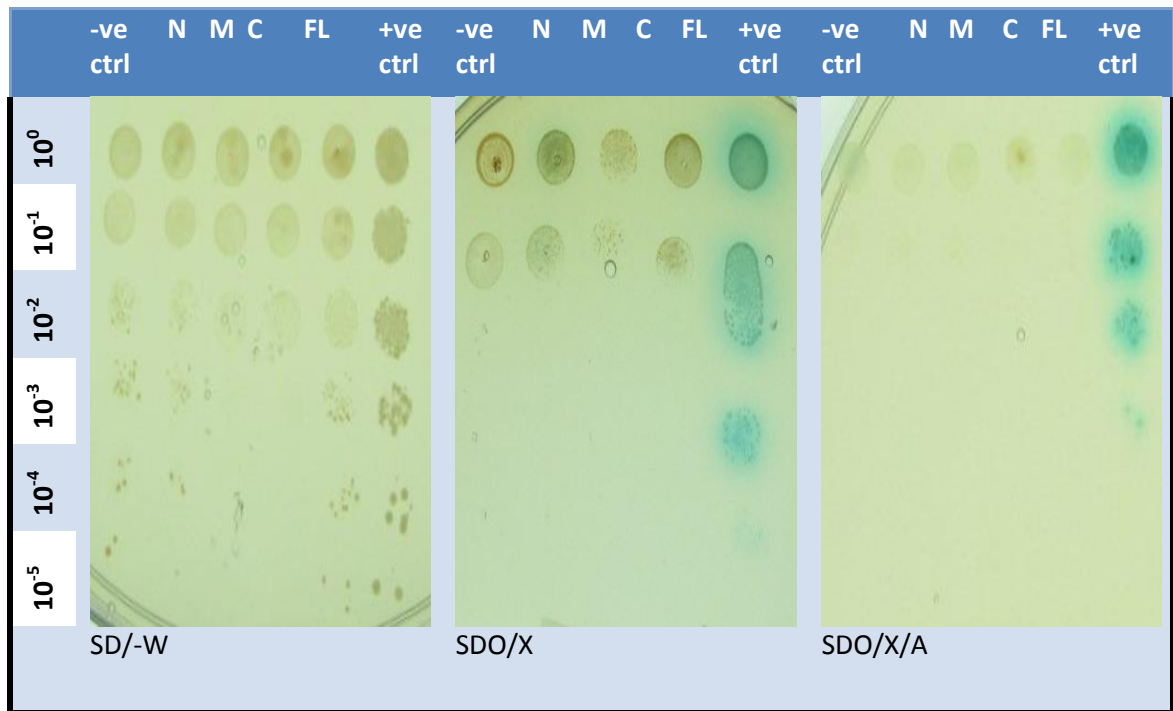


Figure 3-6. Bait auto-activation testing.

Key: -ve ctrl = pGBKT7 only; N = pGBKT7-N-term; M = pGBKT7-mid-*TOPORS*; C = pGBKT7-C-term; FL = pBD-*TOPORS*; +ve ctrl = pGBKT7-p53 x pGADT7-T Ag → reporter activation positive control. Culture dilutions are indicated on the left-hand side. SD/-W medium selects for colonies expressing GAL4 BD-bait proteins; SDO/X medium selects for colonies expressing GAL4 BD-bait proteins, which activate the *Mel1* reporter gene (blue growth phenotype); SDO/X/A medium selects for colonies expressing GAL4 BD-bait proteins, which activate the *Mel1* and *Aur1-C* reporter genes (blue growth phenotype and growth on media with Aba lethal to yeasts that do not express *Aur1-C* respectively).

Table 3-7. Results expected from the bait auto-activation testing.

Media type	SD/-W	SDO/X	SDO/X/A
<b>Media selectivity</b>	Colonies harbouring bait plasmids	Colonies harbouring bait plasmids and activating the <i>Mel1</i> reporter gene for utilisation of X- $\alpha$ -galactose (resulting in blue metabolite being excreted by the yeasts)	Colonies harbouring bait plasmids and activating the <i>Mel1</i> reporter gene for utilisation of X- $\alpha$ -galactose (resulting in blue metabolite being excreted by the yeasts) as well as the <i>Aur1-C</i> reporter gene enabling yeasts to break down the toxic AbA in the media
<b>Expected yeast growth phenotype</b>	White growth of samples and controls	White, or pale blue, growth of samples; blue growth of controls	No growth of samples; blue growth of controls

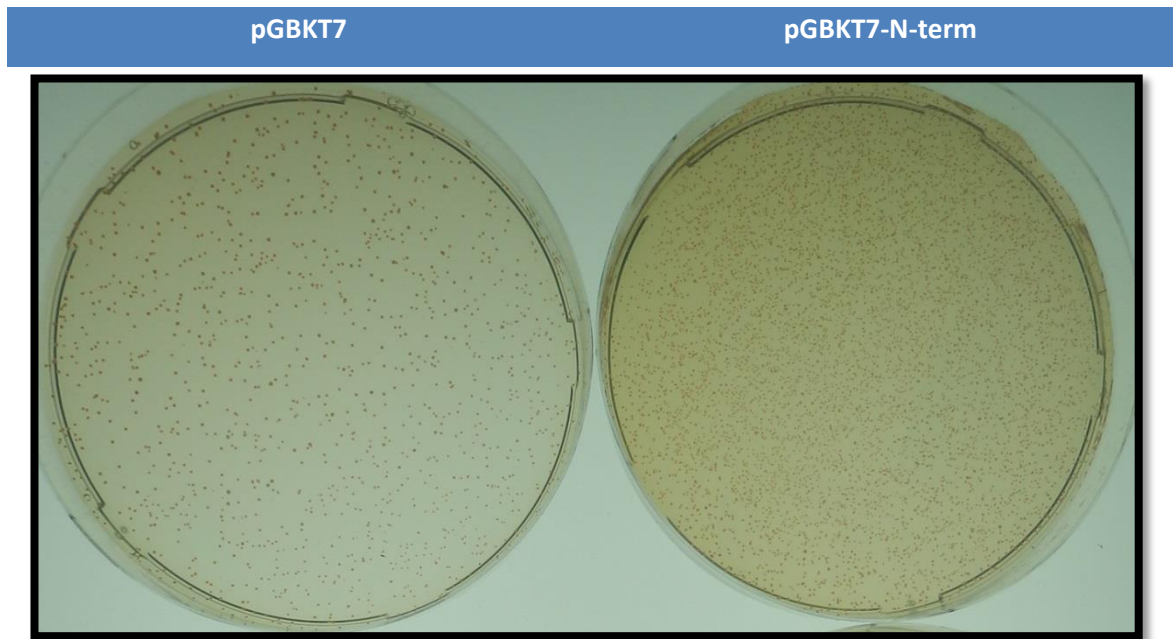


Figure 3-7. Comparison of colony sizes transformed with pGBKT7 vs. pGBKT7-N-term. SD/-W media selects for colonies expressing GAL4 BD-bait proteins. Culture was diluted  $10^{-2}$  prior to spreading on agar media.

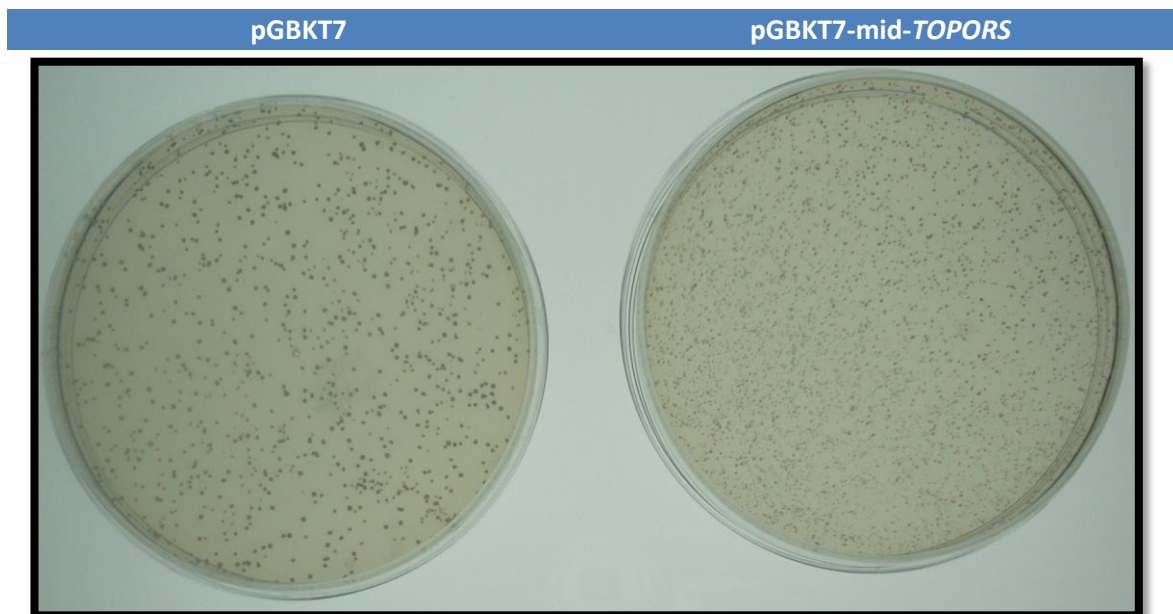


Figure 3-8. Comparison of colony sizes transformed with pGBKT7 vs. pGBKT7-mid-TOPORS. SD/-W media selects for colonies expressing GAL4 BD-bait proteins. Culture was diluted  $10^{-2}$  prior to spreading on agar media.

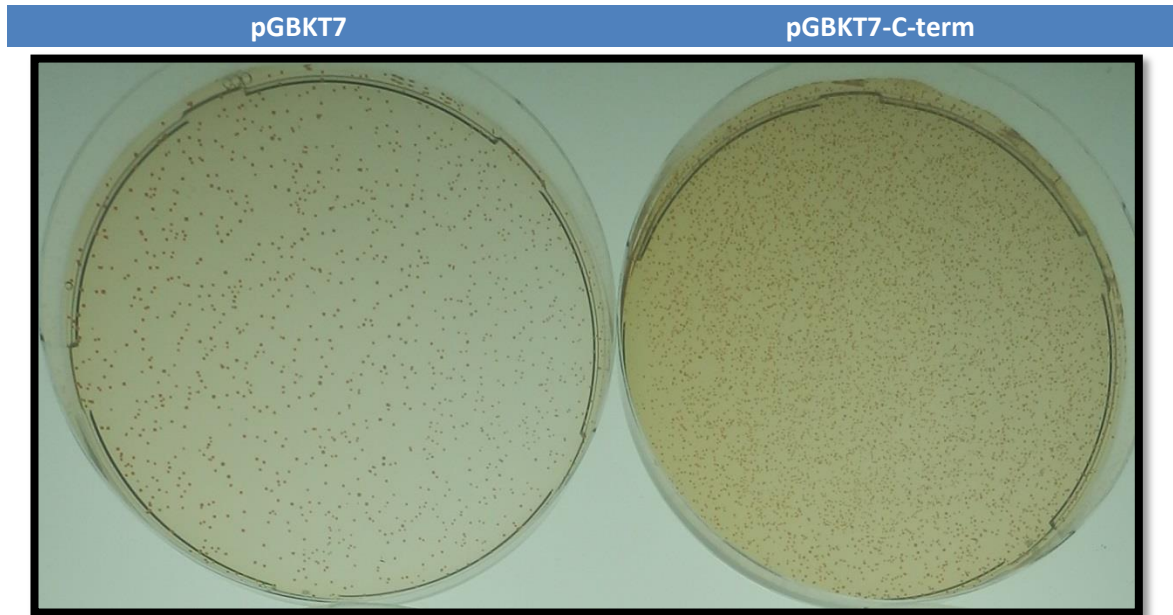


Figure 3-9. Comparison of colony sizes transformed with pGBKT7 vs. pGBKT7-C-term. SD/-W media selects for colonies expressing GAL4 BD-bait proteins. Culture was diluted  $10^{-2}$  prior to spreading on agar media.

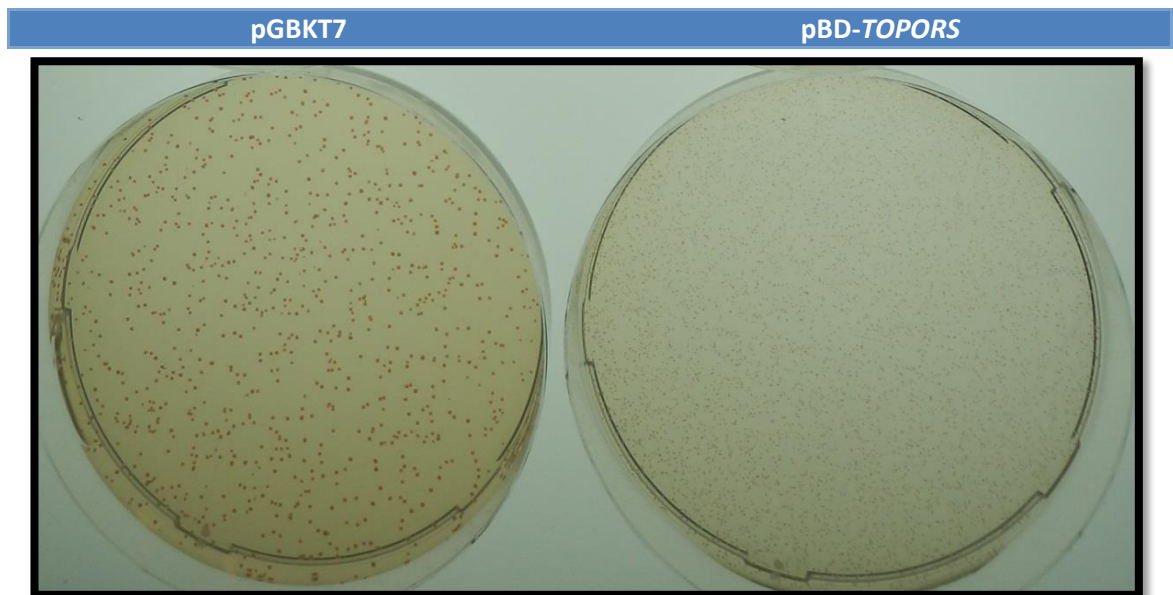


Figure 3-10 Comparison of colony sizes transformed with pGBKT7 vs. pBD-*TOPORS*. SD/-W media selects for colonies expressing GAL4 BD-bait proteins. Culture was diluted  $10^{-2}$  prior to spreading on agar media.



### **3.3 DISCUSSION**

This chapter described the construction and validation of the human retina cDNA libraries as well as the Y2H bait vectors, intended for library screening and subsequent PPI characterisation.

The random- and oligo-dT-primed (R&O-dT) library was constructed in GAL4 activation domain (AD) vectors, and it was thoroughly characterised to determine the content of retina-specific fragments, and hence its suitability for the Y2H screen for retina-expressed interacting partners of TOPORS. The protein-coding retina-specific fragments comprised 1.6 % of total library inserts (n = 668; Table 3-1), which appears to be a high proportion (discussed in section 3.3.1).

The full-length TOPORS cDNA as well as its three fragments (shown in Figure 3-5) were sub-cloned into GAL4 DNA-binding domain (BD). It was indirectly shown by repeating a known PPI that TOPORS protein is expressed within the yeast host cells (section 3.2.2.2). It was additionally demonstrated that TOPORS expression affects the host cells' physiology negatively; however the cells were able to thrive (section 3.2.2.3.2). TOPORS or its fragments did not cause auto-activation of the Y2H reporter genes with the exception of the N-term TOPORS; this fragment activated the 'leaky' *MEL1* reporter gene (but not the more stringent *Aur1-C* reporter gene, which was utilised in all screens and direct interaction testing).

#### **3.3.1 CONSTRUCTION AND VALIDATION OF CDNA LIBRARIES**

Two types of DNA libraries are commonly recognised: genomic libraries and cDNA libraries. By principle the genomic libraries comprise fragments of the whole genome of an organism, including coding as well as non-coding regions. On the other hand, cDNA libraries typically reflect the transcriptome of a single-celled organism, the transcriptome of a cell type, a tissue type, or of a multi-cellular organism. The library, generated using the Make Your Own "Mate & Plate™" Library System (Clontech, CA, USA), although referred to as a cDNA library by the manufacturer, actually also possesses features of genomic libraries.

Total human retina RNA (Clontech, CA, USA) was used for construction of the cDNA library used for the screen, which was a starting point for this project. Hence, the cDNA, reverse-transcribed from the RNA, and used for the library construction, was complimentary not only to messenger RNA (mRNA), but also to other RNA species, including transfer RNA (tRNA) and ribosomal RNA (rRNA). Non-spliced pre-mRNA as well as RNA species in the process of undergoing splicing will also have been included and reverse transcribed, thereby leading to

the inclusion of introns (non-protein-coding DNA). Overall, the rRNA would have comprised the most abundant RNA species within the starting material.

Two cDNA libraries were constructed according to the manufacturer's instructions using two types of primers: oligo-dT (O-dT) only and random (R) and O-dT (R&O-dT). The initial PCR results demonstrated that the R&O-dT library comprised more plasmids with protein-coding cDNA inserts than the O-dT library, i.e. 35/42 (83 %), and 23/45 (51 %), respectively. On average, the insert size was larger in the R&O-dT library (444 bp) than in the O-dT library (315 bp).

It must be noted that the library insert sizes within the approximate range of 300 bp to 450 bp were smaller than expected. An analysis of the human genome organisation demonstrates that the length of an average human transcript or cDNA is 2822.4 bp. The exon sizes range from 77 bp to 850 bp, where the average exon size is 288 bp; whereas the number of exons per gene ranges from one to 363 with the average exon number being 9.8 (Strachan e Read, 2010). This indicates that even within the O-dT&R-primed library the average insert size is over six times smaller (2822.4 bp/444 bp) than the average human cDNA clone.

Such a discrepancy between the expected and observed insert sizes poses severe limitations to the usefulness of the library as a tool for identification of interacting protein partners of TOPORS. The existence of short library inserts indicates that only full-length transcripts of up to 500 bp will be expressed by the yeast (in addition to longer, but truncated, transcripts).

Expression of non-full-length protein may lead to protein mis-folding and hence increase the chances of false-positive interactions being observed. On the other hand, whilst constructing a cDNA library, it is generally rare that many (if any) full-length cDNA clones will be generated. This is due to the fact that the use of an oligo-dT primer will often result in a higher proportion of cDNA clones representing the 3' end transcript regions; whereas the 5' end regions will be underrepresented. The use of a random primer aims to alleviate this issue to result in a more uniform representation of cDNA fragments, but, since it binds randomly, it will rarely result in a generation of a full-length cDNA molecule (Dale e Schantz, 2007).

Still, it would be expected that the library inserts ought to be at least half-length of the average human transcript, given the library construction conditions as well as the positive cDNA synthesis results (Figure 3-1). Because it was demonstrated that fragments of up to 6000 bp were generated by the reverse transcription of human retinal RNA, and the library inserts are significantly smaller (444 bp), this indicates either that the CHROMA SPIN TE-400 purification

was not performed correctly (perhaps the columns were not properly equilibrated prior to use), resulting in excessive loss of the larger cDNA molecules, or that smaller cDNA fragments were preferentially incorporated into the library vectors by the homologous recombination performed by endogenous yeast enzymes.

Figure 3-1 shows the range of cDNA molecules, generated by LD-PCR, prior to the CHROMA SPIN TE-400 procedure; perhaps an electrophoresis of the purified cDNA molecules should have been performed after the CHROMA SPIN TE-400 treatment and prior to homologous recombination in yeast in order to ensure that no errors occurred during the CHROMA SPIN TE-400 purification. Since that was not done, it is not possible to state, what issue potentially prevented the incorporation of the large inserts into the library vectors. These aspects were not addressed by the Make Your Own "Mate & Plate™" Library System User Manual Troubleshooting Guide (Clontech), however, it was previously shown that increasing the length of the homology region between the vector and insert sequences increases the homologous recombination efficiency (Oldenburg *et al.*, 1997). It could be speculated that recombination of the larger inserts was less efficient as they potentially required larger regions of homology (relative to their overall size) to recombine with the vectors. In conclusion, the presence of small library fragments will decrease the chances of identifying putative interacting proteins, as fewer full-length proteins will be expressed within the library.

Further evaluation of the R&O-dT library revealed that the protein-coding library fragments constituted about a fifth of all the total evaluated library fragments (n = 668; Table 3-1 and Appendix 11.1). This was reflected in the relatively high number of prey-sequences pulled out from the Y2H screens, which included fragments of, or comprised exclusively, non-protein coding genomic sequences.

In order to enrich the protein-coding sequences in future cDNA-library construction projects, the RNA, used as starting material for cDNA synthesis, should be pre-filtered using oligo-dT beads prior to reverse transcription, to remove non-coding and immature RNA species. This would lead to generation of a greater number of protein-coding library fragments using not only the oligo-dT, but also the random primer, by limiting, if not completely eliminating, the extent of non-coding RNA inclusion.

Furthermore, elimination of the highly abundant, non-coding sequences would increase the probability that rare inserts would also be isolated via Y2H screens, as they would be enriched in relation to other library clones. Even though no cDNA library can ever be

guaranteed to represent all of the transcriptome of interest, if the rarer transcripts did not have to 'compete' with the more numerous ones for reverse transcription, and later, insertion into the library vectors, it would result in the library being more representative of the tissue in question.

Despite a lack of these potential beneficial changes, the number of independent clones in each one of the two libraries was a million, or higher, satisfying the quality criteria established by the manufacturer.

Conversely, such a pre-filtering procedure would limit a transparent evaluation of the starting material. Nine inserts among the evaluated library clones contained mitochondrial mRNA, encoding ribosomal RNA (rRNA), which, according to the UCSC search results, is expressed only in placental villi. Such a result could indicate a previously unreported expression, or a contamination of the human retinal RNA with material from other tissues, which would otherwise be overlooked.

Another aspect to consider, whilst evaluating cDNA library quality, is whether the inserted fragments were in frame with the GAL4 AD and other upstream vector sequences. Due to the nature of primers used for the library fragments' amplification, the inserts would definitely recombine with the vector DNA in the correct orientation. However, there is just a 33 % chance that the library fragment would be inserted in frame. This feature had not been evaluated whilst characterising the library prior to screening; hence, it was essential to verify the reading frame of all the fragments of interest isolated from the Y2H PPI screen. *ITM2B*, *PTGDS* and *PSMC1*, the novel identified interacting partners of TOPORS, were found to be in frame with the library vector sequence; had they not been inserted in frame, they would have been required to be re-cloned for subsequent experiments, to verify findings.

The library content of the retina-specific transcripts also appears insubstantial considering the total count of evaluated library clones ( $11/668 = 1.6\%$ ; Table 3-1). However, it looks more specific, when it is considered as a proportion of all protein-coding sequences from the library ( $11/117 = 9.4\%$ ). Still, it cannot be determined for certain how representative a sample of 668 clones is of the library, if the total number of independent clones was determined as over a million, i.e. four orders of magnitude higher. However, this provided a somewhat representative overview of its composition.

According to studies by Schulz *et al.* (2004) the retina-specific genes (including the RPE genes) should comprise approximately 0.33 % of total human retina transcriptome (43/13037 genes).

On the other hand, Strunnikova *et al.* (2010) analysed the human RPE transcriptome (exclusive of the neural retina), and found 154 'RPE signature genes', which would comprise 0.62 % - 0.77 % of the total protein-coding human genome (20000 – 25000 genes) (Consortium, 2004). These results suggest that the proportion of the retina-specific protein-coding transcripts contained within the library, constructed for the purposes of this project, is actually rather high: 1.6 % of the evaluated library inserts, or 9.4 % (11/117) of the protein-coding library inserts. This outcome could reflect the fact that the library is not normalised, as according to the transcriptome studies the proportion of retinal genes should be lower.

As a final point it is important to re-emphasise that the overall quality of the library was mediocre due to high content of very short (444 bp average) cDNA fragments as well as a majority of the inserts being non-coding (protein-coding cDNAs comprised only 17.5 % of library inserts). Whilst preparing a cDNA library in the future, it would be recommended to augment the protein-coding content of the starting material. Enriching for mRNA molecules using an oligo dT-based probe would generate a suitably purified template for cDNA synthesis, which would then be incorporated into appropriate vectors by homologous recombination inside the yeast cells. Still, following the manufacturer's instructions, the resulting libraries with its features, described in section 3.1, and discussed here, was used for the Y2H screens and identification of novel interacting protein partners of TOPORS.

### **3.3.2 BAIT CONSTRUCTION AND VALIDATION OF EXPRESSION**

Full-length TOPORS cDNA was cloned into a Y2H vector, and the subsequent goal was to validate the expression of this exogenous human TOPORS protein within the yeast system. It was initially attempted to verify the expression of TOPORS by Western blotting; however, this method did not yield positive results either due to inefficient protein extraction and/or a lack of abundance of the protein expression. It was concluded that the protein extraction was inefficient during the preliminary attempts (rather than that TOPORS was not expressed) since the GAL4 DNA-BD, serving as a control for protein expression, could not be detected either. Following manufacturer's instructions, expression of GAL4 DNA-BD by itself without the bait protein fused to it, was to be used as control. An antibody raised against GAL4 DNA-BD (Clontech) was to be used for detection of both: the sole control GAL4 DNA-BD as well as the GAL4 DNA-BD-TOPORS fusion protein. Neither protein could be detected using this antibody; TOPORS could not be detected using the antibody raised against its amino-terminal epitope (Abnova) either. On the contrary, the Western blot showed a smear in all cases (Appendix 11.4), indicating either impure extracts and/or protein degradation.

Hence, to circumvent this issue, the subsequent aim was to repeat a previously reported protein interaction, involving murine TOPORS and p53 (Zhou, Wen e Ao, 1999), and, thus, indirectly confirming that TOPORS protein (bait) is indeed expressed in yeast. Fragments of TOPORS (Figure 3-5) were also tested for interaction with p53. Results of this experiment provided strong evidence for association between human TOPORS (including its fragments) and p53, thus validating bait expression.

### **3.3.3 CONCLUSIONS**

The human retina cDNA libraries and the Y2H bait plasmids have been constructed and characterised, as described and discussed in this chapter. The quality of the library was mediocre due to high content of very short (444 bp average) cDNA fragments as well as a majority of the inserts being non-coding (protein-coding cDNAs comprised only 17.5 % of library inserts). The bait constructs were of fine quality, and the bait proteins did not activate stringent PPI reporter genes; however, they did have a slight negative impact on the yeasts' growth.

These procedures were essential pre-requisites for the cDNA library screening for interacting partners of TOPORS, which was the primary aim of this work. It was hypothesised that TOPORS must have a retina-specific interacting partner, which leads to a retina-restricted phenotype associated with TOPORS mutations.

The findings of the Y2H cDNA library screening for TOPORS' retinal putative interacting partners are reported in Chapter 4. The interactors identified via the Y2H screen are subsequently verified and characterised as described in Chapters 5-8. The results are discussed in Chapter 9.

## **4 LIBRARY SCREENING AND IDENTIFICATION OF POSITIVE INTERACTIONS**

Chapter 3 provided a description of human retinal cDNA library construction and characterisation as well as it summarised the procedures involved in cloning and characterising of *TOPORS* bait constructs.

Two libraries were constructed; one using only the oligo-dT primer, and one using two primers: the oligo-dT and random. The latter library was characterised in greater depth since preliminary analysis revealed that this library harboured a higher proportion of clones with inserts, and, when present, the inserts were on average 130 bp longer than in the oligo-dT only-primer library. Despite a thorough characterisation of only one library, both libraries were screened for protein interacting partners of TOPORS.

The construction of the human retinal cDNA library and *TOPORS* bait plasmids were critical requirements for fulfilling the major goal of this project, i.e. identifying protein interacting partners of TOPORS using the Y2H screening method (section 2.1). As was already emphasised, identification of proteins, which associate with TOPORS, could help explain the aetiology of retinitis pigmentosa, caused by mutations in the *TOPORS* gene. Due to the ubiquitous expression of TOPORS along with *TOPORS* mutations being linked only to retinal disease, it was hypothesised that a protein, produced only in the retina, must be the critical interactor of TOPORS. The current chapter describes the outcomes of the Y2H screening procedures aiming to detect protein-protein interactions (PPIs) between TOPORS and a retinal protein.

The workflow of the Y2H methods (Figure 4-1) includes the already described cDNA library (Section 3.1) and bait (Section 3.2) construction and characterisation (experimental Chapter 3; Methods and Materials section 2.1), which form the basis for identification of interactions that TOPORS is involved in (Chapter 4).

Prior to performing the Y2H screens against the retina cDNA libraries, the bait was constructed by sub-cloning the *TOPORS* gene into a Y2H vector in frame with the GAL4 binding domain (BD) ('Cloning' in Figure 4-1; Methods and Materials section 2.2.5). The resulting construct was then used for the transformation of the Y2H Gold yeast strain of mating type a (*Mata*); the cDNA library constructs, i.e. preys, had been transformed into the Y187 strain of mating type alpha (*Mata*) in frame with the GAL4 activation domain (AD) ('Yeast transformation' in Figure 4-1; Methods and Materials section 2.1.3).

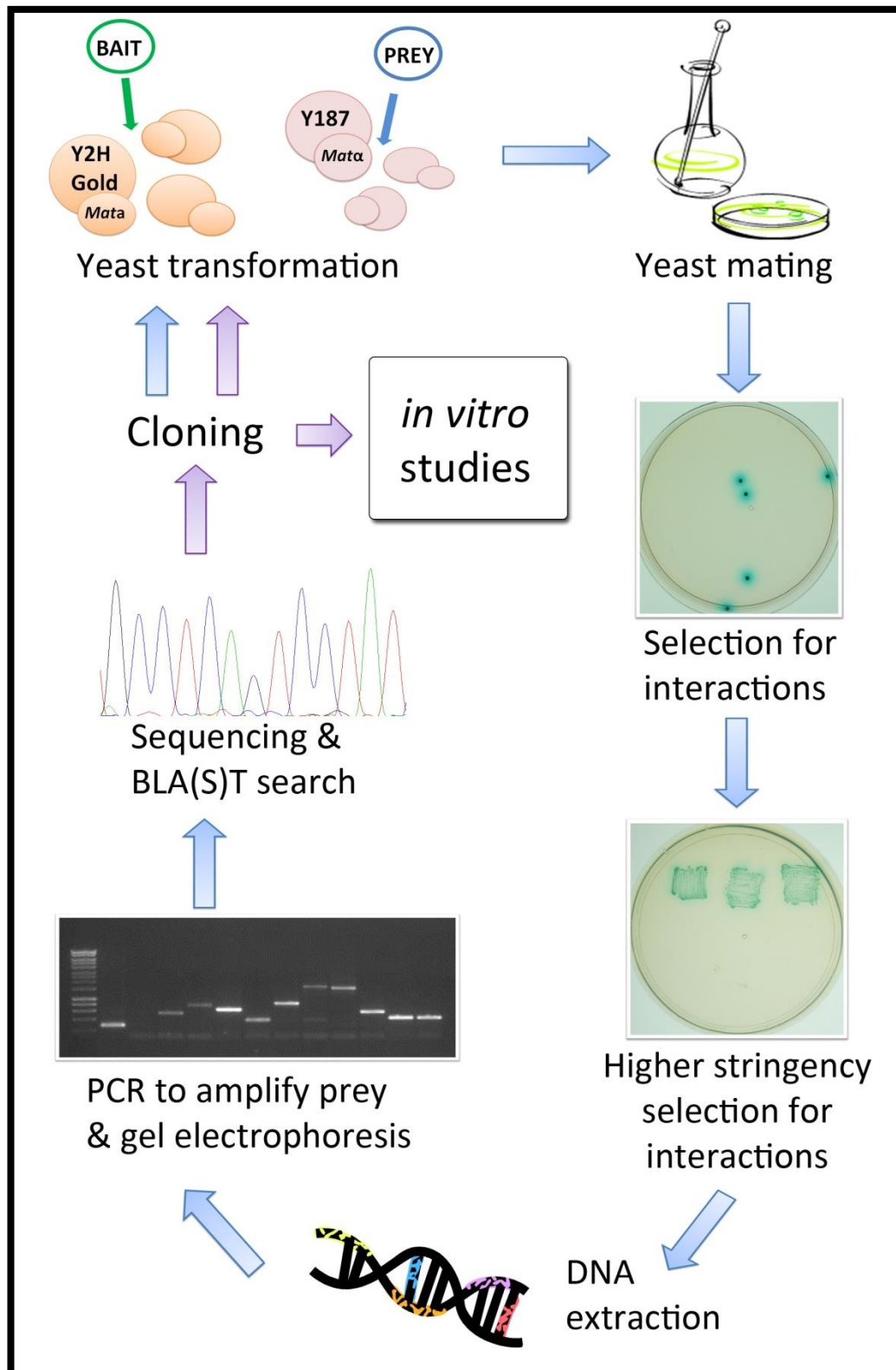


Figure 4-1. Overview of the Y2H library screen workflow.



Both of the transformed strains were subsequently cultured and mated in liquid media ('Yeast mating' in Figure 4-1; Methods and Materials section 2.1.5). The resulting mated cultures were then spread on agar media, selective for bait and prey plasmids as well as for PPIs based on two reporter genes; blue yeast colonies were expected to grow on agar supplemented with AbA and X-alpha-gal ('Selection for interactions' in Figure 4-1).

Blue colonies were patched on higher stringency media, selective for PPIs based on four reporter genes; in addition to breaking down AbA and using X-alpha-gal as carbon source, the yeasts were required to produce histidine and adenine, which were lacking from the selective growth media ('Higher stringency selection for interactions' in Figure 4-1; Methods and Materials section 2.1.1).

DNA was extracted from yeast patches ('DNA extraction' in Figure 4-1; Methods and Materials section 2.1.6), which activated all four reporter genes, and primers, specific to the prey-vector, were used to amplify the cDNA library inserts encoding the potential interacting proteins ('PCR to amplify prey & gel electrophoresis' in Figure 4-1; Methods and Materials sections 2.2.1 and 2.2.2).

The resulting PCR products were purified and sequenced; the UCSC BLAT search engine was used to identify the inserts (NCBI BLAST was used for verification of some of the obtained results; 'Sequencing & BLA(S)T search' in Figure 4-1). The figure also indicates '*in vitro* studies' as part of the workflow; the aim of these studies was to verify the identified interactions, using independent methods, other than the Y2H system (Methods and Materials sections 2.5, 2.6 and 2.7), the outcomes of which were described in Chapters 6 - 8.

#### **4.1 YEAST MATING CONTROL EXPERIMENTS**

The Matchmaker™ Gold Yeast Two-Hybrid System User Manual (Clontech, CA, USA) provides instruction for performing two mating controls alongside the library screen(s). For the positive control the Y2H Gold strain, transformed with the pGBKT7-53 plasmid (carrying the *p53* gene cDNA), was mated with the Y187 strain, and transformed with the pGADT7-T plasmid, encoding the T Ag. In the negative control experiment the pGADT7-Lam-transformed Y187 strain was used instead (Table 2-16 in Methods and Materials).

As full-length TOPORS was cloned using a different vector system (Gateway system; Table 2-33), into pBD rather than pGBKT7 (In-Fusion system; Table 2-32), an additional control was performed to validate the compatibility of the two Y2H vector systems, using p53 in the pBD

Gateway vector and pGADT7-T In-Fusion vector. The p53 gene had previously been cloned into the pDONR vector (Appendix 11.5). The resulting pDONR-p53 entry vector was subsequently used in a Gateway LR recombination with the pBD vector. Resulting constructs were propagated in bacterial cells, and sequenced using p53-specific primers (Table 2-52 in Methods and Materials). The obtained sequences confirmed the successful cloning of p53 into the pBD plasmid.

The control Y2H constructs were transformed into yeast strains of opposite mating types, and the haploid yeast cells were mated as illustrated in Table 4-1. The resulting diploid yeast cells were spread on specific nutrient-limited, selective media (expected results in Table 4-2). All mating experiments were performed in triplicate.

Table 4-1. Control mating to check for Y2H system performance.

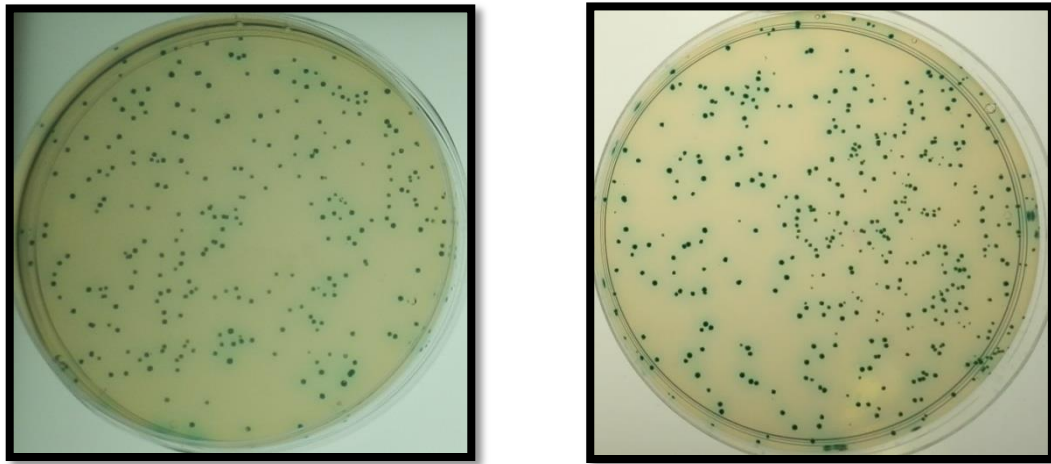
Y187 [pGADT7-T] colony	
Y2H Gold [pGBKT7-p53] colony	Positive control mating (1)
Y2H Gold [pBD-p53] colony	Positive control mating (2)
Y2H Gold [pGBKT7-Lam] colony	Negative control mating (1)
Y2H Gold [pBD-pLC] colony	Negative control mating (2)

Table 4-2. Expected control Y2H PPI results.

Expected growth On selective media	Positive control mating	Negative control mating
SD/-W (bail selection)	White colonies	White colonies
SD/-L (prey selection)	White colonies	White colonies
DDO (diploid selection)	White colonies	White colonies
DDO/X/A (PPI selection in diploid yeasts)	Blue colonies	No colonies

The colonies resulting from both the positive and the negative control mating were all expected to be white, when grown on the SD/-L, the SD/-W, or the DDO media (section 2.1.5 in Methods and Materials), which was observed (data not shown).

Growth on the DDO/X/A positive control agar plates was, as expected; round, blue colonies were observed, without any satellite colonies (Figure 4-2). These results demonstrated that a positive interaction had occurred between the p53 tumour suppressor protein and the large T antigen of the SV40 virus, leading to activation of transcription of the reporter genes, i.e. *Me1* and *Aur-C*.



A.

B.

Figure 4-2. Y2H control p53 x SV40 T Ag PPI: a comparison of *p53* constructs (pBD-p53 vs. pGBKT7-53). A, Y2H Gold [pBD-p53] x Y187 [pGADT7-T] diploid colonies. B, Y2H Gold [pGBKT7-53] x Y187 [pGADT7-T] diploid colonies. Dilutions of  $10^{-2}$  of both cultures were spread on DDO/X/A (selects for colonies, within which a p53-T Ag interaction occurred).

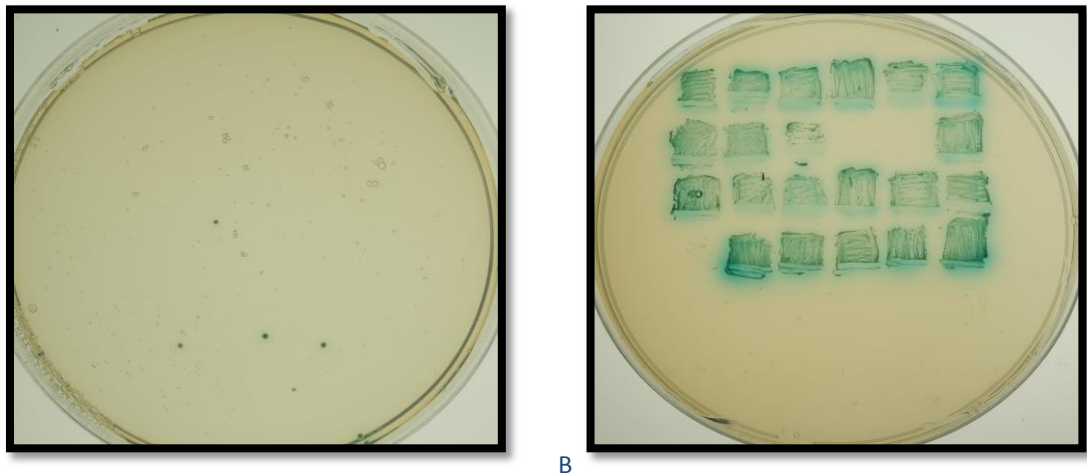
## 4.2 IDENTIFICATION OF POSITIVE INTERACTIONS BY Y2H SCREENS

Two Y2H screens were performed using the pBD-TOPORS bait construct: one against the random-&-oligo-dT-primed (R&O-dT) library, and the other against the oligo-dT-primed (O-dT) library (despite the latter one not having been as thoroughly characterised).

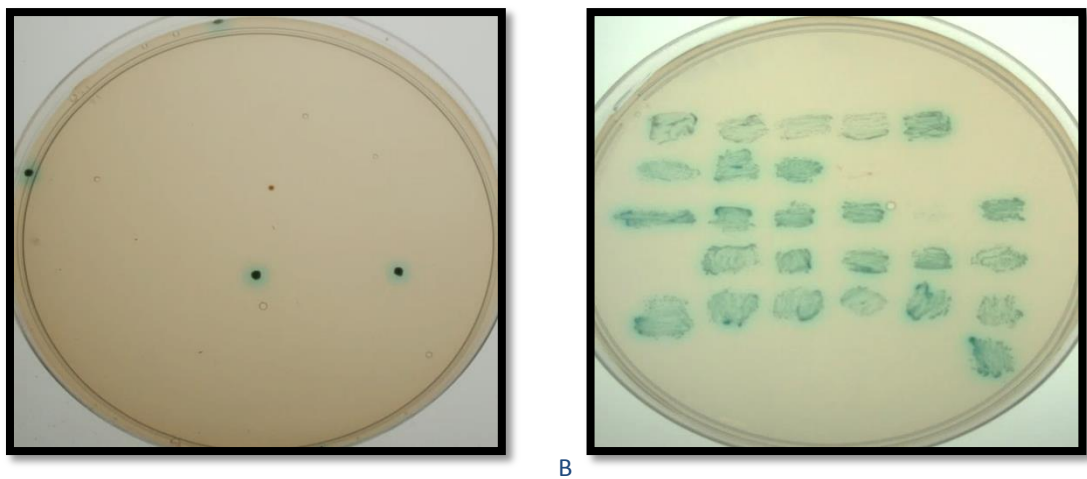
The Y2H screens were subject to a two-tier selection process. Initially, for each Y2H screen, the mated culture was spread over 66 yeast media plates (selecting for activation of PPI reporter genes *Mel1* and *Aur-C*). Between zero and three colonies grew on most plates; more colonies per plate were seldom observed (e.g. plates in Figure 4-3 and Figure 4-4). Over  $10^7$  clones from each of the two human retinal cDNA libraries were screened (Table 4-3). After the first selection 24 and 48 colonies resulted from the screen against O-dT and R&O-dT library, respectively. Following this, each observed colony was picked and patched on higher stringency media, aiming to activate reporter genes *His3* and *Ade2* in addition to *Mel1* and *Aur-C*. Selection with additional two reporter genes led to a successful isolation of 21 and 32 positive clones, respectively.

The findings of the two screens were combined, and DNA was extracted from all 53 yeast patches. Library inserts were amplified by colony PCR using vector-specific primers, and amplicons larger than 300 bp were subsequently purified and sequenced. Figure 4-5 exemplifies the extent of prey insert sizes; amplicons from lanes 2-6 were  $\geq 600$  bp in size, therefore they were extracted from the gel and sequenced. The 300 bp large amplicon from lane 7 was not considered in further analysis, as it was large enough to encompass mainly the insert-flanking regions of the library vector (equating to an empty vector).

Following the PCR-based insert analysis, 19 clones with large enough ( $\geq 300$  bp) inserts were isolated from the O-dT library screen, and all 32 from the R&O-dT library. Among these, 12 and 32, respectively, were found to align with genes; these alignments included 6 and 28 protein-coding regions, respectively, as determined using the BLAT (UCSC) search (Table 4-4). Sequences aligning to intergenic, intronic or UTR were eliminated from further investigation.



A B  
Figure 4-3. A, Example of single plate from Y2H O-dT library screen. Initial selection: PPI reporter genes, Mel1 and Aur-C. Blue colouration suggests interaction of bait with unknown prey. B, All clones, isolated from the initial O-dT selection stage, were patched on to higher stringency media; reporter genes: Mel1, Aur-C, His3 and Ade2. Three of the 24 blue colonies, did not re-grow.



A B  
Figure 4-4. A, Example of single plate from Y2H R&O-dT library screen. Initial selection: PPI reporter genes, Mel1 and Aur-C. Blue colouration suggests interaction of bait with unknown prey. B, All clones, isolated from the initial R&O-dT selection stage, were patched on to higher stringency media; reporter genes: Mel1, Aur-C, His3 and Ade2. Eleven of the 36 blue colonies patched on the plate presented in figure B, did not re-grow.

The clones, which aligned with exonic, protein-coding, gene fragments, were subsequently categorised, using the Swiss-Prot (UniProtKB) annotations, and RefSeq (NCBI) annotations. All clones were also checked against RetNet, a Retinal Information Network.

Retina-associated proteins were categorised together based on their high expression in this tissue, and/or a specific (patho)physiological role (Table 4-6). The cytoskeletal and trafficking proteins were evaluated due to potential involvement in ciliary transport, which is vital to the health of photoreceptor cells, and as several proteins involved in this function have already been implicated in retinal degeneration. The category of protein turnover and modification was crucial due to the function of TOPORS as ubiquitin E3 ligase.

Mitochondrial proteins were given attention due to high energy requirement of photoreceptors.

Nuclear proteins were included based on known functions of TOPORS inside cell nucleus (Table 4-6 and Appendix 11.6).

Table 4-3. Quantitative results of Y2H screens.

	Screen of O-dT library	Screen of R&O-dT library
<b>Number of clones screened</b>	3.29 x 10 <sup>7</sup>	1.63 x 10 <sup>7</sup>
<b>AUR1-C+ve &amp; MEL1+ve</b>	24 (six shown in Figure 4-3: A)	48 (five shown in Figure 4-3: B)
<b>AUR1-C+ve, MEL1+ve, HIS3+ve &amp; ADE2+ve</b>	21 (all shown in Figure 4-4: A)	32 (25 shown in Figure 4-4: B)

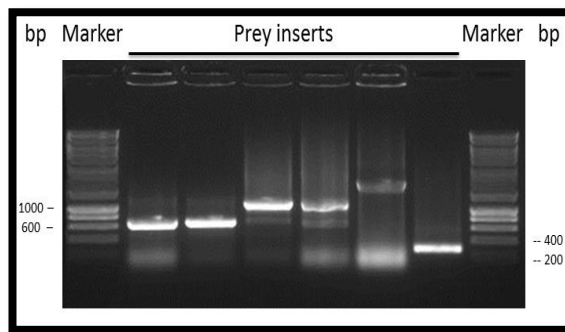


Figure 4-5. PCR amplification of prey inserts, pulled out from the R&O-dT cDNA Y2H library screen (Mango *Taq* polymerase).

Lane 1: Hyper Ladder I marker. Lanes 2-7: Inserts amplified from prey colony patches. Lane 8: Hyper Ladder I marker. Two microliters of the PCR product were loaded per well. Bands ≥300 bp large were purified from the gel and sequenced; size in base pairs (bp) is indicated on either side of the figure. One percent agarose gel with ethidium bromide.

Table 4-4. Quantitative results from prey selection process.

	Screen of O-dT library	Screen of R&O-dT library
<b>Clones obtained from Y2H screen</b>	21	32
<b>Clones with inserts of ≥300 bp in size</b>	19	32
<b>Clones with cistronic inserts</b>	12	32
<b>Clones with exonic inserts</b>	6	28

Table 4-5. Retina-associated Y2H preys. Functional data from UniProtKB and RefSeq (NCBI).

Expression data from UniProtKB, or databases redirected to from protein-specific Swiss-Prot annotation page.

Y2H clone	Gene from BLAT search	RefSeq Gene Summary	Protein name (ID)	Swiss-Prot Protein Function Summary	Protein Expression	Other notes
R&O-dT 27	<i>ITM2B</i> (aka <i>BRI</i> ; <i>abri</i> ; <i>ABRI</i> ; <i>BRI2</i> ; <i>E25B</i> ; <i>E3-16</i> ; <i>imBRI2</i> ; <i>BRICD2B</i> )	Amyloid precursor proteins are processed by beta-secretase and gamma-secretase to produce beta-amyloid peptides which form the characteristic plaques of Alzheimer disease. This gene encodes a transmembrane protein which is processed at the C-terminus by furin or furin-like proteases to produce a small secreted peptide which inhibits the deposition of beta-amyloid. Mutations which result in extension of the C-terminal end of the encoded protein, thereby increasing the size of the secreted peptide, are associated with two neurodegenerative diseases, familial British dementia and familial Danish dementia.	Integral membrane protein 2B (Q9Y287)	Plays a regulatory role in the processing of the beta-amyloid A4 precursor protein (APP) and acts as an inhibitor of the beta-amyloid peptide aggregation and fibrils deposition. Plays a role in the induction of neurite outgrowth. Functions as a protease inhibitor by blocking access of secretases to APP cleavage sites.	Ubiquitous; High in Brain	Recently, <i>ITM2B</i> has also been associated with a dominantly inherited retinal dystrophy (Audo <i>et al.</i> , 2013).
R&O-dT 29						

Y2H clone	Gene from BLAT search	RefSeq Gene Summary	Protein name (ID)	Swiss-Prot Protein Function Summary	Protein Expression	Other notes
R&O-dT 28	<i>PDC</i> (aka <i>PHD</i> ; <i>MEKA</i> ; <i>PhLP</i> ; <i>PhLOP</i> )	This gene encodes a phosphoprotein, which is located in the outer and inner segments of the rod cells in the retina. This protein may participate in the regulation of visual phototransduction or in the integration of photoreceptor metabolism. It modulates the phototransduction cascade by interacting with the beta and gamma subunits of the retinal G-protein transducin. This gene is a potential candidate gene for retinitis pigmentosa and Usher syndrome type II. Alternatively spliced transcript variants encoding different isoforms have been identified.	Phos-ducin (P20941)	May participate in the regulation of visual phototransduction or in the integration of photoreceptor metabolism. Inhibits the transcriptional activation activity of the cone-rod homeobox CRX.	Ubiquitous; High in Retina	Only of very small fragment of the library insert could be sequenced (~60 bp).

Y2H clone	Gene from BLAT search	RefSeq Gene Summary	Protein name (ID)	Swiss-Prot Protein Function Summary	Protein Expression	Other notes
<b>R&amp;O-dT 31</b>		The protein encoded by this gene is a glutathione-independent prostaglandin D synthase that catalyses the conversion of prostaglandin H2 (PGH2) to prostaglandin D2 (PGD2). PGD2 functions as a neuromodulator as well as a trophic factor in the central nervous system. PGD2 is also involved in smooth muscle contraction/relaxation and is a potent inhibitor of platelet aggregation. This gene is preferentially expressed in brain. Studies with transgenic mice overexpressing this gene suggest that this gene may be also involved in the regulation of non-rapid eye movement sleep.		Catalyses the conversion of PGH2 to PGD2, a prostaglandin involved in smooth muscle contraction/relaxation and a potent inhibitor of platelet aggregation. Involved in a variety of CNS functions, such as sedation, NREM sleep and PGE2-induced allodynia, and may have an anti-apoptotic role in oligodendrocytes. Binds small non-substrate lipophilic molecules, including biliverdin, bilirubin, retinal, retinoic acid and thyroid hormone, and may act as a scavenger for harmful hydrophobic molecules and as a secretory retinoid and thyroid hormone transporter. Possibly involved in development and maintenance of the blood-brain, blood-retina, blood-aqueous humor and blood-testis barrier. It is likely to play important roles in both maturation and maintenance of the central nervous system and male reproductive system.	Abundant in brain/CNS; secreted into cerebrospinal fluid. Abundant in heart and chick male reproductive system; secreted into semen. Expressed in eye; secreted into aqueous humour. Lower levels in tissue fluids: serum, normal urine, ascitic fluid, tears. Found in female reproductive system, kidney, leukocytes.	
<b>R&amp;O-dT 45</b>	PTGDS (aka PDS; PGD2; PGDS; LPGDS; PGDS2; L-PGDS)		Prosta-glandin-D2 synthase (P41222)			
<b>R&amp;O-dT 47</b>						



Table 4-6. A summary of genes encoding potential interacting partners of TOPORS, as identified by prey sequencing.

BLAT search (UCSC Genome Browser) was used to identify the sequenced preys, which were categorised according to reviewed Swiss-Prot (Protein Knowledgebase: UniProtKB) and RefSeq (NCBI database) annotations (included in the Appendix).

Retina-Associated	Cytoskeleton & Trafficking	Protein Turnover & Modification	Mitochondrial	Nuclear	Others
<i>ITM2B, PDC, PTGDS</i>	<i>TPT1, DYNC1LI2, DPYSL3</i>	<i>UBA52, UBB, UBC, RPL10, PSMC1, CTSD, PPP1R16A, CSNK1D, MGEA5, NMT1</i>	<i>NDUFB10, NDUFS2, PRDX5</i>	<i>ZNF7, AES, SCAF4, PIAS1</i>	<i>ENO3, RPS7, SLC22A6, LMAN1, RPL31, SOD1</i>
Table 4-5	Appendix 11.6				

The retina-associated clones were prioritised for further studies, which led to a more in depth analysis of alignments of *PDC* and *PTGDS* clones<sup>14</sup> with their annotated sequences (UCSC Genome Browser was used).

*PDC*, an attractive candidate due to its involvement in phototransduction responses, was disregarded, as only approximately 60 bp of the library clone (1.5 kb in size at PCR level) could be sequenced. The remainder of the sequence appeared as a noisy electropherogram (data not shown), a problem not resolved by repeated PCR amplification of the isolated library clone.

*PTGDS*, encoding a brain prostaglandin D2 synthase, highly expressed in the retina, and previously suggested to play a role in retinal homeostasis (Yamakawa e Ogino, 1986; Beuckmann *et al.*, 1996; Shiroma *et al.*, 1996), was also evaluated. The interaction with this clone was picked up in three (out of a final 34) cases. Alignment analysis of the three clones suggested that they had probably originated from three copies of the same cDNA insert during the R&O-dT library construction (Figure 4-6 A-C). It should also be noted that all three clones cover virtually the entire protein-coding region of the *PTGDS* gene, isoform 001 (Ensembl database). This increases the chances of correct protein folding, and hence that probability that the observed interaction is genuine. It was also demonstrated that the *PTGDS* fragment was inserted in frame in all three clones: Figure 4-7 shows the reference sequence that the reading frames were checked against. The results for one of the three clones are summarised in Figure 4-8; the same result was observed in all three cases.

<sup>14</sup> *ITM2B* was originally placed in the ‘Protein Turnover & Modification’ category, as its association with retinal disease emerged only recently (Audo *et al.*, 2013).

The sequence alignment and reading-frame verification procedure, outline in the *PTGDS* example, was applied to all of the candidate genes, which were listed in Table 4-6, and led to selection of additional two candidate interacting partners for Y2H PPI experiments.

A soluble fragment of integral membrane protein 2B (*ITM2B*), previously linked to neurodegenerative disorders, was selected primarily due to its high expression in CNS, and the familial nature of diseases, in which it is involved (Vidal *et al.*, 1999; Vidal *et al.*, 2000). It had firstly been categorised with proteins involved in protein modification and degradation due to its role in APP processing (Matsuda *et al.*, 2008). The association of *ITM2B* with isolated inherited retinal disease is a much more recent finding (Audo *et al.*, 2013), which caused its reclassification as a retina-associated gene.

The interaction with *ITM2B* was found in two (Figure 4-9) of the 34 clones selected through the Y2H screen. The gene fragment in both clones aligns with exons 3-6 of the *ITM2B*, isoform 001 (Ensembl database), which approximately corresponds to the C-terminal fragment of the peptide. This fragment is typically cleaved during *ITM2B* processing; a membrane-bound, full-length *ITM2B* protein should not have been able to interact with TOPORS in a transcription-based Y2H assay, which was used here. The reading frame of both clones was correct; the result for one of the clones is shown in Figure 4-10.

In addition to the two preys, associated with the retina, *PSMC1* (Table 4-6) was also selected for evaluation. The *PSMC1* protein is a regulatory ATPase subunit of the proteasome, essential for its correct function across eukaryotic kingdoms (Köhler *et al.*, 2001; Bedford *et al.*, 2008; Lee *et al.*, 2011); it presumably acts downstream of TOPORS in the ubiquitin-proteasome system (UPS), and it may be directly involved in mediating retinal protein turn-over. Interestingly, the *Arabidopsis* orthologue of *PSMC1*, *RPT2A/RPT2B*, plays a role in mediating light-induced stress in plant cells (Lee, K. H. *et al.*, 2012). It would be exciting to see whether *PSMC1* might accordingly have photoreceptor-specific functions also in the animal kingdom. The amino-terminal half of *PSMC1* (*PSMC1*-001; Ensembl database) was pulled out from the Y2H PPI screen with TOPORS used as bait (Figure 4-11). The gene appeared to be inserted in frame with GAL4 AD (Figure 4-12).

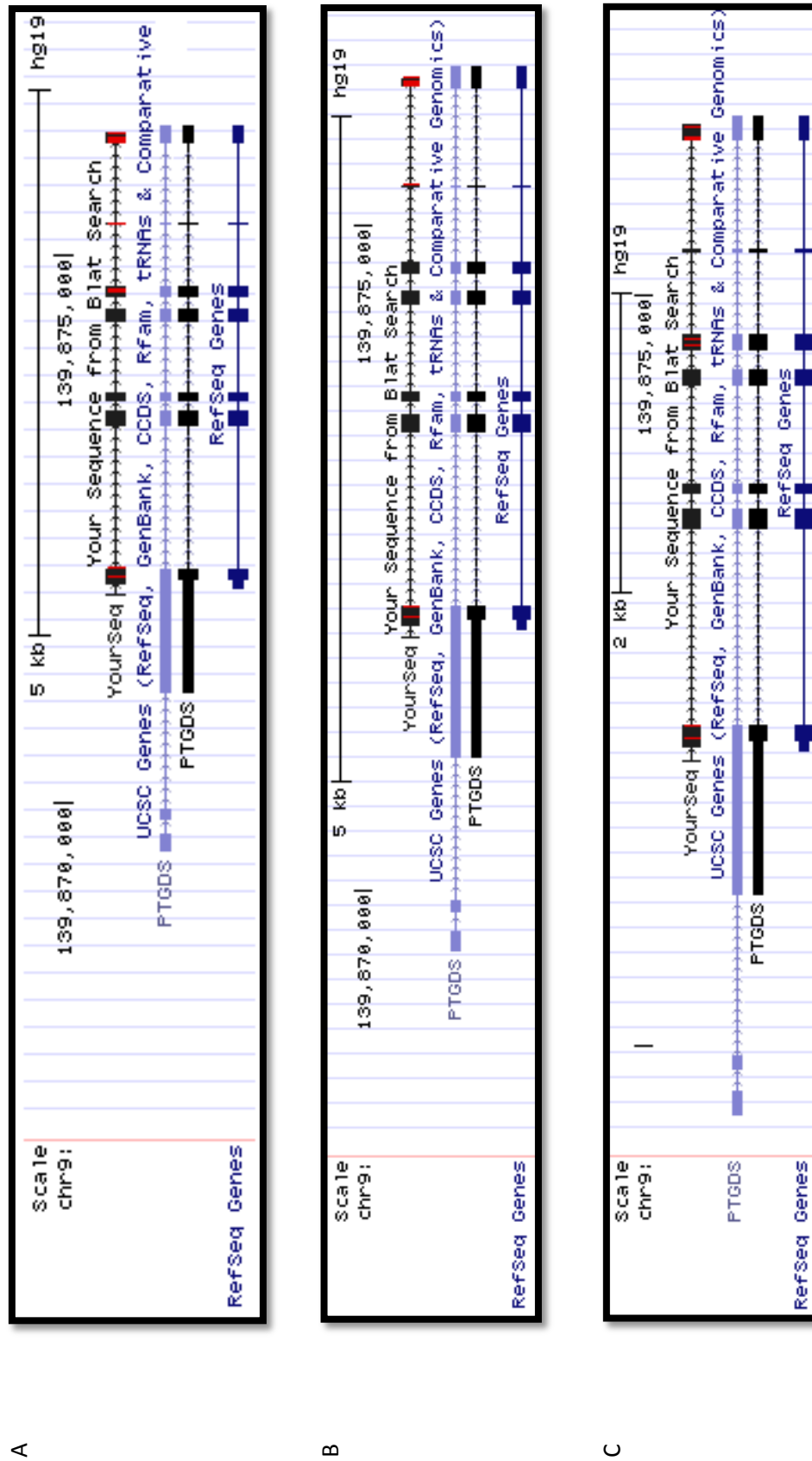


Figure 4-6. *PTGDS* alignments. Snapshot of results obtained from BLAT (UCSC) genome search. A, clone R&O-dT 31; B, clone R&O-dT 45; C, clone R&O-dT 47.

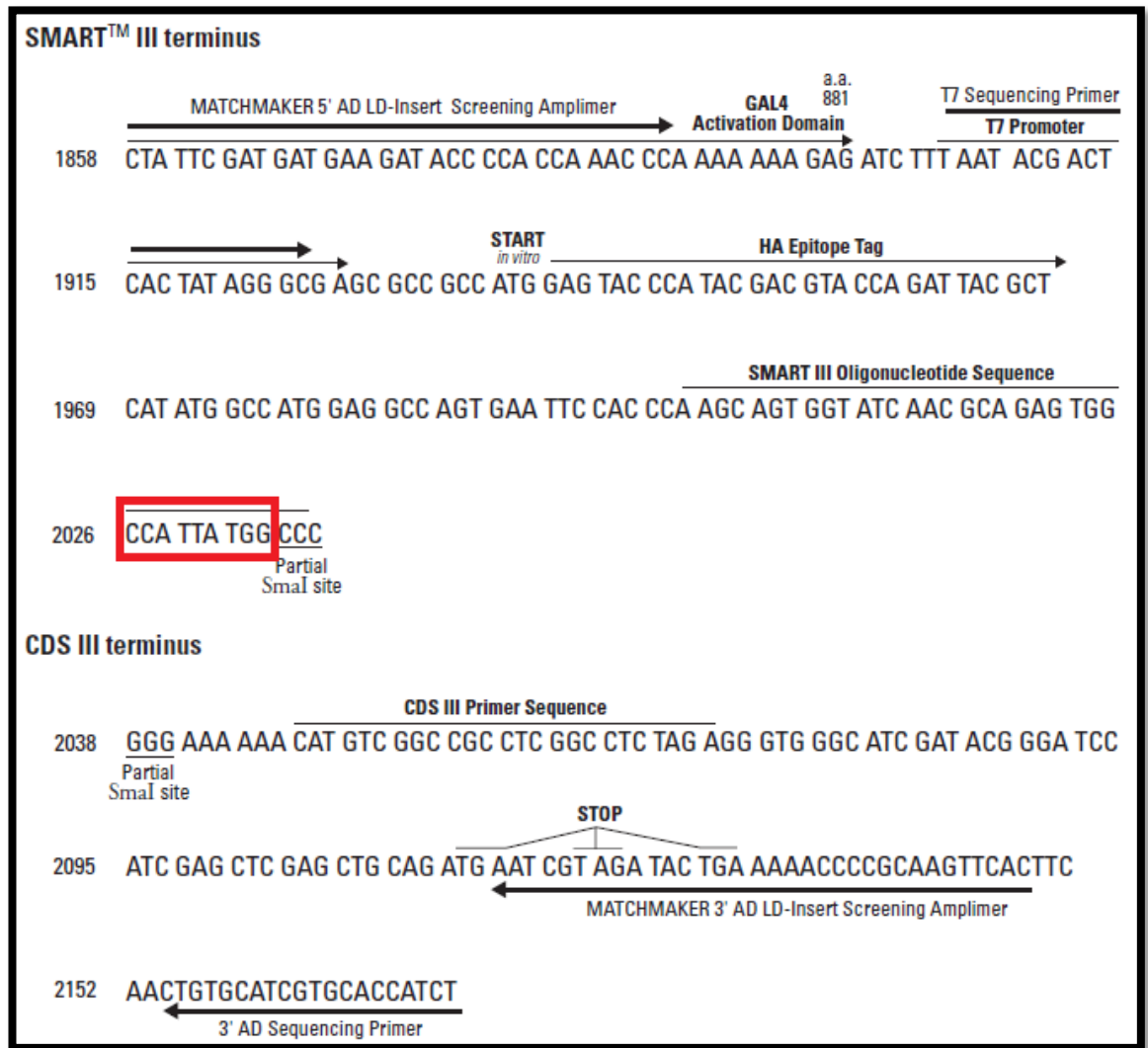


Figure 4-7. Multiple cloning site (MCS) of the pGADT7-Rec Vector, in which the human retinal cDNA library was constructed. The sequence used for reading frame verification of the inserts is highlighted in red. From the pGADT7-Rec Vector Information brochure (Clontech, CA, USA).

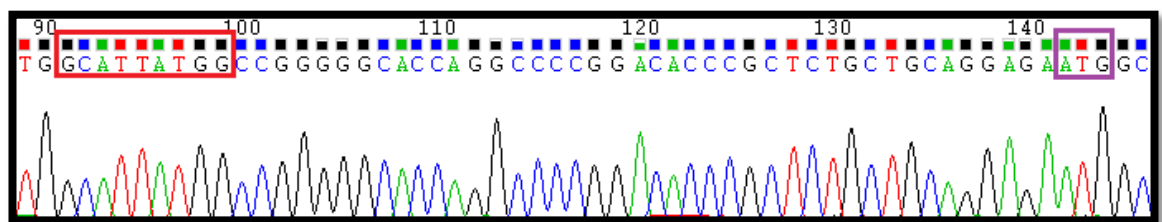


Figure 4-8. One of *PTGDS* library clones: sequence snapshot. The fragment highlighted in red corresponds to the vector reference sequence (Figure 4-7). The ATG start codon of *PTGDS* is highlighted in purple. The gene was inserted in frame with GAL4 AD sequence: 42 nucleotides are included between the vector's reference sequence and the gene's start codon. Identical result was observed for all three clones.

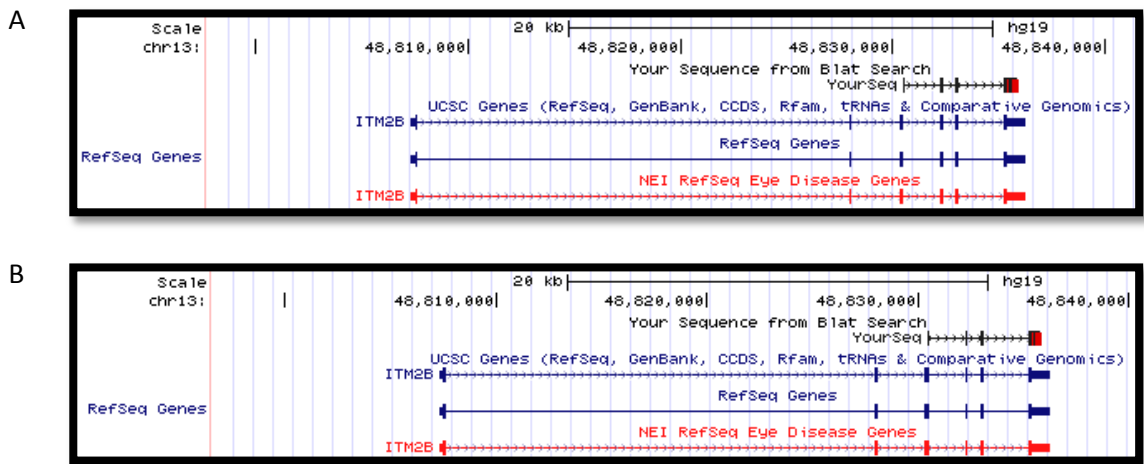


Figure 4-9. *ITM2B* alignments. Snapshot of results obtained from BLAT (UCSC) genome search. A, clone R&O-dT 27; B, clone R&O-dT 29.

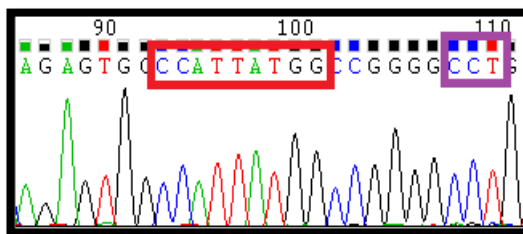


Figure 4-10. One of *ITM2B* library clones: sequence snapshot.

The fragment highlighted in red corresponds to the vector reference sequence (Figure 4-7). The CCT codon of *ITM2B*, which corresponds to Proline 133 of the *ITM2B* peptide, and forms the beginning of the *ITM2B* clone isolated here, is highlighted in purple.

The gene was inserted in frame with GAL4 AD sequence: six nucleotides are included between the vector's reference sequence and the gene's CCT codon. Identical result was observed for both clones.

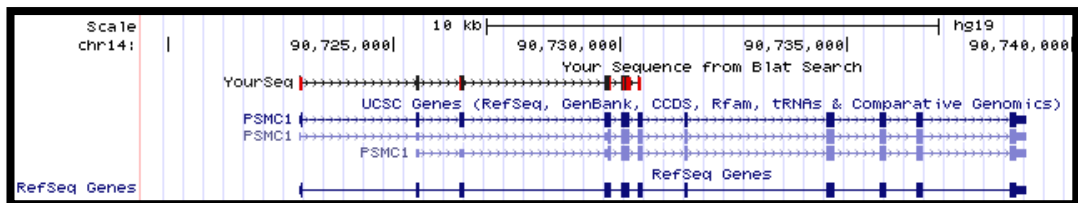


Figure 4-11. *PSMC1* clone R&O-dT 2.2 alignment. Snapshot of results obtained from BLAT (UCSC) genome search.

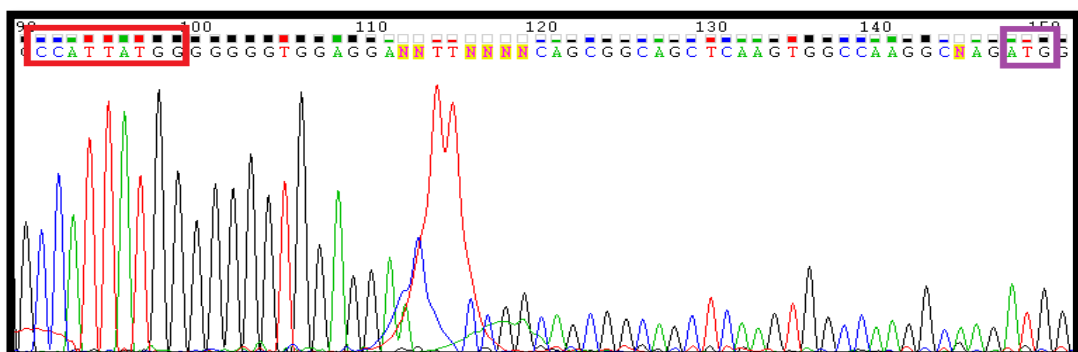


Figure 4-12. *PSMC1* library clone: sequence snapshot.

The fragment highlighted in red corresponds to the vector reference sequence (Figure 4-7). The start codon of *PSMC1*, is highlighted in purple. The gene was inserted in frame with GAL4 AD sequence: 48 nucleotides are included between the vector's reference sequence and the gene's start codon.

### 4.3 DISCUSSION

The goal of the Y2H screening for protein interacting partners of TOPORS was to identify a protein expressed only in the retina, or fulfilling a role specific to this tissue. *TOPORS* is ubiquitously expressed, yet its mutations have only been associated with retinal disease phenotypes. Hence, it was hypothesised that TOPORS must have a retina-specific interacting partner essential for retinal homeostasis.

No such protein, which would have an obvious strong association with either structure or function of the retina, was identified.

However, three of the putative interacting partners of TOPORS, identified via the Y2H screen, were promising candidates, as they were previously shown to be associated with either the retina or, more widely, the central nervous system. These proteins, selected for further protein-protein interaction (PPI) validation studies, were ubiquitously expressed and comprised:

- Integral membrane protein 2B (*ITM2B*);
- Lipocalin-type, glutathione-independent prostaglandin D2 synthase (*PTGDS*);
- 26 S Protease regulatory subunit 4 ATPase (*PSMC1*).

*ITM2B* was an attractive candidate due to its historic involvement in familial dementia (Vidal *et al.*, 1999; Vidal *et al.*, 2000) and, more recently, a retinal dystrophy (Audo *et al.*, 2013). *PTGDS*, a multifunctional protein important for proper function of multiple bodily systems, was selected due to its high expression and activity in the central nervous system, and specifically, the retina as well as a potential role in maintenance of the blood-retina barrier (Beuckmann *et al.*, 1996; Shiroma *et al.*, 1996; Gerashchenko *et al.*, 1998; Irikura *et al.*, 2007). *PSMC1* was selected for further evaluation due to its key role in the proteasomal system and neurodegeneration (Bedford *et al.*, 2008; Bedford *et al.*, 2009; Gómez-Garre *et al.*, 2012; Rezvani *et al.*, 2012). Consequently, in view of the well-established function of TOPORS as an E3 ubiquitin protein ligase, *PSMC1* was an obvious candidate to investigate, despite its ubiquitous expression.

The next section discusses the process of the Y2H screening for interacting partners. The selected candidate interacting partners are evaluated in sections 4.3.2 – 4.3.4.

### 4.3.1 Y2H SCREENS AND PREY IDENTIFICATION

Following library validation and confirmation of bait expression, Y2H screens were performed in order to identify proteins, which interact with TOPORS. Two screens were performed; one of a library constructed using only the O-dT primer, and one using the R&O-dT library, constructed using the o-dT and the additional R primer. Both screens utilised the *Me11* and *Aur-C* reporter genes. Putative positive interacting partners isolated through this first round of screening were subsequently validated on higher stringency media, which in addition to the first two reporters, also required expression of two nutritional reporter genes, *Ade2* and *His3*.

The O-dT and R&O-dT screens yielded a high number of candidate interacting partners, 21 and 32, respectively. However, subsequent analysis showed that only six of the 21 O-dT clones carried protein-coding gene fragments; on the other hand most (28/32) of clones pulled out from the R&O-dT library were protein coding (Table 4-3). This result provides additional indirect evidence for superiority of the R&O-dT library over the O-dT library, as analysed earlier. Genes from the positive clones were prioritised for subsequent validation based on information collated from genomic and protein databases. Such a strategy was necessary, as in view of the great number of candidate interactions, a thorough literature review for each one could not be performed. Three genes were selected for further interaction validation experiments based on the described criteria (section 4.2): *ITM2B*, *PTGDS* and *PSMC1*. The full-length transcript of each gene (isoform corresponding to the one identified in the Y2H screen, and verified in the retinal isoform experiment: section 5.1) was cloned into the relevant Y2H vector for control experiments in yeast. Additionally, known *ITM2B* mutants as well as a gene fragment encoding a soluble ITM2B peptide fragment were also tested. It was, firstly, demonstrated that the PPI-indicative phenotypes, observed in yeast, were not due to interaction with the GAL4 BD (section 4.1). Subsequently, each prey was tested again for direct interaction with TOPORS (section 4.2) to ensure that the resulting full-length peptide was still able to associate with the bait. The preys, identified from the screen, corresponded to fragments of genes only, and consequently the expressed peptides were not representative of full-length proteins. This could have led to incorrect folding, and hence the apparent interaction could have been artificial. The use of full-length proteins increases the likelihood that the encoded proteins will be folded correctly, even when fused to the GAL4 AD; therefore, this experiment provided a valuable validation of the results, observed in the Y2H screens.

### 4.3.2 INTEGRAL MEMBRANE PROTEIN 2B

*Itm2B* was first described in mouse by Pittois *et al.* (1998) who established its ubiquitous expression at mRNA level. This was supported by findings of Pickford *et al.* (2003), who demonstrated *Itm2b* mRNA expression in liver, heart, lung, kidney, and brain of mice with higher levels observed some brain regions, such as Purkinje cells in the cerebellum. At protein level Itm2B was elevated in the cerebellum, midbrain and olfactory bulb, and outside the brain in the lung, heart, kidney, liver, and skeletal muscle. Hippocampal expression was also documented (Meyer, 2014). In human tissues *ITM2B* mRNA was expressed ubiquitously, and at highest levels in kidney, brain, pancreas and placenta. ITM2B protein was detected in the cytoplasm of hippocampal neurons, and cerebellar Purkinje cells (Akiyama *et al.*, 2004).

#### 4.3.2.1 ITM2B IN CONTEXT OF DEMENTIA AND NEURODEGENERATION

In 1999, Vidal *et al.* demonstrated that a point mutation (c.799T>A) in *ITM2B* causes autosomal dominant Familial British Dementia (adFBD). Further symptoms included an overall cognitive impairment, spasticity, and cerebellar ataxia. Pathologically, the disease was characterised by cerebral amyloid angiopathy, non-neuritic and perivascular plaques, neurofibrillary tangles, and hippocampal neurofibrillar degeneration.

The identified mutation occurs in the stop codon of *ITM2B*, resulting in an extension at the C-terminus of the ITM2B protein (p.\*267Argext\*11). In physiological conditions the protein is constitutively cleaved near the C-terminus by furin, or a related protease (Kim *et al.*, 1999), generating a 23-amino acid long peptide. In the FBD mutant, the generated C-terminus peptide, named ABri, is 34-residues long, and forms a component of amyloid complexes (unrelated to A $\beta$  (Ghisso *et al.*, 2000)). Kim *et al.* also demonstrated that the furin cleavage of the British (FBD) mutant is up-regulated, comparing to wild-type ITM2B. ABri formed both fibrillar (amyloid), and non-fibrillar (pre-amyloid) lesions in parenchyma and blood vessels of the nervous system; only the amyloid deposits triggered microglial and astrocytic response (Holton *et al.*, 2001), and were associated with elevated levels of the complement cascade proteins (Rostagno *et al.*, 2007).

Shortly after identification of the British (FBD) mutant, a novel *ITM2B* mutation was identified in a Danish family, causing autosomal dominant Familial Danish Dementia (adFDD). Besides the memory loss, the patients additionally suffered from cataracts, deafness, and ataxia. Similarly to FBD, pathological changes included cerebral amyloid angiopathy, hippocampal plaques, and neurofibrillary tangles.



The ITM2B protein product also resulted in an extended C-terminal amyloid-forming fragment, denoted ADan; however, this was due to a decamer duplication: c.786\_795dupTTTAATTTGT (p.Ser266Pheext\*12). Like in case of the FBD ITM2B, the furin cleavage of the Danish (FDD) mutant was also enhanced in comparison to wild-type (Kim *et al.*, 2002). Interestingly, although ABri presence was both intra- and extra-cellular, ADan was found predominantly inside the cells (Kim *et al.*, 2002).

Furthermore, multiple sclerosis studies showed that decreased levels of wild-type furin-generated ITM2B C-terminal peptide in cerebrospinal fluid, were associated with cognitive problems (Harris *et al.*, 2010). The study also demonstrated that *ITM2B* expression is down-regulated in the cerebellum of multiple sclerosis patients. The documented association of *ITM2B* with diseases of the CNS system suggests it may have a unique role in neurons and/or other cell types of the CNS, despite its ubiquitous expression.

#### 4.3.2.2 *ITM2B IS ASSOCIATED WITH AUTOSOMAL DOMINANT RETINAL DYSTROPHY*

Audo *et al.* (2013) recently demonstrated that a novel point mutation in *ITM2B* causes an isolated, dominantly inherited retinal dystrophy, characterised by defects in the inner retina and the retinal ganglion cells. *ITM2B* mRNA was detected in both INL and GCL, consistently with the affected areas. Moreover, the group also demonstrated ITM2B and APP co-localisation in the GCL of the retina. Table 4-7 summarises the *ITM2B*-associated phenotypes identified to date.

Although the proband experienced night blindness, which could suggest the initial stages of RP, only a sibling of the proband also reported night vision problems. All of the affected family members, including the two with night blindness, consistently experienced photophobia and a progressive loss of central vision. Peripheral vision was unaffected in all patients, and visual acuity varied. Three of the affected members experienced colour vision disorders. Ophthalmoscopic examination revealed pale optic discs and some foveal changes, whereas fundus auto-fluorescence was consistently enhanced around the macula. Optical coherence tomography typically revealed hyper-reflectivity within the inner retina and foveal ONL. The disease onset among the affected members typically occurred between 25 and 40 years of age. Importantly, no systemic symptoms and no dementia were experienced by any of the affected members.

Table 4-7. Summary of mutations identified in *ITM2B* to date.

DNA mutation	Protein mutation	Phenotype	Reference
<b>c.799T&gt;A</b>	p.*267Argext*11	adFBD: dementia/cognitive impairment, spasticity, cerebellar ataxia, cerebral amyloid angiopathy, non-neuritic and perivascular plaques, neurofibrillary tangles, hippocampal neurofibrillar degeneration	(Vidal <i>et al.</i> , 1999)
<b>c.786_795 dupTTTAA TTTG</b>	p.Ser266Phe ext*12	adFDD: cataracts, deafness, ataxia, dementia, cerebral amyloid angiopathy, hippocampal plaques, neurofibrillary tangles	(Vidal <i>et al.</i> , 2000)
<b>c.782A&gt;C</b>	p.Glu261Ala	adRD: retinal dystrophy with inner retinal dysfunction and ganglion cell layer defects; photophobia; decreased vision	(Audo <i>et al.</i> , 2013)

#### 4.3.2.3 *ITM2B HAS A ROLE IN CANCERS*

*ITM2B* is a potential tumour suppressor gene, as loss of heterozygosity (LOH) at its chromosomal location (13q14) is among the most frequent changes associated with sporadic prostate cancer (Latil *et al.*, 2003). *ITM2B* and three other genes found at this location are differentially expressed in prostate cancers; however, the strongest association was found for *ITM2B*, making it the major candidate. Furthermore, *ITM2B* was deleted in an atypical cell lipoma (Creytens *et al.*, 2014), and it was differentially expressed in lung adenocarcinoma metastatic cell lines (Yang *et al.*, 2003).

Additionally, *ITM2B* is among genes differentially expressed in Wilms tumour, a common children's neoplasia, where its expression is regulated by all-*trans* retinoic acid (Zirn *et al.*, 2005). This suggests that *ITM2B* may be a component of the retinoic acid signalling pathway, in which prostaglandin D2 synthase (*PTGDS*), an interacting partner of TOPORS identified during this project, also participates. *PTGDS* directly interacts with RIG1 (retinoic acid-inducible gene 1), and the pair appears to work in concert to suppress testicular cancer development (Wu *et al.*, 2012; Shyu *et al.*, 2013).

In a human bladder cancer model it was shown that *ITM2B* is involved in mediating cell survival responses. Their effects could be silenced by methylation or mutations. Substitution mutations within and a deletion of the apoptosis-associated BH3 domain of *ITM2B*<sub>s</sub> all resulted in loss of regulated cell death activity. Furthermore, hypermethylation of the CpG island within the *ITM2B* promoter was found in six out of twelve bladder cancer cell lines, resulting in a two-fold decrease in *ITM2B* expression; the group also found that hypermethylation of the *ITM2B* promoter occurred in 40 % of tumour samples from transitional cell carcinomas of the bladder.

The involvement of ITM2B in cancer suggests that it may possibly be involved in regulation of the cell cycle. *TOPORS* is also differentially expressed in a range of tumours, as well as it is closely associated with the centrosome. It could be speculated that perhaps this organelle is the site of interaction between ITM2B and *TOPORS*, where they may act in concert to coordinate cell cycle activities.

### **4.3.3 PROSTAGLANDIN D2 SYNTHASE**

Prostaglandin D2 synthase (*PTGDS*) is the main arachidonic acid metabolite (Figure 4-13) produced in neurons and glia of the central nervous system (García-Fernández *et al.*, 1998; Payne *et al.*, 2008).

In mouse brain *Ptgds* was shown to induce morphological changes in glia, resembling reactive gliosis. Glial cell migration enhanced actin filament and focal adhesion formation and activation of AKT, RhoA and JNK signalling pathways. At the same time, *Ptgds* was shown to promote migration and accumulation of astrocytes, possibly via its PPI with myristoylated alanine-rich protein kinase C substrate (MARCKS), which promotes cell migration (Lee, S. *et al.*, 2012).

#### **4.3.3.1 GENETIC INTERACTIONS OF PTGDS**

Notably, an association between *TOPORS* and *PTGDS* might occur, in addition to the identified PPI, also at a genetic level. It was shown in a human cell line, derived from the medulloblastoma of cerebellum (TE671 cells), that *Hes1* (dHairy homologue known to interact with dTopors) binds to the N-box region within the *PTGDS* promoter. The activity of the *PTGDS* promoter increases by 220 % - 300 % due to deletion of the N-box. In agreement, expression of Notch cellular domain leads to an increased *Hes1* expression, but to a decreased *PTGDS* expression; whereas silencing of *Hes1* results in elevated *PTGDS* levels. These results indicate that the Notch-*Hes1* signalling pathway acts to repress *PTGDS* expression (Fujimori, Kadoyama e Urade, 2005).

The deletion of another fragment of the *PTGDS* promoter, the AP-2 element, leads to a significant decrease in the promoter's activity to 10 % of its normal level.



Figure 4-13. Prostaglandin D2 (PGD) synthase as a component of arachidonic acid metabolism. PGG<sub>2</sub>, prostaglandin G<sub>2</sub>; PGH<sub>2</sub>, prostaglandin H<sub>2</sub>; PGF<sub>2α</sub>, prostaglandin F<sub>2α</sub>; PGD<sub>2</sub>, prostaglandin D<sub>2</sub>; PGE<sub>2</sub>, prostaglandin E<sub>2</sub>; PGI<sub>2</sub>, prostaglandin I<sub>2</sub>; TXA<sub>2</sub>, thromboxane A<sub>2</sub>. Figure from Sorokin (2011).

The AP-2 element, is bound by the activator protein 2 (AP-2), a mammalian transcription factor, induced by retinoic acid, and which is specifically regulated during development. It should also be mentioned that retinoic acid also induces *RIG1* expression, whose protein product PTGDS interacts with (Wu *et al.*, 2012). Moreover, an over-expressed protein kinase C (PKC), which phosphorylates PTGDS, has also been shown to phosphorylate Hes1. The Hes1 phosphorylation prevents it from binding to the N-box within the *PTGDS* promoter region. Exogenous expression of PKC has also been associated with up-regulating *PTGDS* expression via AP-2 (Fujimori, Kadoyama e Urade, 2005).

#### 4.3.3.2 ROLE OF PTGDS IN THE RETINA

Prostaglandin D2 synthase was first studied in the retina of a chick by Yamakawa & Ogino (1986), who suggested that the enzyme was not active in the neural retina, but it had a high activity in the RPE. The activity was greatly enhanced by glutathione; however, at a slower rate prostaglandin (PG) D2 was also synthesised from PG H2 in its absence. No PG E2 synthesis (also

from PG H<sub>2</sub>; Figure 4-13), evaluated as a control, was observed either in the presence or absence of glutathione.

It should be noted that two types of prostaglandin D<sub>2</sub> synthase can be distinguished. The one identified in the Y2H screen, as an interacting partner of TOPORS, was the lipocalin-type glutathione-independent neurone (UniProt: P41222), encoded by the *PTGDS* gene. The enzyme activity, originally detected in the chick retina (Yamakawa & Ogino, (1986) was probably generated due to collective action of PTGDS as well as the hematopoietic glutathione-dependent prostaglandin D<sub>2</sub> synthase (UniProt: O60760), encoded by the *HPGDS* gene (UniProt: O60760).

A year later, Goh *et al.* (1987) reported their findings on synthesis and levels of PG D<sub>2</sub>, E<sub>2</sub>, and F<sub>2</sub>α in different regions of the rat ocular system. They dissected the rat eye (Figure 1-1. Structure of the Eye.) into the anterior and posterior segments along the ora serrata, and isolated the 'uveal complex', i. e. the cornea, iris and ciliary body (the lens was removed) from the anterior half of the eye. The posterior part of the eye was further sub-divided into, the 'retinal complex', referring to neural retina and the vitreous, and the 'scleral complex', comprising the RPE, choroid and sclera. Out of the studied PGs, PG D<sub>2</sub> formation was the highest in all three complexes, which was in agreement with the highest activity of soluble brain-type glutathione-independent PG D synthase in all these compartments (the other two detected activities corresponded to membrane-bound glutathione-dependent PG E synthase and to soluble PG F synthase). In fact, the only PG synthase activity, detected in the 'retinal complex', was the PG D synthase activity (Figure 4-13). Shiroma *et al.* (1996) showed that the equivalent is true in cultured chick RPE cells, which produce a larger amount of PG D<sub>2</sub>, than they do of PG E<sub>2</sub>, or PG F<sub>2</sub>α.

At the same time, a study by Beuckmann *et al.* (1996) revealed that the glutathione-independent PG D synthase, generally referred to as the brain-type PG D synthase (*PTGDS*), is significantly more active in the rat RPE and in the inter-photoreceptor matrix (IPM), than in the brain.

Specifically, the enzyme activity was increased six-fold in the RPE, and it was even higher in the IPM. Additionally, the group provided evidence for existence of at least two glycosylation sites within this protein, as Western blot experiments showed that bands of three different sizes were identified in different cellular fractions from the RPE.

Table 4-8. Prostaglandin D2 synthase types.

Gene	PTGDS	HPGDS
<b>UniProt-recommended name</b>	Prostaglandin-H2 D-isomerase	Hematopoietic prostaglandin D synthase
<b>Defined as</b>	<ul style="list-style-type: none"> <li>• Brain-type</li> <li>• Lipocalin-type</li> <li>• Glutathione-independent</li> </ul>	<ul style="list-style-type: none"> <li>• Hematopoietic</li> <li>• Glutathione-requiring</li> </ul>
<b>Enzyme activities</b>	<ul style="list-style-type: none"> <li>• Conversion of PGH2 to PGD2</li> </ul>	<ul style="list-style-type: none"> <li>• Conversion of PGH2 to PGD2</li> <li>• Glutathione S-transfer</li> </ul>
<b>Enzyme cofactor</b>	[none known]	Glutathione (required for PGH2 to PGD2 conversion)
<b>Other activities</b>	<ul style="list-style-type: none"> <li>• Smooth muscle contraction/relaxation</li> <li>• Potent inhibition of platelet aggregation</li> </ul>	[none known]
	<ul style="list-style-type: none"> <li>• Variety of CNS functions</li> <li>• Transport of small hydrophobic molecules, e.g. steroids, bilirubin, retinoids, and lipids.</li> <li>• Possible involvement in development and maintenance of the blood-brain, blood-retina, blood-aqueous humour and blood-testis barrier.</li> </ul>	

The membrane-bound RPE fraction gives rise to immuno-reactive bands of 20 kDa and 23 kDa. The cytosolic RPE fraction also contained the 23 kDa fraction, in addition to a larger 26 kDa species. The latter was also detected in the IPM. The cytosolic fraction of the neural retina cells appeared to contain a glycosylated 25 kDa peptide.

The most intense immuno-histochemical signal was detected in the RPE, and some was also observed in the outer and inner segments of photoreceptors. However, *in situ* hybridisation signal was limited to the RPE, suggesting that these cells are the site of PTGDS synthesis. The protein is subsequently released into the IPM, where it accumulates, and is then taken up by the photoreceptors.

It was subsequently shown that in addition to PG D2 synthesis, PTGDS also has a role as a retinoid transporter. Specifically, the protein binds all-*trans*- or 9-*cis* retinoic acid as well as all-*trans*- or 13-*cis* retinal. However, PTGDS did not bind vitamin A (all-*trans* retinol). Furthermore, the binding pocket for these retinoid compounds was the same as for PG H2

(the substrate for PG D2 synthesis), which, however, bound to a different site within this pocket (Tanaka *et al.*, 1997; Shimamoto *et al.*, 2007).

#### 4.3.3.3 PTGDS MAY BE INVOLVED IN DEVELOPMENT

*PTGDS* has been implicated in the development of male reproductive structures (Fouchécourt, Dacheux e Dacheux, 1999; Fouchécourt *et al.*, 2002; Fouchécourt *et al.*, 2003; Philibert *et al.*, 2013). Furthermore, *PTGDS* interacts with RIG1, which is highly expressed in testicular cells, and which can enhance the activity of *PTGDS*. In cancers, RIG1 can also suppress cell migration via the PGD2 signalling pathway (Wu *et al.*, 2012), similarly to its family member H-rev107, which co-localised with *PTGDS* in testes (Shyu *et al.*, 2013). Interestingly, in catfish *PTGDS* is regulated in developing testes and seminal vesicles by thyroid hormone (Sreenivasulu *et al.*, 2013), which is also known to regulate *PTGDS* expression during rat brain development (García-Fernández *et al.*, 1998). *PTGDS*, in addition to its prostaglandin synthase activity, has a role as a carrier of thyroid hormones as well as other lipophilic molecules such as retinoids (Ruano *et al.*, 2007). It might be via regulating the thyroid hormone availability that *PTGDS* affects testes development. *PTGDS* has been additionally implicated in hair loss and lengthening (Nieves e Garza, 2014).

#### 4.3.4 26 S PROTEASE REGULATORY SUBUNIT 4

The *PSMC1* gene encodes a major regulatory component (RegP) of the 26 S proteasome; the *PSMC1* protein belongs to a family of six ATPases (Tanahashi *et al.*, 1998). The 26 S protease comprises a core barrel-shaped catalytic particle (CP) and either one, or two, flanking regulatory particles (RegP), which lack protease activity, but confer substrate specificity and dependence on ATP (Section 1.7.1.1: The 26 S Protease). The RegP is known to comprise at least twenty protein subunits, constituting a base and a cap. The former includes of a ring of six ATPases, one of which is *PSMC1* (Figure 4-14).

Among members of the ATPase hexameric ring *PSMC1* is the only one of the six *PSMC1-6* hexamer components, whose ATPase activity is essential for peptidase activity of the CP. It is also required for opening of the CP gates, possibly for mediating the movement of the  $\alpha$ 2-4 extensions of CP (Voges, Zwickl e Baumeister, 1999; Lee *et al.*, 2011).

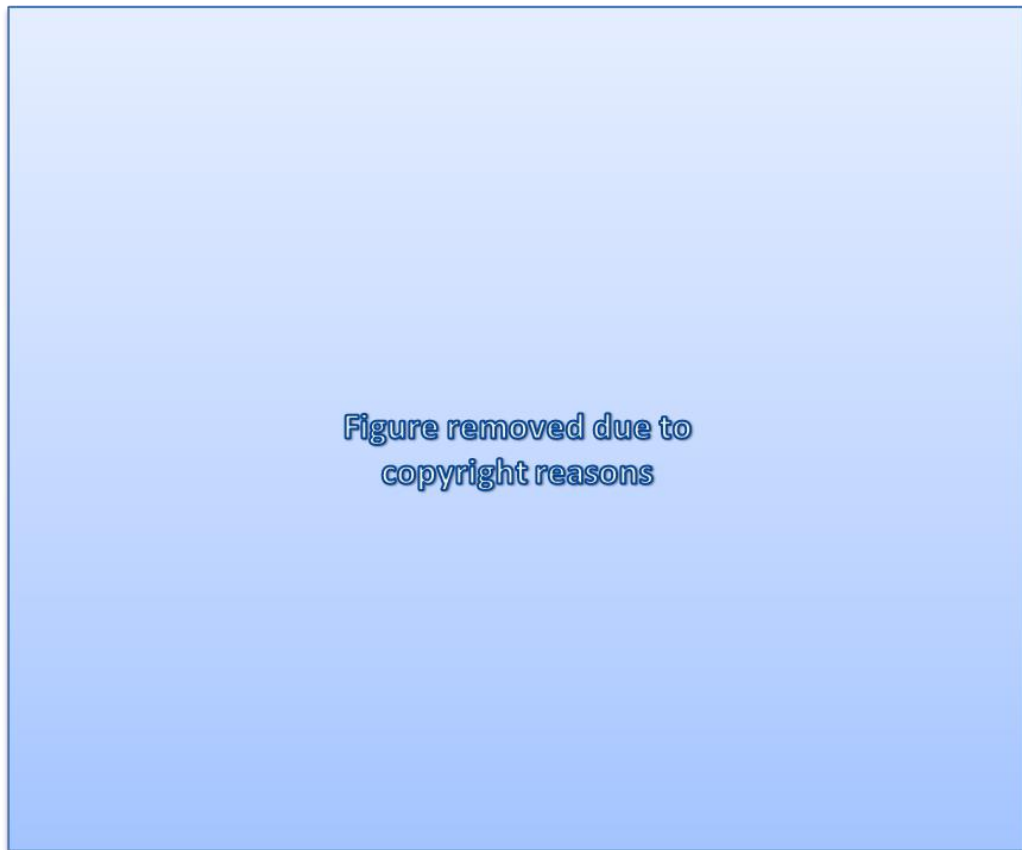


Figure 4-14. PSMC1 forms a key component of the regulatory ATPase ring of the 26 S protease. The labelled ubiquitin moieties are not visible on this modified image. Figure modified from Sullivan *et al.* (2003).

It should also be highlighted that, in addition to its role in the 26 S proteasome function, the hexameric ATPase ring has been shown to exist and function separately (Kodadek, 2010). The yeast homologues of the mammalian hexameric ring components, as well as of the non-ATPase subunits PSMD1 and PSMD2, were shown to bind DNA.

Specifically, they were associated with the nucleotide excision DNA repair proteins; consequently, it was proposed that perhaps the ATPase activity of the ring could be used to remove transcription factors and/or other proteins from chromatin.

This hypothesis would be in agreement with the observation that the *Arabidopsis* orthologue of PSMC1 is required for nucleosome assembly in the plant cells (Lee *et al.*, 2011). Additional evidence from several independent sources suggests that light-induced signalling, involving ubiquitin ligase activity, affects chromatin condensation and de-condensation processes (reviewed in: Fransz e De Jong, 2011).

Moreover, other non-proteasomal activities of the plant homologues were indicated by phenotypes, resulting from its mutations. Lee *et al.* (2011; 2012) provided evidence for a role



for the plant PSMC1 homologue in regulating cell elongation, apical growth (short/tall stature and root length), size and appearance of organs (e.g. leaves), proportion of trichome branching as well as DNA endoreduplication, protection from oxidative stress and zinc deficiency.

The analysis of plant mutants also showed that it is the amino terminal portion of PSMC1, which is responsible for its function, as deletion of its eight carboxy-terminal residues (including the  $\Psi$ YX motif) does not impair the protein's activity. At the same time, the thirteen amino-terminal residues were required for the correct functioning of PSMC1. However, mutation of a consensus N-myristoylation site, also located at the N-terminal, had no effects on function (Lee, K. H. *et al.*, 2012).

#### 4.3.4.1 PSMC1 AND LIGHT-INDUCED STRESS OF PLANT CELLS

Lee *et al.* (2012) demonstrated that an *Arabidopsis* homologue of PSMC1<sup>15</sup> is involved in the plant's responses to light-induced stress. Mutations in the N-terminal portion of the protein affected the seedling morphology of *Arabidopsis* in a light-dependent manner (Figure 4-15).

Specifically, when plants, expressing wild-type and mutant PSMC1 homologue, were grown in continuous light (24 h light), the seedling was developing very readily in the WT, whereas the mutant displayed a delayed and abnormal growth phenotype.

The difference was less pronounced in the long day mode (16 h light and 8 h dark) experiment.

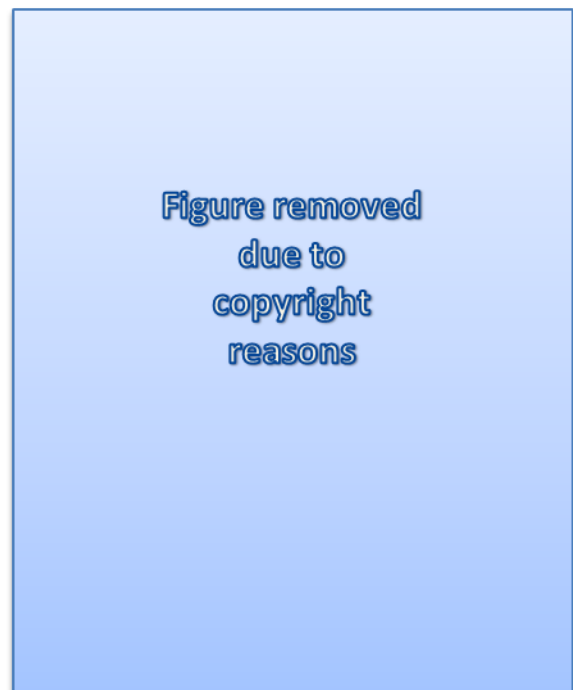


Figure 4-15. *PSMC1* mutation effects on the morphology of *Arabidopsis thaliana* seedlings. Plants expressing either wild-type (WT) or mutant (MU) *PSMC1* homologue, at different light exposure duration periods (indicated on the left hand side of the figure). Figure modified from Lee *et al.* (2012).

---

<sup>15</sup> *PSMC1* orthologue is encoded in *A. thaliana* by the *RPT2A* and *RPT2B* paralogues, which are functionally redundant, but differentially expressed (hence their mutations present with different phenotypes); not to be confused with the *RPT2* gene, which codes for a protein, known as root phototropism 2.

However, the mutant was still developing at a noticeably slower rate. On the other hand, no differences in growth rates of the wild-type and the mutant were detected in plants cultivated in the short day mode (8 h light, 16 h light).

It could be speculated that in animal cells, subject to light-stress, such as the photoreceptors and other retinal neurons, PSMC1 could also play a protective role. Perhaps the mechanism, by which the plant PSMC1 homologue modulates responses to light-stress, is as obvious as degradation of proteins damaged by reactive-oxygen species, generated due to light exposure. Protein turnover is also likely to be a key pathway in the retina, especially in the photoreceptor cells, which are highly metabolically active. This presents a sound hypothesis for PSMC1 being a central player in the retinal cells.

#### 4.3.4.2 PSMC1 HAS BEEN IMPLICATED IN NEURODEGENERATION

*PSMC1* gene has been suggested to have a role in Parkinson's disease (PD). Mouse models demonstrate that proteasomal dysfunction is sufficient to trigger neuro-degeneration, and *Psmc1* is an essential component of this protease complex (Bedford *et al.*, 2008).

However, data from human subjects suggests that the association between *PSMC1* and PD is probably less robust than what the mouse models suggest (Gómez-Garre *et al.*, 2012).

Evidence has been presented, which suggests that ubiquitinated proteins are typically found in neurodegeneration-associated neuronal inclusions, suggesting that proteasomal dysfunction may be involved in disease pathogenesis (Bedford *et al.*, 2009; Watabe *et al.*, 2014).

#### 4.3.4.3 PSMC1 HAS A ROLE IN CANCERS

*PSMC1* has been found among tumour-associated antigens in serum samples from patients with monoclonal gammopathy of undetermined significance (MGUS) (Blotta *et al.*, 2009).

Silencing of *PSMC1* in androgen receptor-positive prostate cancers results in suppression of cancer growth, and it enhances the anti-proliferative function of anti-androgens (Dahlman *et al.*, 2012).

Studies on mouse embryonic fibroblast (MEF) cells demonstrate that heterozygous *PSMC1* knock-down (KD) results in an arrest of these cells at the G2/M cell cycle phase. This is independent evidence for a role of *PSMC1* in regulation of cell growth (Rezvani *et al.*, 2012).

#### 4.3.5 CONCLUSIONS

Chapter 4 described Y2H screening for protein interacting partners of TOPORS. Conversely to what was hypothesised, no retina-specific protein was identified. Nonetheless, three candidate interactors were selected for further validation (Chapter 5) and characterisation (Chapters 6, 7 and 8) studies; namely, ITM2B, PTGDS and PSMC1.

The association of both ITM2B and PSMC1 with the cell cycle was previously described (sections 4.3.2.3 and 4.3.4.3). Since TOPORS associates with the centrosome in dividing cells and ciliary basal body in ciliated cells, experiments aiming to characterise their interactions (if/when validated) would aim to establish whether the molecules co-localise with centriolar markers as well as with each other in a centriole-like pattern in human cell lines (Section 1.8. The Centrosome Cycle).

No evidence for ciliary association of the PTGDS has been found. However, based on the previous findings that it is synthesised in the RPE, released, and then taken up by photoreceptors, it could be hypothesised that it could be transported via the connecting cilium. Hence, if/when the PPI between PTGDS and TOPORS is validated, sub-cellular co-localisation studies to investigate whether PTGDS also associates with centrioles, and/or primary cilium, would be performed.

Evaluation of the putative association of the novel candidate interactors of TOPORS with the centrioles, or specifically, ciliary basal body, was a priority. As the identified proteins are not retina-specific, the next objective would be to investigate whether they co-localise with TOPORS at the primary cilium, which is a key organelle to the photoreceptor homeostasis.

Prior to testing the hypotheses delineated above, validation of interactions in yeast (Chapter 5) and mammalian cells (Chapter 6) needed to be performed. Chapter 5 also describes results of splice variants' identification study, the purpose of which was to determine whether alternatively spliced isoforms of the candidate TOPORS' interactors are expressed in the retina (in addition to the ones identified via the Y2H screen).

## 5 VERIFICATION OF EXPRESSION AND INTERACTIONS

The two previous chapters described construction and characterisation of the Y2H cDNA library and bait constructs used for screening (Chapter 3) as well as the Y2H screen for protein interacting partners of TOPORS (Chapter 4). Findings from the latter led to selection of three candidate interactors for further studies in context of the retinal disease associated with *TOPORS* mutations. This was necessary due to the fact that no retina specific interacting partner of TOPORS was identified (in contrary to what was originally hypothesised).

The primary criterion for selecting the candidate interactors for further validation was a demonstrated link with the retina. This was clear for two of the interacting proteins: ITM2B, associated with a familial retinal dystrophy, and PTGDS, a lipocalin-type transporter of retinoids (and other lipophilic compounds), putatively involved in maintenance of the blood-retina barrier. The third candidate, PSMC1, did not have an evident retinal association; it was selected due to, firstly, its role in neurodegeneration, secondly, mediating responses to light-induced stress in plants, and thirdly, because it is a vital component of the ubiquitin-proteasome system, of which TOPORS is also a member.

In an attempt to further prioritise one of these three candidates an RT-PCR-based screen for alternatively-spliced retinal protein-coding transcripts of the interactors was performed (section 2.4.4. Amplification of Alternative Prey Transcripts). Several protein-coding isoforms of each one of the candidate interacting partners have been documented in genomic databases (Ensembl, NCBI, UCSC); data available from the Ensembl database was used for designed the experiments described here. The objective of this experiment was to attempt to amplify the alternative isoforms (in addition to the ones identified via the Y2H PPI screen) from the human retinal RNA (section 5.1). Amplification of the isoforms pulled out from the Y2H PPI screen would have served as an additional validation of the Y2H results, as only fragments of the isoforms were isolated via the Y2H methods (Chapter 4). This would also have provided valuable information for interpretation of results of immunofluorescence (IF) staining on retinal cryo-sections (Chapter 8). Time-allowing, these isoforms could additionally have been sub-cloned into Y2H and mammalian expression vectors for use in control PPI and localisation experiments.

Validation of interactions between TOPORS and its novel protein partners using the Y2H method was the final one of the Y2H experiments of this project (section 5.2), prior to co-immuno-precipitation (coIP) studies to validate the interactions in human cell lines (section 2.5.4 in Methods and Materials and experimental Chapter 6). Besides the full-length TOPORS

construct, the Y2H PPIs were additionally performed with TOPORS deletion constructs (shown in red, blue and green in Figure 3-5 in Chapter 3). The deletion constructs of TOPORS were designed to correspond to TOPORS regions known to convey a specific function; e.g. E3 ubiquitin ligase (red) vs. E3 SUMO1 ligase (blue), or the mutational hot-spot region (green). The purpose of these additional Y2H PPI experiments was to try to define the putative nature of the interactions between TOPORS and its newly-isolated partners.

Section 5.1 of this chapter describes the identification of the alternative transcripts of the novel candidate interactors, whereas section 5.2 deals with the experiments performed in yeast to validate the interactions identified in the Y2H screen.

## **5.1 SPLICE VARIANTS OF *ITM2B*, *PTGDS* AND *PSMC1* EXPRESSED IN THE RETINA**

The purpose of this section was to determine the expression of protein-coding transcript variants of *ITM2B*, *PTGDS* and *PSMC1* in human retina at mRNA level. Human retina RNA (Clontech, CA, USA) was used to prepare cDNA as described in section 2.4. Primers were designed to identify and differentiate the protein-coding transcripts for each of the genes of interest according to details of splice variants available on the Ensembl database<sup>16</sup> (section 2.4.4 in Methods and Materials). PCRs were performed on retinal cDNA, generated in three independent experiments. Each PCR was performed at least in triplicate and a representative image for each result is presented.

### **5.1.1 *ITM2B* ISOFORM EXPRESSION STUDY**

Two protein-coding transcripts have been reported for *ITM2B* according to the Ensembl database (Appendix: Figure 11-29), whereas the UCSC database contains only the longer isoform (Appendix: Figure 11-30). The UCSC display additionally summarises the reported ESTs from human retina and the RPE, as well as potential retinal disease loci. The UCSC database uses the Human Feb. 2009 (GRCh37/hg19) Assembly of the human genome, hence information

---

<sup>16</sup> Alternative protein-coding transcripts, described and evaluated in this section, were accessible on the Ensembl database till July 2014 inclusive, and have been updated since then. Snapshots of those past database records are included in Appendix 11.7. In context of the retinal isoform evaluation, the update affects only *PTGDS*, as its isoform 201 has been removed from database records. As findings presented in this section will demonstrate, the old *PTGDS*-201 was not detected in the retina, thus, its removal would not significantly influence the analysis. No other changes, relevant to this project, have been noted.

regarding the involvement of ITM2B in retinal degeneration (Audo *et al.*, 2013); is not indicated.

All PCRs resulted in amplification of the longer *ITM2B*-001 isoform. No *ITM2B*-003 PCR products were generated using any of the primer pairs, designed to detect it (Table 2-65 in Methods and Materials). This is a positive result in view of the fact that TOPORS interacted with ITM2B peptide fragments, encoded by exons 3-6, i. e. a region corresponding to isoform 001 (Figure 5-1).

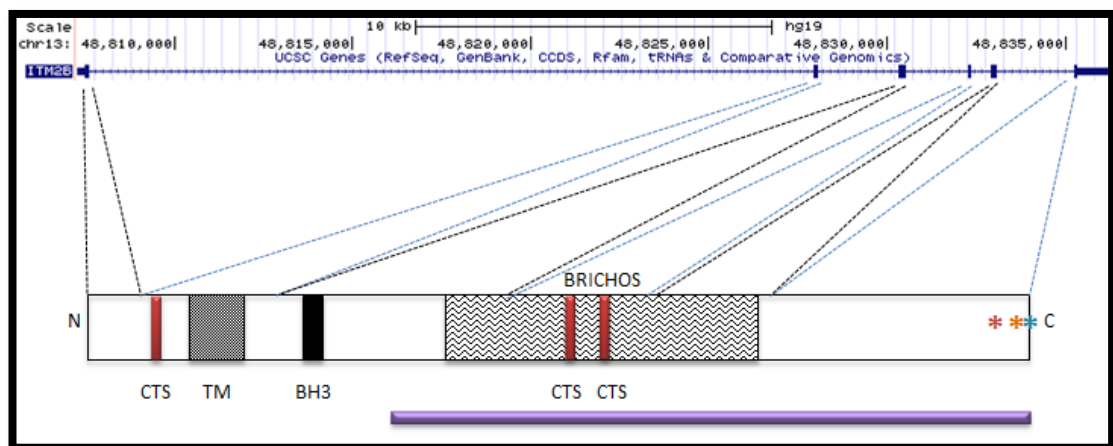


Figure 5-1. ITM2B isoform 001.

Transcript structure from the UCSC database is shown in the top panel. Protein structure is shown in the bottom panel. N, amino-terminus; CTS, ciliary targeting sequence; TM, transmembrane domain; BH3, Bcl 2 homology 3 domain; BRICHOS, BRICHOS domain; C, carboxy-terminus; asterisks indicate known ITM2B mutation sites: retinal mutation (c.782A>C; p.Glu261Ala), FDD mutation (c.795-796insTTTAATTTGT; p.Ser266Phefs\*11), FBD mutation (c.799T>A; p.Stop267Argfs\*11). Protein fragments corresponding to specific exons are indicated using dashed lines, joining an exon in the top panel with a region of ITM2B in the lower panel; alternating exons are differentiated using black and blue paired lines. The horizontal purple bar at the bottom of the figure corresponds to the ITM2B fragment, which was pulled out from the Y2H screen twice as an interacting protein partner of TOPORS (Figure 4-9 in Chapter 4). The alternative protein coding ITM2B isoform 003 differs from isoform 001 in lacking exons 3 and 4. Figure not to scale.

Images of the amplified fragments are presented in Figure 5-2; the amplified fragments are typed in **bold** script in Table 5-1. The identity of the amplified PCR fragments was confirmed by sequencing. Only one sequence per band was identified, and no unexpected sequences were detected.

Importantly, the results demonstrated that *ITM2B*-001, a fragment of which interacted with TOPORS in the Y2H screen, is expressed in the human retina.

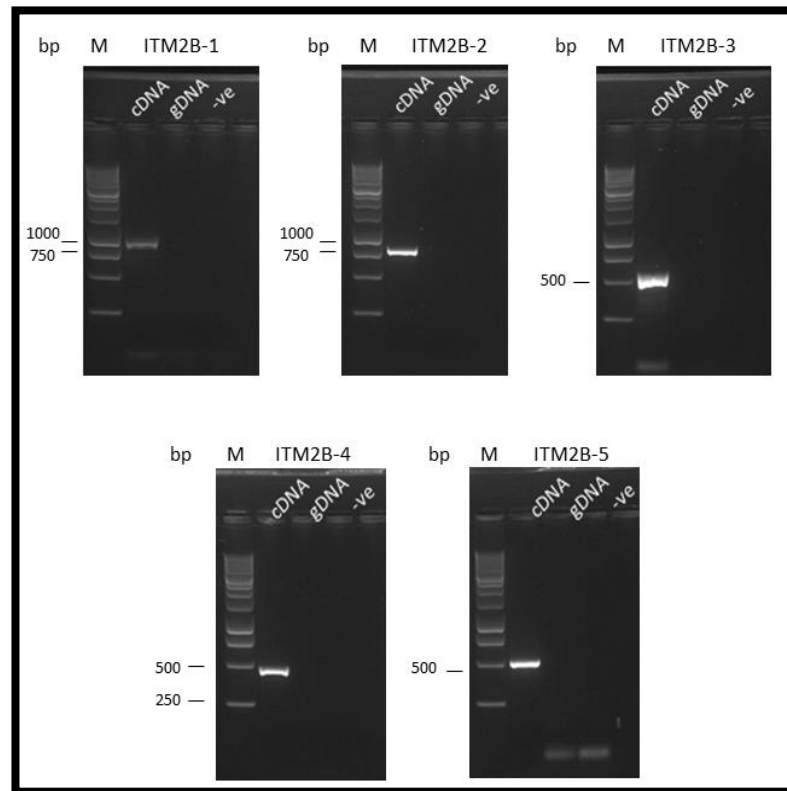


Figure 5-2. Results of *ITM2B* isoform expression study.

Expected band sizes for relevant isoform(s) in each PCR are given in Table 5-1. Five microliters of PCR products were loaded for ITM2B-1, ITM2B-2, and ITM2B-3; two microliters were loaded for ITM2B-4 and ITM2B-5. Key: M (marker): 1 kb DNA Ladder (Promega, WI, USA); cDNA, complementary DNA; gDNA, genomic DNA control; -ve, negative control. ITM2B-[number] corresponds to the PCR name given in Table 5-1. Gels (1.8 %) were run at 120 V for 1h 20'.

Table 5-1. *ITM2B* primer details for isoform amplification.

Primers correspond to those given in Table 2-52. Isoforms expected to be amplified by the designated primer pairs are indicated; and expected amplicon sizes from the corresponding isoforms are given in brackets. Isoforms, whose expression was detected in this experiment are in bold. The first column contains a reference to the corresponding PCR result image Figure 5-2.

PCR name	Primer pair	Expected isoform fragments (size)
ITM2B-1	Ex1F Ex6R	Isoform <b>001</b> (918 bp)
ITM2B-2	Ex1Fb Ex6R	Isoforms <b>001</b> (737 bp) & <b>003</b> (419 bp)
ITM2B-3	Ex1F Ex3R	Isoform <b>001</b> (530 bp)
ITM2B-4	Ex2F Ex5R	Isoform <b>001</b> (445 bp) & <b>003</b> (127 bp)
ITM2B-5	Ex3F Ex6R	Isoform <b>001</b> (490 bp)

### 5.1.2 PTGDS ISOFORM EXPRESSION STUDY

Six protein-coding transcripts have been reported for *PTGDS* according to the Ensembl database (Appendix: Figure 11-31), whereas the UCSC database contains only two variants (Appendix: Figure 11-32). Full-length isoform *PTGDS*-001 (Ensembl) was isolated as an interacting protein partner of TOPORS three times (Chapter 4).

The PCR results have provided strong evidence for retinal expression of *PTGDS* isoforms 001 (PCR PTGDS-1), 004 (PCR PTGDS-3) and 005 (PCR PTGDS-5). As demonstrated in Figure 5-3, the product of PTGDS-1 PCR migrated at approximately 750 bp, very close to the expected *PTGDS*-001 amplicon size of 743 bp. Additionally, the band in PTGDS-4 PCR migrated between the 250 bp and 500 bp markers, at approximately 400 bp; this result also points towards the presence of a *PTGDS*-001 (390 bp); however it may also represent a *PTGDS*-005 amplicon of 360 bp. In either case, evidence from PTGDS-5 PCR clearly demonstrates that *PTGDS*-005 is indeed expressed in the human retina. Primers used in the PTGDS-3 PCR also amplify a product from just one isoform, *PTGDS*-004; the observed band migrated above the 500 bp marker, and the expected band for this isoform was 560 bp, confirming that it was present.

Based on results of PCRs PTGDS-2 and PTGDS-7, it can also be concluded that either isoform 003, or 201, or both, are also expressed in human retina. The band observed in PTGDS-2 PCR migrated slightly below 500 bp; the expected product from this reaction should have been 443 bp long, which could correspond to isoform *PTGDS*-003, *PTGDS*-004 (expression confirmed by PTGDS-3 PCR result), or *PTGDS*-201. However, it must be noted that isoform *PTGDS*-201 was not amplified in PTGDS-1 PCR; therefore, the obtained product is more likely to represent either isoform-004 or 003.

Products of PTGDS-6 PCR include two bands, both migrating between the 250 bp and 500 bp markers, estimated to be between 300 bp and 400 bp in size. The lower faint product could represent either isoform 001 (316 bp), or isoform 005 (313 bp); the expression of both of them is confirmed by products of PCRs PTGDS-1 and PTGDS-5, respectively. The larger strong band could represent isoform 006; the expression of this splice variant has been reported (Ensembl) to result in a processed transcript only; hence, it was not intended for this analysis, as it should not encode a protein potentially interacting with TOPORS.

The amplicons, which resulted from PCRs: PTGDS-8 and PTGDS-9, could both demonstrate the expression of either isoform 001 or 201. In the PTGDS-8 PCR the observed band migrated below 500 bp, showing an estimated size of approximately 400 bp; this band can represent



both isoforms, whose expected products in these reaction would be 399 bp and 396 bp, respectively. In PTGDS-9 PCR, amplification of both isoforms should result in a product of 207 bp; the amplified band migrated below the 250 bp marker, demonstrating the presence of either *PTGDS-001*, or *PTGDS-201*, or both. However, it should again be emphasised that no product, corresponding to isoform 201, was amplified in PTGDS-1 PCR, therefore the band is more likely to represent *PTGDS-001*.

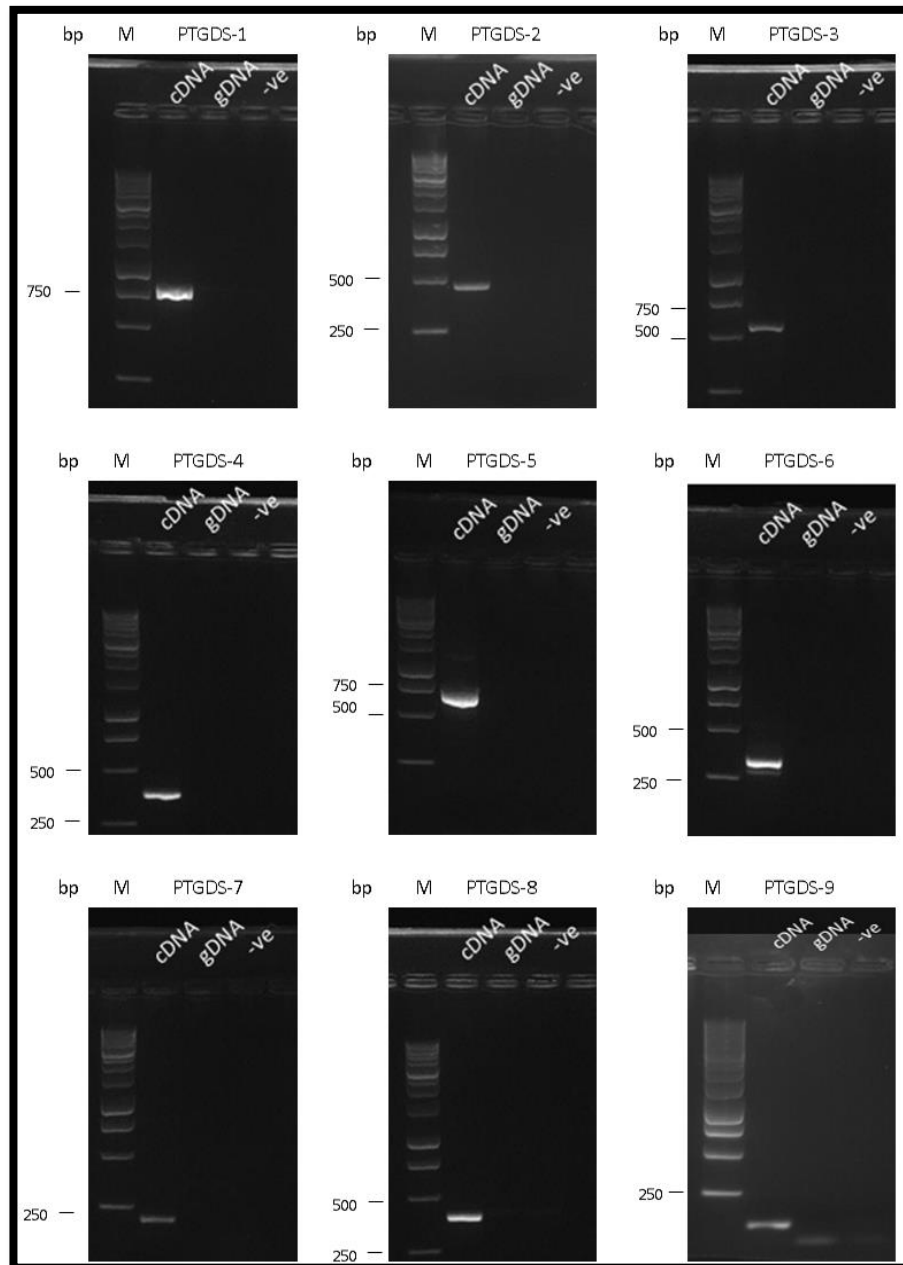


Figure 5-3. Results of *PTGDS* isoform expression study.

Expected band sizes for relevant isoform(s) in each PCR are given in Table 5-2. Five microliters of PCR products were loaded for all PCRs. Key: M (marker): 1 kb DNA Ladder (Promega, WI, USA); cDNA: complementary DNA; gDNA: genomic DNA control; -ve: negative control. PTGDS-[number] corresponds to the PCR name given in Table 5-2. Gels (1.8 % – 2.0 %) were run at 120 V for 1h 20’.

Alternatively, this PCR could have also yielded a larger product (363 bp), which would provide evidence for expression of isoform 008; this was not observed.

These results are also summarised in Table 5-2. The identity of the amplified PCR fragments was confirmed by sequencing. Only one sequence per band was identified, and no unexpected sequences were detected.

The outcomes of this study suggest that, except for *PTGDS*-008 and *PTGDS*-201, all of the reported protein-coding *PTGDS* splice variants, appear to be expressed in the human retina. Of particular note, it was demonstrated that *PTGDS*-001, which interacted with TOPORS in the Y2H screen, is expressed in the human retina.

Table 5-2. *PTGDS* primer details for isoform amplification.

Primers sequences are given in Table 2-53. Isoforms expected to be amplified by the designated primer pairs are indicated; and expected amplicon sizes from the corresponding isoforms are given in brackets. Isoforms, whose expression was detected in this experiment, are in bold (or in bold italics, where a product is not exclusive to the highlighted isoform, but the expression was confirmed by one of the other PCRs). Isoforms, which were potentially detected in this experiment, but their identity was not fully confirmed, are typed in italics. The first column contains a reference to the corresponding PCR result image (Figure 5-3).

PCR name	Primer pair	Expected isoform fragments (size)
PTGDS-1	Ex1F Ex7R	Isoforms 201 (845 bp) & <b>001</b> (743 bp)
PTGDS-2	Ex1F Ex3RII	Isoform <i>003</i> , <b>004</b> , 201 (443 bp)
PTGDS-3	Ex1F Ex3Rb	Isoform <b>004</b> (560 bp)
PTGDS-4	Ex2F Ex5R	Isoforms 201 (462 bp), <b>001</b> (391 bp) & <b>005</b> (360 bp)
PTGDS-5	Ex2Fb Ex7Rb	Isoform <b>005</b> (624 bp)
PTGDS-6	Ex3F Ex6R	Isoforms 201 (418 bp) <b>001</b> (316 bp) <b>005</b> (313 bp)
PTGDS-7	Ex3Fb Ex5Rb	Isoforms 201 & <i>003</i> (213 bp)
PTGDS-8	Ex4F Ex7R	Isoforms 201 (399 bp) & <b>001</b> (396 bp)
PTGDS-9	Ex5F Ex7R	Isoforms 201, <b>001</b> (207 bp) & 008 (363bp)

### 5.1.3 *PSMC1* ISOFORM EXPRESSION STUDY

Three protein-coding transcripts have been reported for *PSMC1* according to the Ensembl database (Appendix: Figure 11-33), whereas the UCSC database contains two of these splice variants (Appendix: Figure 11-34).

All PCRs resulted in amplification of the longest *PSMC1* isoform 001 (Figure 5-4). Results of PCRs PSMC1-5 and PSMC1-6 may also suggest the expression of isoform 002, as sizes of the PCR products would be the same for both: *PSMC1*-001 and *PSMC1*-002 isoforms; however, in view of the findings from the other PCRs, it is more likely that the observed amplicons would indicate the presence of isoform 001. No bands migrating at sizes indicative of isoform 002 expression were detected in PCRs: PSMC1-1, PSMC1-2, or PSMC1-3. Furthermore, no amplicon corresponding to isoform-004 was observed in PCR PSMC1-2 (nonetheless, it could not be excluded that this was a false negative result due to the very small size of the expected amplicon). The amplified fragments are typed in **bold** script in Table 5-3. The identity of the amplified PCR fragments was confirmed by sequencing (only one sequence per band was identified).

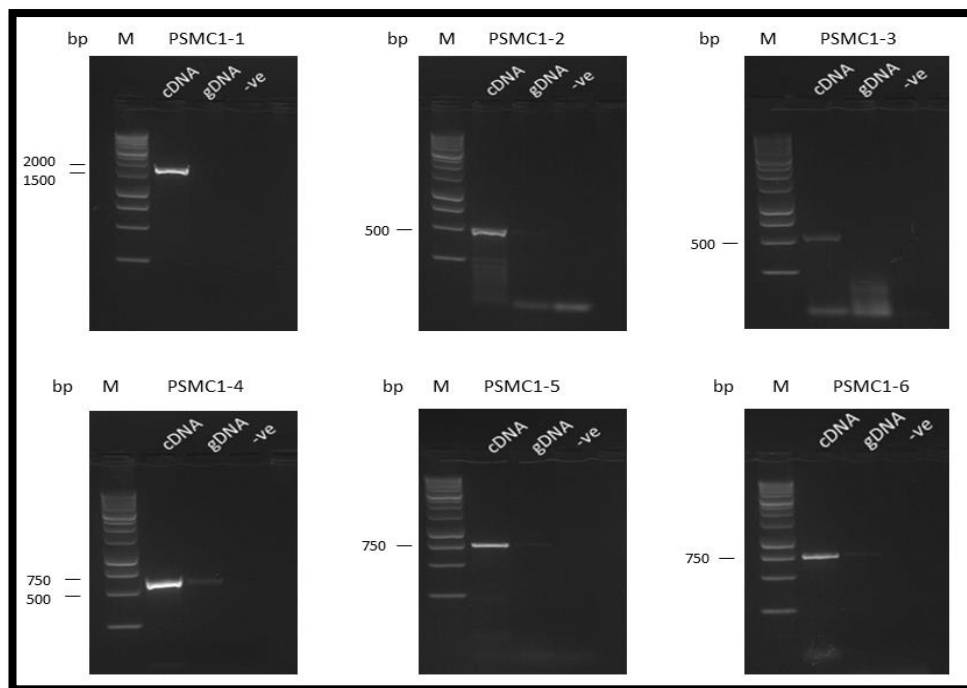


Figure 5-4. Results of *PSMC1* isoform expression study.

Five microliters of PCR products were loaded for all PCRs. Expected band sizes for relevant isoform(s) in each PCR are given in Table 5-3. Key: M (marker): 1 kb DNA Ladder (Promega, WI, USA); cDNA, complementary DNA; gDNA, genomic DNA control; -ve, negative control. PSMC1-[number] corresponds to the PCR name given in Table 5-3. Gels (2 %) were run at 120 V for 1h 20'.

This is a positive result in view of the fact that in the Y2H screen TOPORS interacted with a PSMC1 peptide fragment, encoded by exons 1-6, corresponding to *PSMC1* isoform 001.

Unexpectedly, faint PCR products were also observed in the gDNA lanes in Figure 5-4. These products were purified and sequenced in triplicate. The gDNA band from PSMC1-2 PCR consistently aligned with an intergenic region on chromosome 1, upstream of gene *SAMD11* (Appendix: Figure 11-35). The remaining bands appeared to have no matches in the UCSC database.

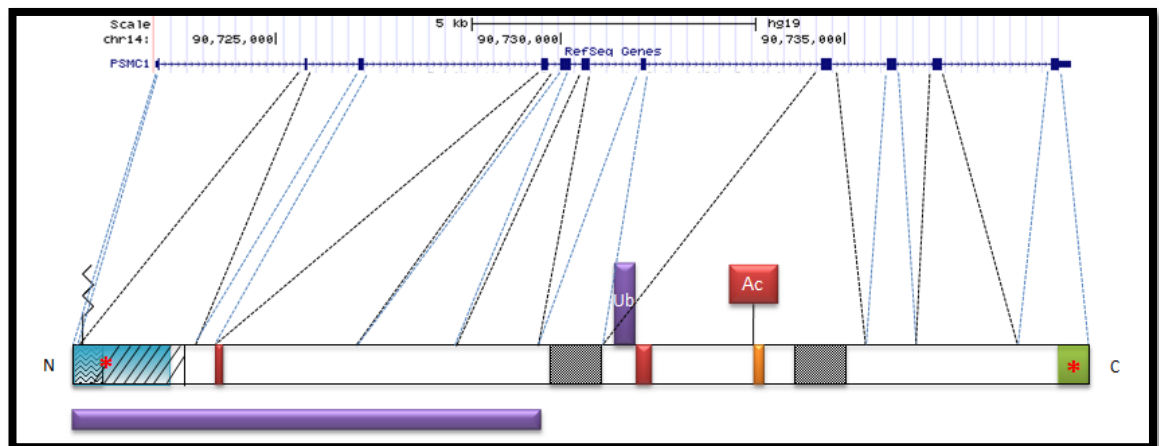


Figure 5-5. PSMC1 isoform 001.

Transcript structure from the UCSC database is shown in the top panel. Protein structure is shown in the bottom panel. N, amino-terminus; Ub, ubiquitin; Ac, acetyl group; C, carboxy-terminus. Starting from the N-terminus: the lipid tail structure indicates N-myristoylation at Gly 2, and the box filled with wavy lines represents a consensus sequence for this modification; the region emphasised with straight diagonal black lines represents an NADH-binding site; the blue box represents a PSMC1 fragment indispensable for plant development. asterisks indicate phosphorylation sites; two red boxes represent ciliary targeting sequences (CTSs); the grey boxes represent regions required for ATP binding and hydrolysis, respectively, whereas the orange box indicates an aromatic loop mediating the hydrolysis of ATP; green box represents the proteasomal anchoring region. Protein fragments corresponding to specific exons are indicated using dashed lines, joining an exon in the top panel with a region of PSMC1 in the lower panel; alternating exons are differentiated using black and blue paired lines. The horizontal purple bar at the bottom of the figure corresponds to the PSMC1 fragment, which was pulled out from the Y2H screen as an interacting protein partner of TOPORS (Figure 4-11 in Chapter 4). The alternative protein coding PSMC1 isoform 002 differs from isoform 001 in lacking exon 3; whereas isoform 004 lacks exons 2, 3, 4, 9, 10 and 11, and fragments of exons 5 and 8, relative to isoform 001. Figure not to scale.

Table 5-3. *PSMC1* primer details for isoform amplification.

Primer sequences are given in Table 2-54. Isoforms expected to be amplified by the designated primer pairs are indicated; and expected amplicon sizes from the corresponding isoforms are given in brackets. Isoforms, whose expression was detected in this experiment, are typed in bold (or in bold italics, where a product is not exclusive to the highlighted isoform, but the expression was confirmed by one of the other PCRs). Isoforms, which were potentially detected in this experiment, but their identity was not fully confirmed, are typed in italics. The first column contains a reference to the corresponding PCR result image (Figure 5-4).

PCR name	Primer name	Expected isoform fragments (size)
PSMC1-1	Ex1F Ex11R	Isoform <b>001</b> (1495 bp), 002 (1389 bp)
PSMC1-2	Ex1F Ex5R	Isoform <b>001</b> (476 bp), 002 (379 bp) & 004 (67 bp)
PSMC1-3	Ex2F Ex6R	Isoform <b>001</b> (520 bp), 002 (423 bp)
PSMC1-4	Ex3F Ex7R	Isoforms <b>001</b> (569 bp)
PSMC1-5	Ex5F Ex9R	Isoforms <b>001</b> & 002 (714 bp)
PSMC1-6	Ex8F Ex11R	Isoforms <b>001</b> & 002 (715 bp)

The current section 5.1 provided a summary of expression of alternatively spliced variants of novel putative interactors of TOPORS in the human retina.

The next section 5.2 includes evidence of direct PPIs between TOPORS and its full-length interactors in yeast.

## 5.2 Y2H PPI VALIDATION EXPERIMENTS

With the exception of PTGDS, preys identified in the Y2H screen comprised only fragments of protein-coding sequences rather than full-length complete transcripts. Consequently, having confirmed their retinal expression (section 5.1), but prior to performing the control experiments in yeast (section 5.1), the relevant transcript variants had to be cloned into the Y2H vectors (Appendix 11.8). The following splice variants (based on the Ensemble database) were used for cloning:

- *ITM2B*-001 (ENST00000378565);
- *PTGDS*-001 (ENST00000371625);
- *PSMC1*-001 (ENST00000261303).

### 5.2.1 CONTROL INTERACTION TESTING WITH GAL4 DNA-BD

The final interacting partners, sub-cloned into GAL4 AD vector, were tested for putative interactions with the GAL4 DNA-BD, to ensure the interactions observed with TOPORS were not false-positives. Each interacting partner was transformed into the relevant yeast strain and then mated with the GAL4 DNA-BD yeast culture. Serial dilutions of the mated cultures were prepared, and seeded on selective media. The test was performed in triplicate, and demonstrated that the preys do not interact with the DNA-BD of GAL4. Representative results from one of the experiment replicates are summarised in two tables (Table 5-7 and Table 5-6). Results of a control experiment, involving p53 (the overall control interacting partner), PSMC1 and PTGDS, are shown in the figures in Table 5-5. Results of a test involving ITM2B and its variants are shown in Table 5-6; full-length ITM2B and its non-membrane-bound fragment were tested, in addition to *ITM2B* mutants, previously described in section 4.3.2 (Chapter 4). The mated cultures were serially diluted ( $10^0 - 10^{-5}$ ) before plating. The expected results are delineated in Table 5-4.

Table 5-4. Expected control Y2H PPI results.

Expected growth On selective media	Positive control mating	Negative control mating
<b>SD/-W (bait selection)</b>	White colonies	White colonies
<b>SD/-L (prey selection)</b>	White colonies	White colonies
<b>DDO (diploid selection)</b>	White colonies	White colonies
<b>DDO/X/A (PPI selection in diploid yeasts)</b>	Blue colonies	No colonies

Table 5-5. Control yeast mating to confirm putative interacting partners (preys) of TOPORS do not bind the GAL4 DNA-BD. Part I.

A putative interaction between p53 and GAL4 DNA-BD is included in the assay as an additional control (TOPORS x p53 Y2H PPI was published previously). All of the putative interacting proteins, as well as p53, are expressed as fusion proteins with GAL AD (preys) just as the cDNA library clones were. GAL4 DNA-BD was used as bait in the putative PPI testing. +ve PPI control: SV40 T Ag x p53. -ve PPI control: SV40 T Ag x Lamin C. SD/-W media selected for BD constructs; SD/-L media selected for AD constructs; DDO media selected for both BD and AD constructs, i.e. controlled for mating efficiency; DDO/X/A media selected for PPIs, as indicated by *Mel1* and *Aur-C* reporters (blue colonies and growth on the anti-fungal AbA agent, respectively); QDO/X/A media selected for PPIs, as indicated by *Mel1*, *Aur-C*, *His3* and *Ade2* reporters (blue colonies, growth on AbA, growth without histidine and growth without adenine, respectively). Key: 'M.' = selective medium; 'sel.' = 'selects for'.

Expect	Sel.	M.	10 <sup>-5</sup> 10 <sup>-4</sup> 10 <sup>-3</sup> 10 <sup>-2</sup> 10 <sup>-1</sup> 10 <sup>0</sup>						+ve	-ve														
			Bait		Prey		Bait + Prey				p53	Lamin C												
			GAL4 DNA-BD		GAL4 DNA-BD		GAL4 DNA-BD		GAL4 DNA-BD															
			p53	PSMC1	PTGDS	SV40 T Ag	SV40 T Ag	p53	PSMC1	PTGDS	SV40 T Ag	SV40 T Ag	p53	PSMC1	PTGDS	SV40 T Ag	SV40 T Ag	p53	PSMC1	PTGDS	SV40 T Ag	SV40 T Ag		
White growth	Bait	SD/-W																						
Blue growth																								
No growth																								
Blue growth																								
No growth																								

Table 5-6. Control yeast mating to confirm putative interacting partners (preys) of TOPORS do not bind the GAL4 DNA-BD. Part II.

All of the putative interacting proteins are expressed as fusion proteins with GAL AD (preys) just as the cDNA library clones were. GAL4 DNA-BD was used as bait in the putative PPI testing. +ve PPI control: SV40 T Ag x p53. -ve PPI control: SV40 T Ag x Lamin C. SD/-W media selected for BD constructs; SD/-L media selected for AD constructs; DDO media selected for both BD and AD constructs, i.e. controlled for mating efficiency; DDO/X/A media selected for PPIs, as indicated by *Mel1* and *Aur-C* reporters (blue colonies and growth on the anti-fungal AbA agent, respectively); QDO/X/A media selected for PPIs, as indicated by *Mel1*, *Aur-C*, *His3* and *Ade2* reporters (blue colonies, growth on AbA, growth without histidine and growth without adenine, respectively). Key: ITM2B: wild-type ITM2B; ITM2B90: soluble wild-type ITM2B fragment; RetMu: ITM2B retinal dystrophy mutant; FBD: ITM2B British Dementia mutant; FDD: ITM2B Danish Dementia mutant; ‘M.’: selective medium; ‘sel.’: ‘selects for’.

Expect	Sel.	M.	10 <sup>0</sup>						+ve		-ve		
			10 <sup>0</sup>	10 <sup>-1</sup>	10 <sup>-2</sup>	10 <sup>-3</sup>	10 <sup>-4</sup>	10 <sup>-5</sup>	p53	Lamin C	p53	Lamin C	
White growth	Bait	SD/-W	GAL4 DNA-BD						p53		Lamin C		
			ITM2B	ITM2B90	RetMu	FBD	FDD	SV40 T Ag	SV40 T Ag	ITM2B	ITM2B90	RetMu	FBD
White growth	Prey	SD/-L	GAL4 DNA-BD						p53		Lamin C		
			ITM2B	ITM2B90	RetMu	FBD	FDD	SV40 T Ag	SV40 T Ag	ITM2B	ITM2B90	RetMu	FBD
White growth	Bait + Prey	DDO	GAL4 DNA-BD						p53		Lamin C		
			ITM2B	ITM2B90	RetMu	FBD	FDD	SV40 T Ag	SV40 T Ag	ITM2B	ITM2B90	RetMu	FBD
No growth	PPI: less stringent	DDO/X/A	GAL4 DNA-BD						p53		Lamin C		
			ITM2B	ITM2B90	RetMu	FBD	FDD	SV40 T Ag	SV40 T Ag	ITM2B	ITM2B90	RetMu	FBD
Blue growth	PPI: more stringent	QDO/X/A	GAL4 DNA-BD						p53		Lamin C		
			ITM2B	ITM2B90	RetMu	FBD	FDD	SV40 T Ag	SV40 T Ag	ITM2B	ITM2B90	RetMu	FBD
No growth	PPI: more stringent	QDO/X/A	GAL4 DNA-BD						p53		Lamin C		
			ITM2B	ITM2B90	RetMu	FBD	FDD	SV40 T Ag	SV40 T Ag	ITM2B	ITM2B90	RetMu	FBD



## 5.2.2 DIRECT PROTEIN-PROTEIN INTERACTIONS (PPIs) IN YEAST

The primary purpose of this experiment was to validate the PPIs, identified by the Y2H cDNA library screening, by re-testing the interaction directly in yeast, using the relevant full-length transcript.

Considering the variable nature of TOPORS and its potential multiple roles, an attempt was also made to understand which of the domains of this protein could be responsible for mediating its interactions with PTGDS, PSMC1 and non-membrane bound fragments of ITM2B. TOPORS deletion constructs, highlighted in Figure 3-4, were designed, cloned in frame with the GAL4 BD, and directly tested, using the Y2H method, for interactions with the three partners identified in the cDNA library screen. *ITM2B* mutants were also tested for PPIs with full-length TOPORS as well as its fragments.

This Y2H-based experiment directly tested the PPIs between full-length TOPORS (FL), and each one of its domain-isolating fragments (N, M and C) with each of the identified interaction partners, i.e. ITM2B, PSMC1 and PTGDS. The interaction between the SV40 large T Ag (fusion protein with GAL4 AD) and p53 (fusion protein with GAL4 DNA-BD) was used as a positive control (AD-T Ag x BD-p53); whereas Lamin C bound to the DNA-BD and the SV40 large T Ag fused with the AD (AD-T Ag x BD-Lamin C) served as the negative control.

In order to determine, which domains are involved, each experiment was repeated six times. The following tables (Table 5-8 – Table 5-15) contain figures with the raw results from one (of the six) representative experiment performed to evaluate the PPIs, whereas Table 5-16 summarises the findings from all six repeats. A result was considered positive overall, if blue growth, indicating a PPI, was observed in at least four out of six experiments at a given stringency level (two or four reporter genes). The raw results are tabulated in the Appendix section 11.9.

The mated cultures were serially diluted ( $10^0 - 10^{-5}$ ) before plating. SD/-W media selected for BD constructs; SD/-L media selected for AD constructs; DDO media selected for both BD and AD constructs, i.e. controlled for mating efficiency; DDO/X/A media selected for PPIs, as indicated by *Mel1* and *Aur-C* reporter activation (blue colonies and growth on the anti-fungal AbA agent, respectively); QDO/X/A media selected for PPIs, as indicated by *Mel1*, *Aur-C*, *His3* and *Ade2* reporter activation (blue colonies, growth on AbA, growth without histidine and growth without adenine, respectively; Table 5-7).

Table 5-7. An overview of expected results in Y2H PPI testing.  
Key: 'Med.' = selective medium; 'Sel.' = 'selects for'.

Med.	SD/-W	SD/-L	DDO	DDO/X/A	QDO/X/A
Sel.	Bait	Prey	Bait + Prey	PPI: less stringent	PPI: more stringent
Expect	White growth	White growth	White growth	PPI: Blue growth No PPI: No growth	PPI: Blue growth No PPI: No growth

Table 5-8. Control yeast mating to test direct TOPORS-p53 PPI (published interaction used as an overall positive control).

Key: FL: full-length TOPORS; N: N-term TOPORS, M: mid-TOPORS; C: C-term TOPORS; Pr.: prey; T, SV40 T Ag. All baits are expressed as fusion proteins with GAL4 DNA-BD. All preys are expressed as fusion proteins with GAL4 AD. '+': PPI control: SV40 T Ag x p53. '-': PPI control: SV40 T Ag x Lamin C.

	Pr.															+		-			
		p53		T		T		p53		T		T		p53		T		T			
		Bait	FL	N	M	C	p53	Lam	FL	N	M	C	p53	Lam	FL	N	M	C	p53	Lam	
10 <sup>0</sup>																					
10 <sup>-1</sup>																					
10 <sup>-2</sup>																					
10 <sup>-3</sup>																					
10 <sup>-4</sup>																					
10 <sup>-5</sup>																					
		SD/-W				SD/-L				DDO				DDO/X/A				QDO/X/A			

Table 5-9. Control yeast mating to test direct TOPORS-ITM2B PPI.

Key: FL: full-length TOPORS; N: N-term TOPORS, M: mid-TOPORS; C: C-term TOPORS; Pr.: prey; T, SV40 T Ag. All baits are expressed as fusion proteins with GAL4 DNA-BD. All preys are expressed as fusion proteins with GAL4 AD. '+': PPI control: SV40 T Ag x p53. '-': PPI control: SV40 T Ag x Lamin C.

	Pr.	ITM2B		T		ITM2B		T		ITM2B		T		ITM2B		T									
		Bait		P53		Lam		P53		Lam		P53		Lam		P53		Lam							
		FL	N	M	C	FL	N	M	C	FL	N	M	C	FL	N	M	C	FL	N	M	C	P53	Lam		
		SD/-W				SD/-L				DDO				DDO/X/A				QDO/X/A							
		10 <sup>0</sup>	10 <sup>-1</sup>	10 <sup>-2</sup>	10 <sup>-3</sup>	10 <sup>-4</sup>	10 <sup>-5</sup>	10 <sup>0</sup>	10 <sup>-1</sup>	10 <sup>-2</sup>	10 <sup>-3</sup>	10 <sup>-4</sup>	10 <sup>-5</sup>	10 <sup>0</sup>	10 <sup>-1</sup>	10 <sup>-2</sup>	10 <sup>-3</sup>	10 <sup>-4</sup>	10 <sup>-5</sup>	10 <sup>0</sup>	10 <sup>-1</sup>	10 <sup>-2</sup>	10 <sup>-3</sup>	10 <sup>-4</sup>	10 <sup>-5</sup>

Table 5-10. Control yeast mating to test direct TOPORS-ITM2B90 PPI.

Key: FL: full-length TOPORS; N: N-term TOPORS, M: mid-TOPORS; C: C-term TOPORS; Pr.: prey; T, SV40 T Ag. All baits are expressed as fusion proteins with GAL4 DNA-BD. All preys are expressed as fusion proteins with GAL4 AD. '+': PPI control: SV40 T Ag x p53. '-': PPI control: SV40 T Ag x Lamin C.

	Pr.	ITM2B90		T		ITM2B90		T		ITM2B90		T		ITM2B90		T									
		Bait		P53		Lam		P53		Lam		P53		Lam		P53		Lam							
		FL	N	M	C	FL	N	M	C	FL	N	M	C	FL	N	M	C	FL	N	M	C	P53	Lam		
		SD/-W				SD/-L				DDO				DDO/X/A				QDO/X/A							
		10 <sup>0</sup>	10 <sup>-1</sup>	10 <sup>-2</sup>	10 <sup>-3</sup>	10 <sup>-4</sup>	10 <sup>-5</sup>	10 <sup>0</sup>	10 <sup>-1</sup>	10 <sup>-2</sup>	10 <sup>-3</sup>	10 <sup>-4</sup>	10 <sup>-5</sup>	10 <sup>0</sup>	10 <sup>-1</sup>	10 <sup>-2</sup>	10 <sup>-3</sup>	10 <sup>-4</sup>	10 <sup>-5</sup>	10 <sup>0</sup>	10 <sup>-1</sup>	10 <sup>-2</sup>	10 <sup>-3</sup>	10 <sup>-4</sup>	10 <sup>-5</sup>

Table 5-11. Control yeast mating to test direct TOPORS-ITM2B-RetMu PPI.

Key: FL: full-length TOPORS; N: N-term TOPORS, M: mid-TOPORS; C: C-term TOPORS; Pr.: prey; T, SV40 T Ag. All baits are expressed as fusion proteins with GAL4 DNA-BD. All preys are expressed as fusion proteins with GAL4 AD. '+': PPI control: SV40 T Ag x p53. '-': PPI control: SV40 T Ag x Lamin C.

	Pr.	ITM2B RetMu										+		-			
		T					T					T	T	T	T		
		FL	N	M	C	P53	Lam	FL	N	M	C	P53	Lam	FL	N	M	C
10 <sup>0</sup>																	
10 <sup>-1</sup>																	
10 <sup>-2</sup>																	
10 <sup>-3</sup>																	
10 <sup>-4</sup>																	
10 <sup>-5</sup>																	
		SD/-W					SD/-L					DDO		DDO/X/A		QDO/X/A	

Table 5-12. Control yeast mating to test direct TOPORS-ITM2B-FBD PPI.

Key: FL: full-length TOPORS; N: N-term TOPORS, M: mid-TOPORS; C: C-term TOPORS; Pr.: prey; T, SV40 T Ag. All baits are expressed as fusion proteins with GAL4 DNA-BD. All preys are expressed as fusion proteins with GAL4 AD. '+': PPI control: SV40 T Ag x p53. '-': PPI control: SV40 T Ag x Lamin C.

	Pr.	ITM2B FBD										+		-			
		T					T					T	T	T	T		
		FL	N	M	C	P53	Lam	FL	N	M	C	P53	Lam	FL	N	M	C
10 <sup>0</sup>																	
10 <sup>-1</sup>																	
10 <sup>-2</sup>																	
10 <sup>-3</sup>																	
10 <sup>-4</sup>																	
10 <sup>-5</sup>																	
		SD/-W					SD/-L					DDO		DDO/X/A		QDO/X/A	

Table 5-13. Control yeast mating to test direct TOPORS-ITM2B-FDD PPI.

Key: FL: full-length TOPORS; N: N-term TOPORS, M: mid-TOPORS; C: C-term TOPORS; Pr.: prey; T, SV40 T Ag. All baits are expressed as fusion proteins with GAL4 DNA-BD. All preys are expressed as fusion proteins with GAL4 AD. '+': PPI control: SV40 T Ag x p53. '-': PPI control: SV40 T Ag x Lamin C.

	Pr.	ITM2B FDD										T	T	+	-																
		ITM2B FDD					ITM2B FDD									T	T	+	-												
		FL	N	M	C	P53	Lam	FL	N	M	C									P53	Lam										
	Bait	FL	N	M	C	P53	Lam	FL	N	M	C	P53	Lam	FL	N	M	C	P53	Lam	FL	N	M	C	P53	Lam						
		SD/-W						SD/-L						DDO						DDO/X/A						QDO/X/A					

Table 5-14. Control yeast mating to test direct TOPORS-PTGDS PPI.

Key: FL: full-length TOPORS; N: N-term TOPORS, M: mid-TOPORS; C: C-term TOPORS; Pr.: prey; T, SV40 T Ag. All baits are expressed as fusion proteins with GAL4 DNA-BD. All preys are expressed as fusion proteins with GAL4 AD. '+': PPI control: SV40 T Ag x p53. '-': PPI control: SV40 T Ag x Lamin C.

	Pr.	PTGDS										T	T	+	-																
		PTGDS					PTGDS									T	T	+	-												
		FL	N	M	C	P53	Lam	FL	N	M	C									P53	Lam										
	Bait	FL	N	M	C	P53	Lam	FL	N	M	C	P53	Lam	FL	N	M	C	P53	Lam	FL	N	M	C	P53	Lam						
		SD/-W						SD/-L						DDO						DDO/X/A						QDO/X/A					

Table 5-15. Control yeast mating to test direct TOPORS-PSMC1 PPI.

Key: FL: full-length TOPORS; N: N-term TOPORS, M: mid-TOPORS; C: C-term TOPORS; Pr.: prey; T, SV40 T Ag. All baits are expressed as fusion proteins with GAL4 DNA-BD. All preys are expressed as fusion proteins with GAL4 AD. '+': PPI control: SV40 T Ag x p53. '-': PPI control: SV40 T Ag x Lamin C.

Pr.	PSMC1		T	T	PSMC1		T	T	PSMC1		T	T	PSMC1		T	T	PSMC1		T	T	PSMC1		T	T
	Bait	FL	N	M	C	P53	Lam	FL	N	M	C	P53	Lam	FL	N	M	C	P53	Lam	FL	N	M	C	P53
	10 <sup>0</sup>				10 <sup>-1</sup>				10 <sup>-2</sup>				10 <sup>-3</sup>				10 <sup>-4</sup>				10 <sup>-5</sup>			
	SD/-W				SD/-L				DDO				DDO/X/A				QDO/X/A							

Table 5-16. PPIs summary.

Key: FL TOPORS = full length TOPORS; N-term TOPORS = amino-terminal TOPORS fragment; Mid-TOPORS = TOPORS middle fragment; C-term TOPORS = carboxy-terminal TOPORS fragment; p53 = tumour protein 53; ITM2B = integral membrane protein 2B; ITM2B90 = soluble fragment of ITM2B (aa90 - aa266); ITM2B\_RetMu = ITM2B retinal dystrophy mutant; ITM2B\_FBD = ITM2B British dementia mutant; ITM2B\_FDD = ITM2B Danish dementia mutant; PSMC1 = 26 protease regulatory subunit 4; PTGDS = prostaglandin D2 synthase; + = PPI; - = No PPI.

BD constructs	FL TOPORS		N-term TOPORS		Mid-TOPORS		C-term TOPORS	
<b>AD constructs</b>	DDO/X/A	QDO/X/A	DDO/X/A	QDO/X/A	DDO/X/A	QDO/X/A	DDO/X/A	QDO/X/A
p53	+	-	+	+	+	+	+	+
ITM2B	+	-	+	+	-	-	+	+
ITM2B90	+	-	+	+	+	-	+	+
ITM2B_RetMu	+	+	+	+	+	-	+	+
ITM2B_FBD	+	-	+	+	+	+	+	+
ITM2B_FDD	-	-	-	-	-	-	+	-
PTGDS	+	-	+	+	+	-	+	-
PSMC1	+	-	+	-	+	+	+	+

All tested proteins apart from the Danish dementia mutant interacted with full-length TOPORS on DDO/X/A media, but only the association with ITM2B retinal dystrophy mutant appeared strong enough to activate the additional two reporters, selected for on the (most stringent) QDO/X/A media.

The amino-terminal fragment of TOPORS (N-term), comprising one PEST domain and the RING finger region required for E3 ubiquitin ligase activity and a ciliary-targeting sequence (CTS), appeared to strongly interact with all, apart from two tested peptides, at both levels of stringency. The ITM2B Danish dementia mutant displayed no association with this TOPORS fragment at all, whereas the interaction with PSMC1 was observed only on the lower stringency media (DDO/X/A).

The mid-TOPORS fragment, consisting of two CTS regions, two PEST domains, RS/SR region, nuclear localisation signal (NLS), within which two mutations are known to occur, interacted at both stringency levels with p53, PSMC1 and with the ITM2B British dementia mutant. A PPI at the lower stringency level was additionally observed with PTGDS, and the other ITM2B constructs, excluding the British mutant.

The carboxy-terminal (C-term) mutational hotspot region of TOPORS (Lys/His domain and two PEST domains) interacted at both stringency levels with all tested proteins apart from the ITM2B Danish mutant and PTGDS, in which cases the interaction occurred only in less stringent conditions.

### 5.3 DISCUSSION

The full-length transcripts of each gene isoform corresponding to the ones identified in the Y2H screen (Chapter 4), and verified in the retinal isoform experiment (section 5.1) were cloned into the relevant Y2H vector for control experiments in yeast (section 5.2). Additionally, known *ITM2B* mutants as well as a gene fragment encoding a soluble ITM2B peptide fragment were also tested. It was, firstly, demonstrated that the PPI-indicative phenotypes, observed in yeast, were not due to an interaction with the GAL4 BD (section 5.2.1). Subsequently, each prey was tested again for direct interaction with TOPORS to ensure that the resulting full-length peptide was still able to associate with the bait. PPIs involving the identified proteins were also tested for interaction with TOPORS fragments (section 5.2.2).

### 5.3.1 ISOFORM EXPRESSION EXPERIMENTS

Identification of alternatively spliced retinal variants was performed by amplification of protein-coding isoforms (as reported on the Ensembl database), from cDNA, which was synthesised from human retinal total RNA (Clontech, CA, USA). The product sheet specified that the RNA was pooled from normal retinae of 25 suddenly deceased individuals (male and female), aged 24-65; however, no information was given, which would specify whether 'retina RNA' referred to RNA originated from neural retina only, or from neural retina and the RPE. For the purposes of this project it was assumed that the RNA was representative of all retinal cell types including the RPE and glial cells.

#### 5.3.1.1 ITM2B ALTERNATIVE RETINAL ISOFORM INVESTIGATION

The Ensembl genomic database reports that two protein-coding isoforms of *ITM2B* were previously identified in human. The experiments described in section 5.1 aimed to determine whether both of these isoforms, namely *ITM2B-001* and *ITM2B-003* were also expressed in the retina. Only the reported protein-coding isoforms were evaluated, however their expression was verified at the mRNA rather than protein level.

In the Y2H screen for human protein interacting partners of TOPORS a peptide corresponding to exons 3-6 of transcript *ITM2B-001* was identified (Figure 5-1). Among the two known protein-coding *ITM2B* transcripts, the identified protein fragment could have been encoded only by isoform 001, as isoform 003 comprises only exons 1, 2, 5 and 6 of the *ITM2B* gene.

Indeed the isoform study on human retinal cDNA did not lead to identification of *ITM2B* isoform 003. This finding could lead to the assumption that only one protein-coding transcript variant of *ITM2B* is expressed in the human retina. Nonetheless, it should be emphasised that as yet unidentified protein-coding isoforms may additionally exist.

For instance, cell work performed by Fleischer *et al.* (2002) suggests that another alternatively spliced protein-coding *ITM2B* variant might exist, which the researchers denoted ITM2B-short (ITM2B<sub>s</sub>). This variant corresponds to a peptide comprising residues 57 – 266 of ITM2B encoded by isoform 001 (Fleischer *et al.*, 2002). The protein structure of isoform 001 shows that methionine 57 is embedded within the transmembrane (TM) domain of this protein (Figure 6-4).

On the other hand, this TM domain is also a site of intramembrane proteolysis by SPPL2a/b (Martin *et al.*, 2008); therefore, rather than resulting from alternative splicing, ITM2B<sub>s</sub> might



be a product of ITM2B isoform 001 protein expression, followed by SPPL2a/b-mediated cleavage. Although the order of ITM2B-001 proteolytic processing was previously shown to commence at the carboxy-terminus with furin, followed by approximately centrally-cleaving ADAM10, and lastly the intramembrane proteolysis by SPPL2a/b, it could be speculated that an alternative order of peptide cleavage might generate the ITM2B<sub>s</sub> peptide.

Pro-apoptotic factors could trigger a signal for ITM2B processing leading to formation of ITM2B<sub>s</sub>, as the latter was shown to play a key part in apoptosis by inducing loss of the mitochondrial membrane potential (Fleischer, Ayllon e Rebollo, 2002). Nonetheless, no transcript corresponding to ITM2B-short was found in the Ensembl database; hence, this protein variant was not tested for retinal expression.

Overall, the study presented in section 5.1.1 demonstrated that the protein-coding *ITM2B* isoform 001 is expressed in human retina at mRNA level; whereas isoform 003 is not. This result supports the findings from the Y2H screen for interacting protein partners of TOPORS, where a peptide, corresponding to a fragment of isoform 001, was isolated twice as a TOPORS' interactor.

#### 5.3.1.2 *PTGDS* ALTERNATIVE RETINAL ISOFORM INVESTIGATION

The alternative *PTGDS* variants, amplified from human retinal cDNA included isoforms 001, 004 and 005. However, it could not be ascertained, in which retinal cell type their expression occurred, as the cDNA used in the isoform study was generated from RNA obtained from suddenly deceased individuals. The manufacturer's datasheet did not specify whether the RNA was extracted only from the neural retinae, therefore, it was assumed that all of the retinal cell types served as a source for the RNA extraction.

This assumption was a necessity; however, it would have been interesting to determine *PTGDS* expression in different retinal cell types, as previous studies in chick and rat showed the mRNA is expressed specifically in the RPE, even though the protein was also observed in the photoreceptors cells (and the interphotoreceptor matrix) (Beuckmann *et al.*, 1996; Shiroma *et al.*, 1996). Nonetheless, those studies did not evaluate alternative *PTGDS* isoforms.

Still, the isoform study showed that, in addition to *PTGDS*-001, pulled out as an interactor of TOPORS from the Y2H screen, the protein-coding isoforms 004 and 005 are also expressed in human retina at the mRNA level. If this mRNA is subsequently translated into protein (as would be expected), this could prove to be a challenge for performing reliable immunohistochemical

(IHC) experiments aiming to determine the localisation of PTGDS-001 protein in retinal cryosections (Chapter 8).

As was mentioned at the end of section 4.3.3.2, PTGDS-001 contains overlapping binding pockets for prostaglandin (PG) H<sub>2</sub> (a PG D<sub>2</sub> precursor) and for lipophilic compounds, such as retinoids (for which the protein serves as a transporter). A representative crystal structure of PTGDS-001 depicts a bucket-shaped protein (Figure 5-6).

The antibody, which will have been used in subsequent immuno-based studies (Chapter 6, 7 and 8) was raised against a peptide corresponding to full-length PTGDS isoform 001.

Figure 5-7 shows sequence alignments of PTGDS isoform 004 with the antigen sequence; and Figure 5-8 shows the alignment of isoform 005 with the antigen sequence. Isoform 004 aligns with approximately the amino-terminal half of isoform 001 (the antigen), whereas isoform 005 corresponds to approximately two thirds of the 001 isoform at its carboxy-terminal end.

No crystal structures have been published for the alternative isoforms 004 and 005. Additionally, it has not been demonstrated that they perform either one of the main known functions of PTGDS-001. Based on the substantial region of sequence dissimilarity between PTGDS variant 001 and either one of the alternative isoforms 004 or 005, it could be expected that their tertiary structures would differ. This in turn should suggest that the antibody against PTGDS-001, used in Chapters 6 - 8, would not detect the alternatively-spliced PTGDS variants. Nonetheless, this could not be categorically excluded.



Figure 5-6. PTGDS-001 protein crystal structure. The canonical PTGDS variant (isoform 001) protein forms a bucket-like structure with internal docking sites for lipophilic compounds, such as retinoids, and prostaglandin H<sub>2</sub>, the precursor of prostaglandin D<sub>2</sub>. Image from PhosphoSitePlus (Hornbeck *et al.*, 2004).

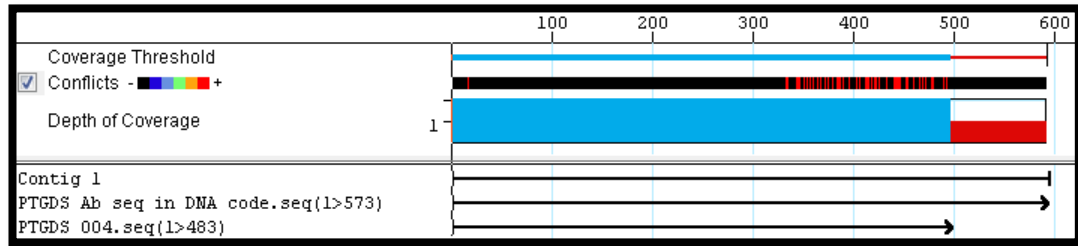


Figure 5-7. *PTGDS*-004 alignment with the sequence of the immunogen, used to generate the antibody against *PTGDS*-001 (sc-30067, Santa Cruz Biotechnology).

Alignment with approximately only with the N-terminal half of *PTGDS* isoform 004 is shown. The red highlighted conflicts represent dissimilarities between the sequence corresponding to the *PTGDS* immunogen, and the sequence of isoform 004. Alignments were generated using SeqMan (DNAStar Inc., WI, USA).

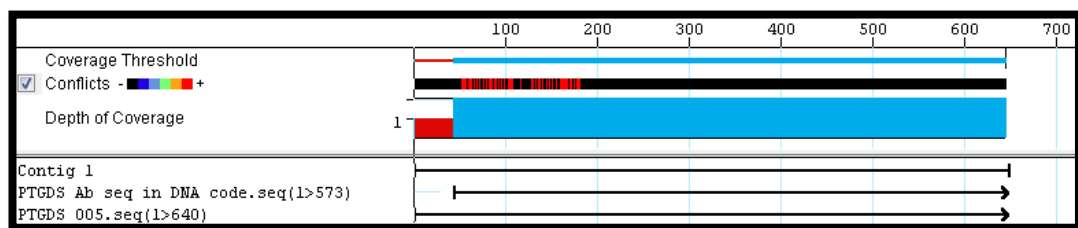


Figure 5-8. *PTGDS*-005 alignment with the sequence of the immunogen, used to generate the antibody against *PTGDS*-001 (sc-30067, Santa Cruz Biotechnology).

Alignment with approximately the C-terminal two-thirds of *PTGDS* isoform 005 is shown. The red highlighted conflicts represent dissimilarities between the sequence corresponding to the *PTGDS* immunogen, and the sequence of isoform 005. Alignments were generated using SeqMan (DNAStar Inc., WI, USA).

### 5.3.1.3 *PSMC1* ALTERNATIVE RETINAL ISOFORM INVESTIGATION

The search for retinal protein-coding isoforms of *PSMC1* confirmed that *PSMC1*-001 is indeed expressed in the retina. On the contrary the study excluded the expression of isoform 002 in retinal cell types and, originally, also the expression of isoform 004. However, judging in retrospect, verification of the existence of protein-coding isoform *PSMC1*-004 in the retina should probably be repeated.

Due to the extremely small size of the expected amplicon (67 bp), it could have been possible that even if this DNA fragment was amplified from the human retinal cDNA, it might have been lost from the 2 % agarose gel during the electrophoresis. In order to definitely confirm that isoform 004 is not expressed in human retina, in future experiments, a higher percentage agarose gel (2.5 %) could be used for separation of the expected PCR product. This would extend the electrophoresis time, but it would also increase resolution, and would additionally lead to retaining very small DNA amplicons that would be lost from the 2 % gel during

electrophoresis. Alternatively, new primer pairs, specific to isoform 004, could be designed, which would lead to amplification of a larger fragment of this *PSMC1* variant. Then, sufficient evidence would have been provided to state that isoform *PSMC1*-004 is not expressed in cells of the human retina.

Overall, the *PSMC1* isoform study confirmed that isoform 001 is expressed in the human retina; therefore, enhancing the significance of results of the Y2H screen, where only a fragment of *PSMC1* isoform 001 was found to interact with TOPORS.

Furthermore, exclusion of the expression of other known protein-coding variants of *PSMC1* in the retina would allow for a more unambiguous interpretation of immunohistochemical protein localisation results in retinal cryo-sections. Still, it must not be overlooked that other as yet unidentified protein-coding variants of *PSMC1* could exist in the retinal cell types.

### 5.3.2 Y2H DIRECT PPI VALIDATION EXPERIMENTS

As is shown in Figure 5-9, the N-term fragment of TOPORS (residues 1-380) comprises the first PEST domain of the protein, the RING domain, and a ciliary targeting sequence (CTS), conserved among primates. The fragment also includes serine 98, which is a target for phosphorylation. A phosphomimetic mutation of serine 98 to asparagine was shown to increase the ubiquitin E3 ligase activity of TOPORS, as well as enhanced its binding to Ubch5a, an E2 conjugating enzyme (Park *et al.*, 2008).

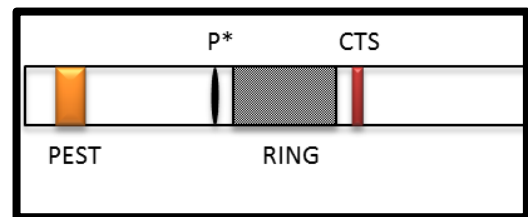


Figure 5-9. Amino-terminus (N) TOPORS bait (residues 1-380).

The orange box indicates a PEST domain; maroon narrow oval at Ser 98 denotes a known phosphorylation site (P\*); dark grey box indicates the RING domain (conveys E3 ubiquitin ligase activity); red narrow box represents a ciliary targeting sequence (CTS). Figure not to scale.

The region required for DNA binding by TOPORS is also found within this fragment (Chu *et al.*, 2001), and it includes two consensus SUMOylation sites (at which, however, SUMO1 attachment has not been demonstrated for TOPORS, which appears to be a true result (Weger, Hammer e Engstler, 2003; Weger, Hammer e Heilbronn, 2005)). No known mutations for *TOPORS*-associated retinal dystrophies are found within this fragment.

The mid-TOPORS fragment (Figure 5-10; residues 373-781) comprises two PEST domains, a ciliary targeting sequence (CTS) conserved among vertebrates, and the SR/RS dipeptide region, divided by the NLS and inclusive of the SUMO1 acceptor site at lysine 560 and a phosphate acceptor site at serine 718. It also includes motifs required for interaction with

SUMO1, as well as residues necessary for SUMOylation of TOPORS at lysine 560. The region required for association with the cytoplasmic domain of syndecan 1 (S1CD), as demonstrated on murine proteins, is also included within this fragment and comprises a consensus site for casein kinase 2 modification (Braun *et al.*, 2012).

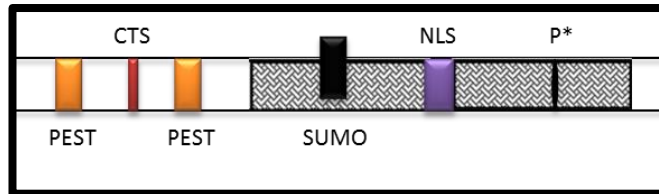


Figure 5-10. Mid-TOPORS (M) bait (residues 373-781). Orange boxes indicate PEST domains; maroon narrow oval at Ser 718 denotes a known phosphorylation sites (P\*); red narrow box represents a ciliary targeting sequence (CTS); dark cross-hatched box represents the arginine- and serine-rich (SR/RS) domain; a SUMO1 acceptor site at Lys 560, with a covalently bound SUMO1 modification (perpendicular black box), is indicated within the first SR/RS domain; a nuclear localisation signal (NLS) is located approximately centrally within the SR/RS domains. The fragment is required for E3 SUMO1 ligase activity. Figure not to scale.

Moreover, this fragment overlaps with the TOPORS fragment (residues 456-882) pulled out in a screen for interacting partners of human topoisomerase 1 (hTop1) (Haluska *et al.*, 1999). A residue mutated in adPRD (p.Q402P) (Schob *et al.*, 2009; Selmer *et al.*, 2010) is also located within this fragment of TOPORS, in addition to two other residues found mutated in panels of adRP patients.

The mutations found in these two residues (p.S606R, N755S) have not however been sufficiently characterised to ascertain that they are of pathological significance, since no family members of the probands were examined, and it has not been ascertained that the probands do not harbour mutations in other putative RP genes (Schob *et al.*, 2009; Sullivan *et al.*, 2013).

The C-term TOPORS fragment (Figure 5-11; residues 705-1045) includes some of the SR/RS dipeptides region, located downstream of the NLS, including serine 718, which is also found within the mid-TOPORS fragment.

Phosphorylation of serine 718 by Plk-1 was shown to increase the E3 ubiquitin ligase activity of TOPORS, resulting in degradation of p53.

A similar effect on ubiquitin E3 ligase activity was observed in case of serine 98 phosphorylation (N-term TOPORS fragment).

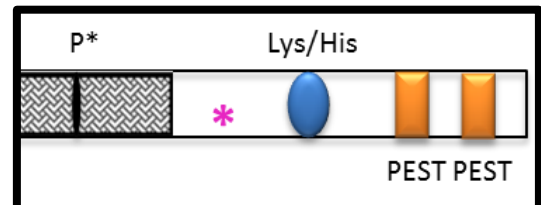


Figure 5-11. Carboxy-terminus (N) TOPORS bait (residues 705-1045). The cross-hatched box represents a fragment of the arginine- and serine-rich (SR/RS) domain with the maroon narrow oval Ser 718 denoting a known phosphorylation site (P\*); the pink asterisk represents the mutational hot spot region of TOPORS; the blue oval indicates the location of a lysine- and histidine-rich motif; the orange boxes indicate PEST domains. Figure not to scale.

However, unlike serine 98 phosphorylation, which had no effect on SUMO1 E3 ligase activity of TOPORS (Park *et al.*, 2008), phosphorylation of serine 718 decreased it (Yang *et al.*, 2009). This C-term fragment also includes the Lys/His motif, associated with speckled nuclear localisation

of TOPORS, and overlaps with the region required for minimal interaction of TOPORS with UBC9 and Rep proteins of AAV2 (residues 871-917). Two C-terminal PEST domains are also found within this fragment. The C-terminal region of TOPORS, required for interaction with SUMO1 overlaps with the two PEST domains as well as the Lys/His motif. This C-terminal fragment additionally harbours a mutational hotspot, associated with retinitis pigmentosa (RP).

### 5.3.2.1 *ITM2B INTERACTIONS*

The interaction between ITM2B and TOPORS fragments was tested using constructs, encoding full-length and a soluble portion of ITM2B. Additionally, known disease-causing mutants were included in the analysis. As was summarised in Table 5-16, a PPI was observed between full-length ITM2B and full-length TOPORS as well as its N- and C-term fragments, but not with mid-TOPORS. Furthermore the interactions between full-length ITM2B and the N- and C-term fragments were stronger than with full-length TOPORS, as shown by activation of four reporter genes, as opposed to two.

Before potential reasons for these findings are discussed, it should also be noted that in endogenous conditions ITM2B forms homodimers via a cystine, formed from residue 89 of each monomer; furthermore, the protein is heavily proteolytically processed (described in section 6.2; briefly depicted in Figure 5-12).

Firstly, ITM2B is cleaved by furin at the C-terminus to generate a mature protein and the CCTP fragment (peptide 7). Subsequent processing by ADAM10 results in shedding of the ITM2B ectodomain (peptide 6). The N-terminal membrane-bound fragment (NTF; peptide 3), which remains, is then cleaved within the membrane domain by SPPL2a/b, yielding a C-terminal secreted domain (SCD; peptide 5) and an intracellular domain (ICD; peptide 4). The GAL4 AD, to which the expressed ITM2B would be fused, is located at the N-terminus of ITM2B. Assuming that proteolytic cleavage of ITM2B in yeast resembles the mammalian processing pathway (if ITM2B becomes cleaved at all), it should be expected that the observed PPI phenotypes would be due to an interaction between TOPORS (and its fragments) and the intracellular domain (ICD; peptide 4) of ITM2B (the intra-cellular fragment remaining after the proteolytic action of SPPL2a/b; Figure 5-12).

This is a necessary assumption as only a non-membrane bound peptide should have been able to reach the nucleus and activate the expression of interaction reporter genes in GAL4-based Y2H system. The ICD contains (peptide 4) one CTS and a cysteine residue, which was previously

shown not to be involved in disulphide bond formation; hence, it should probably be assumed that the expressed GAL4 AD-ICD hybrid, which interacted with TOPORS, was a monomer, unless it formed a homodimer with involvement of non-covalent bonds.

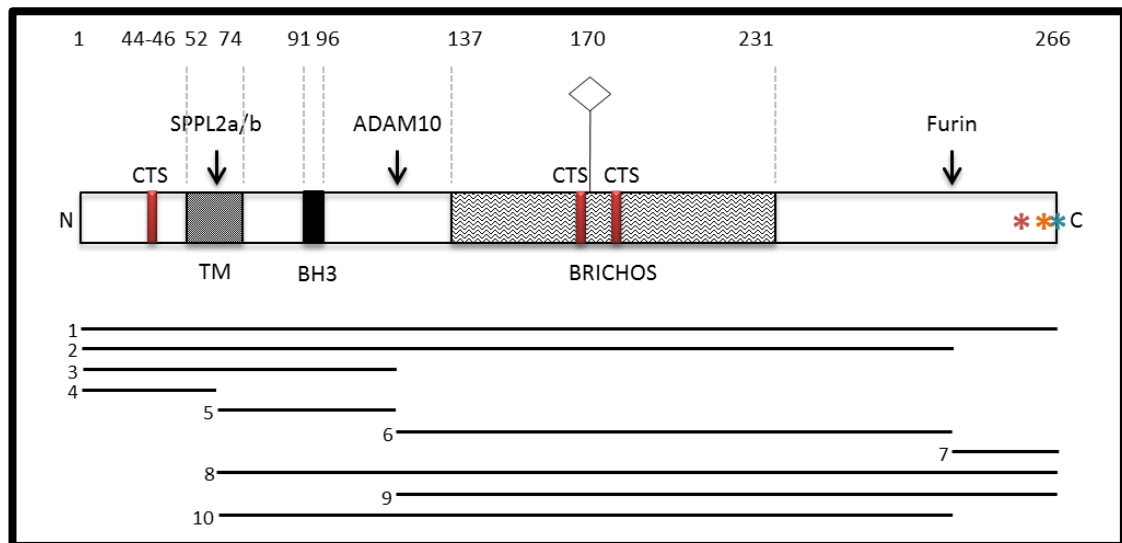


Figure 5-12. ITM2B protein structure and processing details.

Numbers at the top of the figure represent amino acid residues. Protein domains in order from the amino-terminus (N) to the carboxy-terminus (C) include ciliary-targeting sequences (CTS; aa: 44-46, 166-168 and 174-176), indicated by red boxes; a transmembrane (TM) domain (aa 52-75); a Bcl 2 homology 3 (BH3) domain (aa 91-96); a BRICHOS domain (aa 137-231) with an N-glycosylation site at Asn 170, denoted by a diamond. ITM2B is subject to proteolytic cleavage by proteases: SPPL2a/b, ADAM10, and Furin (cleaves between aa 243 and 244, generating a 23-aa peptide). Asterisks indicate mutations identified in ITM2B to date: Retinal mutation (c.782A>C; p.Glu261Ala) in pink; FDD mutation (c.786\_795dupTTTAATTTGT; p.Ser266Pheext\*12) in orange, produces a frameshift generating an 11-residue longer precursor peptide; FBD mutation (c.799T>A; p.\*267Argext\*11) in blue at stop codon causes a read-through of the 3'UTR and also adds 11 additional residues to precursor.

Putative and reported ITM2B peptides are numbered 1-10 in the lower part of the figure. The order of action of the proteases, determined to date, starts with furin cleavage (yielding peptides 2 and 7), followed by ADAM10 (yielding peptides 3 and 6), and subsequently by SPPL2a/b (yielding peptides 4 and 5). The remaining peptides are hypothetical, and, with the exception of peptide 8 (Fleischer *et al.*, 2002), their existence has not been empirically demonstrated. Figure not to scale.

It could be speculated that the strong interaction with N-term TOPORS occurred due to involvement of TOPORS in ICD ubiquitination. The strong interaction with C-term TOPORS could suggest that in the full-length protein the binding actually occurs within this C-terminal region, even if then the N-terminal region mediates ubiquitin attachment to the bound substrate. A region within the C-term TOPORS fragment was previously shown to be required for the SUMOylation activity of TOPORS, and it was also shown to bind proteins of the SUMOylation machinery, so, alternatively, it also could suggest that the ITM2B ICD is a target for SUMO1 modification. Although no known SUMO1 consensus site was found within its sequence, it cannot be excluded that this protein may harbour a yet unidentified SUMO1

site. For instance, TOPORS possess two of the previously-identified SUMO1 sites, but, empirically, SUMO1 binding to TOPORS was shown at different fragments of this protein; this supports the hypothesis that the opposite may be true for ITM2B. It should also be highlighted that a mutational RP hotspot is found within this region. If these mutants are expressed in patients, which was hypothesised not to happen (Chakarova *et al.*, 2007), then premature truncation of the protein could prevent binding of the interacting partners of TOPORS, including the ITM2B fragment: ICD (peptide 4).

A soluble ITM2B90 fragment (residues 90-266, BH3 domain onwards in Figure 5-12) was also tested with TOPORS (and its fragments) for an interaction in yeast. This was considered essential since a membrane-bound protein would not be able to trigger an interaction phenotype in a GAL4-based Y2H system due to being unable to enter the cell nucleus. Residues 90-266 of the ITM2B peptide are inclusive of the ITM2B fragment, which was identified as an interacting partner of TOPORS in the Y2H screen (Figure 5-1).

Depending on the extent of proteolytic processing, which occurs before translocation of the GAL4 AD-ITM2B90 fusion protein to the yeast cell nucleus, the fragment interacting with TOPORS could comprise either full-length of the artificial ITM2B90 protein, or the following peptides, as highlighted in Figure 5-12: peptide 8 (comprising: SCD, ectodomain and CTPP), peptide 10 (comprising: SCD and ectodomain) and/or peptide 5 (comprising: SCD only). If the processing of this artificial ITM2B90 protein resembles that of full-length ITM2B, then it should be assumed that it is probably not peptide 8, which interacts with TOPORS, as furin cleavage of the CTPP was shown to be required for maturation of ITM2B. Thus, it should almost certainly be either peptide 10, or peptide 5 (excluding the amino acids normally found upstream of residue 90).

As in case of the ICD (peptide 4), the strongest interaction for this ITM2B90 species was detected with the N- and C-term TOPORS fragments (activation of four reporter genes). However, it also robustly associated with full-length and mid-TOPORS (activation of two reporter genes). Reasons for association with the N- and C-terminal fragments would be the same as those given for the ICD (peptide 4). On the other hand, the interaction with mid-TOPORS would provide additional evidence that TOPORS participates in its SUMOylation (however, no SUMO1 consensus sites have been found within ITM2B90 sequence).

It should also be noted that ITM2B90 contains two CTS motifs within the BRICHOS domain, which forms a major part of the protein's ectodomain. A potential SUMO1 attachment could



be a signal for changing the localisation of the molecule, for example, for either transporting this ITM2B fragment to the centrioles, or away from them, depending on environmental stimuli. It is also unknown whether glycosylation of this ITM2B fragment at asparagine 170 in yeast resembles the modification, known to occur in mammalian cells, which would certainly affect the observed interactions.

The extent of branching of the attached carbohydrate would also influence the size of the modified ITM2B fragment, and, consequently, its ability to enter the nucleus. Still, the interaction would have been demonstrated in yeast as well as in mammalian cell lines (experimental Chapter 6). This suggests that the PPI is either not affected by asparagine 170 modification; or, if it is, then the yeast glycosylation pattern must have resembled that from mammalian cell lines.

#### 5.3.2.1.1 ITM2B MUTANTS

Experiments with ITM2B mutants showed association between TOPORS (and all its fragments) and the retinal (RetMu) and British dementia (FBD) mutants, but not with the Danish dementia (FDD) mutant.

The mechanism underlying this result could be similar to that identified in mouse brain, where it was shown that, whereas wild-type ITM2B was expressed as a full-length protein, the Danish mutant protein was only detected as small peptides (~4 kDa) (Gibson *et al.*, 2005); the researchers concluded this was due to protein degradation by proteolytic processing. If similar processing occurs in yeast, and the FDD mutant protein becomes degraded by cellular proteases, no blue yeast growth phenotype indicative of an interaction should be observed in the Y2H PPI assay. With regard to the retinal and British dementia mutants, the fact that an interaction is observed suggests that the proteins are expressed, and processed. As all known *ITM2B* mutations occur near its C-terminus, after expression and processing, the fragment(s) ultimately left fused to GAL4 AD should be the same as in case of wild-type ITM2B, i.e. the ICD (peptide 4). Nevertheless, the obtained results are not fully supportive of such reasoning since, unlike the wild-type ITM2B, the retinal and British dementia mutants interacted (to a greater or lesser extent: Table 5-16) with the mid-TOPORS fragment. On the other hand, it cannot be excluded that the mutations could affect the expression and processing via as yet unknown mechanisms.

### 5.3.2.2 PTGDS INTERACTIONS

PTGDS interacted with full-length TOPORS and all its three fragments, as indicated by activation of two reporter genes; however, a strong interaction (demonstrated by activation of four reporter genes) was observed only with the N-term TOPORS fragment (Table 5-16). CoIP experiments showed positive results, confirming PTGDS and TOPORS interaction in mammalian cell lines. As was previously mentioned in the case of ITM2B, it is possible that TOPORS is also involved in ubiquitination of PTGDS. It should be noted that PTGDS contains a signal peptide at its N-terminus. If proteolytic cleavage of this peptide occurs before the GAL4 AD-PTGDS fusion protein is transported into the yeast nucleus, then only the signal peptide would be interacting with TOPORS and its fragments. It could be that the interaction with N-term TOPORS appears stronger due to enhanced requirement for degradation of this signal peptide, which has fulfilled its signalling function, and so was removed from the main portion of the protein.

Alternatively, if un-cleaved PTGDS protein enters the nucleus, its interaction with TOPORS could suggest a role for PTGDS in modulating the DNA binding of TOPORS, and its regulation of RNA polymerase II-transcription, as PTGDS was previously shown to influence gene expression of apoptotic factors (Ragolia, Hall e Palaia, 2007). Studies in the COS-7 cell line on the association between mouse TOPORS and p53 revealed that the association between over-expressed mouse TOPORS and p53 stabilises p53 and enhances its transcription factor activities on p21(Waf1), MDM2 and Bax promoters, of which Bax is a positive regulator of apoptosis. Overall, increased TOPORS levels triggered suppression of cell proliferation, cell cycle arrest and induction of apoptosis (Lin *et al.*, 2005). Independent findings showed that TOPORS interacts with death effector domain of caspase 8 subunit a (DEDa). This results in displacement of p53 from TOPORS, which then becomes available to activate pro-apoptotic genes, including caspase 8 (Yao *et al.*, 2007).

### 5.3.2.3 PSMC1 INTERACTIONS

PPIs between PSMC1 and TOPORS showed the strongest association with the mid-TOPORS and C-term fragments (activation of four reporter genes); however, interactions still occurred with the N-term fragment and full length TOPORS (activation of two reporter genes; Table 5-16). The more readily occurring interactions with regions of TOPORS, implicated in SUMOylation, could suggest that TOPORS acts as a SUMO1 E3 ligase for PSMC1. Such modification by SUMO1 could modulate the activity of PSMC1 within, or independently from the proteasome, such as ATP binding and/or hydrolysis. For example, PSMC1 was shown to act as a key regulator of

sperm surface ATP levels, crucial for successful fertilisation (Yi *et al.*, 2009). SUMOylation could also determine what other post-translational modifications the protein undergoes, e. g. it can serve as a signal for ubiquitin-dependent degradation of SUMO-modified protein (Miteva *et al.*, 2010).

### 5.3.3 CONCLUSIONS

This chapter provided an overview of expression and interaction control experiments performed in order to validate the Y2H screening results. Firstly, it was demonstrated that full-length protein-coding transcripts, corresponding to human retinal cDNA library clones, identified in the screen for interactors of TOPORS, are indeed expressed in the retina at mRNA level.

For *ITM2B* and *PSMC1* the isoforms, pulled out from the Y2H screen, were shown to be the only known protein-coding variants of these respective genes to be expressed in the retina. However, as was discussed, the existence of alternatively spliced variant 004 could not be authoritatively excluded for *PSMC1*. On the other hand, the study of protein-coding *PTGDS* variants indicated that, in addition to *PSMC1*-001, at least two other isoforms are expressed in cells of the human retina.

The second section of this chapter described the results of PPI verification by direct interaction in yeast. The findings confirmed that TOPORS does indeed interact with full-length *PTGDS*-001, *ITM2B*-001 and *PSMC1*-001, to varying extents. Additionally, it was also demonstrated which domains of TOPORS protein, potentially associated with which functions, could be involved in mediating the observed interactions.

On the whole, the results described in Chapter 5 demonstrated that exogenously expressed human TOPORS and its newly-identified human retinal protein partners interact directly in yeast; and their expression in human retina was confirmed at mRNA level. The observed outcomes provided a sound basis for further validation and characterisation experiments. Chapter 6 provides an overview the studies of protein expression of TOPORS, *ITM2B*, *PTGDS* and *PSMC1* in human cell lines, demonstrated by Western blotting (section 2.5.3). The key sections of Chapter 6 also demonstrate that the novel interactors of TOPORS are found in protein complexes precipitated from cell lysates using an antibody against TOPORS (section 2.5.4 Co-immuno-precipitation).

## **6 PROTEIN EXPRESSION AND INTERACTION ANALYSIS IN CELLS**

The experimental chapters so far described the construction and characterisation of the human retinal cDNA library in yeast (Chapter 3); two Y2H screening assays for novel protein interacting partners of TOPORS (Chapter 4); and verification experiments demonstrating retinal mRNA expression of protein-coding isoforms of the identified interactors, as well as direct Y2H PPI experiments confirming the newly-identified interactions in yeast (Chapter 5).

The following objectives were to confirm that the novel PPIs also occur in mammalian cells between endogenous proteins. Prior to this the protein expression of the new interacting partners of TOPORS, namely ITM2B, PTGDS and PSMC1, had to be demonstrated. These experiments utilised sodium-dodecyl sulphate polyacrylamide gel electrophoresis (SDS-PAGE; section 2.5.2 in Methods and Materials) for protein separation, approximately, by size, and then protein transfer and Western blotting (WB; section 2.5.3 in Methods and Materials) for proteins of interest (detection using commercially available antibodies; section 2.8 in Methods and Materials). Evaluation of the PPIs was achieved by precipitating protein complexes using an antibody against TOPORS, separating the mixture by SDS-PAGE, and then Western blotting for one of the identified interacting partners (sections 2.5.2. – 2.5.4 in Methods and Materials).

WB and coIP studies were performed using the HeLa cell line, which is the oldest and most frequently used human cell line. It was derived from the cervix tumour tissue in the early 1950s, and has been dividing autonomously ever since (Rahbari *et al.*, 2009). It should be emphasised that the purpose of this chapter was to demonstrate the interaction between TOPORS and its novel partners in a mammalian host. As no ideal retinal neuronal cell line exists, the HeLa cells were selected for the protein expression and interaction experiments.

Due to the cancerous nature of HeLa cells, it may appear to be an inappropriate cell type for this project. Nonetheless, perhaps counter-intuitively, tumours share many metabolic features with the mammalian retina. Most importantly, as was reviewed by Ng *et al.* (2014), both: neoplastic and retinal tissues are very metabolically active. In fact, they both rely not only on the mitochondrial oxidative phosphorylation for energy generation, but they also perform aerobic glycolysis. This process, also known as the Warburg effect, has been additionally documented in several types of white blood cells and in embryonic stem cells.

The photoreceptors are the predominant retinal cell type involved in aerobic glycolysis. Interestingly, it was shown in pig, that as much 60 % of photoreceptor glucose metabolism is

performed via the glycolytic, rather than oxidative, pathway (Wang, Törnquist e Bill, 1997a; b). This is supported by prominent expression of lactate dehydrogenase (LDH) in the mammalian retina; this enzyme is typically up-regulated in neoplasms (Saavedra e Anderson, 1983).

Another feature of energy metabolism shared by HeLa cells and the photoreceptors is the presence of active brain-type creatine kinase (CK-B). This enzyme catalyses the re-creation of ATP from phospho-creatine (PCr) at sites, where energy is required. In photoreceptors the process typically occurs at synaptic terminals where it is needed for glutamate release (Zhao *et al.*, 1994; Linton *et al.*, 2010). Furthermore, both: the HeLa cell line and retinal cells are enriched in glucose transporters GLUT1 and GLUT3, allowing this sugar to passively and continuously enter cells, where it is used for energy generation (Wong-Riley, 2010).

Biosynthetic requirements are also a characteristic shared by both: cancers and the retina. The photoreceptor homeostasis involves daily outer segment phagocytosis by the retinal pigment epithelial (RPE) cells, resulting in a continuing necessity for synthesis of rhodopsin and other ciliary and outer segment-specific proteins. These biosynthetic demands for renewal of photoreceptor outer segments resemble the physiology of cancer cells, which also rely on constant protein synthesis for cell growth and migration.

Hence, due to reasons outlined above, the use of HeLa cells for investigation of protein expression and verification of the novel PPIs was not considered disadvantageous.

These experiments were necessary prior to performing subsequent studies aiming to better characterise the proteins' relationships. Positive co-immuno-precipitation (coIP; section 2.5.4 in Methods and Materials) results would have demonstrated that, in mammalian cells, TOPORS and its interacting partners are indeed found together in a protein complex within the same cellular compartment, thus strengthening the outcomes of the Y2H screens. The latter demonstrated the occurrence of binary interactions between two exogenously-expressed proteins; however, it provided no evidence that those two proteins could actually encounter each other in native conditions. Hence, the coIP experiments were fundamental for proceeding with further work, such as sub-cellular and tissue localisation studies.

Section 6.1 provides an overview of TOPORS protein expression, and shows a verification of one of its previously published interactions, demonstrated by coIP. Sections 6.2 – 6.4 contain evaluations of expression of ITM2B, PTGDS and PSMC1, as well as coIP experiments demonstrating interactions between TOPORS and its new partners in native conditions.

## 6.1 TOPORS PROTEIN EXPRESSION ANALYSIS

TOPORS monoclonal antibody (M  $\alpha$ -TOPORS), raised in mouse against residues 98-205 of human, GST-tagged TOPORS (Table 2-752-75), was used for Western blot and co-immunoprecipitation (coIP) studies, as well as in immunofluorescent studies (Chapters 7 and 8). Specifically, the immunogen for this antibody includes serine 98, the phosphorylation of which is associated with the ubiquitin ligase (but not SUMO1 ligase) activity of TOPORS (Park *et al.*, 2008); the RING finger domain (residues 103-141), also involved in ubiquitination; and a ciliary targeting sequence (CTS; residues 172-174; identification summarised in section 7.5). Furthermore, the epitope maps to a fragment shown to be required for DNA-binding (residues 51-374) in a zinc-dependent manner (Chu *et al.*, 2001).

An alternative TOPORS polyclonal antibody (Rb  $\alpha$ -TOPORS), raised in rabbit against amino acids 251-377 of human TOPORS, was also evaluated. Just as in case of the mouse antibody, the immunogen of this rabbit antibody forms a part of the zinc-dependent DNA-binding TOPORS fragment. Otherwise, it is not aligned with any distinct functional domains, except for a putative SUMO1 modification site (residues 300-303),  $\Psi$ KxE, where  $\Psi$  is a hydrophobic amino acid, and x can represent any amino acid. TOPORS protein structure and domains were already discussed in detail in the introduction in section 1.6; an overview is summarised and presented in Figure 6-3.

### 6.1.1 TOPORS WESTERN BLOT EXPERIMENTS

Western blot (WB) results (Figure 6-1) demonstrated the pattern of TOPORS bands, detected by both antibodies, is mostly the same; however, their intensity differs significantly. The three most distinct bands, detected using the mouse antibody, migrated at 150 kDa, approximately half way between the 100 kDa and 75 kDa markers, and just below the 50 kDa marker band, respectively. The Rb  $\alpha$ -TOPORS antibody detected the top two of these bands, but the signal was considerably weaker. The strongest band observed with the Rb  $\alpha$ -TOPORS antibody migrated at approximately 75 kDa. The signal for the corresponding Abnova band, using the M  $\alpha$ -TOPORS antibody was considerably weaker.

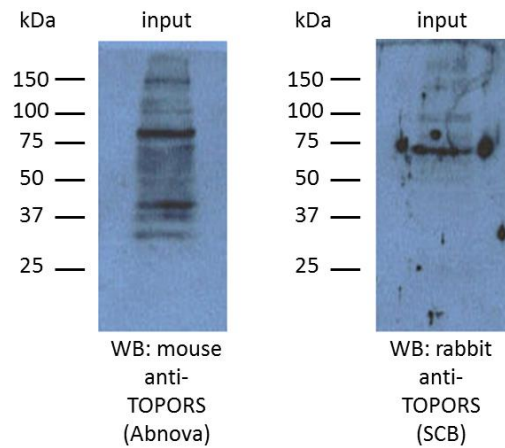


Figure 6-1. Western blots against TOPORS.  
 Input: total endogenous protein extract from non-synchronised HeLa cells. Exposure time: 1 minute.

### 6.1.2 CONTROL COIP EXPERIMENT

It was previously reported (Chakarova *et al.*, 2011) that  $\gamma$ -tubulin was found in complexes immuno-precipitated with TOPORS. This interaction was used as a positive control in the subsequent coIP experiments. The observed results demonstrated a weak interaction (Figure 6-2), but they were reproduced consistently. All of the coIP assays, including the control interaction with  $\gamma$ -tubulin, were performed at least in triplicate, and representative images are presented. Reverse coIP experiments were attempted in triplicate for all interactions, but they did not yield positive results (data not shown). This may have occurred due to the interacting partners of TOPORS being potentially embedded within a protein complex, which would prevent antibodies from accessing them, and consequently from binding. If TOPORS was located on the outside of a complex of proteins, it could be accessed and bound by an antibody raised against it.

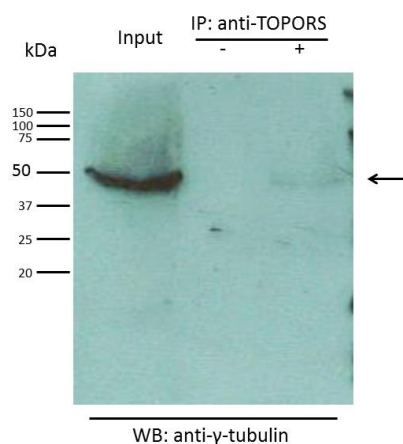


Figure 6-2. Gamma tubulin is detected in complexes precipitated from HeLa cell extract with antibody against TOPORS, raised in mouse.  
 Input: total cell extract; antibody-negative beads control is indicated by a minus (-), whereas complexes, precipitated with mouse anti-TOPORS antibody-conjugated beads, are indicated with a plus (+). A faint  $\gamma$  tubulin band in the positive coIP lane is indicated with an arrow.

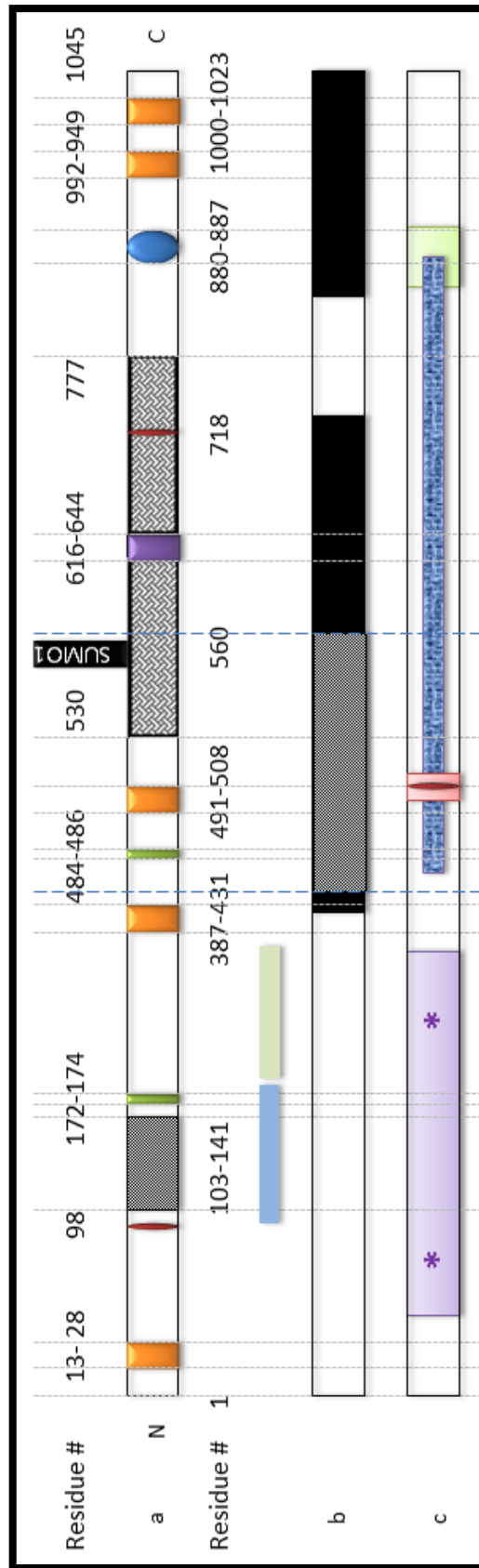


Figure 6-3. TOPORS Protein Domain Structure.

Amino acid (aa) residues are indicated above and below diagram (a). Regions recognised by the mouse (aa: 98-205) and rabbit (aa: 251-377) antibodies are indicated by a blue and a green bar, respectively, shown between diagrams (a) and (b). (a) TOPORS protein domains. Orange boxes indicate PEST domains; maroon narrow ovals at Ser 98 and Ser 718 denote known phosphorylation sites; dark grey box (aa: 103-141) indicates the RING domain; green narrow boxes (aa: 172-4 and 484-6) represent ciliary targeting sequences (CTS); dark cross-hatched box (aa: 530-777) represents the arginine- and serine-rich (SR/RS) domain; a SUMO1 acceptor site at Lys 560, with a covalently bound SUMO1 modification (perpendicular black box), is indicated within the first SR/RS domain; a nuclear localisation signal (NLS; aa: 616-644) is located approximately centrally within the SR/RS domains; the blue oval indicates the location of a lysine- and histidine-rich motif (aa: 880-887). (b) Black boxes (aa: 415-737 and 854-1045) indicate regions required for interaction with SUMO1; grey box (aa: 437-574), partly overlapping with one of the black boxes, represents a fragment required for SUMOylation of TOPORS at Lys 560. (c) Region required for interaction with DNA-binding (aa: 51-374) is denoted by a purple box; two consensus SUMOylation sites ( $\Psi$ KxE; aa: 75-78 and 300-303) are indicated by asterisks within the purple box, and represent putative additional sites for TOPORS modification by SUMO1; the red box signifies a region required for interaction with the cytoplasmic domain of syndecan 1 (S1CD)17 (aa: 493-510), whereas the narrow maroon oval within it represents a consensus casein kinase 2 phosphorylation site (aa: 499-502); the long blue segment (aa 456-882) denotes the region, which interacted with hTop1 in a Y2H screen; the green box (aa: 871-917), overlapping with Lys/His region (diagram 1), represents a region required for minimal interaction with UBC9 and Rep proteins of AAV2. Figure not to scale.

<sup>17</sup> This was demonstrated by a Y2H involving murine TOPORS and S1CD, not human (Braun *et al.*, 2012).



## 6.2 ITM2B PROTEIN EXPRESSION ANALYSIS

Two antibodies against the ITM2B protein were used in this project, both raised in rabbit. An antibody against the carboxy-terminal region of ITM2B, specifically amino acids 218-247 of the human 266-residue long protein (Abgent # AP13163b: ITM2B C-term), was used in the initial stages of cell-based studies. A second antibody, used by Audo *et al.* (2013), was later included in additional analysis (Sigma-Aldrich # HPA029292: ITM2B); this antibody was raised against residues 78-224 of the human ITM2B peptide. ITM2B is synthesised as a full-length trans-membrane protein, which subsequently undergoes regulated proteolytic cleavage. Figure 6-4 delineates the various potential peptides resulting from ITM2B processing, and demonstrates that the Sigma-Aldrich antibody is likely to detect two further putative peptides, which would not be recognised by the C-term antibody, i.e. NFT (fragment 3) and SCD (fragment 5).

### 6.2.1 ITM2B WESTERN BLOT EXPERIMENTS

The Western blot analysis of non-synchronised HeLa cell extracts demonstrated ITM2B is expressed in mammalian cells (Figures 6-5 and 6-6, where the first figure represents endogenous proteins, whereas the latter represents protein extracts from cells transfected using N-terminally six-His-tagged ITM2B).

Specifically, a band migrating at 37 kDa was detected by in all blots. A 50 kDa band was detected only by the  $\alpha$ -ITM2B C-term antibody (Figures 6-5 and 6-6 A). A band, migrating just below the 75 kDa marker, was detected by the  $\alpha$ -ITM2B C-term antibody in the endogenous extract (Figure 6-5), and also by the  $\alpha$ -six-His antibody in the transfected cell extract (Figure 6-6 C). Additionally, some bands were observed between the 37 kDa and 50 kDa markers (Figures 6-6 A and 6-6 C), as well as between the 15 kDa and 20 kDa markers (Figure 6-5). The ITM2B C-term antibody detects several bands (Figure 6-4 and Figure 6-6: A), an observation consistent with the known existence of several ITM2B peptides due to proteolytic cleavage.

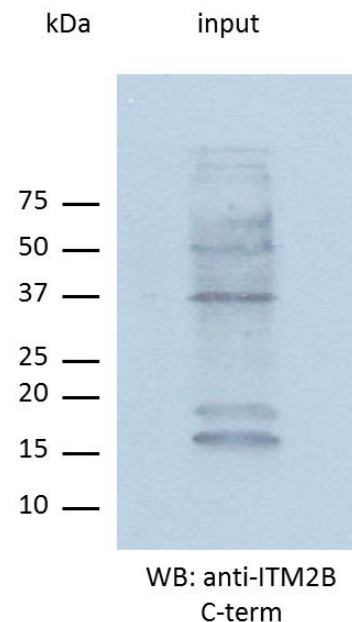


Figure 6-4. Western blot against endogenous ITM2B C-term (Ab diluted 1/250).

Input: total protein extract from non-synchronised HeLa cells. Exposure time: 30 seconds.

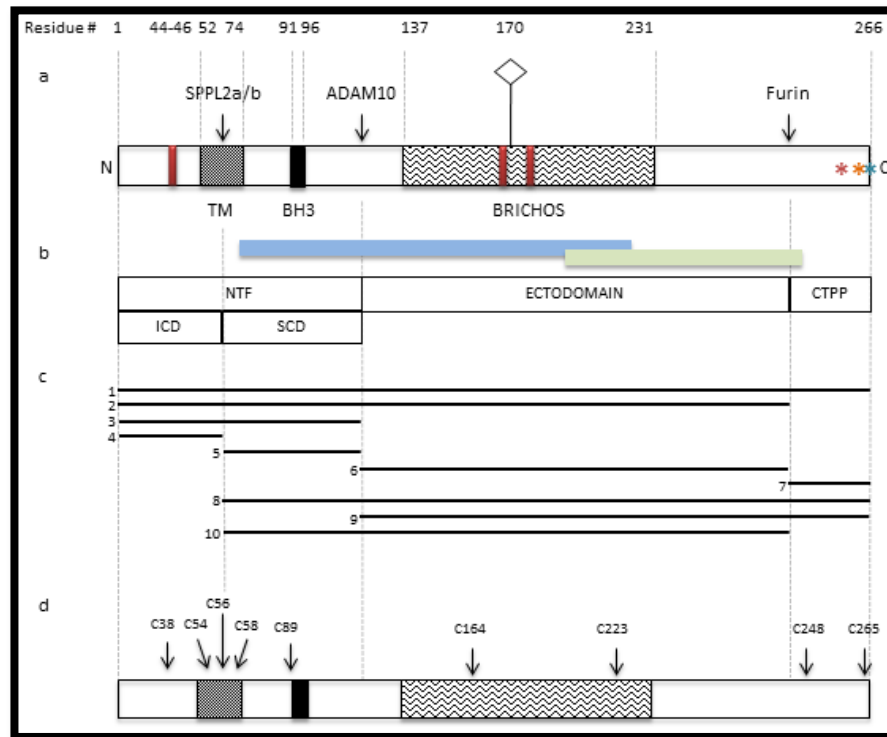


Figure 6-5. ITM2B Protein Domain Structure.

Amino acids (aa) residues are indicated above the figure. (a) Ciliary-targeting sequences (CTS; aa: 44-46, 166-168 and 174-176) are indicated by red boxes. Transmembrane domain (TM: aa 52-75); Bcl 2 homology 3 (BH3: aa 91-96) domain; BRICHOS domain (aa 137-231) N-glycosylation site at Asn 170, denoted by a diamond. ITM2B is subject to proteolytic cleavage by proteases: SPPL2a/b, ADAM10, and Furin (cleaves between aa 243 and 244, generating a 23-aa peptide). Asterisks indicate mutations identified in ITM2B to date: Retinal mutation (c.782A>C; p.Glu261Ala) in pink; FDD mutation (c.786\_795dupTTTAATTGT; p.Ser266Pheext\*12) in orange, produces a frameshift generating an 11-residue longer precursor peptide; FBD mutation (c.799T>A; p.\*267Argext\*11) in blue at stop codon causes a read-through of the 3'UTR and also adds 11 additional residues to precursor. (b) Peptide-nomenclature: Furin-mediated cleavage results in the release of a 23 aa C-terminal pro-peptide (CTPP); a large part of the remaining ectodomain (BRICHOS domain) is shed extracellularly by ADAM10, leaving the membrane-bound N-terminal fragment (NTF). The NTF undergoes intramembrane proteolysis by SPPL2a or SPPL2b, generating the intracellular domain (ICD) and the secreted C-term domain (SCD). Regions (and hence peptides) potentially recognised by antibodies are indicated in blue (residues 78-224) – Sigma-Aldrich; and green (residues 218-247) – Abgent. (c) Putative and reported peptides are numbered 1-10. The order of action of the proteases, determined to date, starts with furin cleavage (yielding peptides 2 and 7), followed by ADAM10 (yielding peptides 3 and 6), and subsequently by SPPL2a/b (yielding peptides 4 and 5). However, it cannot be excluded that in some circumstances the protein may undergo different, not yet known, combinations of proteolytic processing, which could generate additional peptide species (8-10) from the ITM2B full-length protein. For instance, the initiation methionine of ITM2BS corresponds to residue 57 of the full-length protein, i. e. following the known order of proteolysis, it could give rise to peptides 7 and 10, and subsequently to 5 and 6. Peptide 9 is not unlikely to exist either, as the pro-apoptotic activities have been observed only with ITM2BS, suggesting that it would be processed, or modified differently than full-length ITM2B, for which no apoptotic involvement has been shown. Furthermore, protein expression of isoform ITM2B-003 would yield a peptide comprising only ICD (peptide 4) and CTPP (peptide 7), which would result in one more peptide variant (4 + 7); however, the presence of this isoform would not be detected with either of the two antibodies used. (d) Nine cysteine (C, Cys) residues found within the ITM2B peptide. Figure not to scale.

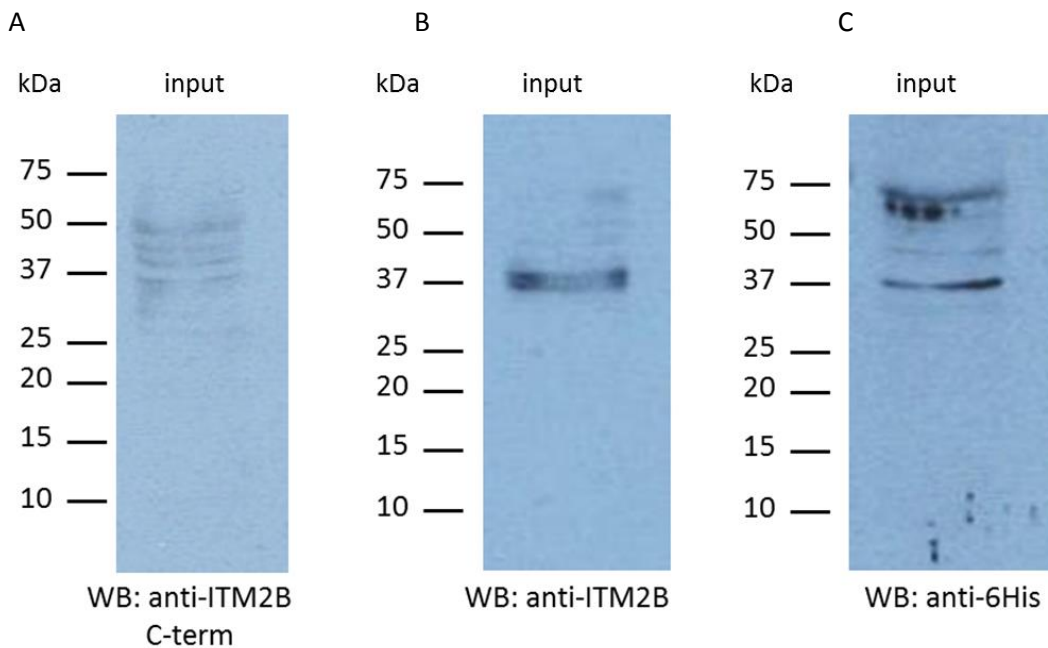


Figure 6-6. Western blot against over-expressed ITM2B.

Input: total protein extract from non-synchronised HeLa cells, transfected with six-His-tagged ITM2B. A, Detected using  $\alpha$ -ITM2B C-term Ab, diluted 1/250 (Abgent); B, detected using  $\alpha$ -ITM2B Ab, diluted 1/250 (Sigma-Aldrich); C, detected using 6His-Ab, diluted 1/250. Exposure time: 3 minutes 30 seconds for all three blots.

Additionally, many of the observed bands are larger than the predicted 29 kDa of the full size protein, which is consistent with the presence of N-acetyl glucosamine modification at asparagine 170 and predicted glycation and phosphorylation sites.

It was previously reported that the full-length ITM2B protein forms homodimers (Tsachaki *et al.*, 2010), therefore, it is also possible that the bands represent dimers (or fragments of the dimers), which perhaps had not been completely denatured prior to electrophoresis. The band, migrating between the 50 kDa and 75 kDa markers, could potentially correspond to ITM2B homodimers, similar to the 66 kDa band, observed by Tsachaki *et al.*

The two bands, which were consistently detected by the ITM2B C-term antibody, migrate at 50 kDa and 37 kDa, respectively. This is consistent with observations by Akiyama *et al.* (2004) who detected bands estimated to migrate at 35 kDa and just above 50 kDa. The observed ~50 kDa bands could represent either a full-length ITM2B protein or ITM2B without the CTPP fragment, with all the potential post-translational modifications. Depending on the exact cleavage point of ADAM10, the 35/37 kDa fragment could represent either the ITM2B ectodomain, or the membrane-bound N-terminal fragment (NTF).

Two smaller bands, migrating between the 20 kDa and 15 kDa size markers (endogenous ITM2B: Figure 6-4), were also observed. They could either represent ITM2B degradation products, or, for instance, the ITM2B ectodomain without any modifications.

The Sigma-Aldrich ITM2B antibody appears to detect predominantly what appear to be two bands around 37 kDa, with fainter bands also observed migrating at approximately 50- and 75 kDa (Figure 6-6 B). These fragments could represent either the ITM2B ectodomain or the NTF domain, or these two fragments joint together. Alternatively, the largest band could even represent non-denaturated dimers of the full-length, or cleaved, ITM2B. These bands, resulting from over-expression of ITM2B, tagged with six-histidines (six-His) at the amino terminus, were also strong, when detected using an antibody against the six-histidine peptide (Figure 6-6 C). This finding would be in support of the 37 kDa band potentially representing the NTF fragment, as the six-His tag would be fused to it directly. The anti-six-His antibody also detected a band migrating between the 50 kDa and 75 kDa markers, which could represent a fragment of ITM2B homodimer, analogous to the 66 kDa band, observed by Tsachaki *et al.* (2010). A band of similar size was also detected by the anti-ITM2B C-term antibody (Figure 6-4) in the endogenous extract.

## 6.2.2 ITM2B IS FOUND IN PROTEIN COMPLEXES WITH TOPORS

CoIP experiments were conducted using mammalian cells to validate the ITM2B interaction identified in the Y2H studies, using HeLa cell extracts (Figure 6-7).

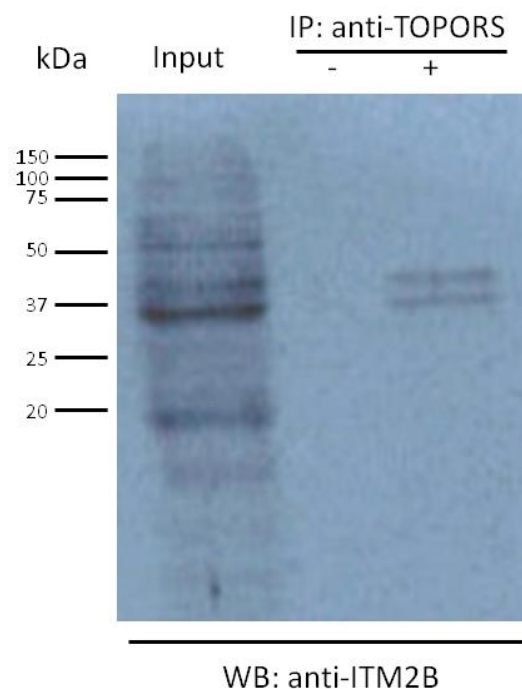


Figure 6-7. ITM2B C-term (Abgent) is detected in complexes precipitated from HeLa cell extracts with antibody against TOPORS, raised in mouse. Input: total cell extract; antibody-negative beads control is indicated by a minus (-), whereas complexes, precipitated with mouse anti-TOPORS antibody-conjugated beads, are indicated with a plus (+). Two bands are detected in the positive coIP lane.

Full-length ITM2B and/or ITM2B proteolytic processing products are found in protein complexes with TOPORS in endogenous extracts from mammalian cells. Western blotting for ITM2B on protein extracts precipitated with TOPORS yielded two bands, one migrating just around the 37 kDa marker band, and a larger one migrating approximately half way between the 37 kDa and 50 kDa markers.

The remaining bands detected in the input with the antibody against ITM2B did not appear to co-precipitate with TOPORS (Figure 6-7). As already analysed above, the 37 kDa could represent the NTF and/or the ectodomain, jointly or separately, depending on post-translational modifications. The larger band is probably more likely to represent these two domains together, or it may represent full length ITM2B with just a few of the potential post-translational modifications.

Other bands, which have been detected multiple times, but inconsistently, include two bands migrating between the 37 kDa and 50 kDa size markers (overexpressed ITM2B: Figure 6-6 A). This double band pattern was shown by Tsachaki *et al.* (2010) in their results figure, demonstrating ITM2B monomers, and both bands were detected here in protein complexes, precipitated with an antibody against TOPORS (Figure 6-7).

They could potentially represent full-length ITM2B (or ITM2B without the CTPP fragment) modified by only some of the predicted post-translational modifications. This coIP result indicates that in mammalian cells ITM2B is found in endogenous protein complexes with TOPORS, and it serves as a validation of the direct PPI between these two proteins, demonstrated in the Y2H system.

### **6.3 PTGDS PROTEIN EXPRESSION ANALYSIS**

An antibody raised in rabbit against full-length human PTGDS (sc-30067, Santa Cruz Biotechnology, TX, USA) was used in all immuno-based experiments.

PTGDS is a small, stable molecule, refolding correctly even after heat and/or protease treatment. It exists as a monomer, and assumes a  $\beta$ -barrel structure with two overlapping hydrophobic pockets: one for hydrophobic ligand binding and another for catalysis of PG D2 synthesis (Åkerström, 2006). PTGDS is known to be glycosylated at three sites, a feature, which has probably greatly affected the range of its reported sizes. It is also known to be phosphorylated, and four potential sites have been predicted for this modification. No other post-translational modifications of this protein have been reported. A summary of PTGDS protein domains and modifications is given in Figure 6-8.

#### **6.3.1 PTGDS WESTERN BLOT EXPERIMENTS**

The Western blot analysis of non-synchronised HeLa cell extracts demonstrated PTGDS is expressed in mammalian cells (Figure 6-9). Two strong bands immuno-reactive for PTGDS are observed: one migrating just above and one just below the 50 kDa marker. The predicted calculated weight of PTGDS is 21 kDa; however, according to published reports, the protein electrophoretic size range spans from 19 kDa to 29 kDa.

Nonetheless, it cannot be excluded that the observed antibody binding is non-specific. The manufacturer validated the antibody only for immunostaining of cultured cells and tissue sections (section 2.8 in Methods and Materials). In those experimental conditions PTGDS would have maintained its native bucket-shaped (or barrel-shaped) conformation, which is probably of key importance for specificity, as the antibody was raised against a full-length protein. As was mentioned in the introduction to section 1.3, PTGDS is a readily refolding protein, thus, since the antibody was raised against the full-length PTGDS peptide, it was probably in its native conformation.

Proteins subject to the denaturing SDS-PAGE would undergo electrophoretic separation as unfolded peptides. This possible change in tertiary structure of PTGDS could have resulted in loss of specificity of the antibody, which was raised against a native bucket-shaped molecule.

Alternatively (although unlikely), the denaturing conditions of SDS-PAGE might be insufficient to trigger (complete) PTGDS unfolding, as this protein is known for structural stability. If PTGDS is not fully denatured (unfolded), then it would be travelling through the porous gel as a more

bukly structure (rather than a linearised peptide). This would lead to its apparent electrophoretic size being significantly larger than expected, as the bulky shape would slow down the proteins passage through the porous acrylamide gel.

In rat retina the reported size range for PTGDS was 20 kDa – 26 kDa (Beuckmann *et al.*, 1996). Some of the lower weight species could potentially be represented by the very faint bands observed between approximately 20 kDa and 37 kDa. Otherwise, they could represent one of the alternative isoforms (004 or 005), identified in the human retinal cDNA (section 5.1.2).

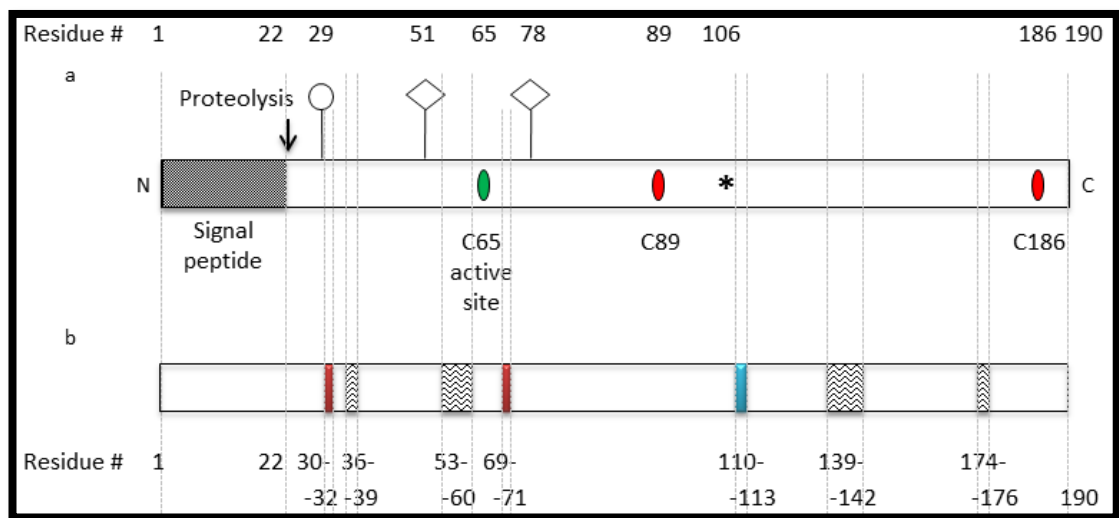


Figure 6-8. PTGDS Protein Domain Structure.

Amino acids (aa) residues are indicated above and below the figure. (a) Signal peptide (aa 1-22) is removed by proteolytic cleavage (indicated with an arrow); PTGDS is modified by glycosylation at three sites: Ser 29 is modified by O-linked glycosylation (denoted by a circle), whereas Asn 51 and Asn 78 are N-glycosylated (denoted by diamonds); catalytic activity of PTGDS is conferred by Cys 65 (denoted by a green oval), whereas Cys 89 and Cys 186 (denoted by red ovals) form a disulphide bridge. Ser106, phosphorylated by PKC, is denoted by an asterisk. (b) Apart from the signal peptide (aa 1-22), PTGDS structure is rich in  $\beta$ -pleated sheets. Exceptions include four  $\alpha$ -helices (indicated by boxes filled with undulating lines: aa 36-39; aa 53-60; aa 139-142; aa 174-176) and a proline-including turn (indicated by a blue box: aa 110-113); ciliary-targeting sequences (CTS; aa: 30-32 and 69-71) are denoted by red boxes. Figure not to scale.

In case of the 19 kDa species, isolated from cerebrospinal fluid (CSF) (Harrington *et al.*, 1993), PTGDS was probably missing its signal peptide (Figure 6-8), resulting in a size below the expected 21 kDa.

The largest PTGDS species that the group observed was migrating at 24 kDa, as demonstrated by two-dimensional electrophoresis (2DE), and the protein pI ranged from 5.2 to 8.5. The researchers determined that the increase in size was due to N-linked modifications, involving sialic acid (also known as neuraminic acid). The larger (up to 29 kDa) PTGDS reactive bands have been reported several times independently (Hoffmann *et al.*, 1993; Hoffmann *et al.*, 1994; Yamashima *et al.*, 1997; Ragolia *et al.*, 2003).

Hoffmann *et al.* (1993; 1994) detected bands ranging from 21 kDa to 29 kDa in samples of human CSF. They determined that the 21 kDa band represents unglycosylated PTGDS, a 24 kDa band is equivalent to a monoglycosylated species, whereas the highest band represented PTGDS, modified at two, or more, glycosylation sites. The authors referred to these N-glycosylation sites as asparagine 29 and asparagine 56, as the existence of the cleavable signal peptide was not known at the time; these residues actually correspond to asparagine 51 and asparagine 78 of PTGDS, respectively (Figure 6-8).

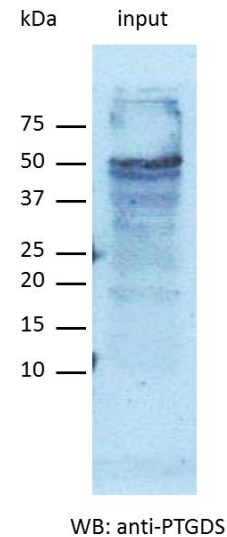


Figure 6-9. Western blot against PTGDS (Ab diluted 1/500).

Input: total endogenous protein extract from non-synchronised HeLa cells. Exposure time: 30 seconds.

### 6.3.2 PTGDS IS FOUND IN PROTEIN COMPLEXES WITH TOPORS

CoIP experiments using HeLa cell extracts confirmed that PTGDS is found in protein complexes with TOPORS in endogenous extracts from mammalian cells.

It should also be emphasised that two bands (rather than one) were consistently observed on PTGDS Western blots, one migrating just above the 50 kDa marker, and one just below it. However, only the PTGDS band migrating just under the 50 kDa marker was found in complexes with TOPORS (Figure 6-10). The slightly smaller size could potentially reflect a lack of the signal peptide, or alternatively, a lack of a posttranslational modification(s), or both. This coIP result indicates that in mammalian cells PTGDS is found in endogenous protein complexes with TOPORS, and it serves as a validation of the direct PPI between these two proteins, demonstrated in the Y2H system.



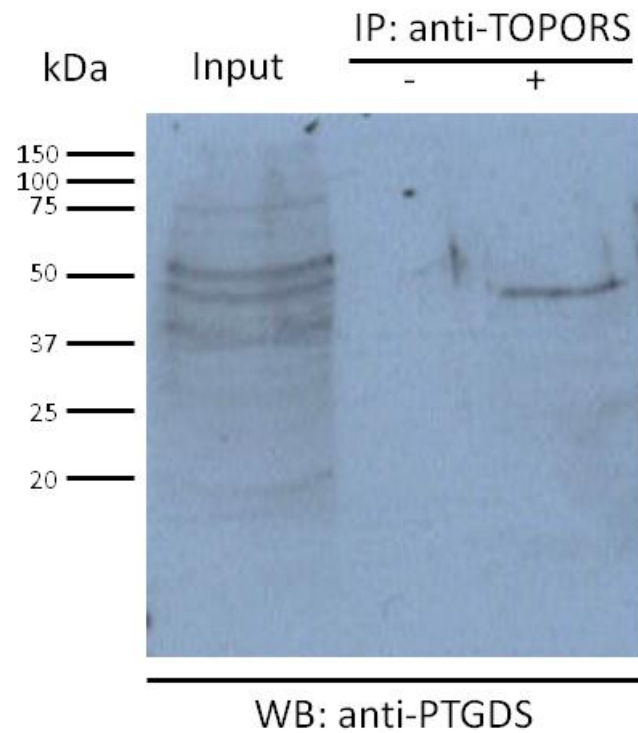


Figure 6-10. PTGDS is detected in complexes precipitated from HeLa cell extract with antibody against TOPORS, raised in mouse. Input: total cell extract; antibody-negative beads control is indicated by a minus (-), whereas complexes, precipitated with mouse anti-TOPORS antibody-conjugated beads, are indicated with a plus (+). The band detected in the positive coIP lane is migrating just below 50 kDa.

## 6.4 PSMC1 PROTEIN EXPRESSION ANALYSIS

An antibody against the carboxy-terminal residues 295-436 of human PSMC1 (Sigma-Aldrich # HPA000872) was used in all immuno-based experiments (Figure 6-11). It should be noted that the antibody recognises a region of PSMC1, located close to the sequence, required for anchoring PSMC1, together with other ATPases of the regulatory proteasomal hexameric ring, onto the core catalytic particle (Figure 6-11). This may pose difficulties in localisation studies, as in its native form, this region might be hidden inside the proteasome.

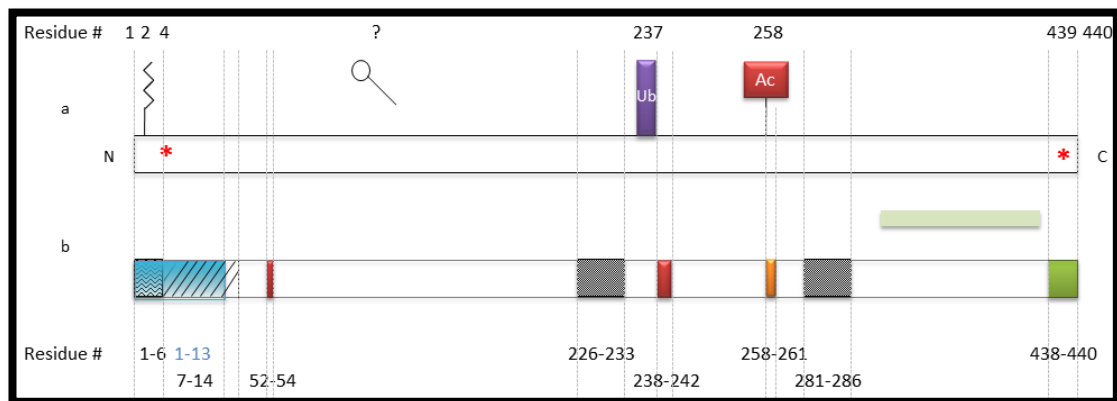


Figure 6-11. PSMC1 Protein Domain Structure.

Amino acids (aa) residues are indicated above and below the figure. Region recognised by the antibody (aa: 295-436), is indicated with a light green bar, shown between diagrams (a) and (b). (a) Post-translational modifications of PSMC1. N-myristoylation at Gly 2 (modification indicated by a lipid notation); two phosphorylation sites, denoted by red asterisks, at Ser4 and Tyr 439; ubiquitination at Lys 237, which forms a glycy l lysine isopeptide bond with a C-terminal peptide of ubiquitin; N-acetylation at Lys 258. Functionally indispensable O-linked glycosylation (represented by a floating lollipop) has also been reported for PSMC1; however, the site of modification has not yet been determined. (b) Functionally-significant sequence motifs. N-myristoylation consensus sequence: MGxxx(S/T) (aa: 1-6); NADH-binding motif: xGxGxxGx (aa: 7-14); Arabidopsis thaliana PSMC1 orthologue fragment of high functional significance for plant development (aa: 1-13) (Lee, K. H. *et al.*, 2012); ciliary-targeting motifs (CTS; aa: 52-54 and 238-242); ATP-binding loop: GxxxxGK(T/S) (aa: 226-233); axially-positioned aromatic loop: (K/M)Y(V/L/I)G (aa: 258-261), coordinated with ATP hydrolysis region: hhhhDE (aa: 281-286; h, hydrophobic residue); proteasomal regulatory ATPase-anchoring sequence: hYx (aa: 438-440). Figure not to scale; compiled based on findings from human and mouse cell lines, and PSMC1 orthologues from *S. cerevisiae* and *A. thaliana*.

On the other hand, the plant orthologue of PSMC1 was shown to exist and function independently in chromatin regulation (section 4.3.4); hence, its detection should not be entirely discounted. In fact, the presence of its NADH-binding activity may signify a role in regulation of gene expression in response to redox stress (Fjeld, Birdsong e Goodman, 2003). The acetyl at residue 258 may be a regulatory component, which competes with ubiquitin and/or ubiquitin-like proteins, for lysine 258 (Caron, Boyault e Khochbin, 2005), and hence defines the purpose of the modified PSMC1 peptide. This lysine acetylation could also directly

influence the activity of the aromatic loop, which follows directly afterwards, and whose function is directly associated with the ATP hydrolysis (site located twenty residues downstream).

These variable activities would require PSMC1 to be differentially, post-translationally modified either to mark it for targeting to a specific cellular location, and/or to perform a specific function. For instance, a SUMOylation could determine whether PSMC1 should be acting as a component of the 26 S proteasome, or whether perhaps it should be mediating an independent process.

#### **6.4.1 PSMC1 WESTERN BLOT EXPERIMENTS**

The Western blot analysis of non-synchronised HeLa cell extracts demonstrated that PSMC1 is expressed in mammalian cells (Figure 6-13).

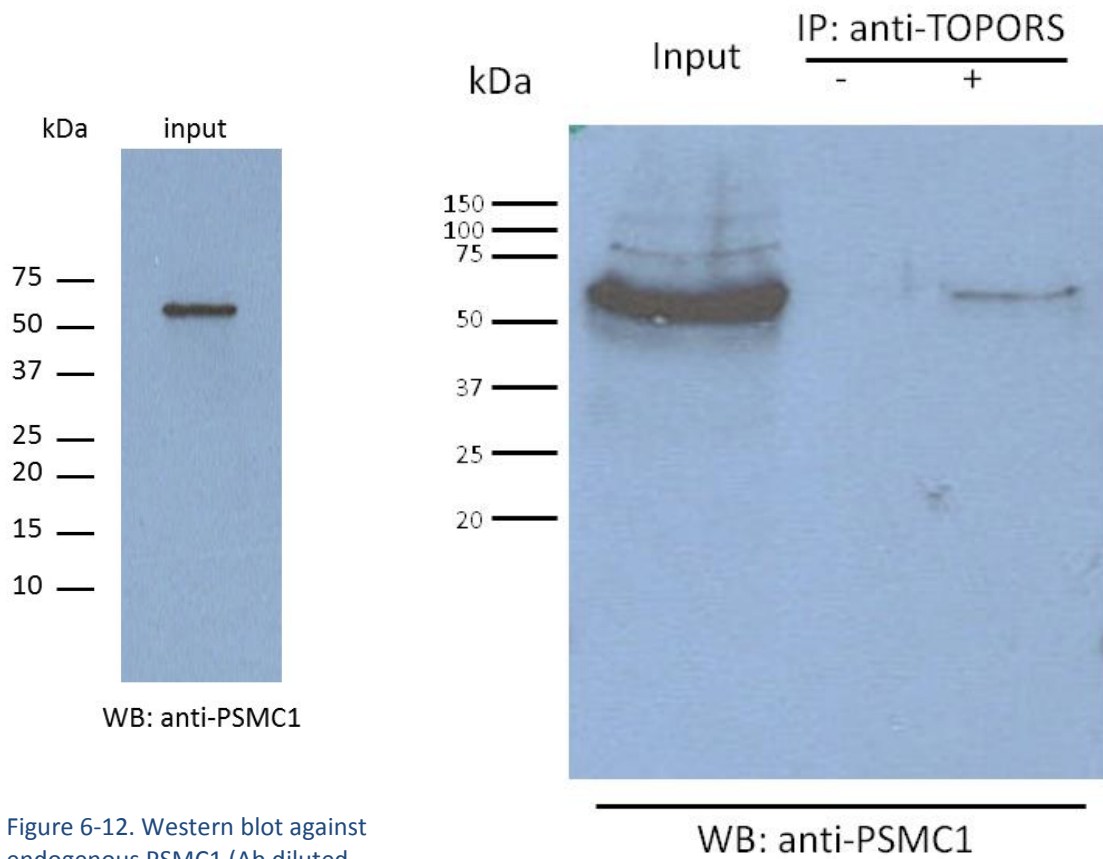
The expected calculated weight of PSMC1 was 48.5 kDa. Western blot analysis demonstrated specifically that the band, immuno-reactive for PSMC1, migrated between the 50 kDa and 75 kDa markers (Figure 6-13), approximately at 55 kDa - 60 kDa. This was observed consistently, and a band of similar size was also shown in studies by Zhang *et al.* (2003).

#### **6.4.2 PSMC1 IS FOUND IN PROTEIN COMPLEXES WITH TOPORS**

CoIP experiments revealed that PSMC1 is found in protein complexes with TOPORS in endogenous extracts from mammalian cells.

The same-sized band, migrating approximately at 55 kDa - 60 kDa, was observed in both the total input lane, as well as in the lane loaded with protein extract precipitated with an antibody against TOPORS (Figure 6-13). This size shift could signify a covalent modification with a monomer or ubiquitin (8.5 kDa), perhaps the modification at lysine 237, which is immediately followed by a CTS.

This coIP result indicates that in mammalian cells PSMC1 is found in endogenous protein complexes with TOPORS, and it serves as a validation of the direct PPI between these two proteins, demonstrated in the Y2H system.



## 6.5 DISCUSSION

The novel interacting partners of TOPORS, namely ITM2B, PTGDS and PSMC1, were shown to be expressed in the human cancerous HeLa cell line. This cell line might not at first appear to be the right choice for experiments conducted in context of this project due to its cancerous nature, as the retina comprises mostly non-dividing neuronal cells.

Nonetheless, as was explained in the introductory section of Chapter 6, the purpose of the experiments described here was predominantly to demonstrate that PPIs between TOPORS and its novel interacting partners do indeed occur between endogenous proteins in its native conditions in mammalian cells.

Secondly, analogies between cancer cells and the retina, especially the photoreceptor cells, were additionally highlighted in order to demonstrate that HeLa cells are not a bad model for these PPI studies. Importantly, both: cancer cells and photoreceptor cells have large energy requirements and high biosynthetic rates. Especially, the latter characteristic appears that HeLa cells are more suitable model cell line than for instance the hTERT-RPE1 cells, which in its native tissue perform predominantly phagocytosis and protein breakdown (rather than synthesis). The neuroblastoma SK-N-SH cell line would also have been adequate for the purposes of this study, or even better, as it is both: of neuronal origin and it is a cancerous cell line. Nonetheless, this cell line was not yet available in the mid-stages of the project when the WB and coIP experiments were being performed.

### 6.5.1 ITM2B PROTEIN EXPRESSION

Based on molecular mass calculations the predicted mass of the full-length ITM2B protein should be approximately 30 kDa; the predictions for the various peptide combinations, potentially recognised by the two ITM2B antibodies, are given in Table 6-1, based on published data on ITM2B structure and processing.

It should also be noted that in addition to the N-glycosylation site, which appears to shift the electrophoretic mass of ITM2B by approximately 2 kDa, bioinformatics research predicted eight glycation (non-enzymatic sugar residue attachment) sites as well as eight phosphorylation sites within the ITM2B peptide sequence (Tsachaki *et al.*, 2011). These additional post-translational modifications, if empirically confirmed, collectively could explain the significantly larger mass shift of approximately 15 kDa – 20 kDa observed for ITM2B (Figure 6-5).

Table 6-1. Expected fragment sizes of ITM2B monomers detected by anti-ITM2B antibodies. Fragments are indicated by numbers and/or names, as shown in Figure 6-4. Length is given as number of amino acid (aa) residues, and it is predicted for fragments, arising due to ADAM10 processing, as the exact cleavage point is not known. The expected size (kDa) was calculated assuming the average weight of an amino acid residue as 110 Da. Antibodies expected to detect the specified fragments are denoted as  $\alpha$ -ITM2B (Sigma-Aldrich) and  $\alpha$ -ITM2B C-term (Abgent).

Fragment	Predicted Length (aa)	Expected size (kDa)	Ab expected to detect fragment(s) of interest
Full length ITM2B/1	266	29	$\alpha$ -ITM2B and $\alpha$ -ITM2B C-term
ICD/4	60	7	Neither
SCD/5	40	4	$\alpha$ -ITM2B
NTF/3	100	11	$\alpha$ -ITM2B
Ecto/6	143	16	$\alpha$ -ITM2B and $\alpha$ -ITM2B C-term
NTF + Ecto/2	243	27	$\alpha$ -ITM2B and $\alpha$ -ITM2B C-term
CTPP/7	23	3	Neither
SCD+Ecto+CTPP/8	206	23	$\alpha$ -ITM2B and $\alpha$ -ITM2B C-term
Ecto+CTPP/9	166	18	$\alpha$ -ITM2B and $\alpha$ -ITM2B C-term
SCD+Ecto/10	183	20	$\alpha$ -ITM2B and $\alpha$ -ITM2B C-term
iso-003/ 4+7	160	18	Neither

It should also not be excluded that ITM2B (or one/several of its proteolytic cleavage products) is modified by a covalent attachment of ubiquitin, or a ubiquitin-like protein, which would result in an apparent size shift of approximately 8 kDa to 10 kDa per single attached molecule.

Proteolytic processing of ITM2B begins in the *cis*- to median-Golgi apparatus, where the protease furin removes the carboxy-terminal peptide of ITM2B (CTPP), triggering its maturation, and subsequent transport in secretory vesicles towards the plasma membrane and endosomes (Choi *et al.*, 2004; Matsuda *et al.*, 2011). Furin cleavage occurs between residues 243 and 244 (Kim *et al.*, 1999), and the resulting CTPP fragment has a predicted weight of only 3 kDa. The glycosylation at asparagine 170 is required for transport of ITM2B to the plasma membrane, and for maintaining the protein's levels there, which suggests that ADAM10 does not cleave ITM2B until it reaches the cell membrane. It was demonstrated that cleavage of ephrin by ADAM10, a single-pass type I protein, occurs in *trans* (Janes *et al.*, 2005); therefore, it could be speculated that also in case of ITM2B cleavage, ADAM10 may be located within the membrane of a neighbouring cell.

The precise cleavage site recognized by ADAM10, which in ITM2B mediates shedding of the BRICHOS-containing ectodomain, remains to be determined. In Figure 6-4 the ADAM10 cleavage site is indicated with an arrow between the BH3 (residues 91-96) and BRICHOS (residues 137-231) domains; however, it may well be found between the TM (residues 52-74) and BH3 domains, or even within the BH3 domain itself. It was shown that residues 46-106 of ITM2B were sufficient for intra-membrane interaction with APP in *cis* (Fotinopoulou *et al.*, 2005), which could suggest that the cleavage should occur beyond amino acid 106; however, the authors did not test smaller constructs, therefore, it cannot be excluded that ADAM10 cleavage site occurs nearer the TM domain.

The membrane-bound N-terminal fragment (NTF), which remains after ADAM10 proteolysis, contains the TM domain, which has a high  $\alpha$ -helical content and four conserved glycine residues. NTF is further split into the intracellular domain (ICD) and a soluble C-terminal domain (SCD), following intra-membrane proteolytic processing by SPPL2a/b. The transmembrane (TM) domain has a high  $\alpha$ -helical content, which has an inhibitory effect on potential proteolysis. The four conserved glycine residues within the TM domain could potentially destabilize the  $\alpha$ -helix, and, therefore, enhance proteolysis; however, only glycine 60 affects the secondary structure of the TM domain, and, thus, its cleavage (Fluhrer *et al.*, 2012). Martin *et al.* (2008; 2009) also determined that ten residues of the ICD, adjacent to membrane, as well as 23 amino acids from the SCD, were additionally involved in mediating the SPPL2b cleavage, which was further enhanced by prior ectodomain shedding by ADAM10.

The 37 kDa band, consistently observed in non-synchronised HeLa extracts, may represent the same peptide fragment, which was detected by Akiyama *et al.* (2004); the researchers generated three different antibodies against ITM2B for the purposes of their study, and all three of those detected a band, which migrated approximately at 35 kDa. Based on the observation by Tsachaki *et al.* (2011) that the *N*-glycosylation at asparagine 170 affects the electrophoretic mass of ITM2B by 2 kDa, the 35 kDa fragment observed by Akiyama *et al.* (2004) may represent a non-glycosylated version of the equivalent fragment, observed in this study, which could in this case be glycosylated. The Akiyama *et al.* (2004) publication also shows a WB band, which could represent the glycosylated form of the protein; however, in opposition of such analysis is the fact that the three antibodies, detecting the 35 kDa band, were raised against residues 7-21, 11-26 and 223-243, respectively. This would suggest that the observed 35 kDa should represent the NTF domain and the ectodomain joint together (i.e. ITM2B without the C-terminal CTPP peptide). This is not consistent with findings from this

project, or with outcomes of the Tsachaki *et al.* (2011) study. However, this could be explained by the possibility that ITM2B is subject to different patterns and/or extents of post-translational modifications, depending on cell or tissue type, in which it is expressed. Akiyama *et al.* (2004) also observed bands migrating at or slightly above 50 kDa, as shown in Figure 6-5, or 6-6 A.

Following ITM2B synthesis, the protein forms homo-dimers with the involvement of an inter-molecular disulphide bridge between cysteine 89 of each monomer. The full-length ITM2B protein additionally comprises a further eight cysteine residues; the total odd number of these amino acids (shown in Figure 6-4 D) initially prompted the investigation into dimer formation (Tsachaki *et al.*, 2010). The authors tested cysteine 38 despite its location in the cytoplasmic region of the protein, a reducing environment, which does not predispose towards disulphide bond formation; it was shown not to form an inter-molecular disulphide bond. Cysteine residues 54, 56 and 58 were disregarded due to their location within the TM domain, within a lipid bilayer, which does not favour disulphide bond formation either. Among the cysteines found in the oxidising extracellular environment, cysteine 246 and cysteine 265 form an intra-molecular disulphide bridge once the CTPP is released; cysteine 164 and cysteine 223 of the BRICHOS domain also form an intra-molecular disulphide bond, allowing for formation of a functional BRICHOS loop. This only left cysteine 89 available for interaction; two cysteine 89 residues were shown to form an inter-molecular disulphide linkage between two ITM2B monomers (Tsachaki *et al.*, 2010). The researchers showed that the dimer molecules migrated at approximately 88 kDa, whereas they assigned the 44 kDa species to monomers. They also observed bands migrating at 22 kDa and 66 kDa, which could be fragments of the dimers and/or monomers. The dimers are additionally stabilized by non-covalent interactions (Tsachaki *et al.*, 2010), and glycosylated at asparagine 170 within the BRICHOS domain (Tsachaki *et al.*, 2011) prior to export from the endoplasmic reticulum (ER). As already mentioned, the 66 kDa band could correspond to the band observed in this study, migrating between the 50 kDa and 75 kDa markers (Figures 6-5 and 6-6 C).

#### 6.5.1.1 ITM2B AND TOPORS CO-IMMUNO-PRECIPITATE FROM CELL LYSATES

Co-immuno-precipitation experiments on human cell lines showed that two large species of ITM2B were consistently found in protein complexes with TOPORS, at 37 kDa and ~42 kDa (Figure 6-7). The 37 kDa species could have represented post-translationally-modified NTF domain together with, or separately from, the ectodomain. On the other hand, the ~42 kDa species could represent both the NTF and ectodomain together, or be indicative of full length



ITM2B. Both, full-length ITM2B and the NTF, are inclusive of the ICD domain, which is hypothetically involved in interactions with TOPORS and its fragments in the Y2H direct PPI experiments.

### 6.5.2 PTGDS PROTEIN EXPRESSION

Hoffmann *et al.* (1993; 1994) analysed the nature of the N-linked carbohydrates, and saw no qualitative differences in the glycan composition at both sites. They determined that 10 % of modifications at both asparagine residues are either bi- or triantennary with lactosamine repeats; of these triantennary structures were twice as numerous at asparagine 51 as at asparagine 78. Ninety percent of all the N-linked carbohydrates are biantennary with different combinations of sialic acid modifications (which were more abundant at asparagine 51), which is in agreement with the findings of Harrington *et al.* (1993). Among them 20 % contain two N-acetyl neuraminic acid residues, 40 % have one, and the remaining 40 % include no such component.

Sialic acid was previously shown to affect the SDS-PAGE migration of human Chorionic Gonadotropin (hCG) (Gam e Latiff, 2005) as well as of esterase's (Small e Hemingway, 2000); in the latter case, a removal of sialic acids caused the proteins to migrate more slowly.

Overall, the modifications involved a substantial amount of fucosylation, which was peripherally located and more abundant at asparagine 78; this is in agreement with the finding by Jia *et al.* (2009) that asparagine 78 of PTGDS is a major fucosylation site. It was demonstrated on viral envelope proteins that a modification by fucose can increase the apparent protein size even by 10 kDa (Ng, Wood e Arlinghaus, 1982). The researches additionally noted that fucosylation is a sugar modification, which occurs in the final stages of glycoprotein maturation. This could indicate that perhaps the small PTGDS reactive bands (20 kDa – 37 kDa in Figure 6-9) represent PTGDS species, which were extracted before they could become mature, and therefore had no fucose modifications.

N-acetyl glucosamine was most frequently identified as the bisecting component of the attached sugar, and it was also more abundant at asparagine 78. N-acetyl glucoseamine and galactose were typically found at terminals of the carbohydrate branches (Hoffmann *et al.*, 1994). Since 90 % of sugar modifications on PTGDS were shown to be biantennary, and N-acetyl glucosamine, the sugar conveying this property was additionally found terminally, this suggests that the N-linked modifications can be rather bulky, and, thus, likely to decrease the speed of SDS-PAGE migration of PTGDS, thus increasing the protein's apparent size.

In a high-throughput analysis of human urinary glycoproteins Halim *et al.* (2012) detected an N-linked glycosylation at asparagine 78 of PTGDS. They additionally determined that 100 % of glycan modifications at this site are of the dHexHex<sub>5</sub>HexNAc<sub>4</sub> type, where 'd' stands for 'deoxy-', Hex denotes a hexose, whereas HexNAc is an abbreviation for N-acetyl hexoseamine. It is noteworthy that fucose, which was shown to greatly delay the migration of viral envelope proteins (Ng, Wood e Arlinghaus, 1982), is an example of a deoxy-hexose sugar. This carbohydrate composition approximately corresponds to the exemplary modification, shown in Figure 6-10 A; the difference is that Halim *et al.* identified a deoxy-hexose in place of the sialic acid on the diagram. Again, if the carbohydrate is branched, as is depicted on the image, and therefore potentially bulky, this would negatively affect the SDS-PAGE migration. The HexNAc component in N-linked glycans of the urinary PTGDS typically contains glucosamine; the hexose could be, for example, a mannose, a fucose or a galactose.




a)	b)	c)
		
<p>Example of an N-linked glycosylation</p> <p>Key: N, asparagine; X, any amino acid; S, serine; T, threonine.</p>	<p>Example of an O-linked glycosylation (core carbohydrates)</p> <p>Key: S, serine; T, threonine.</p>	<p>Key: Neu5Ac, neuraminic acid (sialic acid); Gal, galactose; Hex, hexose; Man, mannose; GlcNAc, acetyl glucosamine; HexNAc, acetyl hexosamine; GalNAc, acetyl galactoseamine</p>

Figure 6-14. Visual representation of putative carbohydrate modifications. Figure modified from Halim *et al.* (2013).

Lack of identified sialic acid components within the asparagine 78 glycan, as shown by Halim *et al.*, may suggest that this type of modification is specific to PTGDS found in urine samples, as Hoffmann *et al.* found sialic acid at asparagine 78 on PTGDS from CSF. This demonstrates that PTGDS is likely to be differentially modified, depending on which cell type it originates from. These differences, even if minor, could affect the migration of PTGDS on SDS-PAGE gels.

N-linked glycosylation at asparagine 51 was also detected by Chen *et al.* (2009) in a mass spectrometry analysis of glycoproteins from human liver tissue. On the other hand, Liu *et al.* (2005) determined that in human plasma asparagine 78 of PTGDS is modified by glycosylation. It was not investigated further, therefore, it not known whether the type of the attached glycan corresponds to the one from urine, or perhaps the one from CSF, or whether it is unique in composition.

An additional *N*-glycosylation modification, containing sialic acid, was also detected at asparagine 87 (Rajagopal *et al.*, 2011). However, this modification was identified on a PTGDS, originating from CSF of children patients with medulloblastoma, and has never been observed on PTGDS originating from healthy CSF; hence, it is not mapped in Figure 6-8. Nonetheless, this indicates that additional glycosylation sites could also be present on PTGDS proteins, expressed by the HeLa cell line, which is also cancerous nature, similarly to the medulloblastoma sample.

In CSF samples from patients with neurological disorders, the PTGDS bands were migrating considerably more slowly between 34 kDa and 64 kDa (2DE) (Harrington *et al.*, 2006). These PTGDS bands are closer in size to those observed using HeLa cell extract (Figure 6-9), which could again be due to the cancerous disease state of this cell line. The control group in the study by Harrington *et al.* (2006) appeared to contain much lighter PTGDS species in their CSF samples, 25 kDa on average ( $4.5 > pI > 8.0$ ); however, in three controls (out of 21) the bands were observed between 28 kDa and 34 kDa, and had a narrower charge range:  $5.8 > pI > 7.5$ . Still, these size are considerably smaller than the major bands, observed in Figure 6-9, which migrated around the 50 kDa marker.

Perhaps this significantly increased apparent size of PTGDS in the disease samples was due to modification by ubiquitin (a ubiquitin monomer would increase the apparent mass by about 8 kDa), or another covalently attached small protein, e. g. NEDD8 (Neural precursor cell Expressed Developmentally Down-regulated protein 8, a monomer of approximately 9 kDa). There is no consensus site for SUMOylation within the PTGDS peptide. It cannot be excluded that such a covalent modification by a ubiquitin, or a ubiquitin-like protein, could also have occurred in the HeLa protein extract, used in this project.

Harrington *et al.* (2006) additionally performed a mass spectrometric analysis to identify potential molecules, affecting the size and charge variations of PTGDS, and identified two peptides. The first peptide comprised residues 23-38 of PTGDS; therefore, it could have arisen

due to the O-glycosylation of serine 29 (Figure 6-8). The second peptide (residues 169-185) is not known to be post-translationally modified; it was also detected by Hoffmann *et al.* (1994), but it was not glycosylated, and hence excluded from downstream analysis. This second peptide is located right upstream of cysteine 186, involved in disulphide bond formation, and includes an  $\alpha$ -helix region; it could be speculated that another, as yet unknown, modification occurs at a residue within this region, whose attachment or removal would influence protein folding, and/or disulphide bond formation. This region includes a lysine, which could serve as an attachment site for e. g. ubiquitin.

The O-glycosylation of serine 29 of PTGDS in human CSF was recently determined to be of the HexHexNAc type (Halim *et al.*, 2013). It should be noted that this study determined just the core of this O-linked glycan, and numerous additional carbohydrates could subsequently be attached to it in physiological conditions (Roth, Yehezkel e Khalaila, 2012). Figure 6-14 B provides a visual representation of a core structure of an O-linked carbohydrate.

Among additional modifications, PTGDS was shown to be phosphorylated by protein kinase C at serine 106 (Ragolia *et al.*, 2003; Ragolia, Hall e Palaia, 2007). Its phosphorylation by casein kinase II was also demonstrated (Angenstein, Buchner e Staak, 1999). However, it is not expected that phosphorylation of PTGDS could affect the apparent size of PTGDS to the extent observed on SDS-PAGE. A summary of the reported post-translational modifications of PTGDS is given in Table 6-2.

The Western blot experiments consistently resulted in bands significantly higher (~50 kDa) than the expected size (21 kDa - 29 kDa) of PTGDS, suggested by literature reports (representative result in Figure 6-9). This could have resulted from differential glycosylation, as observed in various disease states (Lescuyer *et al.*, 2005; Harrington *et al.*, 2006), which could also reflect the cancerous nature of the HeLa cell line, from which the protein complexes were extracted. Further support for differential glycosylation comes from Hoffmann *et al.* (1994) who emphasised that the *N*-glycosylation pattern of proteins expressed in the brain/CNS is different than of those in other body parts, and PTGDS found in CSF was modified by the 'brain-type' *N*-glycosylation. Hence, the glycosylation pattern of PTGDS in cell lines should be expected to differ from that in CSF.

However, an apparent increase of over 20 kDa is probably too high to be justified by differential glycosylation on its own. It is plausible that this increase in size is caused by as yet unidentified covalently attached protein modification(s).

Table 6-2. Summary of reported post-translational modifications of PTGDS. Protein was obtained from a healthy source (tissue or body fluid) unless specifically stated otherwise.

Position	Modification	PTGDS source	Potential size shift	Reference(s)
Asp 51	N-linked carbohydrate; mostly biantennary with sialic acid components	Human CSF	3 kDa - 4 kDa per modified residue	(Harrington <i>et al.</i> , 1993; Hoffmann <i>et al.</i> , 1993; Hoffmann <i>et al.</i> , 1994)
Asp 78				
Asp 78	dHexHex <sub>5</sub> HexNAc <sub>4</sub> No sialic acid.	Human urine	Predicted 3 kDa - 4 kDa or larger <sup>18</sup>	(Halim <i>et al.</i> , 2012) <sup>19</sup>
Asp 51	N-linked carbohydrate	Human liver	Predicted 3 kDa - 4 kDa or larger <sup>18</sup>	(Chen <i>et al.</i> , 2009) <sup>19</sup>
Asp 78	N-linked carbohydrate	Human plasma	Predicted 3 kDa - 4 kDa or larger <sup>18</sup>	(Liu <i>et al.</i> , 2005) <sup>19</sup>
Asp 87	N-linked carbohydrate; with sialic acid components	Human children medulloblastoma CSF	Unknown	(Rajagopal <i>et al.</i> , 2011)
Unknown	Unknown	CSF of human adults with neurological disorders	10 kDa – 40 kDa	(Harrington <i>et al.</i> , 2006)
Ser 29	O-linked carbohydrate modification with a HexHexNAc core	Human CSF	Unknown	(Harrington <i>et al.</i> , 2006; Halim <i>et al.</i> , 2013)
Ser 106	Phosphorylation by PKC	Rat cultured vascular smooth muscle cells	None or minor	(Ragolia, Hall e Palaia, 2007)
Unknown	Phosphorylation by CKII and PKC	Rat hippocampal slices	None or minor	(Angenstein, Buchner e Staak, 1999)

Ubiquitination and neddylation are two candidates with the first one supported by the role of TOPORS as an E3 Ubiquitin ligase. In the central nervous system, neddylation should not be excluded either, especially considering that roles of PTGDS in development have been frequently reported, and only a few substrates of NEDD8 modification have been identified to

<sup>18</sup> This would depend on fucose content – see main text.

<sup>19</sup> Chen *et al.* did not detect a modification at asparagine 78 on PTGDS from human liver cells, whereas Liu *et al.* and Halim *et al.* did not detect a modification at asparagine 51 on PTGDS from human plasma and urine, respectively.

date (UniProtKB: **Q15843**). SUMOylation can probably be excluded as no consensus sites for this modification are found within the PTGDS sequence.

#### 6.5.2.1 PTGDS AND TOPORS CO-IMMUNO-PRECIPITATE FROM CELL LYSATES

It should be highlighted that Western blot analysis of protein complexes from human cell lines consistently showed two bands immuno-reactive for PTGDS, one migrating just above, and one just below the 50 kDa marker (Figure 6-9), which could correspond to PTGDS with and without the signal peptide. The two bands could represent the two largest *PTGDS* isoforms: 001 (peptide corresponding to this isoform was identified in the Y2H screen with TOPORS) as the lower band, and the larger band of the two observed, could represent *PTGDS* isoform 201, which codes for a peptide about twenty residues longer<sup>20</sup>. Only the smaller band was found in complexes immuno-precipitated with an antibody against TOPORS. This could suggest that TOPORS associates with PTGDS following its signal peptide cleavage. Alternatively, the size difference between the two PTGDS bands could also indicate a post-translational modification, such as a bulky fucose glycosylation (PTGDS glycosylation sites were shown in Figure 6-8).

The protein, which interacted in the Y2H screen with TOPORS, was encoded by *PTGDS* isoform 001. DNA sequence alignment (SeqMan, DNA Star) of the protein-coding isoforms of *PTGDS* demonstrates that the sc-30067 antibody immunogen aligns specifically with isoform 001 (Appendix 11.10). It also showed partial alignment with isoforms 003, 004 and 005; however, it is difficult to predict whether the antibody, raised against full-length isoform 001, would bind to them. Unlike for PTGDS 001, no crystal structures of isoforms 003, 004 and 005 are known; it is not known whether they fold in similar manner as 001, as well as whether the properties of their outward-facing amino acids are similar to those in 001. It is not known whether peptides encoded by these additional isoforms also form the characteristic kink, so important in PTGDS 001 for formation of the bucket-shaped docking site for PG H2 and retinoids (summarised in section 4.3.3.2), and, presumably, also important in recognition by the antibody.

According to the Ensembl records the biochemical properties of peptides encoded by the protein-coding *PTGDS* transcripts are rather diverse. The isoelectric point (pI) and charge of

---

<sup>20</sup> *PTGDS* isoform 201 was included in the *PTGDS* gene record, accessible on the Ensembl database until July 2014 inclusive, and has been removed since. Snapshots of those past database records are included in Appendix 11.7.

PTGDS 001 are 7.69 and 2.5, respectively. Similar properties are recorded for PTGDS 003 with a pI of 7.89 and a charge of 3.0. On the other hand, isoform 004 has a similar pI of 9.77; however, its charge is much higher, i.e. 7.0. Moreover, these numbers are even higher for PTGDS 005 (pI: 10.36; charge: 12.5). On the contrary, isoform 008 (which, however, shows almost no sequence alignment with the antibody immunogen, as shown in Appendix 11.10) has a pI as low as 5.69, and carries a slightly negative charge of -0.5. The great diversity of these biochemical properties prompts a speculation that the antibody is probably specific for detection of PTGDS 001 (at least for immuno-staining of tissue sections and cultured cells, as it is not certain that it would detect a denatured protein on a WB membrane). It could also potentially detect isoform 003, however, the sequence dissimilarities between the C-terminal half of this isoform and the immunogen provide evidence against this.

### **6.5.3 PSMC1 PROTEIN EXPRESSION**

The polyclonal antibody against PSMC1 consistently detected only one band, without background, migrating approximately 5 kDa - 10 kDa above its predicted size. The protein is known to form a glycyl lysine isopeptide link with ubiquitin. A single molecule of the latter could increase the apparent PSMC1 by 8.5 kDa. Alternatively, such an increase in size could indicate a covalent attachment of another ubiquitin-like protein, for instance SUMO1, as was suggested in Chapter 5. Other known modifications of PSMC1 include lipidation by *N*-linked myristoyl on glycine 2, two phosphorylation modifications at serine 4 and 439 and acetylation at lysine 258. It is not expected that these modifications, if present, would have a pronounced effect on the apparent electrophoretic size of PSMC1. This protein is also modified by an *O*-linked carbohydrate; however, the attachment site for this modification has not been identified yet. Depending on the extent of carbohydrate branching, a glycosylation could have an effect on the apparent protein size.

#### **6.5.3.1 PSMC1 AND TOPORS CO-IMMUNO-PRECIPITATE FROM CELL LYSATES**

The hypothesis that PSMC1 is probably SUMOylated by TOPORS, as it was shown to interact most strongly with TOPORS regions, associated with SUMOylation activity, could explain the results of Western blot and coIP experiments on protein extracts from human cell lysates, which consistently showed one band immuno-reactive for PSMC1 (Figure 6-13), migrating approximately 10 kDa above its calculated/predicted size. This observation could be indicative of modification by mono-ubiquitin, or another ubiquitin-like molecule, such as SUMO1, as suggested in yeast by the strong direct PPI with mid-TOPORS and C-term TOPORS fragments.

#### 6.5.4 CONCLUSIONS

The findings described in Chapter 6 demonstrated that TOPORS, ITM2B, PTGDS and PSMC1 are endogenously expressed in human cells, specifically the HeLa cell line. Furthermore, it was shown that these novel interacting partners of TOPORS, identified via the Y2H screen, are found in protein complexes immuno-precipitated from cell lysates using the mouse monoclonal antibody against human TOPORS protein (Abnova; Table 2-75 in Methods and Materials).

The evidence for interactions is stronger for ITM2B and PSMC1 than for PTGDS in view of the uncertainty regarding the specificity of the anti-PTGDS antibody (SCB; Table 2-75) for the denatured protein, which would be expected on a Western blot. In the future alternative antibodies against PTGDS should be tested for WB and coIP experiments. Using exogenously expressed tagged proteins could also help identify the reason for the observed size.

Results of coIP experiments with TOPORS and PSMC1 appear to be the most reliable in view of the unquestionable antibody specificity (Sigma-Aldrich; Table 2-75), generating a clean band, within up to 10 kDa of the expected size, and with no background, even when blotted for on total cell lysate.

The interpretation of the coIP results between TOPORS and ITM2B is more ambiguous due to the widespread proteolytic cleavage of the protein. The experiments demonstrated that two bands, corresponding to two of the ITM2B bands observed on the WB for total cell lysates, were also observed within the protein complexes precipitated using the TOPORS antibody raised in mouse. The Abgent ITM2B C-term antibody (Table 2-75) was used to blot for ITM2B, which could be pulling out putative peptides 6, 8, or 9, or perhaps even a full-length protein. Studies on tagged constructs of individual ITM2B fragments would help explain the observed findings and verify the ITM2B peptide identity of the observed bands.

Overall, the results, depicted in Chapter 6, demonstrated that TOPORS and its novel Y2H interacting protein partners: ITM2B (or its fragments) and PSMC1 do interact in human cells as endogenously expressed proteins. The evidence also suggest that an interaction between TOPORS and PTGDS probably occurs as well; however, this requires further verifications, as was specified above.

The subsequent Chapter 7 contains a collection of cellular localisation studies on TOPORS and its interactors from the Y2H system: ITM2B, PTGDS and PSMC1. The goal of Chapter 7 was to identify the cellular compartments and/or organelles that the Y2H-identified interactors



localise to in human cells. The focus of the sub-cellular localisation work was on the centrosome both: in dividing and ciliated cells. This non-membranous organelle was prioritised due to TOPORS' association with it throughout the cell cycle in cultured cells and, at the ciliary basal body in photoreceptor cells (section 1.5).

## **7 CELLULAR LOCALISATION STUDIES**

The previous experimental Chapters 3, 4 and 5 described construction of the human retinal cDNA library, the Y2H screen for interacting protein partners of TOPORS, and validation experiments demonstrating the relevant direct interactions in yeast, as well as confirming the retinal mRNA expression of full-length clones of the Y2H interactors of TOPORS, respectively. This work led to identification of ITM2B, PTGDS and PSMC1 as new protein partners of TOPORS, as demonstrated by the Y2H assay.

The purpose of Chapter 6 was to determine the endogenous expression of the novel interactors in human cells and to demonstrate their interaction with TOPORS in these cells. This was successfully completed for PSMC1 and ITM2B. The outcomes of WB and coIP studies with PTGDS were also positive, however, future experiments should aim to validate the results, as antibody specificity for denatured PTGDS could not be ascertained.

The current chapter aimed to evaluate the sub-cellular localisation of the three newly-identified proteins. Specifically, in view of TOPORS' association with the centrosome and the ciliary basal body (section 1.5), the primary objective of the localisation studies was to show whether the novel interacting partners co-localise with TOPORS at these centriole-based organelles.

As was described in section 1.8, in dividing cells the centrosome forms the microtubule-organising centre (MTOC). It is closely associated with the nucleus as well as with the Golgi apparatus. In the former case it is a key component of the mitotic spindle during nuclear division. During interphase, the microtubules organised by the centrosome serve to preserve the ordered structure of the Golgi apparatus (it becomes dissociated into irregular membrane-enclosed compartments during mitosis and cytokinesis). The microtubules also aid in vesicular trafficking, important here in context of primary cilia formation and function. The centrosome is also closely associated with the 26 S proteasome (section 1.7.1.1), at least in ciliated cells (Gerdes *et al.*, 2007; Liu *et al.*, 2014).

Hence, the goal of this chapter was to determine whether ITM2B, PTGDS and PSMC1 co-localise with TOPORS at the MTOC, either in dividing, or in ciliated cells.

For the purposes of experiments described in this chapter cells were maintained either as mitotic culture, or they were stimulated to exit the cell cycle and become ciliated. The dividing cells were grown either as a non-synchronised culture, approximately 60 % confluent. In order

to produce primary cilia, a culture of dividing cells was subject to serum starvation (0.25 % FCS) for 48 hours.

Several cell lines were used for the optimisation experiments, namely HEK293, hTERT-RPE1 and SK-N-SH cells (Table 2-56 in Methods and Materials).

Prior to immunofluorescent (IF) labelling of TOPORS and its interacting partners the cells were fixed to preserve the proteins of interest.

Preservation of proteins within cells (as well as tissues) is most frequently performed using a solution of 4 % paraformaldehyde (PFA) in PBS, followed by permeabilisation with a detergent, such as Tx100, which removes lipids from membranes. PFA forms methylene (-CH<sub>2</sub>-) cross-links between proteins, thus it is usually the fixative of choice for preserving cellular structures.

However, the cross-linking may prevent access to some antigens; therefore, an alternative fixation method, using ice-cold methanol, was also tested during optimisation procedures. Methanol competes with water for protein hydrogen bonds, and dehydration subsequently triggers protein precipitation on cellular structures. Consequently, cellular localisation of an antigen is less well preserved than in PFA fixation; changes in protein conformation may also affect binding of antibodies to their targets. However, this fixation method could be suitable for detecting cell surface proteins (such as ITM2B) as well as antigens associated with the cytoskeleton, such as actin and tubulin filaments.

Ultimately, the co-localisation studies with TOPORS were performed in the hTERT-RPE1 cells due to their documented readiness to develop primary cilia (Pitaval *et al.*, 2010; Spalluto, Wilson e Hearn, 2013). The 4 % PFA fixation, followed by permeabilisation with 0.3 % Triton X-100, was chosen as the fixation method for the co-localisation studies. Firstly, it is more likely to preserve the proteins' locations at their native sub-cellular structures; secondly, as is shown in the subsequent sections, no major differences were demonstrated in localisation of the tested proteins in the hTERT-RPE1 cells, irrespective of fixation method.

## **7.1 CELLULAR LOCALISATION OF TOPORS**

The TOPORS monoclonal antibody (M01, clone 5G11; Abnova, Taiwan; M  $\alpha$ -TOPORS; section 2.8 in Methods and Materials), raised in mouse was used for immunofluorescence experiments. The antibody was used in previously published studies (Chakarova *et al.*, 2011),

where the centriolar localisation of TOPORS was demonstrated in addition to the previously known nuclear localisation.

TOPORS signal was observed throughout the cytoplasm and in the nucleus in 4 % PFA-fixed hTERT-RPE1 and SK-N-SH cells, permeabilised with 0.3 % Tx100. It is noteworthy that in the hTERT-RPE1 cells, the cytoplasmic staining was almost filamentous, to some extent actin-like (Figure 7-1), which may indicate that a close association exists between TOPORS and the actin cytoskeleton. No distinct staining was observed along the edges of the hTERT-RPE1 cells, unlike what was demonstrated for the mouse Topors protein (Braun *et al.*, 2012); and TOPORS displayed its characteristic punctate pattern of localisation in the nucleus, which is in agreement with its previously demonstrated localisation at the PML bodies (Rasheed *et al.*, 2002).

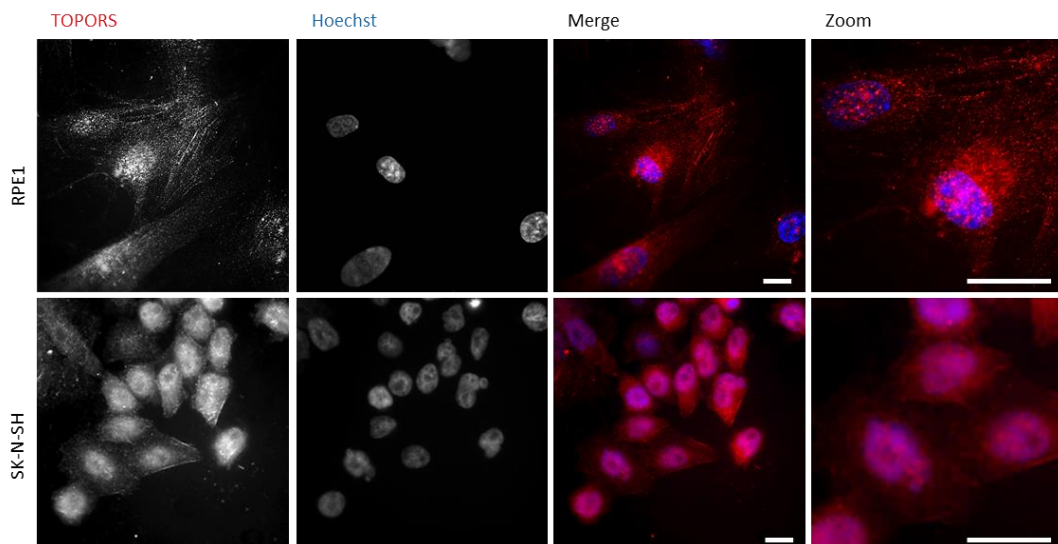


Figure 7-1. Cytoplasmic TOPORS signal appears partly filamentous and partly granular in both retinal epithelial and neuroblastoma cell types.

Dispersed TOPORS signal, partly filamentous-like, is observed in the cytoplasm of the hTERT-RPE1 (RPE1) cells; speckled nuclear localisation is observed simultaneously in addition to sporadic granular signal, which could be indicative of centrioles. The nuclear TOPORS staining in the SK-N-SH cells appears more uniform; the net-like appearance of the cytoplasmic staining, apparent in the magnified image, could be indicative of the endoplasmic reticulum; one cell also appears to be strongly stained on the edges, which could represent an association with the cell membrane as was previously shown in mice (Braun *et al.*, 2012). TOPORS signal (Ab diluted 1/100) observed in non-synchronised dividing cells, grown in complete media, fixed with 4 % PFA and permeabilised with 0.3 % Tx100. Scale bar: 20  $\mu$ m. Fluorescent microscope images.

In the SK-N-SH cells the staining looked less filamentous inside the cells; however, in some cells it was more apparent along their edges. The signal, throughout the cell, appeared more as discreet small points joint by thin threads; this net-like appearance strongly resembled

endoplasmic reticulum (ER) staining. The nuclear speckled localisation was not observed in these cells.

Immunofluorescence (IF) staining of ice cold methanol-fixed cells demonstrated nuclear signal in HEK293 cells, mostly cytoplasmic expression in SK-N-SH cells, and both nuclear and cytoplasmic staining in hTERT-RPE1 (RPE-1) cells (Figure 7-2). Hence, for the latter two cell types, the staining pattern looked very similar here to that in PFA/TritoxX100-fixed cells. The only exception was the appearance of peri-nuclear centriole-like signal in the SK-N-SH cells.

The localisation differences were probably affected by the specific nature of the studied cells and possibly stages of the cell cycle, at which the observed cells were fixed.

HEK293 is an embryonic cell line; hence, it would be constantly dividing until it reaches a signal to specialise, resulting in TOPORS signal being observed mostly in the nucleus. Nonetheless, in the HEK293 cells the nuclear TOPORS signal appeared more diffuse, or less PML-like. The cytoplasmic staining appeared scarce probably due to two major reasons. As was mentioned above, the methanol-fixation method causes soluble proteins to precipitate onto sub-cellular structures. Since the HEK293 cells are dividing rapidly, their organelle contents would be minimal, and the nucleus would be taking up most of the intracellular space. These two aspects may help explain why the cytoplasmic TOPORS staining appeared most intense around the nuclei. Nonetheless, the protein was additionally observed at protrusions, which neighbouring cells extended to each other.

TOPORS signal at cell extensions and at cell edges was also seen in the methanol-fixed hTERT-RPE1 cells, in addition to diffuse cytoplasmic staining, which, however, appeared more punctate throughout the cytoplasm than in the PFA-fixed cells. This could possibly reflect the precipitation of TOPORS protein onto cytoskeletal structures, or membranes of the ER. The nuclear staining in this cell type appeared speckled as was expected.

In ice-cold methanol-fixed samples of SK-N-SH cells some TOPORS signal was observed in cell nuclei; however, it was most intense in the cytoplasm. Distinct peri-nuclear puncta were visible in several cells; these could perhaps represent centrioles.

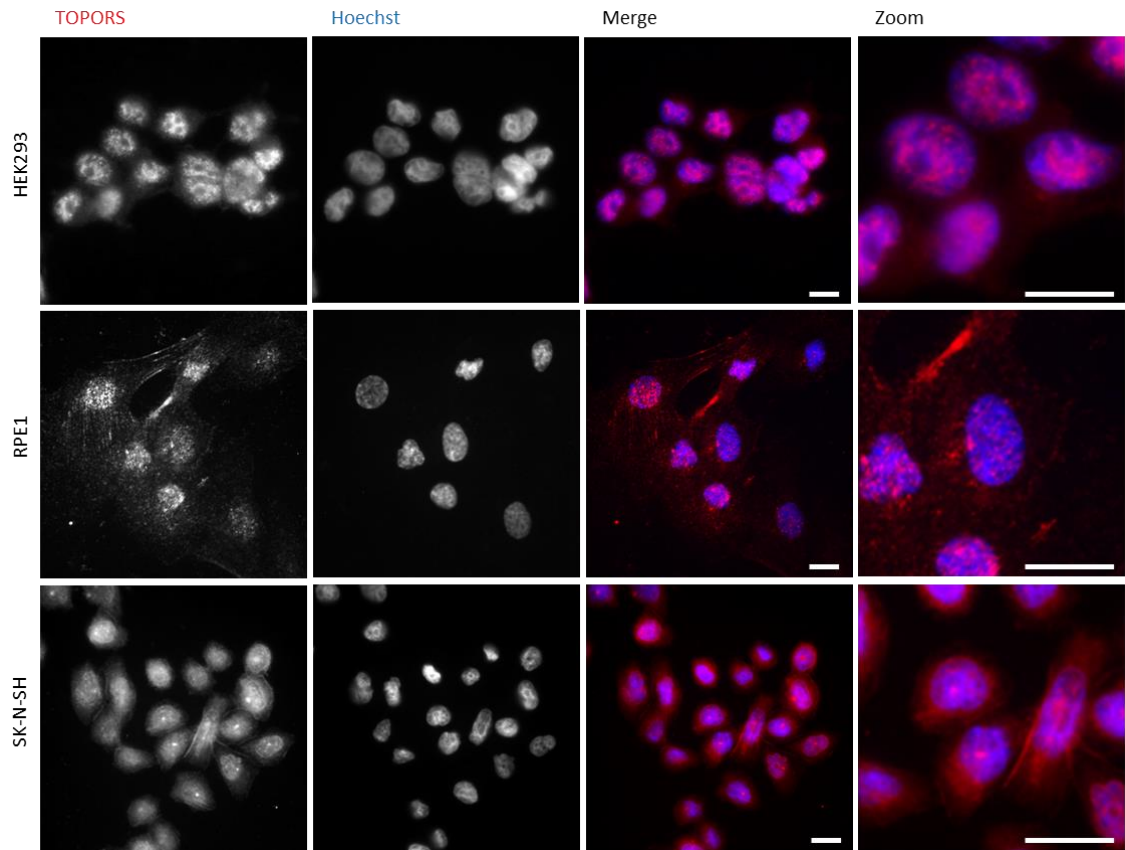


Figure 7-2. TOPORS signal in both retinal epithelial and neuroblastoma cell types appears mostly cytoplasmic: partly filamentous and partly granular; whereas the localisation is mostly nuclear in embryonic cells.

HEK293 cells display mostly nuclear and peri-nuclear staining as opposed to the hTERT-RPE1 (RPE1) cells, in which it is cytoplasmic. Strong diffuse cytoplasmic staining is also observed in the SK-N-SH cells, in addition to sporadic dot-like staining, which could correspond to centrioles. TOPORS signal (Abnova Ab diluted 1/100) observed in non-synchronised dividing cells, grown in complete media, fixed with ice-cold methanol. Scale bar: 20  $\mu$ m. Fluorescent microscope images.

## 7.2 CELLULAR LOCALISATION OF ITM2B

Previous studies in PFA/Tx100-fixed HEK293 cells demonstrated that over-expressed ITM2B localised at the Golgi body together with the SPPL2b protease, which cleaves it at the transmembrane domain (Martin *et al.*, 2008).

Another study showed the protein was found at the ER and plasma membrane (Matsuda *et al.*, 2011). Fluhrer *et al.* (2012) and Audo *et al.* (2013) also independently observed ITM2B at the cell membrane as well as inside the cytoplasm in HEK293 and HeLa cells as well as COS-7 cells, respectively. The overall diffuse cytoplasmic staining, documented by Fluhrer *et al.* also included a peri-nuclear signal of higher intensity.

In mouse T cell line TS1 $\alpha\beta$ , fixed with PFA/Tx100, a shorter ITM2B isoform was observed co-localising with mitochondrial markers (Fleischer, Ayllon e Rebollo, 2002).

Secretion of ITM2B peptides has also been demonstrated (Kim *et al.*, 1999), in addition to localisation in neuronal processes (Akiyama *et al.*, 2004), pre-synaptic terminals (Saul *et al.*, 2013) and synaptic membranes (Matsuda, Tamayev e D'adamio, 2011; Tamayev *et al.*, 2011).

Two antibodies against ITM2B were used throughout the project. An antibody against the carboxy-terminal region of ITM2B (Abgent # AP13163b: ITM2B C-term) was used throughout the cell-based studies. A second additional antibody, used by Audo *et al.* (2013), was used sporadically for additional analysis (Sigma-Aldrich # HPA029292: ITM2B).

Nonetheless, the Abgent # AP13163b: ITM2B C-term antibody was used in most experiments due to its inability to bind the membrane-bound NTF fragment. Since in the Y2H assay TOPORS would have been able to interact only with soluble proteins, here the focus remained on non-membrane-bound ITM2B fragments.

In the hTERT-RPE1 cells the ITM2B C-term antibody generated a cytoplasmic diffuse signal with some punctate regions on higher intensity. This was observed irrespectively of which fixation method was used (top panels in Figures 7-3 and 7-4), and suggests that ITM2B is present within intracellular membranous organelles, such as the ER or Golgi, as well as vesicles. This would be in agreement with previously published findings on ITM2B sub-cellular localisation.

Table 7-1. Comparison of ITM2B antibodies.

ITM2B Fragment	Antibody which probably detects it
Full-length ITM2B	AP13163b (C-term) & HPA029292
NTF + ECTODOMAIN	AP13163b (C-term) & HPA029292
SCD + ECTODOMAIN	AP13163b (C-term) & HPA029292
ECTODOMAIN	AP13163b (C-term) & HPA029292
NTF	HPA029292
SCD	HPA029292

**Key:**

ITM2B protein diagram, highlighting known proteolytic cleavage points (top panel), and the resulting ITM2B peptide fragments (lower panel). The epitope against which the **AP13163b** antibody was raised is denoted by the green bar; the **HPA029292** epitope is denoted by the blue bar. Diagram not to scale.

On the other hand, the SK-N-SH cells did not display such a prominent cytoplasmic localisation. In fact the signal was mostly just peri-nuclear, either dotted, as would be expected for centrioles, or sac-like, which could have represented the Golgi apparatus (lower panels in Figures 7-3 and 7-4). It is not immediately obvious what could be the reasons for the observed dissimilarities. Perhaps they do not reflect differences in the actual localisation, but only appear to convey such a message due to their much smaller size, and putatively more compact morphology.



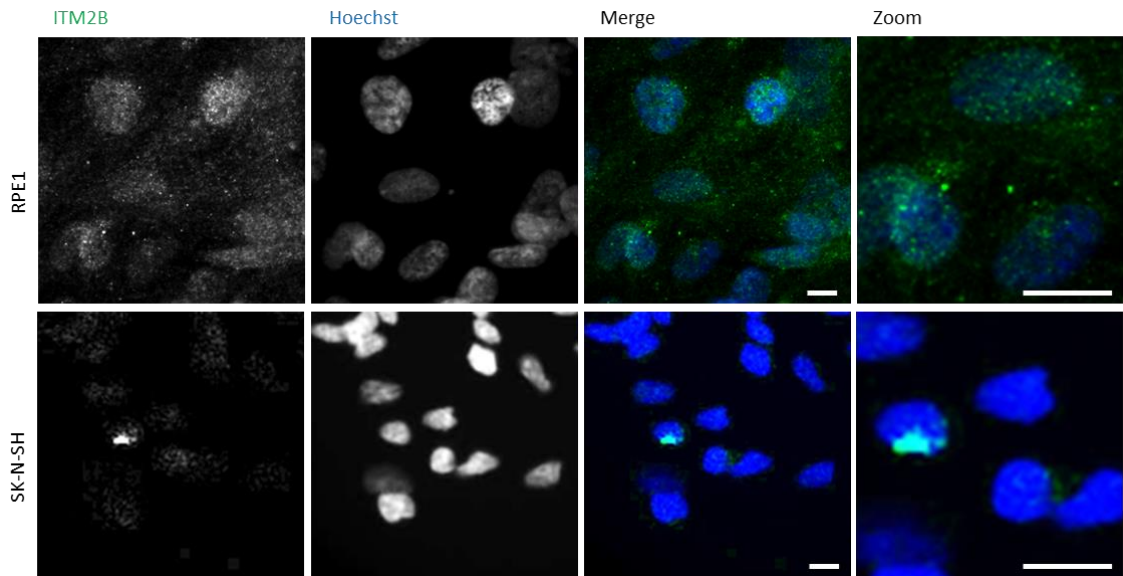


Figure 7-3. ITM2B C-term localises throughout the cytoplasm in retinal epithelial and neuroblastoma cell types.

Dispersed granular cytoplasmic staining is observed in the hTERT-RPE1 (RPE1) and some is also visible in the SK-N-SH cells. Signal in the SK-N-SH cells appears more polarised and resembles the Golgi membranes. Centriole-like dotted regions of higher intensity are observed in the RPE1 cells (magnified in 'zoom'). ITM2B C-term signal (Ab diluted 1/50) observed in non-synchronised dividing cells, grown in complete media, fixed with 4 % PFA and permeabilised with 0.3 % Tx100. Scale bar: 20  $\mu$ m. Fluorescent microscope images.

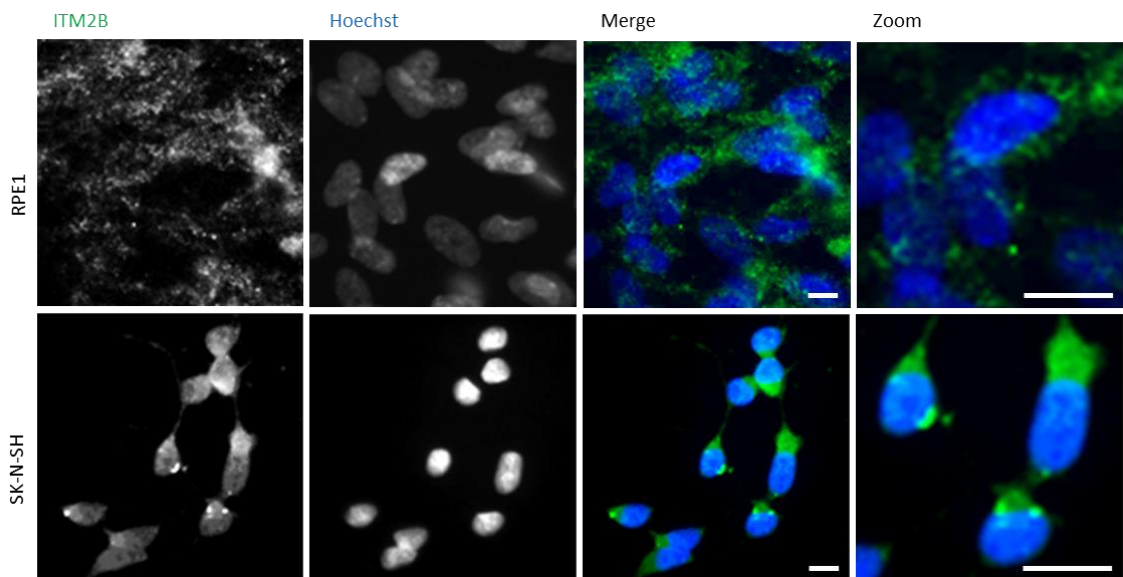


Figure 7-4. ITM2B C-term localises throughout the cytoplasm in retinal epithelial and neuroblastoma cell types; however, the signal appears more polarised in the latter.

Dispersed granular cytoplasmic staining is observed in the hTERT-RPE1 (RPE1) cells. Signal in the SK-N-SH cells appears more polarised and strongly resembles the Golgi apparatus. Centriole-like dotted regions of higher intensity are observed in both cell lines (examples magnified in 'zoom'). ITM2B C-term (Ab diluted 1/100) observed in non-synchronised dividing cells, grown in complete media, fixed with ice-cold methanol. Scale bar: 20  $\mu$ m. Fluorescent microscope images.

Alternatively, if the observed staining really does indicate the highest cellular concentration of ITM2B in the Golgi apparatus, this could reflect potential differential modifications (section 6.2), and hence roles of ITM2B in neuronal versus other cell types. The very polarised localisation could reflect the direction of ITM2B transfer towards a potential synaptic terminal, a localisation demonstrated for this protein previously.

IF staining of PFA-fixed hTERT-RPE1 cells, permeabilised with Tx100, showed that the Sigma-Aldrich ITM2B antibody also detects punctate signal in the cells (Figure 7-5), distributed throughout the cytoplasm with some regions stained more intensely than others. As was shown in Figure 6-5, the Sigma-Aldrich ITM2B antibody can additionally detect the NTF and SCD fragments, which would not be stained for by the Abgent ITM2B C-term antibody, which could explain the more diversified staining pattern in Figure 7-5. Possibly, these are the fragment(s) that remain bound within membranes of transport vesicles, spreading towards more distant sub-cellular localisations.

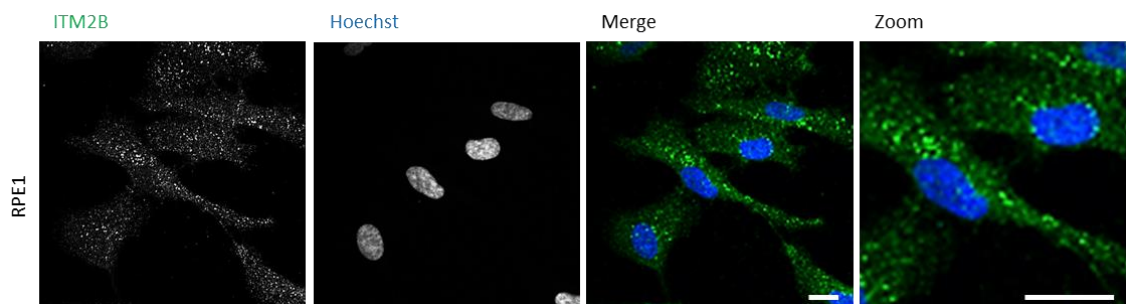


Figure 7-5. ITM2B localises throughout the cytoplasm in a granular pattern in retinal epithelial cells. Dispersed granular cytoplasmic staining is observed. Regions of higher intensity are apparent; some of them might be centrioles; other could represent small transport vesicles. ITM2B (Sigma-Aldrich; Ab diluted 1/200) observed in non-synchronised dividing hTERT-RPE1 (RPE1) cells, grown in complete media, fixed with 4 % PFA and permeabilised with 0.3 % Tx100. Scale bar: 20  $\mu$ m. Fluorescent microscope images.

In cellular co-localisation studies, endogenous ITM2B was observed together with endogenous TOPORS at infrequent punctate locations in hTERT-RPE1 cells (Figure 7-6), with an additional background diffuse cytoplasmic staining, as previously observed. This was demonstrated using the ITM2B C-term antibody (Abgent), and the TOPORS antibody, raised in mouse (Abnova). The punctate signal looks very much centriole-like.

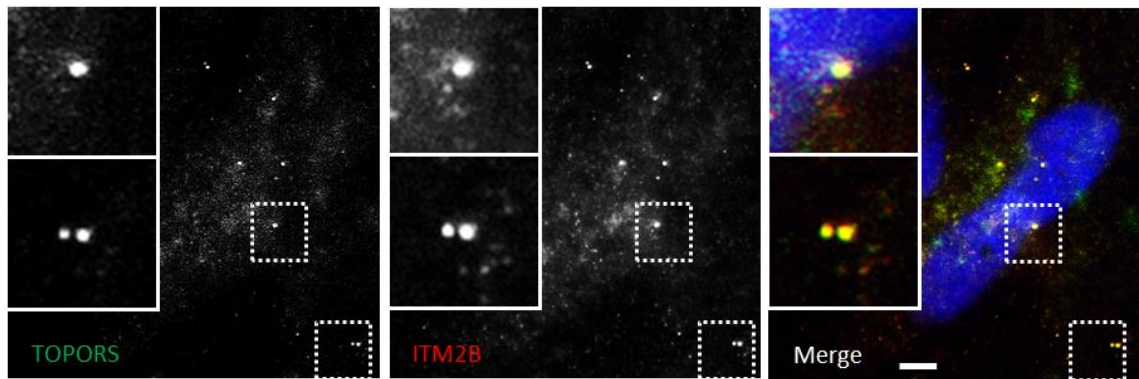


Figure 7-6. ITM2B C-term and TOPORS co-localise in retinal epithelial cells in a centriole-like pattern. Punctate co-localisation of TOPORS and ITM2B C-term is observed at both puncta, presumed to be centrioles. Insets show a magnification of signals enclosed in the dashed squares. Background staining is apparent for both proteins. Unsynchronised dividing hTERT-RPE1 cells, cultured in complete media, fixed with 4 % PFA and permeabilised with 0.3 % Tx100. Scale bar: 10  $\mu$ m. Fluorescent microscope images.

Further imaging showed another distinct localisation: in some cells ITM2B was observed not just co-localising with TOPORS, but also found to form a cloud-like structure around the TOPORS signal (Figure 7-7), in addition to the cytoplasmic staining, surrounding the nucleus. It is known that centrosomes are often found in close proximity to the Golgi apparatus, as the microtubules play a key role in maintaining the stacked structure of this organelle, as well as they are involved in transport of vesicles between the individual Golgi compartments and other membranous organelles.

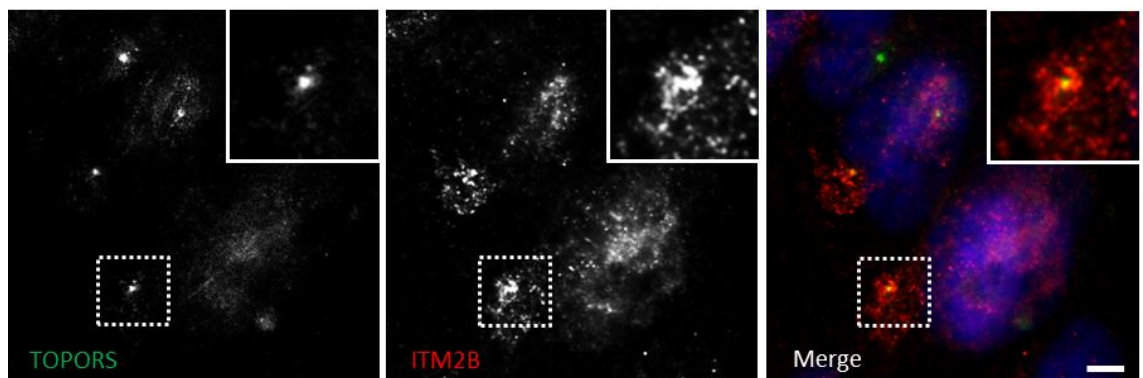


Figure 7-7. ITM2B C-term co-localises with TOPORS and forms an additional cloud-like signal around the region of co-localisation.

ITM2B C-term signal co-localises with as well as surrounds the TOPORS signal in hTERT-RPE1 cells. The observed TOPORS localisation is reminiscent of centrioles. The strongest ITM2B C-term signal is co-localising with TOPORS, but the proximal signal is also substantial. Given that TOPORS marks centrioles in this image, the 'cloud' of ITM2B signal could potentially represent the Golgi apparatus, which is closely associated with the MTOC in most cell types, and which relies on microtubules entirely for preserving its structure. ITM2B is synthesised as a membrane-bound glycoprotein, therefore, its presence in the Golgi complex should be expected. Insets show a magnification of signals enclosed in the dashed squares. Unsynchronised dividing hTERT-RPE1 cells, cultured in complete media, fixed with 4 % PFA and permeabilised with 0.3 % Tx100. Scale bar: 10  $\mu$ m. Fluorescent microscope images.

Furthermore, centrosomes are dynamic structures, constantly dividing throughout the cell cycle (section 1.8). This process requires that an active shuttle of relevant proteins towards and away from the MTOC must be maintained. Figure 7-7 seems to depict a situation in which ITM2B is being transported either towards or away from the centrosome.

The co-localisation of ITM2B with TOPORS in distinct punctate locations was considered strongly reminiscent of centriolar staining. TOPORS itself has been shown to localise to the both centrioles of the centrosome in dividing cells, and at the base of the cilium (the basal body of ciliated cells) (Chakarova *et al.*, 2011), hence centriolar markers were used to better define the observed localisation for ITM2B.

Peri-centriolar material 1 (PCM1) protein, which is a component of centriolar satellites, i.e. electron dense granules scattered around centrosomes (Kubo *et al.*, 1999), was observed co-localising with ITM2B (Figure 7-8).

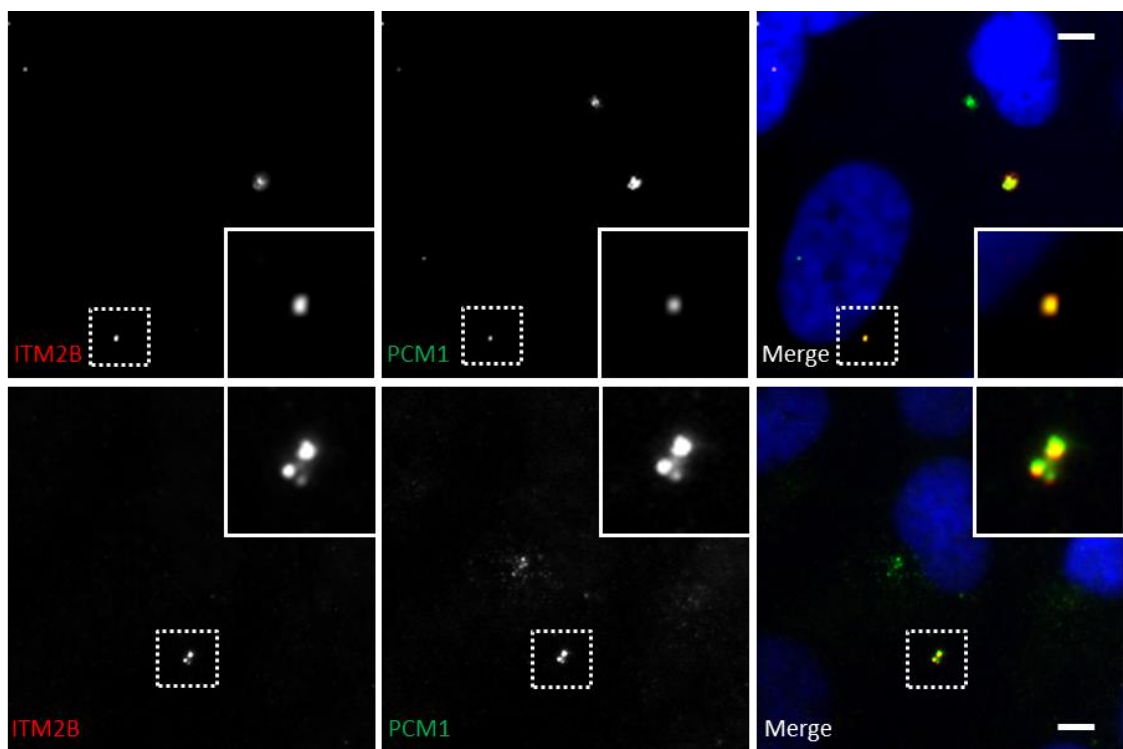


Figure 7-8. ITM2B C-term co-localises with the peri-centriolar marker: PCM1. Both panels show ITM2B C-term co-localising with PCM1 at the centrosome and individual centrioles. Insets show a magnification of signals enclosed in the dashed squares; three dots are observed suggesting that the centrosome was dividing when the cell was fixed, and it was probably in its S phase. Unsynchronised dividing hTERT-RPE1 cells, cultured in complete media, fixed with 4 % PFA and permeabilised with 0.3 % Tx100. Scale bar: 10  $\mu$ m. Fluorescent microscope images.

At times, the co-localisation signal was observed in a 3-4 dotted cluster (insets in lower panel of the figure), but consistently showed localisation to both centrioles. Co-localisation was

additionally observed with a centriolar kinase, PLK4 (Habedanck *et al.*, 2005), and centrin-2 (Salisbury *et al.*, 2002) (Figure 7-9 and Figure 7-10).

Images presented in the lower panel in Figure 7-8 suggest that ITM2B is associated with the centrosome, during its duplication. Specifically, the three PCM1 dots depicted on the micrograph indicate that the cell is probably in its S phase at the time of imaging. ITM2B is co-localising with at least two of the three PCM1 dots. The number of stained puncta is more difficult to delineate in the upper panel; nonetheless, the ITM2B signal is certainly co-localising with the PCM1 signal at one of the dots.

The co-staining with PLK4 generally resulted in the expected centriolar staining with some cytoplasmic background (Figure 7-9). However, there is also a signal, proximal, or overlapping, with the nuclear signal, which potentially suggests the presence of a deuterosome.

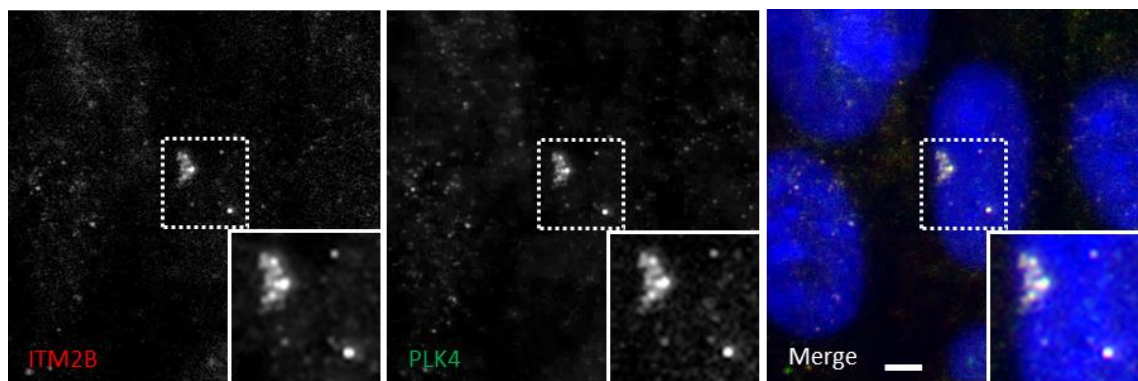


Figure 7-9. ITM2B C-term co-localises with the centriolar and deuterosomal marker: PLK4. ITM2B C-term co-localised with PLK4. Insets show a magnification of signals enclosed in the dashed squares. Most of the signal appears to be centriolar; however, the magnified peri-nuclear structure could potentially be a deuterosome, with which PLK4 is known to associate. Unsynchronised dividing hTERT-RPE1 cells, cultured in complete media, fixed with 4 % PFA and permeabilised with 0.3 % Tx100. Scale bar: 10  $\mu$ m. Fluorescent microscope images.

It was recently shown that PLK4 is involved in centriole biogenesis in multi-ciliated cells (Zhao *et al.*, 2013). It was previously shown that a substantial proportion of the RPE cells in rodent retinae can exist in a binucleated form, as a result of mitoses not followed by cytokineses (Stroeva e Panova, 1983; Al-Hussaini *et al.*, 2008). It is not clear whether, or why, the RPE1 cells would go via the deuterosome pathway (rather than simply the centrosome cycle) to generate another set of centrioles for its putative second nucleus, but at this stage it cannot be excluded that this is indeed happening on the presented image. It could also be speculated that perhaps, when the cells reach a certain age, they will replace their old set of centrioles with new ones via the deuterosome pathway, however, this hypothesis also seems

unlikely. In order to clarify whether ITM2B does localise to deuterosomes, like Figure 7-9 might suggest, the staining could be performed on multi-ciliated cells, for instance, cells of the respiratory tract.

Similarly to PCM1 the observed Centrin-2 staining presents as either a single dot, or as double dots (Figure 7-10). Here again, ITM2B appears to co-localise predominantly (if not only) with just one dot. Overall, there seems to be a larger amount of the Centrin-2 signal at the co-localisation areas, suggesting that ITM2B localises only to a specific part of the centrosome. This was also evident when centrioles were stained with PCM1 (Figure 7-8), but not as much with PLK4 (Figure 7-9), which phosphorylates only specific components of the MTOC.

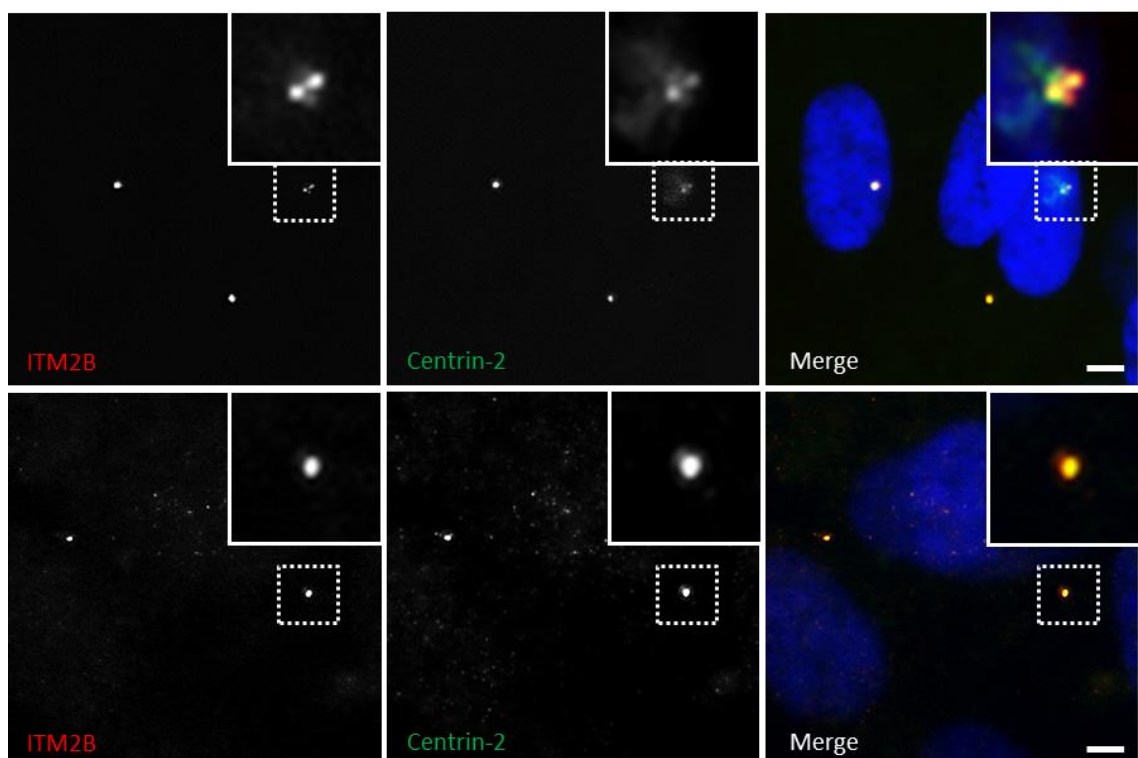


Figure 7-10. ITM2B C-term co-localises with the centriolar marker: Centrin-2.

ITM2B C-term co-localised with Centrin-2; both antibodies appear to stain two centrioles, suggesting that the cell was fixed at the G1 phase. Insets show a magnification of signals enclosed in the dashed squares. Unsynchronised dividing hTERT-RPE1 cells, cultured in complete media, fixed with 4 % PFA and permeabilised with 0.3 % Tx100. Scale bar: 10  $\mu$ m. Fluorescent microscope images.

To understand whether ITM2B, like TOPORS, also associated with the basal body at the base of the primary cilium, further localisation studies were conducted in ciliated cell cultures, using an antibody against  $\alpha$ -tubulin as a marker for the cilium. The markers excluded  $\gamma$  tubulin in this analysis, as the available antibody against it, was raised in rabbit, just like the antibodies against interacting partners of TOPORS.

In ciliated cultures, ITM2B did not show localisation to the basal body (Figure 7-11). However, it co-localised with  $\alpha$ -tubulin at locations other than at the base of primary cilium, at speckles resembling centrioles (indicated by arrows in the figure). These speckles could represent the centrosome/centrioles of un-ciliated cells.

Since in Figures 7-8, 7-9 and 7-10 ITM2B was observed at multi-dotted structures, stained with centriolar markers, that fact that it is absent from the base of the cilium, suggests that it may have a role in centrosome duplication. In view of this hypothesis, once the cells are ciliated, then there is no need for ITM2B at the centrosome anymore.

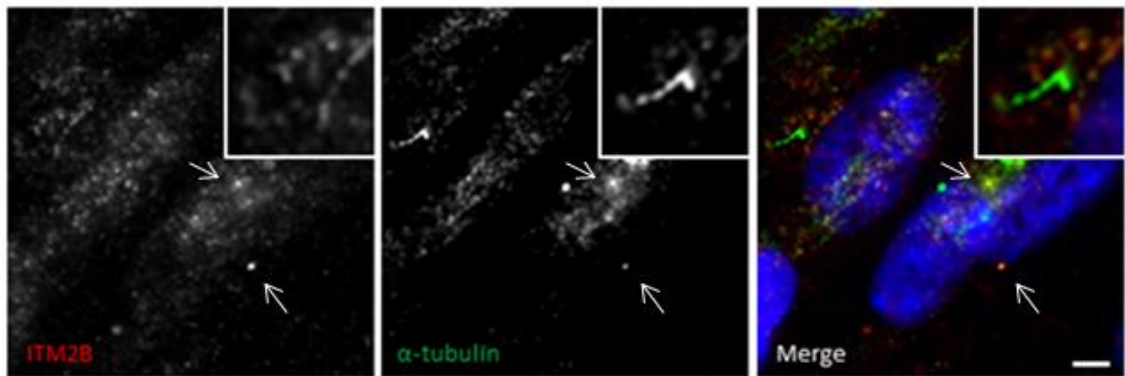


Figure 7-11. ITM2B C-term does not localise to the ciliary basal body.

ITM2B C-term did not localise to the base of the primary cilium (shown here by  $\alpha$ -tubulin staining); however, in non-ciliated cells, ITM2B C-term localised at  $\alpha$ -tubulin-stained puncta, suggesting that it associates with the centrosome in dividing but not in quiescent cells. Inset shows magnification of the primary cilium. Serum-starved ciliated hTERT-RPE1 cells, cultured in media with low serum concentration, fixed with 4 % PFA and permeabilised with 0.3 % Tx100. Scale bar: 10  $\mu$ m. Fluorescent microscope images.

### 7.3 CELLULAR LOCALISATION OF PTGDS

As described in section 4.3.3.2, PTGDS was shown to be produced in retinal epithelial cells of rat and chick retinae. Specifically, PTGDS localised to distinct cytoplasmic structures within the RPE cells.

Urade *et al.* (1987) also showed localisation of PTGDS at rough ER as well as the nuclear envelope of glial cells. Yamashima *et al.* (1997) detected PTGDS in the rough ER and peri-nuclear region in human arachnoid and meningioma cells. In the arachnoid cells it was also detected in the Golgi body and secretory vesicles as well as in spherical cytoplasmic structures.

Additionally, it was found in the microphages and perivascular microglial cells, localising to circular cytoplasmic structures. In 2012, Wu *et al.* demonstrated again that PTGDS showed a predominantly peri-nuclear localisation, with some diffuse staining throughout the cytoplasm of the NTERA-2 cl.D1 (NT2/D1) human testicular carcinoma cell line.

However, PTGDS has mainly been recognised as a protein secreted into various bodily fluids, predominantly the CSF.

The antibody raised in rabbit against full-length human PTGDS (sc-30067, Santa Cruz Biotechnology, TX, USA) was used in all immunofluorescence studies, as well as experiments on cellular protein extracts (section 2.8).

PTGDS displayed some variation in the observed signal, depending on cell fixation method and cell line used. The signal appeared speckled and wide-spread throughout the cytoplasm in hTERT-RPE1 cells fixed with 4 % PFA, with some intense spots of signal visible (and more apparent) closer to the cell nucleus; whereas in the SK-N-SH cells, fixed with PFA, very little signal was observed, if any (Figure 7-12). This closely resembles the signals observed in the same cell lines for ITM2B following 4 % PFA fixation (Figure 7-3).

In methanol-fixed hTERT-RPE1 cells the PTGDS signal in the cytoplasm appeared somehow less granular and more diffuse overall; however, the dot-like signal, which could putatively represent centrioles, appeared more distinct on this background (top panel in Figure 7-13).



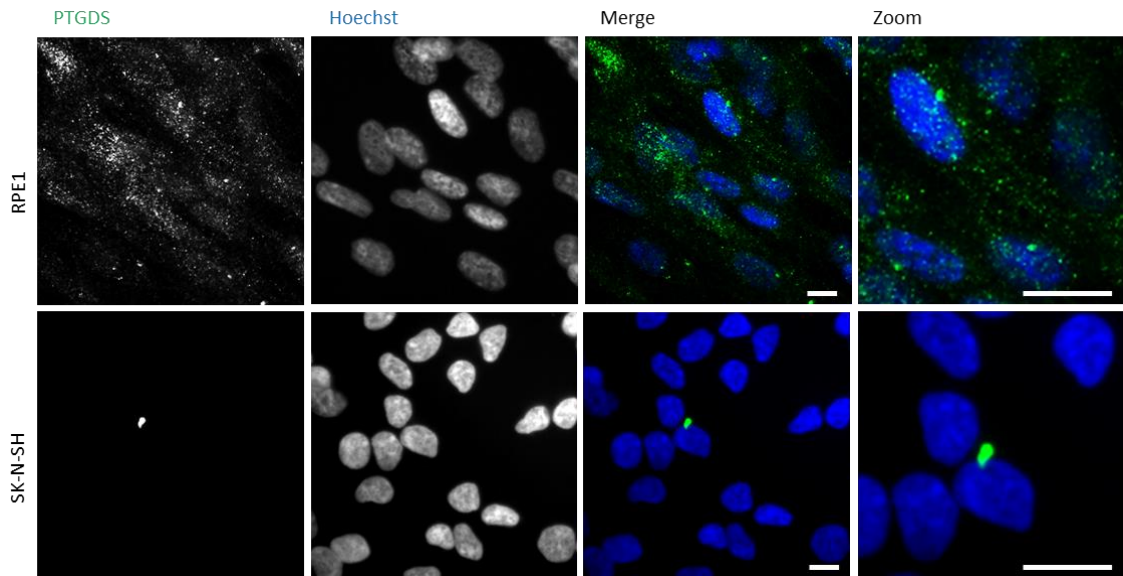


Figure 7-12. PTGDS localises throughout the cytoplasm of retinal epithelial (hTERT-RPE1) cells in a granular pattern, but appears absent from the neuroblastoma (SK-N-SH) cells. PTGDS signal (Ab diluted 1/250) observed in unsynchronised dividing hTERT-RPE1 (RPE1) and SK-N-SH cells, cultured in complete media, fixed with 4 % PFA and permeabilised with 0.3 % Tx100. Scale bar: 20  $\mu$ m. Fluorescent microscope images.

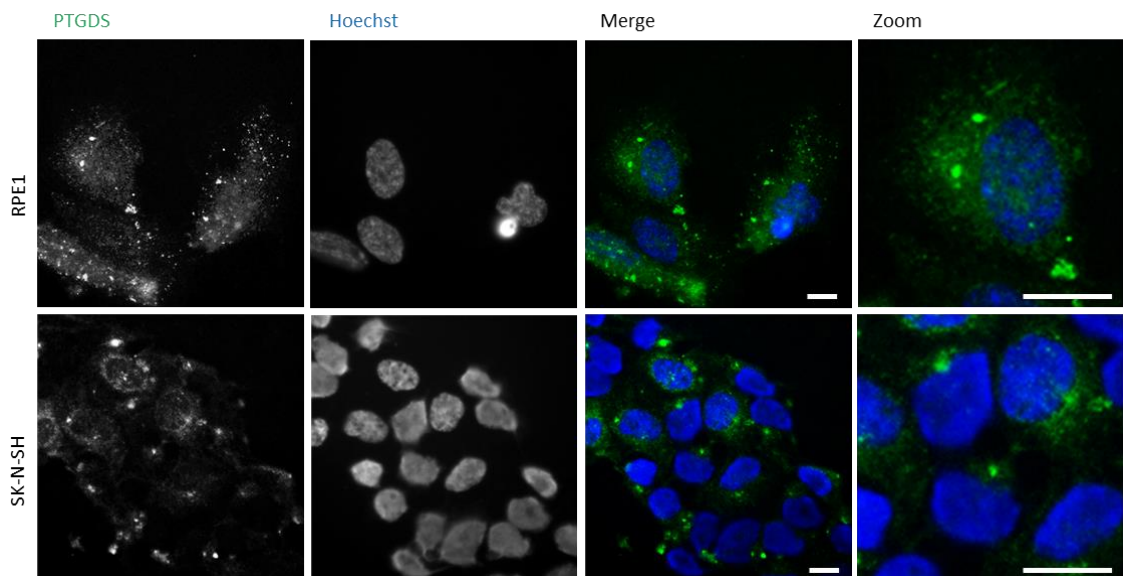


Figure 7-13. PTGDS localises throughout the cytoplasm of retinal epithelial (hTERT-RPE1) and neuroblastoma (SK-N-SH) cells, including more intensely-stained centriole-like puncta. PTGDS (Ab diluted 1/50) observed in unsynchronised dividing hTERT-RPE1 (RPE1) and SK-N-SH cells, cultured in complete media, fixed with ice-cold methanol. Scale bar: 20  $\mu$ m. Fluorescent microscope images.

In methanol-fixed SK-N-SH cells a strong signal was observed in small points located proximally to the nuclei, and additionally a cloud of a more diffuse, wide-spread signal was observed throughout the cells with a slightly more distinct peri-nuclear staining. In some cells PTGDS actually appears to form a ring encircling the nucleus (lower panel in Figure 7-13).

Observations from both cell types are consistent with previously published findings regarding sub-cellular localisation of PTGDS, summarised in the beginning of the current section.

In addition to the peri-nuclear and background cytoplasmic staining, punctate co-localisation with TOPORS was observed in hTERT-RPE1 cells in a pattern, which could be centriolar (Figure 7-14 and Figure 7-15).

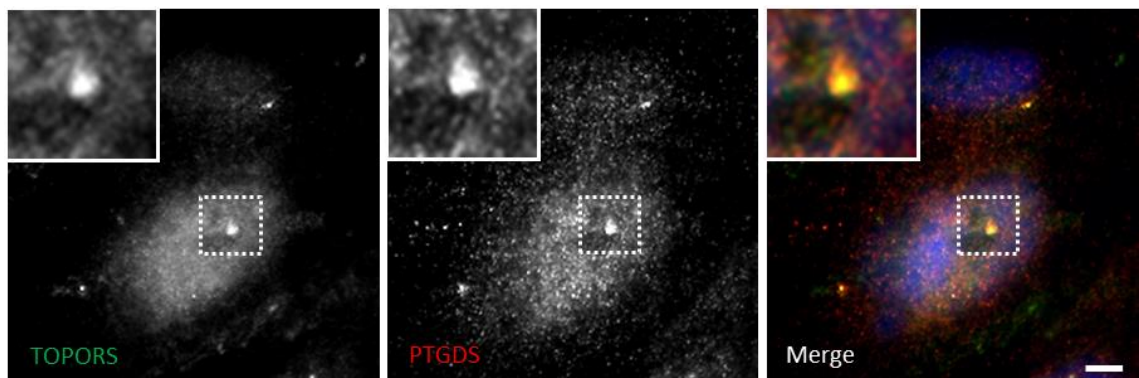


Figure 7-14. PTGDS co-localises with TOPORS in retinal epithelial cells in a centriole-like pattern. PTGDS co-localised with TOPORS, additionally strong cytoplasmic staining was also observed for both proteins. Insets show a magnification of signals enclosed in the dashed squares. Unsynchronised dividing hTERT-RPE1 cells, cultured in complete media, fixed with 4 % PFA and permeabilised with 0.3 % Tx100. Scale bar: 10  $\mu$ m. Fluorescent microscope images.

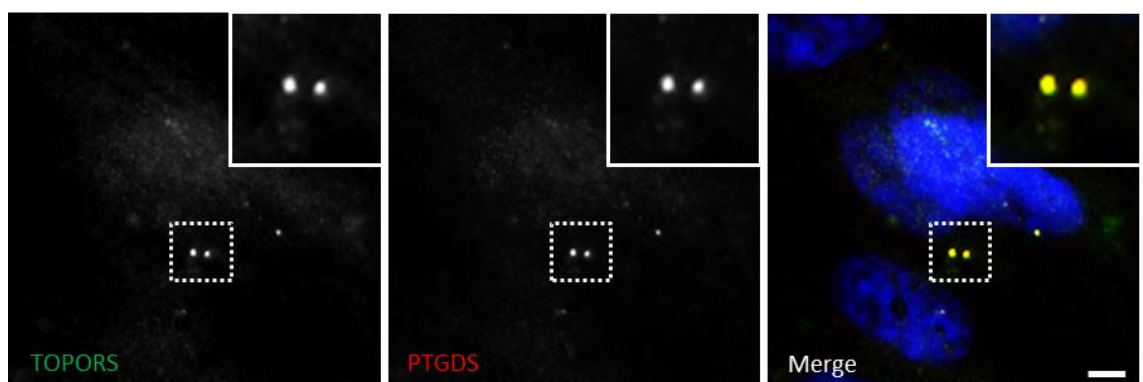


Figure 7-15. PTGDS co-localises with TOPORS in retinal epithelial cells in a centriole-like pattern. PTGDS co-localised with TOPORS at distinct cytoplasmic puncta. Insets show a magnification of signals enclosed in the dashed squares. Unsynchronised dividing hTERT-RPE1 cells, cultured in complete media, fixed with 4 % PFA and permeabilised with 0.3 % Tx100. Scale bar: 10  $\mu$ m. Fluorescent microscope images.

The two images demonstrate two distinct localisation patterns that were observed in cells from the same culture, which were stained with PTGDS. In Figure 7-14 the signal is peri-nuclear and diffuse throughout the cytoplasm (but becoming more widely scattered further away from the nucleus); in addition there are two puncta of higher intensity signal, reminiscent of centrioles, and co-localising with TOPOPRS (which is also showing some nuclear staining).

On the contrary, the sole signal detected using both antibodies (against PTGDS and TOPORS) in Figure 7-15 appeared to look strikingly like centrioles.

Similarly to ITM2B, further localisation studies using centriolar markers confirmed that PTGDS localised to the centrioles, as demonstrated by co-staining with PCM1 (Figure 7-16), PLK4 (Figure 7-17) and centrin-2 (Figure 7-18).

PTGDS and PCM1 co-localised precisely in a centriolar pattern (Figure 7-16); however, PCM1 also stained a peri-nuclear location, from which PTGDS was mostly absent (except for extremely faint speckles at four points). The opposite would be expected, as PTGDS was previously shown (in earlier figures and in referenced studies) to localise around the nucleus. Presumably, PTGDS is targeted to different peri-nuclear domains than PCM1, or at different points in the cell cycle.

Co-localisation between PTGDS and PLK4 was very precise and the two signals overlapped almost entirely (Figure 7-17). Overall, the PTGDS signal appeared to cover a slightly larger surface area, but it is not possible to ascertain at this stage whether it was due to a higher concentration of PTGDS (than PLK4) at the centrioles, or whether perhaps this observation was fluorophore-dependent.

On the contrary, Centrin-2 (Figure 7-18) certainly stained other MTOC components in addition to those, which were also stained by PTGDS. Where a single centriole is visible, the overlap with PTGDS signal is very precise. However, at the structure, which appears to comprise three or more dots (inset in Figure 7-18), PTGDS co-localises only with two of the brighter dots. This structure probably represents a centrosome in the process of becoming duplicated, and perhaps PTGDS is localising to either only the mother centrioles, or the daughter centrioles, of the two resulting centrosomes, or perhaps to mother and daughter centriole of the 'old' centrosome. Nonetheless, it is certainly not co-localising with this structure fully. The three-to-four dotter Centrin-2 staining pattern suggests that the cells were probably in transition from the S phase to the G2 phase at the time of fixation.

Unlike ITM2B, PTGDS was observed at the base of the cilium, as shown by co-staining with  $\alpha$ -tubulin (Figure 7-19). In fact, further analysis showed that in some cells PTGDS signal was observed even along the axoneme of the cilium itself (Figure 7-20).

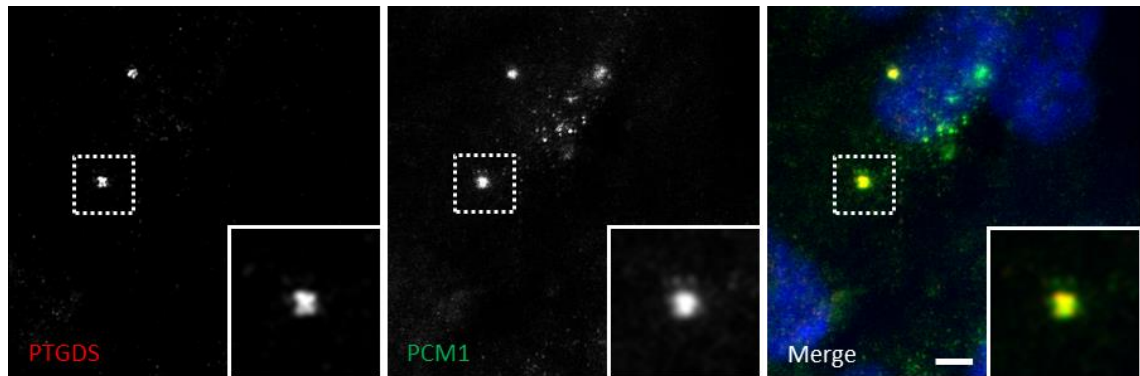


Figure 7-16. PTGDS co-localises with the peri-centriolar marker: PCM1. PTGDS co-localised with PCM1 in a centriole-like pattern. Both proteins additionally localised proximally to the nucleus, but the PCM1 staining was much more intense. Insets show a magnification of signals enclosed in the dashed squares. Unsynchronised dividing hTERT-RPE1 cells, cultured in complete media, fixed with 4 % PFA and permeabilised with 0.3 % Tx100. Scale bar: 10  $\mu$ m. Fluorescent microscope images.

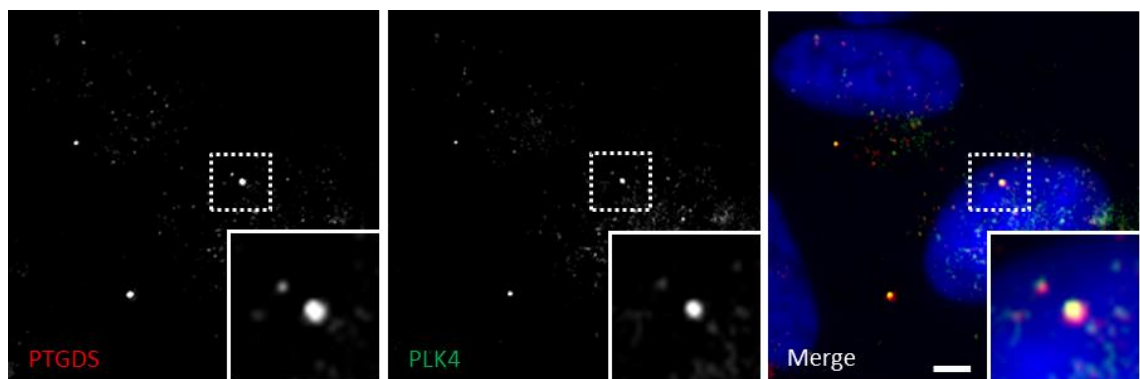


Figure 7-17. PTGDS co-localises with the centriolar and deuterosomal marker: PLK4. PTGDS co-localised with PLK4, as well as appeared to localise around it (the PTGDS signal covers a larger surface area in comparison to PLK4). Insets show a magnification of signals enclosed in the dashed squares. Unsynchronised dividing hTERT-RPE1 cells, cultured in complete media, fixed with 4 % PFA and permeabilised with 0.3 % Tx100. Scale bar: 10  $\mu$ m. Fluorescent microscope images.

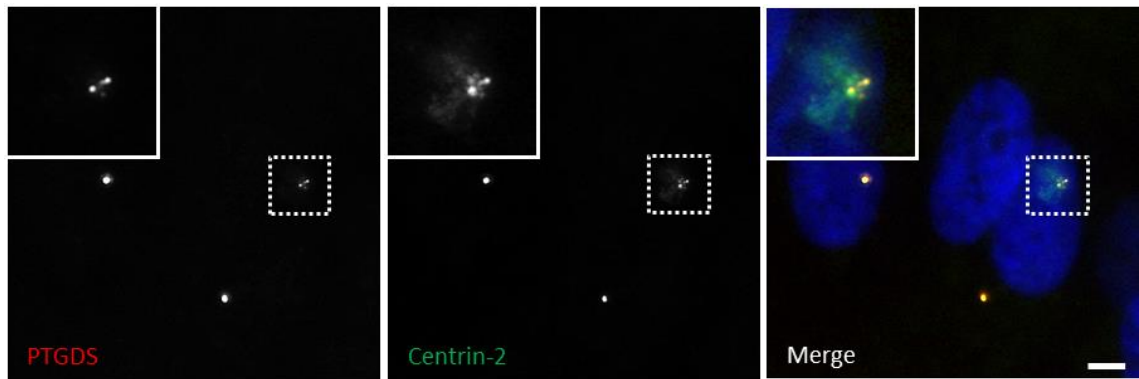


Figure 7-18. PTGDS co-localises with the centriolar marker: Centrin-2. PTGDS co-localised with Centrin-2. Insets show a magnification of signals enclosed in the dashed squares, in which three distinct dots can be discriminated. Unsynchronised dividing hTERT-RPE1 cells, cultured in complete media, fixed with 4 % PFA and permeabilised with 0.3 % Tx100. Scale bar: 10  $\mu$ m. Fluorescent microscope images.

The same images provide evidence for punctate localisation with  $\alpha$ -tubulin away from primary cilia (inset in Figure 7-19), which was also observed for ITM2B.

PTGDS is a highly glycosylated protein, which would support its previously demonstrated localisation within intracellular membranous organelles, which mediate glycosylation, i.e. the endoplasmic reticulum and Golgi apparatus. It was also shown to localise to secretory vesicles and ganglion cell membranes. No PTGDS localisation at the primary cilium was previously shown. Nonetheless, it was demonstrated that prostaglandin (PG) E<sub>2</sub>, a product of PG E<sub>2</sub> synthase, rather than PG D<sub>2</sub> synthase (PTGDS), has important role in ciliary function in development (Jin *et al.*, 2014; Jin, Liu e Zhong, 2015). This information, coupled to the known high PTGDS expression in the rodent RPE layer, suggests that the observed localisation of PTGDS along the cilium can be true.

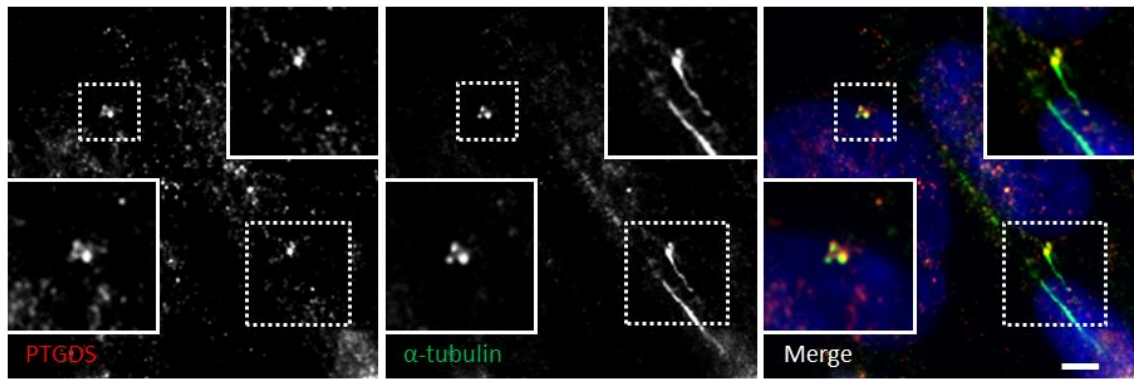


Figure 7-19. PTGDS localises to both centrioles of the ciliary basal body. PTGDS localised to both centrioles at the base of the primary cilium (marked with  $\alpha$ -tubulin). Additionally PTGDS co-localised with  $\alpha$ -tubulin at dotted points other than the base of the cilium. Insets show a magnification of signals enclosed in the dashed squares. More wide-spread peri-nuclear PTGDS staining was also observed. Serum-starved ciliated hTERT-RPE1 cells, cultured in media with low serum concentration, fixed with 4 % PFA and permeabilised with 0.3 % Tx100. Scale bar: 10  $\mu$ m. Fluorescent microscope images.

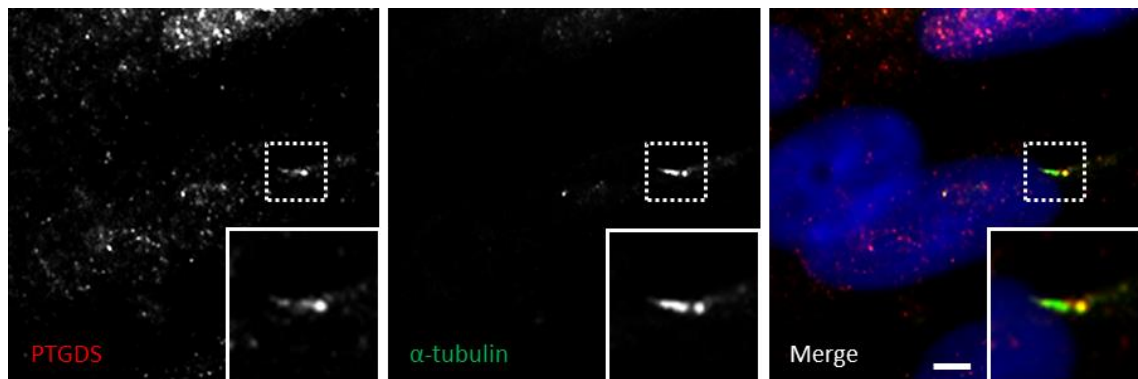


Figure 7-20. PTGDS localises to the ciliary basal body and along the ciliary axoneme. PTGDS localised to the base and along the length of primary cilium (marked with  $\alpha$ -tubulin); Insets show a magnification of signals enclosed in the dashed squares. In addition peri-nuclear PTGDS signal was detected. Serum-starved ciliated hTERT-RPE1 cells, cultured in media with low serum concentration, fixed with 4 % PFA and permeabilised with 0.3 % Tx100. Scale bar: 10  $\mu$ m. Fluorescent microscope images.

## 7.4 CELLULAR LOCALISATION OF PSMC1

Evidence from the Human Protein Atlas (Berglund *et al.*, 2008) demonstrated in three different cell lines (U-2 OS, A-431, and U-251 MG) that PSMC1 localises to the nucleus and throughout the cytoplasm; in all the cell lines the nuclear localisation excludes the nucleoli, which was additionally supported by findings by de Mateo *et al.* (2011).

An antibody against a carboxy-terminal fragment of human PSMC1 (Sigma-Aldrich # HPA000872), as denoted in Figure 6-11, was used in all immuno-based experiments.

The antibody signal was observed in hTERT-RPE1 cells and SK-N-SH cells, fixed with PFA and permeabilised with Tx100 (top panel in Figure 7-21, and Figure 7-22, respectively), as well as hTERT-RPE1 cells fixed with ice-cold methanol (lower panel in Figure 7-21), but it was not detected in methanol-fixed SK-N-SH cells (data not shown).

Figure 7-21 (top panel) shows that in hTERT-RPE1 cells PSMC1 localises throughout the cytoplasm and to the nuclei; however, as in case of the immuno-staining images, recorded in the Human Protein Atlas, the nuclear localisation appears to be exclusive of the nucleoli.

In the ice-cold methanol-fixed hTERT-RPE1 cells the staining was most intense in distinct areas, located adjacently to the nucleus, or inside it, accompanied by peri-nuclear cytoplasmic background staining (Figure 7-22).

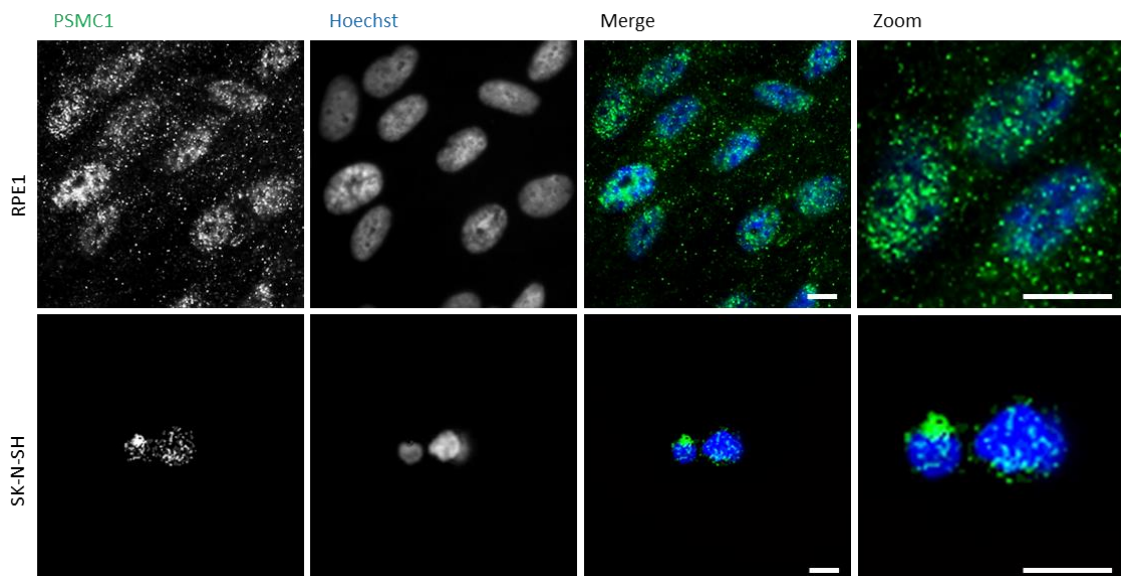


Figure 7-21. PSMC1 localises throughout the cytoplasm of retinal epithelial (hTERT-RPE1) and neuroblastoma (SK-N-SH) cells with a distinct region of higher intensity in the latter. PSMC1 signal (Ab diluted 1/250) observed in unsynchronised dividing hTERT-RPE1 (RPE1) and SK-N-SH cells, cultured in complete media, fixed with 4 % PFA and permeabilised with 0.3 % Tx100. Scale bar: 20  $\mu$ m. Fluorescent microscope images.

In fact, the PSMC1 localisation observed in hTERT-RPE1 cells, fixed with methanol, strongly resembled the PSMC1 signal, detected in SK-N-SH cells, fixed with PFA (lower panel in Figure 7-21). Perhaps the intensely stained regions, observed in these experiments, represent aggregates of the 26 S proteasome, which are recruited to the nucleus in times of stress. It is also possible that they may be artefacts.

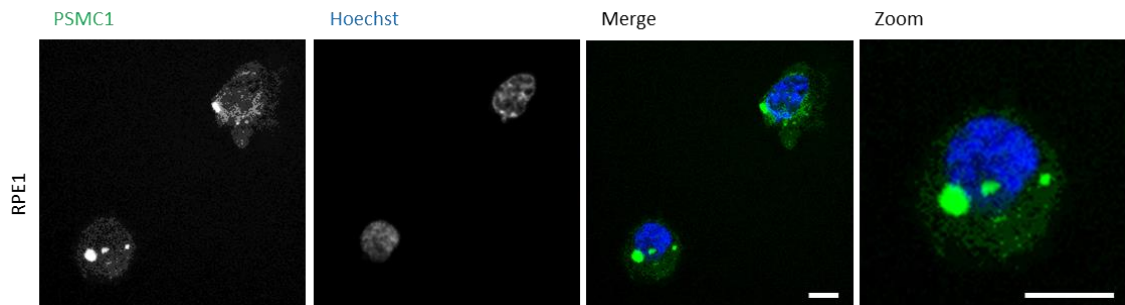


Figure 7-22. PSMC1 localises throughout the cytoplasm of retinal epithelial (hTERT-RPE1) cells with distinct regions of higher intensity. PSMC1 (Ab diluted 1/100) observed in unsynchronised dividing hTERT-RPE1 (RPE1) and SK-N-SH cells, cultured in complete media, fixed with ice-cold methanol. Scale bar: 20  $\mu$ m. Fluorescent microscope images.

Apart from the already demonstrated wide-spread cytoplasmic and nuclear distribution demonstrated in PFA-fixed hTERT-RPE1 cells, punctate signal was also observed, as distinct dots, located proximally to the cell nucleus, in a pattern similar to that of centrioles (Figure 7-23). Subsequent experiments showed that PSMC1 sporadically co-localised with TOPORS (Figure 7-24).

Furthermore, PSMC1 co-localised with centriolar marker PCM1 (Figure 7-25), but not at all times (Figure 7-26). Co-localisation with PLK4 was also observed; however, PSMC1 signal was co-localising with only one of the two centrioles marked by PLK4 (Figure 7-27). PSMC1 and Cenrin-2 co-staining also showed sporadic co-localisation (Figure 7-28).

Additionally, as was also observed for ITM2B and PTGDS on some of the presented micrographs, the PSMC1 signal was sometimes widespread throughout the cell, and other times it appeared extremely specific (compare Figures 7-26 and 7-27).

The outcomes of PSMC1 co-staining with the centriolar markers (PCM1, PLK4, and Centrin-2) were not consistent, even within the same experiment. Co-localisation was always observed in a subset of cells, but never all of the cells, suggesting an association with the cell cycle as unsynchronised cell cultures were used for all localisation experiments.



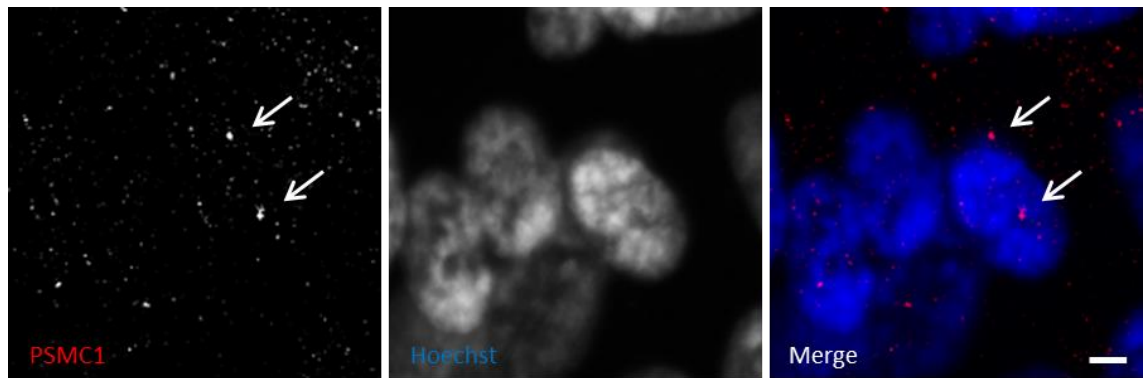


Figure 7-23. PSMC1 localises throughout the cytoplasm in a dotted pattern, some of which is reminiscent of centrioles (arrows). PSMC1 localised throughout the cell, and sometimes more distinct punctate peri-nuclear signal (arrows) was also observed. Unsynchronised dividing hTERT-RPE1 cells, cultured in complete media, fixed with 4 % PFA and permeabilised with 0.3 % Tx100. Scale bar: 10  $\mu$ m. Fluorescent microscope images.

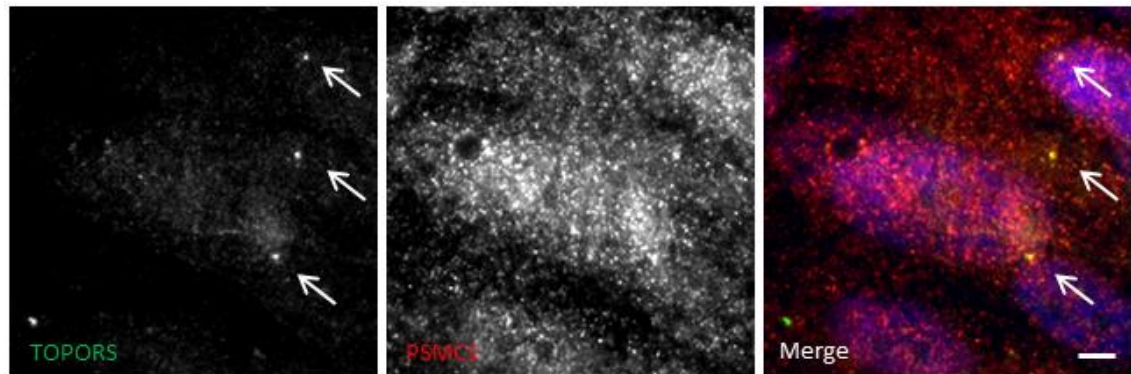


Figure 7-24. PSMC1 co-localises with TOPORS in a centriole-like pattern. PSMC1 localised throughout the cell; the signal included more distinct points, co-localising with TOPORS staining (arrows). Unsynchronised dividing hTERT-RPE1, cultured in complete media, fixed with 4 % PFA and permeabilised with 0.3 % Tx100. Scale bar: 10  $\mu$ m. Fluorescent microscope images.

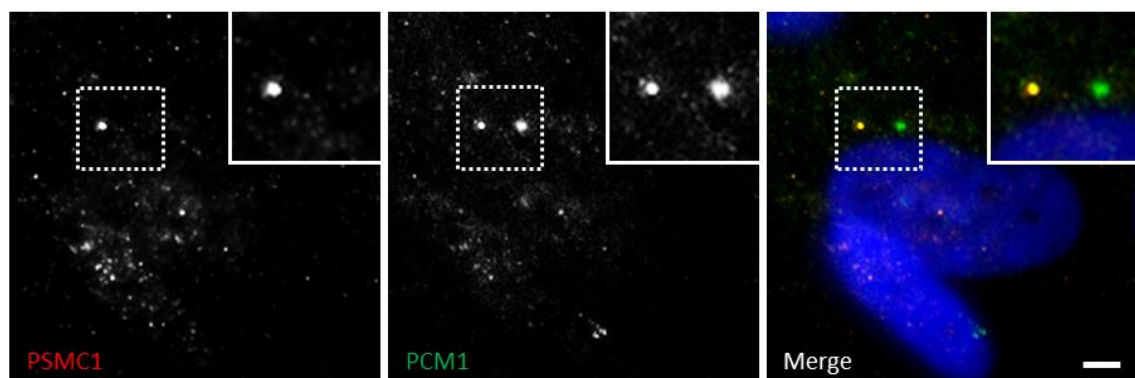


Figure 7-25. In the selected cells PSMC1 co-localises with the peri-centriolar marker: PCM1. PSMC1 co-localised with PCM1 at structures resembling centrioles, but it did not co-localise with a slightly more diffuse spot of PCM1 signal (which could represent a centriole, which is out of focus). Insets show a magnification of signals enclosed in the dashed squares. Unsynchronised dividing hTERT-RPE1 cells, cultured in complete media, fixed with 4 % PFA and permeabilised with 0.3 % Tx100. Scale bar: 10  $\mu$ m. Fluorescent microscope images.

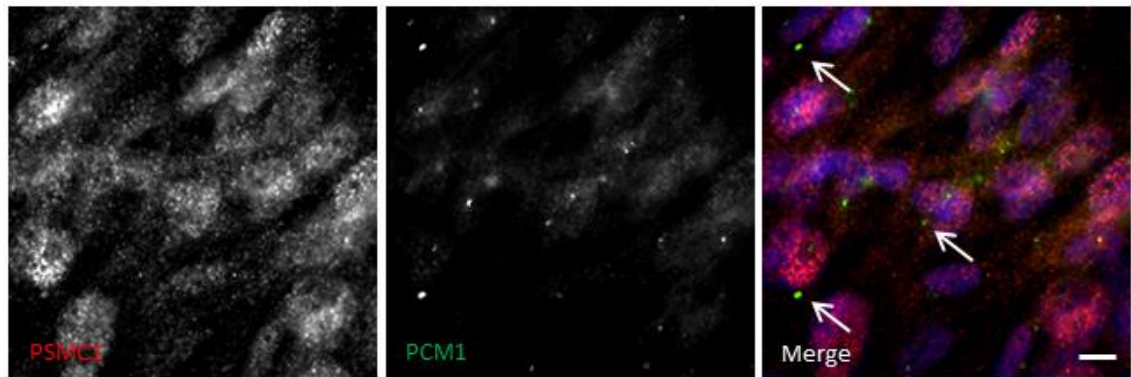


Figure 7-26. In the selected cells PSMC1 does not co-localise with the peri-centriolar marker: PCM1. PSMC1 did not consistently co-localise with PCM1 (arrows); nonetheless, co-localisation with both centrioles one cell in this figure is also apparent. Unsynchronised dividing hTERT-RPE1 cells, cultured in complete media, fixed with 4 % PFA and permeabilised with 0.3 % Tx100. Scale bar: 25  $\mu$ m. Fluorescent microscope images.

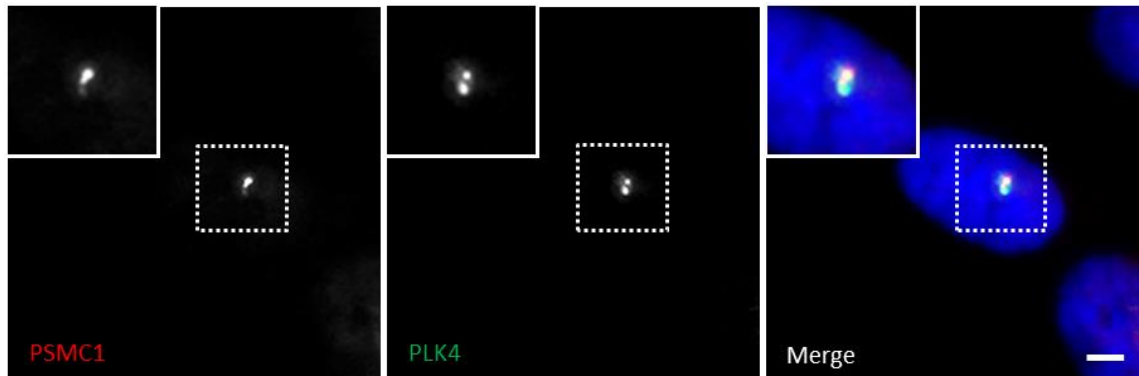


Figure 7-27. PSMC1 co-localises with the centriolar and deuterosomal marker: PLK4. PSMC1 co-localised with PLK4 at one of the two centrioles marked with PLK4. The PSMC1 also appears to co-localise with linker molecules holding the two centrioles together. Insets show a magnification of signals enclosed in the dashed squares. Unsynchronised dividing hTERT-RPE1 cells, cultured in complete media, fixed with 4 % PFA and permeabilised with 0.3 % Tx100. Scale bar: 10  $\mu$ m. Fluorescent microscope images.

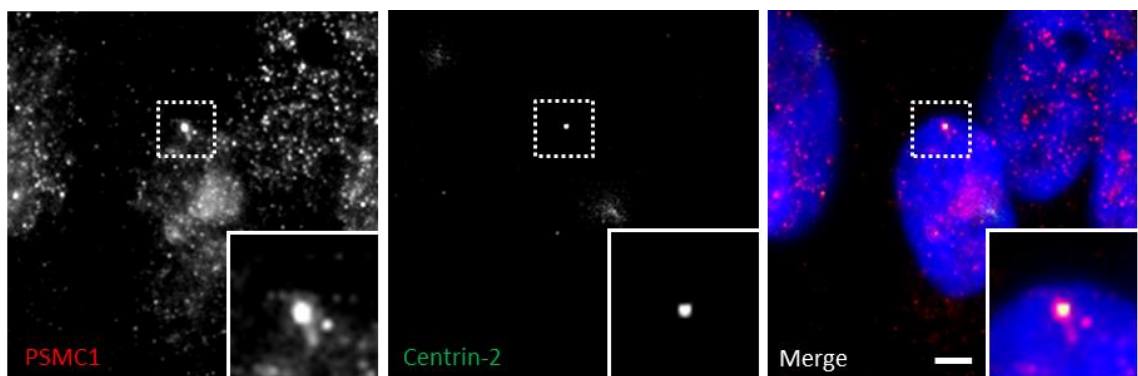


Figure 7-28. In selected cells PSMC1 co-localises with the centriolar marker: Centrin-2. PSMC1 localised peri-nuclearly, sporadically co-localising with Centrin-2; the PSMC1 overlapped with as well as surrounded the Centrin-2 signal. Insets show a magnification of signals enclosed in the dashed squares. Unsynchronised dividing hTERT-RPE1 cells, cultured in complete media, fixed with 4 % PFA and permeabilised with 0.3 % Tx100. Scale bar: 10  $\mu$ m. Fluorescent microscope images.

It is interesting to note that in cells where PSMC1 does localise at the centrioles, there appears to be a stronger signal from one centriole, over the other, suggesting preference for either the mother or daughter centriole, and also suggestive of a cell cycle function. A role for *PSMC1* in the cell cycle has been demonstrated in mouse embryonic fibroblasts (Rezvani *et al.*, 2012).

Furthermore, regulated proteolysis is essential for cell cycle progression, and proteasomal degradation of cyclins, their associated kinases and other accessory proteins has been demonstrated, which would fit with the known role of PSMC1 (reviewed in: Vermeulen, Van Bockstaele e Berneman, 2003).

Similarly, the staining pattern with  $\alpha$ -tubulin did not provide evidence that PSMC1 localises to primary cilium (Figure 7-29); but, like ITM2B, and to some degree PTGDS, it co-localised with  $\alpha$ -tubulin at distinct, solitary points proximal to the cell nucleus (inset in Figure 7-29).

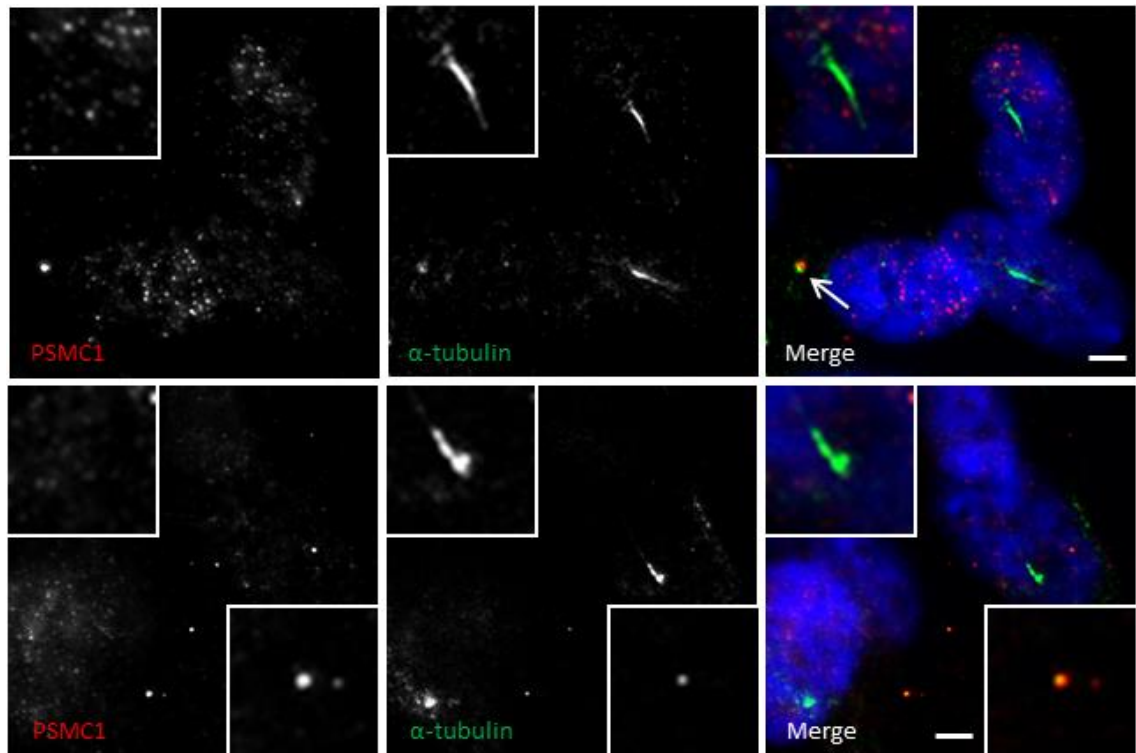


Figure 7-29. PSMC1 does not localise to the ciliary basal body.

PSMC1 did not co-localise with the primary cilium (marked with  $\alpha$ -tubulin, inset); however, it co-localised with  $\alpha$ -tubulin in a punctate, centriole-like pattern, in cells in which no primary cilium was observed, suggesting that it associates with the MTOC at some points in the life cycle of dividing cells but not in quiescent cells. Serum-starved ciliated hTERT-RPE1 cells, cultured in media with low serum concentration, fixed with 4 % PFA and permeabilised with 0.3 % Tx100. Scale bar: 10  $\mu$ m. Fluorescent microscope images.

## 7.5 IDENTIFICATION OF CILIARY TARGETING SEQUENCES

Based on cellular localisation experiments, all three interacting partners of TOPORS, ITM2B, PTGDS and PSMC1, appear to co-localise with TOPORS, at or around the centrioles and/or centrosome. This is a novel observation for each of the three interacting partners, neither of which have been implicated as ciliary, or cilia-related proteins, prior to this work.

Given the unexpected localisation results, an attempt was made to identify potential ciliary targeting sequences (CTS) (Mazelova *et al.*, 2009; Hsiao, Tuz e Ferland, 2012) within these proteins. These motifs were already referred to in Chapter 6, and were mapped onto Figures 6-3, 6-5, 6-8 and 6-11. This section describes why they were searched for, and how they were identified.

Firstly, the amino acid conservation of was determined for each interacting partner, using the PRALINE multiple sequence alignment tool (The Centre for Integrative Bioinformatics VU (IBIVU), University of Amsterdam, Netherlands). Once the alignment files had been generated, the results were saved as .pdf files, and the sequence was annotated manually, as well as employing the 'find' function to identify potential CTS sites. Several different CTS have been identified; these include VxPx, RVxP, KVHPSST, AxEGG and Ax(S/A)xQ, amongst others (Hsiao, Tuz e Ferland, 2012), all of which were searched for.

Based on the bioinformatics analysis human TOPORS contains two VxP sequences. The first CTS is located shortly after the RING finger (Table 7-2), and according to PRALINE is conserved among apes and monkeys. The second CTS, located between the second and third PEST domains, and show an even greater conservation; in addition to primates, it has been found in other vertebrates, such as mouse, the African clawed frog and zebrafish.

Interestingly, three CTS sites were identified in ITM2B, the first before the transmembrane domain, and the latter two closer to the C-terminal end of the protein (shown in Figure 6-5), and showing complete conservation in the species tested (Figures 11-52 and 11-53 in Appendix 11.10).

Two sites were identified in PTGDS, at amino acids 30-32 and 69-71, both of which were conserved in higher mammals, the second of the two, also in dog and frog. PSMC1 showed one VxP CTS site in the N-terminus (amino acids 52-54), the second being the Ax(S/A)xQ site found approximately mid-protein at amino acids 238-242.

The CTS VxP is considered a generic sequence, and was the main CTS identified for TOPORS and the three interacting partners, with the exception of PSMC1 which additionally contained an Ax(S/A)xQ, usually associated with G-protein coupled receptors (Hsiao, Tuz e Ferland, 2012).

Given time this work could be developed further by using SDM to mutagenize each of these putative CTS sites in turn, to better understand the role (if only) they play in determining the localisation of each of the said proteins.

Table 7-2. CTS domains identified in TOPORS and its interacting partners.

PROTEIN	AMINO ACID NUMBER (according to human sequence)	AMINO ACID SEQ
<b>TOPORS</b>	172-174	VTP
	484-486	VKP
<b>ITM2B</b>	44-46	VVP
	166-168	VIP
	174-176	VMP
<b>PTGDS</b>	30-32	VQP
	69-71	VAP
<b>PSMC1</b>	52-54	VTP
	238-242	AVANQ

## 7.6 DISCUSSION

The findings described in this chapter demonstrated that, although not throughout the cell cycle, the novel interactors of TOPORS do indeed localise to the centrioles. The localisation of TOPORS at these strategic organelles was previously demonstrated by Chakarova *et al.* (2011), who showed that this protein associated with centrosomes in both dividing and ciliated cells.

The centrosome was the organelle of interest as the study additionally demonstrated that in retinal sections TOPORS localises to the basal body of rod photoreceptor connecting cilium. It was hypothesised that the localisation of TOPORS at the photoreceptors' literal bottle-neck was the reason why its mutations resulted in retinitis pigmentosa. Hence, it was interesting to evaluate whether the interacting partners of TOPORS also localised to the centrosome, or specifically, the ciliary basal body.

Cellular co-staining studies with TOPORS were indicative of localisation of the interacting proteins to the centrosome, which was confirmed by co-staining for each interacting protein and centriolar markers. As was described in section 1.8, the centrosome comprises two centrioles and forms the microtubule organising centre (MTOC) of the cell. Furthermore, in cells, which have exited the cell cycle, it serves as the basal body of the primary cilium (section 1.9).

### 7.6.1 EVALUATION OF LOCALISATION

Table 7-3 provides a summary of the co-localisation experiments, which show that, in this study, in hTERT-RPE1 cell line only PTGDS was observed at the primary cilium. ITM2B and PSMC1 did indeed localise to centrioles in dividing cells; however, they were both absent from the ciliary basal body in cells at the G0 cell cycle phase.

ITM2B showed co-localisation with TOPORS at the centrosome (Figure 7-6 and 7-7), localising to both centrioles, as confirmed by co-localisation studies with centriolar markers PCM1, PLK4 and Centrin-2 (Figures 7-8, 7-9, and 7-10). It appeared that ITM2B remains associated with both centrioles throughout the cell cycle: ITM2B co-localised with PCM1 and PLK4 in a 3-dotted pattern (Figure 7-8 and Figure 7-9), respectively, which could indicate that it localises to centrioles in S-phase cells (or perhaps G2-phase) cells, given that PCM1 and PLK4 staining could be interpreted similarly to centrin-2 staining.

The signal depicted in Figure 7-9 also shows co-localisation at two dots spread apart on two sides of a nucleus, possibly indicating centrosome separation at the G2/M transition.

Table 7-3. Summary of localisation study with centriolar markers. The cell cycle stages are just hypothetical, they were determined solely based on the appearance of the centriolar staining as indicated by markers.

	ITM2B (C-term)	PTGDS	PSMC1
<b>TOPORS</b>	Co-localised in a centriole-like pattern. In some cells ITM2B displayed additional 'cloud'-like signal around the co-localisation area.	Co-localised in a centriole-like pattern in addition to diffuse cytoplasmic signal observed for both proteins. In some cells the cytoplasmic PTGDS signal appeared very granular, whereas in others it was almost unnoticeable.	Co-localised in a centriole-like (G1 phase) pattern in some cells in addition to diffuse cytoplasmic signal observed for both proteins (much more extensive for PSMC1).
<b>PCM1</b>	Co-localised in cells fixed at S phase.	Co-localised in a centriole-like pattern. Did not co-localise proximally to the nucleus.	Co-localised in a centriole-like pattern in some cells, but did not co-localise at all in others.
<b>PLK4</b>	Co-localised in a centriole-like pattern. Co-localisation at a larger deuterosome-like structure was also observed.	Co-localised in a centriole-like pattern. Additionally, both proteins were observed in the cytoplasm where some of their signals co-localised.	PSMC1 co-localised with one of the two PLK4-stained centrioles (S phase).
<b>Centrin-2</b>	Co-localised in cells fixed at G1 phase.	Co-localised in cells fixed at G1 and S phases.	Co-localised in cells fixed at G1 phase. The PSMC1 signal overlapped with and surrounded the PCM1 signal (but it was continuous rather cloud-like as in case of ITM2B).
<b><math>\alpha</math>-tubulin</b>	Co-localised in a dot-like pattern reminiscent of centrioles. Did not co-localise at the ciliary basal body.	Co-localised in a dot-like pattern reminiscent of centrioles at G1 and S phases. Co-localised at both centrioles of the ciliary basal body and along the axoneme.	Co-localised in a dot-like pattern reminiscent of centrioles. Did not co-localise at the ciliary basal body.

The fact that nuclear staining of the cell, within which the two dots are observed resembles the appearance of chromatin undergoing condensation, supports this hypothesis.

Co-staining with centrin-2, whose localisation at the centrioles/centrosome can be used to determine cell cycle stages, shows a two-dotted pattern (Figure 7-10), suggesting cells were at G1 stage at fixation. No ITM2B signal was observed at the basal body of primary cilia in cells displaying this characteristic (Figure 7-11), which suggests that this protein does not associate with the centrosome in cells, which have exited the cell cycle, and are quiescent at the G0 phase.

PTGDS, like ITM2B, was found localising to the centrioles with TOPORS and the other centriolar markers. PTGDS displayed a 3-4 dotted co-localisation pattern with PCM1 (Figure 7-16); whereas the PLK4 signal appeared mostly as single dots in the same non-synchronised cell batch, putatively indicating the G2/M transition of the cell cycle (Figure 7-17).

PTGDS co-staining with Centrin-2 showed a speckled 3-4 dotted signal, suggesting that the co-localisation occurred either at the S- or in the beginning of G2-phase. However, unlike ITM2B, PTGDS was found to localise to the basal body of ciliated hTERT-RPE1 cells, and it was also observed along the length of the ciliary axoneme (Figure 7-19 and Figure 7-20), demonstrating that it remains localised to the centrosome in quiescent cells, also implying it might remain associated with the centrosome/centrioles throughout the cell cycle.

Interestingly, lack of PTGDS staining in SK-N-SH cells was shown in Figure 7-12. This result could support the previously published findings, stating that, in the retina, PTGDS is not synthesised in the neuronal photoreceptor cells (Beuckmann *et al.*, 1996). The study showed that the protein is synthesised in the retinal pigmented epithelial (RPE) cells, secreted into the interphotoreceptor space, and then taken up by the photoreceptor cells. It could be speculated that perhaps the retina is not the only tissue in the CNS, where PTGDS produced by an epithelial cell type (or another cell type) is at some point taken up by a neuronal cell type.

For example, it was previously reported that PTGDS production by oligodendrocytes protected neighbouring neurons from death by apoptosis (Taniike *et al.*, 2002). Other studies also demonstrated that PTGDS in neurons has an anti-apoptotic activity (Fujimori, Fukuhara, *et al.*, 2012; Fukuhara *et al.*, 2012). High levels of PTGDS were also recorded in detached human retinae (Jaggi *et al.*, 2008), which could be explained by the protective anti-apoptotic function of this protein. Nonetheless, the above speculation must remain purely hypothetical since PTGDS signal was recorded in cells fixed with ice-cold methanol (Figure 7-13).



In contrast to the other two interacting partners, co-localisation of PSMC1 with TOPORS, as well as with centriolar markers, was only observed sporadically, which suggested that its localisation to the centrioles and/or centrosome could be cell cycle phase-dependent. Where a pair of dots was observed, shown by co-staining with PLK4 to be centrioles (Figure 7-27), PSMC1 was observed localising to just one of them, suggesting a preference for either the mother, or the daughter centriole. PSMC1 signal was not detected at the basal body of the primary cilium. Nonetheless, efficient and highly-regulated proteasomal degradation is essential for correct progression of the cell cycle, therefore, the observed co-localisation of PSMC1 with centriolar markers is most likely true.

There is evidence to suggest that centrosomes may act as peri-nuclear scaffold structures, onto which proteasomes are docked (Wigley *et al.*, 1999). Furthermore, it was also demonstrated that proteasomes associated with centrosomes are involved in homeostasis of centrosomal proteins (Didier *et al.*, 2008).

This function could be especially relevant to protein hubs at centrosomes and basal bodies, where proteins are unloaded from and prepared for transport by components of the intraflagellar transport (IFT) system. The exact conditions, determining when the two cellular structures associate, probably depend on cell cycle stage as well as cellular stresses/responses to environmental stimuli, which could help explain the inconsistent localisation of PSMC1 to the centrioles.

The implication of *PSMC1* in cell cycle defects was previously demonstrated (Rezvani *et al.*, 2003; Rezvani *et al.*, 2012); therefore, despite the observed inconsistencies PSMC1 is expected to play an important role in cell cycle regulation.

Remarkably, as was summarised in Table 7-2, all three proteins: ITM2B, PTGDS and PSMC1, as well as TOPORS, possess ciliary-targeting sequences (CTSs) of the same type (VxPx) as those found in rhodopsin, or polycystin-2, both of which are involved in debilitating ciliopathies.

Hence, even though the functionality of these CTS motifs was not demonstrated in this sub-cellular localisation study, it cannot be excluded that they would localise to the primary cilium in different circumstances. For instance, if the experiment was repeated in another cell type, or if the localisation was evaluated within a tissue section harbouring ciliated cells, then perhaps a ciliary signal would have been observed. Specific signalling events, possibly from neighbouring cells of a different type, might be necessary in order to trigger a translocation of

a certain protein at the ciliary base. Clearly, a CTS motif is not the only determinant of a protein's localisation to the primary cilium.

For PTGDS it was previously demonstrated that serum-starvation resulted in an enhanced production of this protein (Fujimori, Aritake e Urade, 2008). In order to simulate the hTERT-RPE1 cells to grow primary cilia, they were firstly subject to serum starvation. On this basis, it could be speculated that the increased synthesis of PTGDS, hypothetically triggered by serum-starvation, was required in order for a subset of the protein to localise to the cilium.

If this could be confirmed as the necessary environmental stimulus for PTGDS, it could be speculated that alternative environmental stimuli exist for ITM2B and/or PSMC1, which could trigger ciliary localisation of these proteins.

Overall, centrioles comprise the main building blocks of the MTOC in mammalian cells. During the interphase cells depend on the centrosomes for maintaining the cellular cytoskeleton as well as the correct positioning of organelles. For instance, when cells are undergoing mitosis and cytokinesis, the stacks of the Golgi apparatus dissociate from each other and diffuse freely throughout the cytosol, as they do not have the cytoskeletal support of microtubules anymore since the centrosomes are participating in the mitotic spindle formation.

Consequently, if a protein, such as TOPORS, which is associated with the centrosome throughout the cell cycle, becomes mutated, this could affect the overall cell physiology, irrespectively of whether the cell is dividing or ciliated. TOPORS, specifically, is believed to be of key importance to the MTOC due to its enzymatic activities. The protein possesses dual E3 ubiquitin and SUMO1 ligase activities, both of which are crucial to regulation of proteasomal degradation, which in turn is key to cell cycle progression in dividing cells and to signalling functions in ciliated cells.

Among the three evaluated interactors PTGDS was the only protein, for which both: the centriolar and ciliary localisations were demonstrated. Roles of prostaglandins (PGs) in signalling, including signalling via the primary cilium, were previously reported (Fujimori, Kadoyama e Urade, 2005; Fujimori, Maruyama, *et al.*, 2012; Lee, S. *et al.*, 2012; Jin *et al.*, 2014; Jin, Liu e Zhong, 2015). Hence, it is not unreasonable for a PG synthase, such PTGDS, to be present at the primary cilium. Nonetheless, the function that it has there does not necessarily need to involve PTGDS synthesis. PTGDS might be involved in signalling cascades conveyed through the cilium through its role as a transporter of lipophilic compounds, here specifically retinoids (section 4.3.3.2).

## 7.6.2 CONCLUSIONS

The data presented in the current Chapter 7 demonstrated that ITM2B, PTGDS and PSMC1 all co-localised with TOPORS as well as centriolar markers (PCM1, PLK4 and Centrin-2) in the human retinal pigmented epithelial cell line: hTERT-RPE1. Furthermore, a bioinformatics analysis revealed that all three interactors as well as TOPORS possess ciliary targeting sequences (CTS) within their peptide chains. These CTF motifs were of the same type as those found in rhodopsin or polycystin-2, in which they were demonstrated to be functional. Nonetheless, PTGDS was the only one of the three interactors, which was observed at the primary cilium of the hTERT-RPE1 cells. This suggests that, in addition to the CTS motifs, other factors must also be involved in targeting of the identified proteins to primary cilia (if the CTS regions are indeed functional).

Still, the localisation of all three proteins to centrioles in dividing cells was evident. These results supported the findings from the Y2H assays as well as coIP studies (even though the later resulted in a less strong evidence of interaction between TOPORS and PTGDS), as they demonstrated that these proteins localise to the same sub-cellular compartments as TOPORS in human cells. Since the proteins are able to encounter each other in the native intracellular environment, this strengthens the importance of the protein interaction findings.

In view of the above as well as due to the previously reported ubiquitous expression of TOPORS, it could be hypothesised that, in the retina, TOPORS associates with its novel interactors not at the ciliary basal bodies of rod photoreceptor cells (or, perhaps for PTGDS, not only there). As the expression of TOPORS' interactors also appears ubiquitous, perhaps the association between them (or one of them) and TOPORS actually occurs in the RPE layer, actively phagocytising the photoreceptor outer segments, which undergo a continual renewal process.

The outcomes of immuno-fluorescent (IF) staining experiments on retinal cryo-sections (Chapter 8), should provide evidence to either support or disregard this hypothesis. A co-staining for each interacting pair will have been performed to determine whether TOPORS and its interactors are found within a reachable proximity to each other within the retinal tissue. The results of these immunohistochemical (IHC) IF studies should aid in interpretation of the other empirical findings described throughout this thesis.

## **8 RETINAL TISSUE LOCALISATION STUDIES**

The results described in the experimental chapters so far described the construction of the human retinal cDNA library in yeast, the identity of which was validated by isolating clones of rhodopsin (*rho*) (Chapter 3). Subsequently, a Y2H screen for human retinal protein interacting partners of TOPORS was performed using the newly constructed retinal cDNA library. The screen led to identification and selection of three novel candidates for validation and characterisation of interactions, namely ITM2B, PTGDS and PSMC1 (Chapter 4).

The Y2H results were subsequently re-demonstrated by direct interaction in yeast, using full length clones as well as relevant deletion constructs. These experiments confirmed that interactions between these human exogenous proteins do indeed occur in yeast. Moreover, it was shown that ITM2B interacts most strongly with the N-terminal and C-terminal fragments of TOPORS, conveying the E3 ubiquitin ligase activity and comprising the mutational hotspot, respectively. PTGDS interacted most strongly with the N-terminal TOPORS fragment, whereas PSMC1 associated most readily with mid-TOPORS fragment (associated with E3 SUMO1 ligase activity) and the C-terminal fragment. An additional study aimed at identifying alternatively spliced retinal variants of the novel Y2H interactors of TOPORS was also performed and showed that at mRNA level one protein-coding isoform is expressed in the retina of both *ITM2B* and *PSMC1* (corresponding to the isoforms pulled out from the Y2H screen); however, a total of three protein-coding *PTGDS* isoforms (including the one pulled out from the Y2H screen) were shown to be expressed in the human retina at mRNA level (Chapter 5).

Co-immuno-precipitation studies (Chapter 6) provided sound evidence that ITM2B and PSMC1 are both found in HeLa endogenous protein complexes with TOPORS. On the other hand, the band observed for PTGDS (for total cell lysates as well as complexes immuno-precipitated with an antibody detecting TOPORS) was consistently migrating about 20 kDa higher than expected, suggesting that, although it did appear in the coIP complex with TOPORS, the interaction with this protein requires further verification.

Findings from cellular localisation studies showed that in the hTERT-RPE1 cells TOPORS co-localised with its three novel interacting partners from the Y2H screen in a punctate pattern resembling centrioles. Further co-immuno-staining of centriolar markers and the TOPORS' interactors did indeed demonstrate that all three: ITM2B, PTGDS and PSMC1 localise to the centrioles, although in variable patterns, which could be cell-cycle dependent.

PTGDS was the only protein, which was observed at the ciliary basal body in ciliated non-dividing cells. In non-ciliated cells within the same population ITM2B and PSMC1 also co-localised with  $\alpha$  tubulin (which was used as the ciliary marker in ciliated cells) in a dotted pattern reminiscent of MTOCs. The results in the previous chapter demonstrated that, in dividing cells, TOPORS and its interacting protein partners localise to the same non-membrane-bound organelles, specifically the centrioles, therefore supporting the outcomes of the coIP studies.

The purpose of the current chapter is to evaluate the localisation of the novel interacting partners of TOPORS in retinal tissue cryo-sections. Although co-IPs and immuno-localisation in cells can provide some degree of confirmation towards the interaction in question, to begin to understand the biological significance and relevance of the identified interacting proteins, it is important to determine how and where they localise in the tissue of interest. In this case the tissue affected by mutations in the gene of interest, *TOPORS*, is the retina. Murine and primate retinae were used for co-localisation studies.

The first objective was to perform an optimisation of the immuno-histochemical staining and the preparatory procedures. This was achieved by repeating the immuno-staining experiment, which previously demonstrated retinal localization of TOPORS at the connecting cilium (Chakarova *et al.*, 2011), using the same antibody (Abnova #H00010210-M01). Additionally, a co-staining was performed with PNA (marker for cone photoreceptors). A signal, strongly resembling the previously demonstrated retinal localisation of TOPORS at the connecting cilium (CC) of the photoreceptor layer, was observed in mouse sections (Figure 8-1). This experiment was used as an overall positive control for subsequent tissue staining studies.

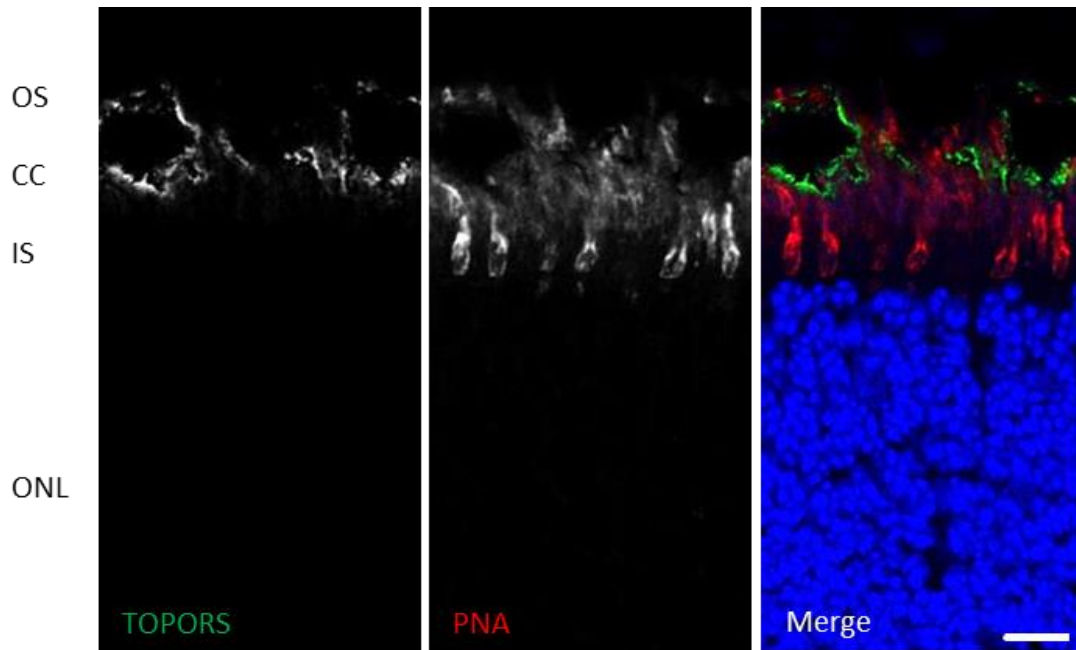


Figure 8-1. TOPORS and PNA staining: C57 Black 6 mouse retina section (2 weeks old at time of tissue collection).

TOPORS signal is observed at the CC, whereas peanut agglutinin (PNA) is a cone marker. OS, rod photoreceptor outer segment; CC, rod photoreceptor connecting cilium; IS, rod photoreceptor inner segment; ONL, outer nuclear layer. Scale bar: 25  $\mu$ m. Nuclei stained using DAPI. Confocal microscope images. Secondary antibody control images were collected using the same settings and generated no signals in the red and green channels.

## 8.1 RETINAL LOCALISATION OF ITM2B

Previously, the localisation of ITM2B in the retina was detected in the inner retinal layers, with highest intensity in the ganglion cell layer (Audo *et al.*, 2013). In this study, immunofluorescence staining experiments were performed using the ITM2B C-term antibody (Abgent # AP13163b). In young mice (2 weeks), the strongest ITM2B signal was observed in the photoreceptor cell layer, in what looks to be the inner segment (IS): however, some signal was also detected in the outer plexiform layer (OPL), inner plexiform layer (IPL), and the ganglion cell layer (GCL) (Figure 8-2). Heat-induced epitope retrieval (HIER) treatment of adult (6.5 months) mouse sections resulted in a higher intensity ITM2B C-term signal also in the GCL (Figure 8-3), as was previously reported.

It must be emphasised that Audo *et al.* (2013) used the Sigma-Aldrich # HPA029292 antibody. As was indicated in Table 7-1 (Chapter 7), in addition to full-length ITM2B presumably detected by both antibodies, the Sigma-Aldrich # HPA029292 antibody is expected to detect ITM2B fragments that the Abgent # AP13163b antibody is not able to bind to; specifically, the membrane-bound ITM2B N-terminal fragment (NTF) and the ITM2B secreted C-term domain (SCD). It cannot be excluded that the differences in the observed localisation patterns result from the possibility that ITM2B NTF is highly abundant within cellular membranes of the ganglion cell layer due to the ITM2B being more readily processed in these neuronal cells (relative to other cell types). Hence, a stronger signal was detected there with the Sigma-Aldrich # HPA029292 antibody in comparison to other retinal layers.

On the contrary, the similar-looking signal presented in this chapter, in the image of the HIER-treated section (Figure 8-3), would be representative of ITM2B protein prior to ADAM10 cleavage, i.e. inclusive of the BRICHOS domain since the Abgent # AP13163b antibody would not bind to ITM2B NTF (Table 7-1).

Co-staining with TOPORS (Figure 8-4) allowed further dissection of the ITM2B signal observed in Figures 8-2 and 8-3 at the photoreceptor cell layer. In Figure 8-4 the most distinct signal appeared to be located in the inner segments, with some overlap with TOPORS signal at the connecting cilium as indicated by the yellow signal (lower panel). A weaker overlap of the TOPORS-ITM2B signals was also observed in the ganglion cell layer and both plexiform layers.

ITM2B localisation was also tested in primate retinal sections (Figure 8-5). The signals co-localised at regions appearing to correspond to rod photoreceptor outer segments, as indicated by the yellow staining. The ITM2B reactivity is particularly distinct at a region, which

could represent either rod inner segments, or cone outer segments, confirming observations in the mouse retinae (Figures 8-2 and 8-3), and it also seems to be present in the RPE (Figure 8-5, lower panel). Intense ITM2B staining is additionally observed in a few cells in the ganglion cell layer; weak TOPORS signal is observed at the same location. Overall, ITM2B immuno-staining of primate retinal sections demonstrated strong immuno-reactivity in the inner and outer segments of photoreceptor cells as well as the ganglion cell layer.

Overall, in retinal sections obtained from mice, which were two weeks old at time of tissue collection, the most intense ITM2B signal was observed in what appear to be the rod inner segments and/or cone outer segments as well as the plexiform layers (Figures 8-2 A and 8-3).

In summary, ITM2B co-localised with TOPORS in the photoreceptor cells as well as the retinal ganglion cells in both: murine and macaque retinae. These findings are discussed at the end of the current experimental chapter (section 8.4.1).



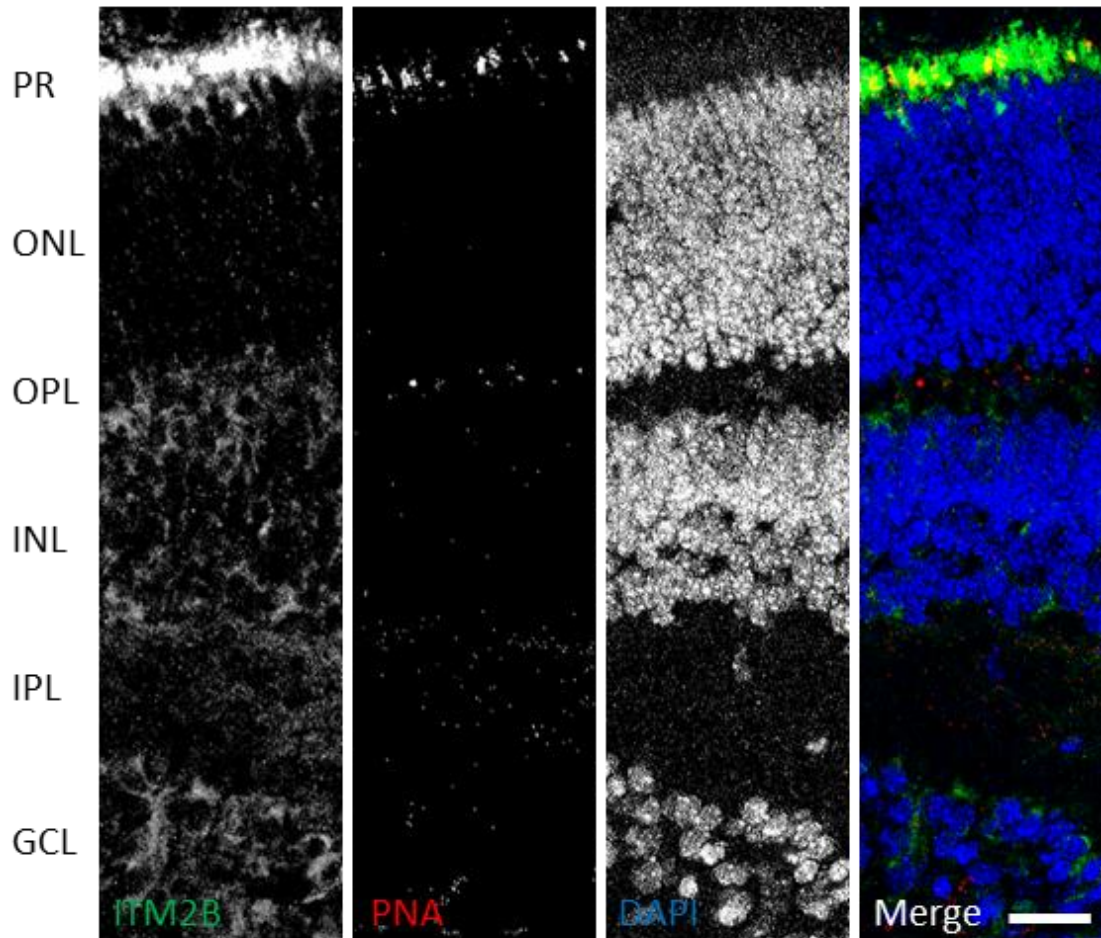


Figure 8-2. ITM2B and PNA (marking cone photoreceptors) staining: C57 Black 6 mouse retina section (2 weeks old at time of tissue collection).

ITM2B and PNA signals overlap partly at the level of the cone cells. Weaker ITM2B signal is additionally observed at both plexiform layers and the GCL. PR, photoreceptor outer and inner segments; ONL, outer nuclear layer; OPL, outer plexiform layer; INL, inner nuclear layer; IPL, inner plexiform layer; GCL, ganglion cell layer. Scale bar: 40  $\mu\text{m}$ . Nuclei stained using DAPI. Confocal microscope images. Secondary antibody control images were collected using the same settings and generated no signals in the red and green channels.

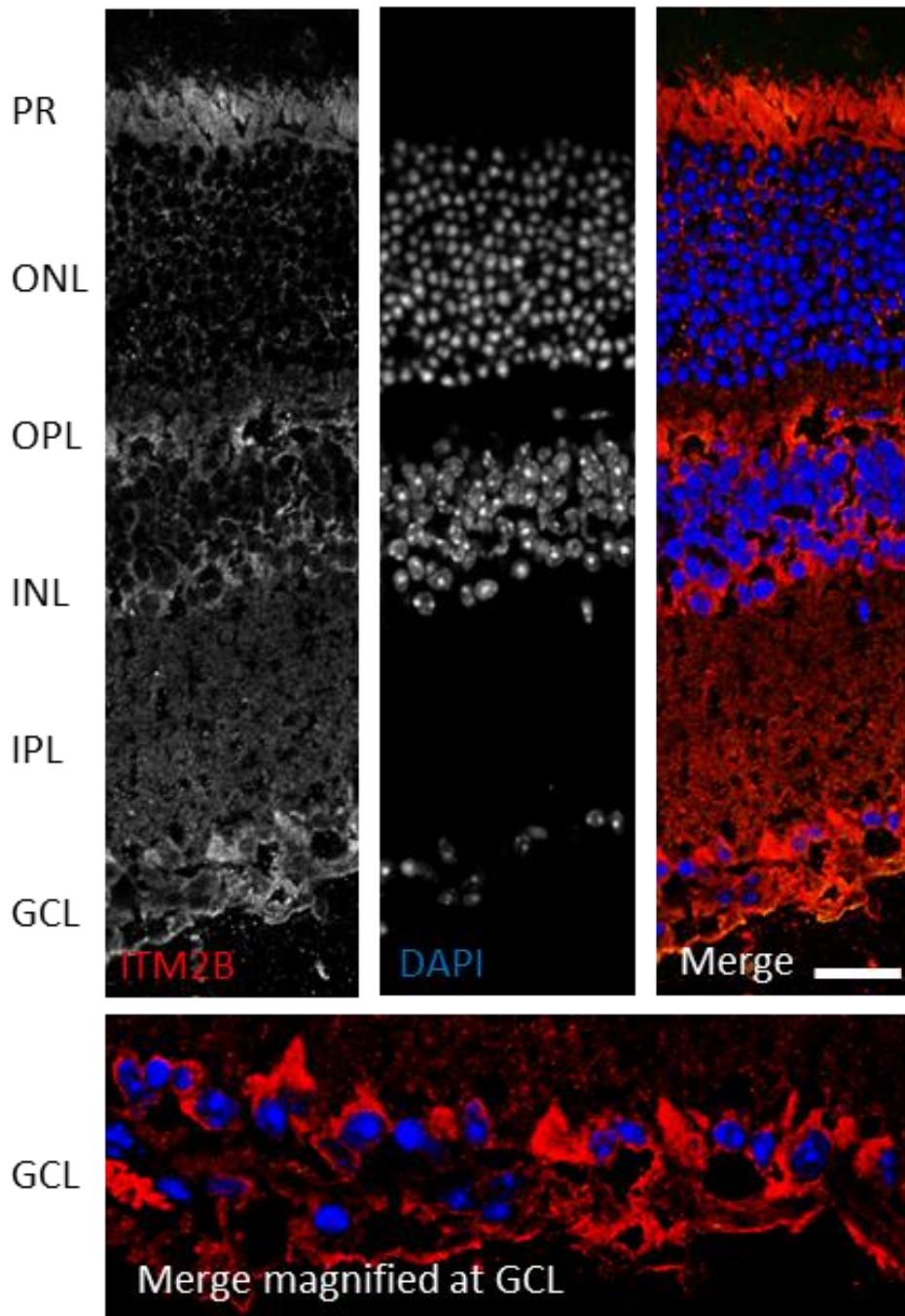


Figure 8-3. ITM2B staining: C57 Black 6 mouse retina section (6.5 weeks old at time of tissue collection) subject to heat-induced epitope retrieval (HIER).

ITM2B immuno-staining is observed throughout the retina; the signal is more distinct in the PR layer, the GCL and the regions of OPL and IPL immediately adjacent to the INL (peri-nuclear staining within the latter is also apparent). The ITM2B immuno-reactive signal at the GCL is magnified in the lower panel. PR, photoreceptor outer and inner segments; ONL, outer nuclear layer; OPL, outer plexiform layer; INL, inner nuclear layer; IPL, inner plexiform layer; GCL, ganglion cell layer. Scale bars: 40  $\mu$ m. Nuclei stained using DAPI. Confocal microscope images. Secondary antibody control images were collected using the same settings and generated no signals in the red and green channels.

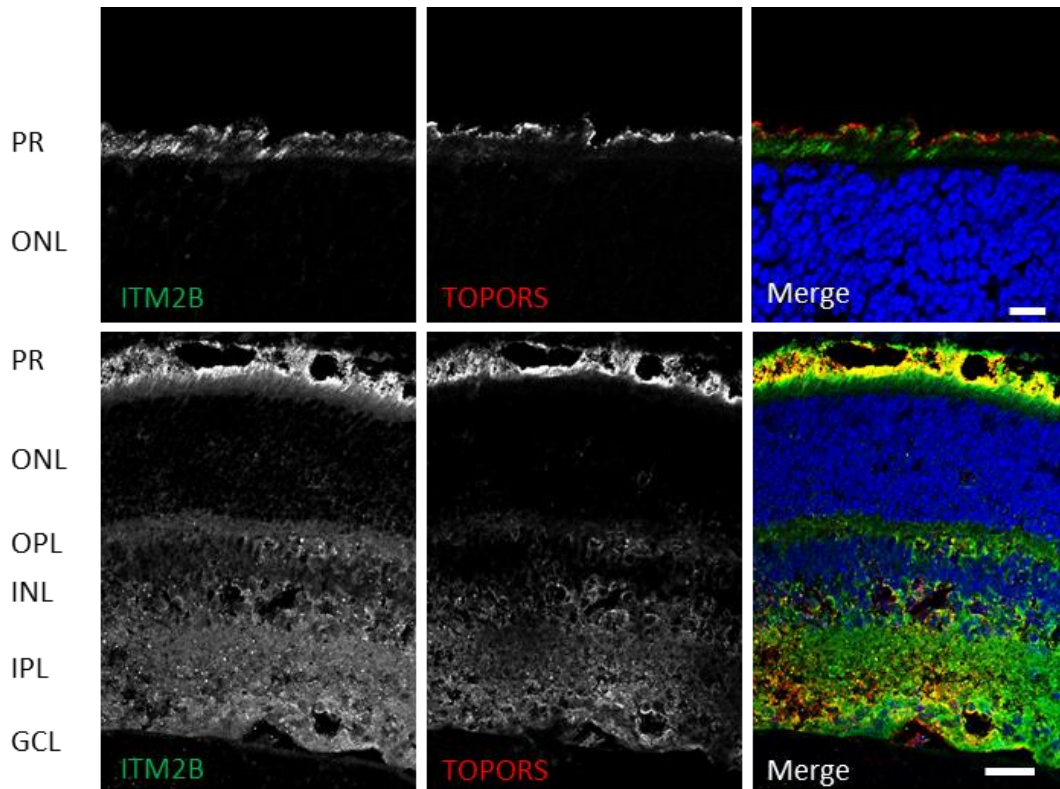


Figure 8-4. TOPORS and ITM2B staining: C57 Black 6 mouse retina sections (2 weeks old at time of tissue collection).

Upper panel: ITM2B and TOPORS signal do not overlap; assuming that TOPORS immuno-staining is specific to the connecting cilium, ITM2B signal is limited to PR inner segments. Lower panel: As in the upper panel, ITM2B signal appears the strongest in the presumed inner segments; however, in this section there is an overlap with TOPORS signal at a region which could represent the connecting cilia and/or the outer segments. Diffuse weak signal, generated by both antibodies is observed in both plexiform layers and the GCL. PR, photoreceptor outer and inner segments; ONL, outer nuclear layer; OPL, outer plexiform layer; INL, inner nuclear layer; IPL, inner plexiform layer; GCL, ganglion cell layer. Scale bars: 38  $\mu$ m. Nuclei stained using DAPI. Confocal microscope images. Secondary antibody control images were collected using the same settings and generated no signals in the red and green channels.

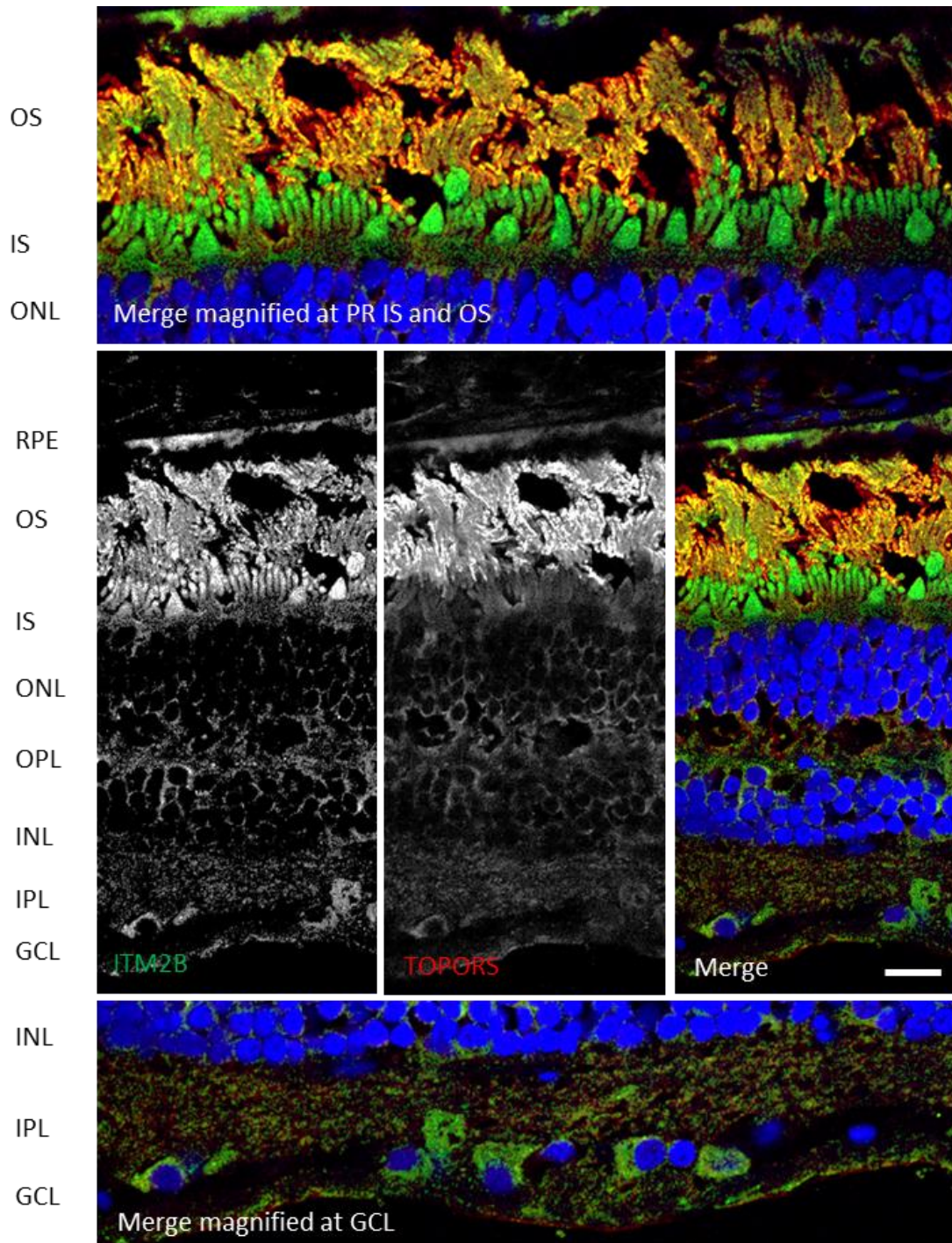


Figure 8-5. ITM2B & TOPORS co-staining in primate (*Macaca fascicularis*) retina section – kindly provided by Prof. Glen Jeffery (section details: #2, 992G, young, 6 & 7, 10  $\mu\text{m}$ , peripheral retina). ITM2B and TOPORS co-localise in the OS and the GCL; TOPORS signal is weaker in the latter, thus the co-localisation is not immediately apparent. OS, rod photoreceptor outer segment; IS, rod photoreceptor inner segment; ONL, outer nuclear layer; OPL, outer plexiform layer; INL, inner nuclear layer; IPL, inner plexiform layer; GCL, ganglion cell layer. Scale bar: 30  $\mu\text{m}$ . Nuclei stained using DAPI. Upper and lower panels show magnified regions of co-localisation. Confocal microscope images. Secondary antibody control images were collected using the same settings and generated no signals in the red channel, but a faint signal was observed in the region of photoreceptor outer segments.

## 8.2 RETINAL LOCALISATION OF PTGDS

Previous studies in chick and rat retinae demonstrated that PTGDS was produced in the RPE, released into the inter-photoreceptor matrix, and taken up by the photoreceptor cells (Yamakawa e Ogino, 1986; Goh *et al.*, 1987; Beuckmann *et al.*, 1996; Shiroma *et al.*, 1996). Here, immunofluorescent staining of the mouse and macaque retinae, using the already described PTGDS antibody, revealed PTGDS immuno-reactivity throughout the retinal layers, but excluding the outer and inner nuclear layers (ONL and INL) (Figures 8-6, 8-7, 8-8 and 8-9).

No co-localisation with PNA was observed (Figure 8-6), whereas co-staining with TOPORS (Figure 8-7) showed some overlap of the two signals at the regions of the inner segment and connecting cilium (indicated by the yellow staining). Further analysis showed consistent signal for PTGDS through the inner segment, co-localising with TOPORS at the region of the connecting cilium (Figure 8-8).

This immuno-staining additionally confirmed the integrity of the outer retina, and revealed faint PTGDS signal from the outer segment. This outer segment signal could have been due to the auto-fluorescence based on the nature of the outer segment themselves; however, there was also some PTGDS signal noted along the axoneme in ciliated hTERT-RPE1 cells (Figure 7-20). Since photoreceptor outer segments (together with the connecting cilia) form highly specialised primary cilia, it is reasonable to assume that the weaker signal seen in the outer segments is true. PTGDS signal was also observed at the plexiform layers, as in earlier figures.

Staining of the primate retinal section revealed PTGDS signal throughout the entire retina (but excluding the inner and outer nuclear layers), with immuno-reactivity observed at the RPE, photoreceptor cells, both plexiform layers and the ganglion cell layer (Figure 8-9). PTGDS and TOPORS signals were co-localising at the photoreceptor outer segments. Some TOPORS signal, which overlapped with PTGDS signal, was also observed in the plexiform layers and the ganglion cell layer, but it was much less abundant than the PTGDS reactivity.

In summary, PTGDS signal was consistently observed in the plexiform layers, the ganglion cell layer and the inner segment, connecting cilium region and outer segment of photoreceptors in both: mouse and primate retinae. Furthermore, in the inner segment/connecting cilium region in mouse the PTGDS and TOPORS signals overlap. Additionally, signal in the adult mouse retina appears much stronger than in sections from the young mouse or the primate. These findings are discussed at the end of the current experimental chapter (section 8.4.2).

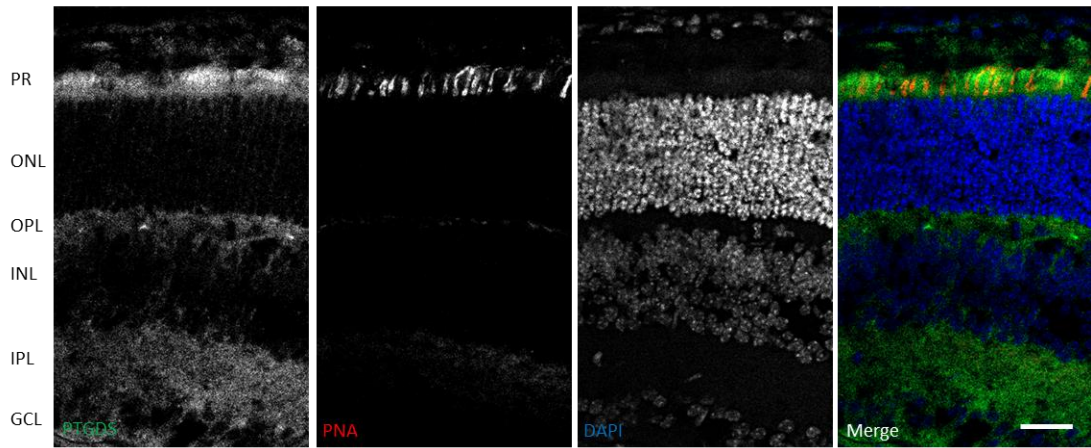


Figure 8-6. PTGDS and PNA staining: C57 Black 6 mouse retina section (2 weeks old at time of tissue collection).

Strongest PTGDS signal is observed in both the plexiform layers, and at the GCL. PTGDS immunoreactivity at the PR layer is weaker. PR, photoreceptor outer and inner segments; ONL, outer nuclear layer; OPL, outer plexiform layer; INL, inner nuclear layer; IPL, inner plexiform layer; GCL, ganglion cell layer. Scale bar: 30  $\mu\text{m}$ . Nuclei stained using DAPI. Confocal microscope images. Secondary antibody control images were collected using the same settings and generated no signals in the red and green channels.

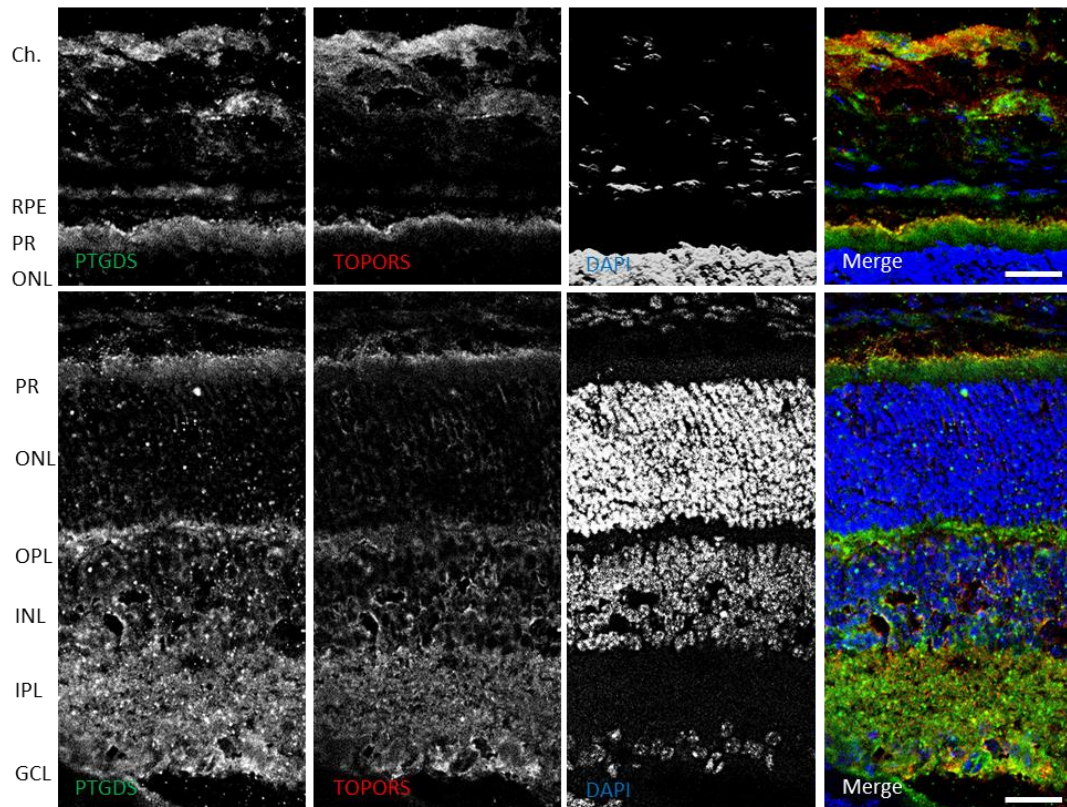


Figure 8-7. TOPORS and PTGDS staining: C57 Black 6 mouse retina sections (2 weeks old at time of tissue collection).

Some overlap of PTGDS and TOPORS signal is observed at the PR layer, possibly at the interface between the inner segments and connecting cilia (both: upper and lower panels). Strong yellow co-localisation signal was also detected in the region most likely to be the choroid (upper panel). TOPORS and PTGDS also co-localised at the GCL; strong PTGDS reactivity was also observed throughout both plexiform layers (lower panel). Ch., choroid; RPE, retinal pigment epithelium; PR, photoreceptor outer and inner segments; ONL, outer nuclear layer; OPL, outer plexiform layer; INL, inner nuclear layer; IPL, inner plexiform layer; GCL, ganglion cell layer. Scale bars: 38  $\mu$ m. Nuclei stained using DAPI. Confocal microscope images. Secondary antibody control images were collected using the same settings and generated no signals in the red and green channels.

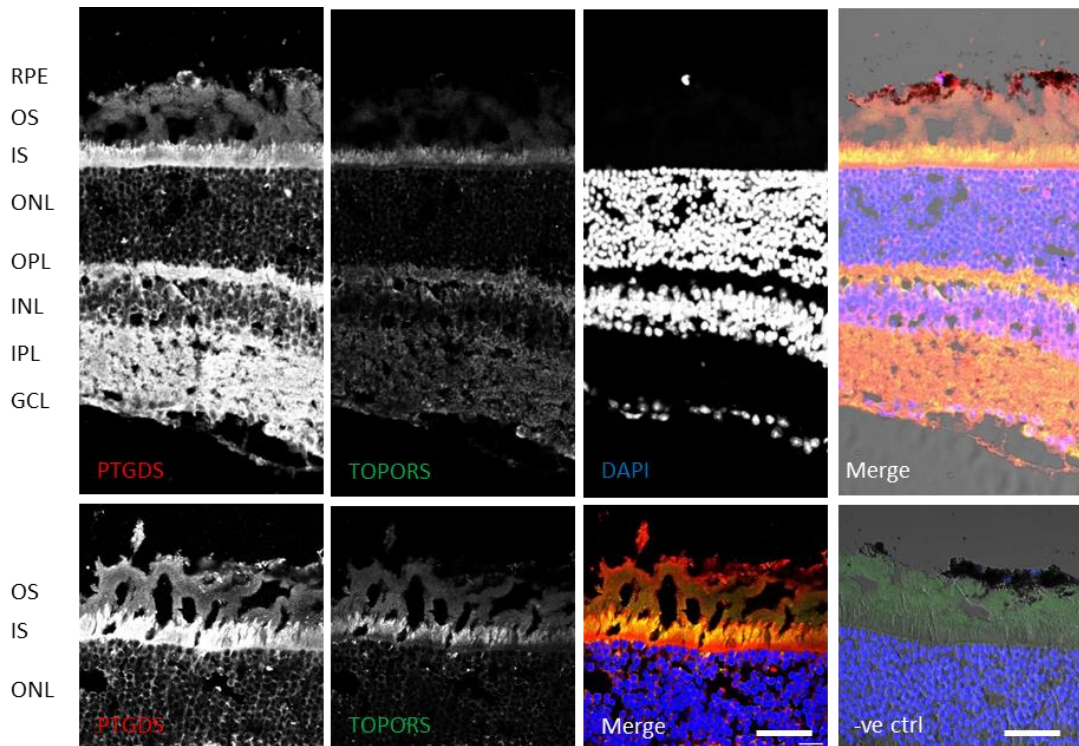


Figure 8-8. PTGDS and TOPORS staining in C57 Black 6 mouse retina sections (6.5 months old at time of tissue collection).

Strong PTGDS signal observed throughout the retinal layers (apparently more intense than in young mouse retina: Figures 8-6 and 8-7), co-localising with TOPORS at the IS and/or the connecting cilia (magnified in the lower panel). RPE, retinal pigmented epithelium; OS, rod photoreceptor outer segment; IS, rod photoreceptor inner segment; ONL, outer nuclear layer; OPL, outer plexiform layer; INL, inner nuclear layer; IPL, inner plexiform layer; GCL, ganglion cell layer. Top panel scale bar: 30  $\mu\text{m}$ . Bottom panel scale bars: 8  $\mu\text{m}$ . Nuclei stained using DAPI. Confocal microscope images. Secondary antibody control images were collected using the same settings and generated no signals in the red channel; some faint signal was observed in the green channel (shown in the lower panel: -ve ctrl, negative control).



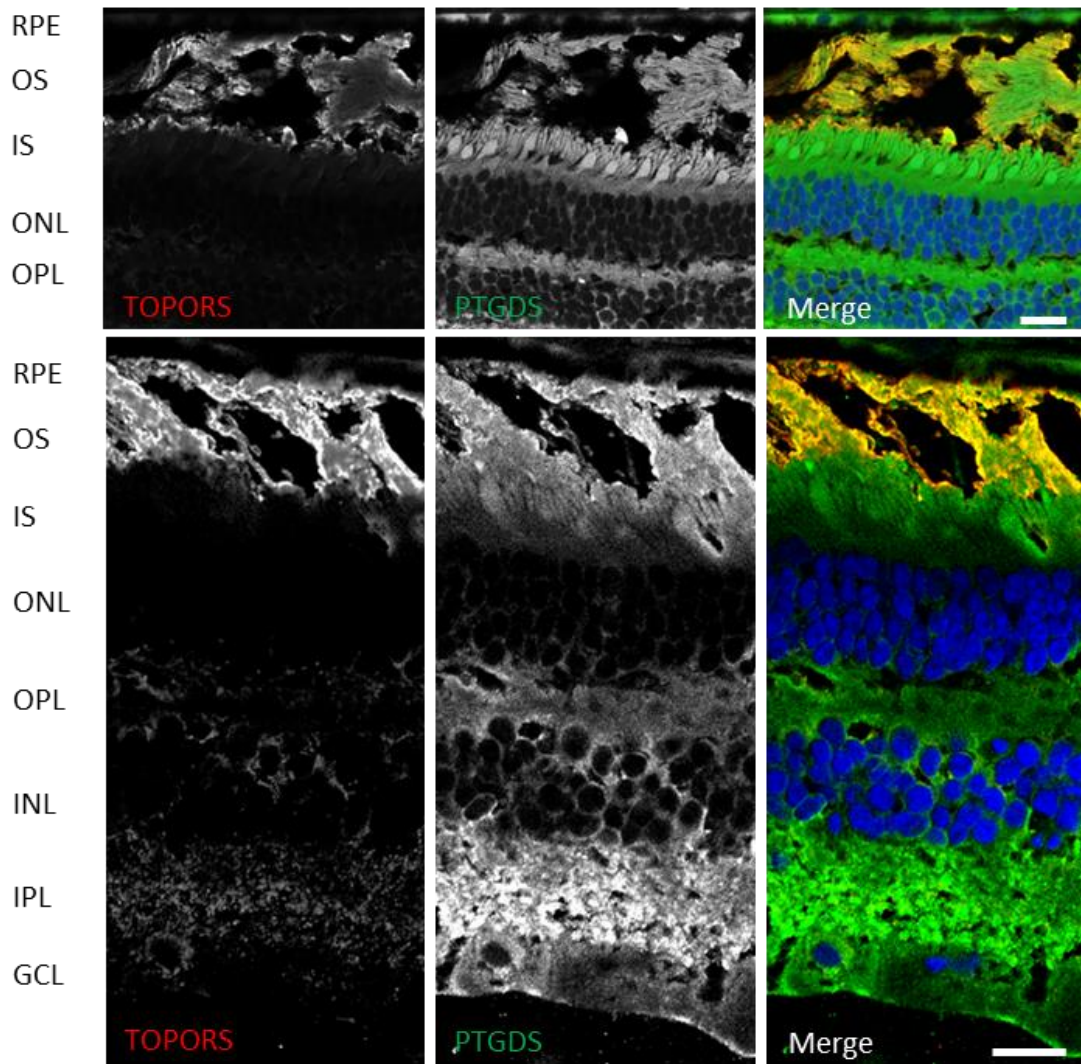


Figure 8-9. PTGDS & TOPORS staining in primate (*Macaca fascicularis*) retina sections (slide details: #2, 992G, young, 6 & 7, 10  $\mu$ m, periphery – kindly provided by Prof. Glen Jeffery). Signals co-localise at OS (both: upper and lower panels) as well as GCL, where TOPORS reactivity was weaker (lower panel). The PTGDS staining was additionally visible at plexiform layers, and it was especially distinct at the IPL. RPE, retinal pigment epithelium; OS, rod photoreceptor outer segment; IS, rod photoreceptor inner segment; ONL, outer nuclear layer; OPL, outer plexiform layer; INL, inner nuclear layer; IPL, inner plexiform layer; GCL, ganglion cell layer. Scale bar: 30  $\mu$ m. Nuclei stained using DAPI. Confocal microscope images. Secondary antibody control images were collected using the same settings and generated no signals in the red channel, but a faint signal was observed in the region of photoreceptor outer segments.

### **8.3 RETINAL LOCALISATION OF PSMC1**

Interestingly, no PSMC1 staining was observed in retinal sections of young (2 weeks old) mice (data not shown). This may be due to inadequate tissue fixation and putative lack of compatibility with the antibody; however, it could also reflect a genuine absence of the PSMC1 protein from the young mouse retina. Attempts to optimise the antibody conditions (i.e. by antigen retrieval, data not shown) did not alleviate this issue.

Staining using the adult mouse retina did however show a signal: the signal observed in the adult appears to be very specifically localised at the interface between the photoreceptor outer segment and the RPE layer (Figure 8-10). This was considered a very promising observation since PSMC1 acts as a regulatory subunit of the proteasome. Moreover, the PSMC1 is involved in the ER-phagosome pathway, in which the ER fuses with the cell membrane to aid in forming nascent phagosomes. This function is conserved in PSMC1 orthologues of yeasts, plants, rodents and humans (UniProtKD).

Thus, its localisation to the tips of the outer segment and/or the apical RPE1 surface could indicate that it is actively involved in recycling of the tips of the outer segments.

The PSMC1 immuno-reactivity at the RPE-OS interface was also observed, when the retinal sections were subject to heat-induced epitope retrieval (HIER). However, this treatment additionally resulted in PSMC1 signal being detected in the photoreceptor inner segments (Figure 8-11). Immuno-staining of a primate retinal section (not subject to HIER treatments) was attempted, but it did not yield positive results (data not shown).

Overall, findings described in this section indicate that PSMC1 is possibly down-regulated in young retinae, as PSMC1 immuno-reactivity was not detected in retinal cryo-sections obtained from the two-week-old mouse (data not shown). Alternatively, this could have been a false negative result, obtained, for instance, due to the antigen being inaccessible to the antibody. The latter could also explain a lack of reactivity with the primate retinal section (data not shown).

In adult mouse retinal sections strong PSMC1 signal was observed at the RPE-OS interface. Additional PSMC1 immuno-staining was detected in the inner segments of photoreceptors, following a heat treatment of the cryo-sections, aiming to retrieve the antigens. These findings are discussed at the end of the current experimental chapter (section 8.4.3).

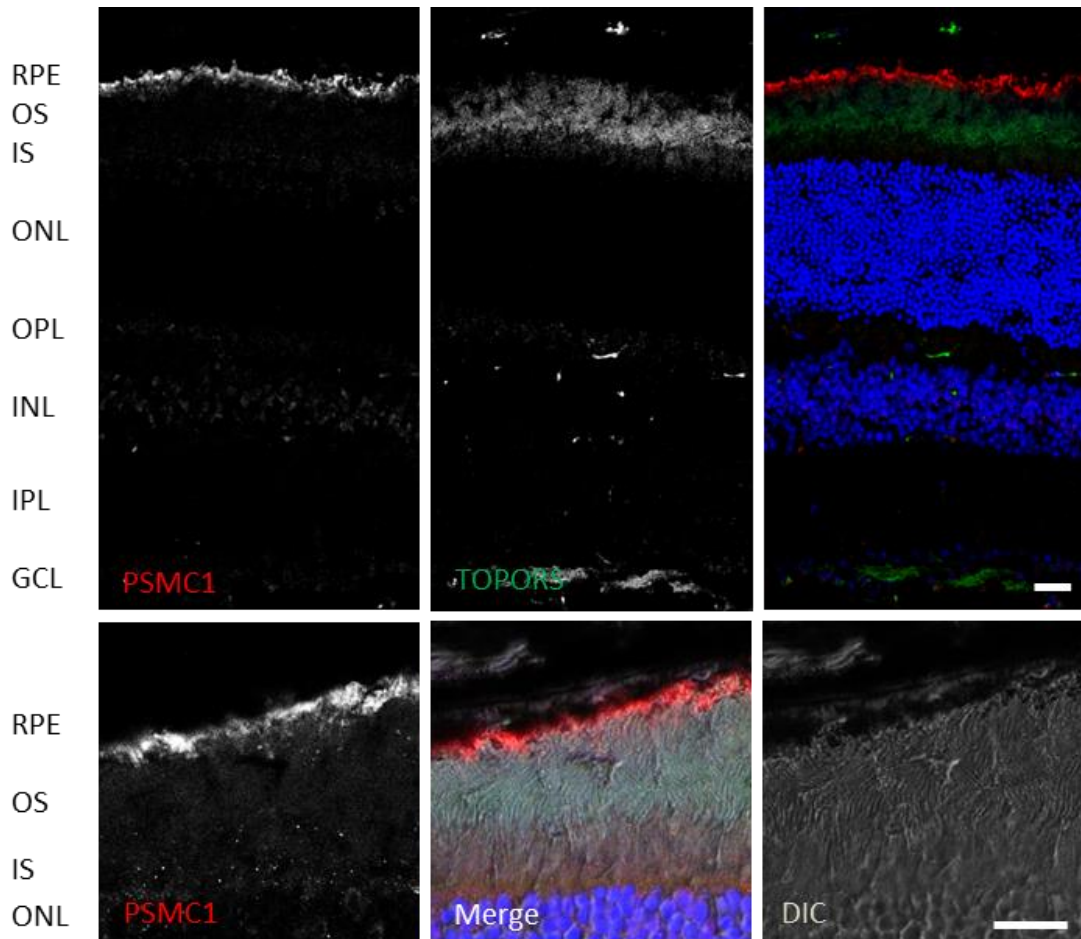


Figure 8-10. PSMC1 and TOPORS co-staining: C57 Black 6 mouse retina sections (6.5 months old at time of tissue collection).

Upper panel: PSMC1 signal was observed at the interface between rod OS and the RPE; whereas TOPORS signal was observed throughout the inner and outer segments (IS and OS) and it was most intense at their interface where the connecting cilia (CC) reside; additional TOPORS signal was seen in the retinal ganglion cell layer (GCL). Scale bar: 30  $\mu\text{m}$ . Lower panel: PSMC1 signal was observed at the interface between rod OS and the RPE; localisation was determined using the DIC image. Scale bar: 10  $\mu\text{m}$ . RPE, retinal pigment epithelium; OS, rod photoreceptor outer segment; IS, rod photoreceptor inner segment; ONL, outer nuclear layer; OPL, outer plexiform layer; INL, inner nuclear layer; IPL, inner plexiform layer; GCL, ganglion cell layer. Nuclei stained using DAPI. Confocal microscope images. Secondary antibody control images were collected using the same settings and generated no signals in the red and green channels.

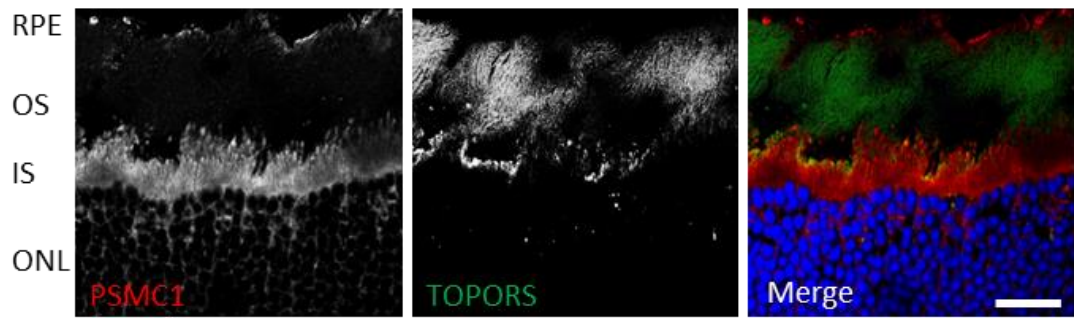


Figure 8-11. PSMC1 and TOPORS co-staining: C57 Black 6 mouse retina section (6.5 months old at time of tissue collection) subject to heat-induced epitope retrieval (HIER).

Some PSMC1 immuno-reactivity is apparent at the interface between the OS and the RPE, as was observed in sections not treated to retrieve antigens (Figure 8-10). However, following antigen retrieval, strong PSMC1 signal was observed in the IS. RPE, retinal pigment epithelium; OS, rod photoreceptor outer segment; IS, rod photoreceptor inner segment; ONL, outer nuclear layer; OPL, outer plexiform layer; INL, inner nuclear layer. Secondary antibody control images were collected using the same settings and generated no signals in the red and green channels.

## 8.4 DISCUSSION

The current chapter described data suggesting that, in mammalian retinae, ITM2B, PTGDS and PSMC1 could all interact with TOPORS at the basal body of the photoreceptor connecting cilium, based on the observed localisation patterns (Figures 8-4, 8-7, 8-8 and 8-11). Furthermore, immuno-reactivity of in the primate retinal sections demonstrated strong TOPORS signal in the photoreceptor outer segments, which overlapped with ITM2B as well as PTGDS signals (Figures 8-5 and 8-9, respectively).

ITM2B immuno-reactivity was additionally observed at the ganglion cell layer (Figures 8-2, 8-3, 8-4 and 8-5), where the signal overlapped with TOPORS staining (Figures 8-4 and 8-5: TOPORS signal weaker in comparison to ITM2B signal). PTGDS immuno-staining also showed reactivity in the plexiform layers and the ganglion cell layer, where co-localisation was seen with the weaker TOPORS signal (Figures 8-7, 8-8 and 8-9).

PSMC1 signal was observed at the interface of distal regions of photoreceptor outer segments and the RPE (Figure 8-10), as well as in photoreceptor inner segments (Figure 8-11), but the latter was observed only following antigen retrieval by heat treatment. Attempts to elucidate the PSMC1 immuno-staining pattern in young mice (2 weeks of age), or in primate retinae, were unsuccessful (data not shown).

A summary of the observed localisation patterns is included in Table 8-1, whereas the putative functions and significance of TOPORS interactors at the observed retinal layers are discussed individually in the following sections.

The phenotype associated with *TOPORS* mutations in human appears to affect predominantly the retina, and, at later stages, also the choroid (Chakarova *et al.*, 2007; Chakarova *et al.*, 2011). This phenotype have been puzzling as, in the retina, TOPORS was shown to localise to the basal body of the connecting cilium in rod photoreceptor cells (Chakarova *et al.*, 2011).

Given the fact that dysfunctions in components of the intraflagellar transport (IFT) system previously showed to affect cilia function overall, leading to syndromic ciliopathies, rather than being limited to photoreceptors (reviewed in: Sung e Chuang, 2010), it should be concluded that TOPORS is not involved in transport of cargo through the cilium, or rather from the cilium to the cytoplasm. The association of TOPORS with the dynein–dynactin complex proteins, demonstrated by Chakarova *et al.* (2011), could have, consequently, represented the involvement of TOPORS in transport of cargoes from the cytoplasm towards the base of the cilium.

Table 8-1. Summary of interactors’ localisation in retinal tissues.

Key: PR, photoreceptor; PNA, peanut agglutinin; RPE, retinal pigment epithelium; OS, rod photoreceptor outer segment; CC, connecting cilium; IS, rod photoreceptor inner segment; ONL, outer nuclear layer; OPL, outer plexiform layer; INL, inner nuclear layer; IPL, inner plexiform layer; GCL, ganglion cell layer; HIER, heat-induced epitope retrieval.

	ITM2B	PTGDS	PSMC1
<b>Mouse sections – 2 weeks old</b>	Localised at the PR cell layer, where partial signal overlap was observed with PNA (cone marker) (Figure 8-2) and TOPORS at the distal/outer part of PR layer, indicating it could be the CC and/or OS (Figure 8-4, lower panel). Localised at the plexiform layers (both OPL and IPL) and the GCL (Figure 8-2), where the signal appeared granular and partial signal overlap was observed with TOPORS (Figure 8-4, lower panel). In one section ITM2B and TOPORS signals were observed adjacent to each other, but not co-localising (Figure 8-4, upper panel).	Localised at both plexiform layers (where some higher intensity granular signals were observed overlaying the overall diffuse signal: Figure 8-7), the GCL and the PR cell layer (Figure 8-6, lower panel), as well as the RPE layer (Figure 8-7). At the PR layer PTGDS did not co-localise with PNA (cone marker; Figure 8-6); however, it did co-localise with TOPORS at the distal/outer part of PR layer, indicating it could be the CC and/or OS (Figure 8-7). Co-localisation of PTGDS and TOPORS signals was also observed within cells of the choroid (Figure 8-7; upper panel).	No PSMC1 signal was observed at all (data not shown).
<b>Mouse sections – 6.5 months old</b>	In sections subject to HIER, ITM2B immuno-staining was observed throughout the retina, where the signal was most distinct within the PR layer, the GCL and the regions of OPL and IPL immediately adjacent to the INL (Figure 8-3).	Localised at the plexiform layers (both OPL and IPL), the GCL and at the PR cell layer (Figure 8-8). At the PR layer PTGDS co-localised with TOPORS in a pattern strongly indicative of the CC (Figure 8-8; lower panel).	Localised at the RPE-OS interface only (Figures 8-10). In sections subject to HIER, PSMC1 immuno-staining was observed in IS as well as the RPE-OS interface; here, an overlap with TOPORS signal was seen at the apical IS regions (Figure 8-11).
<b>Macaque sections – young adult</b>	Co-localised with TOPORS at PR cell layer, resembling the OS, the RPE, and the GCL (peri-nuclear signals). Additionally localised at plexiform layers (both OPL and IPL), where the signal appeared granular; higher intensity signals were also observed at the interface between OPL and INL (Figure 8-5).	Localised at both plexiform layers (stronger signal at IPL), the GCL and at the PR cell layer, as well as the RPE layer (Figure 8-9); signal intensity was the greatest in the OS and in the IPL. TOPORS was observed in the PR OS layer and, to a lesser extent, in the plexiform layers and the GCL. PTGDS and TOPORS co-localised at the OS layer (both strong signals), as well as the GCL (strong PTGDS signal and weak TOPORS signal).	No PSMC1 signal was observed at all (data not shown).

This would be supported by the proteins' Gene Ontology (GO) Biological Processes and Functions, which include:

- Retrograde transport from endosome to Golgi apparatus (p150<sup>glued</sup>, Dynactin subunit 1: Q14203);
- Organelle organisation (p50-dynamitin; dynactin subunit 2: Q13561);
- Vesicle transport along microtubules (cytoplasmic dynein 1 intermediate chain 1: O14576);
- Microtubule-based movement (cytoplasmic dynein 1 intermediate chain 2: Q13409).

Whereas in most cells, which possess primary cilia, a certain extent of redundancy probably exists regarding protein transport towards the cilium, in photoreceptors an impairment of one of the transport systems could be expected to lead to degeneration due to the unusual (for terminally differentiated cells) requirement of these cells for constant biosynthesis and delivery of rhodopsin to their outer segments. In fact, Kong *et al.* (2013) previously showed in mice that a knock-down of dynein light intermediate chain (DLIC, DYNC1LI), a component of the dynein multimer, leads to photoreceptor dysfunction; however, it is not lethal despite ubiquitous expression and function. Specifically, the findings showed that the knock-down resulted in impaired photoreceptor ciliogenesis, as well as an impaired transport of outer segment proteins from the Golgi apparatus to the basal body of the cilium.

Furthermore, the mouse model showed that deficiency of the dynein light intermediate chain resulted in defective trafficking of Rab11 vesicles to the base of the cilium in photoreceptor cells (Kong *et al.*, 2013). The photoreceptor outer segments have a great biosynthetic requirement not only for proteins (mostly rhodopsin), but also for lipids. Mayhew and Astle (1997) showed in rat that in order to maintain the photoreceptor outer segment renewal, 77 cm<sup>2</sup> of disc membrane must be synthesised per day per rat retina (cited in: Sung e Chuang, 2010) containing 3 x 10<sup>7</sup> photoreceptors. Malfunctioning vesicular trafficking to the base of the connecting cilium, which TOPORS appears to be involved in, would negatively affect the renewal of the disc membranes in photoreceptors outer segments.

The associated GO terms (UniProtKB), specifically melanosome transport, also suggest a key role for the dynein–dynactin complex along with the associated TOPORS protein in the retinal pigmented epithelial (RPE) layer due to the involvement of p150<sup>glued</sup> and p50-dynamitin in the above-mentioned process. A dysfunction of the melanosome transport in the RPE would make this cell layer more prone to light-induced stress, and consequently deterioration of RPE function and, eventually, retinal degeneration. This process could to some extent occur

naturally in aging RPE cells, contributing to symptoms of age-related macular degeneration (AMD). The age component would explain why *TOPORS* mutations do not always manifest in early age, especially that protein quality control processes decline with age (Balch *et al.*, 2008; Rezvani *et al.*, 2012).

On the other hand, impaired melanosome transport, could help explain the perivascular retinal dystrophy, observed in children affected by *TOPORS* mutations. With age this phenotype disappeared (but the retina also degenerated further), suggesting that possibly the melanosomes were being subject to autophagy within the RPE cells. Once, this removal system became over-loaded, the RPE cells would begin to die, but they melanin pigment would be visible. Nonetheless, it would be more difficult to explain why this type of dystrophy should display only a peri-vascular pattern. This concept will be evaluated further in section 8.4.3 of this discussion in context of the PSMC1 protein being involved in the ER-phagosome pathway (function conserved in eukaryotes: UniProtKD) as well as in responses to light-induced stress, demonstrated in plant cells (Lee, K. H. *et al.*, 2012).

Finally, given the nature and purpose of photoreceptor cells, it cannot be excluded that the localisation of *TOPORS*' interactors within the photoreceptor cells, is at least partly dependent on light exposure. The light-dependent translocation of transducin, arrestin and recoverin have been established and characterised (Calvert *et al.*, 2006). The light-driven protein translocation process also seems to happen exclusively in photoreceptor cells; notably, it is conserved in the *Drosophila* rhabdomeres, which are actin-based microvilli (Sung e Chuang, 2010), rather than microtubule-based cilia, as is the case in vertebrate photoreceptors, suggesting convergent evolution, and thus an important function.

*TOPORS* was also previously observed to be differentially localised within photoreceptor cells, depending on whether the retina had been exposed to light or not. Specifically, in light-adapted mice *TOPORS* was always observed at the connecting cilium of photoreceptor cells, whereas its localisation was widespread in the retinae of dark-adapted mice, and, notably, it excluded the connecting cilium (Dr Amna Z. Shah: personal communication). It could be speculated that the novel interactors of *TOPORS* may display analogous light-dependent localisation patterns.



### 8.4.1 EVALUATION OF ITM2B LOCALISATION

In all three types of sections tested: the young two-week-old mouse, the adult mouse and the young adult macaque similar ITM2B reactivity pattern was observed. Specifically, ITM2B and TOPORS co-localised in the apical area of photoreceptor inner segments, or the connecting cilia, in mice, and in the outer segments in primate, as well as fragments of the plexiform layers and the ganglion cell layer. No distinct age-related staining pattern was observed, however, HIER treatment significantly enhances ITM2B reactivity in the adult mouse. The focus of this discussion is on the photoreceptor localisation due to the hypothetical key role of TOPORS at the connecting cilium.

Firstly, it appears that the localisation of ITM2B at the apical inner segment region, possibly the ciliary basal body, is not in agreement with findings from the cellular localisation studies (Chapter 7). In the hTERT-RPE1 cells it was shown that ITM2B was associated with centrioles in dividing cells (Figures 7-6, 7-7, 7-8, 7-9 and 7-10); however, it did not localise to the base of primary cilium in quiescent ciliated cells (Figure 7-11). Nonetheless, it cannot be excluded that the result from the cell culture studies as well as the finding from the tissue immuno-staining are both true. For example, it was previously shown by Chuang and Sung (1998) that targeting of rhodopsin to the primary cilia is less efficient in ciliated epithelial cells, in comparison to photoreceptors. Furthermore, the apical localisation of ITM2B in photoreceptors may depend of a post-translational modification, which perhaps does not occur in the hTERT-RPE1 cells.

For instance, Li *et al.* (2012) showed in worm that targeting of sensory receptors to primary cilia depends on SUMOylation of Arl-13 (homologue of Arl13b). TOPORS did not interact with Arl13b in the Y2H screen (which could also be a false negative results, as these can never be excluded); however, it might be involved in SUMOylation of another small GTPase, involved in vesicular trafficking to primary cilia, or specifically the photoreceptor connecting cilia, which in turn could affect the ciliary targeting of other proteins, such as ITM2B. It could be speculated that the pathways of protein interactions and or modifications, necessary for ITM2B targeting to cilia, occur only in neuronal cell types, hence, no localisation to base of the cilium was observed in Figure 7-11.

Furthermore, it was shown that the phosphorylation status of small GTPases involved in ciliary targeting could influence their affinity for ciliary-targeted cargoes; e.g. Rab8-GDP binds ciliary-targeting sequences (CTS) of other proteins more readily than Rab8-GTP does (Hsiao, Tuz e Ferland, 2012). ITM2B possesses a total of three conserved CTS motifs of the same type as

the one found in rhodopsin, i.e. 'VxPx' (Figures 8-12 and 8-13). The precise location of these motifs within the ITM2B protein structure was shown in Figure 6-5 (Chapter 6).

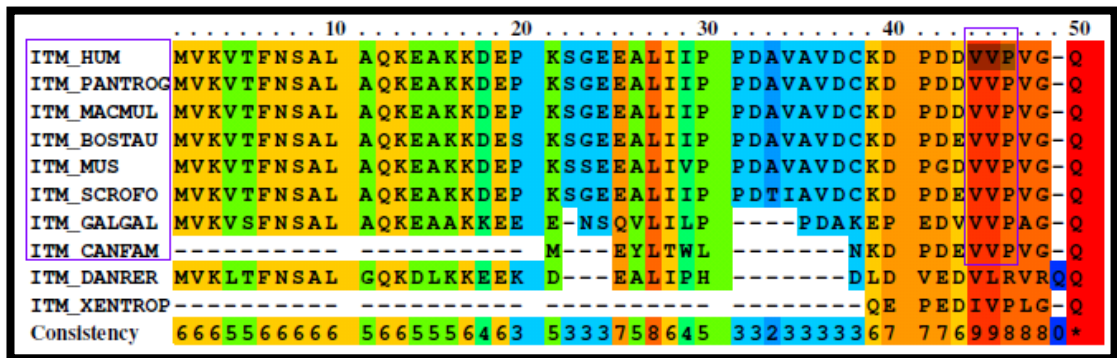


Figure 8-12. ITM2B CTS#1: AA44 – AA46. Species and CTS are boxed inside purple rectangles. Key: Hum, human; Xentrop, western clawed frog (*Xenopus tropicalis*); Musmus, mouse (*Mus musculus*); Pantrog, common chimpanzee (*Pan troglodytes*); Macmul, rhesus macaque (*Macaca mulatta*); Bostau, cattle (*Bos taurus*); Canfam, family Canidae (includes dogs and wolves); Scrofo, wild boar (*Sus scrofa*); Danrer, zebrafish (*Danio rerio*); Galgal, chicken (*Gallus gallus*); Dromel, fruit-fly (*Drosophila melanogaster*). Note: p.Val44del is reported on Ensembl (in frame); source: NHLBI Exome Sequencing Project (ESP). PRALINE alignment – a modified snapshot (Simossis, Kleinjung e Heringa, 2003).

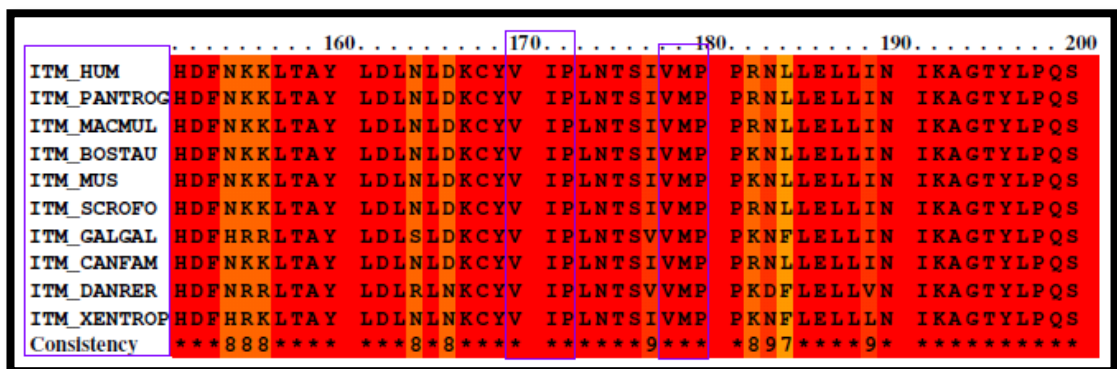


Figure 8-13. ITM2B CTS#2 and #3. Species and CTS are boxed inside purple rectangles. Key: Hum, human; Xentrop, western clawed frog (*Xenopus tropicalis*); Musmus, mouse (*Mus musculus*); Pantrog, common chimpanzee (*Pan troglodytes*); Macmul, rhesus macaque (*Macaca mulatta*); Bostau, cattle (*Bos taurus*); Canfam, family Canidae (includes dogs and wolves); Scrofo, wild boar (*Sus scrofa*); Danrer, zebrafish (*Danio rerio*); Galgal, chicken (*Gallus gallus*); Dromel, fruit-fly (*Drosophila melanogaster*). Note: p. Ile167Thr and p.Val174Ile are reported on Ensembl; source: dbSNP (NCBI). [AA numbers refer to human protein sequence on Ensembl]. The missense change resulting in Ile instead Thr in CTS#1 would probably not affect the ciliary targeting, whereas the change to CTS#2 may well cause disruption as Val is a conserved part of the consensus sequence. PRALINE alignment – a modified snapshot (Simossis, Kleinjung e Heringa, 2003).

Secondly, it is important to emphasise that lack of peri-nuclear ITM2B immuno-reactive staining in rod photoreceptors is not conflicting with the perinuclear staining evident in the second and third order neurons of the inner retinal layer and the ganglion cell layer (Figures 8-2, 8-3, 8-4 and 8-5). Being a membrane-bound protein, ITM2B is synthesised on

the ER membranes and processes in the Golgi apparatus. In canonical nerve cells these membranous organelles are found within the cell body proximally to the nucleus, which is also observed in dividing cells. Photoreceptors are highly specialised neurons, modified in such a way that, except for the nucleus, which resides in the cell body like in typical neurons, the majority of its organelles are located within the inner segments. Hence, the observed retinal localisations actually provide indirect evidence that ITM2B is very likely associated with membranes of the ER and the Golgi body.

It should also be noted that in some of the photographed mouse sections, the ITM2B immunostaining appears restricted to the inner segment and is only proximal to, but not overlapping with, the TOPORS signal marking the connecting cilium (Figure 8-4, upper panel). On the other hand, TOPORS-ITM2B co-staining of other sections from the same animal demonstrated an undisputable co-localisation (Figure 8-5, lower panel). As both of the presented sections originated from the same young mouse, it cannot be speculated that this apparent inconsistency of signals is due to putative light-induced translocation, which would have been an attractive hypothesis. However, it could be speculated that a differential expression gradient of *ITM2B* occurs across the retina, resulting in one localisation pattern nearer the central retina, and changing towards the periphery. Such a spatial expression patterning was previously shown in mouse cones for genes encoding the M and S opsins (Applebury *et al.*, 2000), therefore, it should not be excluded that similar differential patterning occurs also in case of other genes and in other retinal cell types.

Additionally, the ITM2B signal within the plexiform layers appeared granular both in murine and primate retinae (Figures 8-2, 8-3 and 8-5), and appeared especially distinct in the primate (Figure 8-5). This granular staining pattern could be indicative of the association of ITM2B with intracellular vesicles, as was previously demonstrated in neuronal cell cultures (Choi *et al.*, 2004). Nonetheless, according to these previously published findings, only the smallest carboxy-terminal, CTPP (Figure 6-5, Chapter 6) fragment of ITM2B is transported within the vesicles along the neuronal axons. Only a few amino acids from this CTPP are included within the epitope, which was used to raise the Abgent # AP13163b: ITM2B C-term antibody, therefore, it is unlikely that the signal observed in the retinal sections corresponds to this fragment on its own. Nonetheless, impairment of vesicular trafficking has been shown to be a significant contributor to retinal degenerations (Sung e Chuang, 2010; Wright *et al.*, 2010).

As was already specified, photoreceptor cells are modified neurons, and possess some unique features, such as the outer segment acting as a highly specialised primary cilium. This

exceptional organelle is the site of onset of photoreception, i.e. when photons of light hit the opsin molecules within the outer segments, this triggers a cascade of reactions, which result in visual perception upon reaching the brain. Remarkably, photoreceptors lack dendrites, which serve as signal receivers in the canonical neuronal types. Choi *et al.* (2004) showed that in neuronal cell culture, ITM2B stimulates neurite outgrowth. It would be interesting to investigate whether it could similarly stimulate primary cilia growth. If the answer was positive, this would allow speculating that the role of ITM2B in photoreceptor cells is to stimulate the growth of the outer segment, which is a specialised primary cilium, and is functionally analogous to dendrites in context of neurons. The outer segments undergo constant renewal necessary due to the light-induced oxidative stress, which they encounter, and stimuli, which trigger this constant outer segment production must persist for correct photoreceptor functioning.

If the above hypothesis was true, then the role of TOPORS in the described process would be purely regulatory. It would be expected to degrade ITM2B and/or its fragment(s), when the latter is no longer needed, or when less of it is needed. Such a role would be supported by the Y2H study results, which showed that ITM2B interacted most strongly with the N-term TOPORS fragment, conveying its E3 ubiquitin ligase activity, as well as with the C-term TOPORS, within which the mutational hotspot is located (Chapter 5, Table 5-16).

#### **8.4.2 EVALUATION OF PTGDS LOCALISATION**

It was initially surprising to observe PTGDS reactivity in the inner retinal layers (Figures 8-6, 8-7, 8-8 and 8-9) since in a rat retina the immuno-staining for this enzyme generated signal mostly in the RPE and, to a lesser extent, in the photoreceptor outer segments, but not in other regions of this tissue (Beuckmann *et al.*, 1996). Nonetheless, in an earlier study, Goh *et al.* (1987) demonstrated PTGDS ('prostaglandin D synthetase of the brain type' as opposed to the 'GSH-dependent enzyme') activity was present at high levels throughout the rat eye, including its anterior regions and the vitreous humour in addition to the retina and other posterior fractions. Thus it cannot be excluded that this enzyme is present within the inner retinal layers, even if only due to its presence in the vitreous humour, within which the neurons would be immersed. Perhaps lack of reactivity in the tissues tested by Beuckmann *et al.* (1996) could have resulted from a preceding tissue treatment potentially preventing antigen accessibility.

Furthermore, as was shown in Chapter 5, at least three alternatively spliced variants of *PTGDS* are expressed at mRNA level in the human retina (Table 5-2 in section 5-1) (tissue source included both the RPE and the neural retina). It cannot be excluded that the antibody used by Beuckmann *et al.* (1996) could have been specific only to isoform PTGDS-001; whereas the antibody used in this project, which was raised against full-length human PTGDS-001 (sc-30067, Santa Cruz Biotechnology) could perhaps also detect isoforms PTGDS-004 and PTGDS-005, which share a partial sequence overlap with PTGDS-001 (Figures 5-7 and 5-8 in Chapter 5). The specificity of the sc-30067 antibody requires further validation also due to the unexpectedly large bands observed by Western blotting (Figures 6-9 and 6-10 in Chapter 6).

Nonetheless, in this study, in which the antibody raised against full-length human isoform PTGDS-001 (sc-30067) was used, PTGDS immuno-reactivity was observed in all retinal layers except for the outer nuclear layer (Figures 8-6, 8-7, 8-8 and 8-9) of mouse and primate retinae. The signal was strong in both plexiform layers, and weaker in the inner nuclear layer; however, the latter probably reflects the fact this region is dominated by neuronal nuclei, which leaves little space for cytoplasmic components, thus generating weaker reactivity (Figures 8-7, 8-8 and 8-9). In mice the signal was also strong in photoreceptor inner segments (Figures 8-6, 8-7 and 8-8), at the apical end of which the signal co-localised with TOPORS signal (Figures 8-7 and 8-8).

In the adult (6.5 months old) mouse the PTGDS signal was also observed in the outer segments of photoreceptors, but it appeared weaker there. In the primate section (Figure 8-9) PTGDS localised in the plexiform layers and the inner nuclear layer, as already stated, as well as in the inner and outer segments of photoreceptor cells. Notably, TOPORS was also observed localising in the outer segments (most strongly on its edges) as well as at the apical end of the inner segments, assumed to be the connecting cilia. The interesting localisation of TOPORS on the edges of outer segments is also visible in Figure 8-5; the potential significance of this immuno-reactivity pattern will be discussed in Chapter 9. It is worth noting that the ATP-binding cassette transporter (ABCR), involved in the recycling of retinal (section 1.2.4), localises to rim regions of disc membranes, where it translocates all-*trans* retinal from disc lumen to cytosol. It would be interesting to investigate whether PTGDS (known to bind all-*trans* retinal) (section 4.3.3.2) or TOPORS may participate in this process.

It was shown that cyclic nucleotide-gated (CNG) ion channels from rod photoreceptors can be inhibited by 9-*cis* and 11-*cis* retinal. This was prevented by the cellular retinoid binding

protein II (CRBP II) (He *et al.*, 2006). Although PTGDS is not known to bind either the 9-*cis* or the 11-*cis* retinal, it could be speculated that the retinoids, which it was shown to transport, specifically, all-*trans*- or 9-*cis*-retinoic acid as well as all-*trans*- or 13-*cis*-retinal (Tanaka *et al.*, 1997), could have a similar putative inhibitory effect on the ion channels, and PTGDS could serve as their scavenger. It could be speculated further that this protein may have a similar role also in other retinal neurons.

PTGDS has two ciliary-targeting sequences (CTS) of the same type as those found in rhodopsin, i.e. 'VxPx.' The first one is conserved in humans, mice and macaques, and, intriguingly, it is missing in the chimpanzee PTGDS protein along with a longer preceding peptide fragment (Figure 8-14). The second CTS motif appears to be more widely conserved, specifically, in human, cattle, mouse, macaque, dog and chimpanzee. The presence of these motifs supports the observed localisation of PTGDS at the apical region of inner segments, where it co-localised with TOPORS in mouse, as well as in the outer segments, where it co-localised with TOPORS in the primate.

Furthermore, the observed localisation is additionally supported by the findings from cell culture studies (Chapter 7), where PTGDS was seen localising at the basal body and along the primary cilium (Figure 7-20), or at the tip of this organelle (Figure 7-19). It would be interesting to determine whether it is present there as a soluble protein or whether it is perhaps anchored to the ciliary membrane via one of its oligosaccharide modifications (PTGDS is highly glycosylated: Figure 6-8). Live cell imaging experiment would be a useful tool for clarifying this.

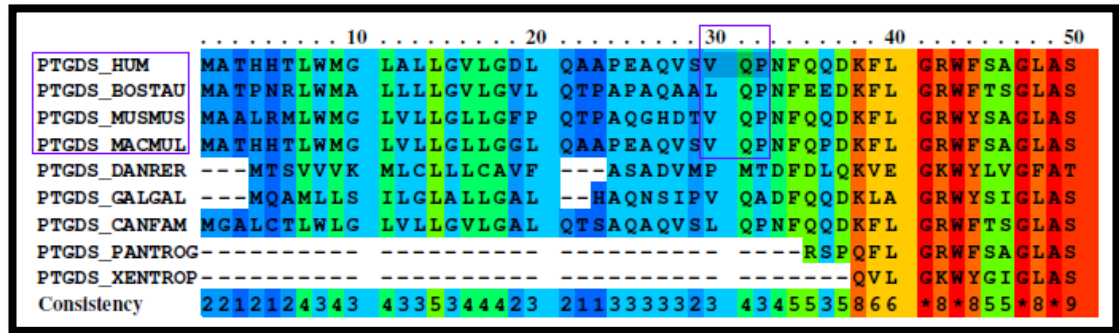


Figure 8-14. PTGDS CTS#1. Species and CTS are boxed inside purple rectangles.

Note: p.Gln31Leu is reported on Ensembl; source: dbSNP (NCBI). Key: Hum, human; Xentrop, western clawed frog (*Xenopus tropicalis*); Musmus, mouse (*Mus musculus*); Pantrog, common chimpanzee (*Pan troglodytes*); Macmul, rhesus macaque (*Macaca mulatta*); Bostau, cattle (*Bos taurus*); Canfam, family Canidae (includes dogs and wolves); Scrofo, wild boar (*Sus scrofa*); Danrer, zebrafish (*Danio rerio*); Galgal, chicken (*Gallus gallus*); Dromel, fruit-fly (*Drosophila melanogaster*). PRALINE alignment – a modified snapshot (Simossis, Kleinjung e Heringa, 2003).

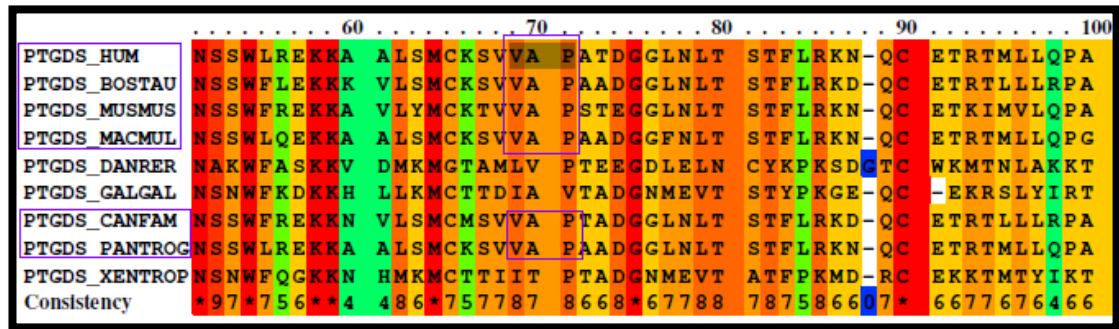


Figure 8-15. PTGDS CTS#2. Species and CTS are boxed inside purple rectangles.

Note: p.Val69Met is reported on Ensembl; source: Somatic mutations found in human cancers from the COSMIC project (release 67). Key: Hum, human; Xentrop, western clawed frog (*Xenopus tropicalis*); Musmus, mouse (*Mus musculus*); Pantrog, common chimpanzee (*Pan troglodytes*); Macmul, rhesus macaque (*Macaca mulatta*); Bostau, cattle (*Bos taurus*); Canfam, family Canidae (includes dogs and wolves); Scrofo, wild boar (*Sus scrofa*); Danrer, zebrafish (*Danio rerio*); Galgal, chicken (*Gallus gallus*); Dromel, fruit-fly (*Drosophila melanogaster*). PRALINE alignment – a modified snapshot (Simossis, Kleinjung e Heringa, 2003).

Involvement of PTGDS in the regulation of sleep was also demonstrated (Urade e Hayaishi, 1999). This finding suggests that PTGDS plays a role in light- and dark-adaptation responses and the circadian regulation in general, which could affect the function of the retina specifically, and an organism overall. This functional association of PTGDS could help explain its observed localisation in retinal tissues. For instance, at the outer-most RPE layer PTGDS could be associated with regulation of timing of photoreceptor outer segment phagocytosis by the RPE cells. On the other hand, in the inner retina it could be linked to the intrinsically photosensitive retinal ganglion cells (ipRGCs), which, among other functions, entrain central circadian clocks and modulate the sleep-wake processes (Lucas, 2013). Some co-localisation

with TOPORS was also noted within the layer of retinal ganglion cells; however, TOPORS' signal was never as strong as the signal of PTGDS (Figures 8-7, 8-8 and 8-9).

### **8.4.3 EVALUATION OF PSMC1 LOCALISATION**

PSMC1 immuno-reactivity was observed at the site of RPE phagocytosis (Figures 8-10 and 8-11) as well as in the photoreceptor inner segments (Figure 8-11); the later signal was detectable only following HIER treatment.

It was previously shown that protein folding is an error-prone process (Guo *et al.*, 2014). It was also shown that photoreceptor cells have extremely high biosynthetic requirements, similar to tumour cells (Ng *et al.*, 2014). Consequently, errors in protein quality control systems, mediated by chaperonins and heat-shock proteins, or in protein degradation systems, such as the ubiquitin-proteasome system or autophagy, would probably lead to cell stress due to aberrant protein folding and/or degradation. TOPORS and PSMC1 are both associated with protein degradation.

At molecular level neurodegeneration is often characterised by neuronal inclusions of protein aggregates, e.g. the neuronal intranuclear inclusion disease (NIID) (Lieberman *et al.*, 1998). It should be highlighted that, whereas in dividing cells nuclear protein aggregates can often be cleared out by autophagy, when the nuclear envelope dissociates during cell division, terminally differentiated neurons can only rely on the intranuclear ubiquitin-proteasome system since their nuclear membrane never dissociates.

The primary cilium was previously shown to be structured as a 'privileged membrane domain,' protected from the surrounding cytosolic contents by the transition zone, forming a ciliary diffusion barrier, or the ciliary necklace (Chih *et al.*, 2012). This barrier comprises nuclear pore-like structures within the ciliary necklace restricting access to the intraciliary compartment (Kee e Verhey, 2013; Nozawa, Lin e Chuang, 2013). Consequently, it is possible that the intraciliary space may be subject to similar stresses due to protein misfolding and aggregation as the intranuclear space. This would be an important point to consider in context of the photoreceptor outer segments, i.e. highly specialised primary cilia.

Even though the outer segments are regularly turned over by RPE phagocytosis at their distal ends, the outer segments' regions proximal to the connecting cilium must rely on another protein degradation pathway, if one is required. Photoreceptor cells are constantly exposed to light-induced stress, which would result in generation of reactive oxygen species, which in turn



would be damaging to both proteins as well as lipids. The RPE phagocytosis serves as the major mechanism of outer segment renewal, thus protecting this highly specialised cilium from prolonged effects of exposure to oxidative damage. However, it cannot be excluded that the ubiquitin-proteasome system is also required to tackle potential protein damage near the base of the outer segment. If this latter mechanism is impaired, this may lead to intraciliary stress due to protein misfolding, analogous to that observed in neuronal nuclei. This hypothetical scenario would justify the co-localisation of TOPORS and PSMC1 at the interface between the inner and outer segments (Figure 8-11).

It would be interesting to determine whether mice heterozygous for *TOPORS* have protein aggregate-containing inclusions in their nuclei and/or proximally to the connecting cilia, perhaps within the outer segments as this TOPORS localisation was observed in primate retinae (Figures 8-5 and 8-9). No PSMC1 signal was detected in the primate tissue (data not shown); however, similarly, no PSMC1 signal was observed in young mice (2 weeks old), whereas inner segment-specific PSMC1 reactivity in adult mice (6.5 months old) was revealed only after HIER treatment. No HIER, or another antigen retrieval method, was attempted on the primate retinal sections, or the young mouse sections, which could help explain the lack of apparent signal. Still, it cannot be excluded that *PSMC1* expression increases with age to compensate for the age-related deterioration of protein quality control processes (Balch *et al.*, 2008).

Still, it would be expected that PSMC1 is targeted to the primary cilia, specifically the rod photoreceptor outer segments, also in the primate retina. Bioinformatics analysis revealed that this conserved eukaryotic protein possesses two ciliary-targeting sequences (CTS) of different types (reviewed in: Hsiao, Tuz e Ferland, 2012), both of which are conserved in human, primates, rodents and other vertebrates (Figures 8-16 and 8-17). The first CTS of PSMC1 is of the same type as the one found in the carboxy-terminal regions of rhodopsin, i.e. 'VxPx' (Figure 8-16), whereas the second CTS of PSMC1 is typical for G protein-coupled receptors, such as: *Sstr3*, *Htr6* and *Mchr1*, and fits the consensus of: 'Ax(S/A)xQ' (Figure 8-17).

The existence of two different CTS motifs within the PSMC1 sequence suggests that different molecular mechanisms are probably involved in their recognition and implementation of the ciliary targeting. Their recognition could depend on the intracellular environment of a specific cell type, an environmental stimulus, or perhaps an energy status of the cell. For instance, the ciliary targeting of the NPHP3 protein is modulated by its GTP-GDP status, as well as myristoylation. The latter is a post-translational lipid modification, which is also found in

PSMC1. Palmitoylation is another form of lipid modification, and it is found in rhodopsin. Myristoylation and palmitoylation both serve as membrane attachment points, and were shown to be required for ciliary targeting of some proteins, such as NPHP3 (but not rhodopsin (Chuang e Sung, 1998) (reviewed in: Hsiao, Tuz e Ferland, 2012).

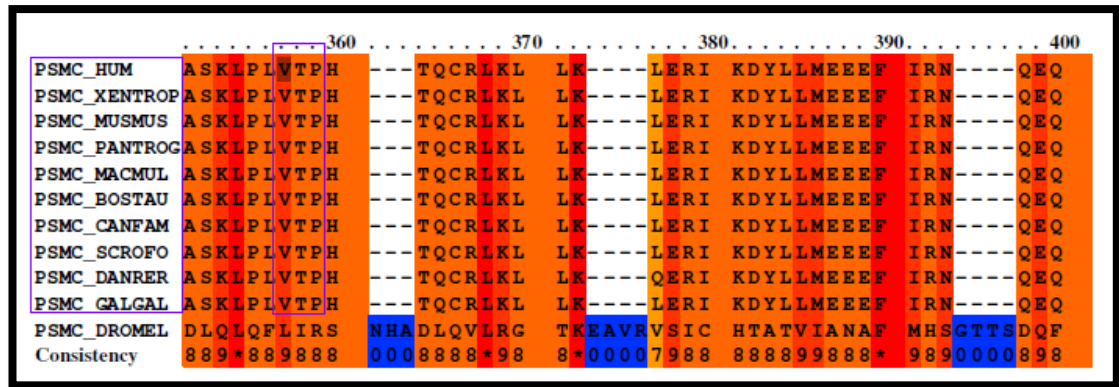


Figure 8-16. PSMC1 CTS#1.

Species and CTS are boxed inside purple rectangles. Key: Hum, human; Xentrop, western clawed frog (*Xenopus tropicalis*); Musmus, mouse (*Mus musculus*); Pantrog, common chimpanzee (*Pan troglodytes*); Macmul, rhesus macaque (*Macaca mulatta*); Bostau, cattle (*Bos taurus*); Canfam, family Canidae (includes dogs and wolves); Scrofo, wild boar (*Sus scrofa*); Danrer, zebrafish (*Danio rerio*); Galgal, chicken (*Gallus gallus*); Dromel, fruit-fly (*Drosophila melanogaster*). PRALINE alignment – a modified snapshot (Simossis, Kleinjung e Heringa, 2003).

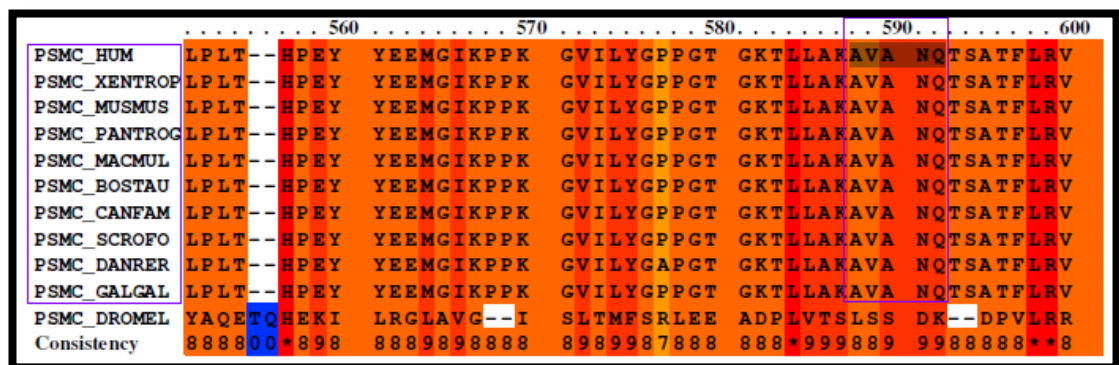


Figure 8-17. PSMC1 CTS#2.

Species and CTS are boxed inside purple rectangles. Key: Hum, human; Xentrop, western clawed frog (*Xenopus tropicalis*); Musmus, mouse (*Mus musculus*); Pantrog, common chimpanzee (*Pan troglodytes*); Macmul, rhesus macaque (*Macaca mulatta*); Bostau, cattle (*Bos taurus*); Canfam, family Canidae (includes dogs and wolves); Scrofo, wild boar (*Sus scrofa*); Danrer, zebrafish (*Danio rerio*); Galgal, chicken (*Gallus gallus*); Dromel, fruit-fly (*Drosophila melanogaster*). PRALINE alignment – a modified snapshot (Simossis, Kleinjung e Heringa, 2003).

The PSMC1 localisation at the outer segment-RPE boundary (Figures 8-10 and 8-11) is consistent with the conserved role of this protein in the ER-phagosome pathway, which is likely to contribute to the overall phagocytic activity of the RPE cell layer. In vertebrates RPE

phagocytosis of rod outer segments was shown to peak two hours after the onset of dawn (La Vail, 1976: referred to by Sung and Chuang, 2010). As was reviewed by Wong-Riley (2010), the RPE microvilli interdigitate with photoreceptor outer segments, and they also release ATP into the sub-retinal space. This ATP could be involved in circadian regulation of outer retina's function. PSMC1 binds as well as hydrolyses ATP (Rezvani *et al.*, 2012), and given its consistently observed localisation at the strategic position, it could be hypothesised that this ATPase may be involved in circadian regulation. This in turn could affect the rhythmicity of phagocytosis by the RPE. If TOPORS acted upstream, e.g. by SUMOylating PSMC1, mutations in the former could lead to impairment in PSMC1-conveyed functions at the boundary regions between the RPE and the outer segments.

It should also be emphasised that a plant orthologue of PSMC1 is involved in mediating responses to light-induced stress (Lee, K. H. *et al.*, 2012). Perhaps the observed high immunoreactivity at the site of RPE phagocytosis reflects an analogous function in the mouse, assuming that distal regions of outer segments would be expected to have undergone substantial light-induced stress, and perhaps even damage, by the time they become phagocytised.

PSMC1 is also involved in regulation of ubiquitin-protein ligase activity in mitotic cell cycle (UniProtKD). It could be speculated that it may also modulate the activity of other ubiquitin ligases involved in mitophagy. Apart from their role in ATP generation, mitochondria also serve as buffering spaces for calcium cations as well as intracellular transducers of apoptotic signals (Schapira, 2010). Molnar *et al.* (2012) previously showed that in saturating light conditions, the level of intracellular calcium cations in rods decreases, which in turn is toxic to these cells.

It cannot be excluded that PSMC1 could play a role in these processes, as its strong reactivity was observed in inner segments of photoreceptors (Figure 8-11), which is rich in mitochondria as well as other 'house-keeping' organelles. It was previously shown to regulate ubiquitin ligases in cell division (UniProtKD), so there is a possibility that it could regulate these enzymes also in other intracellular pathways, especially in terminally differentiated cells such as rods. Finally, PSMC1 is conserved among eukaryotes, and in plants it was shown to mediate responses to cellular stress triggered by light. Photoreceptor cells could also rely on PSMC1 on mediation of these responses, and it could possibly be via the intercellular calcium levels' regulation.

More recently, it was shown in cell culture that PSMC1 binds not only ATP, but also NADH (Tsvetkov *et al.*, 2014). This characteristic provides further evidence that PSMC1 could be associated with mitochondrial structure and function, where it could be mediating light-induced redox stress responses. Moreover, NADH was shown to stabilise 26 S proteasomes in the absence of ATP; this effect was abolished by increasing calcium levels, which, however, did not affect 26 S proteasomes stabilised by ATP rather than NADH. Further cellular studies showed that mitochondrial inhibition lead to increase in the intracellular NADH/NAD<sup>+</sup> ratios and in higher levels of the proteasome complex. Importantly, not only a decrease, but also an increase in calcium levels could also result in cytotoxicity (Kolb *et al.*, 1995).

Moreover, removal of the NADH-binding site from the PSMC1 sequence rendered the host cells less viable during mitochondrial inhibition. It is noteworthy that the central nervous system, which includes the retina, was previously shown to exhibit lower ATP levels and higher NADH/NAD<sup>+</sup> ratios in comparison to other tissues (Veech *et al.*, 1979: referred to in Tsvetkov *et al.*, 2014). Perhaps mutations in TOPORS, an interactor of PSMC1, could lead to an impaired cross-talk between the mitochondria and the ubiquitin-proteasome system (of which they both form a part), which would lead to cell death, as the mitochondria act intracellularly as apoptotic signal transducers.

This would not necessarily need to involve the E3 ubiquitin ligase activity of TOPORS. For instance, the Parkin-mediated mitophagy is independent of its E3 ubiquitin ligase activity (Um *et al.*, 2010). In the Y2H screen PSMC1 interacted most strongly with the mid-TOPORS fragment, linked to the protein's E3 SUMO1 ligase activity, as well as with the C-term TOPORS fragment, which includes the mutational hotspot region of TOPORS (Chapter 5, Table 5-16). Thus, it could be speculated that SUMOylation of PSMC1 is involved in this process (if TOPORS acts upstream of PSMC1). Or hypothetically, perhaps PSMC1 might modulate the E3 SUMO1 ligase activity of TOPORS, perhaps via binding its C-term mutational hot-spot region, if TOPORS acts downstream of PSMC1.

Calcium levels could affect photoreceptor physiology also via a different pathway. The maintenance of the 'dark current' consumes the highest level of energy out of all physiological processes performed by photoreceptor cells (Okawa *et al.*, 2008), and calcium cations contribute to approximately 15 % of this 'dark current' (Kolb *et al.*, 1995). Thus, disruption of calcium levels could lead to defective phototransduction, which eventually could result in processes leading to apoptosis.

Overall, findings presented in this thesis, together with previously published data, indicate that PSMC1 can serve important roles both in the rod inner segments (including their apical regions, where it associates with TOPORS: Figure 8-11), as well as phagocytic region at the interface between the outer segments and the RPE (Figures 8-10 and 8-11).

#### **8.4.4 CONCLUSIONS**

The data presented in this chapter demonstrated that the novel Y2H interactors of TOPORS are detected in mammalian retinae using commercially available antibodies. Furthermore, co-localisation of TOPORS' and the interactors' immuno-reactivity was observed at the apical regions of photoreceptor inner segments, suggesting that they may interact at the basal bodies of connecting cilia. Some co-localisation of detected signals was also observed in the inner retinal layers.

The results from this chapter are crucial for either supporting or rejecting the validity of results obtained in the earlier experimental chapters in context of the retinal environment. The demonstration that TOPORS can co-localise with all: ITM2B, PTGDS and PSMC1 at the ciliary area in the photoreceptors cells of mammalian retinae supports findings from Chapters 4, 5 and 6, showing PPIs and retinal expression, as well as co-localisation in cultured cell lines.

It was hypothesised prior to onset of this project that *TOPORS* mutations lead to photoreceptor degeneration, specifically due to its localisation at the basal body of the connecting cilia of these highly specialised, and equally vulnerable cells. The evidence of co-localisation at this bottle-neck region with the interacting partners of TOPORS may aid in understanding the origin of the observed retina-specific phenotype despite the genes' ubiquitous expression.

The findings obtained throughout the project and presented in the experimental Chapters 3-8 will be collectively summarised and discussed in Chapter 9 in order to try to elucidate the nature of the *TOPORS*-linked autosomal dominant retinitis pigmentosa (adRP) phenotype (*RP31*).

## 9 DISCUSSION

It was very intriguing that despite the ubiquitous expression of *TOPORS* and the multifunctional character of the encoded protein, the mutations in this gene are known to cause disease only in the retina (Chakarova *et al.*, 2007).

A putative explanation for these observations could be that *TOPORS* has a novel, unique role in the retina in one of its homeostatic pathways, or that it has a retina-specific interacting protein partner. In either case the starting point to either accepting or rejecting this hypothesis, was to perform a screen to identify proteins from the retina that associate with *TOPORS*.

Initially human retinal cDNA libraries were constructed in a *Saccharomyces cerevisiae* yeast strain Y187 (Clontech, CA, USA) suitable for yeast two-hybrid (Y2H) screening (Chapter 3). Two libraries were generated: one using an oligo-dT primer (O-dT) only, and one using a random primer and an oligo-dT primer (R&O-dT). A preliminary library characterization revealed that the R&O-dT library appeared to contain more protein-coding sequences and more longer inserts than the O-dT library. Thus the library constructed using both primers was then characterized in greater depth in order to validate its retinal status.

Bait plasmids for Y2H screens were constructed in parallel, and they were tested for auto-activation of Y2H PPI reporter genes, for the effects they have on the host cells (potential toxicity), as well as for bait protein expression (Chapter 3). The final experiment proved to be the most challenging and eventually *TOPORS* bait expression needed to be confirmed indirectly by re-creating a previously published Y2H PPI between *TOPORS* and p53. Attempts to determine protein expression by Western blotting (WB) were not successful (Appendix 11.4). The smudges on images from the WB experiments (Figures 11-25, 11-26 and 11-27) suggest that the procedures were unsuccessful due to inefficient protein extraction from the yeast cells, or possibly protein degradation due to the lengthy extraction process (section 2.1.7 in Methods and Materials). On the contrary, the method of protein extraction from mammalian cells (section 2.5.1 in Methods and Materials) can be performed much faster, making it easier to prevent protein degradation, and subsequently allowing for successful SDS-PAGE and WB procedures (Chapter 6).

Y2H screens were performed once the retinal library and baits were generated and characterised. Both libraries were used: one Y2H screen for interacting partners of *TOPORS* was performed per library (Chapter 4). Due to time constraints the O-dT library had been less thoroughly characterised than the R&O-dT library; the latter had been prioritised due to

an overall higher content of longer inserts, which corresponded to protein-coding gene regions. This had been determined based on an initial evaluation of a small number of samples. Since these few randomly selected samples might not have been representative of all of the library clones, both libraries were screened for interactors of TOPORS.

The Y2H screens resulted in identification of ITM2B and PTGDS proteins among clones of the R&O-dT library, whereas PSMC1 was an interactor pulled out from the O-dT library. The retinal cDNA was subsequently screened for alternatively spliced variants of the identified candidate interactors (Chapter 5). The full-length clones of candidates pulled out from the screen were also generated and re-tested in yeast to confirm that the observed interactions could be reproduced, and that they had not been false positive results, which could have occurred, for instance, due to direct activation of Y2H PPI reporter genes (Chapter 5). The interactions were subsequently verified in mammalian cell cultures (Chapter 6), and their cellular (Chapter 7) and retinal (Chapter 8) localisations were demonstrated.

The next sections summarise and briefly discuss the findings obtained for each individual TOPORS' interactor (sections 9.1 – 9.3). The subsequent two sections, respectively, outline potential future work (section 9.4), which could be performed as a continuation of this PhD project, as well as provide an overview of alternative research methods (section 9.5), which could have been used instead of the approaches applied in this PhD project.

## 9.1 ITM2B COULD HAVE MULTIPLE ROLES IN THE RETINA

*ITM2B* is ubiquitously expressed, and at least two protein-coding isoforms of this gene exist in human. However, just one of them was shown to be expressed at mRNA level in human retinae (section 5.1.1); this was the same isoform as the one pulled out from the Y2H screen and evaluated in this project.

Mutations in *ITM2B* were first identified in patients with familial, Alzheimer-like forms of dementia, and more recently in a family with a dominant retinal dystrophy. This latter disease association made *ITM2B* the most attractive gene to follow up in the context of this project. However, except for the proband and their sibling, who presented with night-blindness, the overall symptoms experienced by the affected family members were indicative of a dystrophy involving the cone photoreceptor pathway. Importantly, as in the case of TOPORS, the observed phenotype was restricted to the retina with no dementia and no systemic symptoms. However, if future functional studies confirm that it is indeed the cone signalling pathway, which is predominantly affected by the retinal *ITM2B* mutation, then the nature of its association with TOPORS, whose mutations appear to initially affect rod cells, will be harder to explain in context of retinal physiology (unless the association occur in the ganglion cell layer).

Once the PPIs between full-length TOPORS and *ITM2B* were demonstrated in yeast, experiments were performed, which aimed to delineate the domains of TOPORS, which mediate its interactions with the newly-identified protein partners. A result was considered positive overall, if blue growth, indicating a PPI, was observed in at least four out of six experiments at a given stringency level (i.e. activation of two reporter genes: D+; and activation of four reporter genes: Q+). Table 9-1 includes a summary of the obtained results for full-length *ITM2B* (which would be expected to be membrane-bound, and thus not able to enter the nucleus until after proteolytic cleavage: Figure 6-5). However, the *ITM2B* protein is heavily proteolytically-processed by at least three different proteases, resulting in a diverse range of peptides (Figure 6-5). Due to the nature of the protein, it is expected that the PPIs observed for the full-length *ITM2B* construct, probably reflect a PPI involving only the amino-terminal cytoplasmic fragment of *ITM2B* (denoted ICD in Figure 6-5 b). The table also summarises the PPI with a construct called *ITM2B90*, which lacks the first ninety residues of *ITM2B*, including the trans-membrane (TM) domain; therefore, *ITM2B90* is expected to be soluble.



Table 9-1. TOPORS and ITM2B interactions in yeast.

Key: D+ = growth on DDO/X/A (a lower stringency medium, indicating a PPI based on activation of two reporter genes); D- = no growth on DDO/X/A, i.e. no PPI; Q+ = growth on QDO/X/A (a higher stringency medium, indicating a PPI based on activation of four reporter genes); Q- = no growth on QDO/X/A, i.e. no PPI. TM, trans-membrane; BH3, Bcl 2 homology 3; PEST, Proline, Glutamate, Serine, and Threonine-rich region; CTS, ciliary-targeting sequence; SR/RS, arginine and serine-rich region; SUMO1, Small ubiquitin-related modifier 1; NLS, nuclear localisation signal; Lys/His, lysine- and histidine-rich region. Refer to Chapter 6 for detailed figures demonstrating the position of motifs within TOPORS and ITM2B proteins.

Construct	Preys		Baits: Full-length TOPORS and its fragments			
	Full-length ITM2B	ITM2B90	Full-length TOPORS	N-term TOPORS	Mid-TOPORS	C-term TOPORS
<b>Motifs</b>	Full-length: CTS # 1, 2 and 3; TM domain; BH3 domain; BRICHOS domain; N-glycosylation site; C-term mutational hot spot (Figure 6-5).	BH3 domain; CTS # 2 and 3; BRICHOS domain; N-glycosylation site; C-term mutational hot spot	Full-length (Figure 6-2, or subsequent columns).	PEST domain # 1; phosphoserine 98; RING finger domain; CTS # 1 (Figure 5-9).	PEST domains # 2 and 3; CTS # 2; SR/RS-rich domain # 1 and # 2; SUMO1 acceptor site; NLS; phosphoserine 718; (Figure 5-10).	SR/RS-rich domain # 2; phosphoserine 718; mutational hot spot; Lys/His motif; PEST domains # 4 and 5 (Figure 5-11).
<b>PPI summary</b>	Full-length ITM2B	n/a	D+ Q-	D+ Q+	D- Q-	D+ Q+
<b>PPI summary</b>	n/a	ITM2B90	D+ Q-	D+ Q+	D+ Q-	D+ Q+

Findings presented in Table 9-1 show that irrespective of the ITM2B fragment tested, the strongest association was observed with the N-term TOPORS and with the C-term TOPORS, containing the RING domain and the mutational hot-spot region, respectively. The RING domain is known to convey the E3 ubiquitin ligase activity of TOPORS, which suggests that TOPORS could be marking ITM2B for degradation. The C-term TOPORS fragment, so frequently mutated in *RP31*, could be acting as an accessory binding region for ubiquitination substrates. This part of TOPORS has also been linked to SUMOylation activities; however, to a lesser extent than the mid-TOPORS fragment (Figure 6-1). Still, it could be speculated that TOPORS is involved specifically in degradation of SUMOylated ITM2B, as it was previously demonstrated that the latter modification is often a pre-requisite for ubiquitination, marking the protein for degradation (Perry, Tainer e Boddy, 2008; Denuc e Marfany, 2010; Miteva *et al.*, 2010).

Due to the proteolytic processing of ITM2B, and the uncertainty regarding ITM2B folding in the yeast cells, especially whilst being bound to the GAL4 AD, makes it difficult to predict whether the observed PPIs represent physiological associations. It is possible that TOPORS is simply involved in degradation of the 'random' ITM2B fragments as they do not represent the native protein. Furthermore, ITM2B is glycosylated at the centre of its BRICHOS domain. It cannot be ensured that this glycosylation occurs in yeast, and if it does not, how this would affect the proteolytic processing and/or PPIs.

The co-immuno-precipitation experiments on mammalian cell extracts tested interactions between endogenous proteins (Chapter 6), which were thought to be full-length (with the exception of the smaller ITM2B band, identified in a protein complex with TOPORS: Figure 6-7). Protein localisations in cultured cells as well as in retinal tissue sections were subsequently evaluated (Chapters 7 and 8) (Table 9-2). It was established in hTERT-RPE1 cells that endogenous ITM2B localises to centrioles in dividing cells, but not in ciliated cells, in which it was absent from the ciliary basal body. This finding was not entirely consistent with results of retinal localisation studies.

ITM2B was observed in the inner segments of rod photoreceptors (Figure 8-2). Furthermore, the signal overlapped with PNA staining (yellow in merged image), thus suggesting that ITM2B could also be expressed in cones. ITM2B signal was also evident in the ganglion cell layer, the outer plexiform layer, and at the interface between the inner plexiform and the inner nuclear layers.

Co-localisation of ITM2B and TOPORS signals at a photoreceptor cell region, which appeared to correspond to the connecting cilia and/or the outer segments was also demonstrated (Figure 8-4). Some signal within the distal area of inner segments cannot be excluded either. The diffuse localisation of both proteins at the plexiform layers and the ganglion cell layer suggests that these may also comprise putative sites of interaction.

This apparent co-localisation at the connecting cilium, as well as in the outer segments of primate photoreceptors (Figure 8-5), indicates that in neuronal cell types ITM2B can be targeted to primary cilia, even if this does not apparently occur in epithelial cell types (Figure 7-11). Thus, the observed discrepancy could be cell-type dependent. The aim of future cell work could be to compare ITM2B targeting in cell lines originating from different tissues.

The ciliary targeting of ITM2B in photoreceptors could be related to its role as a protease inhibitor. Specifically, ITM2B was previously shown to inhibit proteolysis of the amyloid precursor protein (APP) by blocking access of secretases to its cleavage sites (Fotinou et al 2014).

*al.*, 2005; Matsuda *et al.*, 2005); furthermore, it was also shown that the carboxy-terminal ITM2B fragment (CCTP in Figure 6-5 b), which becomes elongated from 23 to 34 amino acids due to the British and Danish familial dementia mutations, in its native form is responsible for preventing deposition and aggregation of amyloid-beta (A $\beta$ ) (Kim *et al.*, 2008).

Table 9-2. ITM2B localisation summary.

Key: PCM1, peri-centriolar material 1; PLK4, polo-like kinase 4; PR, photoreceptor; PNA, peanut agglutinin; CC, connecting cilium; OS, outer segment; RPE, retinal pigmented epithelium; GCL, ganglion cell layer; INL, inner nuclear layer; IPL, inner plexiform layer; OPL, outer plexiform layer; IS, inner segment; OS, outer segment.

Sub-cellular localisation in hTERT-RPE1 cells		Localisation within retinal tissue cryo-sections	
Dividing cells	<p>Co-localised with TOPORS in a centriole-like pattern. In some cells ITM2B displayed additional 'cloud'-like signal around the co-localisation area.</p> <ul style="list-style-type: none"> <li>Co-localised with PCM1 during interphase.</li> <li>Co-localised with PLK4 in a centriole-like pattern, and also at a larger aggregate, possibly representing a deuterosome.</li> <li>Co-localised with Centrin-2 during interphase.</li> </ul>	<p>Mouse – 2 weeks old</p>	<p>Localised at the PR IS/OSI layer, where partial signal overlap was observed with:</p> <ul style="list-style-type: none"> <li>PNA (cone marker) (Figure 8-2);</li> <li>TOPORS at the distal/outer part of PR layer, indicating it could be the CC and/or OS (Figure 8-4, lower panel).</li> </ul> <p>Localised at the plexiform layers (both OPL and IPL) and the GCL (Figure 8-2), where partial signal overlap was observed with TOPORS (Figure 8-4, lower panel).</p>
		<p>Mouse – 6.5 months old</p>	<p>In sections subject to HIER, ITM2B immunostaining was observed throughout the retina, where the signal was most distinct within the PR layer, the GCL and the regions of OPL and IPL immediately adjacent to the INL (Figure 8-3).</p>
Ciliated cells	<ul style="list-style-type: none"> <li>Co-localised with <math>\alpha</math> tubulin (used as a ciliary marker) in a dot-like pattern reminiscent of centrioles, but did not co-localise at the ciliary basal body.</li> </ul>	<p>Macaque</p>	<p>Co-localised with TOPORS at:</p> <ul style="list-style-type: none"> <li>PR OS;</li> <li>RPE (weaker TOPORS signal);</li> <li>GCL (peri-nuclear signals; weaker TOPORS signal).</li> </ul> <p>Additionally localised at plexiform layers (both OPL and IPL) with higher intensity signals observed at the interface between INL and OPL (Figure 8-5).</p>

It was previously demonstrated by Hoh Kam, Lenassi and Jeffery (2010) that A $\beta$  deposition occurs in aging retinæ of mice as well as humans. Based on these published data, it could be speculated that perhaps ITM2B (or its fragment) is targeted to the outer segments in order to modulate APP processing at their surface, and or to act as a scavenger of A $\beta$ . Therefore, an

impairment of ITM2B targeting to photoreceptor outer segments, either due to mutation in *TOPORS* or *ITM2B* itself, could lead to pre-mature cell degeneration due to an excess of A $\beta$  accumulation of the surface of the outer segments.

Moreover, if, after binding A $\beta$ , the secondary role of ITM2B (or its fragment) would be to re-enter the cells to help target it for proteasomal degradation, then *TOPORS* mutations would affect this process. It is less obvious that this would be of significance in mice, in which *TOPORS* localisation appeared to be restricted to the connecting cilia (Chapter 8); however, in primate retinae *TOPORS* immuno-reactivity was observed throughout the outer segments (and was most intense at their edges) (Figures 8-5 and 8-9). Thus, it is probable that *TOPORS* may have a role in degradation of A $\beta$  via the ubiquitin-proteasome system, mediated by ITM2B (or its fragment). However, it would seem more likely that the ITM2B CCTP-bound A $\beta$  would be cleared out by the RPE phagocytosis. Weak *TOPORS* immuno-reactivity was sometimes seen in the RPE retinal layer (Figures 8-5, 8-7 and 8-9), thus it cannot be excluded that this protein may also be important for RPE phagocytosis. This would be supported by its endogenous expression in hTERT-RPE1 cultured cells (Chapter 7) as well as its ubiquitous and multifunctional nature.

The finding by Audo *et al.* (2013) that retinal ITM2B reactivity appears limited to the ganglion cell layer, rather than being detected in most retinal regions (Figures 8-2, 8-3, 8-4 and 8-5), probably reflects differences in specificity of the used antibodies. The antibody used by Audo *et al.* (2013) would detect membrane-bound ITM2B fragments, which perhaps were more easily accessible to the antibody in the ganglion cell layer. Therefore, the signal appeared stronger there, making it harder to detect weaker ITM2B immuno-reactivity in other retinal layers. Moreover, the differences in the obtained immuno-staining results could also reflect difference in the treatment of tissue prior to immuno-staining. For instance, the localisation of PSMC1 in the inner photoreceptor segment was revealed only after HIER treatment; whereas staining of untreated tissues showed PSMC1 immuno-reactivity only at the region of RPE phagocytosis (Figures 8-10 and 8-11).

It should also be noted that unlike the previously identified ITM2B mutants, implicated in dementia, the retinal mutation probably does not lead to amyloid formation. Unlike the dementia mutations, which lead to formation of extended C-terminal peptides, which tend to aggregate, the retinal mutation results in an amino acid substitution (p.Glu261Ala). Glutamic acid is known to have phosphomimetic properties, resembling those of a phosphoserine, or a phosphothreonine. Consequently, this residue is likely to be important for maintaining ITM2B protein activity, which would be abolished by mutating it to alanine; in fact,

in experiments aiming to determine the significance of phosphorylation of serine or threonine residues, they are frequently mutated to alanine to generate phospho-deficient mutants.

If the mutation does not affect cleavage, it might influence intra-molecular bond formation. Cysteines 246 and 265 (Figure 6-4) form a disulphide bridge within the ITM2B C-terminal peptide (CTPP), once it is released by furin cleavage (Tsachaki *et al.*, 2010). Perhaps, the retinal mutation may prevent formation of this bond due to incorrect peptide folding; however, the hydrophobic side chain of alanine is small (as opposed to a charged side chain found in glutamate). In fact, it was demonstrated that an aspartate residue within a furin precursor peptide forms an active site, which is essential for auto-proteolytic activation of furin at its consensus cleavage site (Leduc *et al.*, 1992). Perhaps substrates for furin processing, such as ITM2B, also comprise glutamate active sites, required to trigger proteolysis by this enzyme at the consensus cleavage site.

If the above hypothesis is true, this would indicate that the retinal dystrophy mutant (ITM2B RetMu) is never processed at its C-terminus, which prevents the formation of mature ITM2B. Only mature protein should be able to leave the Golgi body, where proteolytic processing was shown to occur (Choi *et al.*, 2004). If ITM2B never matures, but the protein is expressed, then it would probably accumulate in the Golgi complex, stressing this organelle, and thus preventing correct and efficient processing of other proteins. By extrapolation, it could for instance be hypothesised that retinal ITM2B mutations impair the processing and/or transport of photoreceptor opsins, which could eventually lead to apoptosis and retinal degeneration.

In context of the interaction with TOPORS, if it is indeed the N-terminal fragment of ITM2B and/or the intracellular domain (NTF and ICD, respectively, in Figure 6-4), which are/is involved in the PPI with TOPORS, it could be speculated that the nature of this interaction is analogous to that between murine Topors and the cytoplasmic domain of syndecan 1 (Braun *et al.*, 2012). Specifically, ITM2B may serve as a membrane receptor, and TOPORS binding may be involved in signal transduction, possibly serving to maintain the differentiated state of the photoreceptor cells. Disruption of such signalling might trigger the photoreceptor cells to attempt to re-enter the cell cycle, eventually resulting in apoptosis, as growth and division would not be supported within cellular environment of the retina. This would be supported by the observed localisation of TOPORS on the edges of OS (Figure 8-5 and 8-9).

Alternatively, the association between ITM2B and TOPORS may be related to regulating the energy metabolism of retinal cells. A short mouse *Itm2B* splice variant (*Itm2B<sub>S</sub>*)<sup>21</sup>, for which as yet no orthologue has been confirmed in human, is able to induce apoptosis. The long transcript (*Itm2B* aka *Itm2B<sub>L</sub>*) appears to have no such function (Fleischer *et al.*, 2002). This mouse *Itm2B<sub>S</sub>* protein contains a Bcl 2 homology 3 (BH3) domain, found in members of Bcl-2 protein family, e. g. in Bax, whose transcription is activated by p53 due to *TOPORS* over-expression (Lin *et al.*, 2005). *Itm2B<sub>S</sub>* interacts with anti-apoptotic protein Bcl-2, but not with the pro-apoptotic BH3-containing protein Bad.

The BH3 domain includes key leucine and aspartic acid residues; an identical sequence is not conserved in human ITM2B, which contains isoleucine (Ile91) rather than leucine, found at the corresponding position in mice. Leucine and isoleucine are isomers, which differ in the attachment position of a methyl group on a side chain; this appears to be a minor modification, however, the associated conformational and spatial change may as well prevent a BH3 domain-associated apoptotic function.

Despite this, Lee *et al.* (2007) reported that *ITM2B<sub>S</sub>* and *ITM2B<sub>L</sub>* alternatively spliced variants are both expressed in human urothelial and bladder cancer cells at the protein level. They also demonstrated that exogenous expression of *ITM2B<sub>S</sub>* triggers apoptosis (based on pro-caspase 3 processing and DNA fragmentation), whereas exogenously expressed *ITM2B<sub>L</sub>* caused no such effects. This supports the results obtained with the mouse orthologues (Fleischer *et al.*, 2002), and also provides evidence that the isoleucine in the human sequence is sufficient for reconstituting a functional BH3 domain.

Fleischer *et al.* (2002) showed that localisation of *Itm2B<sub>S</sub>* to mitochondria was associated with the loss of mitochondrial membrane potential, and accompanied by a release of cytochrome C to the cytoplasm, which triggered apoptosis, even when cells were stimulated by IL-2, acting as a growth factor.

Photoreceptors are metabolically highly active cells, therefore, any problems with the energy-generating mitochondria may manifest as degeneration. RP disease pathways all converge on apoptosis irrespective of the causative mutation(s). It cannot be excluded that *ITM2B<sub>S</sub>* also

---

<sup>21</sup> This mouse *Itm2B* transcript is found only in the UCSC Genome Browser Assembly: Dec 2011 (GRCm38/mm10) and corresponds to mRNA AB030204, covering mouse exons 2-6. It is not homologous to the short protein-coding splice variant of human *ITM2B* (ITM2B-003 ENST00000378549) recoded in the Ensembl Genome Browser, which covers human exons 1-2 and 5-6.

exists in photoreceptor cells, where it associates with mitochondria, and possibly mediates the final apoptotic cell death.

TOPORS could then be involved in mitophagy, i.e. autophagy of damaged mitochondria, similarly to the E3 ubiquitin ligase, Parkin (encoded by *PARK2*), associated with familial Parkinson's disease (Deas, Wood e Plun-Favreau, 2011). Furthermore, Parkin activity is modulated by phosphorylation; this modification was also shown to regulate the E3 ubiquitin and SUMO1 ligase activities of TOPORS (Park *et al.*, 2008; Yang *et al.*, 2009). This hypothesis is supported by the preliminary Y2H findings from this project, where several proteins with key mitochondrial functions were also identified as putative interacting partners of TOPORS (Table 11-7 in Appendix 11-6).

## 9.2 PTGDS COULD BE REQUIRED FOR INTRA-RETINAL SIGNALLING

PTGDS is ubiquitously expressed, however, it has been commonly named the 'brain-type' prostaglandin D2 synthase to differentiate it from the glutathione-dependent prostaglandin D2 synthase (Table 4-8), which was initially purified from rat spleen (referred to in: Goh *et al.*, 1987). No direct PTGDS involvement in retinal diseases has ever been shown; but the protein plays a role in maintenance of the blood-retina barrier, as well as it acts as a transporter of retinoid compounds. It also mediates the sleep-wake cycle processes, which would be expected to affect retinal homeostasis.

Once the PPIs between full-length TOPORS and PTGDS were demonstrated in yeast, experiments were performed, which aimed to delineate the domains of TOPORS, which mediate its interactions with this newly-identified protein partner. A result was considered positive overall, if blue growth, indicating a PPI, was observed in at least four out of six experiments at a given stringency level (i.e. activation of two reporter genes: D+; and activation of four reporter genes: Q+).

In the Y2H direct PPI experiments (Table 9-3) PTGDS interacted most strongly with the N-term TOPORS fragment, which comprises the RING domain, and therefore, conveys the ubiquitin E3 ligase activity of this enzyme (Table 5-16). Nonetheless, it should be noted that full-length *PTGDS-001* construct was used for this experiment, which would result in synthesis of full-length PTGDS protein, which would include the amino-terminal signal peptide. Since the GAL4 AD, expressed as a hybrid protein with PTGDS, was fused to its amino-terminal, it cannot be excluded that the observed strong interaction involved the amino-terminal signal peptide of PTGDS rather than the whole protein. Since TOPORS is a component of the ubiquitin-proteasome system, it is very possible that it could be involved in degrading signal peptides, which have fulfilled their roles. Future experiments should aim to repeat this interaction, using a PTGDS construct, which would lack the signal peptide. Nonetheless, the TOPORS-PTGDS co-localisation signals observed in the hTERT-RPE1 cells, as well as the murine and primate retinal sections, indicate that an association with full-length PTGDS probably also occurs in mammalian systems.

Cellular localisation studies (Chapter 7 and Table 9-4) showed that endogenous PTGDS localised along the axoneme as well as at the base of primary cilia in cultured hTERT-RPE1 cells. Furthermore, at the basal body it co-localised with TOPORS, whereas the findings did not provide evidence for co-localisation in other cellular compartments, which, however, should not be excluded. If PTGDS is taken up by the photoreceptors near the site of its origin, the RPE



cell layer, then it would be taken up by the outer segments, which are modified primary cilia. However, this would suggest that PTGDS moved through the cilia in a retrograde direction, whereas the observation of the PTGDS along the axoneme in the cultured RPE1 cells, suggests that it was transported into the cilium in the anterograde direction. Still, it could also be possible that PTGDS was released by a population of the hTERT-RPE1 cells (the cells were not synchronised) into the media, and was subsequently taken up by another population of cells, following binding to receptors on the primary cilia. In order to better define these observations, it would be necessary to determine whether PTGDS interacts with molecules of the anterograde or retrograde IFT proteins.

Table 9-3. TOPORS and PTGDS interactions in yeast.

Key: D+ = growth on DDO/X/A (a lower stringency medium, indicating a PPI based on activation of two reporter genes); D- = no growth on DDO/X/A, i.e. no PPI; Q+ = growth on QDO/X/A (a higher stringency medium, indicating a PPI based on activation of four reporter genes); Q- = no growth on QDO/X/A, i.e. no PPI. TM, trans-membrane; BH3, Bcl 2 homology 3; PEST, Proline, Glutamate, Serine, and Threonine-rich region; CTS, ciliary-targeting sequence; SR/RS, arginine and serine-rich region; SUMO1, Small ubiquitin-related modifier 1; NLS, nuclear localisation signal; Lys/His, lysine- and histidine-rich region. Refer to Chapter 6 for detailed figures demonstrating the position of motifs within TOPORS and PTGDS proteins.

Prey		Baits: Full-length TOPORS and its fragments			
Construct	PTGDS	Full-length TOPORS	N-term TOPORS	Mid-TOPORS	C-term TOPORS
<b>Motifs</b>	Full-length: N-term signal peptide; O-linked glycosylation site; N-linked glycosylation sites # 1 and 2; CTS # 1 and 2; catalytic active site at cysteine 65; cysteines 89 and 186, forming an intramolecular disulphide bridge; phosphoserine 106; four α helix regions and a proline-containing turn motif (Figure 6-8).	Full-length (Figure 6-2, or the subsequent columns).	PEST domain # 1; phosphoserine 98; RING finger domain; CTS # 1 (Figure 5-9).	PEST domains # 2 and 3; CTS # 2; SR/RS-rich domain # 1 and # 2; SUMO1 acceptor site; NLS; phosphoserine 718; (Figure 5-10).	SR/RS-rich domain # 2; phosphoserine 718; mutational hot spot; Lys/His motif; PEST domains # 4 and 5 (Figure 5-11).
<b>PPI summary</b>		<b>D+ Q-</b>	<b>D+ Q+</b>	<b>D+ Q-</b>	<b>D+ Q-</b>

PTGDS localisation at the RPE and the photoreceptor inner and outer segment layers is in agreement with the previous findings from immuno-staining studies (Beuckmann *et al.*, 1996). Prominent PTGDS presence in the inner retinal layers, ranging from the ganglion cell layer to the outer plexiform layer (Figures 8-6, 8-7, 8-8 and 8-9), is in agreement with data, obtained by

measuring the enzyme activity of 'brain-type' prostaglandin D2 synthase in the eye, in which it was wide-spread and high (Goh *et al.*, 1987). Furthermore, the immuno-staining pattern (Figures 8-6, 8-7, 8-8 and 8-9), which was not observed before, could suggest that the antibody (sc-30067) might also bind to PTGDS isoforms other than PTGDS-001. It was shown (Chapter 5) that at least two more protein-coding PTGDS isoforms are expressed in human retina at the mRNA level, therefore, cross-reactivity cannot be excluded.

It could be worth investigating where RIG1/RARRES3 (retinoid-inducible gene 1/retinoic acid receptor responder protein 3; UniProt # Q9UL19) localises in hTERT-RPE1 and neuronal cell lines and in the retina; it may be possible that this receptor is enriched on the ciliary (outer segment) membrane. Wu *et al.* (2012) showed that PTGDS and RIG1 interacted in a Y2H screen. If PTGDS is important for transport of retinoid compounds in the retina, it would be expected that PTGDS would deliver the retinoids to specific receptors. In rat PTGDS was shown to be produced in the RPE, from where it was released into the inter-photoreceptor matrix, and then taken up by the photoreceptors (Beuckmann *et al.*, 1996). RIG1 is a single pass membrane receptor protein, which belongs to a family of H-rev107 proteins, which has five members in humans, including lecithin retinol acyltransferase (LRAT).

Proteins of the H-rev107 family have been shown to be actively involved in cell differentiation processes and suppression of cell migration and invasion (in malignant cells). This function of H-rev107 family proteins, to which RIG1 and LRAT both belong, would be important in highly specialised terminally differentiated cells such as photoreceptors in order to prevent them from re-entering the cell cycle.

Furthermore, the suppression of cell migration and invasion is very relevant in context of the highly energetically- and biosynthetically-demanding and constantly turning over photoreceptor outer segments. These highly modified primary cilia are structures undergoing continuous growth and phagocytosis by the RPE cells. It is probable that RIG1 and/or LRAT might act to prevent the outer segments from invading the space of neighbouring outer segments.

Table 9-4. PTGDS localisation summary.

Key: PCM1, peri-centriolar material 1; PLK4, polo-like kinase 4; PR, photoreceptor; PNA, peanut agglutinin; CC, connecting cilium; OS, outer segment; RPE, retinal pigmented epithelium; GCL, ganglion cell layer; INL, inner nuclear layer; IPL, inner plexiform layer; OPL, outer plexiform layer; IS, inner segment; OS, outer segment.

Sub-cellular localisation in hTERT-RPE1 cells		Localisation within retinal tissue cryo-sections	
Dividing cells	<p>Co-localised with TOPORS in a centriole-like pattern in addition to diffuse cytoplasmic signal observed for both proteins (sometimes having a granular appearance in case of PTGDS).</p> <ul style="list-style-type: none"> <li>Co-localised with PCM1 during interphase, but distally from the cell nucleus.</li> <li>Co-localised with PLK4 in a centriole-like pattern. Additionally, both proteins localised in the cytoplasm where some of their signals overlapped.</li> <li>Co-localised with Centrin-2 during interphase.</li> </ul>	Mouse – 2 weeks old	<p>Localised at the plexiform layers (both OPL and IPL), the GCL and at the PR IS/OS layer (Figure 8-6, lower panel), as well as the RPE layer (Figure 8-7). At the PR IS/OS layer PTGDS:</p> <ul style="list-style-type: none"> <li>Did not co-localise with PNA (cone marker; Figure 8-6);</li> <li>Co-localised with TOPORS at the distal/outer part of PR IS/OS layer, indicating it could be the CC and/or OS (Figure 8-7).</li> </ul> <p>Co-localisation of PTGDS and TOPORS signals was also observed within cells of the choroid (Figure 8-7; upper panel).</p>
		Mouse – 6.5 months old	<p>Localised at the plexiform layers (both OPL and IPL), the GCL and at the PR IS/OS layer (Figure 8-8). At the PR IS/OS layer PTGDS co-localised with TOPORS in a pattern strongly indicative of the CC (Figure 8-8; lower panel).</p>
Ciliated cells	<ul style="list-style-type: none"> <li>Co-localised with <math>\alpha</math> tubulin (used as a ciliary marker) in a dot-like pattern reminiscent of centrioles, and co-localised at both centrioles of the ciliary basal body as well as along the primary cilium.</li> </ul>	Macaque	<p>Localised at the plexiform layers (both OPL and IPL), the GCL and at the PR IS/OS layer, as well as the RPE layer (Figure 8-9); signal intensity was the highest at the RPE-OS interface and in the IPL. TOPORS was observed in the PR OS layer and, to a lesser extent, in the plexiform layers and the GCL. PTGDS and TOPORS co-localised at:</p> <ul style="list-style-type: none"> <li>OS layer (both strong signals);</li> <li>GCL (strong PTGDS signal and weak TOPORS signal).</li> </ul>

Proteins from this family also display a phospholipase A1/A2 activity, i. e. they are able to hydrolyse acyl bonds of membrane phospholipids, such as phosphatidylcholine (PC/lecithin), or phosphatidylethanolamine (PE/cephalin). It is noteworthy that RIG1 is indeed involved in hydrolysis of PC and PE, and LRAT uses PC as a donor of acyl group for esterification of retinol in the processes of replenishing 11-*cis* retinal during the visual cycle (section 1.2.4). It cannot be excluded that PTGDS is also involved in this retinoid metabolism even though it has not been shown to bind 11-*cis* retinal. Since TOPORS immuno-reactivity was also observed in primate outer segments, especially on the cell edges (Figures 8-5 and 8-9), it could be speculated that this dual E3 ubiquitin and SUMO1 ligase can be also involved in retinoid metabolism, even if only by regulating the amounts and/or quality of retinoid transporters and/or isomerases.

On the other hand, assuming that PTGDS, released from the RPE, enters the photoreceptor outer segments and is then transported via the cilium in the retrograde direction, it would potentially interact with TOPORS prior to being transported to its subsequent destination. Possibly a specific ubiquitin modification by TOPORS (other than with ubiquitin-48- and -63-linked chains, which would target for degradation by the proteasome and lysosome, respectively) (reviewed in: Komander e Rape, 2012), would direct PTGDS to its intended destination, where it could play an as yet unidentified role.

As was already described in section 4.3.3.2, PTGDS was shown to have a high affinity for binding all-*trans*-retinoic acid and 9-*cis* retinoic acid as well as all-*trans* retinal and 13-*cis* retinal, but not vitamin A (all-*trans* retinol) (Tanaka *et al.*, 1997). The authors additionally highlighted that nuclear receptors for retinoids also bind 9-*cis* retinoid acid and all-*trans* retinoic acid, resulting in transcription of retinoid-responsive genes.

Overall, two types of retinoid transporters can be differentiated: extracellular, such as plasma retinol-binding protein (RBP), and intracellular, e. g. cellular RBP, or cellular retinoic acid binding protein (CRABP). PTGDS has been detected in various body fluids, in and outside of the CNS, as well as inside the cells. Consequently, it could be involved in retinoid transport both: intra- and extracellularly. It could be speculated that PTGDS may work as a messenger molecule between the RPE cells and the photoreceptors. Perhaps it is released from the RPE cells, with a retinoic acid bound within its pocket, and it is subsequently taken up by the photoreceptors, putatively following recognition by RIG1. Subsequently, it could travel towards the nucleus where it may transfer the retinoic acid compound to a specific nuclear retinoid receptor (or to another transporter, which would in turn dock it onto a nuclear

receptor); depending on the conformation of the retinoic acid (*all-trans* or *9-cis*), a message to transcribe, or suppress, specific genes could be conveyed.

PTGDS was previously shown to possess both: pro- as well as anti-apoptotic activities depending on the environment (Ragolia *et al.*, 2001; Ragolia *et al.*, 2003; Fujimori, Fukuhara, *et al.*, 2012; Fukuhara *et al.*, 2012; Maesaka *et al.*, 2013). It could be speculated that PTGDS affects expression of genes involved in regulation of cell survival and apoptosis. Regulation of PTGDS levels by ubiquitination by TOPORS could act upstream to indirectly regulate this putative pathway. Since, photoreceptor degenerations are known to converge on a common apoptotic pathway (Wright *et al.*, 2010), this option forms a reasonable possibility.

### 9.3 PSMC1 COULD HAVE PROTECTIVE FUNCTIONS IN THE RETINA

*PSMC1* is a ubiquitously expressed essential component of the 26 S protease. *PSMC1* appears to have no direct link to the retina, according to literature published to date; however, it is often purposefully knocked down in a conditional manner to generate neurodegeneration mouse models (Bedford *et al.*, 2008; Gómez-Garre *et al.*, 2012; Paine *et al.*, 2013). Hence it could also be involved in retinal neurodegeneration.

Remarkably, a *PSMC1* orthologue was shown to mediate responses to light-induced stress in plants. It would be interesting to investigate whether *PSMC1* is perhaps of similar functional importance in tissues, such as the retina, which are exposed to light stress in the animal kingdom. The structure of *PSMC1* and its orthologues is conserved among plant, animal and fungi kingdoms, which presents a sound basis for consequent conservation of its function. Indeed, its role in proteasomal degradation in these three kingdoms has been documented (Hartmann-Petersen, Tanaka e Hendil, 2001; Takeuchi e Tamura, 2004; Park *et al.*, 2009; Bar-Nun e Glickman, 2012; Lee, K. H. *et al.*, 2012), and is supportive of its interaction with TOPORS, which is also involved in protein homeostasis via its E3 ubiquitin ligase activity.

Once the PPIs between full-length TOPORS and *PSMC1* were demonstrated in yeast, experiments were performed to delineate the domains of TOPORS, which mediate its interactions with this newly-identified protein partner. A result was considered positive overall, if blue growth, indicating a PPI, was observed in at least four out of six experiments at a given stringency level (i.e. activation of two reporter genes: D+; and activation of four reporter genes: Q+).

Findings presented in Table 9-5 show that *PSMC1* interacted most strongly with the mid-TOPORS and the C-term TOPORS fragments. Both of these fragments are involved in SUMOylation activities; in addition the mutational hotspot of TOPORS is located within the C-term TOPORS fragment (Figure 6-1). These results suggest that TOPORS may be important for SUMOylation of *PSMC1*. This could hypothetically regulate the proteasomal function. At least one SUMO-interacting motif (SIM:  $\Psi Kx E$ , where  $\Psi$  is a hydrophobic amino acid, K is lysine, x is any amino acid, and E is glutamate) is found within human *PSMC1* sequence at residues 63LKLE66 (where L is leucine). It is possible that fragment 174MKVE177 (where M is methionine, and V is valine) could act as another SIM, however, methionine is only weakly hydrophobic, making this region less likely to be involved in SUMO binding. *PSMC1* SUMOylation has never been demonstrated empirically; however, based on the bioinformatics data, future work should aim to investigate this possibility.

Table 9-5. TOPORS and PSMC1 interactions in yeast.

Key: D+ = growth on DDO/X/A (a lower stringency medium, indicating a PPI based on activation of two reporter genes); D- = no growth on DDO/X/A, i.e. no PPI; Q+ = growth on QDO/X/A (a higher stringency medium, indicating a PPI based on activation of four reporter genes); Q- = no growth on QDO/X/A, i.e. no PPI. TM, trans-membrane; BH3, Bcl 2 homology 3; PEST, Proline, Glutamate, Serine, and Threonine-rich region; CTS, ciliary-targeting sequence; SR/RS, arginine and serine-rich region; SUMO1, Small ubiquitin-related modifier 1; NLS, nuclear localisation signal; Lys/His, lysine- and histidine-rich region. Refer to Chapter 6 for detailed figures demonstrating the position of motifs within TOPORS and PSMC1 proteins.

Prey		Baits: Full-length TOPORS and its fragments			
Construct	PSMC1	Full-length TOPORS	N-term TOPORS	Mid-TOPORS	C-term TOPORS
<b>Motifs</b>	Full-length: N-myristoylation site and consensus motif; NADH-binding site; CTS # 1 and 2; ATP-binding loop; ATP-hydrolysis site and aromatic loop; proteasomal ATPase-anchoring region; phosphoserine 4; phospho-tyrosine 439; ubiquitin acceptor site; N-acetylation site; O-linked glycosylation site(Figure 6-11).	Full-length (Figure 6-2, or the subsequent columns).	PEST domain # 1; phosphoserine 98; RING finger domain; CTS # 1 (Figure 5-9).	PEST domains # 2 and 3; CTS # 2; SR/RS-rich domain # 1 and # 2; SUMO1 acceptor site; NLS; phosphoserine 718; (Figure 5-10).	SR/RS-rich domain # 2; phosphoserine 718; mutational hot spot; Lys/His motif; PEST domains # 4 and 5 (Figure 5-11).
<b>PPI summary</b>		<b>D+ Q-</b>	<b>D+ Q-</b>	<b>D+ Q+</b>	<b>D+ Q+</b>

Similarly to the mitochondrial hypothesis, mentioned in case of ITM2Bs, robust protein turnover mechanisms are also critical to correct functioning of highly active cellular systems, such as the retina. In specialised cell types with such high metabolic rates proteins need to keep undergoing constant quality control, which would involve protein degradation pathways.

PSMC1 orthologues, studied thoroughly in plant systems, were additionally shown to perform functions, such as regulation of cell growth, histone dynamics and nucleosome assembly (Sonoda *et al.*, 2009; Lee *et al.*, 2011; Lee, K. H. *et al.*, 2012).

Work in plants also showed that a PSMC1 homologue is involved in regulation of the cell cycle, specifically DNA replication and regulation of the G2/M checkpoint, which is in agreement with its involvement in nucleosome and histone regulation; the mutation phenotype is associated with an abnormal polyploidy, and leading to an enlarged leaf phenotype due to increased cell size. RNAi-mediated knock-down of PSMC1 in mammalian cells could be used to investigate, whether similar effects are observed in mammalian systems. In fact, the involvement of

PSMC1 in cell cycle defects was documented in mammals (Rezvani *et al.*, 2003; Rezvani *et al.*, 2012), which is in agreement with localisation of PSMC1 to centrosomes in human cell lines; this was, however, observed inconsistently (Chapter 7 and Table 9-7).

Table 9-6. PSMC1 localisation summary.

Key: PCM1, peri-centriolar material 1; PLK4, polo-like kinase 4; OS, photoreceptor outer segment; RPE, retinal pigmented epithelium.

Sub-cellular localisation in hTERT-RPE1 cells		Localisation within retinal tissue cryo-sections	
Dividing cells	<p>Co-localised with TOPORS in a centriole-like pattern in some cells at interphase; diffuse cytoplasmic signal was also observed for both proteins (PSMC1 signal appeared stronger).</p> <ul style="list-style-type: none"> <li>Co-localised with PCM1 during interphase in some cells, but no co-localisation at all was observed in others.</li> <li>Co-localised with PLK4 at interphase in a centriole-like pattern; however, where two PLK4-stained dots were stained, PSMC1 always co-localised with only one of them.</li> <li>Co-localised with Centrin-2 during interphase, as well as surrounded it (the surrounding signal was uniformly continuous with the area of signals' co-localisation; not cloud-like, or granular).</li> </ul>	Mouse – 2 weeks old	No PSMC1 signal was observed at all (data not shown).
		Mouse – 6.5 months old	Localised at the RPE-OS interface only in sections not treated to retrieve antigen (Figure 8-10). In sections subject to HIER, PSMC1 immuno-staining was observed in IS as well as the RPE-OS interface (Figure 8-11).
Ciliated cells	Co-localised with $\alpha$ tubulin (used as a ciliary marker) in a dot-like pattern reminiscent of centrioles, but was not observed at the ciliary basal body.	Macaque	No PSMC1 signal was observed at all (data not shown).

It could be speculated that in photoreceptors, or in neurons, in general, which are non-dividing, differentiated cells, PSMC1 is additionally required for mediating signalling pathways, which prevent cellular growth. SUMOylation by TOPORS could modulate such a function, and its impairment might result in cells attempting to re-enter the cell cycle and start growing and dividing again. Within the retina this would eventually trigger apoptotic pathways, leading to photoreceptor cell death.

The PSMC1 protein contains a consensus *N*-myristoylation sequence (residues 1-6), conserved in humans, *Saccharomyces cerevisiae* (yeast), *Drosophila melanogaster* (fruit-fly), and in *Arabidopsis thaliana* (mouse-ear cress); this modification was demonstrated in yeast and plants (Kimura, Kato e Hirano, 2012; Lee, K. H. *et al.*, 2012). It is noteworthy that in the initial Y2H screen TOPORS interacted with glycopeptide N-tetradecanoyltransferase 1 (NMT1; Table



11-6 in Appendix 11-6), which catalyses the myristoylation of certain cellular and viral proteins (UniProt: P30419). This putative interaction was never confirmed, but it could be speculated that TOPORS acts upstream of NMT1 to stimulate, or prevent, PSMC1 myristoylation.

*N*-myristoylation of PSMC1 is required for localisation of the proteasomal complex to the nucleus, potentially by anchoring it within the nuclear envelope. Mutations of glycine 2, otherwise modified by the myristoyl attachment, trigger re-location of the proteasome from the nucleus to the cytoplasm (Kimura, Kato e Hirano, 2012). However, modification of this glycine does not appear to affect protein function, as even transgenes lacking this residue, were able to rescue the developmental phenotype and proteasomal stress, induced by silencing of the PSMC1 orthologue in plants (Lee *et al.*, 2011). Conversely, a transgene lacking the N-terminal thirteen residues was not able to rescue the developmental phenotype, and plants still displayed abnormal leaf morphology, delayed root growth, and an excess of trichome branching (Lee, K. H. *et al.*, 2012).

Importantly, the myristoylation modification may be important for docking PSMC1 onto cellular vesicles targeted for the primary cilium and/or photoreceptor outer segments. It may also allow for 'hitch-hiking' of other 26 S protease components to the OS. There the proteins could work in concert with TOPORS to tackle protein degradation requirements near the basolateral outer segment membrane.

## 9.4 FUTURE PERSPECTIVES

Three interacting partners of TOPORS were identified using a Y2H-based screen of human retinal cDNA library. The interactions were validated and evaluated in mammalian cells and tissues in addition to further experiments in yeast. Two of these interacting proteins have documented functions in the retina: ITM2B has been implicated in autosomal dominant retinal dystrophy; whereas PTGDS was suggested to play a role in maintaining the blood-retina barrier as well as in transport of retinoid compounds. The third interacting partner of TOPORS, PSMC1, was selected for evaluation since, like TOPORS, it participates in protein turnover by the ubiquitin-proteasome system, in which it plays a key regulatory function; it had a strong association with neurodegeneration in mammals, and was shown to play crucial roles in responses to light-induced stress in plants.

Neither one of these three proteins displays a specific retina expression pattern. On the contrary, just like TOPORS, all three are ubiquitous.

Based on findings from direct interactions in yeast, involving TOPORS fragments, it can be speculated that the interactions between TOPORS and ITM2B, as well as between TOPORS and PTGDS, would likely involve ubiquitination of these interacting partners by TOPORS. An alternative scenario, in which TOPORS participated in a putative ITM2B signalling pathway, could also occur. The strongest associations between TOPORS and PSMC1, involved fragments required for the SUMO1 E3 ligase activity of TOPORS, thus it was speculated that TOPORS SUMOylated PSMC1. Future experiments, aiming to verify these findings could include ubiquitination and SUMOylation assays in mammalian cell lines. A basal level of modification of the proteins of interest by ubiquitin and/or SUMO1 would first be determined. In subsequent experiments TOPORS would be over-expressed and/or silenced, and effects of this manipulation on levels on ubiquitination and/or SUMOylation would be determined by Western blotting.

Further work, planned to explain the observed results, involves Western blotting and coIP of proteins from cellular lysates, extracted from specific cellular fractions. Additionally, treatment of these protein extracts with enzymes, which would remove the putative glycosylation (and other) modifications, would also help clarify the observations from current Western blot and co-IP experiments. This could be especially helpful in understanding the processing of ITM2B and PTGDS, which are subject to proteolytic cleavage and heavy post-translational modification. Additionally, these post-translational features may be related to the presence of the proteins of interest in specific cellular compartments. For instance, it would be interesting

to determine whether glycosylation is at all important for ciliary targeting of these proteins in a similar manner to lipidation (reviewed in: Hsiao, Tuz e Ferland, 2012). The glycosylation site of ITM2B is located very closely to two of its ciliary-targeting sequences (CTS) on the BRICHOS domain (Figure 6-5). Two of the three confirmed carbohydrate modifications of PTGDS are also found proximally to the protein's CTS motifs (Figure 6-8). The site of PSMC1 glycosylation has not been established yet; however, its myristoylation modification (Figure 6-11) could play a role in ciliary targeting, as is known to happen for NPHP3.

It is noteworthy that in the initial Y2H screen TOPORS interacted with bifunctional protein NCOAT (*MGEA5*; Table 10-6 in Appendix 10-6), which catalyses the cleavage of N-acetyl glucosamine, but not N-acetyl galactosamine, from glycopeptides; it was also shown to possess hyaluronidase and acetylase activities (UniProt: O60502). However, the putative interaction between TOPORS and this enzyme was never confirmed. If *MGEA5* became validated as a true interacting partner of TOPORS, it would be interesting to investigate whether perhaps it works in concert with TOPORS to modulate the glycosylation modifications of ITM2B, PTGDS and PSMC1. It could also be required for the acetyl modification of PSMC1 (Figure 6-11).

Furthermore, TOPORS and its three interacting partners were observed to co-localise at the centrosomes in the human RPE1 cell line. This indicates a potential involvement of these proteins in the cell cycle and/or centrosome replication cycle. Nonetheless, only PTGDS was observed along the axoneme and at the basal bodies of primary cilia as well as co-localising with TOPORS at the connecting cilium in retinal sections, suggesting that this one interacting partner may have a more specific role in quiescent differentiated cells, whereas ITM2B and PSMC1 are perhaps more important for centrosomal homeostasis of dividing cells.

Still, in mouse retinal sections, some co-localisation was observed between TOPORS and ITM2B in the region of connecting cilia. Nonetheless, this observation requires a further, more thorough investigation. This could be achieved by silencing and/or over-expressing TOPORS to evaluate how the localisation of its interacting partners is affected (if at all) in mammalian cell culture systems. Additionally, future cell work with the three interacting partners of TOPORS should incorporate cell cycle arrest experiments to delineate the relevant cell cycle stages more precisely. RNA interference (RNAi)-mediated knock-down of each interacting protein could be used to observe the effects on the cell cycle of losing that particular interacting partner. For example, the pattern of co-staining with centriolar markers (Table 7-3 or Tables 9-2, 9-4 and 9-6) indicated that the association of the TOPORS' interactors with centrioles occurred at very precise cell cycle stages, and sometimes with a preference for only one of

the two centrioles of a centrosome (Figures 7-27 and 7-28). Yet, this was concluded solely on the observations of fluorescent micrographs, depicting non-synchronised cell cultures.

If cells were synchronised by serum starvation (which blocks them at G<sub>0</sub>, which triggers cilia growth), and then simultaneously released from the starvation, this would help to more precisely distinguish the cell cycle stage(s), at which co-localisation with centrioles occurs. Cell cycle arrest at specific phases, using chemical compounds would ensure an even greater accuracy; however, this method may be more detrimental to the overall physiology of the cell cycle-arrested cell.

Furthermore, studies in cells cultured at different confluence levels could also help characterise the cellular localisations observed for all three interacting proteins. For instance, in ciliated cells cultured to a high confluence levels TOPORS localises to the basal bodies of primary cilia. However, in dividing cells, which have not experienced contact-induced inhibition, TOPORS is observed throughout the cytoplasm, where it is associated with the actin cytoskeleton (Dr Amna Z. Shah: personal communication). This observation may reflect the sub-cellular localisation of TOPORS in a differentiated and growing tissue, respectively. It is possible that the interactors of TOPORS would display analogous changes in apparent cellular localisations depending on cell culture confluence level, or on the tissue type that they are expressed in.

Site-directed mutagenesis (SDM) of the ciliary-targeting sequences (CTS) within TOPORS, as well as those identified in ITM2B, PTGDS and PSMC1, could also be performed in order to determine whether these bioinformatics-predicted sequences do indeed affect the localisation of the proteins of interest to the primary cilia. Additionally, the fate of ITM2B, PTGDS and PSMC1 could be studied in a *TOPORS* knock-down mouse model, which should provide additional explanations regarding the nature of associations between TOPORS and these interacting partners.

Defining the basal protein levels of TOPORS and its interacting partners in different cellular compartments, preferably by extracting proteins from cellular fraction of synchronised cells at specific cell cycle stages, would also help delineate their potential roles, and, thus, the nature of the observed interactions. This would be especially relevant to PTGDS and ITM2B, as they are both expected to carry different post-translational modifications, depending on whether they are still undergoing processing in intracellular compartments, or whether they are excreted, or bound to plasma membrane, respectively. With regard to ITM2B, represented by

several peptides on Western blotted membranes (Figures 6-4, 6-6 and 6-7), this would additionally serve to verify the published data about where and when the protein undergoes specific proteolytic processing steps. In order to obtain more definite results the protein extracts should additionally be treated with de-glycosylation enzymes prior to SDS-PAGE.

To test the hypothetical effects of the *ITM2B* retinal mutant, an experiment could be performed, which would involve silencing of endogenous *ITM2B* in cell lines, followed by over-expression of wild-type *ITM2B* (as control) and the retinal mutant *ITM2B*, tagged at the C-terminus. Western blots could then be performed, using an antibody against the tag. The tagged CCTP fragment should be detected in cells, expressing the wild-type protein; however, no corresponding band should be observed for the retinal mutant, if the retinal *ITM2B* mutation does indeed impair proteolytic cleavage by furin.

Further work, to better understand the nature of the interaction between TOPORS, *ITM2B* and *PSMC1* could focus on mitochondrial homeostasis. Mitochondrial localisation of a shorter *ITM2B* isoform was associated with loss of membrane potential of this organelle and apoptosis, which could suggest converging functions of *ITM2B* and TOPORS at this organelle (Fleischer, Ayllon e Rebollo, 2002; Fleischer *et al.*, 2002; Fleischer e Rebollo, 2004). In mouse models of neurodegeneration *PSMC1* has also been implicated in mitochondrial protein quality control and homeostasis, providing further support for focusing on this organelle in context of the retina (Paine *et al.*, 2013). Additionally, mitochondrial DNA damage might occur due to light-induced oxidative stress. If *PSMC1* was found to mediate responses to these stresses, this would provide evidence of a functional correlation with the plant orthologue of *PSMC1*.

This section provided an overview of experiments, which could be performed as a continuation of this PhD project. The next section offers a different outlook at the initial question of the project; i.e. why mutations in ubiquitously expressed genes, here *TOPORS*, result in retina-restricted disease.

## 9.5 ALTERNATIVE APPROACHES

Mutations, which were originally identified in TOPORS in German and French Canadian families presenting with autosomal dominant retinitis pigmentosa (adRP), concentrate closer to the C-terminal region of the TOPORS protein: after the RS/SR domain, but before the Lys/His domain. They lead to a shift of the protein reading frame, resulting in early termination codons. Thus they are believed to cause the production of truncated TOPORS proteins, which become immediately degraded, or perhaps the transcripts are subject to nonsense-mediated decay. Hence, haploinsufficiency was proposed as the disease mechanism for these mutants.

More recently, a Scandinavian study identified a missense mutation in TOPORS, located within the second PEST domain in close proximity to the second CTS region. The mutation, also inherited in a dominant manner, causes a single amino acid change, and the resulting disease, a pericentral retinal dystrophy, is less severe than adRP.

The specific pericentral retinal degeneration may reflect a putative differential expression of *TOPORS* across the retina. Perhaps the rod photoreceptors located pericentrally naturally express a lower level of TOPORS, compared to those towards the periphery. This could explain why the periphery is not affected by the 'mild' p.Glu402Pro mutation, as sufficient wild-type protein is probably produced from the un-mutated gene copy. It is also possible that the mutant is still able to retain some functions of TOPORS, conveyed by residues located away from the mutation site.

On the other hand, complete removal of a copy of TOPORS due to a potential truncating mutation, results in a more severe RP phenotype.

In order to better understand the nature of the retinal phenotypes, associated with *TOPORS* mutations, several alternative approaches could have been undertaken.

Firstly, bioinformatics methods could have been implemented to evaluate conservation of *TOPORS* between species. Creation of a phylogenetic tree for this gene would allow for determining how long ago it evolved and in what types of organisms it is present, and hence it would at least help determine its putative importance, if not delineate its function. Identification of expression profiles of *TOPORS* in different tissues would also help characterise the gene; for instance, it would be interesting to determine whether it perhaps came into existence as a fusion between two genes (phylogeny study would aid in determining this), giving rise to a "Rosetta stone protein," and what it could mean. Such an event could

be expected to have occurred, as very few proteins exist, which possess a dual E3 ubiquitin as well as SUMO1 ligase activity. In fact, TOPORS was the first protein known to perform both these enzymatic activities. Understanding the origin of this gene, and determining whether or not it came to exist as a fusion between two genes, could help recognize why it emerged and thus what its roles are.

Bioinformatics could also be used as an alternative to the Y2H screen for trying to predict the protein-protein interactions (PPIs) *in silico*. Various algorithms could be utilised for determining the PPIs. For instance, compatibility of the tertiary structures of different proteins could be determined; the emphasis on tertiary structure is key, as proteins can sometime display homology of their three-dimensional structures, even if they lack homology at the level of the amino acid sequence (primary structure). Additionally, primary structure evaluation could be used for identifying “signature sequences” of the protein of interest, available in genomic databases, based on empirically verified data, which could then be linked to “signature sequences” of putative interactors. Alternatively, the focus could be on specific domains of the protein of interest, aiming to identify other domains (and thus indirectly proteins), which the domain of the protein of interest would interact with.

Affinity chromatography-based approaches, coupled to mass spectrometry based peptide sequencing would aid in delineating whole putative protein networks rather than solely binary interactions. It would be helpful to elucidate wider protein networks, which TOPORS forms a part of within the different cell types of the retina, not only neuronal, but also glial and epithelial. It would also help establish the basis of this interaction, e.g. to determine whether TOPORS participates in ubiquitination and/or SUMOylation of certain components of the network.

Gene expression profiling would be a very informative alternative to PPI studies. Microarray experiments could be performed, for instance, to compare gene expression a wild-type animal and a mutant *TOPORS* animal model. Alternatively, gene expression in different regions of the retina, e.g. centre vs. periphery, or from different retinal cell types, could help explain the peri-central retinal dystrophy observed in the Scandinavian pedigree. Furthermore, a comparison of gene expression in light- and dark-adapted animals (both: wild-type and mutant) could perhaps explain the light-dependent translocation pattern of TOPORS within photoreceptor cells.

An animal model should also be studied at the protein level. Specifically, the histology of tissues, hypothetically affected by TOPORS mutations, should be compared between the wild-type and mutant animals. Gene profiling in tissues affected at protein level could then also be performed. Moreover, electron microscopy imaging should be performed in the affected tissues in order to accurately examine and compare the structure of primary cilia between wild-type animals and mutants. It would also be important to conduct the described experiments at different developmental stages, focusing on the tissue of primary interest, here: the retina.

At the cell culture level constructs of *TOPORS*, carrying mutations, identified in patients could be studied. Firstly, to re-confirm the truncating mutations of the *RP31* phenotype, and secondly to characterize the Scandinavian *TOPORS* mutant, which is expected to be expressed. Alternatively, *TOPORS* plasmids could be constructed, in which the proteins' functional domains would be individually removed. If they were then expressed in a cell line, stably transfected with a plasmid encoding the shRNA against *TOPORS*, aiming to knock-down the endogenous *TOPORS*, this could help determine the significance of individual TOPORS protein domains for cellular functions and survival.

Finally, *TOPORS* regulatory DNA sequences could also be studied in different tissues, or cell types, to try to determine whether anything unique happens in the retina in terms of *TOPORS* expression due to a difference in its regulation at genetic level. Perhaps retina-specific DNA-binding regulatory elements are involved.

Many of the approaches described in this section could have been used instead of the Y2H as well as the following verification procedures. For instance, a thorough characterisation of the mouse model would probably comprise a whole separate project on its own. Similarly, the procedures and analysis involved in affinity chromatography- and mass spectrometry-based peptide sequencing, which would include identification of proteins found in a complex with TOPORS as well as their modifications, would probably also require a substantial amount of time and resources. This would also to a large extent be true for micro-array based gene profiling studies.

On the other hand, many of the bioinformatics methods could have been used as an alternative to the Y2H screening only, and the results of these *in silico* experiments could then have been verified empirically, using many of the same procedures involved in validation of Y2H screening results. An initial affinity chromatography- and mass spectrometry-based



identification of TOPORS' interactors could also have been performed instead of the Y2H screen (yet, it would result in identification of constituents of whole protein complexes rather than binary interactions), which could have been followed by a characterisation in cell lines and tissue sections.

Overall, a thorough characterisation of a gene, and its protein product(s), should probably include most, if not all, of the approaches referred to in this section. No one method can ever give a full picture of genes and/or proteins roles; therefore, diverse complementary methods should probably be used in order to answer such an ambiguous research question as: why mutations in a widely-expressed gene appear to result in tissue-restricted phenotypes.

## 9.6 CONCLUSIONS

The primary aim of this PhD project was to determine why mutations in *TOPORS*, which is a ubiquitously expressed gene, cause a phenotype specific to the retina. It was hypothesised that TOPORS protein associates with a retina-specific protein at the basal body of the rod photoreceptor connecting cilium; when the interaction is impaired, this leads to photoreceptor degeneration and cell death.

The results generated throughout this project contribute only a minute component to the overall knowledge of retinal functions, or a specific role of TOPORS in the retina. Thus, the answer to the initial research question remains largely elusive.

The work led to identification of ITM2B, PTGDS and PSMC1 proteins as interacting partners of TOPORS using the Y2H screen. They were all shown to be expressed in the human retina at mRNA levels, were found together in protein complexes precipitated from human HeLa cells, and co-localised with TOPORS in human hTERT-RPE1 cell lines as well as mammalian retinal cryo-sections. Their precise functions in the retina require further elucidation; however, findings from this project have made it possible to develop several novel hypotheses, regarding the association between TOPORS and its interactors, and their significance in context of retinal homeostasis.

ITM2B was shown to be involved in regulation of APP processing and A $\beta$  levels in cell (Fotinopoulou *et al.*, 2005; Matsuda *et al.*, 2008); thus, it could be hypothesised that it has the same role in photoreceptors outer segments, which are affected by increasing A $\beta$  deposition, correlated with aging (Hoh Kam, Lenassi e Jeffery, 2010). TOPORS mutations could affect the retrograde transport of ITM2B-containing vesicles from the Golgi membranes to the base of the connecting cilium, or their docking at the base of the cilium. This in turn could result in impaired trafficking of ITM2B to outer segments, and photoreceptor dysfunction due to the A $\beta$  deposition.

PTGDS could possibly be involved in recycling of retinoid compounds between the RPE cell layer and the photoreceptor outer segments lines (Tanaka *et al.*, 1997; Shimamoto *et al.*, 2007), as well as it could be involved in inter-cellular signalling from the RPE cells to the photoreceptor cells. In the latter case it may need to interact with TOPORS at the basal body of primary cilium, whilst being transported from the RPE, via the outer segment to the inner segment of a photoreceptor cell. There, it might affect gene expression by, e.g. docking retinoic acid molecules on specific nuclear receptors.

PSMC1 is conserved across eukaryotes and has a documented protective role in plants subjected to light-induced stress (Lee, K. H. *et al.*, 2012). Furthermore, the protein and its orthologues have been associated with ER-phagosomes (UniProtKD), which is supportive of the prominent presence of PSMC1 at the region of RPE phagocytosis in the retina. TOPORS is an E3 ubiquitin ligase, expressed in the RPE layer (although to a lesser extent than PSMC1); therefore, it could also possibly be involved in RPE phagocytosis.

Hence, the obtained data allowed for speculating about putative roles of TOPORS' interactors in the retina, and thus, indirectly, about hypothetical retina-specific roles of TOPORS. Yet, no definitive conclusions could be drawn as to why mutations in *TOPORS*, which is a ubiquitously expressed gene, cause a retina-restricted disease. Instead, the findings resulted in generation of new hypotheses summarised above.

The data obtained throughout this project contributes to the general knowledge about the retina, even if it does not accurately determine the role of the ubiquitous gene *TOPORS* in causing a retina-restricted disease. An in-depth insight into the tissue of interest, here the retina, forms a pre-requisite for inventing treatments for tissue-specific diseases, such as retinitis pigmentosa. Consequently, the results presented in this thesis could indirectly aid in development of future therapies for retinal dystrophies by complementing our current understanding of the highly specialised and complex retinal tissue.

## 10 BIBLIOGRAPHY

AKIYAMA, H. *et al.* Expression of BRI, the normal precursor of the amyloid protein of familial British dementia, in human brain. *Acta Neuropathol*, v. 107, n. 1, p. 53-8, Jan 2004. ISSN 0001-6322. Disponível em: < <http://www.ncbi.nlm.nih.gov/pubmed/14586629> >.

AL-HUSSAINI, H. *et al.* Mature retinal pigment epithelium cells are retained in the cell cycle and proliferate in vivo. *Mol Vis*, v. 14, p. 1784-91, 2008. ISSN 1090-0535. Disponível em: < <http://www.ncbi.nlm.nih.gov/pubmed/18843376> >.

ALLER, E. *et al.* The USH2A c.2299delG mutation: dating its common origin in a Southern European population. *Eur J Hum Genet*, v. 18, n. 7, p. 788-93, Jul 2010. ISSN 1476-5438. Disponível em: < <http://www.ncbi.nlm.nih.gov/pubmed/20145675> >.

\_\_\_\_\_. Genetic analysis of 2299delG and C759F mutations (USH2A) in patients with visual and/or auditory impairments. *Eur J Hum Genet*, v. 12, n. 5, p. 407-10, May 2004. ISSN 1018-4813. Disponível em: < <http://www.ncbi.nlm.nih.gov/pubmed/14970843> >.

ANGENSTEIN, F.; BUCHNER, K.; STAAK, S. Age-dependent differences in glutamate-induced phosphorylation systems in rat hippocampal slices. *Hippocampus*, v. 9, n. 2, p. 173-85, 1999. ISSN 1050-9631. Disponível em: < <http://www.ncbi.nlm.nih.gov/pubmed/10226777> >.

APPLEBURY, M. L. *et al.* The murine cone photoreceptor: a single cone type expresses both S and M opsins with retinal spatial patterning. *Neuron*, v. 27, n. 3, p. 513-23, Sep 2000. ISSN 0896-6273. Disponível em: < <http://www.ncbi.nlm.nih.gov/pubmed/11055434> >.

ARAKI, M. *et al.* Centrosome protein centrin 2/caltractin 1 is part of the xeroderma pigmentosum group C complex that initiates global genome nucleotide excision repair. *J Biol Chem*, v. 276, n. 22, p. 18665-72, Jun 2001. ISSN 0021-9258. Disponível em: < <http://www.ncbi.nlm.nih.gov/pubmed/11279143> >.

ARSHAVSKY, V. Y. Vision: the retinoid cycle in *Drosophila*. *Curr Biol*, v. 20, n. 3, p. R96-8, Feb 2010. ISSN 1879-0445. Disponível em: < <http://www.ncbi.nlm.nih.gov/pubmed/20144777> >.

AUDO, I. *et al.* The familial dementia gene revisited: a missense mutation revealed by whole-exome sequencing identifies ITM2B as a candidate gene underlying a novel autosomal dominant retinal dystrophy in a large family. *Hum Mol Genet*, Sep 2013. ISSN 1460-2083. Disponível em: < <http://www.ncbi.nlm.nih.gov/pubmed/24026677> >.

ÅKERSTRÖM, B. *Lipocalins*. Georgetown, Tex.: Landes Bioscience ; Eurekah.com, 2006. 204 p. ISBN 9781587062971  
1587062976.

BADANO, J. L. *et al.* The ciliopathies: an emerging class of human genetic disorders. *Annu Rev Genomics Hum Genet*, v. 7, p. 125-48, 2006. ISSN 1527-8204. Disponível em: < <http://www.ncbi.nlm.nih.gov/pubmed/16722803> >.

BALCH, W. E. *et al.* Adapting proteostasis for disease intervention. *Science*, v. 319, n. 5865, p. 916-9, Feb 2008. ISSN 1095-9203. Disponível em: < <http://www.ncbi.nlm.nih.gov/pubmed/18276881> >.

BAR-NUN, S.; GLICKMAN, M. H. Proteasomal AAA-ATPases: structure and function. *Biochim Biophys Acta*, v. 1823, n. 1, p. 67-82, Jan 2012. ISSN 0006-3002. Disponível em: < <http://www.ncbi.nlm.nih.gov/pubmed/21820014> >.

BARON, B. W.; BARON, R. M.; BARON, J. M. The ITM2B (BRI2) gene is a target of BCL6 repression: Implications for lymphomas and neurodegenerative diseases. *Biochim Biophys Acta*, Dec 2014. ISSN 0006-3002. Disponível em: < <http://www.ncbi.nlm.nih.gov/pubmed/25557390> >.

BARRETT, K. E. *et al.* Ganong's Review of Medical Physiology. 23rd edition. McGraw-Hill, 2010.

BEDFORD, L. *et al.* Depletion of 26 S proteasomes in mouse brain neurons causes neurodegeneration and Lewy-like inclusions resembling human pale bodies. *J Neurosci*, v. 28, n. 33, p. 8189-98, Aug 2008. ISSN 1529-2401. Disponível em: < <http://www.ncbi.nlm.nih.gov/pubmed/18701681> >.

\_\_\_\_\_. The UPS and autophagy in chronic neurodegenerative disease: six of one and half a dozen of the other--or not? *Autophagy*, v. 5, n. 2, p. 224-7, Feb 2009. ISSN 1554-8635. Disponível em: < <http://www.ncbi.nlm.nih.gov/pubmed/19077533> >.

BERGLUND, L. *et al.* A genecentric Human Protein Atlas for expression profiles based on antibodies. *Mol Cell Proteomics*, v. 7, n. 10, p. 2019-27, Oct 2008. ISSN 1535-9484. Disponível em: < <http://www.ncbi.nlm.nih.gov/pubmed/18669619> >.

BETTENCOURT-DIAS, M.; CARVALHO-SANTOS, Z. Double life of centrioles: CP110 in the spotlight. *Trends Cell Biol*, v. 18, n. 1, p. 8-11, Jan 2008. ISSN 1879-3088. Disponível em: < <http://www.ncbi.nlm.nih.gov/pubmed/18068367> >.

BEUCKMANN, C. T. *et al.* Lipocalin-type prostaglandin D synthase (beta-trace) is located in pigment epithelial cells of rat retina and accumulates within interphotoreceptor matrix. *J Neurosci*, v. 16, n. 19, p. 6119-24, Oct 1996. ISSN 0270-6474. Disponível em: < <http://www.ncbi.nlm.nih.gov/pubmed/8815894> >.

\_\_\_\_\_. Cellular localization of lipocalin-type prostaglandin D synthase (beta-trace) in the central nervous system of the adult rat. *J Comp Neurol*, v. 428, n. 1, p. 62-78, Dec 2000. ISSN 0021-9967. Disponível em: < <http://www.ncbi.nlm.nih.gov/pubmed/11058225> >.

BLAIN, D. *et al.* eyeGENE®: a vision community resource facilitating patient care and paving the path for research through molecular diagnostic testing. *Clin Genet*, v. 84, n. 2, p. 190-7, Aug 2013. ISSN 1399-0004. Disponível em: < <http://www.ncbi.nlm.nih.gov/pubmed/23662816> >.

BLOTTA, S. *et al.* Identification of novel antigens with induced immune response in monoclonal gammopathy of undetermined significance. *Blood*, v. 114, n. 15, p. 3276-84, Oct 2009. ISSN 1528-0020. Disponível em: < <http://www.ncbi.nlm.nih.gov/pubmed/19587378> >.

BOUGHMAN, J. A.; VERNON, M.; SHAVER, K. A. Usher syndrome: definition and estimate of prevalence from two high-risk populations. *J Chronic Dis*, v. 36, n. 8, p. 595-603, 1983. ISSN 0021-9681. Disponível em: < <http://www.ncbi.nlm.nih.gov/pubmed/6885960> >.

BOUTELL, C. *et al.* Reciprocal activities between herpes simplex virus type 1 regulatory protein ICP0, a ubiquitin E3 ligase, and ubiquitin-specific protease USP7. *J Virol*, v. 79, n. 19, p. 12342-54, Oct 2005. ISSN 0022-538X. Disponível em: < <http://www.ncbi.nlm.nih.gov/pubmed/16160161> >.

BOUTELL, C.; ORR, A.; EVERETT, R. D. PML residue lysine 160 is required for the degradation of PML induced by herpes simplex virus type 1 regulatory protein ICP0. *J Virol*, v. 77, n. 16, p. 8686-94, Aug 2003. ISSN 0022-538X. Disponível em: < <http://www.ncbi.nlm.nih.gov/pubmed/12885887> >.

BOWNE, S. J. *et al.* Mutations in the TOPORS gene cause 1% of autosomal dominant retinitis pigmentosa. *Mol Vis*, v. 14, p. 922-7, 2008. ISSN 1090-0535. Disponível em: < <http://www.ncbi.nlm.nih.gov/pubmed/18509552> >.

BRAUN, K. R. *et al.* Inhibition of PDGF-B induction and cell growth by syndecan-1 involves the ubiquitin and SUMO-1 ligase, Topors. *PLoS One*, v. 7, n. 8, p. e43701, 2012. ISSN 1932-6203. Disponível em: < <http://www.ncbi.nlm.nih.gov/pubmed/22912899> >.

BRÜCKNER, A. *et al.* Yeast two-hybrid, a powerful tool for systems biology. *Int J Mol Sci*, v. 10, n. 6, p. 2763-88, Jun 2009. ISSN 1422-0067. Disponível em: < <http://www.ncbi.nlm.nih.gov/pubmed/19582228> >.

BUCH, H. *et al.* Prevalence and causes of visual impairment and blindness among 9980 Scandinavian adults: the Copenhagen City Eye Study. *Ophthalmology*, v. 111, n. 1, p. 53-61, Jan 2004. ISSN 0161-6420. Disponível em: < <http://www.ncbi.nlm.nih.gov/pubmed/14711714> >.

CALVERT, P. D. *et al.* Light-driven translocation of signaling proteins in vertebrate photoreceptors. *Trends Cell Biol*, v. 16, n. 11, p. 560-8, Nov 2006. ISSN 1879-3088. Disponível em: < <http://www.ncbi.nlm.nih.gov/pubmed/16996267> >.

CAPELSON, M.; CORCES, V. G. The ubiquitin ligase dTopors directs the nuclear organization of a chromatin insulator. *Mol Cell*, v. 20, n. 1, p. 105-16, Oct 2005. ISSN 1097-2765. Disponível em: < <http://www.ncbi.nlm.nih.gov/pubmed/16209949> >.

CARBONE, M. *et al.* Simian virus-40 large-T antigen binds p53 in human mesotheliomas. *Nat Med*, v. 3, n. 8, p. 908-12, Aug 1997. ISSN 1078-8956. Disponível em: < <http://www.ncbi.nlm.nih.gov/pubmed/9256284> >.

CARON, C.; BOYAUULT, C.; KHOCHBIN, S. Regulatory cross-talk between lysine acetylation and ubiquitination: role in the control of protein stability. *Bioessays*, v. 27, n. 4, p. 408-15, Apr 2005. ISSN 0265-9247. Disponível em: < <http://www.ncbi.nlm.nih.gov/pubmed/15770681> >.

CHAKAROVA, C. F. *et al.* TOPORS, implicated in retinal degeneration, is a cilia-centrosomal protein. *Hum Mol Genet*, v. 20, n. 5, p. 975-87, Mar 2011. ISSN 1460-2083. Disponível em: < <http://www.ncbi.nlm.nih.gov/pubmed/21159800> >.

\_\_\_\_\_. Mutations in TOPORS cause autosomal dominant retinitis pigmentosa with perivascular retinal pigment epithelium atrophy. *Am J Hum Genet*, v. 81, n. 5, p. 1098-103, Nov 2007. ISSN 0002-9297. Disponível em: < <http://www.ncbi.nlm.nih.gov/pubmed/17924349> >.

CHATTERJEE, V.; GASHEV, A. A. Aging-associated shifts in functional status of mast cells located by adult and aged mesenteric lymphatic vessels. *Am J Physiol Heart Circ Physiol*, v. 303, n. 6, p. H693-702, Sep 2012. ISSN 1522-1539. Disponível em: < <http://www.ncbi.nlm.nih.gov/pubmed/22796537> >.

CHEN, R. *et al.* Glycoproteomics analysis of human liver tissue by combination of multiple enzyme digestion and hydrazide chemistry. *J Proteome Res*, v. 8, n. 2, p. 651-61, Feb 2009. ISSN 1535-3893. Disponível em: < <http://www.ncbi.nlm.nih.gov/pubmed/19159218> >.

CHEUNG, C. L. *et al.* Reduced serum beta-trace protein is associated with metabolic syndrome. *Atherosclerosis*, v. 227, n. 2, p. 404-7, Apr 2013. ISSN 1879-1484. Disponível em: < <http://www.ncbi.nlm.nih.gov/pubmed/23375684> >.

CHIH, B. *et al.* A ciliopathy complex at the transition zone protects the cilia as a privileged membrane domain. *Nat Cell Biol*, v. 14, n. 1, p. 61-72, Jan 2012. ISSN 1476-4679. Disponível em: < <http://www.ncbi.nlm.nih.gov/pubmed/22179047> >.

CHOI, S. C. *et al.* Cloning and characterization of a type II integral transmembrane protein gene, *Itm2c*, that is highly expressed in the mouse brain. *Mol Cells*, v. 12, n. 3, p. 391-7, Dec 2001. ISSN 1016-8478. Disponível em: < <http://www.ncbi.nlm.nih.gov/pubmed/11804340> >.

CHOI, S. I. *et al.* Axonal transport of British and Danish amyloid peptides via secretory vesicles. *FASEB J*, v. 18, n. 2, p. 373-5, Feb 2004. ISSN 1530-6860. Disponível em: < <http://www.ncbi.nlm.nih.gov/pubmed/14656991> >.

CHU, D. *et al.* Cloning and characterization of LUN, a novel ring finger protein that is highly expressed in lung and specifically binds to a palindromic sequence. *J Biol Chem*, v. 276, n. 17, p. 14004-13, Apr 2001. ISSN 0021-9258. Disponível em: < <http://www.ncbi.nlm.nih.gov/pubmed/11278651> >.

CHU, Y.; YANG, X. SUMO E3 ligase activity of TRIM proteins. *Oncogene*, v. 30, n. 9, p. 1108-16, Mar 2011. ISSN 1476-5594. Disponível em: < <http://www.ncbi.nlm.nih.gov/pubmed/20972456> >.

CHUANG, J. Z.; SUNG, C. H. The cytoplasmic tail of rhodopsin acts as a novel apical sorting signal in polarized MDCK cells. *J Cell Biol*, v. 142, n. 5, p. 1245-56, Sep 1998. ISSN 0021-9525. Disponível em: < <http://www.ncbi.nlm.nih.gov/pubmed/9732285> >.

COELHO, P. A. *et al.* Spindle formation in the mouse embryo requires Plk4 in the absence of centrioles. *Dev Cell*, v. 27, n. 5, p. 586-97, Dec 2013. ISSN 1878-1551. Disponível em: < <http://www.ncbi.nlm.nih.gov/pubmed/24268700> >.

COLWILL, K. *et al.* The Clk/Sty protein kinase phosphorylates SR splicing factors and regulates their intranuclear distribution. *EMBO J*, v. 15, n. 2, p. 265-75, Jan 1996. ISSN 0261-4189. Disponível em: < <http://www.ncbi.nlm.nih.gov/pubmed/8617202> >.

CONSORTIUM, I. H. G. S. Finishing the euchromatic sequence of the human genome. *Nature*, v. 431, n. 7011, p. 931-45, Oct 2004. ISSN 1476-4687. Disponível em: < <http://www.ncbi.nlm.nih.gov/pubmed/15496913> >.

COWPER, A. E. *et al.* Serine-arginine (SR) protein-like factors that antagonize authentic SR proteins and regulate alternative splicing. *J Biol Chem*, v. 276, n. 52, p. 48908-14, Dec 2001. ISSN 0021-9258. Disponível em: < <http://www.ncbi.nlm.nih.gov/pubmed/11684676> >.

CREYTENS, D. *et al.* Atypical spindle cell lipoma: a clinicopathologic, immunohistochemical, and molecular study emphasizing its relationship to classical spindle cell lipoma. *Virchows Arch*, Mar 2014. ISSN 1432-2307. Disponível em: < <http://www.ncbi.nlm.nih.gov/pubmed/24659226> >.

CUNNINGHAM, C. N. *et al.* Human TREX2 components PCID2 and centrin 2, but not ENY2, have distinct functions in protein export and co-localize to the centrosome. *Exp Cell Res*, v. 320, n. 2, p. 209-18, Jan 2014. ISSN 1090-2422. Disponível em: < <http://www.ncbi.nlm.nih.gov/pubmed/24291146> >.

DAHLMAN, K. B. *et al.* Modulators of prostate cancer cell proliferation and viability identified by short-hairpin RNA library screening. *PLoS One*, v. 7, n. 4, p. e34414, 2012. ISSN 1932-6203. Disponível em: < <http://www.ncbi.nlm.nih.gov/pubmed/22509301> >.

DALE, J.; SCHANTZ, M. V. *From genes to genomes : concepts and applications of DNA technology*. 2nd. Chichester, West Sussex ; Hoboken, NJ: John Wiley & Sons, 2007. x, 384 p. ISBN 9780470017333 (cloth alk. paper)  
0470017333 (cloth alk. paper)  
9780470017340 (pbk. alk. paper)  
0470017341 (pbk. alk. paper).

DAVENPORT, J. R.; YODER, B. K. An incredible decade for the primary cilium: a look at a once-forgotten organelle. *Am J Physiol Renal Physiol*, v. 289, n. 6, p. F1159-69, Dec 2005. ISSN 1931-857X. Disponível em: < <http://www.ncbi.nlm.nih.gov/pubmed/16275743> >.

DE MATEO, S. *et al.* Proteomic characterization of the human sperm nucleus. *Proteomics*, v. 11, n. 13, p. 2714-26, Jul 2011. ISSN 1615-9861. Disponível em: < <http://www.ncbi.nlm.nih.gov/pubmed/21630459> >.

DEAS, E.; WOOD, N. W.; PLUN-FAVREAU, H. Mitophagy and Parkinson's disease: the PINK1-parkin link. *Biochim Biophys Acta*, v. 1813, n. 4, p. 623-33, Apr 2011. ISSN 0006-3002. Disponível em: < <http://www.ncbi.nlm.nih.gov/pubmed/20736035> >.

DENUÇ, A.; MARFANY, G. SUMO and ubiquitin paths converge. *Biochem Soc Trans*, v. 38, n. Pt 1, p. 34-9, Feb 2010. ISSN 1470-8752. Disponível em: < <http://www.ncbi.nlm.nih.gov/pubmed/20074031> >.

DIDIER, C. *et al.* Inhibition of proteasome activity impairs centrosome-dependent microtubule nucleation and organization. *Mol Biol Cell*, v. 19, n. 3, p. 1220-9, Mar 2008. ISSN 1939-4586. Disponível em: < <http://www.ncbi.nlm.nih.gov/pubmed/18094058> >.

DORTA-CONTRERAS, A. J. *et al.* [Beta trace protein in the cerebrospinal fluid and serum in meningoencephalitis]. *Rev Neurol*, v. 26, n. 151, p. 386-8, Mar 1998. ISSN 0210-0010. Disponível em: < <http://www.ncbi.nlm.nih.gov/pubmed/9585948> >.

DREYER, B. *et al.* A common ancestral origin of the frequent and widespread 2299delG USH2A mutation. *Am J Hum Genet*, v. 69, n. 1, p. 228-34, Jul 2001. ISSN 0002-9297. Disponível em: < <http://www.ncbi.nlm.nih.gov/pubmed/11402400> >.

DURCAN, T. M. *et al.* Centrosome duplication proceeds during mimosine-induced G1 cell cycle arrest. *J Cell Physiol*, v. 215, n. 1, p. 182-91, Apr 2008. ISSN 1097-4652. Disponível em: < <http://www.ncbi.nlm.nih.gov/pubmed/17960592> >.

ENGELHARDT, O. G. *et al.* Interferon-induced antiviral Mx1 GTPase is associated with components of the SUMO-1 system and promyelocytic leukemia protein nuclear bodies. *Exp Cell Res*, v. 271, n. 2, p. 286-95, Dec 2001. ISSN 0014-4827. Disponível em: < <http://www.ncbi.nlm.nih.gov/pubmed/11716541> >.

EVERETT, R. D. Trans activation of transcription by herpes virus products: requirement for two HSV-1 immediate-early polypeptides for maximum activity. *EMBO J*, v. 3, n. 13, p. 3135-41, Dec 1984. ISSN 0261-4189. Disponível em: < <http://www.ncbi.nlm.nih.gov/pubmed/6098466> >.

EYESAGE. SAGE data from the Duke University Eye Center's EyeSAGE project. <http://neibank.nei.nih.gov/EyeSAGE/index.shtml>, National Eye Institute, [Accessed 03/02/2015]. Disponível em: < <http://neibank.nei.nih.gov/EyeSAGE/index.shtml> >.

FAHIM, A.; DAIGER, S.; WELEBER, R. Retinitis Pigmentosa Overview. In: Pagon RA, Adam MP, Ardinger HH, *et al.*, editors. *GeneReviews*® [Internet]: Seattle (WA): University of Washington, Seattle; 1993-2014., 2000 Aug 4 [Updated 2013 Mar 21].

FIELDS, S.; SONG, O. A novel genetic system to detect protein-protein interactions. *Nature*, v. 340, n. 6230, p. 245-6, Jul 1989. ISSN 0028-0836. Disponível em: < <http://www.ncbi.nlm.nih.gov/pubmed/2547163> >.

FJELD, C. C.; BIRDSONG, W. T.; GOODMAN, R. H. Differential binding of NAD<sup>+</sup> and NADH allows the transcriptional corepressor carboxyl-terminal binding protein to serve as a metabolic sensor. *Proc Natl Acad Sci U S A*, v. 100, n. 16, p. 9202-7, Aug 2003. ISSN 0027-8424. Disponível em: < <http://www.ncbi.nlm.nih.gov/pubmed/12872005> >.

FLEISCHER, A.; AYLLON, V.; REBOLLO, A. ITM2BS regulates apoptosis by inducing loss of mitochondrial membrane potential. *Eur J Immunol*, v. 32, n. 12, p. 3498-505, Dec 2002. ISSN 0014-2980. Disponível em: < <http://www.ncbi.nlm.nih.gov/pubmed/12442332> >.

FLEISCHER, A. *et al.* Proapoptotic activity of ITM2B(s), a BH3-only protein induced upon IL-2-deprivation which interacts with Bcl-2. *Oncogene*, v. 21, n. 20, p. 3181-9, May 2002. ISSN 0950-9232. Disponível em: < <http://www.ncbi.nlm.nih.gov/pubmed/12082633> >.



FLEISCHER, A.; REBOLLO, A. Induction of p53-independent apoptosis by the BH3-only protein ITM2Bs. *FEBS Lett*, v. 557, n. 1-3, p. 283-7, Jan 2004. ISSN 0014-5793. Disponível em: < <http://www.ncbi.nlm.nih.gov/pubmed/14741382> >.

FLIEGAUF, M.; BENZING, T.; OMRAN, H. When cilia go bad: cilia defects and ciliopathies. *Nat Rev Mol Cell Biol*, v. 8, n. 11, p. 880-93, Nov 2007. ISSN 1471-0080. Disponível em: < <http://www.ncbi.nlm.nih.gov/pubmed/17955020> >.

FLUHRER, R. *et al.* The  $\alpha$ -helical content of the transmembrane domain of the British dementia protein-2 (Bri2) determines its processing by signal peptide peptidase-like 2b (SPPL2b). *J Biol Chem*, v. 287, n. 7, p. 5156-63, Feb 2012. ISSN 1083-351X. Disponível em: < <http://www.ncbi.nlm.nih.gov/pubmed/22194595> >.

FOTINOPOULOU, A. *et al.* BRI2 interacts with amyloid precursor protein (APP) and regulates amyloid beta (Abeta) production. *J Biol Chem*, v. 280, n. 35, p. 30768-72, Sep 2005. ISSN 0021-9258. Disponível em: < <http://www.ncbi.nlm.nih.gov/pubmed/16027166> >.

FOUCHÉCOURT, S. *et al.* Prostaglandin D2 synthase secreted in the caput epididymidis displays spatial and temporal delay between messenger RNA and protein expression during postnatal development. *Biol Reprod*, v. 68, n. 1, p. 174-9, Jan 2003. ISSN 0006-3363. Disponível em: < <http://www.ncbi.nlm.nih.gov/pubmed/12493710> >.

\_\_\_\_\_. Mammalian lipocalin-type prostaglandin D2 synthase in the fluids of the male genital tract: putative biochemical and physiological functions. *Biol Reprod*, v. 66, n. 2, p. 458-67, Feb 2002. ISSN 0006-3363. Disponível em: < <http://www.ncbi.nlm.nih.gov/pubmed/11804963> >.

FOUCHÉCOURT, S.; DACHEUX, F.; DACHEUX, J. L. Glutathione-independent prostaglandin D2 synthase in ram and stallion epididymal fluids: origin and regulation. *Biol Reprod*, v. 60, n. 3, p. 558-66, Mar 1999. ISSN 0006-3363. Disponível em: < <http://www.ncbi.nlm.nih.gov/pubmed/10026099> >.

FRANSZ, P.; DE JONG, H. From nucleosome to chromosome: a dynamic organization of genetic information. *Plant J*, v. 66, n. 1, p. 4-17, Apr 2011. ISSN 1365-313X. Disponível em: < <http://www.ncbi.nlm.nih.gov/pubmed/21443619> >.

FUJIMORI, K.; ARITAKE, K.; URADE, Y. Enhancement of prostaglandin D(2) production through cyclooxygenase-2 and lipocalin-type prostaglandin D synthase by upstream stimulatory factor 1 in human brain-derived TE671 cells under serum starvation. *Gene*, v. 426, n. 1-2, p. 72-80, Dec 2008. ISSN 0378-1119. Disponível em: < <http://www.ncbi.nlm.nih.gov/pubmed/18817855> >.

FUJIMORI, K. *et al.* Prevention of paraquat-induced apoptosis in human neuronal SH-SY5Y cells by lipocalin-type prostaglandin D synthase. *J Neurochem*, v. 120, n. 2, p. 279-91, Jan 2012. ISSN 1471-4159. Disponível em: < <http://www.ncbi.nlm.nih.gov/pubmed/22043816> >.

FUJIMORI, K.; KADOYAMA, K.; URADE, Y. Protein kinase C activates human lipocalin-type prostaglandin D synthase gene expression through de-repression of notch-HES signaling and enhancement of AP-2 beta function in brain-derived TE671 cells. *J Biol Chem*, v. 280, n. 18, p. 18452-61, May 2005. ISSN 0021-9258. Disponível em: < <http://www.ncbi.nlm.nih.gov/pubmed/15743775> >.

FUJIMORI, K. *et al.* Activation of adipogenesis by lipocalin-type prostaglandin D synthase-generated  $\Delta^{12}$ -PGJ<sub>2</sub> acting through PPAR $\gamma$ -dependent and independent pathways. *Gene*, v. 505, n. 1, p. 46-52, Aug 2012. ISSN 1879-0038. Disponível em: < <http://www.ncbi.nlm.nih.gov/pubmed/22664386> >.

FUJITA, H. *et al.* Rapid decrease in active tension generated by C2C12 myotubes after termination of artificial exercise. *J Muscle Res Cell Motil*, v. 31, n. 4, p. 279-88, Dec 2010. ISSN 1573-2657. Disponível em: < <http://www.ncbi.nlm.nih.gov/pubmed/21120590> >.

FUKUHARA, A. *et al.* Lipocalin-type prostaglandin D synthase protects against oxidative stress-induced neuronal cell death. *Biochem J*, v. 443, n. 1, p. 75-84, Apr 2012. ISSN 1470-8728. Disponível em: < <http://www.ncbi.nlm.nih.gov/pubmed/22248185> >.

GAM, L. H.; LATIFF, A. SDS-PAGE electrophoretic property of human chorionic gonadotropin (hCG) and its beta-subunit. *Int J Biol Sci*, v. 1, n. 3, p. 103-9, 2005. ISSN 1449-2288. Disponível em: < <http://www.ncbi.nlm.nih.gov/pubmed/16094462> >.

GARCÍA-FERNÁNDEZ, L. F. *et al.* Identification of a thyroid hormone response element in the promoter region of the rat lipocalin-type prostaglandin D synthase (beta-trace) gene. *Brain Res Mol Brain Res*, v. 55, n. 2, p. 321-30, Apr 1998. ISSN 0169-328X. Disponível em: < <http://www.ncbi.nlm.nih.gov/pubmed/9582446> >.

GEISS-FRIEDLANDER, R.; MELCHIOR, F. Concepts in sumoylation: a decade on. *Nat Rev Mol Cell Biol*, v. 8, n. 12, p. 947-56, Dec 2007. ISSN 1471-0080. Disponível em: < <http://www.ncbi.nlm.nih.gov/pubmed/18000527> >.

GELMAN, I. H.; SILVERSTEIN, S. Co-ordinate regulation of herpes simplex virus gene expression is mediated by the functional interaction of two immediate early gene products. *J Mol Biol*, v. 191, n. 3, p. 395-409, Oct 1986. ISSN 0022-2836. Disponível em: < <http://www.ncbi.nlm.nih.gov/pubmed/3029383> >.

GERASHCHENKO, D. Y. *et al.* Localization of lipocalin-type prostaglandin D synthase (beta-trace) in iris, ciliary body, and eye fluids. *Invest Ophthalmol Vis Sci*, v. 39, n. 1, p. 198-203, Jan 1998. ISSN 0146-0404. Disponível em: < <http://www.ncbi.nlm.nih.gov/pubmed/9430563> >.

GERDES, J. M.; DAVIS, E. E.; KATSANIS, N. The vertebrate primary cilium in development, homeostasis, and disease. *Cell*, v. 137, n. 1, p. 32-45, Apr 2009. ISSN 1097-4172. Disponível em: < <http://www.ncbi.nlm.nih.gov/pubmed/19345185> >.

GERDES, J. M. *et al.* Disruption of the basal body compromises proteasomal function and perturbs intracellular Wnt response. *Nat Genet*, v. 39, n. 11, p. 1350-60, Nov 2007. ISSN 1546-1718. Disponível em: < <http://www.ncbi.nlm.nih.gov/pubmed/17906624> >.

GHERMAN, A.; DAVIS, E. E.; KATSANIS, N. The ciliary proteome database: an integrated community resource for the genetic and functional dissection of cilia. *Nat Genet*, v. 38, n. 9, p. 961-2, Sep 2006. ISSN 1061-4036. Disponível em: < <http://www.ncbi.nlm.nih.gov/pubmed/16940995> >.

GHISO, J. *et al.* Amyloidogenesis in familial British dementia is associated with a genetic defect on chromosome 13. *Ann N Y Acad Sci*, v. 920, p. 84-92, 2000. ISSN 0077-8923. Disponível em: < <http://www.ncbi.nlm.nih.gov/pubmed/11193180> >.

GHISO, J. A. *et al.* Systemic amyloid deposits in familial British dementia. *J Biol Chem*, v. 276, n. 47, p. 43909-14, Nov 2001. ISSN 0021-9258. Disponível em: < <http://www.ncbi.nlm.nih.gov/pubmed/11557758> >.

GIBSON, G. *et al.* Structure and neurotoxicity of novel amyloids derived from the BRI gene. *Biochem Soc Trans*, v. 33, n. Pt 5, p. 1111-2, Nov 2005. ISSN 0300-5127. Disponível em: < <http://www.ncbi.nlm.nih.gov/pubmed/16246057> >.

GIETZ, R. D.; SCHIESTL, R. H. Applications of high efficiency lithium acetate transformation of intact yeast cells using single-stranded nucleic acids as carrier. *Yeast*, v. 7, n. 3, p. 253-63, Apr 1991. ISSN 0749-503X. Disponível em: < <http://www.ncbi.nlm.nih.gov/pubmed/1882550> >.

GOETZ, K. E. *et al.* eyeGENE(R): a novel approach to combine clinical testing and researching genetic ocular disease. *Curr Opin Ophthalmol*, v. 23, n. 5, p. 355-63, Sep 2012. ISSN 1531-7021. Disponível em: < <http://www.ncbi.nlm.nih.gov/pubmed/22847030> >.

GOH, Y. *et al.* Content and formation of prostaglandins and distribution of prostaglandin-related enzyme activities in the rat ocular system. *Biochim Biophys Acta*, v. 921, n. 2, p. 302-11, Sep 1987. ISSN 0006-3002. Disponível em: < <http://www.ncbi.nlm.nih.gov/pubmed/3477292> >.

GRABENHORST, E.; CONRADT, H. S. The cytoplasmic, transmembrane, and stem regions of glycosyltransferases specify their *in vivo* functional sublocalization and stability in the Golgi. *J Biol Chem*, v. 274, n. 51, p. 36107-16, Dec 1999. ISSN 0021-9258. Disponível em: < <http://www.ncbi.nlm.nih.gov/pubmed/10593893> >.

GROSS, T. *et al.* Functional analysis of the fission yeast Prp4 protein kinase involved in pre-mRNA splicing and isolation of a putative mammalian homologue. *Nucleic Acids Res*, v. 25, n. 5, p. 1028-35, Mar 1997. ISSN 0305-1048. Disponível em: < <http://www.ncbi.nlm.nih.gov/pubmed/9102632> >.

GUAN, B. *et al.* Ubiquitination by TOPORS regulates the prostate tumor suppressor NKX3.1. *J Biol Chem*, v. 283, n. 8, p. 4834-40, Feb 2008. ISSN 0021-9258. Disponível em: < <http://www.ncbi.nlm.nih.gov/pubmed/18077445> >.

GUI, J. F.; LANE, W. S.; FU, X. D. A serine kinase regulates intracellular localization of splicing factors in the cell cycle. *Nature*, v. 369, n. 6482, p. 678-82, Jun 1994. ISSN 0028-0836. Disponível em: < <http://www.ncbi.nlm.nih.gov/pubmed/8208298> >.

GUNGE, N.; NAKATOMI, Y. Genetic Mechanisms of Rare Matings of the Yeast *SACCHAROMYCES CEREVISIAE* Heterozygous for Mating Type. *Genetics*, v. 70, n. 1, p. 41-58, Jan 1972. ISSN 0016-6731. Disponível em: < <http://www.ncbi.nlm.nih.gov/pubmed/17248555> >.

GUO, L. *et al.* A Cellular System that Degrades Misfolded Proteins and Protects against Neurodegeneration. *Mol Cell*, v. 55, n. 1, p. 15-30, Jul 2014. ISSN 1097-4164. Disponível em: < <http://www.ncbi.nlm.nih.gov/pubmed/24882209> >.

GÓMEZ-GARRE, P. *et al.* PSMC1 Gene in Parkinson's Disease. *Eur Neurol*, v. 68, n. 4, p. 193-8, 2012. ISSN 1421-9913. Disponível em: < <http://www.ncbi.nlm.nih.gov/pubmed/22948515> >.

HABEDANCK, R. *et al.* The Polo kinase Plk4 functions in centriole duplication. *Nat Cell Biol*, v. 7, n. 11, p. 1140-6, Nov 2005. ISSN 1465-7392. Disponível em: < <http://www.ncbi.nlm.nih.gov/pubmed/16244668> >.

HAIM, M. Prevalence of retinitis pigmentosa and allied disorders in Denmark. II. Systemic involvement and age at onset. *Acta Ophthalmol (Copenh)*, v. 70, n. 4, p. 417-26, Aug 1992. ISSN 0001-639X. Disponível em: < <http://www.ncbi.nlm.nih.gov/pubmed/1414285> >.

HALIM, A. *et al.* Human urinary glycoproteomics; attachment site specific analysis of N- and O-linked glycosylations by CID and ECD. *Mol Cell Proteomics*, v. 11, n. 4, p. M111.013649, Apr 2012. ISSN 1535-9484. Disponível em: < <http://www.ncbi.nlm.nih.gov/pubmed/22171320> >.

\_\_\_\_\_. LC-MS/MS characterization of O-glycosylation sites and glycan structures of human cerebrospinal fluid glycoproteins. *J Proteome Res*, v. 12, n. 2, p. 573-84, Feb 2013. ISSN 1535-3907. Disponível em: < <http://www.ncbi.nlm.nih.gov/pubmed/23234360> >.

HALUSKA, P. *et al.* Interaction between human topoisomerase I and a novel RING finger/arginine-serine protein. *Nucleic Acids Res*, v. 27, n. 12, p. 2538-44, Jun 1999. ISSN 0305-1048. Disponível em: < <http://www.ncbi.nlm.nih.gov/pubmed/10352183> >.

HAMEL, C. Retinitis pigmentosa. *Orphanet J Rare Dis*, v. 1, p. 40, 2006. ISSN 1750-1172 (Electronic). Disponível em: < [http://www.ncbi.nlm.nih.gov/entrez/query.fcgi?cmd=Retrieve&db=PubMed&dopt=Citation&list\\_uids=17032466](http://www.ncbi.nlm.nih.gov/entrez/query.fcgi?cmd=Retrieve&db=PubMed&dopt=Citation&list_uids=17032466) >.

HAMMER, E.; HEILBRONN, R.; WEGER, S. The E3 ligase Topors induces the accumulation of polysumoylated forms of DNA topoisomerase I in vitro and in vivo. *FEBS Lett*, v. 581, n. 28, p. 5418-24, Nov 2007. ISSN 0014-5793. Disponível em: < <http://www.ncbi.nlm.nih.gov/pubmed/17976381> >.

HARRINGTON, M. G. *et al.* Identification of a brain-specific human cerebrospinal fluid glycoprotein, beta-trace protein. *Appl Theor Electrophor*, v. 3, n. 5, p. 229-34, 1993. ISSN 0954-6642. Disponível em: < <http://www.ncbi.nlm.nih.gov/pubmed/7692978> >.

\_\_\_\_\_. Prostaglandin D synthase isoforms from cerebrospinal fluid vary with brain pathology. *Dis Markers*, v. 22, n. 1-2, p. 73-81, 2006. ISSN 0278-0240. Disponível em: < <http://www.ncbi.nlm.nih.gov/pubmed/16410653> >.

HARRIS, V. K. *et al.* Bri2-23 is a potential cerebrospinal fluid biomarker in multiple sclerosis. *Neurobiol Dis*, v. 40, n. 1, p. 331-9, Oct 2010. ISSN 1095-953X. Disponível em: < <http://www.ncbi.nlm.nih.gov/pubmed/20600910> >.

HARTMANN-PETERSEN, R.; TANAKA, K.; HENDIL, K. B. Quaternary structure of the ATPase complex of human 26 S proteasomes determined by chemical cross-linking. *Arch Biochem Biophys*, v. 386, n. 1, p. 89-94, Feb 2001. ISSN 0003-9861. Disponível em: < <http://www.ncbi.nlm.nih.gov/pubmed/11361004> >.

HARTONG, D. T.; BERSON, E. L.; DRYJA, T. P. Retinitis pigmentosa. *Lancet*, v. 368, n. 9549, p. 1795-809, Nov 2006. ISSN 1474-547X. Disponível em: < <http://www.ncbi.nlm.nih.gov/pubmed/17113430> >.

HE, Q. *et al.* Cyclic nucleotide-gated ion channels in rod photoreceptors are protected from retinoid inhibition. *J Gen Physiol*, v. 128, n. 4, p. 473-85, Oct 2006. ISSN 0022-1295. Disponível em: < <http://www.ncbi.nlm.nih.gov/pubmed/17001087> >.

HOFFMANN, A. *et al.* Purification and chemical characterization of beta-trace protein from human cerebrospinal fluid: its identification as prostaglandin D synthase. *J Neurochem*, v. 61, n. 2, p. 451-6, Aug 1993. ISSN 0022-3042. Disponível em: < <http://www.ncbi.nlm.nih.gov/pubmed/8336134> >.

HOFFMANN, A.; NIMTZ, M.; CONRADT, H. S. Molecular characterization of beta-trace protein in human serum and urine: a potential diagnostic marker for renal diseases. *Glycobiology*, v. 7, n. 4, p. 499-506, Jun 1997. ISSN 0959-6658. Disponível em: < <http://www.ncbi.nlm.nih.gov/pubmed/9184830> >.

HOFFMANN, A. *et al.* Carbohydrate structures of beta-trace protein from human cerebrospinal fluid: evidence for "brain-type" N-glycosylation. *J Neurochem*, v. 63, n. 6, p. 2185-96, Dec 1994. ISSN 0022-3042. Disponível em: < <http://www.ncbi.nlm.nih.gov/pubmed/7525874> >.

HOH KAM, J.; LENASSI, E.; JEFFERY, G. Viewing ageing eyes: diverse sites of amyloid Beta accumulation in the ageing mouse retina and the up-regulation of macrophages. *PLoS One*, v. 5, n. 10, 2010. ISSN 1932-6203. Disponível em: < <http://www.ncbi.nlm.nih.gov/pubmed/20957206> >.

HOLTON, J. L. *et al.* Regional distribution of amyloid-Bri deposition and its association with neurofibrillary degeneration in familial British dementia. *Am J Pathol*, v. 158, n. 2, p. 515-26, Feb 2001. ISSN 0002-9440. Disponível em: < <http://www.ncbi.nlm.nih.gov/pubmed/11159188> >.

HORNBECK, P. V. *et al.* PhosphoSite: A bioinformatics resource dedicated to physiological protein phosphorylation. *Proteomics*, v. 4, n. 6, p. 1551-61, Jun 2004. ISSN 1615-9853. Disponível em: < <http://www.ncbi.nlm.nih.gov/pubmed/15174125> >.

HSIAO, Y. C.; TUZ, K.; FERLAND, R. J. Trafficking in and to the primary cilium. *Cilia*, v. 1, n. 1, p. 4, 2012. ISSN 2046-2530. Disponível em: < <http://www.ncbi.nlm.nih.gov/pubmed/23351793> >.

IRIKURA, D. *et al.* Characterization of a major secretory protein in the cane toad (*Bufo marinus*) choroid plexus as an amphibian lipocalin-type prostaglandin D synthase. *J Biochem*, v. 141, n. 2, p. 173-80, Feb 2007. ISSN 0021-924X. Disponível em: < <http://www.ncbi.nlm.nih.gov/pubmed/17167040> >.

JAGGI, G. P. *et al.* Lipocalin-like prostaglandin D synthase in subretinal fluid of detached retinas in humans. *Retina*, v. 28, n. 6, p. 858-63, Jun 2008. ISSN 0275-004X. Disponível em: < <http://www.ncbi.nlm.nih.gov/pubmed/18536603> >.

JANES, P. W. *et al.* Adam meets Eph: an ADAM substrate recognition module acts as a molecular switch for ephrin cleavage in trans. *Cell*, v. 123, n. 2, p. 291-304, Oct 2005. ISSN 0092-8674. Disponível em: < <http://www.ncbi.nlm.nih.gov/pubmed/16239146> >.

JIA, W. *et al.* A strategy for precise and large scale identification of core fucosylated glycoproteins. *Mol Cell Proteomics*, v. 8, n. 5, p. 913-23, May 2009. ISSN 1535-9484. Disponível em: < <http://www.ncbi.nlm.nih.gov/pubmed/19139490> >.

JIN, D.; LIU, P.; ZHONG, T. P. Prostaglandin signaling in ciliogenesis during development. *Cell Cycle*, v. 14, n. 1, p. 1-2, 2015. ISSN 1551-4005. Disponível em: < <http://www.ncbi.nlm.nih.gov/pubmed/25551273> >.

JIN, D. *et al.* Prostaglandin signalling regulates ciliogenesis by modulating intraflagellar transport. *Nat Cell Biol*, v. 16, n. 9, p. 841-51, Sep 2014. ISSN 1476-4679. Disponível em: < <http://www.ncbi.nlm.nih.gov/pubmed/25173977> >.

KAJIWARA, K.; BERSON, E. L.; DRYJA, T. P. Digenic retinitis pigmentosa due to mutations at the unlinked peripherin/RDS and ROM1 loci. *Science*, v. 264, n. 5165, p. 1604-8, Jun 1994. ISSN 0036-8075. Disponível em: < <http://www.ncbi.nlm.nih.gov/pubmed/8202715> >.

KAPLAN, J. *et al.* Clinical and genetic heterogeneity in retinitis pigmentosa. *Hum Genet*, v. 85, n. 6, p. 635-42, Oct 1990. ISSN 0340-6717. Disponível em: < <http://www.ncbi.nlm.nih.gov/pubmed/2227956> >.

KEE, H. L.; VERHEY, K. J. Molecular connections between nuclear and ciliary import processes. *Cilia*, v. 2, n. 1, p. 11, 2013. ISSN 2046-2530. Disponível em: < <http://www.ncbi.nlm.nih.gov/pubmed/23985042> >.

KEEN, T. J. *et al.* Autosomal dominant retinitis pigmentosa: four new mutations in rhodopsin, one of them in the retinal attachment site. *Genomics*, v. 11, n. 1, p. 199-205, Sep 1991. ISSN 0888-7543. Disponível em: < <http://www.ncbi.nlm.nih.gov/pubmed/1765377> >.

KHANNA, H. *et al.* A common allele in RPEGRIPL1 is a modifier of retinal degeneration in ciliopathies. *Nat Genet*, v. 41, n. 6, p. 739-45, Jun 2009. ISSN 1546-1718. Disponível em: < <http://www.ncbi.nlm.nih.gov/pubmed/19430481> >.

KIM, J. *et al.* BRI2 (ITM2b) inhibits Abeta deposition in vivo. *J Neurosci*, v. 28, n. 23, p. 6030-6, Jun 2008. ISSN 1529-2401. Disponível em: < <http://www.ncbi.nlm.nih.gov/pubmed/18524908> >.

KIM, S. H. *et al.* Proteolytic processing of familial British dementia-associated BRI variants: evidence for enhanced intracellular accumulation of amyloidogenic peptides. *J Biol Chem*, v. 277, n. 3, p. 1872-7, Jan 2002. ISSN 0021-9258. Disponível em: < <http://www.ncbi.nlm.nih.gov/pubmed/11709554> >.

\_\_\_\_\_. Furin mediates enhanced production of fibrillogenic ABri peptides in familial British dementia. *Nat Neurosci*, v. 2, n. 11, p. 984-8, Nov 1999. ISSN 1097-6256. Disponível em: < <http://www.ncbi.nlm.nih.gov/pubmed/10526337> >.

KIM, Y. C.; DEMARTINO, G. N. C termini of proteasomal ATPases play nonequivalent roles in cellular assembly of mammalian 26 S proteasome. *J Biol Chem*, v. 286, n. 30, p. 26652-66, Jul 2011. ISSN 1083-351X. Disponível em: < <http://www.ncbi.nlm.nih.gov/pubmed/21628461> >.

KIMURA, A.; KATO, Y.; HIRANO, H. N-myristoylation of the Rpt2 subunit regulates intracellular localization of the yeast 26 S proteasome. *Biochemistry*, v. 51, n. 44, p. 8856-66, Nov 2012. ISSN 1520-4995. Disponível em: < <http://www.ncbi.nlm.nih.gov/pubmed/23102099> >.

KLOS DEHRING, D. A. *et al.* Deuterosome-mediated centriole biogenesis. *Dev Cell*, v. 27, n. 1, p. 103-12, Oct 2013. ISSN 1878-1551. Disponível em: < <http://www.ncbi.nlm.nih.gov/pubmed/24075808> >.

KODADEK, T. No Splicing, no dicing: non-proteolytic roles of the ubiquitin-proteasome system in transcription. *J Biol Chem*, v. 285, n. 4, p. 2221-6, Jan 2010. ISSN 1083-351X. Disponível em: < <http://www.ncbi.nlm.nih.gov/pubmed/19955182> >.

KOLB, H. *et al.* *Webvision*  
the organization of the retina and visual system. Salt Lake City, Utah: University of Utah Health Sciences Center, 1995.

KOMANDER, D.; RAPE, M. The ubiquitin code. *Annu Rev Biochem*, v. 81, p. 203-29, 2012. ISSN 1545-4509. Disponível em: < <http://www.ncbi.nlm.nih.gov/pubmed/22524316> >.

KONG, S. *et al.* Dlic1 deficiency impairs ciliogenesis of photoreceptors by destabilizing dynein. *Cell Res*, v. 23, n. 6, p. 835-50, Jun 2013. ISSN 1748-7838. Disponível em: < <http://www.ncbi.nlm.nih.gov/pubmed/23628724> >.

KREMER, H. *et al.* Usher syndrome: molecular links of pathogenesis, proteins and pathways. *Hum Mol Genet*, v. 15 Spec No 2, p. R262-70, Oct 2006. ISSN 0964-6906. Disponível em: < <http://www.ncbi.nlm.nih.gov/pubmed/16987892> >.

KUBO, A. *et al.* Centriolar satellites: molecular characterization, ATP-dependent movement toward centrioles and possible involvement in ciliogenesis. *J Cell Biol*, v. 147, n. 5, p. 969-80, Nov 1999. ISSN 0021-9525. Disponível em: < <http://www.ncbi.nlm.nih.gov/pubmed/10579718> >.

KURIYAMA, R. Centriole assembly in CHO cells expressing Plk4/SAS6/SAS4 is similar to centriogenesis in ciliated epithelial cells. *Cell Motil Cytoskeleton*, v. 66, n. 8, p. 588-96, Aug 2009. ISSN 1097-0169. Disponível em: < <http://www.ncbi.nlm.nih.gov/pubmed/19402176> >.

KÖHLER, A. *et al.* The substrate translocation channel of the proteasome. *Biochimie*, v. 83, n. 3-4, p. 325-32, 2001 Mar-Apr 2001. ISSN 0300-9084. Disponível em: < <http://www.ncbi.nlm.nih.gov/pubmed/11295493> >.

LA VAIL, M. M. Survival of some photoreceptor cells in albino rats following long-term exposure to continuous light. *Invest Ophthalmol*, v. 15, n. 1, p. 64-70, Jan 1976. ISSN 0020-9988. Disponível em: < <http://www.ncbi.nlm.nih.gov/pubmed/1245384> >.

LATIL, A. *et al.* Extensive analysis of the 13q14 region in human prostate tumors: DNA analysis and quantitative expression of genes lying in the interval of deletion. *Prostate*, v. 57, n. 1, p. 39-50, Sep 2003. ISSN 0270-4137. Disponível em: < <http://www.ncbi.nlm.nih.gov/pubmed/12886522> >.

LEDUC, R. *et al.* Activation of human furin precursor processing endoprotease occurs by an intramolecular autoproteolytic cleavage. *J Biol Chem*, v. 267, n. 20, p. 14304-8, Jul 1992. ISSN 0021-9258. Disponível em: < <http://www.ncbi.nlm.nih.gov/pubmed/1629222> >.

LEE, K. H. *et al.* Genetic analyses of the Arabidopsis 26 S proteasome regulatory particle reveal its importance during light stress and a specific role for the N-terminus of RPT2 in development. *Plant Signal Behav*, v. 7, n. 8, p. 973-8, Aug 2012. ISSN 1559-2324. Disponível em: < <http://www.ncbi.nlm.nih.gov/pubmed/22836496> >.

\_\_\_\_\_. The RPT2 subunit of the 26 S proteasome directs complex assembly, histone dynamics, and gametophyte and sporophyte development in Arabidopsis. *Plant Cell*, v. 23, n. 12, p. 4298-317, Dec 2011. ISSN 1532-298X. Disponível em: < <http://www.ncbi.nlm.nih.gov/pubmed/22158466> >.

LEE, S. *et al.* Lipocalin-type prostaglandin D2 synthase protein regulates glial cell migration and morphology through myristoylated alanine-rich C-kinase substrate: prostaglandin D2-independent effects. *J Biol Chem*, v. 287, n. 12, p. 9414-28, Mar 2012. ISSN 1083-351X. Disponível em: < <http://www.ncbi.nlm.nih.gov/pubmed/22275363> >.

\_\_\_\_\_. Forerunner genes contiguous to RB1 contribute to the development of in situ neoplasia. *Proc Natl Acad Sci U S A*, v. 104, n. 34, p. 13732-7, Aug 2007. ISSN 0027-8424. Disponível em: < <http://www.ncbi.nlm.nih.gov/pubmed/17702869> >.

LEMOS, T. A.; KOBARG, J. CGI-55 interacts with nuclear proteins and co-localizes to p80-coilin positive-coiled bodies in the nucleus. *Cell Biochem Biophys*, v. 44, n. 3, p. 463-74, 2006. ISSN 1085-9195. Disponível em: < <http://www.ncbi.nlm.nih.gov/pubmed/16679534> >.

LESCUYER, P. *et al.* Prostaglandin D2 synthase and its post-translational modifications in neurological disorders. *Electrophoresis*, v. 26, n. 23, p. 4563-70, Dec 2005. ISSN 0173-0835. Disponível em: < <http://www.ncbi.nlm.nih.gov/pubmed/16259013> >.

LI, J. *et al.* USP33 regulates centrosome biogenesis via deubiquitination of the centriolar protein CP110. *Nature*, v. 495, n. 7440, p. 255-9, Mar 2013. ISSN 1476-4687. Disponível em: < <http://www.ncbi.nlm.nih.gov/pubmed/23486064> >.

\_\_\_\_\_. Neurl4, a novel daughter centriole protein, prevents formation of ectopic microtubule organizing centres. *EMBO Rep*, v. 13, n. 6, p. 547-53, Jun 2012. ISSN 1469-3178. Disponível em: < <http://www.ncbi.nlm.nih.gov/pubmed/22441691> >.

LI, Y. *et al.* SUMOylation of the small GTPase ARL-13 promotes ciliary targeting of sensory receptors. *J Cell Biol*, v. 199, n. 4, p. 589-98, Nov 2012. ISSN 1540-8140. Disponível em: < <http://www.ncbi.nlm.nih.gov/pubmed/23128241> >.

LIEBERMAN, A. P. *et al.* Polyglutamine-containing aggregates in neuronal intranuclear inclusion disease. *Lancet*, v. 351, n. 9106, p. 884, Mar 1998. ISSN 0140-6736. Disponível em: < <http://www.ncbi.nlm.nih.gov/pubmed/9525376> >.

LIM, W. *et al.* Prostaglandin D2 synthase related to estrogen in the female reproductive tract. *Biochem Biophys Res Commun*, v. 456, n. 1, p. 355-60, Jan 2015. ISSN 1090-2104. Disponível em: < <http://www.ncbi.nlm.nih.gov/pubmed/25475724> >.

LIN, L. *et al.* topors, a p53 and topoisomerase I-binding RING finger protein, is a coactivator of p53 in growth suppression induced by DNA damage. *Oncogene*, v. 24, n. 21, p. 3385-96, May 2005. ISSN 0950-9232. Disponível em: < <http://www.ncbi.nlm.nih.gov/pubmed/15735665> >.

LINTON, J. D. *et al.* Flow of energy in the outer retina in darkness and in light. *Proc Natl Acad Sci U S A*, v. 107, n. 19, p. 8599-604, May 2010. ISSN 1091-6490. Disponível em: < <http://www.ncbi.nlm.nih.gov/pubmed/20445106> >.

LIPSON, C. *et al.* A proteasomal ATPase contributes to dislocation of endoplasmic reticulum-associated degradation (ERAD) substrates. *J Biol Chem*, v. 283, n. 11, p. 7166-75, Mar 2008. ISSN 0021-9258. Disponível em: < <http://www.ncbi.nlm.nih.gov/pubmed/18174173> >.

LIU, T. *et al.* Human plasma N-glycoproteome analysis by immunoaffinity subtraction, hydrazide chemistry, and mass spectrometry. *J Proteome Res*, v. 4, n. 6, p. 2070-80, 2005 Nov-Dec 2005. ISSN 1535-3893. Disponível em: < <http://www.ncbi.nlm.nih.gov/pubmed/16335952> >.

LIU, Y. P. *et al.* Ciliopathy proteins regulate paracrine signaling by modulating proteasomal degradation of mediators. *J Clin Invest*, v. 124, n. 5, p. 2059-70, May 2014. ISSN 1558-8238. Disponível em: < <http://www.ncbi.nlm.nih.gov/pubmed/24691443> >.

LUCAS, R. J. Mammalian inner retinal photoreception. *Curr Biol*, v. 23, n. 3, p. R125-33, Feb 2013. ISSN 1879-0445. Disponível em: < <http://www.ncbi.nlm.nih.gov/pubmed/23391390> >.

MAESAKA, J. K. *et al.* Prostaglandin D2 synthase: Apoptotic factor in alzheimer plasma, inducer of reactive oxygen species, inflammatory cytokines and dialysis dementia. *J Nephropathol*, v. 2, n. 3, p. 166-80, Jul 2013. ISSN 2251-8363. Disponível em: < <http://www.ncbi.nlm.nih.gov/pubmed/24475446> >.

MARIEB, E. N.; HOEHN, K. *Human Anatomy & Physiology*. 7th Edition. Pearson Benjamin Cumming, 2007.

MARTIN, L.; FLUHRER, R.; HAASS, C. Substrate requirements for SPPL2b-dependent regulated intramembrane proteolysis. *J Biol Chem*, v. 284, n. 9, p. 5662-70, Feb 2009. ISSN 0021-9258. Disponível em: < <http://www.ncbi.nlm.nih.gov/pubmed/19114711> >.

MARTIN, L. *et al.* Regulated intramembrane proteolysis of Bri2 (Itm2b) by ADAM10 and SPPL2a/SPPL2b. *J Biol Chem*, v. 283, n. 3, p. 1644-52, Jan 2008. ISSN 0021-9258. Disponível em: < <http://www.ncbi.nlm.nih.gov/pubmed/17965014> >.

MARTINDILL, D. M. *et al.* Nucleolar release of Hand1 acts as a molecular switch to determine cell fate. *Nat Cell Biol*, v. 9, n. 10, p. 1131-41, Oct 2007. ISSN 1465-7392. Disponível em: < <http://www.ncbi.nlm.nih.gov/pubmed/17891141> >.

MARTINEZ-SANZ, J. *et al.* Binding of human centrin 2 to the centrosomal protein hSfi1. *FEBS J*, v. 273, n. 19, p. 4504-15, Oct 2006. ISSN 1742-464X. Disponível em: < <http://www.ncbi.nlm.nih.gov/pubmed/16956364> >.

MARTINI, F. H.; NATH, J. L. *Fundamentals of Anatomy & Physiology*. 7th edition. Pearson Benjamin Cummings, 2006.

MASLAND, R. H. The fundamental plan of the retina. *Nat Neurosci*, v. 4, n. 9, p. 877-86, Sep 2001. ISSN 1097-6256. Disponível em: < <http://www.ncbi.nlm.nih.gov/pubmed/11528418> >.

MATSUDA, S. *et al.* The familial dementia BRI2 gene binds the Alzheimer gene amyloid-beta precursor protein and inhibits amyloid-beta production. *J Biol Chem*, v. 280, n. 32, p. 28912-6, Aug 2005. ISSN 0021-9258. Disponível em: < <http://www.ncbi.nlm.nih.gov/pubmed/15983050> >.

\_\_\_\_\_. BRI2 inhibits amyloid beta-peptide precursor protein processing by interfering with the docking of secretases to the substrate. *J Neurosci*, v. 28, n. 35, p. 8668-76, Aug 2008. ISSN 1529-2401. Disponível em: < <http://www.ncbi.nlm.nih.gov/pubmed/18753367> >.

\_\_\_\_\_. Maturation of BRI2 generates a specific inhibitor that reduces APP processing at the plasma membrane and in endocytic vesicles. *Neurobiol Aging*, v. 32, n. 8, p. 1400-8, Aug 2011. ISSN 1558-1497. Disponível em: < <http://www.ncbi.nlm.nih.gov/pubmed/19748705> >.

MATSUDA, S.; TAMAYEV, R.; D'ADAMIO, L. Increased A $\beta$ PP processing in familial Danish dementia patients. *J Alzheimers Dis*, v. 27, n. 2, p. 385-91, 2011. ISSN 1875-8908. Disponível em: < <http://www.ncbi.nlm.nih.gov/pubmed/21841249> >.

MATSUI, M. *et al.* Nuclear structure and chromosome segregation in Drosophila male meiosis depend on the ubiquitin ligase dTopors. *Genetics*, v. 189, n. 3, p. 779-93, Nov 2011. ISSN 1943-2631. Disponível em: < <http://www.ncbi.nlm.nih.gov/pubmed/21900273> >.



MAYHEW, T. M.; ASTLE, D. Photoreceptor number and outer segment disk membrane surface area in the retina of the rat: stereological data for whole organ and average photoreceptor cell. *J Neurocytol*, v. 26, n. 1, p. 53-61, Jan 1997. ISSN 0300-4864. Disponível em: < <http://www.ncbi.nlm.nih.gov/pubmed/9154529> >.

MAZELOVA, J. *et al.* Ciliary targeting motif VxPx directs assembly of a trafficking module through Arf4. *EMBO J*, v. 28, n. 3, p. 183-92, Feb 2009. ISSN 1460-2075. Disponível em: < <http://www.ncbi.nlm.nih.gov/pubmed/19153612> >.

MELEGOS, D. N.; YU, H.; DIAMANDIS, E. P. Prostaglandin D2 synthase: a component of human amniotic fluid and its association with fetal abnormalities. *Clin Chem*, v. 42, n. 7, p. 1042-50, Jul 1996. ISSN 0009-9147. Disponível em: < <http://www.ncbi.nlm.nih.gov/pubmed/8674187> >.

MERALDI, P.; NIGG, E. A. The centrosome cycle. *FEBS Lett*, v. 521, n. 1-3, p. 9-13, Jun 2002. ISSN 0014-5793. Disponível em: < <http://www.ncbi.nlm.nih.gov/pubmed/12067716> >.

MEYER, M. A. Highly Expressed Genes within Hippocampal Sector CA1: Implications for the Physiology of Memory. *Neurol Int*, v. 6, n. 2, p. 5388, Apr 2014. ISSN 2035-8385. Disponível em: < <http://www.ncbi.nlm.nih.gov/pubmed/24987507> >.

MITEVA, M. *et al.* Sumoylation as a signal for polyubiquitylation and proteasomal degradation. *Subcell Biochem*, v. 54, p. 195-214, 2010. ISSN 0306-0225. Disponível em: < <http://www.ncbi.nlm.nih.gov/pubmed/21222284> >.

MOHRI, I. *et al.* Lipocalin-type prostaglandin D synthase is up-regulated in oligodendrocytes in lysosomal storage diseases and binds gangliosides. *J Neurochem*, v. 97, n. 3, p. 641-51, May 2006. ISSN 0022-3042. Disponível em: < <http://www.ncbi.nlm.nih.gov/pubmed/16515539> >.

MOLNAR, T. *et al.* Store-operated channels regulate intracellular calcium in mammalian rods. *J Physiol*, v. 590, n. Pt 15, p. 3465-81, Aug 2012. ISSN 1469-7793. Disponível em: < <http://www.ncbi.nlm.nih.gov/pubmed/22674725> >.

MORITA, Y. *et al.* TRAF7 sequesters c-Myb to the cytoplasm by stimulating its sumoylation. *Mol Biol Cell*, v. 16, n. 11, p. 5433-44, Nov 2005. ISSN 1059-1524. Disponível em: < <http://www.ncbi.nlm.nih.gov/pubmed/16162816> >.

MÜLLER, D. *et al.* A molecular link between Hairless and Pros26.4, a member of the AAA-ATPase subunits of the proteasome 19S regulatory particle in *Drosophila*. *J Cell Sci*, v. 119, n. Pt 2, p. 250-8, Jan 2006. ISSN 0021-9533. Disponível em: < <http://www.ncbi.nlm.nih.gov/pubmed/16410550> >.

NAGATA, N. *et al.* De novo synthesis, uptake and proteolytic processing of lipocalin-type prostaglandin D synthase, beta-trace, in the kidneys. *FEBS J*, v. 276, n. 23, p. 7146-58, Dec 2009. ISSN 1742-4658. Disponível em: < <http://www.ncbi.nlm.nih.gov/pubmed/19878301> >.

NAVARATNAM, D. S. Yeast two-hybrid screening to test for protein-protein interactions in the auditory system. *Methods Mol Biol*, v. 493, p. 257-68, 2009. ISSN 1064-3745. Disponível em: < <http://www.ncbi.nlm.nih.gov/pubmed/18839352> >.

NEURINGER, M. Infant vision and retinal function in studies of dietary long-chain polyunsaturated fatty acids: methods, results, and implications. *Am J Clin Nutr*, v. 71, n. 1 Suppl, p. 256S-67S, Jan 2000. ISSN 0002-9165. Disponível em: < <http://www.ncbi.nlm.nih.gov/pubmed/10617981> >.

NG, S. K. *et al.* Cancer-like metabolism of the mammalian retina. *Clin Experiment Ophthalmol*, Oct 2014. ISSN 1442-9071. Disponível em: < <http://www.ncbi.nlm.nih.gov/pubmed/25330055> >.

NG, V. L.; WOOD, T. G.; ARLINGHAUS, R. B. Processing of the env gene products of Moloney murine leukaemia virus. *J Gen Virol*, v. 59, n. Pt 2, p. 329-43, Apr 1982. ISSN 0022-1317. Disponível em: < <http://www.ncbi.nlm.nih.gov/pubmed/7077302> >.

NIEVES, A.; GARZA, L. A. Does prostaglandin D2 hold the cure to male pattern baldness? *Exp Dermatol*, v. 23, n. 4, p. 224-7, Apr 2014. ISSN 1600-0625. Disponível em: < <http://www.ncbi.nlm.nih.gov/pubmed/24521203> >.

NOZAWA, Y. I.; LIN, C.; CHUANG, P. T. Hedgehog signaling from the primary cilium to the nucleus: an emerging picture of ciliary localization, trafficking and transduction. *Curr Opin Genet Dev*, v. 23, n. 4, p. 429-37, Aug 2013. ISSN 1879-0380. Disponível em: < <http://www.ncbi.nlm.nih.gov/pubmed/23725801> >.

OH, Y.; CHUNG, K. C. UHRF2, a ubiquitin E3 ligase, acts as a small ubiquitin-like modifier E3 ligase for zinc finger protein 131. *J Biol Chem*, v. 288, n. 13, p. 9102-11, Mar 2013. ISSN 1083-351X. Disponível em: < <http://www.ncbi.nlm.nih.gov/pubmed/23404503> >.

OKAWA, H. *et al.* ATP consumption by mammalian rod photoreceptors in darkness and in light. *Curr Biol*, v. 18, n. 24, p. 1917-21, Dec 2008. ISSN 1879-0445. Disponível em: < <http://www.ncbi.nlm.nih.gov/pubmed/19084410> >.

OLDENBURG, K. R. *et al.* Recombination-mediated PCR-directed plasmid construction in vivo in yeast. *Nucleic Acids Res*, v. 25, n. 2, p. 451-2, Jan 1997. ISSN 0305-1048. Disponível em: < <http://www.ncbi.nlm.nih.gov/pubmed/9016579> >.

PAINE, S. M. *et al.* Pale body-like inclusion formation and neurodegeneration following depletion of 26 S proteasomes in mouse brain neurones are independent of  $\alpha$ -synuclein. *PLoS One*, v. 8, n. 1, p. e54711, 2013. ISSN 1932-6203. Disponível em: < <http://www.ncbi.nlm.nih.gov/pubmed/23382946> >.

PAPAIIOANNOU, M. *et al.* A new locus (RP31) for autosomal dominant retinitis pigmentosa maps to chromosome 9p. *Hum Genet*, v. 118, n. 3-4, p. 501-3, Dec 2005. ISSN 0340-6717. Disponível em: < <http://www.ncbi.nlm.nih.gov/pubmed/16189705> >.

PARK, H. J. *et al.* Identification of phosphorylation sites of TOPORS and a role for serine 98 in the regulation of ubiquitin but not SUMO E3 ligase activity. *Biochemistry*, v. 47, n. 52, p. 13887-96, Dec 2008. ISSN 1520-4995. Disponível em: < <http://www.ncbi.nlm.nih.gov/pubmed/19053840> >.

PARK, S. *et al.* Hexameric assembly of the proteasomal ATPases is templated through their C termini. *Nature*, v. 459, n. 7248, p. 866-70, Jun 2009. ISSN 1476-4687. Disponível em: < <http://www.ncbi.nlm.nih.gov/pubmed/19412160> >.

PAYNE, C. A. *et al.* Loss of prostaglandin D2 synthase: a key molecular event in the transition of a low-grade astrocytoma to an anaplastic astrocytoma. *Mol Cancer Ther*, v. 7, n. 10, p. 3420-8, Oct 2008. ISSN 1535-7163. Disponível em: < <http://www.ncbi.nlm.nih.gov/pubmed/18852145> >.

PERRY, J. J.; TAINER, J. A.; BODDY, M. N. A simultaneous role for SUMO and ubiquitin. *Trends Biochem Sci*, v. 33, n. 5, p. 201-8, May 2008. ISSN 0968-0004. Disponível em: < <http://www.ncbi.nlm.nih.gov/pubmed/18403209> >.

PETIT, C. Usher syndrome: from genetics to pathogenesis. *Annu Rev Genomics Hum Genet*, v. 2, p. 271-97, 2001. ISSN 1527-8204. Disponível em: < <http://www.ncbi.nlm.nih.gov/pubmed/11701652> >.

PHILIBERT, P. *et al.* Unilateral cryptorchidism in mice mutant for Ptgds. *Hum Mutat*, v. 34, n. 2, p. 278-82, Feb 2013. ISSN 1098-1004. Disponível em: < <http://www.ncbi.nlm.nih.gov/pubmed/23076868> >.

PICKFORD, F. *et al.* Expression of mBRI2 in mice. *Neurosci Lett*, v. 338, n. 2, p. 95-8, Feb 2003. ISSN 0304-3940. Disponível em: < <http://www.ncbi.nlm.nih.gov/pubmed/12566161> >.

PITAVAL, A. *et al.* Cell shape and contractility regulate ciliogenesis in cell cycle-arrested cells. *J Cell Biol*, v. 191, n. 2, p. 303-12, Oct 2010. ISSN 1540-8140. Disponível em: < <http://www.ncbi.nlm.nih.gov/pubmed/20956379> >.

PITTOIS, K.; DELEERSNIJDER, W.; MERREGAERT, J. cDNA sequence analysis, chromosomal assignment and expression pattern of the gene coding for integral membrane protein 2B. *Gene*, v. 217, n. 1-2, p. 141-9, Sep 1998. ISSN 0378-1119. Disponível em: < <http://www.ncbi.nlm.nih.gov/pubmed/9795190> >.

PUNGALIYA, P. *et al.* TOPORS functions as a SUMO-1 E3 ligase for chromatin-modifying proteins. *J Proteome Res*, v. 6, n. 10, p. 3918-23, Oct 2007. ISSN 1535-3893. Disponível em: < <http://www.ncbi.nlm.nih.gov/pubmed/17803295> >.

PURAM, S. V. *et al.* The ubiquitin receptor S5a/Rpn10 links centrosomal proteasomes with dendrite development in the mammalian brain. *Cell Rep*, v. 4, n. 1, p. 19-30, Jul 2013. ISSN 2211-1247. Disponível em: < <http://www.ncbi.nlm.nih.gov/pubmed/23831032> >.

RAGOLIA, L.; HALL, C. E.; PALAIA, T. Post-translational modification regulates prostaglandin D2 synthase apoptotic activity: characterization by site-directed mutagenesis. *Prostaglandins Other Lipid Mediat*, v. 83, n. 1-2, p. 25-32, Feb 2007. ISSN 1098-8823. Disponível em: < <http://www.ncbi.nlm.nih.gov/pubmed/17259069> >.

RAGOLIA, L. *et al.* Prostaglandin D2 synthase induces apoptosis in PC12 neuronal cells. *Neuroreport*, v. 12, n. 12, p. 2623-8, Aug 2001. ISSN 0959-4965. Disponível em: < <http://www.ncbi.nlm.nih.gov/pubmed/11522937> >.

\_\_\_\_\_. Elevated L-PGDS activity contributes to PMA-induced apoptosis concomitant with downregulation of PI3-K. *Am J Physiol Cell Physiol*, v. 284, n. 1, p. C119-26, Jan 2003. ISSN 0363-6143. Disponível em: < <http://www.ncbi.nlm.nih.gov/pubmed/12388064> >.

RAHBARI, R. *et al.* A novel L1 retrotransposon marker for HeLa cell line identification. *Biotechniques*, v. 46, n. 4, p. 277-84, Apr 2009. ISSN 1940-9818. Disponível em: < <http://www.ncbi.nlm.nih.gov/pubmed/19450234> >.

RAHIMI, N. The ubiquitin-proteasome system meets angiogenesis. *Mol Cancer Ther*, v. 11, n. 3, p. 538-48, Mar 2012. ISSN 1538-8514. Disponível em: < <http://www.ncbi.nlm.nih.gov/pubmed/22357635> >.

RAJAGOPAL, M. U. *et al.* Proteomic profiling of cerebrospinal fluid identifies prostaglandin D2 synthase as a putative biomarker for pediatric medulloblastoma: A pediatric brain tumor consortium study. *Proteomics*, v. 11, n. 5, p. 935-43, Mar 2011. ISSN 1615-9861. Disponível em: < <http://www.ncbi.nlm.nih.gov/pubmed/21271676> >.

RAJENDRA, R. *et al.* Topors functions as an E3 ubiquitin ligase with specific E2 enzymes and ubiquitinates p53. *J Biol Chem*, v. 279, n. 35, p. 36440-4, Aug 2004. ISSN 0021-9258. Disponível em: < <http://www.ncbi.nlm.nih.gov/pubmed/15247280> >.

RASHEED, Z. A. *et al.* The topoisomerase I-binding RING protein, topors, is associated with promyelocytic leukemia nuclear bodies. *Exp Cell Res*, v. 277, n. 2, p. 152-60, Jul 2002. ISSN 0014-4827. Disponível em: < <http://www.ncbi.nlm.nih.gov/pubmed/12083797> >.

RECHSTEINER, M.; ROGERS, S. W. PEST sequences and regulation by proteolysis. *Trends Biochem Sci*, v. 21, n. 7, p. 267-71, Jul 1996. ISSN 0968-0004. Disponível em: < <http://www.ncbi.nlm.nih.gov/pubmed/8755249> >.

RETNET. Retinal Information Network. <http://www.sph.uth.tmc.edu/retnet/>, v. [accessed: 18 March 2011], 1996-2010.

REZVANI, K. *et al.* Proteasomal interactors control activities as diverse as the cell cycle and glutaminergic neurotransmission. *Biochem Soc Trans*, v. 31, n. 2, p. 470-3, Apr 2003. ISSN 0300-5127. Disponível em: < <http://www.ncbi.nlm.nih.gov/pubmed/12653665> >.

REZVANI, N. *et al.* Heterozygosity for the proteasomal Psmc1 ATPase is insufficient to cause neuropathology in mouse brain, but causes cell cycle defects in mouse embryonic fibroblasts. *Neurosci Lett*, v. 521, n. 2, p. 130-5, Jul 2012. ISSN 1872-7972. Disponível em: < <http://www.ncbi.nlm.nih.gov/pubmed/22677101> >.

ROORYCK, C.; LACOMBE, D. [Bardet-Biedl syndrome]. *Ann Endocrinol (Paris)*, v. 69, n. 6, p. 463-71, Dec 2008. ISSN 0003-4266. Disponível em: < <http://www.ncbi.nlm.nih.gov/pubmed/19019343> >.

ROSARIO, C. O. *et al.* A novel role for Plk4 in regulating cell spreading and motility. *Oncogene*, Sep 2014. ISSN 1476-5594. Disponível em: < <http://www.ncbi.nlm.nih.gov/pubmed/25174401> >.

ROSE, M. D.; WINSTON, F.; HIETER, P. *Methods in Yeast Genetics: A Laboratory Course Manual*. Cold Spring Harbor Laboratory Press, 1990.

ROSTAGNO, A. *et al.* Preferential association of serum amyloid P component with fibrillar deposits in familial British and Danish dementias: similarities with Alzheimer's disease. *J Neurol Sci*, v. 257, n. 1-2, p. 88-96, Jun 2007. ISSN 0022-510X. Disponível em: < <http://www.ncbi.nlm.nih.gov/pubmed/17374542> >.

ROTH, Z.; YEHEZKEL, G.; KHALAILA, I. *Identification and Quantification of Protein Glycosylation*. International Journal of Carbohydrate Chemistry: Hindawi Publishing Corporation. 2012: 1-10 p. 2012.

RUANO, D. *et al.* Family-based and case-control studies reveal no association of lipocalin-type prostaglandin D2 synthase with schizophrenia. *Am J Med Genet B Neuropsychiatr Genet*, v. 144B, n. 5, p. 642-6, Jul 2007. ISSN 1552-4841. Disponível em: < <http://www.ncbi.nlm.nih.gov/pubmed/17230501> >.

SAAVEDRA, R. A.; ANDERSON, G. R. A cancer-associated lactate dehydrogenase is expressed in normal retina. *Science*, v. 221, n. 4607, p. 291-2, Jul 1983. ISSN 0036-8075. Disponível em: < <http://www.ncbi.nlm.nih.gov/pubmed/6857286> >.

SALISBURY, J. L. *et al.* Centrin-2 is required for centriole duplication in mammalian cells. *Curr Biol*, v. 12, n. 15, p. 1287-92, Aug 2002. ISSN 0960-9822. Disponível em: < <http://www.ncbi.nlm.nih.gov/pubmed/12176356> >.

SAMBROOK, J.; RUSSELL, D. W. *Molecular cloning: a laboratory manual*. Third. New York: Cold Spring Harbor Laboratory Press, 2001.

SAMPAIO, M. H. *et al.* Predictability of quantification of beta-trace protein for diagnosis of cerebrospinal fluid leak: cutoff determination in nasal fluids with two control groups. *Am J Rhinol Allergy*, v. 23, n. 6, p. 585-90, 2009 Nov-Dec 2009. ISSN 1945-8932. Disponível em: < <http://www.ncbi.nlm.nih.gov/pubmed/19958607> >.

SANDBERG, M. A.; GAUDIO, A. R.; BERSON, E. L. Disease course of patients with pericentral retinitis pigmentosa. *Am J Ophthalmol*, v. 140, n. 1, p. 100-6, Jul 2005. ISSN 0002-9394. Disponível em: < <http://www.ncbi.nlm.nih.gov/pubmed/15953579> >.

SAUL, A. *et al.* Abundant pyroglutamate-modified ABri and ADan peptides in extracellular and vascular amyloid deposits in familial British and Danish dementias. *Neurobiol Aging*, v. 34, n. 5, p. 1416-25, May 2013. ISSN 1558-1497. Disponível em: < <http://www.ncbi.nlm.nih.gov/pubmed/23261769> >.

SCHAPIRA, A. H. Complex I: inhibitors, inhibition and neurodegeneration. *Exp Neurol*, v. 224, n. 2, p. 331-5, Aug 2010. ISSN 1090-2430. Disponível em: < <http://www.ncbi.nlm.nih.gov/pubmed/20362572> >.

SCHOB, C. *et al.* Mutations in TOPORS: a rare cause of autosomal dominant retinitis pigmentosa in continental Europe? *Ophthalmic Genet*, v. 30, n. 2, p. 96-8, Jun 2009. ISSN 1744-5094. Disponível em: < <http://www.ncbi.nlm.nih.gov/pubmed/19373681> >.

SCHULZ, H. L. *et al.* The Retinome - defining a reference transcriptome of the adult mammalian retina/retinal pigment epithelium. *BMC Genomics*, v. 5, n. 1, p. 50, Jul 2004. ISSN 1471-2164. Disponível em: < <http://www.ncbi.nlm.nih.gov/pubmed/15283859> >.

SCHULZE-BONSEL, K. *et al.* Visual acuities "hand motion" and "counting fingers" can be quantified with the freiburg visual acuity test. *Invest Ophthalmol Vis Sci*, v. 47, n. 3, p. 1236-40, Mar 2006. ISSN 0146-0404. Disponível em: < <http://www.ncbi.nlm.nih.gov/pubmed/16505064> >.

SECOMBE, J.; PARKHURST, S. M. Drosophila Topors is a RING finger-containing protein that functions as a ubiquitin-protein isopeptide ligase for the hairy basic helix-loop-helix repressor protein. *J Biol Chem*, v. 279, n. 17, p. 17126-33, Apr 2004. ISSN 0021-9258. Disponível em: < <http://www.ncbi.nlm.nih.gov/pubmed/14871887> >.

SELMER, K. K. *et al.* Autosomal dominant pericentral retinal dystrophy caused by a novel missense mutation in the TOPORS gene. *Acta Ophthalmol*, v. 88, n. 3, p. 323-8, May 2010. ISSN 1755-3768. Disponível em: < <http://www.ncbi.nlm.nih.gov/pubmed/19183411> >.

SHIKI, Y. *et al.* Changes of lipocalin-type prostaglandin D synthase level during pregnancy. *J Obstet Gynaecol Res*, v. 30, n. 1, p. 65-70, Feb 2004. ISSN 1341-8076. Disponível em: < <http://www.ncbi.nlm.nih.gov/pubmed/14718024> >.

SHIMAMOTO, S. *et al.* NMR solution structure of lipocalin-type prostaglandin D synthase: evidence for partial overlapping of catalytic pocket and retinoic acid-binding pocket within the central cavity. *J Biol Chem*, v. 282, n. 43, p. 31373-9, Oct 2007. ISSN 0021-9258. Disponível em: < <http://www.ncbi.nlm.nih.gov/pubmed/17715133> >.

SHINBO, Y. *et al.* Proper SUMO-1 conjugation is essential to DJ-1 to exert its full activities. *Cell Death Differ*, v. 13, n. 1, p. 96-108, Jan 2006. ISSN 1350-9047. Disponível em: < <http://www.ncbi.nlm.nih.gov/pubmed/15976810> >.

\_\_\_\_\_. DJ-1 restores p53 transcription activity inhibited by Topors/p53BP3. *Int J Oncol*, v. 26, n. 3, p. 641-8, Mar 2005. ISSN 1019-6439. Disponível em: < <http://www.ncbi.nlm.nih.gov/pubmed/15703819> >.

SHIROMA, T. *et al.* [Production and metabolism of prostaglandin D2 by cultured chick retinal pigment epithelial cells]. *Nihon Ganka Gakkai Zasshi*, v. 100, n. 7, p. 501-6, Jul 1996. ISSN 0029-0203. Disponível em: < <http://www.ncbi.nlm.nih.gov/pubmed/8741332> >.

SHYU, R. Y. *et al.* H-rev107 regulates prostaglandin D2 synthase-mediated suppression of cellular invasion in testicular cancer cells. *J Biomed Sci*, v. 20, p. 30, 2013. ISSN 1423-0127. Disponível em: < <http://www.ncbi.nlm.nih.gov/pubmed/23687991> >.

SIEBEL, C. W. *et al.* Conservation in budding yeast of a kinase specific for SR splicing factors. *Proc Natl Acad Sci U S A*, v. 96, n. 10, p. 5440-5, May 1999. ISSN 0027-8424. Disponível em: < <http://www.ncbi.nlm.nih.gov/pubmed/10318902> >.

SIMOSSIS, V.; KLEINJUNG, J.; HERINGA, J. An overview of multiple sequence alignment. *Curr Protoc Bioinformatics*, v. Chapter 3, p. Unit 3.7, Nov 2003. ISSN 1934-340X. Disponível em: < <http://www.ncbi.nlm.nih.gov/pubmed/18428699> >.

SINGLA, V.; REITER, J. F. The primary cilium as the cell's antenna: signaling at a sensory organelle. *Science*, v. 313, n. 5787, p. 629-33, Aug 2006. ISSN 1095-9203. Disponível em: < <http://www.ncbi.nlm.nih.gov/pubmed/16888132> >.

SMALL, G. J.; HEMINGWAY, J. Differential glycosylation produces heterogeneity in elevated esterases associated with insecticide resistance in the brown planthopper *Nilaparvata lugens* Stål. *Insect Biochem Mol Biol*, v. 30, n. 6, p. 443-53, Jun 2000. ISSN 0965-1748. Disponível em: < <http://www.ncbi.nlm.nih.gov/pubmed/10802235> >.

SONODA, Y. *et al.* Regulation of leaf organ size by the Arabidopsis RPT2a 19S proteasome subunit. *Plant J*, v. 60, n. 1, p. 68-78, Oct 2009. ISSN 1365-313X. Disponível em: < <http://www.ncbi.nlm.nih.gov/pubmed/19500299> >.

SOROKIN, A. (2011) Glomerulonephritis and Cellular Regulation of Prostaglandin Synthesis. In: PRABHAKAR, S. (Ed.). *An Update on Glomerulopathies - Etiology and Pathogenesis*. ISBN: 978-953-307-388-0, InTech, Available from: <http://www.intechopen.com/books/an-update-on-glomerulopathies-etiology-andpathogenesis/glomerulonephritis-and-cellular-regulation-of-prostaglandin-synthesis>

\_\_\_\_\_. (2011) Glomerulonephritis and Cellular Regulation of Prostaglandin Synthesis. In: PRABHAKAR, S. (Ed.). *An Update on Glomerulopathies - Etiology and Pathogenesis*. ISBN: 978-953-307-388-0, InTech (, Available from: <http://www.intechopen.com/books/an-update-on-glomerulopathies-etiology-andpathogenesis/glomerulonephritis-and-cellular-regulation-of-prostaglandin-synthesis>

SPALLUTO, C.; WILSON, D. I.; HEARN, T. Evidence for reciliation of RPE1 cells in late G1 phase, and ciliary localisation of cyclin B1. *FEBS Open Bio*, v. 3, p. 334-40, 2013. ISSN 2211-5463. Disponível em: < <http://www.ncbi.nlm.nih.gov/pubmed/24251092> >.

SREENIVASULU, G. *et al.* Modulation of lipocalin-type prostaglandin D2 synthase expression in catfish seminal vesicles by thyroid disrupting agents and hormones. *Comp Biochem Physiol C Toxicol Pharmacol*, v. 158, n. 4, p. 199-206, Nov 2013. ISSN 1532-0456. Disponível em: < <http://www.ncbi.nlm.nih.gov/pubmed/23973827> >.

STRACHAN, T.; READ, A. P. *Human molecular genetics*. 4th ed. New York: Garland Science, 2010. ISBN 9780815341499 (pbk.) : 149.00  
0815341490 (pbk.) : 149.00.

STRAUSS, O. The retinal pigment epithelium in visual function. *Physiol Rev*, v. 85, n. 3, p. 845-81, Jul 2005. ISSN 0031-9333. Disponível em: < <http://www.ncbi.nlm.nih.gov/pubmed/15987797> >.

STROEVA, O. G.; PANOVA, I. G. Retinal pigment epithelium: pattern of proliferative activity and its regulation by intraocular pressure in postnatal rats. *J Embryol Exp Morphol*, v. 75, p. 271-91, Jun 1983. ISSN 0022-0752. Disponível em: < <http://www.ncbi.nlm.nih.gov/pubmed/6886613> >.

STRUNNIKOVA, N. V. *et al.* Transcriptome analysis and molecular signature of human retinal pigment epithelium. *Hum Mol Genet*, v. 19, n. 12, p. 2468-86, Jun 2010. ISSN 1460-2083. Disponível em: < <http://www.ncbi.nlm.nih.gov/pubmed/20360305> >.

SULLIVAN, J. A.; SHIRASU, K.; DENG, X. W. The diverse roles of ubiquitin and the 26 S proteasome in the life of plants. *Nat Rev Genet*, v. 4, n. 12, p. 948-58, Dec 2003. ISSN 1471-0056. Disponível em: < <http://www.ncbi.nlm.nih.gov/pubmed/14631355> >.

SULLIVAN, L. S. *et al.* Prevalence of Mutations in eyeGENE(R) Proband with a Diagnosis of Autosomal Dominant Retinitis Pigmentosa. *Invest Ophthalmol Vis Sci*, Aug 2013. ISSN 1552-5783. Disponível em: < <http://www.ncbi.nlm.nih.gov/pubmed/23950152> >.

SUNG, C. H.; CHUANG, J. Z. The cell biology of vision. *J Cell Biol*, v. 190, n. 6, p. 953-63, Sep 2010. ISSN 1540-8140. Disponível em: < <http://www.ncbi.nlm.nih.gov/pubmed/20855501> >.

SYED, N. *et al.* Transcriptional silencing of Polo-like kinase 2 (SNK/PLK2) is a frequent event in B-cell malignancies. *Blood*, v. 107, n. 1, p. 250-6, Jan 2006. ISSN 0006-4971. Disponível em: < <http://www.ncbi.nlm.nih.gov/pubmed/16160013> >.

TAKEUCHI, J.; TAMURA, T. Recombinant ATPases of the yeast 26 S proteasome activate protein degradation by the 20S proteasome. *FEBS Lett*, v. 565, n. 1-3, p. 39-42, May 2004. ISSN 0014-5793. Disponível em: < <http://www.ncbi.nlm.nih.gov/pubmed/15135049> >.

TAMAYEV, R. *et al.* APP heterozygosity averts memory deficit in knockin mice expressing the Danish dementia BRI2 mutant. *EMBO J*, v. 30, n. 12, p. 2501-9, Jun 2011. ISSN 1460-2075. Disponível em: < <http://www.ncbi.nlm.nih.gov/pubmed/21587206> >.

TANAHASHI, N. *et al.* Chromosomal localization and immunological analysis of a family of human 26 S proteasomal ATPases. *Biochem Biophys Res Commun*, v. 243, n. 1, p. 229-32, Feb 1998. ISSN 0006-291X. Disponível em: < <http://www.ncbi.nlm.nih.gov/pubmed/9473509> >.

TANAKA, T. *et al.* Lipocalin-type prostaglandin D synthase (beta-trace) is a newly recognized type of retinoid transporter. *J Biol Chem*, v. 272, n. 25, p. 15789-95, Jun 1997. ISSN 0021-9258. Disponível em: < <http://www.ncbi.nlm.nih.gov/pubmed/9188476> >.

TANIIKE, M. *et al.* Perineuronal oligodendrocytes protect against neuronal apoptosis through the production of lipocalin-type prostaglandin D synthase in a genetic demyelinating model. *J Neurosci*, v. 22, n. 12, p. 4885-96, Jun 2002. ISSN 1529-2401. Disponível em: < <http://www.ncbi.nlm.nih.gov/pubmed/12077186> >.

THOMPSON, D. A.; GAL, A. Vitamin A metabolism in the retinal pigment epithelium: genes, mutations, and diseases. *Prog Retin Eye Res*, v. 22, n. 5, p. 683-703, Sep 2003. ISSN 1350-9462. Disponível em: < <http://www.ncbi.nlm.nih.gov/pubmed/12892646> >.

TIN, A. *et al.* Genome-wide significant locus of beta-trace protein, a novel kidney function biomarker, identified in European and African Americans. *Nephrol Dial Transplant*, Jan 2013. ISSN 1460-2385. Disponível em: < <http://www.ncbi.nlm.nih.gov/pubmed/23328707> >.

TSACHAKI, M. *et al.* BRI2 homodimerizes with the involvement of intermolecular disulfide bonds. *Neurobiol Aging*, v. 31, n. 1, p. 88-98, Jan 2010. ISSN 1558-1497. Disponível em: < <http://www.ncbi.nlm.nih.gov/pubmed/18440095> >.

\_\_\_\_\_. Glycosylation of BRI2 on asparagine 170 is involved in its trafficking to the cell surface but not in its processing by furin or ADAM10. *Glycobiology*, v. 21, n. 10, p. 1382-8, Oct 2011. ISSN 1460-2423. Disponível em: < <http://www.ncbi.nlm.nih.gov/pubmed/21752865> >.

TSVETKOV, P. *et al.* NADH binds and stabilizes the 26 S proteasomes independent of ATP. *J Biol Chem*, v. 289, n. 16, p. 11272-81, Apr 2014. ISSN 1083-351X. Disponível em: < <http://www.ncbi.nlm.nih.gov/pubmed/24596095> >.

TUMANI, H. *et al.* Beta-trace protein concentration in cerebrospinal fluid is decreased in patients with bacterial meningitis. *Neurosci Lett*, v. 242, n. 1, p. 5-8, Feb 1998. ISSN 0304-3940. Disponível em: < <http://www.ncbi.nlm.nih.gov/pubmed/9509992> >.

UJIHARA, M. *et al.* Prostaglandin D2 formation and characterization of its synthetases in various tissues of adult rats. *Arch Biochem Biophys*, v. 260, n. 2, p. 521-31, Feb 1988. ISSN 0003-9861. Disponível em: < <http://www.ncbi.nlm.nih.gov/pubmed/3124755> >.

UM, J. W. *et al.* Parkin directly modulates 26 S proteasome activity. *J Neurosci*, v. 30, n. 35, p. 11805-14, Sep 2010. ISSN 1529-2401. Disponível em: < <http://www.ncbi.nlm.nih.gov/pubmed/20810900> >.

URADE, Y. *et al.* Postnatal changes in the localization of prostaglandin D synthetase from neurons to oligodendrocytes in the rat brain. *J Biol Chem*, v. 262, n. 31, p. 15132-6, Nov 1987. ISSN 0021-9258. Disponível em: < <http://www.ncbi.nlm.nih.gov/pubmed/3117794> >.

\_\_\_\_\_. Biochemical and immunological characterization of rat spleen prostaglandin D synthetase. *J Biol Chem*, v. 262, n. 8, p. 3820-5, Mar 1987. ISSN 0021-9258. Disponível em: < <http://www.ncbi.nlm.nih.gov/pubmed/3102495> >.

URADE, Y.; HAYAISHI, O. Prostaglandin D2 and sleep regulation. *Biochim Biophys Acta*, v. 1436, n. 3, p. 606-15, Jan 1999. ISSN 0006-3002. Disponível em: < <http://www.ncbi.nlm.nih.gov/pubmed/9989291> >.

URADE, Y. *et al.* Primary structure of rat brain prostaglandin D synthetase deduced from cDNA sequence. *J Biol Chem*, v. 264, n. 2, p. 1041-5, Jan 1989. ISSN 0021-9258. Disponível em: < <http://www.ncbi.nlm.nih.gov/pubmed/2642896> >.

VEECH, R. L. *et al.* Cytosolic phosphorylation potential. *J Biol Chem*, v. 254, n. 14, p. 6538-47, Jul 1979. ISSN 0021-9258. Disponível em: < <http://www.ncbi.nlm.nih.gov/pubmed/36399> >.

VERMEULEN, K.; VAN BOCKSTAELE, D. R.; BERNEMAN, Z. N. The cell cycle: a review of regulation, deregulation and therapeutic targets in cancer. *Cell Prolif*, v. 36, n. 3, p. 131-49, Jun 2003. ISSN 0960-7722. Disponível em: < <http://www.ncbi.nlm.nih.gov/pubmed/12814430> >.

VIDAL, R. *et al.* A stop-codon mutation in the BRI gene associated with familial British dementia. *Nature*, v. 399, n. 6738, p. 776-81, Jun 1999. ISSN 0028-0836. Disponível em: < <http://www.ncbi.nlm.nih.gov/pubmed/10391242> >.

\_\_\_\_\_. A decamer duplication in the 3' region of the BRI gene originates an amyloid peptide that is associated with dementia in a Danish kindred. *Proc Natl Acad Sci U S A*, v. 97, n. 9, p. 4920-5, Apr 2000. ISSN 0027-8424. Disponível em: < <http://www.ncbi.nlm.nih.gov/pubmed/10781099> >.

VITHANA, E. N. *et al.* Expression of PRPF31 mRNA in patients with autosomal dominant retinitis pigmentosa: a molecular clue for incomplete penetrance? *Invest Ophthalmol Vis Sci*, v. 44, n. 10, p. 4204-9, Oct 2003. ISSN 0146-0404. Disponível em: < <http://www.ncbi.nlm.nih.gov/pubmed/14507862> >.

VOGES, D.; ZWICKL, P.; BAUMEISTER, W. The 26 S proteasome: a molecular machine designed for controlled proteolysis. *Annu Rev Biochem*, v. 68, p. 1015-68, 1999. ISSN 0066-4154. Disponível em: < <http://www.ncbi.nlm.nih.gov/pubmed/10872471> >.

VULSTEKE, V. *et al.* Inhibition of spliceosome assembly by the cell cycle-regulated protein kinase MELK and involvement of splicing factor NIPP1. *J Biol Chem*, v. 279, n. 10, p. 8642-7, Mar 2004. ISSN 0021-9258. Disponível em: < <http://www.ncbi.nlm.nih.gov/pubmed/14699119> >.

WADE, N. J. Image, eye, and retina (invited review). *J Opt Soc Am A Opt Image Sci Vis*, v. 24, n. 5, p. 1229-49, May 2007. ISSN 1084-7529. Disponível em: < <http://www.ncbi.nlm.nih.gov/pubmed/17429470> >.

WANG, L.; TÖRNQUIST, P.; BILL, A. Glucose metabolism in pig outer retina in light and darkness. *Acta Physiol Scand*, v. 160, n. 1, p. 75-81, May 1997a. ISSN 0001-6772. Disponível em: < <http://www.ncbi.nlm.nih.gov/pubmed/9179314> >.

\_\_\_\_\_. Glucose metabolism of the inner retina in pigs in darkness and light. *Acta Physiol Scand*, v. 160, n. 1, p. 71-4, May 1997b. ISSN 0001-6772. Disponível em: < <http://www.ncbi.nlm.nih.gov/pubmed/9179313> >.



WATABE, K. *et al.* Adenoviral expression of TDP-43 and FUS genes and shRNAs for protein degradation pathways in rodent motoneurons in vitro and in vivo. *Neuropathology*, v. 34, n. 1, p. 83-98, Feb 2014. ISSN 1440-1789. Disponível em: < <http://www.ncbi.nlm.nih.gov/pubmed/23937386> >.

WEGER, S.; HAMMER, E.; ENGSTLER, M. The DNA topoisomerase I binding protein topors as a novel cellular target for SUMO-1 modification: characterization of domains necessary for subcellular localization and sumolation. *Exp Cell Res*, v. 290, n. 1, p. 13-27, Oct 2003. ISSN 0014-4827. Disponível em: < <http://www.ncbi.nlm.nih.gov/pubmed/14516784> >.

WEGER, S.; HAMMER, E.; HEILBRONN, R. Topors, a p53 and topoisomerase I binding protein, interacts with the adeno-associated virus (AAV-2) Rep78/68 proteins and enhances AAV-2 gene expression. *J Gen Virol*, v. 83, n. Pt 3, p. 511-6, Mar 2002. ISSN 0022-1317. Disponível em: < <http://www.ncbi.nlm.nih.gov/pubmed/11842245> >.

\_\_\_\_\_. Topors acts as a SUMO-1 E3 ligase for p53 in vitro and in vivo. *FEBS Lett*, v. 579, n. 22, p. 5007-12, Sep 2005. ISSN 0014-5793. Disponível em: < <http://www.ncbi.nlm.nih.gov/pubmed/16122737> >.

WELCHMAN, R. L.; GORDON, C.; MAYER, R. J. Ubiquitin and ubiquitin-like proteins as multifunctional signals. *Nat Rev Mol Cell Biol*, v. 6, n. 8, p. 599-609, Aug 2005. ISSN 1471-0072. Disponível em: < <http://www.ncbi.nlm.nih.gov/pubmed/16064136> >.

WIGLEY, W. C. *et al.* Dynamic association of proteasomal machinery with the centrosome. *J Cell Biol*, v. 145, n. 3, p. 481-90, May 1999. ISSN 0021-9525. Disponível em: < <http://www.ncbi.nlm.nih.gov/pubmed/10225950> >.

WILSON, V. G.; HEATON, P. R. Ubiquitin proteolytic system: focus on SUMO. *Expert Rev Proteomics*, v. 5, n. 1, p. 121-35, Feb 2008. ISSN 1744-8387. Disponível em: < <http://www.ncbi.nlm.nih.gov/pubmed/18282128> >.

WISTOW, G. *et al.* NEIBank: genomics and bioinformatics resources for vision research. *Mol Vis*, v. 14, p. 1327-37, 2008. ISSN 1090-0535. Disponível em: < <http://www.ncbi.nlm.nih.gov/pubmed/18648525> >.

WONG-RILEY, M. T. Energy metabolism of the visual system. *Eye Brain*, v. 2, p. 99-116, 2010. ISSN 1179-2744. Disponível em: < <http://www.ncbi.nlm.nih.gov/pubmed/23226947> >.

WRIGHT, A. F. *et al.* Photoreceptor degeneration: genetic and mechanistic dissection of a complex trait. *Nat Rev Genet*, v. 11, n. 4, p. 273-284, Mar 2010. ISSN 1471-0064. Disponível em: < <http://www.ncbi.nlm.nih.gov/pubmed/20212494> >.

WU, C. C. *et al.* Involvement of the prostaglandin D2 signal pathway in retinoid-inducible gene 1 (RIG1)-mediated suppression of cell invasion in testis cancer cells. *Biochim Biophys Acta*, v. 1823, n. 12, p. 2227-36, Dec 2012. ISSN 0006-3002. Disponível em: < <http://www.ncbi.nlm.nih.gov/pubmed/22960220> >.

YAMAKAWA, R.; OGINO, N. Chick retinal pigment epithelium exhibits glutathione requiring prostaglandin D2 synthetase activity. *Invest Ophthalmol Vis Sci*, v. 27, n. 7, p. 1058-62, Jul 1986. ISSN 0146-0404. Disponível em: < <http://www.ncbi.nlm.nih.gov/pubmed/3721784> >.

YAMASHIMA, T. *et al.* Prostaglandin D synthase (beta-trace) in human arachnoid and meningioma cells: roles as a cell marker or in cerebrospinal fluid absorption, tumorigenesis, and calcification process. *J Neurosci*, v. 17, n. 7, p. 2376-82, Apr 1997. ISSN 0270-6474. Disponível em: < <http://www.ncbi.nlm.nih.gov/pubmed/9065498> >.

YANG, H. J. *et al.* [Sequence analysis and expression study of BRI gene in two lung adenocarcinoma cell lines with different metastatic potential]. *Zhonghua Yi Xue Yi Chuan Xue Za Zhi*, v. 20, n. 4, p. 292-6, Aug 2003. ISSN 1003-9406. Disponível em: < <http://www.ncbi.nlm.nih.gov/pubmed/12903036> >.

YANG, X. *et al.* Plk1 phosphorylation of Topors is involved in its degradation. *Mol Biol Rep*, v. 37, n. 6, p. 3023-8, Jul 2010. ISSN 1573-4978. Disponível em: < <http://www.ncbi.nlm.nih.gov/pubmed/19821153> >.

\_\_\_\_\_. Plk1-mediated phosphorylation of Topors regulates p53 stability. *J Biol Chem*, v. 284, n. 28, p. 18588-92, Jul 2009. ISSN 0021-9258. Disponível em: < <http://www.ncbi.nlm.nih.gov/pubmed/19473992> >.

YAO, Z. *et al.* Death effector domain DEDa, a self-cleaved product of caspase-8/Mch5, translocates to the nucleus by binding to ERK1/2 and upregulates procaspase-8 expression via a p53-dependent mechanism. *EMBO J*, v. 26, n. 4, p. 1068-80, Feb 2007. ISSN 0261-4189. Disponível em: < <http://www.ncbi.nlm.nih.gov/pubmed/17290218> >.

YI, Y. J. *et al.* Sperm-surface ATP in boar spermatozoa is required for fertilization: relevance to sperm proteasomal function. *Syst Biol Reprod Med*, v. 55, n. 2, p. 85-96, 2009 Mar-Apr 2009. ISSN 1939-6376. Disponível em: < <http://www.ncbi.nlm.nih.gov/pubmed/19462288> >.

YING, M. *et al.* Comprehensively surveying structure and function of RING domains from *Drosophila melanogaster*. *PLoS One*, v. 6, n. 9, p. e23863, 2011. ISSN 1932-6203. Disponível em: < <http://www.ncbi.nlm.nih.gov/pubmed/21912646> >.

YOUNG, R. W. The renewal of photoreceptor cell outer segments. *J Cell Biol*, v. 33, n. 1, p. 61-72, Apr 1967. ISSN 0021-9525. Disponível em: < <http://www.ncbi.nlm.nih.gov/pubmed/6033942> >.

ZAGHLOUL, N. A.; KATSANIS, N. Mechanistic insights into Bardet-Biedl syndrome, a model ciliopathy. *J Clin Invest*, v. 119, n. 3, p. 428-37, Mar 2009. ISSN 1558-8238. Disponível em: < <http://www.ncbi.nlm.nih.gov/pubmed/19252258> >.

ZAREBA, M. *et al.* Photobleaching of melanosomes from retinal pigment epithelium: II. Effects on the response of living cells to photic stress. *Photochem Photobiol*, v. 83, n. 4, p. 925-30, 2007 Jul-Aug 2007. ISSN 0031-8655. Disponível em: < <http://www.ncbi.nlm.nih.gov/pubmed/17645665> >.

ZHANG, F. *et al.* O-GlcNAc modification is an endogenous inhibitor of the proteasome. *Cell*, v. 115, n. 6, p. 715-25, Dec 2003. ISSN 0092-8674. Disponível em: < <http://www.ncbi.nlm.nih.gov/pubmed/14675536> >.

ZHAO, H. *et al.* The Cep63 paralogue Deup1 enables massive de novo centriole biogenesis for vertebrate multiciliogenesis. *Nat Cell Biol*, v. 15, n. 12, p. 1434-44, Dec 2013. ISSN 1476-4679. Disponível em: < <http://www.ncbi.nlm.nih.gov/pubmed/24240477> >.

ZHAO, J. *et al.* Mouse p53 represses the rat brain creatine kinase gene but activates the rat muscle creatine kinase gene. *Mol Cell Biol*, v. 14, n. 12, p. 8483-92, Dec 1994. ISSN 0270-7306. Disponível em: < <http://www.ncbi.nlm.nih.gov/pubmed/7969181> >.

ZHOU, R.; WEN, H.; AO, S. Z. Identification of a novel gene encoding a p53-associated protein. *Gene*, v. 235, n. 1-2, p. 93-101, Jul 1999. ISSN 0378-1119. Disponível em: < <http://www.ncbi.nlm.nih.gov/pubmed/10415337> >.

ZHU, Y. Y. *et al.* Reverse transcriptase template switching: a SMART approach for full-length cDNA library construction. *Biotechniques*, v. 30, n. 4, p. 892-7, Apr 2001. ISSN 0736-6205. Disponível em: < <http://www.ncbi.nlm.nih.gov/pubmed/11314272> >.

ZIRN, B. *et al.* All-trans retinoic acid treatment of Wilms tumor cells reverses expression of genes associated with high risk and relapse in vivo. *Oncogene*, v. 24, n. 33, p. 5246-51, Aug 2005. ISSN 0950-9232. Disponível em: < <http://www.ncbi.nlm.nih.gov/pubmed/15897880> >.

## 11 APPENDIX

### 11.1 RETINAL cDNA LIBRARY CHARACTERISATION

Table 11-1. Genes identified in the R&O-dT human cDNA library.  
Protein-coding sequences are highlighted in green.

Clone #	Gene symbol	BLAT (UCSC) highest score result	Sequencing file(s)
<b>A</b>	-	No matches	A09_AS9_2011-06-16_1_23-34-22.ab1
<b>B</b>	-	No matches	B09_AS10_2011-06-16_1_23-34-22.ab1
<b>C</b>	<i>GALNTL6</i>	Chr. 4: Intronic region of Homo sapiens UDP-N-acetyl-alpha-D-galactosamine:polypeptide N-acetylgalactosaminyltransferase-like 6 ( <i>GALNTL6</i> ), mRNA.	C09_AS11_2011-06-16_1_23-34-22.ab1
<b>D</b>	-	Chr. M: Homo sapiens mRNA expressed only in placental villi, clone <i>SMAP47</i> , encoding mitochondrial rRNA.	D09_AS12_2011-06-16_1_23-34-22.ab1
<b>E</b>	-	Homo sapiens RNA, tRNaseZL-interacting RNA B1.	E09_AS13_2011-06-16_1_23-34-22.ab1
<b>F</b>	<i>MTRNR2L8</i>	Chr. 11: 5'UTR Homo sapiens MT-RNR2-like 8 ( <i>MTRNR2L8</i> ), mRNA.	F09_AS14_2011-06-16_1_23-34-22.ab1
<b>G</b>	<i>SH3PXD2B</i>	Chr. 5: Intronic region of Homo sapiens SH3 and PX domains 2B ( <i>SH3PXD2B</i> ), mRNA.	G09_AS15_2011-06-16_1_23-34-22.ab1
<b>H</b>	<i>LARP4B</i>	Chr. 10: Intronic region of Homo sapiens La ribonucleoprotein domain family, member 4B ( <i>LARP4B</i> ), mRNA.	G02_AS7_2011-06-29_1_19-23-56.ab1
<b>I</b>	<i>LUC7L</i>	Chr. 16: Intronic region of Homo sapiens LUC7-like ( <i>S. cerevisiae</i> ) ( <i>LUC7L</i> ), transcript variant 1, mRNA.	H02_AS8_2011-06-29_1_19-23-56.ab1
<b>J</b>	-	Homo sapiens uncharacterized LOC100507412 ( <i>LOC100507412</i> ), non-coding RNA.	A04_AS9_2011-06-29_1_19-23-56.ab1
<b>K</b>	-	No matches	B04_AS10_2011-06-29_1_19-23-56.ab1
<b>L</b>	-	No matches	C04_AS11_2011-06-29_1_19-23-56.ab1
<b>M</b>	<i>ZBTB16</i>	Chr. 11: Intronic region of Homo sapiens zinc finger and BTB domain containing 16 ( <i>ZBTB16</i> ), transcript variant 1, mRNA.	D04_AS12_2011-06-29_1_19-23-56.ab1
<b>N</b>	-	Homo sapiens cDNA FLJ38039 fis, clone CTONG2013934. mRNA AK095358	A02_AS1_2011-10-11_1_20-46-43.ab1
<b>O</b>	<i>TSNAX-DISC1</i>	Chr. 1: Homo sapiens TSNAX-DISC1 read-through ( <i>TSNAX-DISC1</i> ), transcript variant 1, non-coding RNA.	B02_AS2_2011-10-11_1_20-46-43.ab1
<b>P</b>	<i>INPP5A</i>	Chr. 10: Intronic region of Homo sapiens inositol polyphosphate-5-phosphatase, 40kDa ( <i>INPP5A</i> ), mRNA.	C02_AS3_2011-10-11_1_20-46-43.ab1
<b>R</b>	-	Homo sapiens uncharacterized LOC100507412 ( <i>LOC100507412</i> ), non-coding RNA.	D02_AS4_2011-10-11_1_20-46-43.ab1
<b>S</b>	<i>EPAS1</i>	Chr. 2: 3' UTR of Homo sapiens endothelial PAS domain protein 1 ( <i>EPAS1</i> ), mRNA.	E02_AS5_2011-10-11_1_20-46-43.ab1
<b>T</b>	<i>PLEKHA7</i>	Chr. 11: Intronic region of Homo sapiens pleckstrin homology domain containing, family A member 7 ( <i>PLEKHA7</i> ), mRNA.	F02_AS6_2011-10-11_1_20-46-43.ab1
<b>U</b>	<i>MAP4</i>	Chr. 3: Intronic region of Homo sapiens microtubule-associated protein 4 ( <i>MAP4</i> ), transcript variant 4, mRNA.	G02_AS7_2011-10-11_1_20-46-43.ab1
<b>V</b>	-	Homo sapiens uncharacterized LOC100507412 ( <i>LOC100507412</i> ), non-coding RNA.	A04_AS9_2011-10-11_1_20-46-43.ab1
<b>W</b>	-	Homo sapiens RNA, tRNaseZL-interacting RNA B1.	B04_AS10_2011-10-11_1_20-46-43.ab1
<b>X</b>	-	Homo sapiens RNA, tRNaseZL-interacting	C04_AS11_2011-10-11_1_20-46-43.ab1

Clone #	Gene symbol	BLAT (UCSC) highest score result	Sequencing file(s)
Y	-	Homo sapiens RNA, tRNaseZL-interacting RNA B1.	D04_AS12_2011-10-11_1_20-46-43.ab1
Z	<i>C2orf71</i>	Chr. 2: Homo sapiens chromosome 2 open reading frame 71 (C2orf71), mRNA.	E04_AS13_2011-10-11_1_20-46-43.ab1
AA	-	No matches	F04_AS14_2011-10-11_1_20-46-43.ab1
AB	-	Chr. 8: Unannotated region	G04_AS15_2011-10-11_1_20-46-43.ab1
AC	<i>TAGLN</i>	Chr. 11: Homo sapiens transgelin (TAGLN), transcript variant 2, mRNA.	H04_AS16_2011-10-11_1_20-46-43.ab1
AD	-	Homo sapiens uncharacterized LOC100507412 (LOC100507412), non-coding RNA.	A05_AS17_2011-11-11_1_16-20-46.ab1
AE	<i>HFM1</i>	Chr. 1: Intronic region of Homo sapiens HFM1, ATP-dependent DNA helicase homolog ( <i>S. cerevisiae</i> ) (HFM1), mRNA.	B05_AS18_2011-11-11_1_16-20-46.ab1
AF	-	No matches	C05_AS19_2011-11-11_1_16-20-46.ab1
AG	<i>CBX5</i>	Chr. 12: Intronic region of Homo sapiens chromobox homolog 5 (CBX5), transcript variant 3, mRNA.	D05_AS20_2011-11-11_1_16-20-46.ab1
AH	-	Chr. 1: Unannotated region	E05_AS21_2011-11-11_1_16-20-46.ab1
AI	<i>KLHL21</i>	3'UTR of Homo sapiens kelch-like family member 21 (KLHL21), mRNA.	F05_AS22_2011-11-11_1_16-20-46.ab1
AJ	-	No matches	G05_AS23_2011-11-11_1_16-20-46.ab1
1	<i>IGFBP7</i>	Chr. 4: Homo sapiens insulin-like growth factor binding protein 7 (IGFBP7), transcript variant 1, mRNA.	A01_AS1_2011-11-18_1_18-20-29.ab1
2	<i>SLC4A7</i>	Chr. 3: Intronic region of Homo sapiens solute carrier family 4, sodium bicarbonate cotransporter, member 7 (SLC4A7), transcript variant 1, mRNA.	A03_AS9_2011-11-18_1_18-20-29.ab1
3	-	Chr. M: Homo sapiens mRNA expressed only in placental villi, clone SMAP47.	B01_AS2_2011-11-18_1_18-20-29.ab1
4	<i>TTR</i>	Chr. 18: 3'UTR of Homo sapiens transthyretin (TTR), mRNA.	B03_AS10_2011-11-18_1_18-20-29.ab1
5	<i>ROMO1</i>	Chr. 20: Homo sapiens reactive oxygen species modulator 1 (ROMO1), nuclear gene encoding mitochondrial protein, mRNA.	C01_AS3_2011-11-18_1_18-20-29.ab1
6	-	Homo sapiens uncharacterized LOC100507412 (LOC100507412), non-coding RNA.	C03_AS11_2011-11-18_1_18-20-29.ab1
7	<i>GAPDH</i>	Retro-GAPDH. Retroposed gene: Homo sapiens glyceraldehyde-3-phosphate dehydrogenase (GAPDH), transcript variant 1, mRNA.	D01_AS4_2011-11-18_1_18-20-29.ab1
8	-	No matches	D03_AS12_2011-11-18_1_18-20-29.ab1
9	<i>TRAFD1</i>	Chr. 12: Intronic region of Homo sapiens TRAF-type zinc finger domain containing 1 (TRAFD1), transcript variant 2, mRNA.	E01_AS5_2011-11-18_1_18-20-29.ab1
10	<i>ARL8B</i>	Chr. 3: Intronic region of Homo sapiens ADP-ribosylation factor-like 8B (ARL8B), mRNA.	F01_AS6_2011-11-18_1_18-20-29.ab1
11	-	Homo sapiens uncharacterized LOC100507412 (LOC100507412), non-coding RNA.	G01_AS7_2011-11-18_1_18-20-29.ab1
12	<i>ZNHIT1</i>	Chr. 7: 3'UTR of Homo sapiens zinc finger, HIT-type containing 1 (ZNHIT1), mRNA.	H01_AS8_2011-11-18_1_18-20-29.ab1
13	<i>SLC4A7</i>	Chr. 3: Intronic region of Homo sapiens solute carrier family 4, sodium bicarbonate cotransporter, member 7 (SLC4A7), transcript variant 1, mRNA.	A03_AS9_2011-11-18_1_18-20-29.ab1
14	<i>TTR</i>	Chr. 18: 3'UTR of Homo sapiens transthyretin (TTR), mRNA.	B03_AS10_2011-11-18_1_18-20-29.ab1

Clone #	Gene symbol	BLAT (UCSC) highest score result	Sequencing file(s)
15	-	Homo sapiens uncharacterized LOC100507412 (LOC100507412), non-coding RNA.	C03_AS11_2011-11-18_1_18-20-29.ab1
16	-	No matches	D03_AS12_2011-11-18_1_18-20-29.ab1
17	<i>SLC25A6</i>	Chr. X & Chr. Y: 3'UTR of Homo sapiens solute carrier family 25 (mitochondrial carrier; adenine nucleotide translocator), member 6 (SLC25A6), nuclear gene encoding mitochondrial protein, mRNA.	E03_AS13_2011-11-18_1_18-20-29.ab1
18	<i>TIAM2</i>	Chr. 6: 3'UTR of Homo sapiens T-cell lymphoma invasion and metastasis 2 (TIAM2), transcript variant 1, mRNA.	F03_AS14_2011-11-18_1_18-20-29.ab1
19	<i>ATG7</i>	Chr. 3: Homo sapiens autophagy related 7 (ATG7), transcript variant 1, mRNA.	G03_AS15_2011-11-18_1_18-20-29.ab1
20	-	Homo sapiens uncharacterized LOC100507412 (LOC100507412), non-coding RNA.	H03_AS16_2011-11-18_1_18-20-29.ab1
21	-	No matches	A01_BC1_2011-11-30_1_16-20-47.ab1
22	-	Homo sapiens uncharacterized LOC100507412 (LOC100507412), non-coding RNA.	A03_BC9_2011-11-30_1_16-20-47.ab1
23	-	No matches	A05_BC17_2011-11-30_1_16-20-47.ab1
24	<i>MIR143HG</i>	Chr. 5: Intronic region of Homo sapiens MIR143 host gene (non-protein coding) (MIR143HG), non-coding RNA.	A07_BC25_2011-11-30_1_16-20-47.ab1
25	-	Homo sapiens uncharacterized LOC100507412 (LOC100507412), non-coding RNA.	A09_BC33_2011-11-30_1_16-20-47.ab1
26	-	No matches	B01_BC2_2011-11-30_1_16-20-47.ab1
27	<i>SEMA3F</i>	Chr. 3: 3'UTR of Homo sapiens sema domain, immunoglobulin domain (Ig), short basic domain, secreted, (semaphorin) 3F (SEMA3F), mRNA.	B03_BC10_2011-11-30_1_16-20-47.ab1
28	-	Homo sapiens similar to ubiquitin-associated protein 1 (predicted), mRNA (cDNA clone IMAGE:6471394).	B05_BC18_2011-11-30_1_16-20-47.ab1
29	-	Homo sapiens uncharacterized LOC100507412 (LOC100507412), non-coding RNA.	B07_BC26_2011-11-30_1_16-20-47.ab1
30	-	Chr. 10: mRNA AF205216: Homo sapiens clone KC9 Alu repeat sequence.	B09_BC34_2011-11-30_1_16-20-47.ab1
31	<i>COL4A3BP</i>	Chr. 5: Intronic region of Homo sapiens collagen, type IV, alpha 3 (Goodpasture antigen) binding protein (COL4A3BP), transcript variant 1, mRNA.	C01_BC3_2011-11-30_1_16-20-47.ab1
32	<i>SEMA3F</i>	Chr. 3: 3'UTR of Homo sapiens sema domain, immunoglobulin domain (Ig), short basic domain, secreted, (semaphorin) 3F (SEMA3F), mRNA.	C03_BC11_2011-11-30_1_16-20-47.ab1
33	-	Homo sapiens uncharacterized LOC100507412 (LOC100507412), non-coding RNA.	C05_BC19_2011-11-30_1_16-20-47.ab1
34	-	Homo sapiens uncharacterized LOC100507412 (LOC100507412), non-coding RNA.	C07_BC27_2011-11-30_1_16-20-47.ab1
35	<i>TTR</i>	Chr. 18: 3'UTR of Homo sapiens transthyretin (TTR), mRNA.	D01_BC4_2011-11-30_1_16-20-47.ab1
36	<i>UPF2</i>	Chr. 10: Intronic region of Homo sapiens UPF2 regulator of nonsense transcripts homolog (yeast) (UPF2), transcript variant 2, mRNA.	D03_BC12_2011-11-30_1_16-20-47.ab1
37	<i>EPHX2</i>	Chr. 8: 3'UTR of Homo sapiens epoxide hydrolase 2, cytoplasmic (EPHX2), transcript variant 1, mRNA.	D05_BC20_2011-11-30_1_16-20-47.ab1
38	-	Homo sapiens uncharacterized LOC100507412 (LOC100507412), non-coding RNA.	D07_BC28_2011-11-30_1_16-20-47.ab1
39	-	Homo sapiens uncharacterized LOC100507412 (LOC100507412), non-coding RNA.	E01_BC5_2011-11-30_1_16-20-47.ab1
40	<i>ZNF625</i>	Chr. 19: Intronic region of Homo sapiens zinc finger protein 625 (ZNF625), transcript variant 2, non-coding RNA.	E03_BC13_2011-11-30_1_16-20-47.ab1

Clone #	Gene symbol	BLAT (UCSC) highest score result	Sequencing file(s)
41	-	Chr. 12: Unannotated region.	E05_BC21_2011-11-30_1_16-20-47.ab1
42	-	No matches	E07_BC29_2011-11-30_1_16-20-47.ab1
43	<i>SH3RF3</i>	Chr. 2: Intronic region of Homo sapiens SH3 domain containing ring finger 3 (SH3RF3), mRNA.	F01_BC6_2011-11-30_1_16-20-47.ab1
44	<i>UBR1</i>	Chr. 15: Intronic region of Homo sapiens ubiquitin protein ligase E3 component n-recognin 1 (UBR1), mRNA.	F03_BC14_2011-11-30_1_16-20-47.ab1
45	-	No matches	F05_BC22_2011-11-30_1_16-20-47.ab1
46	-	Homo sapiens mRNA, HERV-K LTR element, isolate:HKL-FB8.	F07_BC30_2011-11-30_1_16-20-47.ab1
47	-	No matches	G01_BC7_2011-11-30_1_16-20-47.ab1
48	-	Homo sapiens uncharacterized LOC100507412 (LOC100507412), non-coding RNA.	G03_BC15_2011-11-30_1_16-20-47.ab1
49	<i>FTH1</i>	Chr. 11: Homo sapiens ferritin, heavy polypeptide 1 (FTH1), mRNA.	G05_BC23_2011-11-30_1_16-20-47.ab1
50	-	Homo sapiens uncharacterized LOC100507412 (LOC100507412), non-coding RNA.	G07_BC31_2011-11-30_1_16-20-47.ab1
51	-	Homo sapiens uncharacterized LOC100507412 (LOC100507412), non-coding RNA.	H01_BC8_2011-11-30_1_16-20-47.ab1
52	-	No matches	H03_BC16_2011-11-30_1_16-20-47.ab1
53	-	Homo sapiens RNA, tRNaseZL-interacting RNA B1.	H05_BC24_2011-11-30_1_16-20-47.ab1
54	<i>FTO</i>	Chr. 16: Intronic region of Homo sapiens fat mass and obesity associated (FTO), mRNA.	H07_BC32_2011-11-30_1_16-20-47.ab1
55	<i>KALRN</i>	Chr. 3: Intronic region of Homo sapiens kalirin, RhoGEF kinase (KALRN), transcript variant 1, mRNA.	A02_BC1_2011-12-02_1_20-02-54.ab1
56	-	Homo sapiens uncharacterized LOC100507412 (LOC100507412), non-coding RNA.	B02_BC2_2011-12-02_1_20-02-54.ab1
57	<i>FTL</i>	Chr. 19: Homo sapiens ferritin, light polypeptide (FTL), mRNA.	A01_BC1_2011-12-05_1_17-10-32.ab1
58	-	No matches	A03_BC9_2011-12-05_1_17-10-32.ab1
59	-	No matches	B01_BC2_2011-12-05_1_17-10-32.ab1
60	-	No matches	B03_BC10_2011-12-05_1_17-10-32.ab1
61	<i>RAB2B</i>	Chr. 14: 3'UTR of Homo sapiens RAB2B, member RAS oncogene family (RAB2B), transcript variant 2, mRNA.	C01_BC3_2011-12-05_1_17-10-32.ab1
62	<i>ENO3</i>	Chr. 17: Homo sapiens enolase 3 (beta, muscle) (ENO3), transcript variant 2, mRNA.	C03_BC11_2011-12-05_1_17-10-32.ab1
63	<i>TPT1</i>	Chr. 13: Homo sapiens tumour protein, translationally-controlled 1 (TPT1), mRNA.	D01_BC4_2011-12-05_1_17-10-32.ab1
64	<i>PTGDS</i>	Chr. 9: Homo sapiens prostaglandin D2 synthase 21kDa (brain) (PTGDS), mRNA.	D03_BC12_2011-12-05_1_17-10-32.ab1
65	<i>NLK</i>	Chr. 17: Intronic region of Homo sapiens nemo-like kinase (NLK), mRNA.	E01_BC5_2011-12-05_1_17-10-32.ab1
66	<i>TMEM57</i>	Chr. 1: Intronic regions of Homo sapiens transmembrane protein 57 (TMEM57), mRNA.	F01_BC6_2011-12-05_1_17-10-32.ab1
67	<i>RBM48</i>	Chr. 7: Last exon and 3'UTR of Homo sapiens RNA binding motif protein 48 (RBM48), mRNA.	G01_BC7_2011-12-05_1_17-10-32.ab1
68	<i>TAPBP</i>	Chr. 6: 3'UTR of Homo sapiens TAP binding protein (tapasin) (TAPBP), transcript variant 1, mRNA.	H01_BC8_2011-12-05_1_17-10-32.ab1
69	-	Homo sapiens uncharacterized LOC100507412 (LOC100507412), non-coding RNA.	A01_BC1_2011-12-07_1_19-30-29.ab1

Clone #	Gene symbol	BLAT (UCSC) highest score result	Sequencing file(s)
70	<i>CTSD</i>	Chr. 11: Homo sapiens cathepsin D (CTSD), mRNA.	A03_BC9_2011-12-07_1_19-30-29.ab1
71	<i>PDC</i>	Chr. 1: Intronic region of Homo sapiens phosphatidylinositol-3-OH kinase class I domain containing 1 (PDK1), transcript variant 1, mRNA & Homo sapiens microRNA 548f-1 (MIR548F1), microRNA.	A05_BC17_2011-12-07_1_19-30-29.ab1
72	<i>CDH23</i>	Chr. 10: Intronic region of Homo sapiens cadherin-related 23 (CDH23), transcript variant 5, mRNA.	A07_BC25_2011-12-07_1_19-30-29.ab1
73	<i>ABS</i>	Chr. 19: 3'UTR of Homo sapiens amino-terminal enhancer of split (AES), transcript variant 2, mRNA.	B01_BC2_2011-12-07_1_19-30-29.ab1
74	-	Homo sapiens uncharacterized LOC100507412 (LOC100507412), non-coding RNA.	B03_BC10_2011-12-07_1_19-30-29.ab1
75	<i>ITM2B</i>	Chr. 13: Homo sapiens integral membrane protein 2B (ITM2B), mRNA.	B05_BC18_2011-12-07_1_19-30-29.ab1
76	-	Chr. 7: Homo sapiens uncharacterized LOC402483 (FLJ45340), non-coding RNA.	B07_BC26_2011-12-07_1_19-30-29.ab1
77	<i>DYNC1LI2</i>	Chr. 16: 3'UTR of Homo sapiens dynein, cytoplasmic 1, light intermediate chain 2 (DYNC1LI2), mRNA.	C01_BC3_2011-12-07_1_19-30-29.ab1
78	-	Homo sapiens uncharacterized LOC100507412 (LOC100507412), non-coding RNA.	C03_BC11_2011-12-07_1_19-30-29.ab1
79	-	mRNA AF205216: Homo sapiens clone KC9 Alu repeat sequence.	C05_BC19_2011-12-07_1_19-30-29.ab1
80	-	Chr. 7: Unannotated region	C07_BC27_2011-12-07_1_19-30-29.ab1
81	<i>TGFBR2</i>	Chr. 3: Intronic region of Homo sapiens transforming growth factor, beta receptor II (70/80kDa) (TGFBR2), transcript variant 2, mRNA.	D01_BC4_2011-12-07_1_19-30-29.ab1
82	<i>DPYSL3</i>	Chr. 5: Intronic region of Homo sapiens dihydropyrimidinase-like 3 (DPYSL3), transcript variant 1, mRNA.	D03_BC12_2011-12-07_1_19-30-29.ab1
83	<i>PTGDS</i>	Chr. 9: Homo sapiens prostaglandin D2 synthase 21kDa (brain) (PTGDS), mRNA.	D05_BC20_2011-12-07_1_19-30-29.ab1
84	-	Chr. 17: Unannotated region	D07_BC28_2011-12-07_1_19-30-29.ab1
85	<i>HECTD1</i>	Chr. 14: Intronic region of Homo sapiens HECT domain containing E3 ubiquitin protein ligase 1 (HECTD1), mRNA.	E01_BC5_2011-12-07_1_19-30-29.ab1
86	<i>SCAF4</i>	Chr. 21: Last exon and 3'UTR of Homo sapiens SR-related CTD-associated factor 4 (SCAF4), transcript variant 1, mRNA.	E03_BC13_2011-12-07_1_19-30-29.ab1
87	<i>MGEA5</i>	Chr. 10: 5'UTR, exon and intron of Homo sapiens meningioma expressed antigen 5 (hyaluronidase) (MGEA5), transcript variant 1, mRNA.	E05_BC21_2011-12-07_1_19-30-29.ab1
88	<i>SERPINB1</i>	Chr. 6: 3'UTR of Homo sapiens serpin peptidase inhibitor, clade B (ovalbumin), member 1 (SERPINB1), transcript variant 2, non-coding RNA.	F01_BC6_2011-12-07_1_19-30-29.ab1
89	-	No matches	F03_BC14_2011-12-07_1_19-30-29.ab1
90	<i>RPL31</i>	Chr. 2: Homo sapiens ribosomal protein L31 (RPL31), transcript variant 1, mRNA.	F05_BC22_2011-12-07_1_19-30-29.ab1
91	<i>MIR210HG</i>	Chr. 11: Homo sapiens MIR210 host gene (non-protein coding) (MIR210HG), non-coding RNA.	G01_BC7_2011-12-07_1_19-30-29.ab1
92	-	Homo sapiens uncharacterized LOC100507412 (LOC100507412), non-coding RNA.	G03_BC15_2011-12-07_1_19-30-29.ab1
93	<i>RPL31</i>	Chr. 2: Homo sapiens ribosomal protein L31 (RPL31), transcript variant 1, mRNA.	G05_BC23_2011-12-07_1_19-30-29.ab1
94	<i>RPL31</i>	Chr. 2: Homo sapiens ribosomal protein L31 (RPL31), transcript variant 1, mRNA	H01_BC8_2011-12-07_1_19-30-29.ab1
95	<i>ITM2B</i>	Chr. 13: Homo sapiens integral membrane protein 2B (ITM2B), mRNA.	H03_BC16_2011-12-07_1_19-30-29.ab1

Clone #	Gene symbol	BLAT (UCSC) highest score result	Sequencing file(s)
96	<i>RPL31</i>	Chr. 2: Homo sapiens ribosomal protein L31 (RPL31), transcript variant 1, mRNA	H05_BC24_2011-12-07_1_19-30-29.ab1
97	<i>SAR1B</i>	Chr. 5: 3'UTR of Homo sapiens SAR1 homolog B ( <i>S. cerevisiae</i> ) (SAR1B), transcript variant 1, mRNA.	A01_BC1_2011-12-20_1_23-16-12.ab1
98	<i>PRDX5</i>	Chr. 11: Homo sapiens peroxiredoxin 5 (PRDX5), nuclear gene encoding mitochondrial protein, transcript variant 1, mRNA.	A03_BC9_2011-12-20_1_23-16-12.ab1
99	<i>HFM1</i>	Chr. 1: Homo sapiens HFM1, ATP-dependent DNA helicase homolog ( <i>S. cerevisiae</i> ) (HFM1), mRNA.	A05_BC17_2011-12-20_1_23-16-12.ab1
100	-	No matches	B01_BC2_2011-12-20_1_23-16-12.ab1
101	<i>PTGDS</i>	Chr. 9: Homo sapiens prostaglandin D2 synthase 21kDa (brain) (PTGDS), mRNA.	B03_BC10_2011-12-20_1_23-16-12.ab1
102	<i>LMF1</i>	Chr. 16: Intronic region of Homo sapiens lipase maturation factor 1 (LMF1), transcript variant 3, non-coding RNA.	B05_BC18_2011-12-20_1_23-16-12.ab1
103	-	Homo sapiens uncharacterized LOC100507412 (LOC100507412), non-coding RNA.	C01_BC3_2011-12-20_1_23-16-12.ab1
104	<i>SCAF4</i>	Chr. 21: Last exon and 3'UTR of Homo sapiens SR-related CTD-associated factor 4 (SCAF4), transcript variant 1, mRNA.	C03_BC11_2011-12-20_1_23-16-12.ab1
105	-	No matches	C05_BC19_2011-12-20_1_23-16-12.ab1
106	<i>ABCA11P</i> , <i>ZNF721</i>	Chr. 4: Intronic region of two genes: Homo sapiens ATP-binding cassette, sub-family A (ABC1), member 11, pseudogene (ABCA11P), non-coding RNA & Homo sapiens zinc finger protein 721 (ZNF721), mRNA.	D01_BC4_2011-12-20_1_23-16-12.ab1
107	<i>PTGDS</i>	Chr. 9: Homo sapiens prostaglandin D2 synthase 21kDa (brain) (PTGDS), mRNA.	D03_BC12_2011-12-20_1_23-16-12.ab1
108	<i>SRPK2</i>	Chr. 7: Intronic region of Homo sapiens SRSF protein kinase 2 (SRPK2), transcript variant 2, mRNA.	E01_BC5_2011-12-20_1_23-16-12.ab1
109	<i>CLSTN2</i>	Chr. 3: Intronic region of Homo sapiens calyntenin 2 (CLSTN2), mRNA.	E03_BC13_2011-12-20_1_23-16-12.ab1
110	-	Homo sapiens uncharacterized LOC100507412 (LOC100507412), non-coding RNA.	F01_BC6_2011-12-20_1_23-16-12.ab1
111	<i>RBM33</i>	Chr. 7: 3'UTR of Homo sapiens RNA binding motif protein 33 (RBM33), mRNA.	F03_BC14_2011-12-20_1_23-16-12.ab1
112	-	Homo sapiens uncharacterized LOC100507412 (LOC100507412), non-coding RNA.	G01_BC7_2011-12-20_1_23-16-12.ab1
113	-	Chr. 14: Sequences coding for parts of antibodies, mostly variable regions.	G03_BC15_2011-12-20_1_23-16-12.ab1
114	<i>SRPK2</i>	Chr. 7: Intronic region of Homo sapiens SRSF protein kinase 2 (SRPK2), transcript variant 2, mRNA.	H01_BC8_2011-12-20_1_23-16-12.ab1
115	<i>XRCC1</i>	Chr. 19: Homo sapiens X-ray repair complementing defective repair in Chinese hamster cells 1 (XRCC1), mRNA.	H03_BC16_2011-12-20_1_23-16-12.ab1
116	<i>HFM1</i>	Chr. 1: Intronic region of Homo sapiens HFM1, ATP-dependent DNA helicase homolog ( <i>S. cerevisiae</i> ) (HFM1), mRNA.	A01_BC1_2012-01-05_1_17-26-31.ab1
117	-	No matches	A03_BC9_2012-01-05_1_17-26-31.ab1
118	<i>LMF1</i>	Chr. 16: Intronic region of Homo sapiens lipase maturation factor 1 (LMF1), transcript variant 3, non-coding RNA.	B01_BC2_2012-01-05_1_17-26-31.ab1
119	-	No matches	B03_BC10_2012-01-05_1_17-26-31.ab1
120	-	Homo sapiens uncharacterized LOC100507412 (LOC100507412), non-coding RNA.	C01_BC3_2012-01-05_1_17-26-31.ab1



Clone #	Gene symbol	BLAT (UCSC) highest score result	Sequencing file(s)
121	<i>SLC26A5</i>	Chr. 7: Intronic region of Homo sapiens solute carrier family 26, member 5 (prestin) (SLC26A5), transcript variant b, mRNA.	C03_BC11_2012-01-05_1_17-26-31.ab1
122	-	No matches	D01_BC4_2012-01-05_1_17-26-31.ab1
123	-	No matches	D03_BC12_2012-01-05_1_17-26-31.ab1
124	-	Homo sapiens uncharacterized LOC100507412 (LOC100507412), non-coding RNA.	E01_BC5_2012-01-05_1_17-26-31.ab1
125	<i>RPS15</i>	Retro-RPS15. Retroposed gene: Homo sapiens ribosomal protein S15 (RPS15), mRNA.	F01_BC6_2012-01-05_1_17-26-31.ab1
126	-	Chr. 17: Homo sapiens RNASEK-C17orf49 read-through (RNASEK-C17orf49), non-coding RNA.	G01_BC7_2012-01-05_1_17-26-31.ab1
127	-	Homo sapiens uncharacterized LOC100507412 (LOC100507412), non-coding RNA.	H01_BC8_2012-01-05_1_17-26-31.ab1
128	-	Homo sapiens uncharacterized LOC100507412 (LOC100507412), non-coding RNA.	A02_BC1_2012-01-06_1_19-25-37.ab1
129	<i>HFM1</i>	Chr. 1: Intronic region of Homo sapiens HFM1, ATP-dependent DNA helicase homolog ( <i>S. cerevisiae</i> ) (HFM1), mRNA.	A04_BC9_2012-01-06_1_19-25-37.ab1
130	<i>CHCHD6</i>	Chr. 3: Homo sapiens coiled-coil-helix-coiled-coil-helix domain containing 6 (CHCHD6), mRNA.	A06_BC17_2012-01-06_1_19-25-37.ab1
131	-	Homo sapiens RNA, tRNaseZL-interacting RNA B1.	B02_BC2_2012-01-06_1_19-25-37.ab1
132	-	Homo sapiens uncharacterized LOC100507412 (LOC100507412), non-coding RNA.	B04_BC10_2012-01-06_1_19-25-37.ab1
133	<i>SFRP2</i>	Chr. 4: 3'UTR of Homo sapiens secreted frizzled-related protein 2 (SFRP2), mRNA.	B06_BC18_2012-01-06_1_19-25-37.ab1
134	-	Homo sapiens uncharacterized LOC100507412 (LOC100507412), non-coding RNA.	C02_BC3_2012-01-06_1_19-25-37.ab1
135	<i>EIF4H</i>	Chr. 7: Intronic region of Homo sapiens eukaryotic translation initiation factor 4H (EIF4H), transcript variant 1, mRNA.	C04_BC11_2012-01-06_1_19-25-37.ab1
136	<i>GNA11</i>	Chr. 19: Homo sapiens mRNA; cDNA DKFZp434J194 (from clone DKFZp434J194) & Homo sapiens guanine nucleotide binding protein (G protein), alpha 11 (Gq class) (GNA11), mRNA.	D02_BC4_2012-01-06_1_19-25-37.ab1
137	-	Chr. 5: Intronic region of Homo sapiens NR2F1 antisense RNA 1 (NR2F1-AS1), non-coding RNA.	D04_BC12_2012-01-06_1_19-25-37.ab1
138	-	Homo sapiens uncharacterized LOC100507412 (LOC100507412), non-coding RNA.	E02_BC5_2012-01-06_1_19-25-37.ab1
139	-	Homo sapiens uncharacterized LOC100507412 (LOC100507412), non-coding RNA.	E04_BC13_2012-01-06_1_19-25-37.ab1
140	<i>RPS2</i>	Chr. 16: Homo sapiens ribosomal protein S2 (RPS2), mRNA.	F02_BC6_2012-01-06_1_19-25-37.ab1
141	-	Chr. 9: Sequence from an article: PubmedCentral and Elsevier (2006277966)	F04_BC14_2012-01-06_1_19-25-37.ab1
142	-	No matches	G02_BC7_2012-01-06_1_19-25-37.ab1
143	<i>NUMA1</i>	Chr. 11: 3'UTR of Homo sapiens nuclear mitotic apparatus protein 1 (NUMA1), mRNA.	G04_BC15_2012-01-06_1_19-25-37.ab1
144	<i>RGR</i>	Chr. 10: Intronic region of Homo sapiens retinal G protein coupled receptor (RGR), transcript variant 1, mRNA.	H02_BC8_2012-01-06_1_19-25-37.ab1
145	<i>PXN</i>	Chr. 12: 3'UTR of Homo sapiens paxillin (PXN), transcript variant 3, mRNA.	H04_BC16_2012-01-06_1_19-25-37.ab1
146	-	No matches	A02_BC1_2012-01-11_1_01-47-48.ab1

Clone #	Gene symbol	BLAT (UCSC) highest score result	Sequencing file(s)
147	<i>NFKBIA</i>	Chr. 14: Homo sapiens nuclear factor of kappa light polypeptide gene enhancer in B-cells inhibitor, alpha ( <i>NFKBIA</i> ), mRNA.	A04_BC9_2012-01-11_1_01-47-48.ab1
148	-	No matches	A06_BC17_2012-01-11_1_01-47-48.ab1
149	-	Homo sapiens uncharacterized LOC100507412 (LOC100507412), non-coding RNA.	A08_BC25_2012-01-11_1_01-47-48.ab1
150	-	Homo sapiens uncharacterized LOC100507412 (LOC100507412), non-coding RNA.	A10_BC33_2012-01-11_1_01-47-48.ab1
151	-	Chr. 7: Unannotated sequence	A12_BC41_2012-01-11_1_01-47-48.ab1
152	<i>ATP6V1E1</i>	Chr. 22: 3'UTR of Homo sapiens ATPase, H+ transporting, lysosomal 31kDa, V1 subunit E1 ( <i>ATP6V1E1</i> ), transcript variant 1, mRNA.	B02_BC2_2012-01-11_1_01-47-48.ab1
153	<i>NDUFA13</i> , <i>YJEFN3</i>	Chr. 19: Intronic region of Homo sapiens NADH dehydrogenase (ubiquinone) 1 alpha subcomplex, 13 ( <i>NDUFA13</i> ), nuclear gene encoding mitochondrial protein, mRNA & Homo sapiens YjeF N-terminal domain containing 3 ( <i>YJEFN3</i> ), transcript variant 2, mRNA.	B04_BC10_2012-01-11_1_01-47-48.ab1
154	<i>TOP1</i>	Chr. 20: Intronic region of Homo sapiens topoisomerase (DNA) I ( <i>TOP1</i> ), mRNA.	B06_BC18_2012-01-11_1_01-47-48.ab1
155	-	Chr. M: Intronic region of Homo sapiens piRNA piR-34804, complete sequence & Homo sapiens potential LAG1 interactor mRNA, partial cds.	B08_BC26_2012-01-11_1_01-47-48.ab1
156	<i>TUBD1</i>	Chr. 17: Intronic region of Homo sapiens tubulin, delta 1 ( <i>TUBD1</i> ), transcript variant 5, mRNA.	B10_BC34_2012-01-11_1_01-47-48.ab1
157	-	No matches	B12_BC42_2012-01-11_1_01-47-48.ab1
158	-	Homo sapiens uncharacterized LOC100507412 (LOC100507412), non-coding RNA.	C02_BC3_2012-01-11_1_01-47-48.ab1
159	-	Chr. 1: mRNA S77581: HERVK10/HUMMTV reverse transcriptase homolog (clone RT211)	C04_BC11_2012-01-11_1_01-47-48.ab1
160	<i>PARVA</i>	Chr. 11: Intronic region of Homo sapiens parvin, alpha ( <i>PARVA</i> ), mRNA.	C06_BC19_2012-01-11_1_01-47-48.ab1
161	-	Homo sapiens uncharacterized LOC100507412 (LOC100507412), non-coding RNA.	C08_BC27_2012-01-11_1_01-47-48.ab1
162	-	Chr. 17: Homo sapiens RNASEK-C17orf49 read-through ( <i>RNASEK-C17orf49</i> ), non-coding RNA.	C10_BC35_2012-01-11_1_01-47-48.ab1
163	-	Homo sapiens uncharacterized LOC100507412 (LOC100507412), non-coding RNA.	C12_BC43_2012-01-11_1_01-47-48.ab1
164	-	Homo sapiens uncharacterized LOC100507412 (LOC100507412), non-coding RNA.	D02_BC4_2012-01-11_1_01-47-48.ab1
165	<i>NESH</i>	Chr. 3: Intronic region of Homo sapiens ABI family, member 3 ( <i>NESH</i> ) binding protein ( <i>ABI3BP</i> ), mRNA.	D04_BC12_2012-01-11_1_01-47-48.ab1
166	<i>FTH1</i>	Chr. 11: Homo sapiens ferritin, heavy polypeptide 1 ( <i>FTH1</i> ), mRNA.	D06_BC20_2012-01-11_1_01-47-48.ab1
167	-	Homo sapiens uncharacterized LOC100507412 (LOC100507412), non-coding RNA.	D08_BC28_2012-01-11_1_01-47-48.ab1
168	-	Chr. 12: Unannotated region.	D10_BC36_2012-01-11_1_01-47-48.ab1
169	-	No matches	D12_BC44_2012-01-11_1_01-47-48.ab1
170	<i>PPARA</i>	Chr. 22: Homo sapiens peroxisome proliferator-activated receptor alpha ( <i>PPARA</i> ), transcript variant 5, mRNA.	E02_BC5_2012-01-11_1_01-47-48.ab1
171	<i>RAB2B</i>	Chr. 14: 3'UTR of Homo sapiens RAB2B, member RAS oncogene family ( <i>RAB2B</i> ), transcript variant 1, mRNA.	E04_BC13_2012-01-11_1_01-47-48.ab1
172	<i>OPHN1</i>	Chr. X. Intronic region of Homo sapiens oligophrenin 1 ( <i>OPHN1</i> ), mRNA.	E06_BC21_2012-01-11_1_01-47-48.ab1

Clone #	Gene symbol	BLAT (UCSC) highest score result	Sequencing file(s)
173	-	No match	E08_BC29_2012-01-11_1_01-47-48.ab1
174	-	Chr. 17: Homo sapiens RNASEK-C17orf49 read-through (RNASEK-C17orf49), non-coding RNA.	E10_BC37_2012-01-11_1_01-47-48.ab1
175	CA10	Chr. 17: Intronic region of Homo sapiens carbonic anhydrase X (CA10), transcript variant 1, mRNA.	F02_BC6_2012-01-11_1_01-47-48.ab1
176	-	No match	F04_BC14_2012-01-11_1_01-47-48.ab1
177	SLC16A3	Chr. 17: Homo sapiens solute carrier family 16 (monocarboxylate transporter), member 3 (SLC16A3), transcript variant 2, mRNA.	F06_BC22_2012-01-11_1_01-47-48.ab1
178	RASSF4, C10orf10	Chr. 10: Intronic region of Homo sapiens Ras association (RalGDS/AF-6) domain family member 4 (RASSF4), mRNA & 3'UTR of Homo sapiens chromosome 10 open reading frame 10 (C10orf10), mRNA.	F08_BC30_2012-01-11_1_01-47-48.ab1
179	-	Chr. 17: Homo sapiens RNASEK-C17orf49 read-through (RNASEK-C17orf49), non-coding RNA.	F10_BC38_2012-01-11_1_01-47-48.ab1
180	TCF12	Chr. 15: Intronic region of Homo sapiens transcription factor 12 (TCF12), transcript variant 2, mRNA.	G02_BC7_2012-01-11_1_01-47-48.ab1
181	-	Homo sapiens uncharacterized LOC100507412 (LOC100507412), non-coding RNA.	G04_BC15_2012-01-11_1_01-47-48.ab1
182	TTR	Chr. 18: Homo sapiens transthyretin (TTR), mRNA.	G06_BC23_2012-01-11_1_01-47-48.ab1
183	ANO6	Chr. 12: Homo sapiens anoctamin 6 (ANO6), transcript variant 3, mRNA.	G08_BC31_2012-01-11_1_01-47-48.ab1
184	-	Chr. 10: Unannotated sequence.	G10_BC39_2012-01-11_1_01-47-48.ab1
185	-	Homo sapiens uncharacterized LOC100507412 (LOC100507412), non-coding RNA.	H02_BC8_2012-01-11_1_01-47-48.ab1
186	-	Homo sapiens uncharacterized LOC100507412 (LOC100507412), non-coding RNA.	H04_BC16_2012-01-11_1_01-47-48.ab1
187	JUN	Chr. 1: Homo sapiens jun proto-oncogene (JUN), mRNA.	H06_BC24_2012-01-11_1_01-47-48.ab1
188	-	Homo sapiens uncharacterized LOC100507412 (LOC100507412), non-coding RNA.	H08_BC32_2012-01-11_1_01-47-48.ab1
189	-	Homo sapiens uncharacterized LOC100507412 (LOC100507412), non-coding RNA.	H10_BC40_2012-01-11_1_01-47-48.ab1
190	-	Homo sapiens uncharacterized LOC100507412 (LOC100507412), non-coding RNA.	A03_BC7_2012-01-25_1_01-24-53.ab1
191	ZC3H7A	Chr. 16: Homo sapiens zinc finger CCCH-type containing 7A (ZC3H7A), mRNA.	B03_BC8_2012-01-25_1_01-24-53.ab1
192	MMP15	Chr. 16: 3'UTR of Homo sapiens matrix metalloproteinase 15 (membrane-inserted) (MMP15), mRNA.	C01_BC1_2012-01-25_1_01-24-53.ab1
193	PITPNC1	Chr. 17: Intronic region of Homo sapiens phosphatidylinositol transfer protein, cytoplasmic 1 (PITPNC1), transcript variant 2, mRNA.	D01_BC2_2012-01-25_1_01-24-53.ab1
194	-	Homo sapiens uncharacterized LOC100507412 (LOC100507412), non-coding RNA.	E01_BC3_2012-01-25_1_01-24-53.ab1
195	RPS11	Chr. 19: Homo sapiens ribosomal protein S11 (RPS11), mRNA.	F01_BC4_2012-01-25_1_01-24-53.ab1
196	-	Homo sapiens uncharacterized LOC100507412 (LOC100507412), non-coding RNA.	G01_BC5_2012-01-25_1_01-24-53.ab1
197	GOT2	Chr. 16: Intronic region of Homo sapiens glutamic-oxaloacetic transaminase 2, mitochondrial (GOT2), nuclear gene encoding mitochondrial protein, mRNA.	H01_BC6_2012-01-25_1_01-24-53.ab1
198	LMF1	Chr. 16: Intronic region of Homo sapiens lipase maturation factor 1 (LMF1), transcript variant 3, non-coding RNA.	A01_BC1_2012-01-26_1_24-37-39.ab1

Clone #	Gene symbol	BLAT (UCSC) highest score result	Sequencing file(s)
199	<i>FAM120A</i>	Chr. 9: Homo sapiens family with sequence similarity 120A (FAM120A), mRNA.	A03_BC9_2012-01-26_1_24-37-39.ab1
200	-	No matches	B01_BC2_2012-01-26_1_24-37-39.ab1
201	<i>CKB</i>	Chr. 14: Homo sapiens creatine kinase, brain (CKB), mRNA.	B03_BC10_2012-01-26_1_24-37-39.ab1
202	<i>TAOK3</i>	Chr. 12: Intronic region of Homo sapiens TAO kinase 3 (TAOK3), mRNA.	C01_BC3_2012-01-26_1_24-37-39.ab1
203	<i>TMEM117</i>	Chr. 12: Intronic region of Homo sapiens transmembrane protein 117 (TMEM117), mRNA.	C03_BC11_2012-01-26_1_24-37-39.ab1
204	<i>TAOK3</i>	Chr. 12: Intronic region of Homo sapiens TAO kinase 3 (TAOK3), mRNA.	D01_BC4_2012-01-26_1_24-37-39.ab1
205	-	Chr. M: Alignment with several published sequences	D03_BC12_2012-01-26_1_24-37-39.ab1
206	<i>FAM120A</i>	Chr. 9: Homo sapiens family with sequence similarity 120A (FAM120A), mRNA.	E01_BC5_2012-01-26_1_24-37-39.ab1
207	<i>SAR1B</i>	Chr. 5: 3'UTR of Homo sapiens SAR1 homolog B (S. cerevisiae) (SAR1B), transcript variant 1, mRNA.	F01_BC6_2012-01-26_1_24-37-39.ab1
208	-	Chr. M: Homo sapiens mRNA expressed only in placental villi, clone SMAP47.	G01_BC7_2012-01-26_1_24-37-39.ab1
209	-	Chr. M: Alignment with several published sequences	H01_BC8_2012-01-26_1_24-37-39.ab1
210	-	Homo sapiens uncharacterized LOC100507412 (LOC100507412), non-coding RNA.	A01_1_2012-01-27_1_01-08-38.ab1
211	-	Homo sapiens uncharacterized LOC100507412 (LOC100507412), non-coding RNA.	A03_9_2012-01-27_1_01-08-38.ab1
212	-	Chr. M: Alignment with several published sequences	B01_2_2012-01-27_1_01-08-38.ab1
213	<i>HBA2</i>	Chr. 16: Homo sapiens haemoglobin, alpha 2 (HBA2), mRNA.	B03_10_2012-01-27_1_01-08-38.ab1
214	-	Homo sapiens RNA, tRNaseZL-interacting RNA B1.	C01_3_2012-01-27_1_01-08-38.ab1
215	-	Homo sapiens uncharacterized LOC100507412 (LOC100507412), non-coding RNA.	C03_11_2012-01-27_1_01-08-38.ab1
216	<i>FTO</i>	Chr. 16: Intronic region of Homo sapiens fat mass and obesity associated (FTO), mRNA.	D01_4_2012-01-27_1_01-08-38.ab1
217	-	Homo sapiens RNA, tRNaseZL-interacting RNA B1.	E01_5_2012-01-27_1_01-08-38.ab1
218	-	Homo sapiens uncharacterized LOC100507412 (LOC100507412), non-coding RNA.	F01_6_2012-01-27_1_01-08-38.ab1
219	<i>CCDC50</i>	Chr. 3: mRNA AK096400: Homo sapiens cDNA FLJ39081 fis, clone NT2RP7018340 & mRNA HQ448050: Synthetic construct Homo sapiens clone IMAGE:100071429; CCSB012307_01 coiled-coil domain containing 50 (CCDC50) gene, encodes complete protein.	G01_7_2012-01-27_1_01-08-38.ab1
220	<i>GSTM1</i>	Chr. 1: Homo sapiens glutathione S-transferase mu 1 (GSTM1), transcript variant 1, mRNA	H01_8_2012-01-27_1_01-08-38.ab1
221	-	Homo sapiens uncharacterized LOC100507412 (LOC100507412), non-coding RNA.	A01_BC1_2012-02-03_1_18-18-36.ab1
222	<i>MFRP</i>	Chr. 11: Homo sapiens membrane frizzled-related protein (MFRP), mRNA.	A03_BC9_2012-02-03_1_18-18-36.ab1
223	<i>RDH8</i>	Chr. 19: Homo sapiens retinol dehydrogenase 8 (all-trans) (RDH8), mRNA.	A05_BC17_2012-02-03_1_18-18-36.ab1
224	<i>GSTM1</i>	Chr. 1: Homo sapiens glutathione S-transferase mu 1 (GSTM1), transcript variant 1, mRNA	B01_BC2_2012-02-03_1_18-18-36.ab1
225	<i>FAM81A</i>	Chr. 15: 3'UTR of Homo sapiens family with sequence similarity 81, member A (FAM81A), mRNA.	B03_BC10_2012-02-03_1_18-18-36.ab1
226	<i>GBA</i>	Chr. 1: Homo sapiens glucosidase, beta, acid (GBA), transcript variant 1, mRNA.	B05_BC18_2012-02-03_1_18-18-36.ab1

Clone #	Gene symbol	BLAT (UCSC) highest score result	Sequencing file(s)
227	VAC14	Chr. 16: 3'UTR of Homo sapiens Vac14 homolog (S. cerevisiae) (VAC14), mRNA.	C01_BC3_2012-02-03_1_18-18-36.ab1
228	COX7A1	Chr. 19: Homo sapiens cytochrome c oxidase subunit VIIa polypeptide 1 (muscle) (COX7A1), nuclear gene encoding mitochondrial protein, mRNA.	C03_BC11_2012-02-03_1_18-18-36.ab1
229	RPL19	Chr. 5: Retro-RPL19. Retroposed gene: Homo sapiens ribosomal protein L19 (RPL19), mRNA.	C05_BC19_2012-02-03_1_18-18-36.ab1
230	RPL7A	Chr. 9: Homo sapiens ribosomal protein L7a (RPL7A), mRNA.	D01_BC4_2012-02-03_1_18-18-36.ab1
231	CAP1	Chr. 1: 3'UTR of Homo sapiens CAP, adenylate cyclase-associated protein 1 (yeast) (CAP1), transcript variant 1, mRNA.	D03_BC12_2012-02-03_1_18-18-36.ab1
232	GAB2	Chr. 11: Intronic region of Homo sapiens GRB2-associated binding protein 2 (GAB2), transcript variant 1, mRNA.	D05_BC20_2012-02-03_1_18-18-36.ab1
233	-	Homo sapiens uncharacterized LOC100507412 (LOC100507412), non-coding RNA.	E01_BC5_2012-02-03_1_18-18-36.ab1
234	UBC	Chr. 12: Homo sapiens ubiquitin C (UBC), mRNA.	E03_BC13_2012-02-03_1_18-18-36.ab1
235	-	Homo sapiens uncharacterized LOC100507412 (LOC100507412), non-coding RNA.	E05_BC21_2012-02-03_1_18-18-36.ab1
236	-	No matches	F01_BC6_2012-02-03_1_18-18-36.ab1
237	-	Homo sapiens uncharacterized LOC100507412 (LOC100507412), non-coding RNA.	F03_BC14_2012-02-03_1_18-18-36.ab1
238	GPR124	Chr. 8: 3'UTR of Homo sapiens G protein-coupled receptor 124 (GPR124), mRNA.	F05_BC22_2012-02-03_1_18-18-36.ab1
239	TMTC1	Chr. 12: Intronic region of Homo sapiens transmembrane and tetratricopeptide repeat containing 1 (TMTC1), transcript variant 1, mRNA.	G01_BC7_2012-02-03_1_18-18-36.ab1
240	-	Chr. M: Homo sapiens cDNA: FLJ22894 fis, clone KAT04907.	G03_BC15_2012-02-03_1_18-18-36.ab1
241	MICAL3	Chr. 22: Intronic region of Homo sapiens microtubule associated monoxygenase, calponin and LIM domain containing 3 (MICAL3), transcript variant 1, mRNA.	H01_BC8_2012-02-03_1_18-18-36.ab1
242	NRL	Chr. 14: 3'UTR of Homo sapiens neural retina leucine zipper (NRL), mRNA.	H03_BC16_2012-02-03_1_18-18-36.ab1
243	LPHN1	Chr. 19: Intronic region of Homo sapiens latrophilin 1 (LPHN1), transcript variant 1, mRNA.	A02_BC17_2012-02-10_1_20-41-28.ab1
244	EEF2	Chr. 19: 3'UTR of Homo sapiens eukaryotic translation elongation factor 2 (EEF2), mRNA.	A04_BC25_2012-02-10_1_20-41-28.ab1
245	-	No matches	A06_BC33_2012-02-10_1_20-41-28.ab1
246	MOB3B	Chr. 9: Intronic region of Homo sapiens MOB kinase activator 3B (MOB3B), mRNA.	A08_BC41_2012-02-10_1_20-41-28.ab1
247	COA3	Chr. 17: Homo sapiens cytochrome c oxidase assembly factor 3 (COA3), mRNA.	A09_BC1_2012-02-10_1_18-25-29
248	SAR1B	Chr. 5: 3' UTR of Homo sapiens SAR1 homolog B (S. cerevisiae) (SAR1B), transcript variant 1, mRNA.	A10_BC49_2012-02-10_1_20-41-28
249	DNAJC1	Chr. 10: Intronic region of Homo sapiens Dnal (Hsp40) homolog, subfamily C, member 1 (DNAJC1), mRNA.	A11_BC9_2012-02-10_1_18-25-29
250	-	Homo sapiens uncharacterized LOC100507412 (LOC100507412), non-coding RNA.	A12_BC57_2012-02-10_1_20-41-28
251	-	Homo sapiens uncharacterized LOC100507412 (LOC100507412), non-coding RNA.	B02_BC18_2012-02-10_1_20-41-28
252	-	Homo sapiens uncharacterized LOC100507412 (LOC100507412), non-coding RNA.	B04_BC26_2012-02-10_1_20-41-28
253	-	Homo sapiens uncharacterized LOC100507412 (LOC100507412), non-coding RNA.	B06_BC34_2012-02-10_1_20-41-28

Clone #	Gene symbol	BLAT (UCSC) highest score result	Sequencing file(s)
254	<i>STAB2</i>	Chr. 12: Intronic region of Homo sapiens stabilin 2 ( <i>STAB2</i> ), mRNA.	B08_BC42_2012-02-10_1_20-41-28
255	-	Homo sapiens uncharacterized LOC100507412 (LOC100507412), non-coding RNA.	B09_BC2_2012-02-10_1_18-25-29
256	-	Homo sapiens uncharacterized LOC100507412 (LOC100507412), non-coding RNA.	B10_BC50_2012-02-10_1_20-41-28
257	-	No matches	B11_BC10_2012-02-10_1_18-25-29
258	-	Homo sapiens uncharacterized LOC100507412 (LOC100507412), non-coding RNA.	B12_BC58_2012-02-10_1_20-41-28
259	<i>SPG7</i>	Chr. 16: 3' UTR of Homo sapiens spastic paraplegia 7 (pure and complicated autosomal recessive) ( <i>SPG7</i> ), nuclear gene encoding mitochondrial protein, transcript variant 1, mRNA.	C02_BC19_2012-02-10_1_20-41-28
260	-	Chr. M: Homo sapiens mRNA expressed only in placental villi, clone SMAP47.	C04_BC27_2012-02-10_1_20-41-28
261	-	Chr. 11: Unannotated region.	C06_BC35_2012-02-10_1_20-41-28
262	-	Chr. M: Sequences from articles: PubMed Central and Elsevier	C08_BC43_2012-02-10_1_20-41-28
263	-	No matches	C09_BC3_2012-02-10_1_18-25-29
264	<i>OPTC</i>	Chr. 1: 3' UTR of Homo sapiens opticin ( <i>OPTC</i> ), mRNA.	C10_BC51_2012-02-10_1_20-41-28
265	-	Homo sapiens uncharacterized LOC100507412 (LOC100507412), non-coding RNA.	C11_BC11_2012-02-10_1_18-25-29
266	-	Homo sapiens uncharacterized LOC100507412 (LOC100507412), non-coding RNA.	C12_BC59_2012-02-10_1_20-41-28
267	<i>NUDC</i>	Chr. 1: Homo sapiens nuclear distribution C homolog (A. nidulans) ( <i>NUDC</i> ), mRNA.	D02_BC20_2012-02-10_1_20-41-28
268	<i>RSF1</i>	Chr. 11: Intronic region of Homo sapiens remodelling and spacing factor 1 ( <i>RSF1</i> ), mRNA.	D04_BC28_2012-02-10_1_20-41-28
269	<i>PMEL</i>	Chr. 12: Homo sapiens premelanosome protein ( <i>PMEL</i> ), transcript variant 1, mRNA.	D06_BC36_2012-02-10_1_20-41-28
270	-	Homo sapiens uncharacterized LOC100507412 (LOC100507412), non-coding RNA.	D08_BC44_2012-02-10_1_20-41-28
271	<i>RAB7A</i>	Chr. 3: Intronic region of Homo sapiens RAB7A, member RAS oncogene family ( <i>RAB7A</i> ), mRNA.	D09_BC4_2012-02-10_1_18-25-29
272	-	Chr. 2: Unannotated region.	D10_BC52_2012-02-10_1_20-41-28
273	-	Homo sapiens uncharacterized LOC100507412 (LOC100507412), non-coding RNA.	D11_BC12_2012-02-10_1_18-25-29
274	-	No matches	D12_BC60_2012-02-10_1_20-41-28
275	-	Homo sapiens uncharacterized LOC100507412 (LOC100507412), non-coding RNA.	E02_BC21_2012-02-10_1_20-41-28
276	-	Homo sapiens uncharacterized LOC100507412 (LOC100507412), non-coding RNA.	E04_BC29_2012-02-10_1_20-41-28
277	-	Homo sapiens uncharacterized LOC100507412 (LOC100507412), non-coding RNA.	E06_BC37_2012-02-10_1_20-41-28
278	-	Chr. 15: Unannotated region.	E08_BC45_2012-02-10_1_20-41-28
279	<i>ILK</i>	Chr. 11: Homo sapiens integrin-linked kinase ( <i>ILK</i> ), transcript variant 2, mRNA.	E09_BC5_2012-02-10_1_18-25-29
280	<i>C1QB</i>	Chr. 1: Homo sapiens complement component 1, q subcomponent, B chain ( <i>C1QB</i> ), mRNA.	E10_BC53_2012-02-10_1_20-41-28
281	-	No matches	E11_BC13_2012-02-10_1_18-25-29

Clone #	Gene symbol	BLAT (UCSC) highest score result	Sequencing file(s)
282	<i>RBM39</i>	Chr. 20: Intronic region of Homo sapiens RNA binding motif protein 39 (RBM39), transcript variant 1, mRNA.	F02_BC22_2012-02-10_1_20-41-28
283	<i>ZCCHC11</i>	Chr. 1: Intronic region of Homo sapiens zinc finger, CCHC domain containing 11 (ZCCHC11), transcript variant 1, mRNA.	F04_BC30_2012-02-10_1_20-41-28
284	<i>FTX</i>	Chr. X: Intronic region of Homo sapiens FTX transcript, XIST regulator (non-protein coding) (FTX), non-coding RNA.	F06_BC38_2012-02-10_1_20-41-28
285	-	No matches	F08_BC46_2012-02-10_1_20-41-28
286	-	No matches	F09_BC6_2012-02-10_1_18-25-29
287	-	Chr. M: Sequences from articles: PubMed Central and Elsevier	F10_BC54_2012-02-10_1_20-41-28
288	<i>GPI</i>	Chr. 19: Intronic region of Homo sapiens glucose-6-phosphate isomerase (GPI), transcript variant 1, mRNA.	F11_BC14_2012-02-10_1_18-25-29
289	<i>BAP1</i>	Chr. 3: 3' UTR of Homo sapiens BRCA1 associated protein-1 (ubiquitin carboxy-terminal hydrolase) (BAP1), mRNA.	G02_BC23_2012-02-10_1_20-41-28
290	-	Homo sapiens uncharacterized LOC100507412 (LOC100507412), non-coding RNA.	G04_BC31_2012-02-10_1_20-41-28
291	-	Homo sapiens uncharacterized LOC100507412 (LOC100507412), non-coding RNA.	G06_BC39_2012-02-10_1_20-41-28
292	<i>ASB1</i>	Chr. 2: 3' UTR of Homo sapiens ankyrin repeat and SOCS box containing 1 (ASB1), mRNA.	G08_BC47_2012-02-10_1_20-41-28
293	<i>C10orf11</i>	Chr. 10: Intronic region of Homo sapiens chromosome 10 open reading frame 11 (C10orf11), mRNA.	G09_BC7_2012-02-10_1_18-25-29
294	<i>C1QB</i>	Chr. 1: Homo sapiens complement component 1, q subcomponent, B chain (C1QB), mRNA.	G10_BC55_2012-02-10_1_20-41-28
295	-	Chr. 9: Unannotated region.	G11_BC15_2012-02-10_1_18-25-29
296	<i>GCC2</i>	Chr. 2: Intronic region of Homo sapiens GRIP and coiled-coil domain containing 2 (GCC2), transcript variant 2, non-coding RNA.	H02_BC24_2012-02-10_1_20-41-28
297	-	Homo sapiens uncharacterized LOC100507412 (LOC100507412), non-coding RNA.	H04_BC32_2012-02-10_1_20-41-28
298	<i>RNASE1</i>	Chr. 14: Intronic region of Homo sapiens ribonuclease, RNase A family, 1 (pancreatic) (RNASE1), transcript variant 3, mRNA.	H06_BC40_2012-02-10_1_20-41-28
299	-	Homo sapiens uncharacterized LOC100507412 (LOC100507412), non-coding RNA.	H08_BC48_2012-02-10_1_20-41-28
300	-	No matches	H09_BC8_2012-02-10_1_18-25-29
301	<i>LRP2</i>	Chr. 2: 3' UTR of Homo sapiens low density lipoprotein receptor-related protein 2 (LRP2), mRNA.	H10_BC56_2012-02-10_1_20-41-28
302	<i>MYL6</i>	Chr. 12: Homo sapiens myosin, light chain 6, alkali, smooth muscle and non-muscle (MYL6), transcript variant 2, mRNA.	H11_BC16_2012-02-10_1_18-25-29
303	-	Chr. 19: Unannotated sequence	A01_BC1_2012-02-17_1_21-47-04.ab1
304	-	Chr. 14: Intronic region of Homo sapiens cDNA FLJ36573 fis, clone TRACH2012370.	A02_BC49_2012-02-17_1_23-44-30.ab1
305	-	Chr. M: Homo sapiens mRNA expressed only in placental villi, clone SMAP47.	A03_BC9_2012-02-17_1_21-47-04.ab1
306	-	Chr. 21: Unannotated sequence	A04_BC57_2012-02-17_1_23-44-30.ab1
307	<i>SLC6A13</i>	Chr. 12: 3' UTR of Homo sapiens solute carrier family 6 (neurotransmitter transporter, GABA), member 13 (SLC6A13), transcript variant 1, mRNA.	A05_BC17_2012-02-17_1_21-47-04.ab1

Clone #	Gene symbol	BLAT (UCSC) highest score result	Sequencing file(s)
308	-	Chr. 12: Unannotated sequence	A06_BC65_2012-02-17_1_23-44-30.ab1
309	ZCCHC11	Chr. 1: Intronic region of Homo sapiens zinc finger, CCHC domain containing 11 (ZCCHC11), transcript variant 1, mRNA.	A07_BC25_2012-02-17_1_21-47-04.ab1
310	CCP110	Chr. 16: 3' UTR of Homo sapiens centriolar coiled coil protein 110kDa (CCP110), transcript variant 1, mRNA.	A08_BC73_2012-02-17_1_23-44-30.ab1
311	COX4I1	Chr. 16: Homo sapiens cytochrome c oxidase subunit IV isoform 1 (COX4I1), nuclear gene encoding mitochondrial protein, mRNA.	A09_BC33_2012-02-17_1_21-47-04.ab1
312	MFSD11	Chr. 17: Intronic region of Homo sapiens major facilitator superfamily domain containing 11 (MFSD11), transcript variant 3, mRNA.	A10_BC81_2012-02-17_1_23-44-30.ab1
313	PDC	Chr. 1: Homo sapiens phosphatidylinositol-3-OH kinase 1B (PDK1), transcript variant 2, mRNA.	A11_BC41_2012-02-17_1_21-47-04.ab1
314	-	Chr. 16: Unannotated sequence	B01_BC2_2012-02-17_1_21-47-04.ab1
315	ANKRD30BL	Chr. 2: Intronic region of Homo sapiens ankyrin repeat domain 30B-like (ANKRD30BL), transcript variant 2, non-coding RNA.	B02_BC50_2012-02-17_1_23-44-30.ab1
316	NOTCH2	Chr. 1: Intronic region of Homo sapiens notch 2 (NOTCH2), transcript variant 1, mRNA.	B03_BC10_2012-02-17_1_21-47-04.ab1
317	-	No matches	B04_BC58_2012-02-17_1_23-44-30.ab1
318	-	No matches	B05_BC18_2012-02-17_1_21-47-04.ab1
319	ATP1B1	Chr. 1: Intronic region of Homo sapiens ATPase, Na <sup>+</sup> /K <sup>+</sup> transporting, beta 1 polypeptide (ATP1B1), mRNA.	B06_BC66_2012-02-17_1_23-44-30.ab1
320	ENO3	Chr. 17: Homo sapiens enolase 3 (beta, muscle) (ENO3), transcript variant 2, mRNA.	B07_BC26_2012-02-17_1_21-47-04.ab1
321	-	Chr. 2: Unannotated sequence	B08_BC74_2012-02-17_1_23-44-30.ab1
322	SPSWAP	Chr. 12: Intronic region of Homo sapiens splicing factor, suppressor of white-apricot homolog (Drosophila) (SFSWAP), transcript variant 1, mRNA.	B09_BC34_2012-02-17_1_21-47-04.ab1
323	-	No matches	B10_BC82_2012-02-17_1_23-44-30.ab1
324	PDC	Chr. 1: Homo sapiens phosphatidylinositol-3-OH kinase 1B (PDK1), transcript variant 2, mRNA.	B11_BC42_2012-02-17_1_21-47-04.ab1
325	CBLB	Chr. 3: Intronic region of Homo sapiens Cbl proto-oncogene, E3 ubiquitin protein ligase B (CBLB), mRNA.	C01_BC3_2012-02-17_1_21-47-04.ab1
326	MEF2D	Chr. 1: 3' UTR of Homo sapiens myocyte enhancer factor 2D (MEF2D), transcript variant 2, mRNA.	C02_BC51_2012-02-17_1_23-44-30.ab1
327	DAPK1	Chr. 9: Intronic region of Homo sapiens death-associated protein kinase 1 (DAPK1), mRNA.	C03_BC11_2012-02-17_1_21-47-04.ab1
328	GSN	Chr. 9: Intronic region of Homo sapiens gelsolin (GSN), transcript variant 2, mRNA.	C04_BC59_2012-02-17_1_23-44-30.ab1
329	-	Chr. 5: Unannotated sequence	C05_BC19_2012-02-17_1_21-47-04.ab1
330	-	Chr. 18: Unannotated sequence	C06_BC67_2012-02-17_1_23-44-30.ab1
331	RHO	Chr. 3: Homo sapiens rhodopsin (RHO), mRNA.	C07_BC27_2012-02-17_1_21-47-04.ab1
332	-	Chr. 3: Unannotated sequence	C08_BC75_2012-02-17_1_23-44-30.ab1
333	RBM5	Chr. 3: Intronic region of Homo sapiens RNA binding motif protein 5 (RBM5), transcript variant 1, mRNA.	C09_BC35_2012-02-17_1_21-47-04.ab1
334	PDC	Chr. 1: Homo sapiens phosphatidylinositol-3-OH kinase 1B (PDK1), transcript variant 2, mRNA.	C11_BC43_2012-02-17_1_21-47-04.ab1



Clone #	Gene symbol	BLAT (UCSC) highest score result	Sequencing file(s)
335	<i>PLD3</i>	Chr. 19: 3' UTR of Homo sapiens phospholipase D family, member 3 (PLD3), transcript variant 1, mRNA.	D01_BC4_2012-02-17_1_21-47-04.ab1
336	<i>FAM222B</i>	Chr. 17: Homo sapiens family with sequence similarity 222, member B (FAM222B), transcript variant 1, mRNA.	D02_BC52_2012-02-17_1_23-44-30.ab1
337	<i>ZSCAN32</i>	Chr. 16: Intronic region of Homo sapiens zinc finger and SCAN domain containing 32 (ZSCAN32), mRNA.	D03_BC12_2012-02-17_1_21-47-04.ab1
338	<i>CBLB</i>	Chr. 3: Intronic region of Homo sapiens Cbl proto-oncogene, E3 ubiquitin protein ligase B (CBLB), mRNA.	D04_BC60_2012-02-17_1_23-44-30.ab1
339	-	Chr. 21: Unannotated sequence	D05_BC20_2012-02-17_1_21-47-04.ab1
340	<i>TXNL4A</i>	Chr. 18: Intronic region of Homo sapiens thioredoxin-like 4A (TXNL4A), mRNA.	D06_BC68_2012-02-17_1_23-44-30.ab1
341	-	mRNA DL491865	D07_BC28_2012-02-17_1_21-47-04.ab1
342	<i>RHO</i>	Chr. 3: Homo sapiens rhodopsin (RHO), mRNA.	D08_BC76_2012-02-17_1_23-44-30.ab1
343	-	No matches	D09_BC36_2012-02-17_1_21-47-04.ab1
344	<i>PDC</i>	Chr. 1: Homo sapiens phosducin (PDC), transcript variant 2, mRNA.	D11_BC44_2012-02-17_1_21-47-04.ab1
345	-	mRNA L09269: Human dinucleotide repeat polymorphism at the D11S982E locus mRNA.	E01_BC5_2012-02-17_1_21-47-04.ab1
346	-	No matches	E02_BC53_2012-02-17_1_23-44-30.ab1
347	-	Chr. 9: Unannotated sequence	E03_BC13_2012-02-17_1_21-47-04.ab1
348	-	No matches	E04_BC61_2012-02-17_1_23-44-30.ab1
349	<i>EPN2</i>	Chr. 17: Intronic region of Homo sapiens epsin 2 (EPN2), transcript variant 1, mRNA.	E05_BC21_2012-02-17_1_21-47-04.ab1
350	<i>NOTCH2NL</i>	Chr. 1: Intronic region of Homo sapiens notch 2 N-terminal like (NOTCH2NL), mRNA.	E06_BC69_2012-02-17_1_23-44-30.ab1
351	<i>DUOX1</i>	Chr. 15: Intronic region of Homo sapiens dual oxidase 1 (DUOX1), transcript variant 1, mRNA.	E07_BC29_2012-02-17_1_21-47-04.ab1
352	<i>SUCLG2</i>	Chr. 3: Intronic region of Homo sapiens succinate-CoA ligase, GDP-forming, beta subunit (SUCLG2), nuclear gene encoding mitochondrial protein, transcript variant 1, mRNA.	E08_BC77_2012-02-17_1_23-44-30.ab1
353	-	Chr. 16: Unannotated sequence	E09_BC37_2012-02-17_1_21-47-04.ab1
354	<i>PDC</i>	Chr. 1: Homo sapiens phosducin (PDC), transcript variant 2, mRNA.	E11_BC45_2012-02-17_1_21-47-04.ab1
355	<i>CLASP2</i>	Chr. 3: Homo sapiens cytoplasmic linker associated protein 2 (CLASP2), transcript variant 1, mRNA.	F01_BC6_2012-02-17_1_21-47-04.ab1
356	-	No matches	F02_BC54_2012-02-17_1_23-44-30.ab1
357	-	Homo sapiens uncharacterized LOC100507412 (LOC100507412), non-coding RNA.	F03_BC14_2012-02-17_1_21-47-04.ab1
358	<i>EHBP1</i>	Chr. 2: Intronic region of Homo sapiens EH domain binding protein 1 (EHBP1), transcript variant 3, mRNA.	F04_BC62_2012-02-17_1_23-44-30.ab1
359	<i>TRIOBP</i>	Chr. 22: Intronic region of Homo sapiens TRIO and F-actin binding protein (TRIOBP), transcript variant 6, mRNA.	F05_BC22_2012-02-17_1_21-47-04.ab1
360	<i>NOTCH2NL</i>	Chr. 1: Intronic region of Homo sapiens notch 2 N-terminal like (NOTCH2NL), mRNA.	F06_BC70_2012-02-17_1_23-44-30.ab1
361	-	No matches	F07_BC30_2012-02-17_1_21-47-04.ab1
362	<i>RPL13A</i>	Chr. 19: 3' UTR of Homo sapiens ribosomal protein L13a (RPL13A), transcript variant 1, mRNA.	F08_BC78_2012-02-17_1_23-44-30.ab1

Clone #	Gene symbol	BLAT (UCSC) highest score result	Sequencing file(s)
363	<i>NOTCH2</i>	Chr. 1: Intronic region of Homo sapiens notch 2 (NOTCH2), transcript variant 1, mRNA.	F09_BC38_2012-02-17_1_21-47-04.ab1
364	<i>PDC</i>	Chr. 1: Homo sapiens phosducin (PDC), transcript variant 2, mRNA.	F11_BC46_2012-02-17_1_21-47-04.ab1
365	-	Chr. 19: Unannotated sequence	G01_BC7_2012-02-17_1_21-47-04.ab1
366	<i>CHTOP</i>	Chr. 1: 3' UTR of Homo sapiens chromatin target of PRMT1 (CHTOP), transcript variant 1, mRNA.	G02_BC55_2012-02-17_1_23-44-30.ab1
367	-	Chr. 16: Unannotated sequence	G03_BC15_2012-02-17_1_21-47-04.ab1
368	-	Chr. 16: Unannotated sequence	G04_BC63_2012-02-17_1_23-44-30.ab1
369	<i>PTPRG</i>	Chr. 3: Intronic region of Homo sapiens protein tyrosine phosphatase, receptor type, G (PTPRG), mRNA.	G05_BC23_2012-02-17_1_21-47-04.ab1
370	<i>NOTCH2</i>	Chr. 1: Intronic region of Homo sapiens notch 2 (NOTCH2), transcript variant 1, mRNA.	G06_BC71_2012-02-17_1_23-44-30.ab1
371	-	Chr. Y: Unannotated sequence	G07_BC31_2012-02-17_1_21-47-04.ab1
372	<i>NOTCH2</i>	Chr. 1: Intronic region of Homo sapiens notch 2 (NOTCH2), transcript variant 1, mRNA.	G08_BC79_2012-02-17_1_23-44-30.ab1
373	-	No matches	G09_BC39_2012-02-17_1_21-47-04.ab1
374	<i>PDC</i>	Chr. 1: Homo sapiens phosducin (PDC), transcript variant 2, mRNA.	G11_BC47_2012-02-17_1_21-47-04.ab1
375	-	Chr. X: Unannotated sequence	H01_BC8_2012-02-17_1_21-47-04.ab1
376	-	Chr. M: Unannotated sequence	H02_BC56_2012-02-17_1_23-44-30.ab1
377	<i>ATRX</i>	Chr. X: Intronic region of Homo sapiens alpha thalassemia/mental retardation syndrome X-linked (ATRX), transcript variant 1, mRNA.	H03_BC16_2012-02-17_1_21-47-04.ab1
378	-	Chr. 21: Unannotated sequence	H04_BC64_2012-02-17_1_23-44-30.ab1
379	<i>TXNL4A</i>	Chr. 18: Intronic region of Homo sapiens thioredoxin-like 4A (TXNL4A), mRNA.	H05_BC24_2012-02-17_1_21-47-04.ab1
380	<i>SLC6A9</i>	Chr. 1: 3' UTR of Homo sapiens solute carrier family 6 (neurotransmitter transporter, glycine), member 9 (SLC6A9), transcript variant 2, mRNA.	H06_BC72_2012-02-17_1_23-44-30.ab1
381	-	Chr. 19: Unannotated sequence	H07_BC32_2012-02-17_1_21-47-04.ab1
382	-	No matches	H08_BC80_2012-02-17_1_23-44-30.ab1
383	-	No matches	H09_BC40_2012-02-17_1_21-47-04.ab1
384	-	No matches	H11_BC48_2012-02-17_1_21-47-04.ab1
385	-	Chr. M: Sequences from articles: PubMed Central and Elsevier	A01_1_2012-03-01_1_23-37-43
386	-	No matches	A03_17_2012-03-01_1_23-37-43
387	<i>TBC1D23</i>	Chr. 3: Intronic region of Homo sapiens TBC1 domain family, member 23 (TBC1D23), transcript variant 1, mRNA.	A05_33_2012-03-01_1_23-37-43
388	-	Homo sapiens uncharacterized LOC100507412 (LOC100507412), non-coding RNA.	A07_49_2012-03-01_1_23-37-43
389	-	Homo sapiens uncharacterized LOC100507412 (LOC100507412), non-coding RNA.	A09_65_2012-03-01_1_23-37-43
390	-	Chr. 5: Unannotated sequence.	A11_81_2012-03-01_1_23-37-43

Clone #	Gene symbol	BLAT (UCSC) highest score result	Sequencing file(s)
391	-	Chr. M: Sequences from articles: PubMed Central and Elsevier	B01_2_2012-03-01_1_23-37-43
392	<i>UBAP1L</i>	Chr. 15: Intronic region of Homo sapiens ubiquitin associated protein 1-like (UBAP1L), mRNA.	B03_18_2012-03-01_1_23-37-43
393	-	Homo sapiens uncharacterized LOC100507412 (LOC100507412), non-coding RNA.	B05_34_2012-03-01_1_23-37-43
394	-	No matches	B07_50_2012-03-01_1_23-37-43
395	-	Chr. 3: Unannotated region.	B09_66_2012-03-01_1_23-37-43
396	-	Homo sapiens uncharacterized LOC100507412 (LOC100507412), non-coding RNA.	B11_82_2012-03-01_1_23-37-43
397	-	No matches	C01_3_2012-03-01_1_23-37-43
398	-	Homo sapiens uncharacterized LOC100507412 (LOC100507412), non-coding RNA.	C03_19_2012-03-01_1_23-37-43
399	-	Homo sapiens uncharacterized LOC100507412 (LOC100507412), non-coding RNA.	C05_35_2012-03-01_1_23-37-43
400	-	Homo sapiens uncharacterized LOC100507412 (LOC100507412), non-coding RNA.	C07_51_2012-03-01_1_23-37-43
401	-	No matches	C09_67_2012-03-01_1_23-37-43
402	<i>MOB3B</i>	Chr. 9: Intronic region of Homo sapiens MOB kinase activator 3B (MOB3B), mRNA.	C11_83_2012-03-01_1_23-37-43
403	<i>SAG</i>	Chr. 2: Homo sapiens S-antigen; retina and pineal gland (arrestin) (SAG), mRNA.	D01_4_2012-03-01_1_23-37-43
404	-	Homo sapiens uncharacterized LOC100507412 (LOC100507412), non-coding RNA.	D03_20_2012-03-01_1_23-37-43
405	<i>HFM1</i>	Chr. 1: Intronic region of Homo sapiens HFM1, ATP-dependent DNA helicase homolog ( <i>S. cerevisiae</i> ) (HFM1), mRNA.	D05_36_2012-03-01_1_23-37-43
406	-	Chr. 2: Unannotated region.	D07_52_2012-03-01_1_23-37-43
407	-	No matches	D09_68_2012-03-01_1_23-37-43
408	-	No matches	D11_84_2012-03-01_1_23-37-43
409	-	Chr. 19: Alignments with several ZNF proteins	E01_5_2012-03-01_1_23-37-43
410	-	Homo sapiens uncharacterized LOC100507412 (LOC100507412), non-coding RNA.	E03_21_2012-03-01_1_23-37-43
411	<i>MPV17L</i>	Chr. 16: Intronic region of Homo sapiens MPV17 mitochondrial membrane protein-like (MPV17L), nuclear gene encoding mitochondrial protein, transcript variant 1, mRNA.	E05_37_2012-03-01_1_23-37-43
412	-	Chr. 9: Unannotated region.	E07_53_2012-03-01_1_23-37-43
413	-	Chr. 2: Unannotated region.	E09_69_2012-03-01_1_23-37-43
414	<i>CLU</i>	Chr. 8: Homo sapiens clusterin (CLU), transcript variant 4, non-coding RNA.	E11_85_2012-03-01_1_23-37-43
415	<i>PEA15</i>	Chr. 1: 3' UTR of Homo sapiens phosphoprotein enriched in astrocytes 15 (PEA15), mRNA.	F01_6_2012-03-01_1_23-37-43
416	<i>MECOM</i>	Chr. 3: Intronic region of Homo sapiens MDS1 and EVI1 complex locus (MECOM), transcript variant 4, mRNA.	F03_22_2012-03-01_1_23-37-43
417	<i>CPE</i>	Chr. 4: Intronic region of Homo sapiens carboxypeptidase E (CPE), mRNA.	F05_38_2012-03-01_1_23-37-43
418	-	Chr. M: Homo sapiens mRNA expressed only in placental villi, clone SMAP47.	F07_54_2012-03-01_1_23-37-43

Clone #	Gene symbol	BLAT (UCSC) highest score result	Sequencing file(s)
419	<i>ABR</i>	Chr. 17: Intronic region of Homo sapiens active BCR-related ( <i>ABR</i> ), transcript variant 2, mRNA.	F09_70_2012-03-01_1_23-37-43
420	<i>KIAA2022</i>	Chr. X: Intronic region of Homo sapiens <i>KIAA2022</i> ( <i>KIAA2022</i> ), mRNA.	F11_86_2012-03-01_1_23-37-43
421	-	Homo sapiens uncharacterized LOC100507412 (LOC100507412), non-coding RNA.	G01_7_2012-03-01_1_23-37-43
422	-	Homo sapiens uncharacterized LOC100507412 (LOC100507412), non-coding RNA.	G03_23_2012-03-01_1_23-37-43
423	<i>DCAF11</i>	Chr. 14: 3' UTR of Homo sapiens DDB1 and CUL4 associated factor 11 ( <i>DCAF11</i> ), transcript variant 3, mRNA.	G05_39_2012-03-01_1_23-37-43
424	<i>RPS27A</i>	Chr. 2: Homo sapiens ribosomal protein S27a ( <i>RPS27A</i> ), transcript variant 2, mRNA.	G07_55_2012-03-01_1_23-37-43
425	<i>RPS6KA5</i>	Chr. 14: Intronic region of Homo sapiens ribosomal protein S6 kinase, 90kDa, polypeptide 5 ( <i>RPS6KA5</i> ), transcript variant 1, mRNA.	G09_71_2012-03-01_1_23-37-43
426	<i>KIAA2022</i>	Chr. X: Intronic region of Homo sapiens <i>KIAA2022</i> ( <i>KIAA2022</i> ), mRNA.	G11_87_2012-03-01_1_23-37-43
427	-	No matches	H01_8_2012-03-01_1_23-37-43
428	<i>ANKRD34A</i>	Chr. 1: Homo sapiens ankyrin repeat domain 34A ( <i>ANKRD34A</i> ), mRNA.	H03_24_2012-03-01_1_23-37-43
429	-	Chr. M: Homo sapiens piRNA piR-34804, complete sequence.	H05_40_2012-03-01_1_23-37-43
430	-	Homo sapiens uncharacterized LOC100507412 (LOC100507412), non-coding RNA.	H07_56_2012-03-01_1_23-37-43
431	<i>KIF13A</i>	Chr. 6: Intronic region of Homo sapiens kinesin family member 13A ( <i>KIF13A</i> ), transcript variant 4, mRNA.	H09_72_2012-03-01_1_23-37-43
432	<i>CTNNA2</i>	Chr. 2: Intronic region of Homo sapiens catenin (cadherin-associated protein), alpha 2 ( <i>CTNNA2</i> ), transcript variant 1, mRNA.	H11_88_2012-03-01_1_23-37-43
433	-	No matches	A02_9_2012-03-02_1_24-33-05
434	<i>ST6GALNAC3</i>	Chr. 1: Intronic region of Homo sapiens ST6 (alpha-N-acetyl-neuraminyl-2,3-beta-galactosyl-1, 3)-N-acetylgalactosaminide alpha-2,6-sialyltransferase 3 ( <i>ST6GALNAC3</i> ), transcript variant 1, mRNA.	A04_25_2012-03-02_1_24-33-05
435	<i>CPE</i>	Chr. 4: Intronic region of Homo sapiens carboxypeptidase E ( <i>CPE</i> ), mRNA.	A06_41_2012-03-02_1_24-33-05
436	-	Homo sapiens uncharacterized LOC100507412 (LOC100507412), non-coding RNA.	A08_57_2012-03-02_1_24-33-05
437	<i>HSPE1</i>	Chr. 2: Homo sapiens heat shock 10kDa protein 1 (chaperonin 10) ( <i>HSPE1</i> ), nuclear gene encoding mitochondrial protein, mRNA.	A10_73_2012-03-02_1_24-33-05
438	<i>GLYR1</i>	Chr. 16: 3' UTR of Homo sapiens glyoxylate reductase 1 homolog ( <i>Arabidopsis</i> ) ( <i>GLYR1</i> ), mRNA.	A12_89_2012-03-02_1_24-33-05
439	<i>STARD13</i>	Chr. 13: Intronic region of Homo sapiens StAR-related lipid transfer (START) domain containing 13 ( <i>STARD13</i> ), transcript variant 4, mRNA.	B02_10_2012-03-02_1_24-33-05
440	<i>ANK2</i>	Chr. 4: Intronic region of Homo sapiens ankyrin 2, neuronal ( <i>ANK2</i> ), transcript variant 3, mRNA.	B04_26_2012-03-02_1_24-33-05
441	<i>RPL13A</i>	Chr. 19: Intronic region of Homo sapiens ribosomal protein L13a ( <i>RPL13A</i> ), transcript variant 1, mRNA.	B06_42_2012-03-02_1_24-33-05
442	-	No matches	B08_58_2012-03-02_1_24-33-05
443	-	Homo sapiens uncharacterized LOC100507412 (LOC100507412), non-coding RNA.	B10_74_2012-03-02_1_24-33-05
444	<i>MINOS1-NBL1</i>	Chr. 1: 3' UTR of Homo sapiens <i>MINOS1-NBL1</i> read-through ( <i>MINOS1-NBL1</i> ), transcript variant 1, mRNA.	B12_90_2012-03-02_1_24-33-05

Clone #	Gene symbol	BLAT (UCSC) highest score result	Sequencing file(s)
445	<i>RCS1</i>	Chr. 1: 3' UTR of Homo sapiens RCS1 domain containing 1 (RCS1), mRNA.	C02_11_2012-03-02_1_24-33-05
446	-	Homo sapiens uncharacterized LOC100507412 (LOC100507412), non-coding RNA.	C04_27_2012-03-02_1_24-33-05
447	<i>MYL6</i>	Chr. 12: Homo sapiens myosin, light chain 6, alkali, smooth muscle and non-muscle (MYL6), transcript variant 1, mRNA.	C06_43_2012-03-02_1_24-33-05
448	<i>LIN54</i>	Chr. 4: Intronic region of Homo sapiens lin-54 homolog (C. elegans) (LIN54), transcript variant 1, mRNA.	C08_59_2012-03-02_1_24-33-05
449	<i>ARID2</i>	Chr. 12: Intronic region of Homo sapiens AT rich interactive domain 2 (ARID, RFX-like) (ARID2), mRNA.	C10_75_2012-03-02_1_24-33-05
450	<i>SMARCC1</i>	Chr. 3: Intronic region of Homo sapiens SWI/SNF related, matrix associated, actin dependent regulator of chromatin, subfamily c, member 1 (SMARCC1), mRNA.	C12_91_2012-03-02_1_24-33-05
451	-	mRNA S77581: HERVK10/HUMMTV reverse transcriptase homolog	D02_12_2012-03-02_1_24-33-05
452	<i>RAB1A</i>	Chr. 2: Intronic region of Homo sapiens RAB1A, member RAS oncogene family (RAB1A), transcript variant 2, mRNA.	D04_28_2012-03-02_1_24-33-05
453	<i>VPS28</i>	Chr. 8: Homo sapiens vacuolar protein sorting 28 homolog (S. cerevisiae) (VPS28), transcript variant 1, mRNA.	D06_44_2012-03-02_1_24-33-05
454	<i>WDR33</i>	Chr. 2: Intronic region of Homo sapiens WD repeat domain 33 (WDR33), transcript variant 1, mRNA.	D08_60_2012-03-02_1_24-33-05
455	<i>COX6C</i>	Chr. 8: Homo sapiens cytochrome c oxidase subunit VIc (COX6C), nuclear gene encoding mitochondrial protein, mRNA.	D10_76_2012-03-02_1_24-33-05
456	<i>CST3</i>	Chr. 20: Homo sapiens cystatin C (CST3), mRNA.	D12_92_2012-03-02_1_24-33-05
457	-	Homo sapiens uncharacterized LOC100507412 (LOC100507412), non-coding RNA.	E02_13_2012-03-02_1_24-33-05
458	<i>FMOD</i>	Chr. 1: 3' UTR of Homo sapiens fibromodulin (FMOD), mRNA.	E04_29_2012-03-02_1_24-33-05
459	-	Chr. 6: Unannotated region.	E06_45_2012-03-02_1_24-33-05
460	<i>WDR33</i>	Chr. 2: Intronic region of Homo sapiens WD repeat domain 33 (WDR33), transcript variant 1, mRNA.	E08_61_2012-03-02_1_24-33-05
461	-	Homo sapiens uncharacterized LOC100507412 (LOC100507412), non-coding RNA.	E10_77_2012-03-02_1_24-33-05
462	<i>MAP1B</i>	Chr. 5: Homo sapiens microtubule-associated protein 1B (MAP1B), mRNA.	E12_93_2012-03-02_1_24-33-05
463	-	Homo sapiens uncharacterized LOC100507412 (LOC100507412), non-coding RNA.	F02_14_2012-03-02_1_24-33-05
464	-	No matches	F04_30_2012-03-02_1_24-33-05
465	-	Chr. 2: Unannotated region.	F06_46_2012-03-02_1_24-33-05
466	<i>POLR2G</i>	Chr. 11: Intronic region of Homo sapiens polymerase (RNA) II (DNA directed) polypeptide G (POLR2G), mRNA.	F08_62_2012-03-02_1_24-33-05
467	-	Chr. 6: Unannotated region.	F10_78_2012-03-02_1_24-33-05
468	-	Chr. M Sequences from articles: PubmedCentral and Elsevier	F12_94_2012-03-02_1_24-33-05
469	<i>NFAT5</i>	Chr. 16: Intronic region of Homo sapiens nuclear factor of activated T-cells 5, tonicity-responsive (NFAT5), transcript variant 1, mRNA.	G02_15_2012-03-02_1_24-33-05
470	-	Chr. M: Homo sapiens piRNA piR-34804, complete sequence.	G04_31_2012-03-02_1_24-33-05

Clone #	Gene symbol	BLAT (UCSC) highest score result	Sequencing file(s)
471	<i>RAB28</i>	Chr. 4: Intronic region of Homo sapiens RAB28, member RAS oncogene family (RAB28), transcript variant 2, mRNA.	G06_47_2012-03-02_1_24-33-05
472	-	Homo sapiens uncharacterized LOC100507412 (LOC100507412), non-coding RNA.	G08_63_2012-03-02_1_24-33-05
473	<i>FTH1</i>	Chr. 11: Homo sapiens ferritin, heavy polypeptide 1 (FTH1), mRNA.	G10_79_2012-03-02_1_24-33-05
474	-	Homo sapiens uncharacterized LOC100507412 (LOC100507412), non-coding RNA.	H02_16_2012-03-02_1_24-33-05
475	-	Sequences from Articles: PubmedCentral and Elsevier	H04_32_2012-03-02_1_24-33-05
476	<i>EI24</i>	Chr. 11: 3' UTR of Homo sapiens etoposide induced 2.4 (EI24), transcript variant 1, mRNA.	H06_48_2012-03-02_1_24-33-05
477	-	mRNA U61101: Human NTera2D1 cell line mRNA containing L1 retroposon, clone R5.	H08_64_2012-03-02_1_24-33-05
478	-	Homo sapiens uncharacterized LOC100507412 (LOC100507412), non-coding RNA.	H10_80_2012-03-02_1_24-33-05
479	-	No matches	A01_1_2012-03-02_1_01-29-04
480	-	Homo sapiens uncharacterized LOC100507412 (LOC100507412), non-coding RNA.	A03_9_2012-03-02_1_01-29-04
481	-	No matches	A05_17_2012-03-02_1_01-29-04
482	-	No matches	A07_25_2012-03-02_1_01-29-04
483	-	Chr. 22: Unannotated region.	A09_33_2012-03-02_1_01-29-04
484	-	Chr. M Sequences from articles: PubmedCentral and Elsevier	A11_41_2012-03-02_1_01-29-04
485	-	No matches	B01_2_2012-03-02_1_01-29-04
486	-	Homo sapiens uncharacterized LOC100507412 (LOC100507412), non-coding RNA.	B03_10_2012-03-02_1_01-29-04
487	-	Homo sapiens uncharacterized LOC100507412 (LOC100507412), non-coding RNA.	B05_18_2012-03-02_1_01-29-04
488	<i>NTN1</i>	Chr. 17: 3' UTR of Homo sapiens netrin 1 (NTN1), mRNA.	B07_26_2012-03-02_1_01-29-04
489	-	Homo sapiens uncharacterized LOC100507412 (LOC100507412), non-coding RNA.	B09_34_2012-03-02_1_01-29-04
490	-	No matches	B11_42_2012-03-02_1_01-29-04
491	<i>FOXJ2</i>	Chr. 12: Intronic region of Homo sapiens forkhead box J2 (FOXJ2), mRNA.	C01_3_2012-03-02_1_01-29-04
492	-	Homo sapiens uncharacterized LOC100507412 (LOC100507412), non-coding RNA.	C03_11_2012-03-02_1_01-29-04
493	-	No matches	C05_19_2012-03-02_1_01-29-04
494	<i>HFM1</i>	Chr. 1: Intronic region of Homo sapiens HFM1, ATP-dependent DNA helicase homolog ( <i>S. cerevisiae</i> ) (HFM1), mRNA.	C07_27_2012-03-02_1_01-29-04
495	-	Homo sapiens uncharacterized LOC100507412 (LOC100507412), non-coding RNA.	C09_35_2012-03-02_1_01-29-04
496	<i>OSBPL9</i>	Chr. 1: Intronic region of Homo sapiens oxysterol binding protein-like 9 (OSBPL9), transcript variant 5, mRNA.	C11_43_2012-03-02_1_01-29-04
497	-	Chr. 11: EST N85959 and EST DB454841	D01_4_2012-03-02_1_01-29-04
498	<i>MMP2</i>	Chr. 16: Homo sapiens matrix metalloproteinase 2 (gelatinase A, 72kDa gelatinase, 72kDa type IV collagenase) (MMP2), transcript variant 1, mRNA.	D03_12_2012-03-02_1_01-29-04

Clone #	Gene symbol	BLAT (UCSC) highest score result	Sequencing file(s)
499	-	mRNA S77581: HERVK10/HUMMTV reverse transcriptase homolog (clone RT211) [human, multiple sclerosis, brain plaques, mRNA Partial, 90 nt].	D05_20_2012-03-02_1_01-29-04
500	<i>RFNG</i>	Chr. 17: 3' UTR of Homo sapiens RFNG O-fucosylpeptide 3-beta-N-acetylglucosaminyltransferase (RFNG), mRNA.	D07_28_2012-03-02_1_01-29-04
501	-	mRNA S77581: HERVK10/HUMMTV reverse transcriptase homolog (clone RT211) [human, multiple sclerosis, brain plaques, mRNA Partial, 90 nt].	D09_36_2012-03-02_1_01-29-04
502	-	No matches	D11_44_2012-03-02_1_01-29-04
503	<i>TAOK3</i>	Chr. 12: Intronic region of Homo sapiens TAO kinase 3 (TAOK3), mRNA.	E01_5_2012-03-02_1_01-29-04
504	-	No matches	E03_13_2012-03-02_1_01-29-04
505	<i>ABI3BP</i>	Chr. 3: Intronic region of Homo sapiens ABI family, member 3 (NESH) binding protein (ABI3BP), mRNA.	E05_21_2012-03-02_1_01-29-04
506	<i>CEP68</i>	Chr. 2: Intronic region of Homo sapiens centrosomal protein 68kDa (CEP68), mRNA.	E07_29_2012-03-02_1_01-29-04
507	-	Chr. M: Homo sapiens mRNA expressed only in placental villi, clone SMAP47.	E09_37_2012-03-02_1_01-29-04
508	<i>TMTC1</i>	Chr. 12: Intronic region of Homo sapiens transmembrane and tetratricopeptide repeat containing 1 (TMTC1), transcript variant 1, mRNA.	E11_45_2012-03-02_1_01-29-04
509	-	Homo sapiens uncharacterized LOC100507412 (LOC100507412), non-coding RNA.	F01_6_2012-03-02_1_01-29-04
510	<i>CUL1</i>	Chr. 7: Intronic region of Homo sapiens cullin 1 (CUL1), mRNA.	F03_14_2012-03-02_1_01-29-04
511	-	No matches	F05_22_2012-03-02_1_01-29-04
512	<i>CST3</i>	Chr. 20: Homo sapiens cystatin C (CST3), mRNA.	F07_30_2012-03-02_1_01-29-04
513	-	Chr. M: Homo sapiens mRNA expressed only in placental villi, clone SMAP47.	F09_38_2012-03-02_1_01-29-04
514	-	Homo sapiens uncharacterized LOC100507412 (LOC100507412), non-coding RNA.	F11_46_2012-03-02_1_01-29-04
515	<i>BEST1</i>	Chr.11: Homo sapiens bestrophin 1 (BEST1), transcript variant 2, mRNA.	G01_7_2012-03-02_1_01-29-04
516	<i>CUL1</i>	Chr. 7: Intronic region of omo sapiens cullin 1 (CUL1), mRNA.	G03_15_2012-03-02_1_01-29-04
517	<i>ABI3BP</i>	Chr. 3: Intronic region of Homo sapiens ABI family, member 3 (NESH) binding protein (ABI3BP), mRNA.	G05_23_2012-03-02_1_01-29-04
518	-	Homo sapiens uncharacterized LOC100507412 (LOC100507412), non-coding RNA.	G07_31_2012-03-02_1_01-29-04
519	-	Homo sapiens uncharacterized LOC100507412 (LOC100507412), non-coding RNA.	G09_39_2012-03-02_1_01-29-04
520	-	No matches	G11_47_2012-03-02_1_01-29-04
521	<i>COMMD2</i>	Chr. 3: Homo sapiens COMM domain containing 2 (COMMD2), mRNA.	H01_8_2012-03-02_1_01-29-04
522	<i>CUL1</i>	Chr. 7: Intronic region of omo sapiens cullin 1 (CUL1), mRNA.	H03_16_2012-03-02_1_01-29-04
523	<i>ABI3BP</i>	Chr. 3: Intronic region of Homo sapiens ABI family, member 3 (NESH) binding protein (ABI3BP), mRNA.	H05_24_2012-03-02_1_01-29-04
524	<i>TNIK</i>	Chr. 3: Intronic region of Homo sapiens TRAF2 and NCK interacting kinase (TNK1), transcript variant 5, mRNA.	H07_32_2012-03-02_1_01-29-04
525	<i>PTPRM</i>	Chr. 18: Intronic region of Homo sapiens protein tyrosine phosphatase, receptor type, M (PTPRM), transcript variant 2, mRNA.	H09_40_2012-03-02_1_01-29-04

Clone #	Gene symbol	BLAT (UCSC) highest score result	Sequencing file(s)
526	-	No matches	H11_48_2012-03-02_1_01-29-04
527	<i>TNPO1</i>	Chr. 5: Intronic region of Homo sapiens transportin 1 (TNPO1), transcript variant 1, mRNA.	A02_49_2012-03-02_1_03-26-30
528	<i>PPM1G</i>	Chr. 2: 3' UTR of Homo sapiens protein phosphatase, Mg <sup>2+</sup> /Mn <sup>2+</sup> dependent, 1G (PPM1G), mRNA.	A04_57_2012-03-02_1_03-26-30
529	-	Chr. M: Homo sapiens piRNA piR-34804, complete sequence.	B02_50_2012-03-02_1_03-26-30
530	-	No matches	B04_58_2012-03-02_1_03-26-30
531	<i>CKB</i>	Chr. 14: 3' UTR of Homo sapiens creatine kinase, brain (CKB), mRNA.	C02_51_2012-03-02_1_03-26-30
532	<i>MRPS11</i>	Chr. 15: Homo sapiens mitochondrial ribosomal protein S11 (MRPS11), nuclear gene encoding mitochondrial protein, transcript variant 2, mRNA.	C04_59_2012-03-02_1_03-26-30
533	<i>RPL7A</i>	Chr. (: Homo sapiens ribosomal protein L7a (RPL7A), mRNA.	D02_52_2012-03-02_1_03-26-30
534	-	No matches	D04_60_2012-03-02_1_03-26-30
535	-	Chr. 2: Unannotated region.	E02_53_2012-03-02_1_03-26-30
536	-	Chr. M: Homo sapiens mRNA expressed only in placental villi, clone SMAP47.	E04_61_2012-03-02_1_03-26-30
537	-	Homo sapiens uncharacterized LOC100507412 (LOC100507412), non-coding RNA.	F02_54_2012-03-02_1_03-26-30
538	-	No matches	F04_62_2012-03-02_1_03-26-30
539	-	No matches	G02_55_2012-03-02_1_03-26-30
540	<i>WDR33</i>	Chr. 2: 3' UTR of Homo sapiens WD repeat domain 33 (WDR33), transcript variant 1, mRNA.	H02_56_2012-03-02_1_03-26-30
541	<i>GIT1</i>	Chr. 17: 3' UTR of Homo sapiens G protein-coupled receptor kinase interacting ArfGAP 1 (GIT1), transcript variant 1, mRNA.	A02_BC1_2012-03-07_1_18-53-57.ab1
542	-	Chr. 16: Unannotated sequence	A04_BC9_2012-03-07_1_18-53-57.ab1
543	<i>GUSBP11</i>	Chr. 22: Intronic region of Homo sapiens glucuronidase, beta pseudogene 11 (GUSBP11), non-coding RNA.	A06_BC17_2012-03-07_1_18-53-57.ab1
544	<i>CAPNS1</i>	Chr. 19: 3' UTR of Homo sapiens calpain, small subunit 1 (CAPNS1), transcript variant 1, mRNA.	B02_BC2_2012-03-07_1_18-53-57.ab1
545	-	No matches	B04_BC10_2012-03-07_1_18-53-57.ab1
546	-	No matches	B06_BC18_2012-03-07_1_18-53-57.ab1
547	-	No matches	C02_BC3_2012-03-07_1_18-53-57.ab1
548	<i>ASTN2</i>	Chr. 9: Intronic region of Homo sapiens astrotactin 2 (ASTN2), transcript variant 1, mRNA.	C04_BC11_2012-03-07_1_18-53-57.ab1
549	<i>GLC1N</i>	Chr. 15: Intronic region of Homo sapiens KCC, mRNA; and Homo sapiens GLC1N, mRNA.	C06_BC19_2012-03-07_1_18-53-57.ab1
550	<i>PPP1R16A</i>	Chr. 8: Homo sapiens protein phosphatase 1, regulatory subunit 16A (PPP1R16A), mRNA.	D02_BC4_2012-03-07_1_18-53-57.ab1
551	-	Human foetal eye ESTs BM676228 and BM715662	D04_BC12_2012-03-07_1_18-53-57.ab1
552	<i>NDUFS2</i>	Chr. 1: Homo sapiens NADH dehydrogenase (ubiquinone) Fe-S protein 2, 49kDa (NADH-coenzyme Q reductase) (NDUFS2), nuclear gene encoding mitochondrial protein, transcript variant 1, mRNA.	E02_BC5_2012-03-07_1_18-53-57.ab1



Clone #	Gene symbol	BLAT (UCSC) highest score result	Sequencing file(s)
553	-	Homo sapiens uncharacterized LOC100507412 (LOC100507412), non-coding RNA.	E04_BC13_2012-03-07_1_18-53-57.ab1
554	-	Human foetal eye ESTs BM676228 and BM715662	F02_BC6_2012-03-07_1_18-53-57.ab1
555	-	No matches	F04_BC14_2012-03-07_1_18-53-57.ab1
556	<i>KCC, GLC1N</i>	Chr. 15: Intronic region of Homo sapiens KCC, mRNA; and Homo sapiens GLC1N, mRNA.	G02_BC7_2012-03-07_1_18-53-57.ab1
557	<i>CSNK1D</i>	Chr. 17: Homo sapiens casein kinase 1, delta (CSNK1D), transcript variant 2, mRNA.	G04_BC15_2012-03-07_1_18-53-57.ab1
558	<i>PLEKHA7</i>	Chr. 11: Intronic region of Homo sapiens pleckstrin homology domain containing, family A member 7 (PLEKHA7), mRNA.	H02_BC8_2012-03-07_1_18-53-57.ab1
559	-	No matches	H04_BC16_2012-03-07_1_18-53-57.ab1
560	<i>CAPNS1</i>	Chr. 19: 3' UTR of Homo sapiens calpain, small subunit 1 (CAPNS1), transcript variant 2, mRNA.	A02_BC1_2012-04-13_1_17-15-21
561	-	Human brain EST HY324267	A04_BC9_2012-04-13_1_17-15-21
562	<i>PDDC1</i>	Chr. 11: 3' UTR of Homo sapiens Parkinson disease 7 domain containing 1 (PDDC1), mRNA.	A06_BC17_2012-04-13_1_17-15-21
563	<i>CCDC174</i>	Chr. 3: 3' UTR of Homo sapiens coiled-coil domain containing 174 (CCDC174), mRNA.	A08_BC25_2012-04-13_1_17-15-21
564	-	No matches	A10_BC33_2012-04-13_1_17-15-21
565	<i>NDUFS2</i>	Chr. 1: Homo sapiens NADH dehydrogenase (ubiquinone) Fe-S protein 2, 49kDa (NADH-coenzyme Q reductase) (NDUFS2), nuclear gene encoding mitochondrial protein, transcript variant 1, mRNA.	B02_BC2_2012-04-13_1_17-15-21
566	-	Human brain EST HY324267	B04_BC10_2012-04-13_1_17-15-21
567	-	Brain hippocampus mRNA BC045622: Homo sapiens uncharacterized serine/threonine-protein kinase Sgk494, mRNA (cDNA clone MGC:39533 IMAGE:5259536), complete cds.	B06_BC18_2012-04-13_1_17-15-21
568	<i>UBA52</i>	Chr. 19: Homo sapiens ubiquitin A-52 residue ribosomal protein fusion product 1 (UBA52), transcript variant 1, mRNA.	B08_BC26_2012-04-13_1_17-15-21
569	-	Human brain EST HY324267	C02_BC3_2012-04-13_1_17-15-21
570	-	Human brain EST HY324267	C04_BC11_2012-04-13_1_17-15-21
571	<i>DOCK5</i>	Chr. 8: Intronic region of Homo sapiens dedicator of cytokinesis 5 (DOCK5), mRNA.	C06_BC19_2012-04-13_1_17-15-21
572	<i>PIAS1</i>	Chr. 15: Homo sapiens protein inhibitor of activated STAT, 1 (PIAS1), mRNA.	C08_BC27_2012-04-13_1_17-15-21
573	<i>TBC1D2B</i>	Chr. 15: 3' UTR of Homo sapiens TBC1 domain family, member 2B (TBC1D2B), transcript variant 1, mRNA.	D02_BC4_2012-04-13_1_17-15-21
574	-	No matches	D04_BC12_2012-04-13_1_17-15-21
575	<i>SLC22A6</i>	Chr. 11: Homo sapiens solute carrier family 22 (organic anion transporter), member 6 (SLC22A6), transcript variant 1, mRNA.	D06_BC20_2012-04-13_1_17-15-21
576	<i>NMT1</i>	Chr. 17: Homo sapiens N-myristoyltransferase 1 (NMT1), mRNA.	D08_BC28_2012-04-13_1_17-15-21
577	<i>PLEKHA7</i>	Chr. 11: Intronic region of Homo sapiens pleckstrin homology domain containing, family A member 7 (PLEKHA7), mRNA.	E02_BC5_2012-04-13_1_17-15-21

Clone #	Gene symbol	BLAT (UCSC) highest score result	Sequencing file(s)
578	<i>CSNK1D</i>	Chr. 17: Homo sapiens casein kinase 1, delta ( <i>CSNK1D</i> ), transcript variant 2, mRNA.	E04_BC13_2012-04-13_1_17-15-21
579	<i>UBC</i>	Chr. 12: Homo sapiens mRNA for ubiquitin C variant protein.	E06_BC21_2012-04-13_1_17-15-21
580	<i>PLEKHA7</i>	Chr. 11: Intronic region of Homo sapiens pleckstrin homology domain containing, family A member 7 ( <i>PLEKHA7</i> ), mRNA.	E08_BC29_2012-04-13_1_17-15-21
581	<i>RPS27A</i>	Chr. 2: Homo sapiens ribosomal protein S27a ( <i>RPS27A</i> ), transcript variant 2, mRNA.	F02_BC6_2012-04-13_1_17-15-21
582	<i>GUSBP11</i>	Chr. 22: Homo sapiens glucuronidase, beta pseudogene 11 ( <i>GUSBP11</i> ), non-coding RNA.	F04_BC14_2012-04-13_1_17-15-21
583	-	Brain hippocampus mRNA BC045622: Homo sapiens uncharacterized serine/threonine-protein kinase Sgk494, mRNA (cDNA clone MGC:39533 IMAGE:5259536), complete cds.	F06_BC22_2012-04-13_1_17-15-21
584	<i>LMAN1</i>	Chr. 18: Homo sapiens lectin, mannose-binding, 1 ( <i>LMAN1</i> ), mRNA.	F08_BC30_2012-04-13_1_17-15-21
585	<i>UBA52</i>	Chr. 19: Homo sapiens ubiquitin A-52 residue ribosomal protein fusion product 1 ( <i>UBA52</i> ), transcript variant 1, mRNA.	G02_BC7_2012-04-13_1_17-15-21
586	-	Human brain EST HY324267	G04_BC15_2012-04-13_1_17-15-21
587	<i>NDUFB10</i>	Chr. 16: Homo sapiens NADH dehydrogenase (ubiquinone) 1 beta subcomplex, 10, 22kDa ( <i>NDUFB10</i> ), nuclear gene encoding mitochondrial protein, mRNA.	G06_BC23_2012-04-13_1_17-15-21
588	-	Homo sapiens uncharacterized LOC100507412 ( <i>LOC100507412</i> ), non-coding RNA.	G08_BC31_2012-04-13_1_17-15-21
589	<i>ASTN2</i>	Chr. 9: Intronic region of Homo sapiens astrotactin 2 ( <i>ASTN2</i> ), transcript variant 1, mRNA.	H02_BC8_2012-04-13_1_17-15-21
590	-	Homo sapiens uncharacterized LOC100507412 ( <i>LOC100507412</i> ), non-coding RNA.	H04_BC16_2012-04-13_1_17-15-21
591	-	Homo sapiens uncharacterized LOC100507412 ( <i>LOC100507412</i> ), non-coding RNA.	H06_BC24_2012-04-13_1_17-15-21
592	<i>PSMC1</i>	Chr. 14: Homo sapiens proteasome (prosome, macropain) 26 S subunit, ATPase, 1 ( <i>PSMC1</i> ), mRNA.	H08_BC32_2012-04-13_1_17-15-21
593	-	No matches	A02_BC1_2012-04-19_1_17-22-10
594	<i>PLEKHA7</i>	Chr. 11: Intronic region of Homo sapiens pleckstrin homology domain containing, family A member 7 ( <i>PLEKHA7</i> ), mRNA.	A04_BC9_2012-04-19_1_17-22-10
595	<i>CSNK1D</i>	Chr. 17: Homo sapiens casein kinase 1, delta ( <i>CSNK1D</i> ), transcript variant 2, mRNA.	A06_BC17_2012-04-19_1_17-22-10
596	<i>CAPNS1</i>	Chr. 19: 3' UTR of Homo sapiens calpain, small subunit 1 ( <i>CAPNS1</i> ), transcript variant 1, mRNA.	A08_BC25_2012-04-19_1_17-22-10
597	-	Human brain EST HY324267	A10_BC33_2012-04-19_1_17-22-10
598	<i>GIT1</i>	Chr. 17: 3' UTR of Homo sapiens G protein-coupled receptor kinase interacting ArfGAP 1 ( <i>GIT1</i> ), transcript variant 1, mRNA.	B02_BC2_2012-04-19_1_17-22-10
599	<i>RPS27A</i>	Chr. 2: Homo sapiens ribosomal protein S27a ( <i>RPS27A</i> ), transcript variant 2, mRNA.	B04_BC10_2012-04-19_1_17-22-10
600	-	No matches	B06_BC18_2012-04-19_1_17-22-10
601	<i>NDUFS2</i>	Chr. 1: Homo sapiens NADH dehydrogenase (ubiquinone) Fe-S protein 2, 49kDa (NADH-coenzyme Q reductase) ( <i>NDUFS2</i> ), nuclear gene encoding mitochondrial protein, transcript variant 2, mRNA.	B08_BC26_2012-04-19_1_17-22-10
602	-	Human brain EST HY324267	B10_BC34_2012-04-19_1_17-22-10

Clone #	Gene symbol	BLAT (UCSC) highest score result	Sequencing file(s)
603	<i>CAPNS1</i>	Chr. 19: 3' UTR of Homo sapiens calpain, small subunit 1 (CAPNS1), transcript variant 2, mRNA.	C02_BC3_2012-04-19_1_17-22-10
604	<i>UBA52</i>	Chr. 19: Homo sapiens ubiquitin A-52 residue ribosomal protein fusion product 1 (UBA52), transcript variant 1, mRNA.	C04_BC11_2012-04-19_1_17-22-10
605	<i>GUSBP11</i>	Chr. 22: Intronic region of Homo sapiens glucuronidase, beta pseudogene 11 (GUSBP11), non-coding RNA.	C06_BC19_2012-04-19_1_17-22-10
606	-	Human brain EST HY324267	C08_BC27_2012-04-19_1_17-22-10
607	-	No matches	C10_BC35_2012-04-19_1_17-22-10
608	-	No matches	D02_BC4_2012-04-19_1_17-22-10
609	<i>RPL10</i>	Chr. X: Homo sapiens ribosomal protein L10 (RPL10), transcript variant 1, mRNA.	D04_BC12_2012-04-19_1_17-22-10
610	<i>CSNK1D</i>	Chr. 17: Homo sapiens casein kinase 1, delta (CSNK1D), transcript variant 2, mRNA.	D06_BC20_2012-04-19_1_17-22-10
611	-	No matches	D08_BC28_2012-04-19_1_17-22-10
612	-	No matches	D10_BC36_2012-04-19_1_17-22-10
613	<i>PPP1R16A</i>	Chr. 8: Homo sapiens protein phosphatase 1, regulatory subunit 16A (PPP1R16A), mRNA.	E02_BC5_2012-04-19_1_17-22-10
614	-	Human brain EST HY324267	E04_BC13_2012-04-19_1_17-22-10
615	-	Chr. M: Homo sapiens piRNA piR-34804, complete sequence.	E06_BC21_2012-04-19_1_17-22-10
616	-	No matches	E08_BC29_2012-04-19_1_17-22-10
617	-	No matches	E10_BC37_2012-04-19_1_17-22-10
618	<i>NDUFS2</i>	Chr. 1: Homo sapiens NADH dehydrogenase (ubiquinone) Fe-S protein 2, 49kDa (NADH-coenzyme Q reductase) (NDUFS2), nuclear gene encoding mitochondrial protein, transcript variant 2, mRNA.	F02_BC6_2012-04-19_1_17-22-10
619	-	Human brain EST HY324267	F04_BC14_2012-04-19_1_17-22-10
620	<i>TBC1D2B</i>	Chr. 15: 3' UTR of Homo sapiens TBC1 domain family, member 2B (TBC1D2B), transcript variant 1, mRNA.	F06_BC22_2012-04-19_1_17-22-10
621	<i>RPS27A</i>	Chr. 2: Homo sapiens ribosomal protein S27a (RPS27A), transcript variant 2, mRNA.	F08_BC30_2012-04-19_1_17-22-10
622	-	No matches	F10_BC38_2012-04-19_1_17-22-10
623	-	Human brain EST HY324267	G02_BC7_2012-04-19_1_17-22-10
624	-	No matches	G04_BC15_2012-04-19_1_17-22-10
625	-	Human brain EST HY324267	G06_BC23_2012-04-19_1_17-22-10
626	<i>UBA52</i>	Chr. 19: Homo sapiens ubiquitin A-52 residue ribosomal protein fusion product 1 (UBA52), transcript variant 1, mRNA.	G08_BC31_2012-04-19_1_17-22-10
627	-	No matches	G10_BC39_2012-04-19_1_17-22-10
628	<i>TBC1D2B</i>	Chr. 15: 3' UTR of Homo sapiens TBC1 domain family, member 2B (TBC1D2B), transcript variant 1, mRNA.	H02_BC8_2012-04-19_1_17-22-10
629	-	No matches	H04_BC16_2012-04-19_1_17-22-10

Clone #	Gene symbol	BLAT (UCSC) highest score result	Sequencing file(s)
630	-	Human brain EST HY324267	H06_BC24_2012-04-19_1_17-22-10
631	-	mRNA L09269: Human dinucleotide repeat polymorphism at the D11S982E locus mRNA.	H08_BC32_2012-04-19_1_17-22-10

## **11.2 SUMMARY OF INITIAL ATTEMPTS TO CLONE TOPORS**

The initial objective was to clone full-length *TOPORS* and its shorter fragments, using the In-fusion method marketed by Clontech (CA, USA), which was therefore most suitable for the Matchmaker™ Gold Yeast Two-Hybrid (Y2H) System (Clontech, CA, USA) used throughout this project. This cloning procedure worked efficiently only for the shorter fragments (*TOPORS* deletion constructs), whereas other methods, such as ‘traditional’ cloning and the Gateway system (Life Technologies, CA, USA), had to be employed for the purpose of cloning the full-length gene.

### **11.2.1 IN-FUSION CLONING**

*TOPORS* and its fragments were amplified from a cDNA clone, using the In-fusion primers, which have 15 nt homology to pGBKT7 (Table 2-34). A range of primer annealing temperatures was used in order to optimise the reaction, i.e. 75 °C – 85 °C for the full-length gene, and 65 °C – 75 °C for the three shorter fragments (Figure 3-4). Amplifications of all fragments were successful. Full-length *TOPORS* amplification products are shown in Figure 11-1, whereas Figure 11-2, Figure 11-3 and Figure 11-4 illustrate the results of amplification of DNA fragments, encoding the short ‘baits’, i.e. the N-terminus *TOPORS* (N), the middle *TOPORS* (M) and the C-terminus *TOPORS* (C), respectively. Amplification of full-length *TOPORS* was successful only once, and was not possible to repeat.

The PCR amplicons were purified and then used for the In-Fusion reaction, the aim of which was to clone the full-length *TOPORS* gene, as well as its three fragments (highlighted in Figure 3-4) into the Clontech pGBKT7 vector, in-frame with the GAL4 DNA BD. DH5α *Escherichia coli* cells (Life Technologies, CA, USA) were transformed with the In-fusion reaction products, the aim of which was to clone the full-length *TOPORS* gene, as well as its three fragments. The bacterial transformations resulted in growth of 2 to 33 colonies per plate (data not shown). In addition, there were approximately thirty colonies growing on each of the transformed positive control plates, and no growth was observed on the negative control plates (data not shown; please refer to sections IX and X of the In-Fusion® Advantage PCR Cloning Kit User Manual, Clontech, CA, USA).

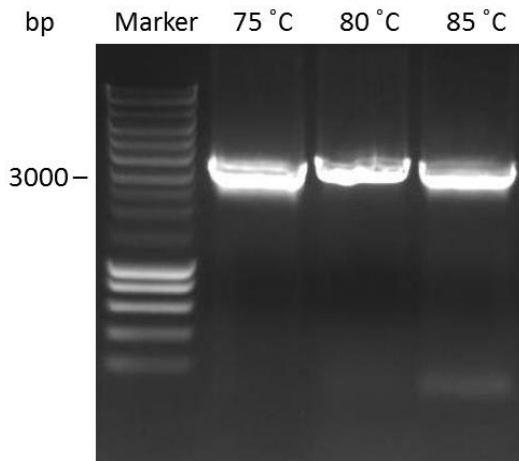


Figure 11-1. PCR amplification of full-length TOPORS, using KOD polymerase. Lane 1: Smart Ladder marker. Lanes 2-4: PCR products achieved at the different primer annealing temperatures (75 °C, 80 °C and 85 °C, respectively). 15 µl of the PCR product were loaded per well. The expected band size was approximately 3.1 kb. One per cent agarose gel with ethidium bromide.

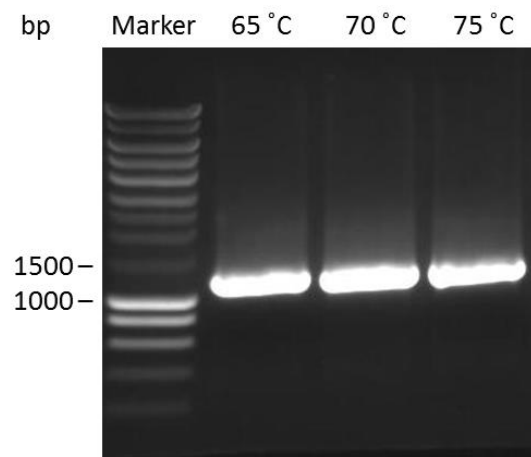


Figure 11-2. PCR amplification of the N-terminal TOPORS fragment, using KOD polymerase. Lane 1: Smart Ladder marker. Lanes 2-4: PCR products achieved at the different primer annealing temperatures (65 °C, 70 °C and 75 °C, respectively). 15 µl of the PCR product were loaded per well. The expected band size was approximately 1.1 kb. One per cent agarose gel with ethidium bromide.

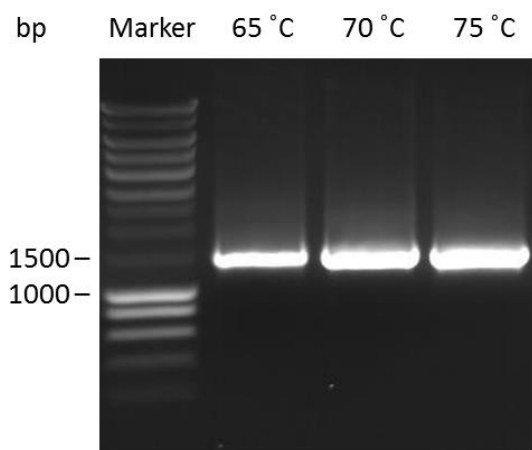


Figure 11-3. PCR amplification of the Mid-TOPORS fragment, using KOD polymerase. Lane 1: Smart Ladder marker. Lanes 2-4: PCR products achieved at the different primer annealing temperatures (65 °C, 70 °C and 75 °C, respectively). 15 µl of the PCR product were loaded per well. The expected band size was approximately 1.2 kb. One per cent agarose gel with ethidium bromide.

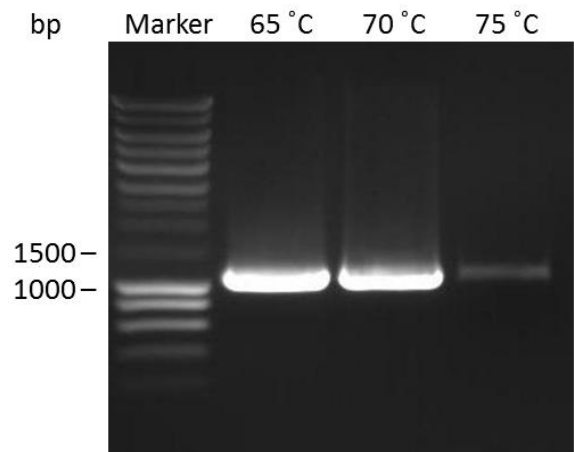


Figure 11-4. PCR amplification of the C-terminal TOPORS fragment, using KOD polymerase. Lane 1: Smart Ladder marker. Lanes 2-4: PCR products achieved at the different primer annealing temperatures (65 °C, 70 °C and 75 °C, respectively). 15 µl of the PCR product were loaded per well. The expected band size was approximately 1.0 kb. One per cent agarose gel with ethidium bromide.

According to the manual the presence of a low number of colonies on both control plates indicates that either too much of the In-fusion reaction products were used per transformation, or the quality of the DNA was poor; there should have been several hundred of colonies observed on the positive control plate, and a few colonies were to be expected on

the negative control plate. Despite the fact that the observed results for the control transformations did not correlate with the expected results for the control transformation, the transformation of the In-fusion reaction products was successful for the three *TOPORS* fragments. The results were verified by sequencing.

Eight experiments were performed in an attempt to clone the full-length *TOPORS* gene, using the In-fusion method, all unsuccessful. Hence, the next attempts to clone *TOPORS*, focused on more traditional methods, i.e. the use of restriction enzymes (Promega, WI, USA) and T4 DNA ligase (Promega, WI, USA).

### **11.2.2 ECORI & SALI RESTRICTION DIGEST AND LIGATION**

Cloning *TOPORS* using the In-fusion method was not successful; however, the amplicons, generated for the purpose of In-fusion cloning (Figure 11-1), contained specific restriction sites, which were utilised in the subsequent cloning experiments. Details of the primers containing the relevant restriction sequences are summarised in Table 2-34.

The sequence of the TOP-in-fusion-1-pGBKT7-F primer contains an *EcoRI* restriction site, whereas the TOP-in-fusion-6-pGBKT7-R primer comprises the *SalI* restriction site; hence, both restriction sites become incorporated into the resulting PCR amplicon. Both of these sites are also found on the pGBKT7 vector, as the primers for the In-fusion reaction are based on homology to the target vector, and allow the insert to be cloned in-frame.

In order to prevent digestion of *TOPORS* itself, restriction sites found within the pGBKT7 plasmid sequence were consecutively checked for their presence within the gene, using the SeqBuilder software (DNASTAR Lasergene 8). Restriction sites found within the plasmid, but not within the gene are listed in Table 11-2.

Table 11-2. Restriction enzymes which have been shown not to cut TOPORS (DNASTAR SeqBuilder, Lasergene 8).

The reference TOPORS sequence submitted to the software analysis was obtained from the Ensembl database.

Restriction enzyme	Restriction site sequence	Conditions (Promega, WI, USA)
<b><i>NdeI</i></b>	CA'TATG	Buffer D; 37 °C
<b><i>SfiI</i></b>	GGCCNNNN'NGGCC	Buffer B; 50 °C
<b><i>EcoRI</i></b>	G'AATTC	Buffer H; 37 °C
<b><i>SmaI</i></b>	CCC'GGG	Buffer J; 25 °C
<b><i>XmaI</i></b>	GCC'GGG	Buffer B; 37 °C
<b><i>SalI</i></b>	G'TCGAC	Buffer D; 37 °C
<b><i>PstI</i></b>	CTGCA'G	Buffer H; 37 °C

The full-length *TOPORS* PCR product (Figure 11-1) and the pGBKT7 vector were both digested with the *EcoRI* and *SalI* restriction enzymes (Promega, WI, USA). The digestion was performed sequentially in order to avoid the potential 'star activity' caused by certain reaction buffers. It was confirmed by agarose gel electrophoresis that the digestion reaction worked successfully (Figure 11-5 and Figure 11-6); the DNA bands representing the linearised molecules were expected to appear larger than the band corresponding to the circular plasmid, which can super-coil, and, thus, travel through the agarose gel faster.

The digestion reaction products were purified, and the inserts and vectors were ligated together at a 3:1 insert: vector ratio, using the T4 DNA ligase (Promega, WI, USA). In order to confirm that the ligation reaction had worked, PCR was performed, using a vector-specific primer, such as T7 (Table 2-50), and a *TOPORS*-specific primer, such as S8 (Table 2-51) to amplify across the 5' ligation site as shown in Figure 11-7.



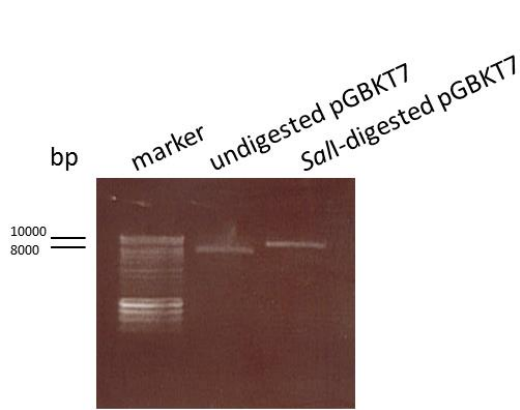


Figure 11-5. Gel electrophoresis of undigested and digested pGBKT7 vectors. Lane 1: Hyper Ladder I; Lane 2: undigested vector; Lane 3: Sall-digested vector. 1  $\mu$ l of the respective digestion products was loaded into each well.

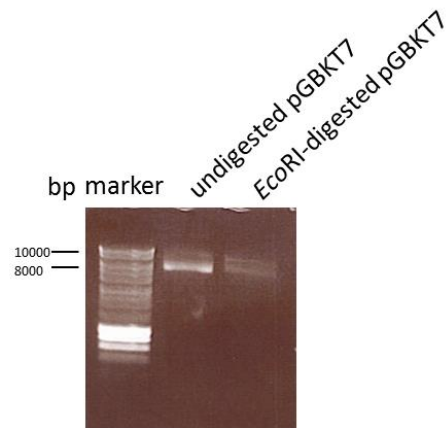


Figure 11-6. Gel electrophoresis of undigested and digested pGBKT7 vector. Lane 1: Hyper Ladder I; Lane 2: undigested vector; Lane 3: EcoRI-digested vector. 1  $\mu$ l of the respective digestion products was loaded into each well.

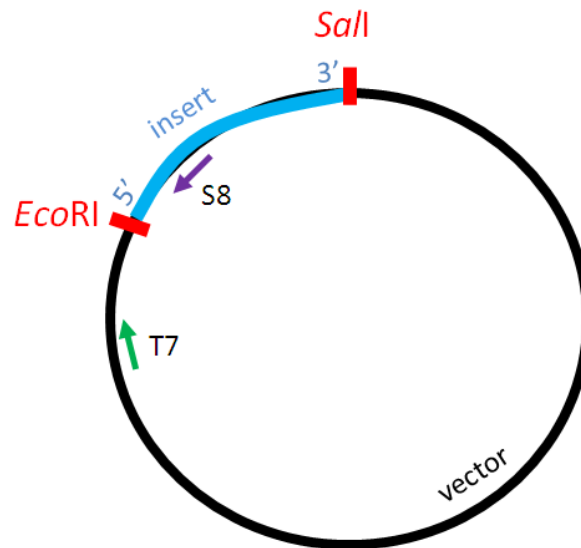


Figure 11-7. Schematic representation of the region of the vector-insert construct, which would be amplified using the T7 and S8 primers.

Results of one of two separate ligation reactions verified in this way are shown in Figure 11-8. Although this confirms the ligation reaction has worked, the sensitive nature of PCR means that a single molecule can be amplified exponentially, therefore results have to be interpreted carefully.

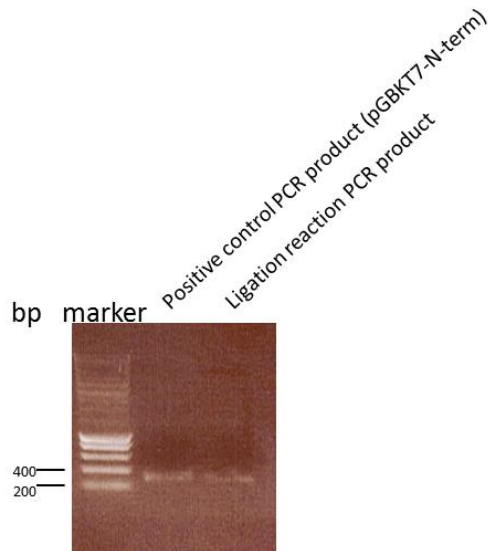


Figure 11-8. PCR amplification using the ligation reaction as template (vector and insert digestion with *EcoRI* and *SalI*), using vector-specific primer T7 (Table 2-50), and *TOPORS*-specific primer S8 (Table 2-51).

Lane 1: Smart Ladder marker. Lane 2: PCR product amplified from N-term *TOPORS* fragment (positive control). Lane 3: PCR product amplified from the ligation reaction products. 5  $\mu$ l of the PCR product were loaded per well.

The ligation reaction product was used to transform DH5 $\alpha$  *E. coli* cells (Life Technologies, CA, USA). In order to optimise the transformation procedure different amounts of the ligation reaction product were used; i.e. 10 ng, 20 ng and 50 ng. Half of the plates were incubated at 37  $^{\circ}$ C overnight, and the other half were incubated at 30  $^{\circ}$ C for approximately 48 hours; the purpose of the extended incubation time at the lower temperature was to enhance the growth of colonies, expressing *TOPORS*, in case they were growing slower than those, which did not express the insert. Abundant growth was observed on all transformation plates (hundreds of colonies). A total of 60 colonies were screened by colony PCR, using either the pair of T7 and S8 primers, or the S9 and R primers (for primer sequences please refer to Table 2-50 and Table 2-51), amplifying across the 5' and adjacent to the 3' ligation sites, respectively.

Primers T7 and S8 serve to amplify a fragment of the pGBKT7 vector, which commences with the T7 Promoter, and includes the first 198 nucleotides of the inserted DNA fragment. This part of the insert is located near the 5' end of the gene, which corresponds to the amino terminus of the protein; hence, the pGBKT7 vector, carrying an insert, which encodes a confirmed N-terminus *TOPORS* fragment, was used as a control in the PCR screening procedure.

Primers S9 and R serve to amplify a DNA fragment, consisting of the last 354 nucleotides of the *TOPORS* gene. This part of the gene sequence is located near its 3' end, which corresponds to the carboxyl terminus of the protein; hence, the pGBKT7 vector, carrying an insert, which encodes a confirmed C-terminus *TOPORS* fragment, was used as a control in this PCR screening

procedure. Several colonies tested positive; results from one of the experiments are shown in Figure 11-9.

Glycerol stocks were made of each of the selected clones, and their plasmids were isolated and sequenced. The result of the sequencing reaction was unexpected. As shown in Figure 11-10, some of the vectors contained inserted fragments, which comprised two approximately 20 nucleotides long sequences, identical to the sequences found at the beginning and at the end of full-length *TOPORS*; however, the majority of the gene sequence from in between these two very short sequences was missing. This result suggests that the restriction enzymes had probably cut *TOPORS* at unspecific sequences, which were perhaps similar to their canonical restriction sites.

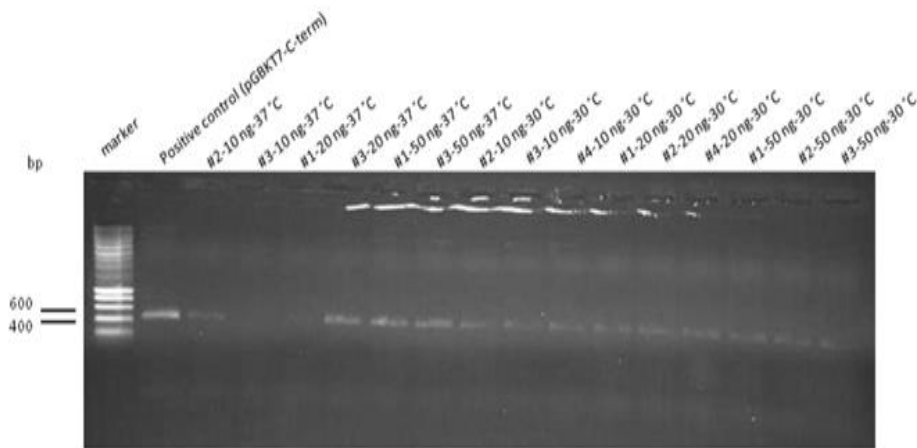


Figure 11-9. Colony PCR screening of DH5 $\alpha$  bacterial cells transformed with the ligation reaction (following vector and insert digestion with *EcoRI* and *Sall*). *TOPORS* sequencing primers S9 and R (Table 2-51). Lane 1: Smart Ladder marker. Lane 2: PCR product amplified from C-term *TOPORS* fragment (positive control). Lanes 3-15: PCR products (1.5  $\mu$ l in each) amplified from bacterial clones from the transformation. Key: example: #2-10 ng-37  $^{\circ}$ C  $\rightarrow$  clone #2 from DH5 $\alpha$  bacterial transformation.

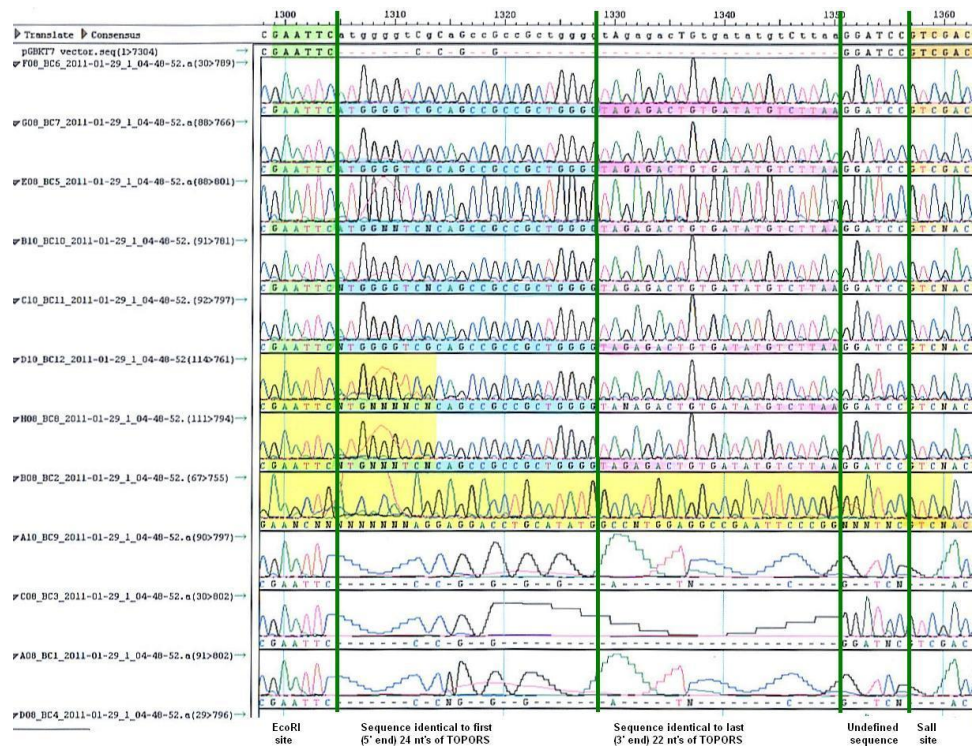


Figure 11-10. Result obtained from sequencing of plasmids, isolated from colonies, which appeared to contain the *TOPORS* insert, based on the colony PCR results (Figure 11-9).

The first 6-nucleotides long sequence represents the *EcoRI* restriction site (highlighted in green). The section, between the first two green bars, corresponds to a 23-nucleotides long fragment, identical to the sequence found at the beginning of the full-length *TOPORS*; whereas the section, between the second and third green bar, corresponds to 21-nucleotides long fragment, identical to the sequence found at the end of the full-length *TOPORS*; the sequence shown between bars three and four is unknown, whereas the last six nucleotides correspond to the *Sall* restriction site (highlighted in orange).

The sequencing results (Figure 11-10) were not consistent with the ligation reaction (Figure 11-8) and colony PCR (Figure 11-9) results; therefore, another experiment was performed in order to verify whether the pGBKT7 DNA fragments may have been amplified in these screening experiments (Figure 11-11). For all of the tested samples it was expected that no amplicons would be generated.

The S8 primer (Table 2-51) used in the first primer pair (T7 & S8) is a *TOPORS* gene-specific primer, therefore it was not expected that this primer would anneal to and lead to amplification of a fragment of the pGBKT7 vector. Although the sizes of the obtained products were not identical with the size of the positive control fragment, the PCR amplicon of pGBKT7-N-*TOPORS* plasmid, a part of the vector was still amplified.

The S9 and R primers (Table 2-51) used as the second primer pair, are also *TOPORS*-specific primers, thus no amplification of any fragment of the pGBKT7 plasmid was expected.

The obtained products were of the exact same size as the positive control fragment, the PCR amplicon of pGBKT7-C-TOPORS plasmid.

This experiment demonstrated that the S8, S9 and R primers anneal to and amplify fragments of the pGBKT7 vector DNA (Figure 11-11), despite being designed specifically for the *TOPORS* sequence. Hence, these primers cannot be used in screening experiments for *TOPORS*, when using this particular vector.

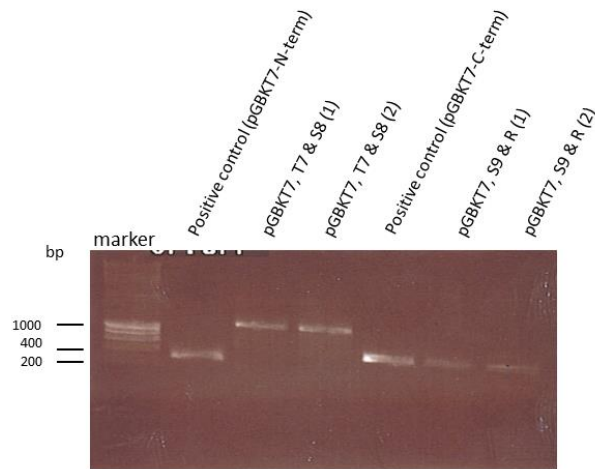


Figure 11-11. Control experiment to clarify the inconsistency of results (obtained amplicon sizes) between the ligation reaction PCR (Figure 11-8) and the colony PCR (Figure 11-9).

Lane 1: Hyper Ladder I marker. Lane 2: PCR product amplified from an N-term *TOPORS* fragment; a positive control for products amplified using the vector-specific primer T7 (Table 2-50) and the *TOPORS*-specific primer S8 (Table 2-51). Lanes 3-4: PCR products amplified from the empty vector using the T7 and S8 primers. Lane 5: PCR product amplified from a C-term *TOPORS* fragment; a positive control for products amplified using the *TOPORS*-specific primers S9 and R (Table 2-51). Lanes 6-7: PCR products amplified from the empty vector using the S9 and R primers. 5 µl of the PCR product were loaded per well.

### 11.2.3 *NDEI* & *PSTI* RESTRICTION DIGEST AND LIGATION

It was deduced from the sequencing results shown in Figure 11-10 that despite inactivation of the *EcoRI* and *Sall* enzymes *TOPORS* had probably been digested by the *EcoRI* and/or *Sall* enzymes at sites similar to the actual respective recognition sites. As a consequence a different set of restriction endonucleases was chosen from Table 11-2 for further cloning experiments.

The *NdeI* and *PstI* restriction enzymes were selected from Table 11-2, as an alternative to the previously used *EcoRI* and *Sall*. New primers for *TOPORS* amplification were designed, which would include these two alternative restriction sites and maintained the correct reading frame (FL F and FL R; Table 2-36).

The annealing temperatures for the FL F and the FL R primers were calculated, yielding 70.5 °C and 50.1 °C, respectively. In order to optimise the PCR conditions the primers were tested for *TOPORS* amplification at three different annealing temperatures within the range of 50.0-70.0 °C; a pCATCH-*TOPORS* (22.5 ng/µl) vector (containing a full-length verified *TOPORS*

sequence), and a full-length *TOPORS* PCR product from a previous amplification were used as templates. The KOD polymerase was used; conditions were kept, as previously described (section 2.2.1 and Table 2-30).

Amplification from the pCATCH-*TOPORS* at an annealing temperature of 57 °C resulted in the best outcome (Figure 11-12).

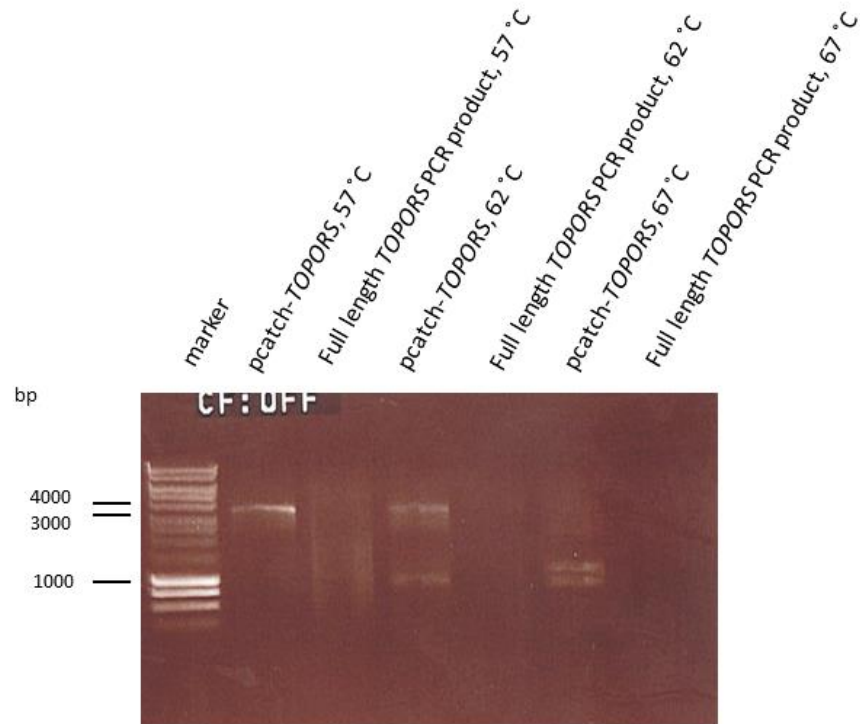


Figure 11-12. PCR amplification of TOPORS using the FL F and FL R primers (Table 2-36). Lane 1: Hyper Ladder I marker. Lane 2: pCATCH-TOPORS as template; 57 °C. Lane 3: PCR product; 57 °C. Lane 4: pCATCH-TOPORS; 62 °C. Lane 5: PCR product; 62 °C. Lane 6: pCATCH-TOPORS; 67 °C. Lane 7: PCR product; 67 °C. 1.5 µl of products were loaded into each well. The expected band size was approximately 3.1 kb.

The reaction was successfully repeated (Figure 11-13) and a substantial amount of *TOPORS* was amplified, which could be used for subsequent sub-cloning. In order to confirm that the obtained PCR product was indeed *TOPORS*, the beginning and the end of the gene were sequenced using primers FL F and FL R. The results were verified by sequencing.

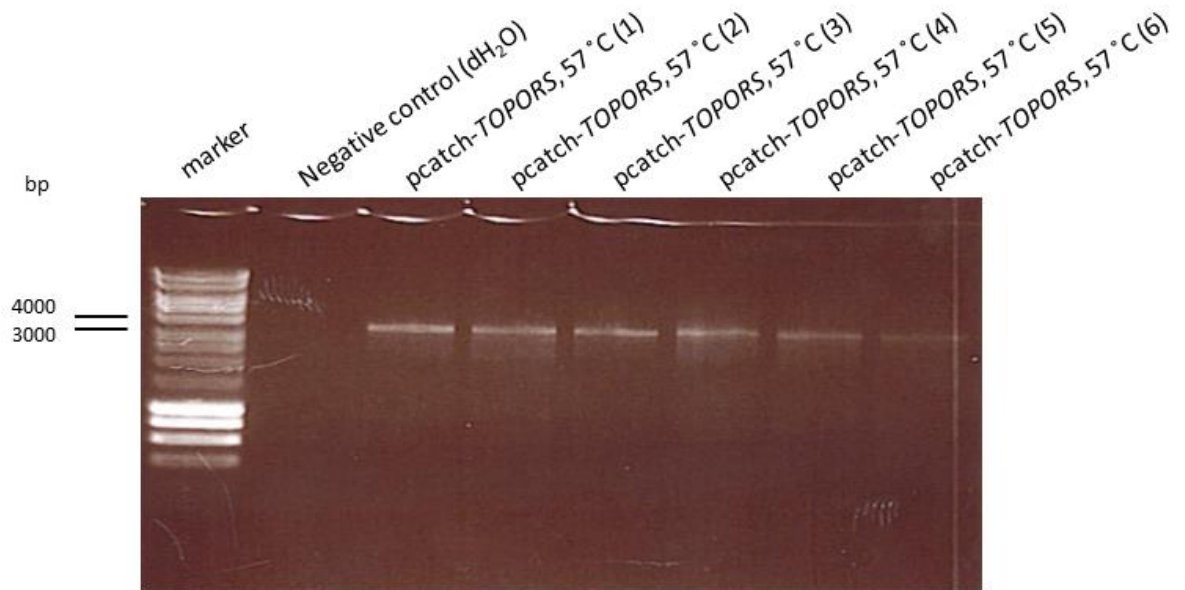


Figure 11-13. PCR amplification of TOPORS using the FL F and FL R primers. Lane 1: Marker: Hyper Ladder I. Lane 2: Negative control; Lanes 3-8: PCR products of TOPORS amplification from pCATCH-TOPORS (57 °C). 1 µl of each product was loaded per well. Expected band size: ~3.1 kb.

PCR amplification of TOPORS with the FL F and FL R primers resulted in generation of DNA fragments with restriction enzyme sites at both ends of the DNA molecule. The sequence of the FL F primer encodes the *NdeI* restriction site, whereas the FL R primer comprises the *PstI* restriction site. Both of these sites are also found in the pGBKT7 MCS, and both restriction enzymes have previously been shown, using a bioinformatics analysis, not to cut *TOPORS* (Table 11-2).

The full-length *TOPORS* amplicon and the pGBKT7 vector were both digested with the *NdeI* and *PstI* restriction enzymes (Promega, WI, USA). The digestion was performed sequentially in order to avoid the potential 'star activity' caused by certain reaction buffers. It was confirmed after every digestion reaction that it had worked by visualising the digested and undigested vectors on an agarose gel following electrophoresis (Figure 11-14); the DNA bands representing the linearised molecules were expected to appear larger than the band corresponding to the circular plasmid, which can super-coil, and, thus, travel through the agarose gel faster.

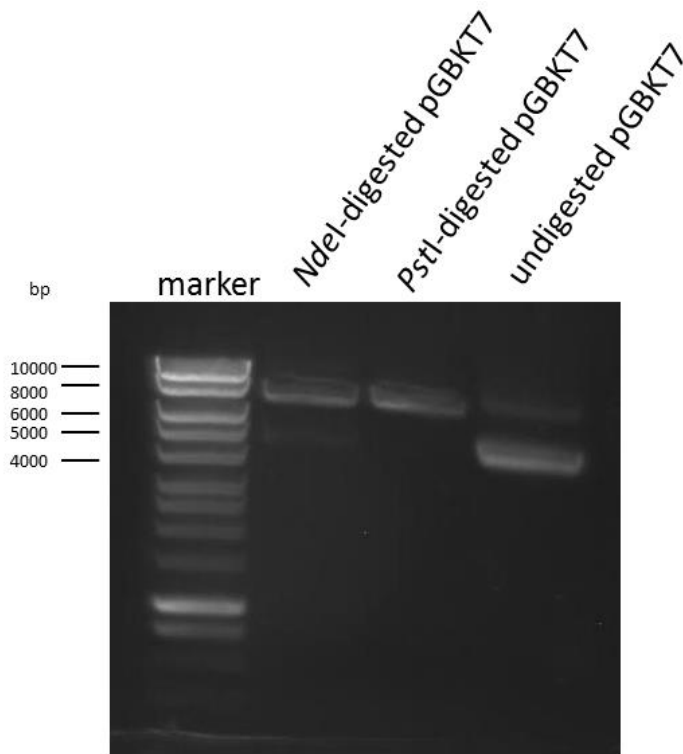


Figure 11-14. Gel electrophoresis of digested and undigested pGBKT7 vector.

Lane 1: Hyper Ladder I; Lane2: *NdeI*-digested vector; Lane 3: *PstI*-digested vector; Lane 4: undigested vector. 1  $\mu$ l of the respective digestion products was loaded into each well. The digested reaction products were purified, and the inserts and vectors were ligated together at a 3:1 insert: vector ratio, using the T4 DNA ligase (Promega, WI, USA). In order to confirm that the ligation reaction had worked, a fragment of the purified product was amplified by PCR, using a vector-specific primer, such as the pGBKT7 R1 primer (Table 2-50) and a *TOPORS*-specific primer, such as S9 (Table 2-51), amplifying across the 3' ligation site (Figure 11-15). Fragments of the expected size (0.7 kb) were amplified (Figure 11-16).

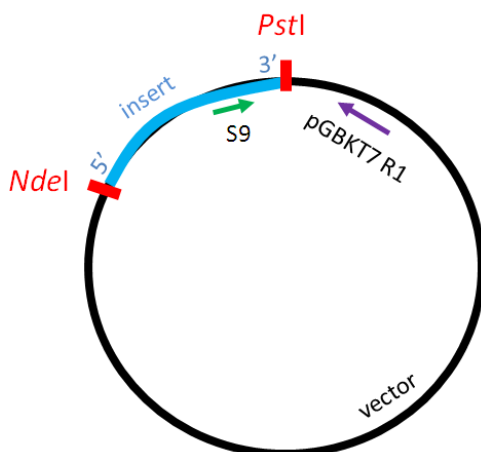


Figure 11-15. Schematic representation of the region of the vector-insert construct, which would be amplified using the S9 and pGBKT7 R1 primers.



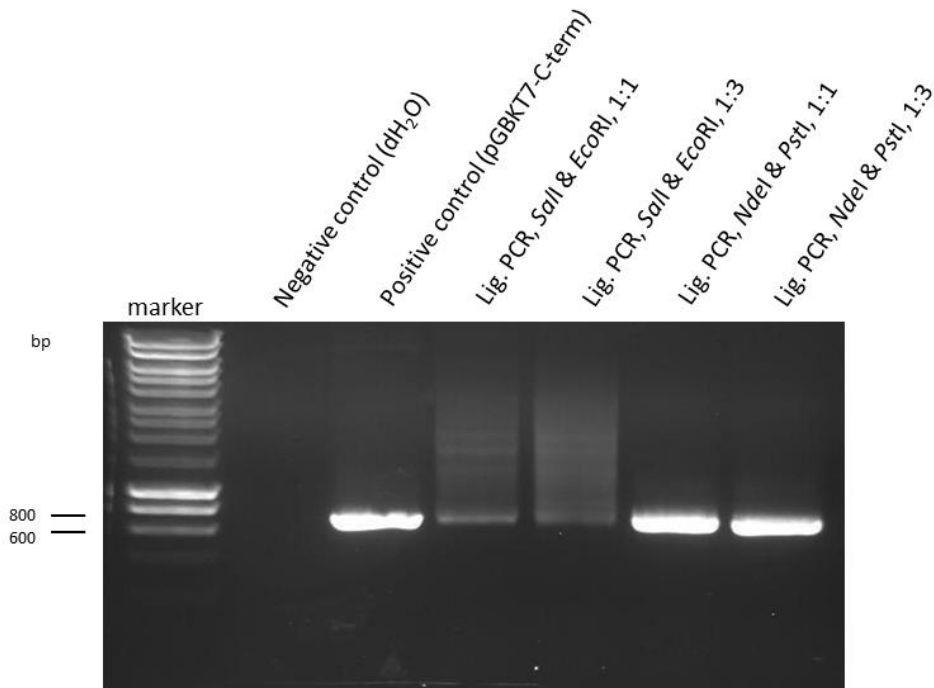


Figure 11-16. PCR amplification using the ligation reaction as template, (vector and insert digestion with EcoRI and Sall as well as NdeI and PstI).

Lane 1: Hyper Ladder I marker. Lane 2: negative control, i.e. dH<sub>2</sub>O was used instead of DNA. Lane 3: PCR product amplified from a C-term TOPORS fragment (positive control). Lane 4-5: PCR products amplified from the ligation reaction products following digestion with EcoRI and Sall. Lanes 6-7: PCR products amplified from the ligation reaction products following digestion with NdeI and PstI. 5 µl of the PCR product were loaded per well.

The ligation reaction was used for transformation of the competent DH5α *E. coli* cells (Life Technologies, CA, USA), the super-competent XL-1 Blue *E. coli* cells (Stratagene, CA, USA) and the Y2H Gold yeast cells (Clontech, CA, USA). All types of cells were transformed, or, where appropriate, made competent, according to the respective manufacturer's instructions.

Initially, DH5α cells were used for all transformations; however, as was shown by scarce growth of cells transformed with plasmids, carrying short TOPORS fragments, these DNA molecules appeared to have a toxic effect on their host bacterial cells, as indicated by low number of colonies growing after the transformations. The DH5α cells did not appear to take up the pGBKT7-TOPORS plasmid; therefore, the super-competent XL-1 Blue cells (less sensitive to potential toxic effects of plasmids, which they take up) were used subsequently. The use of super-competent bacterial cells did not lead to better outcomes either. Since the pGBKT7-TOPORS construct appeared to exert significantly toxic effects on both of the previously used bacterial cell types, transformation of competent yeast cells with the ligation reaction directly was considered as an alternative viable option.

Ten nanograms of DNA were used per each transformation of the DH5 $\alpha$  cells (Life Technologies, CA, USA), and all plates were incubated overnight at 37 °C; abundant growth (hundreds of colonies) was observed. One hundred and eight colonies were screened by colony PCR, using *TOPORS*-specific primers. All results were negative (data not shown).

The XL-1 Blue cells (Stratagene, CA, USA) were transformed with several different amounts of DNA in order to determine what amount was optimal (based on the manufacturer's information the cells can be transformed with any amount of DNA within the range of 0.1-50.0 ng). All plates were incubated overnight at 37 °C; abundant growth was observed. One hundred and eighty eight clones were screened by colony PCR. Half of the colonies was screened using a vector-specific primer, such as the pGBKT7 R1 (Table 2-50), and a *TOPORS*-specific primer, such as S9 (Table 2-51). The other half was screened using two vector specific primers, i.e. the pGBKT7 F and the pGBKT7 R1 primers (Table 2-50). All results were negative (data not shown).

The transformation of the yeast cells (Clontech, CA, USA) was performed using 100 ng of DNA, and plates were incubated at 30 °C until colonies appeared, i.e. for approximately 72 hours. Nine clones were screened by yeast colony PCR, using the pGBKT7 R1 primer (Table 2-50), and the S9 primer (Table 2-51); one colony tested positive (Figure 11-17).

The positive clone was purified and sequenced. The results were negative, no primers appeared to have annealed (data not shown). The plasmids were isolated from the colony-PCR-positive clone, and another attempt was made to sequence this time the isolated DNA; the result was negative again (data not shown).

The isolated DNA was then amplified by PCR in order to verify that the vector with the insert had indeed been isolated; the same primers were used as for the yeast colony PCR, which resulted in the original positive band as seen in Figure 11-17. The PCR results indicated that the pGBKT7-*TOPORS* plasmid was present (Figure 11-18).

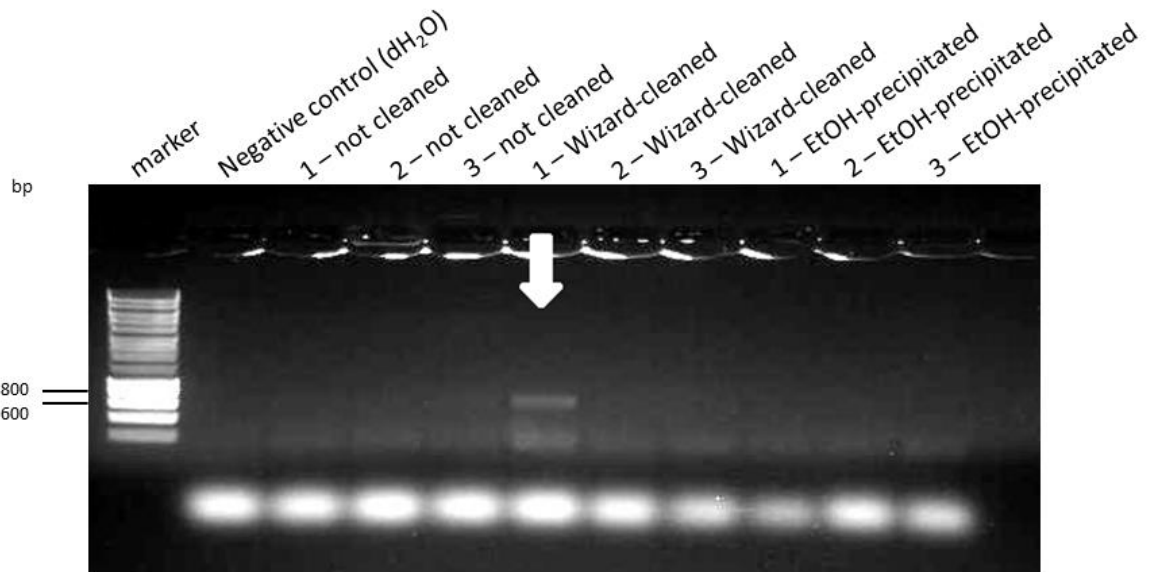


Figure 11-17. Yeast colony PCR screening for *TOPORS* (the ligation reaction products were used for a pilot transformation of the yeast, following unsuccessful attempts to transform bacteria). Lane 1: Hyper Ladder I marker. Lane 2: negative control, i.e. dH<sub>2</sub>O was used instead of DNA. Lanes 3-11: PCR products amplified from the selected yeast colonies. 5  $\mu$ l were loaded per well. The expected fragment size was 657 bp (indicated by white arrow). Key: not cleaned: the PCR product was used directly in the ligation reaction without prior treatment; Wizard-cleaned: the PCR product was purified using the Wizard<sup>®</sup> SV Gel and PCR Clean-Up System (Promega, WI, USA); ethanol-precipitated: the PCR product was precipitated using ethanol to concentrate it prior to ligation.

The presumed pGBKT7-*TOPORS* plasmid was then used for transformation of the XL-1 Blue supercompetent cells (Stratagene, CA, USA). Thirty two colonies were picked and screened by yeast colony PCR, using the pGBKT7 F and the pGBKT7 R1 primers (Table 2-50). The obtained bands' sizes indicated that, although the vector was present, it contained no insert (Figure 11-19). The conclusion was that the original yeast clone must have taken up several plasmids (it was shown by Gietz and Schiestl (1991) competent yeast cells are able to take up more than one DNA vector during a transformation reaction), some without the insert, and the one with the insert was consequently lost over generations.

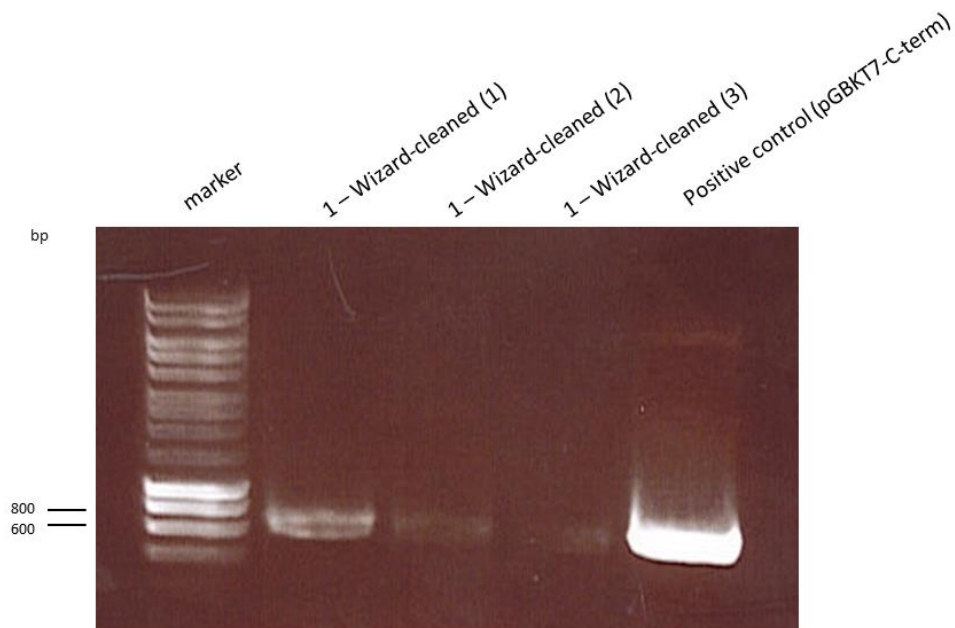


Figure 11-18. PCR amplification of plasmids isolated from the yeast colony PCR positive clone (see Figure 11-17).

Lane 1: Marker: Hyper Ladder I. Lanes 2-4: PCR products amplified from three different samples of the isolated plasmids. Lane 5: Positive control: PCR product amplified from a pGBKT7-C-TOPORS plasmid. 5  $\mu$ l were loaded per well. Expected fragment size: ~0.7 kb. Key: Wizard-cleaned: the PCR product was purified using the Wizard<sup>®</sup> SV Gel and PCR Clean-Up System (Promega, WI, USA).

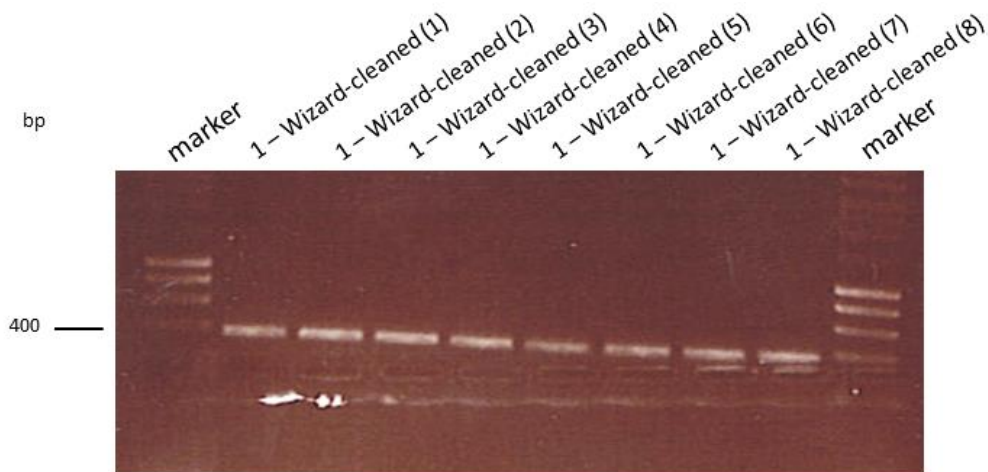


Figure 11-19. Colony PCR screening for *TOPORS* in the plasmids isolated from bacteria, previously transformed with plasmid isolated from positive yeast clone (see Figure 11-17).

Lane 1 and 10: Hyper Ladder I marker. Lanes 2-9: PCR products amplified from the screened bacterial colonies. 10  $\mu$ l were loaded per well. The expected fragment size was over 3 kb. Wizard-cleaned: the PCR product was purified using the Wizard<sup>®</sup> SV Gel and PCR Clean-Up System (Promega, WI, USA).

### 11.2.4 GATEWAY CLONING

Attempts to clone *TOPORS* using traditional methods or the In-fusion system (Clontech, CA, USA) failed. A Gateway system developed by Life Technologies (CA, USA) was used as an alternative; the technique is based on the endogenous recombination system used by bacteriophage  $\lambda$  in order to incorporate itself into the *E. coli* genome (described in section 2.2.5.3).

Primers for *TOPORS* amplification for Gateway cloning were designed to incorporate the *attB1* and *attB2* sites (section 2.2.5.3; Table 2-40). The pCATCH-*TOPORS* construct (containing previously cloned full-length *TOPORS* cDNA sequence) was used as template for the PCR amplification by KOD polymerase (section 2.2.1; Table 2-30), and the optimum annealing temperature for this primer pair was determined to be 60 °C. The gene was successfully amplified (Figure 11-20), using KOD polymerase, yielding a band of the expected size of 3.1 kb.

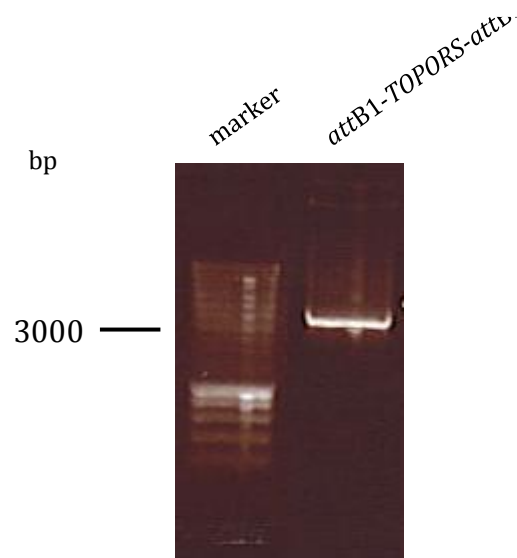


Figure 11-20. Full-length *TOPORS* PCR product amplified using Gateway-specific primers. Lane 1: Smart Ladder marker was used. Lane 2: PCR products of the expected fragments size at approximately 3.2 kb.

The amplified PCR product was cloned into the pDONR/Zeo vector (Table 2-33) during the Gateway BP reaction (section 2.2.5.3). The resulting entry vectors were then transformed into DH5 $\alpha$  bacterial cells, spread on selective media, and incubated overnight at 37 °C.

The nature of the pDONR/Zeo vectors is that they do not allow growth of their host cell unless an insert has become incorporated during the BP reaction, replacing the lethal *ccdB* gene;

i.e. all colonies that have grown following the transformation should contain only the recombinant entry vectors. The entry vectors (pDONR-*TOPORS*) were then purified and used in the Gateway LR reaction with the pBD destination vector (Table 2-33). The reaction products were used for transformation of bacteria (DH5 $\alpha$ ), which were subsequently grown on selective media. The plasmids were isolated from the clones, and sequenced using *TOPORS*-specific primers (Table 2-51). The sequencing reactions were not efficient (22 primers were needed to cover the ~3.1 kb of full-length *TOPORS*), most likely due to its GC-rich and

somewhat repetitive sequence; however, the obtained sequence was correct: *TOPORS* was sub-cloned successfully into the pBD destination vector (Figure 11-21).

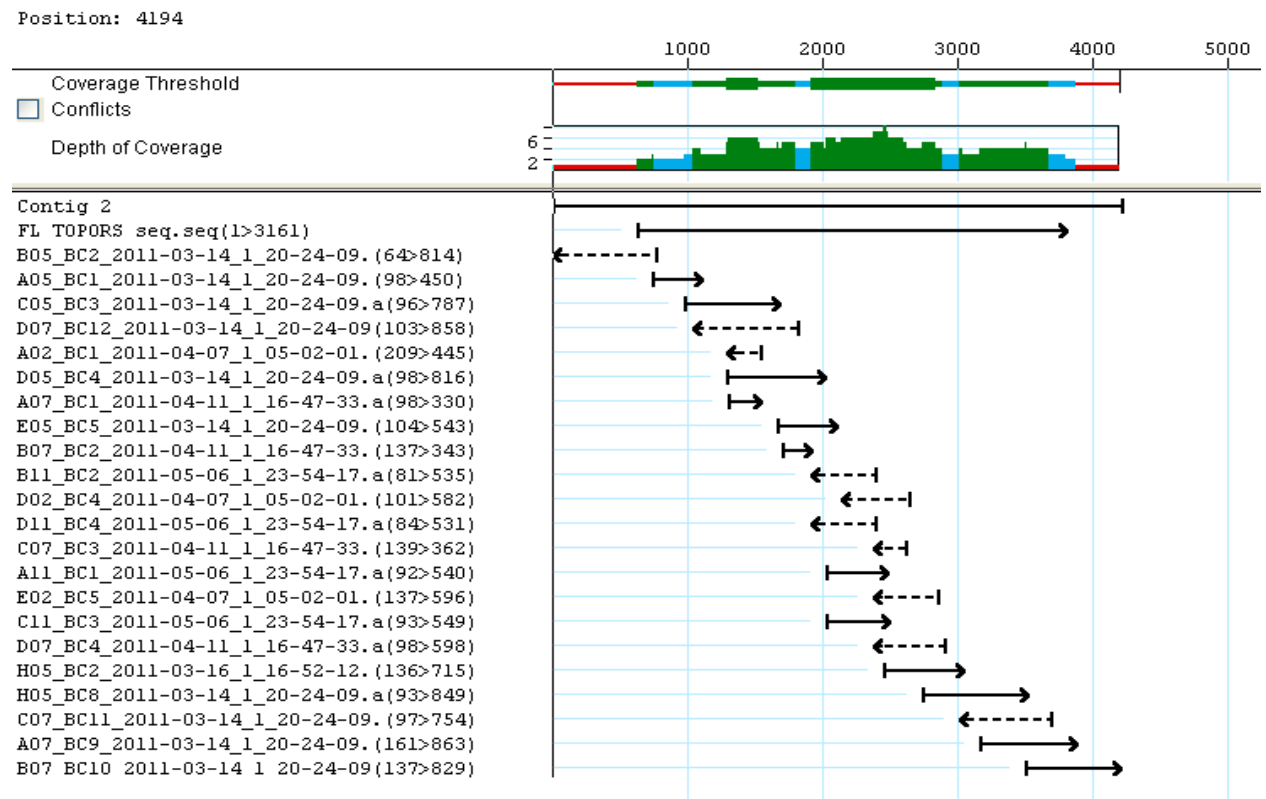


Figure 11-21. Complete full-length *TOPORS* sequence cloned into the pBD vector.

### 11.3 Y2H GOLD YEAST TRANSFORMATION RESULTS

The obtained *TOPORS* constructs (full length and fragments) were then used for transformation of yeast cells prior to the Y2H screens. Each transformation was verified by plasmid isolation from the resulting colonies, PCR amplification (Figure 11-22, Figure 11-23, Figure 11-24), and sequencing.

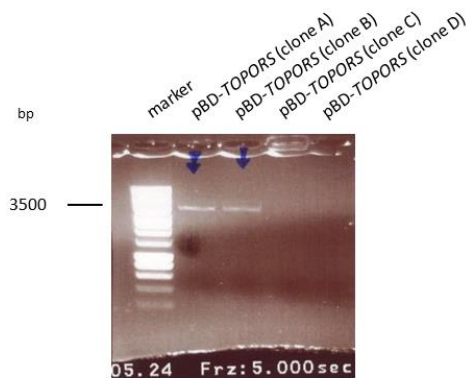


Figure 11-22. PCR amplification product of *TOPORS* from pBD-*TOPORS* vectors isolated from yeast (clones A-D). Lane 1: Hyper Ladder I was used as the band size marker. Lanes 2-5: PCR products from the four different plasmid preparations, amplified using vector-specific primers (Table 2-50; 5 µl per well).

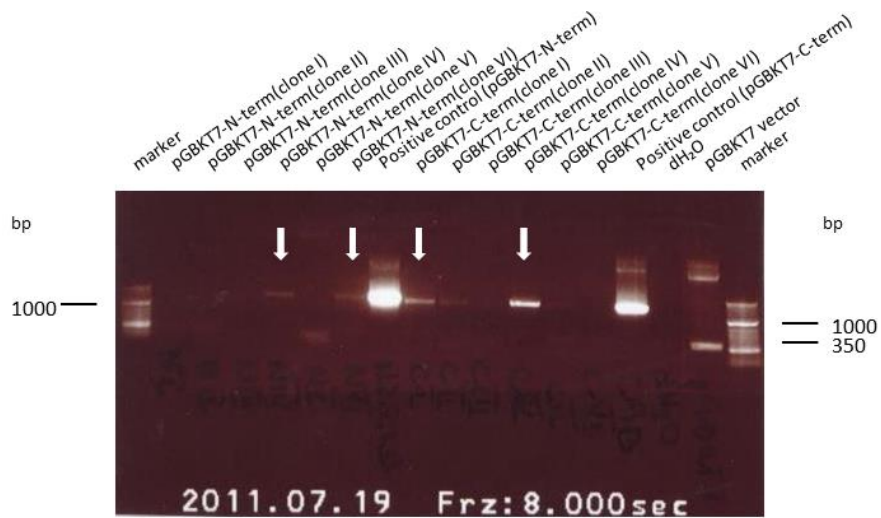


Figure 11-23. PCR amplification product of N-term and C-term TOPORS fragments from the pGBKT7-TOPORS vectors isolated from yeast. Hyper Ladder I was used as the band size marker. Samples from six N-term and six C-term clones were prepared, and the plasmid preparations were amplified using vector-specific primers. 10  $\mu$ l of each PCR product were loaded per well.

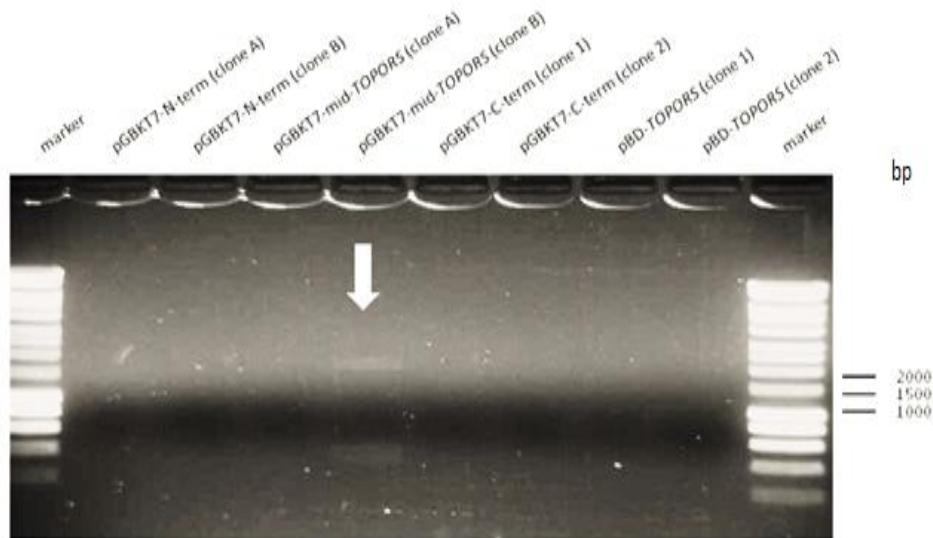


Figure 11-24. PCR amplification products of the short TOPORS fragments cloned into pGBKT7 constructs isolated from yeast. Lanes 1 and 10: Hyper Ladder I was used as the band size marker. Samples from two N-term, two C-term and two mid-TOPORS clones were prepared, and the plasmid preparations were amplified using vector-specific primers. 10  $\mu$ l of each PCR product were loaded per well.

#### **11.4 SUMMARY OF INITIAL ATTEMPTS TO CONFIRM BAIT AND DELETION CONSTRUCT PROTEIN EXPRESSION IN TRANSFORMED YEAST CELLS**

Several attempts were made to detect protein expression by Western blotting, however the results were not successful (Figure 11-25-Figure 11-27). The denatured protein extracts, obtained from yeast cells transformed with pBD-TOPORS were subject to SDS-PAGE on a 7.5 % gel; whereas protein extracts, isolated from yeast cells transformed with pBD-wt and pGBKT7 (for both plasmids' details please refer to Table 2-33 and Table 2-32, respectively) underwent electrophoresis on a 12.0 % gel. Protein extracts obtained from untransformed yeast cells were used as negative control in all experiments. Semi-dry transfer from the acrylamide gels onto a nitrocellulose membrane was subsequently performed; membranes on which GAL4 BD-TOPORS hybrid proteins were expected to have bound were incubated with antibodies against GAL4 BD (Figure 11-25) as well as against TOPORS (Figure 11-26). The membrane with proteins transferred from the 12 % gel, where only GAL4 BD peptide was expected, was incubated only with the anti GAL4 BD antibody (Figure 11-27). Protein sizes are not indicated due to the fact that marker was not visible on the membrane. When membranes, on which the proteins were blotted are aligned next to each other, the proteins visualised on the blots shown in Figure 11-25 and Figure 11-26 appear to have travelled a similar, short distance down the gel; on the contrary the proteins shown in Figure 11-27 appear to have travelled at least three times as far down the gel, indicating that they are indeed significantly smaller. These results would appear promising despite lack of the size marker, if the same blotting pattern was not observed in the negative control well. It is possible that the antibodies did not bind selectively enough; however, problems were being experienced whilst setting up the electrophoresis tanks, and some protein samples spilt over into the neighbouring wells. Nonetheless, such error would only explain the patterns observed in Figure 11-25 and Figure 11-26. In Figure 11-27 an empty well was left between wells, into which the sample and the control were loaded.





Figure 11-25. Anti GAL4 BD Ab. 7.5 % gel. Western blot results. M = marker, Precision Plus Protein Standards, Dual Color (BioRad); T/A = Full-length TOPORS protein, clone T/A, conjugated with GAL4 BD (~131 kDa); T/B = Full-length TOPORS protein, clone T/B, conjugated with GAL4 BD (~131 kDa); -ve = negative control, untransformed Y2H Gold yeast cells. Protein sizes are not indicated as marker faded away from the membrane.



Figure 11-26. Anti TOPORS Ab. 7.5 % gel. Western blot results. M = marker, Precision Plus Protein Standards, Dual Color (BioRad); T/A = Full-length TOPORS protein, clone T/A, conjugated with GAL4 BD (~131 kDa); T/B = Full-length TOPORS protein, clone T/B, conjugated with GAL4 BD (~131 kDa); -ve = negative control, untransformed Y2H Gold yeast cells. Protein sizes are not indicated as marker faded away from the membrane.

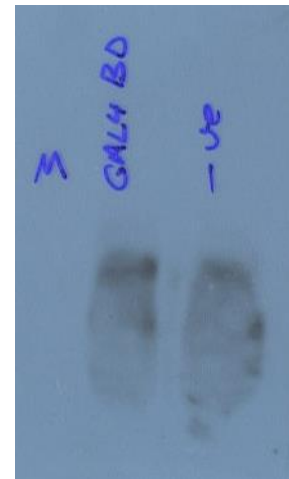


Figure 11-27. Anti GAL4 BD Ab. 12.0 % gel. Western blot results. M = marker, Precision Plus Protein Standards, Dual Color (BioRad); GAL4 BD = GAL4 BD on its own (~16 kDa); -ve = negative control, untransformed Y2H Gold yeast cells. Protein sizes are not indicated as marker faded away from the membrane.

### 11.5 *p53* CLONING USING GATEWAY SYSTEM

Primers for *p53* amplification for Gateway cloning had been designed to incorporate the *attB1* and *attB2* sites essential for this cloning method (Table 2-41).

The pGBKT7-53 vector (Clontech, CA, USA, provided as a separate positive control for this system) was used as template for the PCR amplification. The optimum annealing temperature for this primer pair was determined to be 60 °C (section 2.2.1 and Table 2-30). The gene was successfully amplified (Figure 11-28).

The amplified PCR product was cloned into the pDONR/Zeo vector (for details see Table 2-33) using the Gateway BP reaction (section 2.2.5.3).

The reaction was transformed into DH5 $\alpha$  cells, spread on selective media, and incubated overnight at 37 °C. Single colonies were picked and inoculated into liquid culture.

The entry vectors were subsequently isolated from the bacteria, confirmed via sequencing and used in the Gateway LR reaction with destination vectors (Table 2-33). The *p53* gene was cloned into a pAD vector for indirect TOPORS expression experiments (section 3.2.2.2), and it was simultaneously cloned into a pBD vector for experiments demonstrating the compatibility of In-Fusion and Gateway Y2H vectors (section 4.1).

The reaction products were again used to transform bacteria, which were subsequently grown on selective media. After the incubation plasmids were isolated from the cells, and sequenced using *p53*-specific primers (Table 2-52). The obtained sequences were correct: *p53* was cloned successfully into the pAD and pBD vectors. The cloning outcomes were confirmed by sequencing.

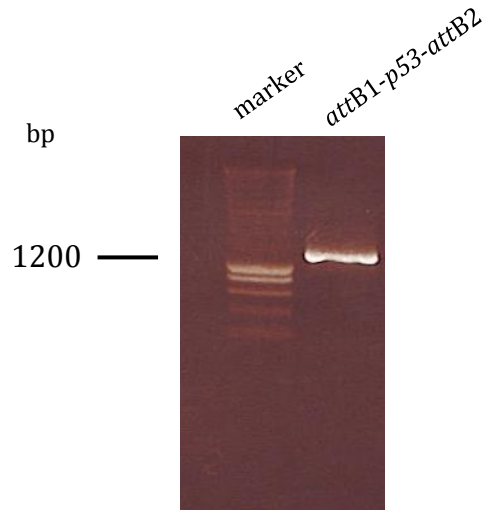


Figure 11-28. Full-length *p53* PCR product amplified using Gateway-specific primers.

Lane 1: Smart Ladder marker. Lane 2: PCR product of the expected fragment size, at approximately 1.2 kb.

## 11.6 CANDIDATE INTERACTING PARTNERS OF TOPORS

A total of 34 potential candidates were identified as interacting partners of TOPORS in the two Y2H library screens (Table 11-3 and Table 11-4). A summary of their key characteristics is provided in the subsequent tables.

Table 11-3. Identities of prey clones from the O-dT library screen, as identified by BLAT (UCSC) genome search.

Key: #, number of O-dT Y2H screen clone; D., date sequenced; F., file identifier.

#	D.	F.	Top BLAT (UCSC) search result
2	2012.03.07	BC	1 Chr. 17. 3' UTR of gene <i>GIT1</i> (99.9 % identity; Homo sapiens G protein-coupled receptor kinase interacting ArfGAP 1 (GIT1), transcript variant 1)
3		BC	2 Chr. 19. 3' UTR of gene <i>CAPNS1</i> (99.9 % identity; Homo sapiens calpain, small subunit 1 (CAPNS1), transcript variant 2) and numerous ESTs
4	2012.04.16	BC	1 Chr. 19. 3' UTR of gene <i>CAPNS1</i> (99.2 % identity; Homo sapiens calpain, small subunit 1 (CAPNS1), transcript variant 2) and numerous ESTs
5	2012.03.07	BC	4 Chr. 8. <i>PPP1R16A</i> (100% identity; Homo sapiens protein phosphatase 1, regulatory subunit 16A) and numerous ESTs
6		BC	5 Chr. 1. <i>NDUFS2</i> (99.8% identity; Homo sapiens NADH dehydrogenase (ubiquinone) Fe-S protein 2, 49kDa (NADH-coenzyme Q reductase) (NDUFS2), nuclear gene encoding mitochondrial protein, transcript variant 1)
7	2012.04.16	BC	2 Chr. 1. <i>NDUFS2</i> (99.8% identity; Homo sapiens NADH dehydrogenase (ubiquinone) Fe-S protein 2, 49kDa (NADH-coenzyme Q reductase) (NDUFS2), nuclear gene encoding mitochondrial protein, transcript variant 1 and numerous ESTs
8		BC	3 Chr. 19. Some ESTs, including from eye and retina: BM676228
9		BC	4 Chr. 15. 3' UTR of gene <i>TBC1D2B</i> (98 % identity; Homo sapiens TBC1 domain family, member 2B (TBC1D2B), transcript variant 2) and numerous ESTs
10	2012.03.07	BC	9 Chr. 16. Two pseudogenes and about 20 ESTs
10	2012.04.16	BC	5 Chr. 11. intronic region of gene <i>PLEKHA7</i> (100 % identity; Homo sapiens pleckstrin homology domain containing, family A member 7 (PLEKHA7)) and some ESTs
11		BC	6 Chr. 16. Two pseudogenes and about 20 ESTs
12		BC	7 Chr. 19. <i>UBA52</i> (99.7% identity; Homo sapiens ubiquitin A-52 residue ribosomal protein fusion product 1 (UBA52), transcript variant 2) and numerous ESTs
14	2012.04.16	BC	8 Chr. X. <i>RPL10</i> (99.0 % identity; Homo sapiens ribosomal protein L10 (RPL10), transcript variant 1, CYTOPLASMIC)
15		BC	9 Chr. 19. Some ESTs, including from eye and retina: BM715662

#	D.	F.	Top BLAT (UCSC) search result
16	BC	10	Chr. 19. Some ESTs, including from eye and retina: BM676228
17	BC	11	Homo sapiens uncharacterized LOC100507412 (LOC100507412), non-coding RNA
18	BC	12	seq. Not readable
19	BC	13	Chr. 17. <i>CSNK1D</i> (99.8% identity; Homo sapiens casein kinase 1, delta ( <i>CSNK1D</i> ), transcript variant 2) and numerous ESTs
22	BC	14	Chr. 22. intronic region of gene <i>GUSBP11</i> (100 % identity; Homo sapiens glucuronidase, beta <u>pseudogene</u> 11 ( <i>GUSBP11</i> ), non-coding RNA) and some ESTs

Table 11-4. Identities of prey clones from the R&amp;O-dT library screen, as identified by BLAT (UCSC) genome search.

Key: #, number of R&amp;O-dT Y2H screen clone; D., date sequenced; F., file identifier.

#	D.	F.	Top BLAT (UCSC) search result
2	2011.11.30	BC35	Chr. 8. <i>ZNF7</i> (zinc finger protein 7) and numerous ESTs
4		BC37	Chr. 17. <i>UBB</i> (99.5 % identity; ubiquitin B precursor) and numerous ESTs
7	2011.12.05	BC11	Chr. 17. <i>ENO3</i> (99.8 % identity; enolase) and numerous ESTs
8		BC12	Chr. 13. <i>TPT1</i> (99.7 % identity; tumour protein, translationally controlled 1)
10		BC2	Chr. 19. <i>AES</i> (100 % identity; amino-terminal enhancer of split isoform b) and numerous ESTs
11		BC3	Chr. 16. <i>DYNC1LI2</i> (99.6 % identity; dynein, cytoplasmic, light intermediate) and numerous ESTs
15		BC6	Chr. 6. 5' UTR of gene <i>SERPINB1</i> (100 % identity; serine (or cysteine) proteinase inhibitor, clade) and numerous ESTs
17		BC8	Chr. 2. <i>RPL31</i> (100 % identity; ribosomal protein L31 isoform 3) and numerous ESTs
18		BC9	Chr. 11. <i>CTSD</i> (99.7 % identity; cathepsin D preproprotein) and numerous ESTs
23		BC12	Chr. 5. <i>DPYSL3</i> (97.1 % identity; dihydropyrimidinase-like 3) and numerous ESTs
24		BC13	Chr. 21. <i>SCAF4</i> (99.9 % identity; splicing factor, arginine/serine-rich 15 isoform; Homo sapiens SR-related CTD-associated factor 4 (SCAF4), transcript variant 3, mRNA) and numerous ESTs
27		BC16	Chr. 13. <i>ITM2B</i> (99.9 % identity; integral membrane protein 2B) and numerous ESTs
28		BC17	Chr. 1. <i>PDC</i> (98.0 % identity; phosducin isoform a) and numerous ESTs.
29		BC18	Chr. 13. <i>ITM2B</i> (99.9 % identity; integral membrane protein 2B) and numerous ESTs
31	2011.12.06	BC20	Chr. 9. <i>PTGDS</i> (99.7 % identity; prostaglandin D2 synthase, brain) and numerous ESTs
32		BC21	Chr. 10. <i>MGEA5</i> (99.9 % identity; meningioma expressed antigen 5 (hyaluronidase) and numerous ESTs
36		BC1	Chr. 5. 3' UTR of gene <i>SAR1B</i> (99.9 % identity) and some ESTs including brain and foetal
44	2011.12.21	BC9	Chr. 11. <i>PRDX5</i> (100 % identity; peroxiredoxin 5 isoform a precursor) and numerous ESTs
45		BC10	Chr. 9. <i>PTGDS</i> (99.7 % identity; prostaglandin D2 synthase, brain) and numerous ESTs

#	D.	F.	Top BLAT (UCSC) search result
46		BC11	Chr.21. <i>SOD1</i> (99.4% identity; superoxide dismutase 1, soluble) and numerous ESTs
47		BC12	Chr. 9. <i>PTGDS</i> (99.7 % identity; prostaglandin D2 synthase, brain) and numerous ESTs
2.3		BC 17	Chr. 11. 3' UTR of gene <i>PDDC1</i> (89.8 % identity; Homo sapiens Parkinson disease 7 domain containing 1 (PDDC1)) and numerous ESTs
2.5		BC 18	Chr. 2. <i>RPS7</i> (100 % identity; Homo sapiens ribosomal protein S7 (RPS7); <b>CYTOPLASMIC</b> ) and numerous ESTs
2.6		BC 19	Chr. 8. intronic region of gene <i>DOCK5</i> (100 % identity; Homo sapiens dedicator of cytokinesis 5 (DOCK5)) and some ESTs
2.7		BC 20	Chr. 2. <i>SLC22A6</i> (99.8 % identity; Homo sapiens solute carrier family 22 (organic anion transporter), member 6 (SLC22A6), transcript variant 1) and numerous ESTs
2.8		BC 21	Chr. 2. <i>UBC</i> (99.8 % identity; Homo sapiens ubiquitin C (UBC)) and numerous ESTs
2.10		BC 23	Chr. 16. <i>NDUFB10</i> (99.6 % identity; Homo sapiens NADH dehydrogenase (ubiquinone) 1 beta subcomplex, 10, 22kDa (NDUFB10), nuclear gene encoding mitochondrial protein) and numerous ESTs
2.13		BC 26	Chr. 15. <i>UBA52</i> (99.7 % identity; Homo sapiens ubiquitin A-52 residue ribosomal protein fusion product 1 (UBA52), transcript variant 2) and numerous ESTs
2.14		BC 27	Chr. 15. <i>PIAS1</i> (100 % identity; Homo sapiens protein inhibitor of activated STAT, 1 (PIAS1)) and numerous ESTs
2.15		BC 28	Chr. 17. <i>NMT1</i> (100 % identity; Homo sapiens N-myristoyltransferase 1 (NMT1)) and numerous ESTs
2.18		BC 30	Chr. 18. <i>LMAN1</i> (99.7 % identity; Homo sapiens lectin, mannose-binding, 1 (LMAN1)) and numerous ESTs
2.20		BC 32	Chr. 14. <i>PSMC1</i> (99.5 % identity; Homo sapiens proteasome (prosome, macropain) 26 S subunit, ATPase, 1 (PSMC1)) and numerous ESTs

Table 11-5. Y2H preys associated with cytoskeleton and trafficking. Functional data from UniProtKB and RefSeq (NCBI).

Expression data from UniProtKB, or databases redirected to from protein-specific Swiss-Prot annotation page.

Clone	Gene from BLAT search	RefSeq Gene Summary	Protein name	Swiss-Prot Protein Function Summary	Protein Expression
R&O-dT 8	<b>TPT1</b> (aka <i>HRF</i> ; <i>p02</i> ; <i>p23</i> ; <i>TCTP</i> )	-	<b>Translationally-controlled tumour protein</b>	Involved in calcium binding and microtubule stabilization.	Ubiquitous
R&O-dT 11	<b>DYNC1L2</b> (aka <i>LIC2</i> ; <i>DNCL2</i> )	Cytoplasmic dynein is a microtubule-associated motor protein (Hughes <i>et al.</i> , 1995 [PubMed 7738094]). See DYNC1H1 (MIM 600112) for general information about dyneins.	<b>Cytoplasmic dynein 1 light intermediate chain 2</b>	Acts as one of several non-catalytic accessory components of the cytoplasmic dynein 1 complex that are thought to be involved in linking dynein to cargos and to adapter proteins that regulate dynein function. Cytoplasmic dynein 1 acts as a motor for the intracellular retrograde motility of vesicles and organelles along microtubules. May play a role in binding dynein to membranous organelles or chromosomes.	Ubiquitous
R&O-dT 23	<b>DPYSL3</b> (aka <i>DRP3</i> ; <i>ULIP</i> ; <i>CRMP4</i> ; <i>DRP-3</i> ; <i>LCRMP</i> ; <i>CRMP-4</i> ; <i>ULIP-1</i> )	-	<b>Dihydropyrimidinase-related protein 3</b>	Necessary for signalling by class 3 semaphorins and subsequent remodelling of the cytoskeleton. Plays a role in axon guidance, neuronal growth cone collapse and cell migration.	Mainly expressed in heart and skeletal muscle. Also strongly expressed in CNS.

Table 11-6. Y2H preys associated with protein turnover and modification. Functional data from UniProtKB and RefSeq (NCBI). Expression data from UniProtKB, or databases redirected to from protein-specific Swiss-Prot annotation page.

Clone	Gene from	RefSeq Gene Summary	Swiss-Prot	Protein
Protein name	BLAT search		Protein Function Summary	Expression
<b>R&amp;O-dT 2.13</b>		Ubiquitin is a highly conserved nuclear and cytoplasmic protein that has a major role in targeting cellular proteins for degradation by the 26 S proteasome. It is also involved in the maintenance of chromatin structure, the regulation of gene expression, and the stress response.	Ubiquitin: exists either covalently attached to another protein, or free (unanchored). When covalently bound, it is conjugated to target proteins via an isopeptide bond either as a monomer (mono-ubiquitin), a polymer linked via different Lys residues of the ubiquitin (poly-ubiquitin chains) or a linear polymer linked via the initiator Met of the ubiquitin (linear poly-ubiquitin chains). Poly-ubiquitin chains, when attached to a target protein, have different functions depending on the Lys residue of the ubiquitin that is linked: Lys-6-linked may be involved in DNA repair; Lys-11-linked is involved in ERAD (endoplasmic reticulum-associated degradation) and in cell-cycle regulation; Lys-29-linked is involved in lysosomal degradation; Lys-33-linked is involved in kinase modification; Lys-48-linked is involved in protein degradation via the proteasome; Lys-63-linked is involved in endocytosis, DNA-damage responses as well as in signalling processes leading to activation of the transcription factor NF-kappa-B. Linear polymer chains formed via attachment by the initiator Met lead to cell signalling. Ubiquitin is usually conjugated to Lys residues of target proteins, however, in rare cases, conjugation to Cys or Ser residues has been observed. When poly-ubiquitin is free (unanchored-poly-ubiquitin), it also has distinct roles, such as in activation of protein kinases, and in signalling.	
<b>O-dT 12</b> Ubiquitin-60S ribosomal protein L40	<b>UBA52</b> (aka <i>L40</i> ; <i>CEP52</i> ; <i>RPL40</i> ; <i>HUBCEP52</i> )	Ubiquitin is synthesized as a precursor protein consisting of either poly-ubiquitin chains or a single ubiquitin moiety fused to an unrelated protein. This gene encodes a fusion protein consisting of ubiquitin at the N terminus and ribosomal protein L40 at the C terminus, a C-terminal extension protein (CEP). Multiple processed pseudogenes derived from this gene are present in the genome.		Ubiquitous



Clone	Gene from BLAT search	RefSeq Gene Summary	Swiss-Prot Protein Function Summary	Protein Expression
<b>R&amp;O-dT 4</b> Poly-ubiquitin-B	<b>UBB</b>	This gene encodes ubiquitin, one of the most conserved proteins known. Ubiquitin has a major role in targeting cellular proteins for degradation by the 26 S proteasome. It is also involved in the maintenance of chromatin structure, the regulation of gene expression, and the stress response. Ubiquitin is synthesized as a precursor protein consisting of either poly-ubiquitin chains or a single ubiquitin moiety fused to an unrelated protein. This gene consists of three direct repeats of the ubiquitin coding sequence with no spacer sequence. Consequently, the protein is expressed as a poly-ubiquitin precursor with a final amino acid after the last repeat. An aberrant form of this protein has been detected in patients with Alzheimer's disease and Down syndrome. Pseudogenes of this gene are located on chromosomes 1, 2, 13, and 17. Alternative splicing results in multiple transcript variants.	As above	Ubiquitous
<b>R&amp;O-dT 2.8</b> Poly-ubiquitin-C	<b>UBC (aka HMG20)</b>	This gene represents a ubiquitin gene, ubiquitin C. The encoded protein is a poly-ubiquitin precursor. Conjugation of ubiquitin monomers or polymers can lead to various effects within a cell, depending on the residues to which ubiquitin is conjugated. Ubiquitination has been associated with protein degradation, DNA repair, cell cycle regulation, kinase modification, endocytosis, and regulation of other cell signalling pathways.	As above	Ubiquitous

Clone	Gene from BLAT search	RefSeq Gene Summary	Swiss-Prot Protein Function Summary	Protein Expression
<b>O-dT 14</b>  60S ribosomal protein L10	<b>RPL10</b> (aka <i>QM</i> ; <i>L10</i> ; <i>NOV</i> ; <i>AUTSX5</i> ; <i>DXS648</i> ; <i>DXS648E</i> )	Ribosomes, the organelles that catalyse protein synthesis, consist of a small 40S subunit and a large 60S subunit. Together these subunits are composed of four RNA species and approximately 80 structurally distinct proteins. This gene encodes a ribosomal protein that is a component of the 60S subunit. The protein belongs to the L10E family of ribosomal proteins. It is located in the cytoplasm. In vitro studies have shown that the chicken protein can bind to c-Jun and can repress c-Jun-mediated transcriptional activation, but these activities have not been demonstrated in vivo. This gene was initially identified as a candidate for a Wilms tumour suppressor gene, but later studies determined that this gene is not involved in the suppression of Wilms tumour. This gene has been referred to as 'laminin receptor homolog' because a chimeric transcript consisting of sequence from this gene and sequence from the laminin receptor gene was isolated; however, it is not believed that this gene encodes a laminin receptor. Alternative splicing results in multiple transcript variants. This gene also uses multiple polyA signals, with the 3'-most polyA signal overlapping the deoxyribonuclease I-like 1 gene on the opposite strand. This gene is co-transcribed with the small nucleolar RNA gene U70, which is located in its fifth intron. As is typical for genes encoding ribosomal proteins, there are multiple processed pseudogenes of this gene dispersed through the genome.	Component of the large ribosomal subunit. Mature ribosomes consist of a small (40S) and a large (60S) subunit. The 40S subunit contains about 33 different proteins and 1 molecule of RNA (18S). The 60S subunit contains about 49 different proteins and 3 molecules of RNA (28S, 5.8S and 5S).	Ubiquitous
<b>R&amp;O-dT 18</b>  Cathepsin D	<b>CTSD</b> (aka <i>CPSD</i> ; <i>CLN10</i> ; <i>HEL-S-</i> <i>130P</i> )	This gene encodes a lysosomal aspartyl protease composed of a dimer of disulphide-linked heavy and light chains, both produced from a single protein precursor. This proteinase, which is a member of the peptidase C1 family, has a specificity similar to but narrower than that of pepsin A. Transcription of this gene is initiated from several sites, including one which is a start site for an oestrogen-regulated transcript. Mutations in this gene are involved in the pathogenesis of several diseases, including breast cancer and possibly Alzheimer disease.	Acid protease active in intracellular protein breakdown. Involved in the pathogenesis of several diseases such as breast cancer and possibly Alzheimer disease.	Ubiquitous

Clone	Gene from BLAT search	RefSeq Gene Summary	Swiss-Prot Protein Function Summary	Protein Expression
<p><b>R&amp;O-dT 2.2</b></p> <p>26 S protease regulatory subunit 4</p>	<p><b>PSMC1</b> (aka <i>S4</i>; <i>p56</i>; <i>P26 S4</i>)</p>	<p>The 26 S proteasome is a multicatalytic proteinase complex with a highly ordered structure composed of 2 complexes, a 20S core and a 19S regulator. The 20S core is composed of 4 rings of 28 non-identical subunits; 2 rings are composed of 7 alpha subunits and 2 rings are composed of 7 beta subunits. The 19S regulator is composed of a base, which contains 6 ATPase subunits and 2 non-ATPase subunits, and a lid, which contains up to 10 non-ATPase subunits. Proteasomes are distributed throughout eukaryotic cells at a high concentration and cleave peptides in an ATP/ubiquitin-dependent process in a non-lysosomal pathway. An essential function of a modified proteasome, the immuno-proteasome, is the processing of class I MHC peptides. This gene encodes one of the ATPase subunits, a member of the triple-A family of ATPases which have a chaperone-like activity. This subunit and a 20S core alpha subunit interact specifically with the hepatitis B virus X protein, a protein critical to viral replication. This subunit also interacts with the adenovirus E1A protein and this interaction alters the activity of the proteasome. Finally, this subunit interacts with ataxin-7, suggesting a role for the proteasome in the development of spinocerebellar ataxia type 7, a progressive neurodegenerative disorder.</p>	<p>The 26 S protease is involved in the ATP-dependent degradation of ubiquitinated proteins. The regulatory (or ATPase) complex confers ATP dependency and substrate specificity to the 26 S complex.</p>	<p>Ubiquitous</p>
<p><b>O-dT 5</b></p> <p>Protein phosphatase 1 regulatory subunit 16A</p>	<p><b>PPP1R16A</b> (aka <i>MYPT3</i>)</p>	<p>-</p>	<p>Inhibits protein phosphatase 1 activity toward phosphorylase, myosin light chain and myosin substrates.</p>	<p>Ubiquitous</p>

Clone	Gene from BLAT search	RefSeq Gene Summary	Swiss-Prot Protein Function Summary	Protein Expression
O-dT 19  Casein kinase I isoform delta	<b>CSNK1D</b> (aka <i>ASPS</i> ; <i>HCKID</i> ; <i>FASPS2</i> ; <i>CK1delta</i> )	This gene is a member of the casein kinase I (CKI) gene family whose members have been implicated in the control of cytoplasmic and nuclear processes, including DNA replication and repair. The encoded protein may also be involved in the regulation of apoptosis, circadian rhythm, microtubule dynamics, chromosome segregation, and p53-mediated effects on growth. The encoded protein is highly similar to the mouse and rat CK1 delta homologs. Three transcript variants encoding different isoforms have been found for this gene.	Essential serine/threonine-protein kinase that regulates diverse cellular growth and survival processes including Wnt signalling, DNA repair and circadian rhythms. It can phosphorylate a large number of proteins. Casein kinases are operationally defined by their preferential utilization of acidic proteins such as caseins as substrates. Phosphorylates connexin-43/GJA1, MAP1A, SNAPIN, MAPT/TAU, TOP2A, DCK, HIF1A, EIF6, p53/TP53, DVL2, DVL3, ESR1, AIB1/NCOA3, DNMT1, PKD2, YAP1, PER1 and PER2. Central component of the circadian clock. In balance with PP1, determines the circadian period length through the regulation of the speed and rhythmicity of PER1 and PER2 phosphorylation. Controls PER1 and PER2 nuclear transport and degradation. YAP1 phosphorylation promotes its SCF(beta-TRCP) E3 ubiquitin ligase-mediated ubiquitination and subsequent degradation. DNMT1 phosphorylation reduces its DNA-binding activity. Phosphorylation of ESR1 and AIB1/NCOA3 stimulates their activity and co-activation. Phosphorylation of DVL2 and DVL3 regulates WNT3A signalling pathway that controls neurite outgrowth. EIF6 phosphorylation promotes its nuclear export. Triggers down-regulation of dopamine receptors in the forebrain. Activates DCK in vitro by phosphorylation. TOP2A phosphorylation favours DNA cleavable complex formation. May regulate the formation of the mitotic spindle apparatus in extravillous trophoblast. Modulates connexin-43/GJA1 gap junction assembly by phosphorylation. Probably involved in lymphocyte physiology. Regulates fast synaptic transmission mediated by glutamate.	Ubiquitous

Clone	Gene from BLAT search	RefSeq Gene Summary	Swiss-Prot Protein Function Summary	Protein Expression
<b>R&amp;O-dT 32</b> Bifunctional protein NCOAT	<b>MGEA5</b> (aka <i>OGA</i> ; <i>MEA5</i> ; <i>NCOAT</i> )	The dynamic modification of cytoplasmic and nuclear proteins by O-linked N-acetyl glucosamine (O-GlcNAc) addition and removal on serine and threonine residues is catalysed by OGT (MIM 300255), which adds O-GlcNAc, and MGEA5, a glycosidase that removes O-GlcNAc modifications.	Cleaves GlcNAc but not GalNAc from glycopeptides. Can use p-nitrophenyl-beta-GlcNAc as substrate but not p-nitrophenyl-beta-GalNAc or p-nitrophenyl-alpha-GlcNAc. Possesses hyaluronidase activity. Acetylates 'Lys-8' of histone H4 and 'Lys-14' of histone H3.	Ubiquitous; Abundant in brain, placenta and pancreas
<b>R&amp;O-dT 2.15</b> Glycyl-peptide N-tetra-decanoyl-transferase 1	<b>NMT1</b> (aka: <i>NMT</i> )	Myristate, a rare 14-carbon saturated fatty acid, is co-translationally attached by an amide linkage to the N-terminal glycine residue of cellular and viral proteins with diverse functions. N-myristoyltransferase (NMT; EC 2.3.1.97) catalyses the transfer of myristate from CoA to proteins. N-myristoylation appears to be irreversible and is required for full expression of the biologic activities of several N-myristoylated proteins, including the alpha subunit of the signal-transducing guanine nucleotide-binding protein (G protein) GO (GNAO1; MIM 139311).	Adds a myristoyl group to the N-terminal glycine residue of certain cellular and viral proteins.	Ubiquitous

Table 11-7. Y2H preys associated with mitochondrial function. Functional data from UniProtKB and RefSeq (NCBI). Expression data from UniProtKB, or databases redirected to from protein-specific Swiss-Prot annotation page.

Clone	Gene from BLAT search	RefSeq Gene Summary	Protein name	Swiss-Prot Protein Function Summary	Protein Expression
R&O-dT 2.1	<b>NDUFB10</b> (aka <i>PDSW</i> )	-	<b>NADH dehydrogenase [ubiquinone] 1 beta subcomplex subunit 10</b>	Accessory subunit of the mitochondrial membrane respiratory chain NADH dehydrogenase (Complex I), that is believed not to be involved in catalysis. Complex I functions in the transfer of electrons from NADH to the respiratory chain. The immediate electron acceptor for the enzyme is believed to be ubiquinone.	Ubiquitous
O-dT 6	<b>NDUFS2</b> (aka <i>Cl-49</i> )	The protein encoded by this gene is a core subunit of the mitochondrial membrane respiratory chain NADH dehydrogenase (complex I). Mammalian mitochondrial complex I is composed of at least 43 different subunits, 7 of which are encoded by the mitochondrial genome, and the rest are the products of nuclear genes. The iron-sulphur protein fraction of complex I is made up of 7 subunits, including this gene product. Complex I catalyses the NADH oxidation with concomitant ubiquinone reduction and proton ejection out of the mitochondria. Mutations in this gene are associated with mitochondrial complex I deficiency for this gene.	<b>NADH dehydrogenase [ubiquinone] iron-sulphur protein 2, mitochondrial</b>	Core subunit of the mitochondrial membrane respiratory chain NADH dehydrogenase (Complex I) that is believed to belong to the minimal assembly required for catalysis. Complex I functions in the transfer of electrons from NADH to the respiratory chain. The immediate electron acceptor for the enzyme is believed to be ubiquinone.	Ubiquitous
O-dT 7					

Clone	Gene from BLAT search	RefSeq Gene Summary	Protein name	Swiss-Prot Protein Function Summary	Protein Expression
R&O- dT 44	<i>PRDX5</i> (aka <i>PLP</i> ; <i>ACR1</i> ; <i>B166</i> ; <i>PRXV</i> ; <i>PMP20</i> ; <i>PRDX6</i> ; <i>prx-</i> <i>V</i> ; <i>SBB110</i> ; <i>AOEB166</i> ; <i>HEL-S-55</i> )	<p>This gene encodes a member of the peroxiredoxin family of antioxidant enzymes, which reduce hydrogen peroxide and alkyl hydroperoxides.</p> <p>The encoded protein may play an antioxidant protective role in different tissues under normal conditions and during inflammatory processes. This protein interacts with peroxisome receptor 1. The crystal structure of this protein in its reduced form has been resolved to 1.5 angstrom resolution. This gene uses alternate in-frame translation initiation sites to generate mitochondrial or peroxisomal/cytoplasmic forms. Three transcript variants encoding distinct isoforms have been identified for this gene.</p>	<b>Peroxi- redoxin-5, mito- chondrial</b>	Reduces hydrogen peroxide and alkyl hydroperoxides with reducing equivalents provided through the thio-redoxin system. Involved in intracellular redox signalling.	Ubiquitous

Table 11-8. Y2H preys associated with cell nucleus.

Functional data from UniProtKB and RefSeq (NCBI). Expression data from UniProtKB, or databases redirected to from protein-specific Swiss-Prot annotation page.

Clone	Gene from BLAT search	RefSeq Gene Summary	Protein name	Swiss-Prot Protein Function Summary	Protein Expression
R&O-dT 2	<b>ZNF7</b> (aka KOX4; zf30; HF.16)	-	<b>Zinc finger protein 7</b>	May be involved in transcriptional regulation.	Ubiquitous
R&O-dT 10	<b>AES</b> (aka GRG; ESP1; GRG5; TLE5; AES-1; AES-2)	The protein encoded by this gene is similar in sequence to the amino terminus of Drosophila enhancer of split Groucho, a protein involved in neurogenesis during embryonic development. The encoded protein, which belongs to the groucho/TLE family of proteins, can function as a homooligomer or as a heterooligomer with other family members to dominantly repress the expression of other family member genes. Three transcript variants encoding different isoforms have been found for this gene.	<b>Amino-terminal enhancer of split</b>	Acts as dominant repressor towards other family members. Inhibits NF-kappa-B-regulated gene expression. May be required for the initiation and maintenance of the differentiated state.	Ubiquitous
R&O-dT 24	<b>SCAF4</b> (aka SRA4; SFRS15)	This gene likely encodes a member of the arginine/serine-rich splicing factor family. A similar protein in Rat appears to bind the large subunit of RNA polymerase II and provide a link between transcription and pre-mRNA splicing. Alternatively spliced transcript variants have been described.	<b>Splicing factor, arginine/serine-rich 15</b>	May act to physically and functionally link transcription and pre-mRNA processing.	Ubiquitous



Clone	Gene from BLAT search	RefSeq Gene Summary	Protein name	Swiss-Prot Protein Function Summary	Protein Expression
R&O-dT 2.14	<b>PIAS1</b> (aka <i>GBP</i> ; <i>ZMIZ3</i> ; <i>DDXBP1</i> ; <i>GU/RH-II</i> )	This gene encodes a member of the mammalian PIAS [protein inhibitor of activated STAT-1 (signal transducer and activator of transcription-1)] family. This member contains a putative zinc-binding motif and a highly acidic region. It inhibits STAT1-mediated gene activation and the DNA binding activity, binds to Gu protein/RNA helicase II/DEAD box polypeptide 21, and interacts with androgen receptor (AR). It functions in testis as a nuclear receptor transcriptional co-regulator and may have a role in AR initiation and maintenance of spermatogenesis.	<b>E3 SUMO-protein ligase PIAS1</b>	Functions as an E3-type small ubiquitin-like modifier (SUMO) ligase, stabilizing the interaction between UBE2I and the substrate, and as a SUMO-tethering factor. Plays a crucial role as a transcriptional co-regulation in various cellular pathways, including the STAT pathway, the p53 pathway and the steroid hormone signalling pathway. In vitro, binds A/T-rich DNA. The effects of this transcriptional co-regulation, transactivation or silencing, may vary depending upon the biological context. Together with PRMT1, may repress STAT1 transcriptional activity, in the late phase of interferon gamma (IFN-gamma) signalling. SUMOylates PML (at 'Lys-65' and 'Lys-160') and PML-RAR and promotes their ubiquitin-mediated degradation. PIAS1-mediated SUMOylation of PML promotes its interaction with CSNK2A1/CK2 which in turn promotes PML phosphorylation and degradation.	Ubiquitous

Table 11-9. Y2H preys – not categorised.

Functional data from UniProtKB and RefSeq (NCBI). Expression data from UniProtKB, or databases redirected to from protein-specific Swiss-Prot annotation page.

Clone	Gene from BLAT search	RefSeq Gene Summary	Protein name	Swiss-Prot Protein Function Summary	Protein Expression
R&O-dT 7	<b>ENO3</b>	This gene encodes one of the three enolase isoenzymes found in vertebrates. Enolase is a dimeric enzyme that converts 2-phosphoglycerate to phosphoenolpyruvate as part of the glycolytic pathway. This isozyme is found in skeletal muscle where it is involved in muscle development and regeneration. Alternative splicing results in multiple transcript variants.	<b>Beta-enolase</b>	Appears to have a function in striated muscle development and regeneration.	Ubiquitous; Abundant in Muscle
R&O-dT 2.5	<b>RPS7</b> (aka S7; DBA8)	Ribosomes, the organelles that catalyse protein synthesis, consist of a small 40S subunit and a large 60S subunit. Together these subunits are composed of 4 RNA species and approximately 80 structurally distinct proteins. This gene encodes a ribosomal protein that is a component of the 40S subunit. The protein belongs to the S7E family of ribosomal proteins. It is located in the cytoplasm. As is typical for genes encoding ribosomal proteins, there are multiple processed pseudogenes of this gene dispersed through the genome.	<b>40S ribosomal protein S7</b>	Required for rRNA maturation.	Brain, heart, kidney, liver, testis, spleen, lung

Clone	Gene from BLAT search	RefSeq Gene Summary	Protein name	Swiss-Prot Protein Function Summary	Protein Expression
R&O-dT 2.7	<i>SLC22A6</i>	The protein encoded by this gene is involved in the sodium-dependent transport and excretion of organic anions, some of which are potentially toxic. The encoded protein is an integral membrane protein and may be localized to the basolateral membrane. Four transcript variants encoding four different isoforms have been found for this gene.	<b>Solute carrier family 22 member 6</b>	Involved in the renal elimination of endogenous and exogenous organic anions. Functions as organic anion exchanger when the uptake of one molecule of organic anion is coupled with an efflux of one molecule of endogenous dicarboxylic acid (glutarate, ketoglutarate, etc). Mediates the sodium-independent uptake of 2,3-dimercapto-1-propanesulfonic acid (DMPS). Mediates the sodium-independent uptake of p-aminohippurate (PAH), ochratoxin (OTA), acyclovir (ACV), 3'-azido-3'-deoxythymidine (AZT), cimetidine (CMD), 2,4-dichlorophenoxyacetate (2,4-D), hippurate (HA), indoleacetate (IA), indoxyl sulphate (IS) and 3-carboxy-4-methyl-5-propyl-2-furanpropionate (CMPF), cidofovir, adefovir, 9-(2-phosphonylmethoxyethyl) guanine (PMEG), 9-(2-phosphonylmethoxyethyl) diaminopurine (PMEDAP) and edaravone sulphate. PAH uptake is inhibited by p-chloromercuribenzenesulphonate (PCMBs), diethyl pyrocarbonate (DEPC), sulindac, diclofenac, carprofen, glutarate and okadaic acid. PAH uptake is inhibited by benzothiazolylcysteine (BTC), S-chlorotrifluoroethylcysteine (CTFC), cysteine S-conjugates S-dichlorovinylcysteine (DCVC), furosemide, steviol, phorbol 12-myristate 13-acetate (PMA), calcium ionophore A23187, benzylpenicillin, furosemide, indomethacin, bumetamide, losartan, probenecid, phenol red, urate, and alpha-ketoglutarate.	CNS, kidney, skeletal muscle, eye (incl. retina), adipose tissue, blood, male and female reproductive structures

Clone	Gene from BLAT search	RefSeq Gene Summary	Protein name	Swiss-Prot Protein Function Summary	Protein Expression
R&O-dT 2.18	<b>LMAN1</b> (aka <i>MR60</i> ; <i>gp58</i> ; <i>F5F8D</i> ; <i>FMFD1</i> ; <i>MCFD1</i> ; <i>ERGIC53</i> ; <i>ERGIC-53</i> )	The protein encoded by this gene is a type I integral membrane protein localized in the intermediate region between the endoplasmic reticulum and the Golgi, presumably recycling between the two compartments. The protein is a mannose-specific lectin and is a member of a novel family of plant lectin homologs in the secretory pathway of animal cells. Mutations in the gene are associated with a coagulation defect. Using positional cloning, the gene was identified as the disease gene leading to combined factor V-factor VIII deficiency, a rare, autosomal recessive disorder in which both coagulation factors V and VIII are diminished.	<b>Protein ERGIC-53</b>	Mannose-specific lectin. May recognize sugar residues of glycoproteins, glycolipids, or glycosylphosphatidyl inositol anchors and may be involved in the sorting or recycling of proteins, lipids, or both. The LMAN1-MCFD2 complex forms a specific cargo receptor for the ER-to-Golgi transport of selected proteins.	Ubiquitous
R&O-dT 17	<b>RPL31</b>	Ribosomes, the organelles that catalyse protein synthesis, consist of a small 40S subunit and a large 60S subunit. Together these subunits are composed of 4 RNA species and approximately 80 structurally distinct proteins. This gene encodes a ribosomal protein that is a component of the 60S subunit. The protein belongs to the L31E family of ribosomal proteins. It is located in the cytoplasm. Higher levels of expression of this gene in familial adenomatous polyyps compared to matched normal tissues have been observed. As is typical for genes encoding ribosomal proteins, there are multiple processed pseudogenes of this gene dispersed through the genome. Alternatively spliced transcript variants encoding distinct isoforms have been found for this gene.	<b>60S ribosomal protein L31</b>	-	Ubiquitous

Clone	Gene from BLAT search	RefSeq Gene Summary	Protein name	Swiss-Prot Protein Function Summary	Protein Expression
R&O-dT 46	<b>SOD1</b> (aka ALS; SOD; ALS1; IPOA; hSod1; HEL-S-44)	The protein encoded by this gene binds copper and zinc ions and is one of two isozymes responsible for destroying free superoxide radicals in the body. The encoded isozyme is a soluble cytoplasmic protein, acting as a homodimer to convert naturally-occurring but harmful superoxide radicals to molecular oxygen and hydrogen peroxide. The other isozyme is a mitochondrial protein. Mutations in this gene have been implicated as causes of familial amyotrophic lateral sclerosis. Rare transcript variants have been reported for this gene.	Superoxide dismutase [Cu-Zn]	Destroys radicals which are normally produced within the cells and which are toxic to biological systems.	Ubiquitous

## 11.7 DETERMINATION OF RETINAL EXPRESSION

An overview of isoforms of *ITM2B*, *PTGDS* and *PSMC1* in the Ensembl and UCSC data bases is summarised in the subsequent figures (Figure 11-29 - Figure 11-34). A sequencing result of a PCR product of genomic origin, which emerged during the *PSMC1* expression analysis, is also included (Figure 11-35).

**Gene: ITM2B** ENSG00000136156

Description integral membrane protein 2B [Source:HGNC Symbol;Acc:6174]  
 Location [Chromosome 13: 48,807,294-48,837,063](#) forward strand.  
 INSDC coordinates chromosome:GRCh37:CM000675.1:48807294:48837063:1  
 Transcripts This gene has 4 transcripts (splice variants) [Hide transcript table](#)

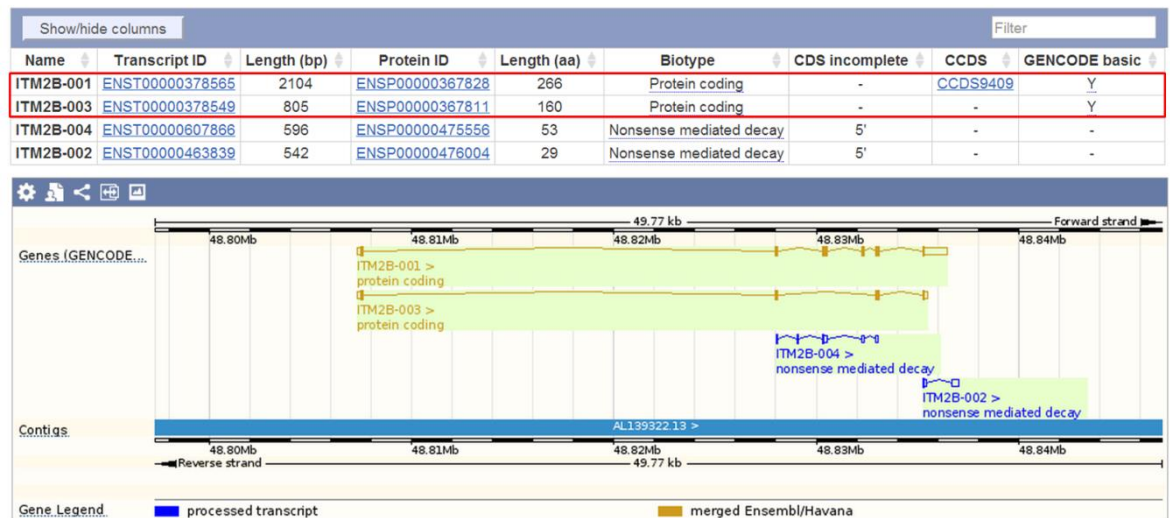


Figure 11-29. Snapshot of *ITM2B* transcript details and the resulting splice variants from the Ensembl database.

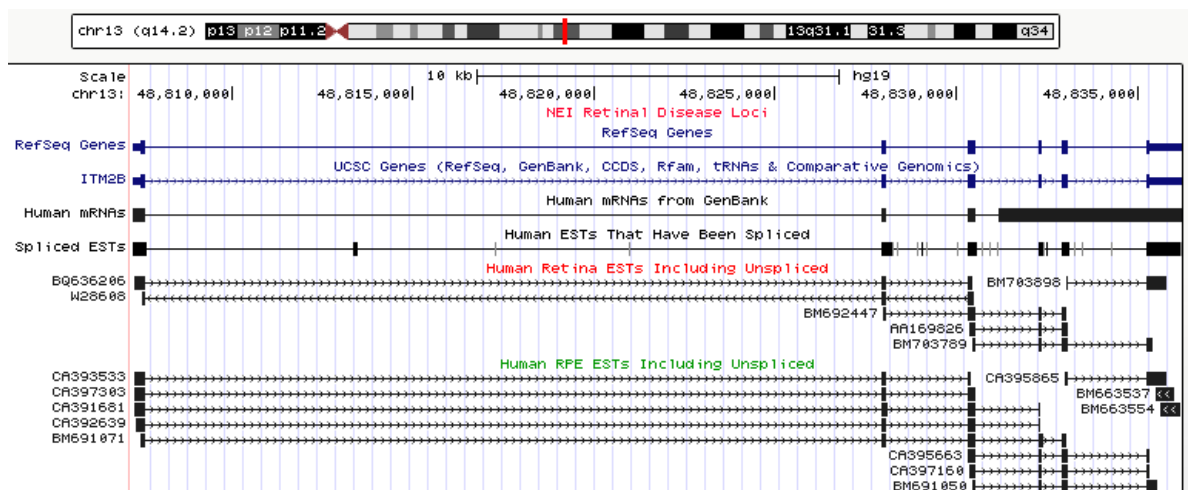


Figure 11-30. Snapshot of *ITM2B* transcript details from the EyeBrowse Gateway, powered by the UCSC database.

**Gene: PTGDS** ENSG00000107317

Description: prostaglandin D2 synthase 21kDa (brain) [Source:HGNC Symbol;Acc:9592]  
 Location: [Chromosome 9: 139,871,956-139,879,887](#) forward strand.  
 INSDC coordinates: chromosome:GRCh37:CM000671.1:139871956:139879887:1  
 Transcripts: This gene has 11 transcripts (splice variants) [Hide transcript table](#)

Name	Transcript ID	Length (bp)	Protein ID	Length (aa)	Biotype	CDS incomplete	CCDS	GENCODE basic
PTGDS-001	<a href="#">ENST00000371625</a>	807	<a href="#">ENSP00000360687</a>	190	Protein coding	-	<a href="#">CCDS7019</a>	Y
PTGDS-004	<a href="#">ENST00000371623</a>	921	<a href="#">ENSP00000360685</a>	160	Protein coding	-	-	-
PTGDS-201	<a href="#">ENST00000224167</a>	913	<a href="#">ENSP00000224167</a>	224	Protein coding	-	-	Y
PTGDS-005	<a href="#">ENST00000446677</a>	754	<a href="#">ENSP00000397468</a>	213	Protein coding	5'	-	-
PTGDS-003	<a href="#">ENST00000457950</a>	661	<a href="#">ENSP00000392633</a>	195	Protein coding	3'	-	-
PTGDS-008	<a href="#">ENST00000444903</a>	369	<a href="#">ENSP00000392692</a>	62	Protein coding	5'	-	-
PTGDS-006	<a href="#">ENST00000460340</a>	616	No protein product	-	Processed transcript	-	-	Y
PTGDS-007	<a href="#">ENST00000462514</a>	593	No protein product	-	Processed transcript	-	-	-
PTGDS-010	<a href="#">ENST00000492068</a>	553	No protein product	-	Processed transcript	-	-	-
PTGDS-009	<a href="#">ENST00000467871</a>	183	No protein product	-	Processed transcript	-	-	-
PTGDS-002	<a href="#">ENST00000471521</a>	989	<a href="#">ENSP00000435033</a>	190	Nonsense mediated decay	-	<a href="#">CCDS7019</a>	-

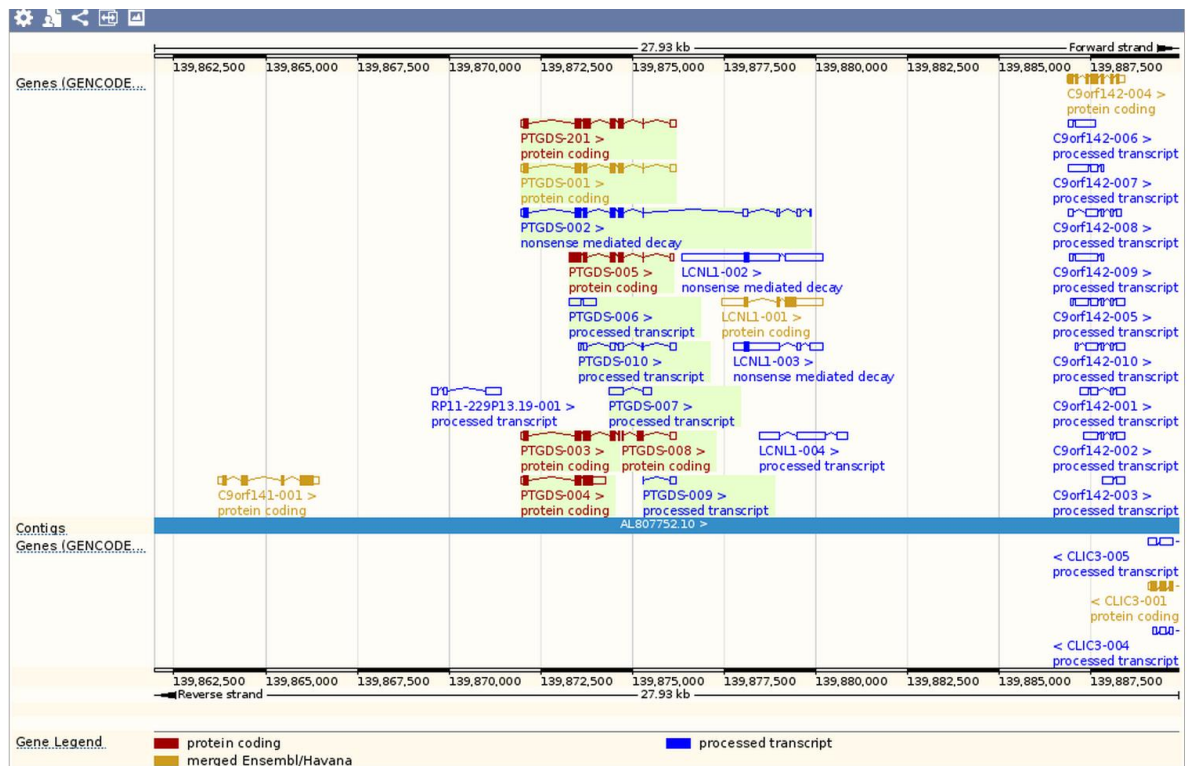


Figure 11-31. Snapshot of *PTGDS* transcript details and the resulting splice variants from the Ensembl database.



Figure 11-32. Snapshot of *PTGDS* transcript details from the EyeBrowse Gateway, powered by the UCSC database. The image was trimmed: not all of the RPE ESTs are displayed.



**Gene: PSMC1** ENSG00000100764

**Description** proteasome (prosome, macropain) 26S subunit, ATPase, 1 [Source:HGNC Symbol;Acc:9547]  
**Location** [Chromosome 14: 90,722,839-90,738,968](#) forward strand.  
**INSDC coordinates** chromosome:GRCh37:CM000676.1:90722839:90738968:1  
**Transcripts** This gene has 7 transcripts (splice variants) [Hide transcript table](#)

Name	Transcript ID	Length (bp)	Protein ID	Length (aa)	Biotype	CDS incomplete	CCDS	GENCODE basic
PSMC1-001	<a href="#">ENST00000261303</a>	1641	<a href="#">ENSP00000261303</a>	440	Protein coding	-	<a href="#">CCDS32139</a>	Y
PSMC1-002	<a href="#">ENST00000543772</a>	1389	<a href="#">ENSP00000445147</a>	367	Protein coding	-	-	Y
PSMC1-004	<a href="#">ENST00000553835</a>	390	<a href="#">ENSP00000452049</a>	84	Protein coding	3'	-	-
PSMC1-003	<a href="#">ENST00000555787</a>	2246	No protein product	-	Retained intron	-	-	-
PSMC1-006	<a href="#">ENST00000555679</a>	606	No protein product	-	Retained intron	-	-	-
PSMC1-007	<a href="#">ENST00000557357</a>	581	No protein protein	-	Retained intron	-	-	-
PSMC1-005	<a href="#">ENST00000554624</a>	577	No protein product	-	Retained intron	-	-	-

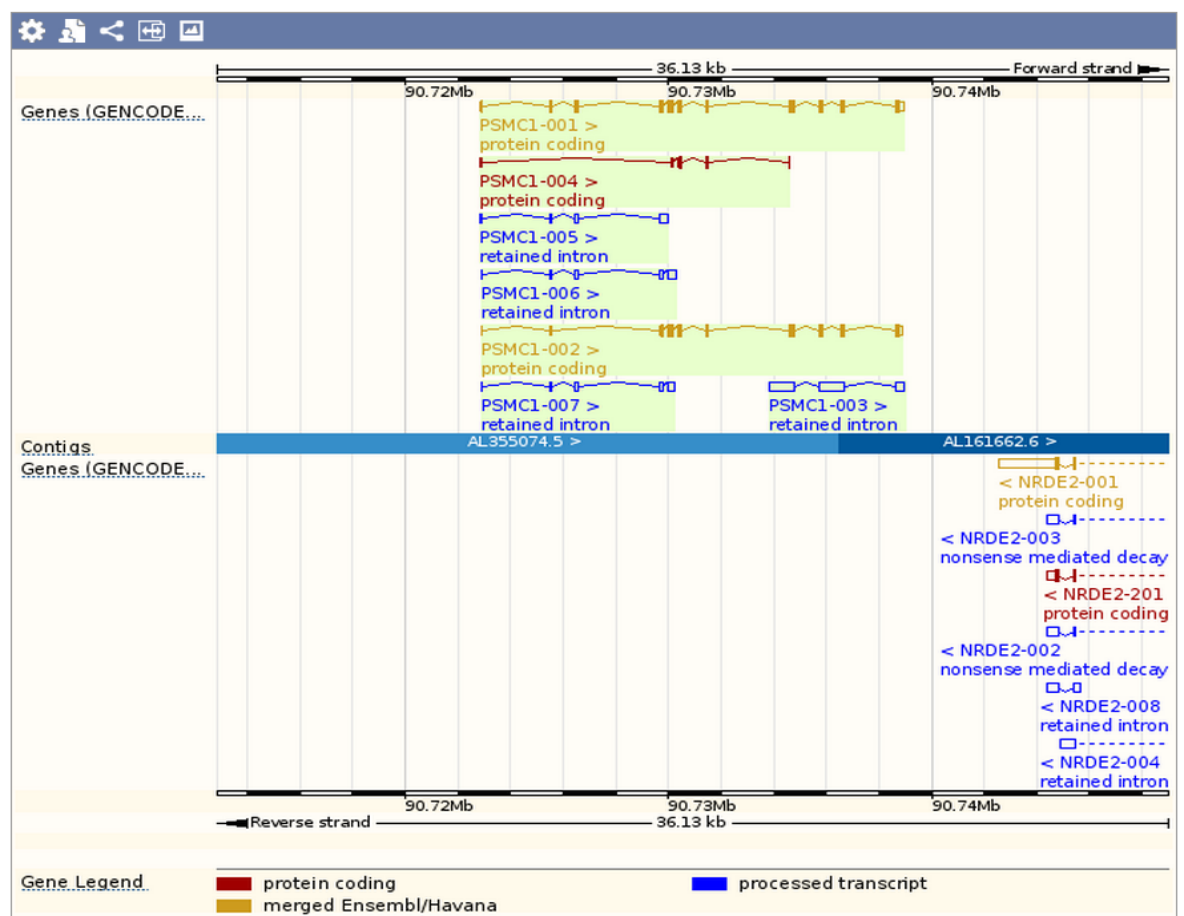


Figure 11-33. Snapshot of PSMC1 transcript details and the resulting splice variants from the Ensembl database.

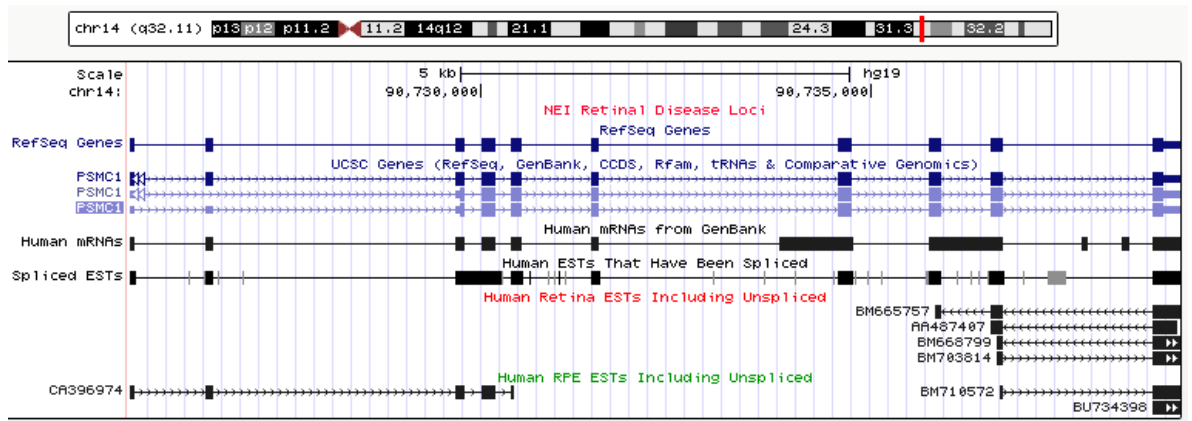


Figure 11-34. Snapshot of PSMC1 transcript details from the EyeBrowse Gateway, powered by the UCSC database.

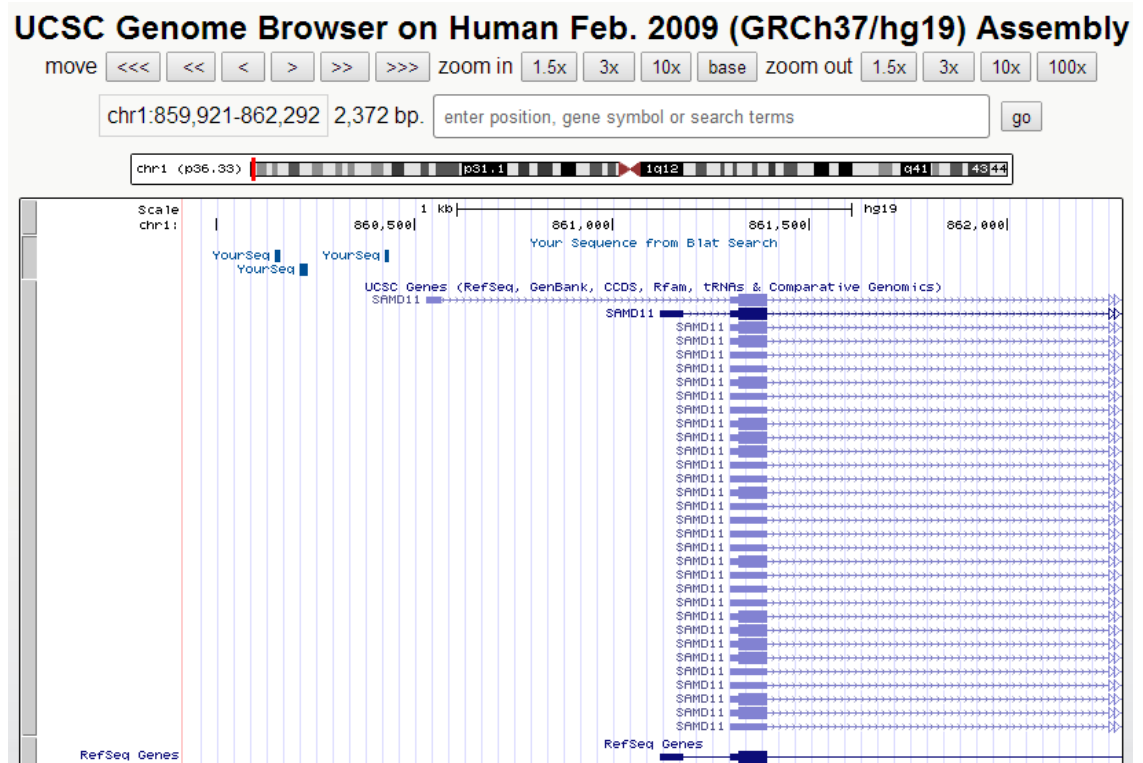


Figure 11-35. Genomic alignments of PCR products amplified from gDNA, using PSMC1 exon-specific primers.

## 11.8 CLONING OF *ITM2B*, *PTGDS* AND *PSMC1*

*ITM2B* is a membrane-bound protein; therefore, it is highly unlikely that the full-length protein would interact with TOPORS in the transcription-based Y2H system. In fact, the *ITM2B* fragments inserted into the library vectors, both comprise exons 3-6 of *ITM2B* isoform 001 (Figure 4-9), which roughly correspond to the ectodomain of *ITM2B*, shedded during its processing. Therefore, the direct PPI was tested not only using full-length *ITM2B* (residues 1-266), but also using its non-membrane-associated ectodomain (residues 90-266), encoded by *ITM2B-001* whose retinal expression was confirmed. Additionally, neurodegeneration-associated *ITM2B* mutants were also cloned into the GAL4 AD vector to further characterise the TOPORS-*ITM2B* interactions. Full-length *PTGDS* isoform 001 and *PSMC1* isoform 001, which appeared to correspond to cDNA library clones identified in the Y2H screen against TOPORS, and whose retinal expression was confirmed, were used in the other two interactions. For cloning purposes, total RNA was extracted from hTERT-RPE1 cells, and reverse-transcribed for cDNA synthesis, which was in turn used for amplification of the prey genes for subsequent experiments. The amplified *PSMC1*, *PTGDS* and *ITM2B* transcripts were sub-cloned in frame with GAL4 AD using the Gateway system (LifeTechnologies, CA, USA, section 2.2.5.3).

### 11.8.1 RNA EXTRACTION AND CHARACTERISATION

The RNA was extracted from hTERT-RPE1 cell line, as described in section 2.4.1. Three variations of the extraction method were tested in order to evaluate, which protocol is optimal for removal of any potentially contaminating DNA. On the one hand, the RNA extraction was performed without any DNase treatment during the procedure; after extraction a half of the resulting RNA sample was treated with DNase (Sample A), and the other half was left untreated (Sample B). On the other hand, the RNA extraction method incorporated the DNase on-column treatment during the extraction procedure (Sample C). The determined RNA yields and purity ratios for each sample are summarised in Table 11-10.

Table 11-10. Yields and purity ratios of the extracted RNA samples.

Ratio results written in green are representative of clean RNA samples (typically  $\geq 2.00$ ). Ratios written in red are much lower than expected in a clean sample, and here indicate the presence of organic compound impurities, absorbing at the 230 nm wavelength.

Sample	[RNA] (ng/ $\mu$ l)	260/280	260/230
A	180	1.66	0.85
B	751	2.11	1.82
C	397	1.80	1.27

All three samples were subsequently evaluated by gel electrophoresis. It was expected that three bands corresponding to the ribosomal RNA molecules, i.e. 28 S, 18 S and 5 S/5.8 S, which collectively make up approximately 80 % of total RNA of a cell, would be observed. A DNA Hyper Ladder I was loaded as reference.

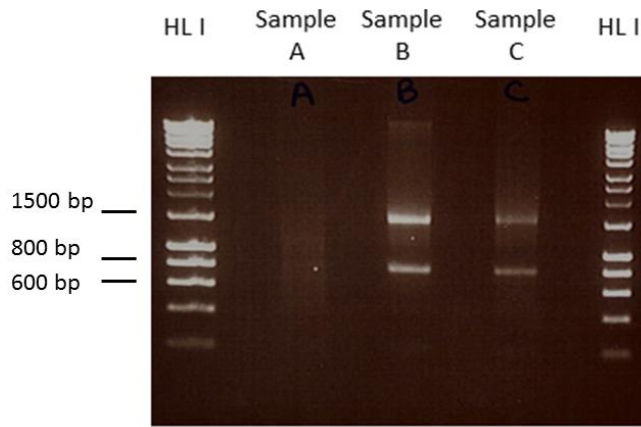


Figure 11-36. Extracted RNA samples A-C. 1.2 % gel, run at 80 V for 1 h. Marker: HL I (Hyper Ladder I - DNA size marker).

### 11.8.2 COMPLEMENTARY DNA GENERATION AND CHARACTERISATION

The cDNA was synthesised as described in section 2.4.2. The results of a subsequent control experiment, aiming to confirm the content of house-keeping genes (HPRT), as well as genes closer in size to the Y2H interacting partners of TOPORS, are summarised in Figure 11-37.

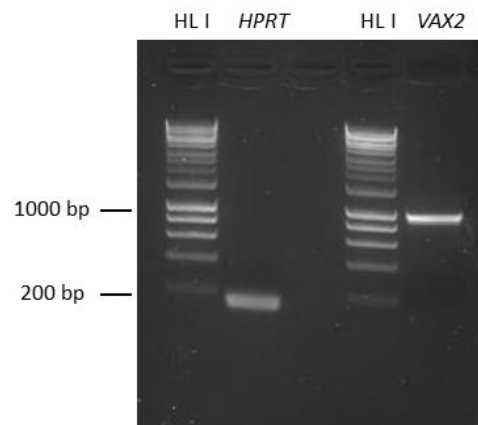


Figure 11-37. HPRT and VAX2 amplicons, generated to test the quality of the newly synthesised cDNA. Marker: HL I (Hyper Ladder I). 1.5 % agarose gel, run at: 150 V for thirty minutes.

### 11.8.3 AMPLIFICATION OF *ITM2B* AND ITS FRAGMENTS

Primers (ITM2B-PCR-F and -R in Table 2-53) were designed for amplification of the longest protein coding transcript of the ITM2B (transcript: ITM2B-001 ENSG00000136156) from human cDNA (Clontech, CA, USA). The resulting PCR product (Figure 11-38) was used as template for PCR using the Gateway BP reaction-specific primers with the attb tails (ITM2B-attb-F and -R in Table 2-53). The soluble fragment of ITM2B (referred to as ITM2B90) was amplified using the same forward primers as the full-length transcript; details of the reverse primers for amplification from cDNA as well as for Gateway cloning are given in section 2.2.5.3 (Methods PhD Thesis 2015 || Appendix

and Materials). All amplicons were sequenced (data not shown) to confirm their identity prior to Gateway cloning.

*ITM2B* mutant constructs, encoding the FBD, FDD and retinal dystrophy mutants, were kindly provided by Audo *et al.* (2013) in pBUD vectors. These constructs were used as templates for amplification by KOD polymerase (Novagen, Merck KGaA, Germany) for sub-cloning into tagged Gateway vectors. The constructs were verified by sequencing (Figure 11-42, Figure 11-43, Figure 11-44) prior to downstream experiments.

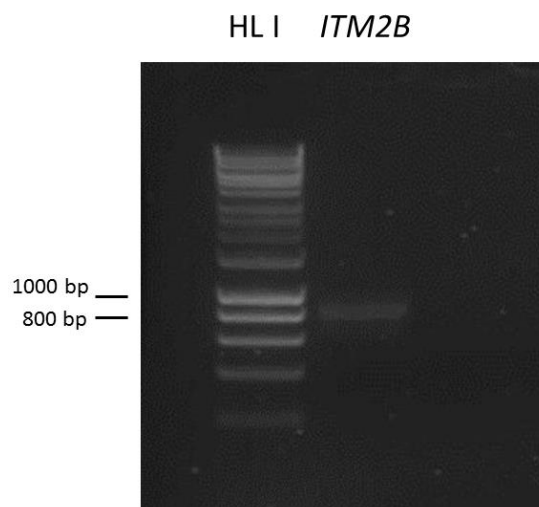


Figure 11-38. *ITM2B* amplicon from RPE1 cDNA. Expected size: 801 bp. Marker: HL I (Hyper Ladder I).

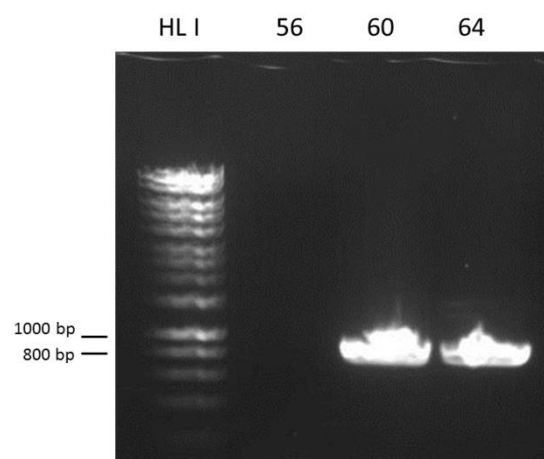


Figure 11-39. *attb-ITM2B-attb* amplicons. Expected size: 861 bp. Marker: HL I (Hyper Ladder I). PCR optimisation run at three annealing temperatures for the primer pair: 56 °C, 60 °C, and 64 °C.

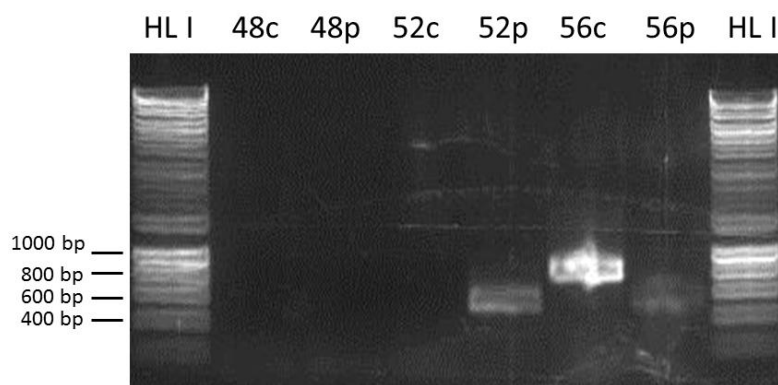


Figure 11-40. Putative *attb-ITM2B90-attb* amplicons. Expected size: 594 bp. Marker: HL I (Hyper Ladder I). PCR optimisation run at three different annealing temperatures for the primer pair, at 48 °C, 52 °C and 56 °C. PCR template used is denoted by 'c' (RPE1 cDNA), or 'p' (PCR amplicon from Figure 11-38).

SL ctrl R60 R64 R68 B60 B64 B68 D60 D64 D68 SL

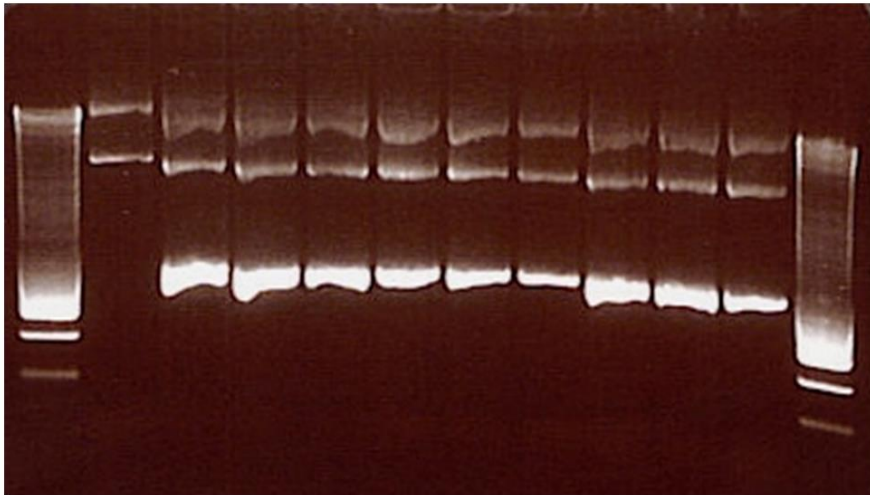


Figure 11-41. Mutant ITM2B Gateway amplicons.

Marker: SL (Smart Ladder). PCR optimisation run at three different annealing temperatures for each primer pair, at 60 °C, 64 °C and 68 °C. PCR template used is denoted by 'c' (RPE1 cDNA), or 'p' (PCR amplicon from Figure 11-38). Ctrl: PCR positive control (did not work). 'R' denotes ITM2B retinal dystrophy mutant construct; 'B', ITM2B British Dementia mutant construct; 'D', ITM2B Danish Dementia mutant construct. Expected band sizes: Retinal dystrophy mutant with attb tails 861 bp; British Dementia mutant with attb tails 894 bp; Danish Dementia mutant with attb tails 894 bp.

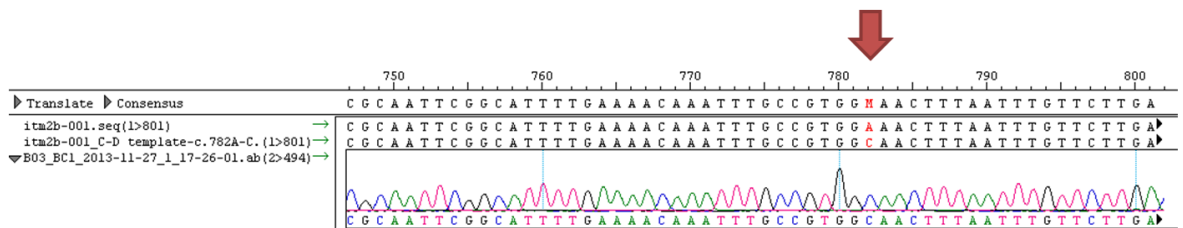


Figure 11-42. Confirmed sequence of the attb-ITM2B\_RetMu-attb amplicon (ITM2B retinal dystrophy mutant).

itm2b-001(1>801): wild-type ITM2B reference sequence. itm2b-001\_C-D template-c.782A-C(1>801): retinal dystrophy mutant ITM2B sequence. Mutation indicated by arrow.

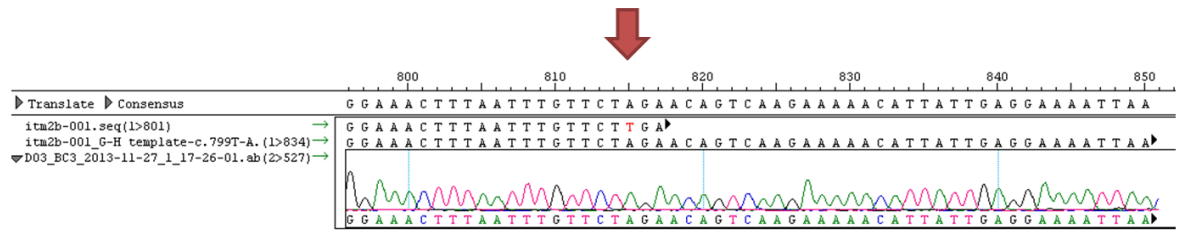


Figure 11-43. Confirmed sequence of the attb-ITM2B\_FBD-attb amplicon (ITM2B Familial British Dementia mutant).

Itm2b-001(1>801): wild-type ITM2B reference sequence. Itm2b-001\_G-H template-c.799T-A(1>834): British Dementia mutant ITM2B sequence. Mutation indicated by arrow.

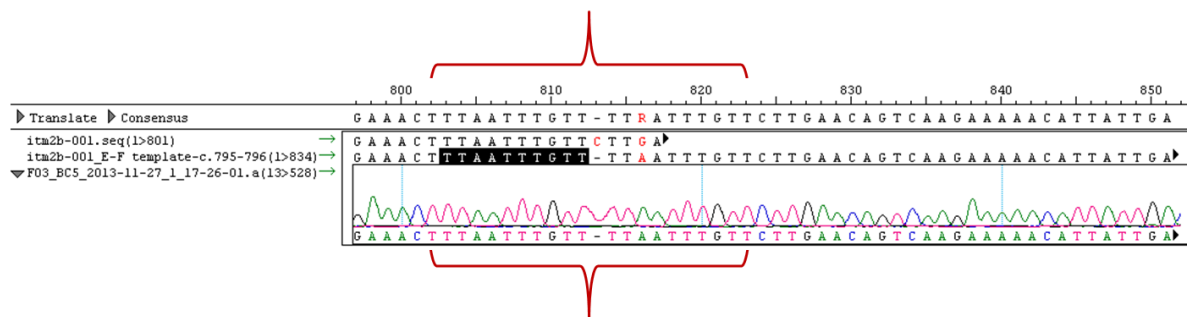


Figure 11-44. Confirmed sequence of the attb-ITM2B\_FDD\_Mu-attb amplicon (ITM2B Familial Danish Dementia mutant).

Itm2b-001(1>801): wild-type ITM2B reference sequence. Itm2b-001\_E-F template-c.795-796(1>834): Danish Dementia mutant ITM2B sequence. The decamer sequence highlighted in black is duplicated in the Danish mutant. The duplicated region is indicated by the brackets.

### 11.8.4 PTGDS AMPLIFICATION

Primers (Table 2-54) were designed for amplification of the second longest protein coding transcript of the PTGDS (transcript: PTGDS-001 ENSG00000107317). The resulting amplicon (Figure 11-45) was then used as template for nested PCR using the Gateway BP reaction-specific primers with attb tails (Table 2-54). The full-length *PTGDS* transcript was amplified as shown in Figure 11-46. All amplicons were sequenced (data not shown) prior to Gateway cloning to confirm their identity and ensure sequence integrity.

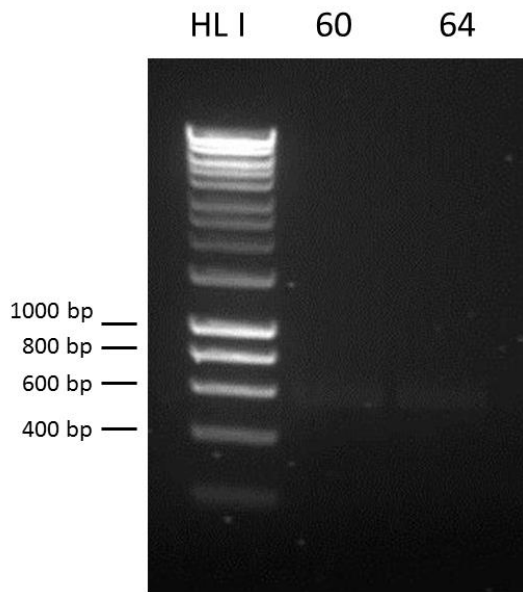


Figure 11-45. *PTGDS* amplicons from RPE1 cDNA. Expected size: 573 bp. Marker: HLI (Hyper Ladder I). PCR optimisation run at two annealing temperatures for the primer pair, at 60 °C and 64 °C.

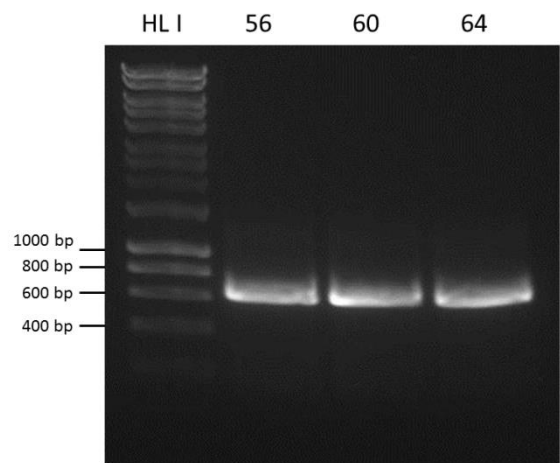


Figure 11-46. *attb-PTGDS-attb* amplicons. Expected size: 633 bp. Marker: HLI (Hyper Ladder I). PCR optimisation run at three annealing temperatures for the primer pair, at 56 °C, 60 °C and 64 °C.



### 11.8.5 *PSMC1* AMPLIFICATION

The longest protein coding transcript of the *PSMC1* (transcript: PSMC1-001 ENST00000261303) was kindly provided in a pBluescript (pBS) vector by T. Jake Liang, MD, and Zhensheng Zhang from the Intramural Research Program (IRP) of the National Institutes of Health (NIH). The pBS-*PSMC1* construct was used as template for PCR with the Gateway BP reaction-specific primers with attb tails (Table 2-55). All amplicons were sequenced (data not shown) prior to Gateway cloning to confirm their identity.

Gel electrophoresis revealed several amplicons, two bands additional to and above the desired band (Figure 11-47), therefore the amplicon of the expected size was excised from the gel, purified and sequenced (Figure 11-48).

A missense mutation was identified, which was also confirmed in the original pBS-*PSMC1* construct. However, the purified mutant amplicon was still used for the Gateway cloning, and the mutation corrected, after the BP recombination step, in the resulting pDONR constructs, using site-directed mutagenesis (Figure 11-49). The corrected pDONR\_*PSMC1* construct was subsequently used for Gateway LR recombination. The cloning outcomes were verified by sequencing.

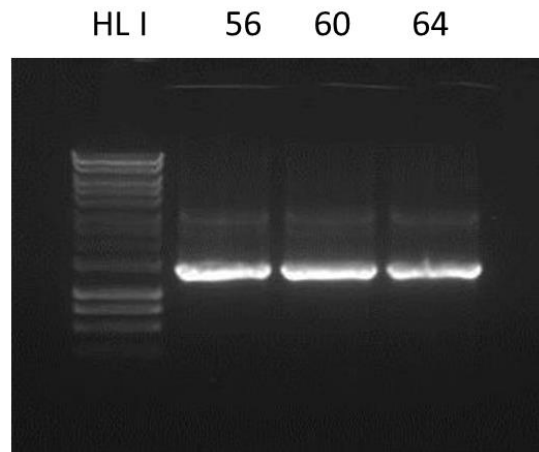


Figure 11-47. *attb-PSMC1-attb* amplicons. Expected size: 1383 bp. HL I: Hyper Ladder I. 56: PCR denaturation step at 56 °C. 60: PCR denaturation step at 60 °C. 64: PCR denaturation step at 64 °C.

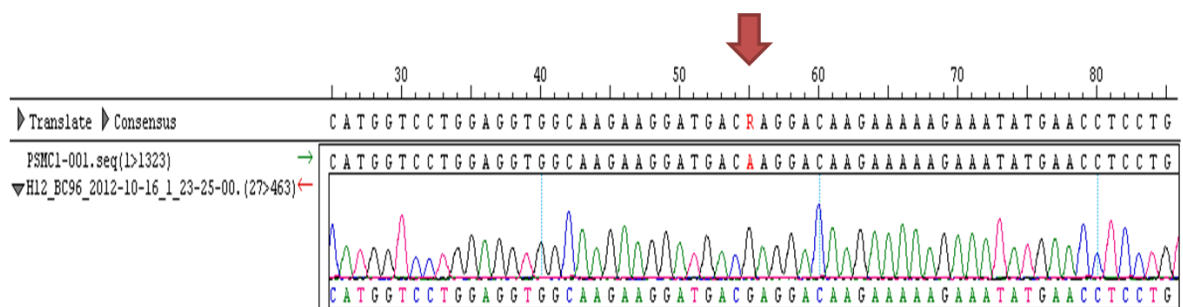


Figure 11-48. Missense mutation (c.55A>G → p.Lys19Glu) was identified in the *PSMC1* amplicon of the expected size, as well as the construct.

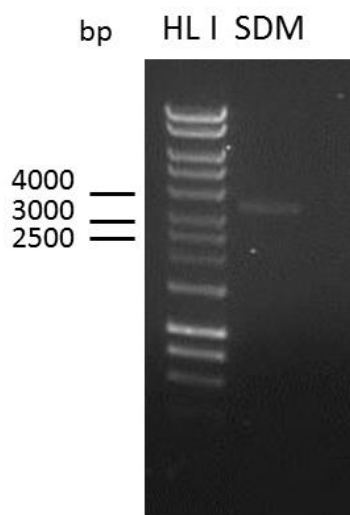


Figure 11-49. pDONR\_PSMC1 amplicon (linear vector).  
 Expected size: 3168 bp (1785 bp vector + 1383 bp insert). Marker: HL I (Hyper Ladder I). SDM: site-directed mutagenesis PCR product (full-length construct amplified with mutation-correcting constructs).

## 11.9 FULL-LENGTH TOPORS AND DOMAIN FRAGMENTS (N, M AND C) INTERACTIONS IN YEAST – RAW RESULTS

Six experiments were performed to delineate the domains of TOPORS, which mediate its interactions with the newly-identified protein partners. A result was considered positive overall, if blue growth, indicating a PPI, was observed in at least four out of six experiments at a given stringency level.

Table 11-11. TOPORS x p53 interactions.

Key: D+ = growth on DDO/X/A; D- = no growth on DDO/X/A; Q+ = growth on QDO/X/A; Q- = no growth on QDO/X/A.

#	Experiment date	Results of tested interactions				+ve	-ve
		pBD- TOPORS	pGBKT7-N	pGBKT7- M	pGBKT7- C	pBD- p53	pBD- Lam
			pAD_p53			pGADT7- T	pGADT7- T
1	28-Oct-13	D+ Q-	D+ Q-	D+ Q+	D+ Q+	D+ Q+	n/a
2	06-Nov-13	D+ Q-	D+ Q-	D+ Q+	D+ Q+	D+ Q+	n/a
3	12-Nov-13	D+ Q+	D+ Q+	D+ Q-	D+ Q+	D+ Q+	n/a
4	23-Jan-14	D- Q-	D+ Q+	D+ Q+	D+ Q+	D+ Q+	D- Q-
5	08-Apr-14	D+ Q+	D+ Q+	D+ Q+	D- Q+	D+ Q+	D- Q-
6	23-Apr-14	D+ Q+	D+ Q+	D+ Q-	D+ Q-	D+ Q+	D- Q-
	<b>Overall Result</b>	<b>D+ Q-</b>	<b>D+ Q+</b>	<b>D+ Q+</b>	<b>D+ Q+</b>	<b>D+ Q+</b>	<b>D- Q-</b>

Table 11-12. TOPORS x ITM2B interactions.

Key: D+ = growth on DDO/X/A; D- = no growth on DDO/X/A; Q+ = growth on QDO/X/A; Q- = no growth on QDO/X/A.

#	Experiment date	Results of tested interactions				+ve	-ve
		pBD- TOPORS	pGBKT7-N	pGBKT7- M	pGBKT7- C	pBD-p53	pBD- Lam
		pAD_ITM2B				pGADT7- T	pGADT7- T
1	28-Oct-13	D- Q-	D+ Q+	D- Q-	D+ Q+	D+ Q+	n/a
2	06-Nov-13	D- Q-	D+ Q+	D- Q-	D+ Q+	D+ Q+	n/a
3	12-Nov-13	D+ Q+	D+ Q+	D+ Q-	D+ Q+	D+ Q+	n/a
4	23-Jan-14	D+ Q+	D+ Q+	D- Q-	D- Q+	D+ Q+	D- Q-
5	08-Apr-14	D+ Q+	D- Q-	D+ Q+	D+ Q+	D+ Q+	D- Q-
6	23-Apr-14	D+ Q-	D+ Q+	D+ Q-	D+ Q-	D+ Q+	D- Q-
	<b>Overall Result</b>	<b>D+ Q-</b>	<b>D+ Q+</b>	<b>D- Q-</b>	<b>D+ Q+</b>	<b>D+ Q+</b>	<b>D- Q-</b>

Table 11-13. TOPORS x ITM2B90 interactions.

Key: D+ = growth on DDO/X/A; D- = no growth on DDO/X/A; Q+ = growth on QDO/X/A; Q- = no growth on QDO/X/A.

#	Experiment date	Results of tested interactions				+ve	-ve
		pBD- TOPORS	pGBKT7-N	pGBKT7- M	pGBKT7- C	pBD- p53	pBD- Lam
		pAD_ITM2B90				pGADT7- T	pGADT7- T
1	28-Oct-13	D+ Q-	D+ Q+	D- Q-	D+ Q+	D+ Q+	n/a
2	06-Nov-13	D+ Q-	D+ Q+	D- Q-	D+ Q+	D+ Q+	n/a
3	12-Nov-13	D+ Q+	D+ Q+	D+ Q+	D+ Q-	D+ Q+	n/a
4	23-Jan-14	D+ Q+	D+ Q+	D+ Q+	D+ Q+	D+ Q+	D- Q-
5	08-Apr-14	D+ Q+	D- Q-	D+ Q+	D+ Q+	D+ Q+	D- Q-
6	23-Apr-14	D+ Q-	D+ Q+	D+ Q-	D+ Q-	D+ Q+	D- Q-
	<b>Overall result</b>	<b>D+ Q-</b>	<b>D+ Q+</b>	<b>D+ Q-</b>	<b>D+ Q+</b>	<b>D+ Q+</b>	<b>D- Q-</b>

Table 11-14. TOPORS x ITM2B\_Ret interactions.

Key: D+ = growth on DDO/X/A; D- = no growth on DDO/X/A; Q+ = growth on QDO/X/A; Q- = no growth on QDO/X/A.

#	Experiment date	Results of tested interactions				+ve	-ve
		pBD- TOPORS	pGBKT7-N	pGBKT7- M	pGBKT7- C	pBD- p53	pBD- Lam
			pAD_ITM2B_Ret			pGADT7- T	pGADT7- T
1	28-Oct-13	n/a	n/a	n/a	n/a	n/a	n/a
2	06-Nov-13	n/a	n/a	n/a	n/a	n/a	n/a
3	12-Nov-13	n/a	n/a	n/a	n/a	n/a	n/a
4	23-Jan-14	D+ Q+	D+ Q+	D+ Q-	D+ Q+	D+ Q+	D- Q-
5	08-Apr-14	D+ Q+	D+ Q+	D- Q+	D- Q+	D+ Q+	D- Q-
6	23-Apr-14	D+ Q-	D+ Q+	D+ Q-	D+ Q-	D+ Q+	D- Q-
	<b>Overall result</b>	<b>D+ Q+</b>	<b>D+ Q+</b>	<b>D+ Q-</b>	<b>D+ Q+</b>	<b>D+ Q+</b>	<b>D- Q-</b>

Table 11-15. TOPORS x ITM2B\_FBDinteractions.

Key: D+ = growth on DDO/X/A; D- = no growth on DDO/X/A; Q+ = growth on QDO/X/A; Q- = no growth on QDO/X/A.

#	Experiment date	Results of tested interactions				+ve	-ve
		pBD- TOPORS	pGBKT7-N	pGBKT7- M	pGBKT7- C	pBD- p53	pBD- Lam
			pAD_ITM2B_ABri			pGADT7- T	pGADT7- T
1	28-Oct-13	n/a	n/a	n/a	n/a	n/a	n/a
2	06-Nov-13	n/a	n/a	n/a	n/a	n/a	n/a
3	12-Nov-13	n/a	n/a	n/a	n/a	n/a	n/a
4	23-Jan-14	D+ Q+	D+ Q+	D+ Q+	D+ Q+	D+ Q+	D- Q-
5	08-Apr-14	D+ Q-	D+ Q+	D+ Q+	D- Q-	D+ Q+	D- Q-
6	23-Apr-14	D+ Q-	D+ Q+	D+ Q-	D+ Q-	D+ Q+	D- Q-
	<b>Overall result</b>	<b>D+ Q-</b>	<b>D+ Q+</b>	<b>D+ Q+</b>	<b>D+ Q+</b>	<b>D+ Q+</b>	<b>D- Q-</b>

Table 11-16. TOPORS x ITM2B\_FDD interactions.

Key: D+ = growth on DDO/X/A; D- = no growth on DDO/X/A; Q+ = growth on QDO/X/A; Q- = no growth on QDO/X/A.

#	Experiment date	Results of tested interactions				+ve	-ve
		pBD- TOPORS	pGBKT7-N	pGBKT7- M	pGBKT7- C	pBD- p53	pBD- Lam
			pAD_ITM2B_FDD			pGADT7- T	pGADT7- T
1	28-Oct-13	n/a	n/a	n/a	n/a	n/a	n/a
2	06-Nov-13	n/a	n/a	n/a	n/a	n/a	n/a
3	12-Nov-13	n/a	n/a	n/a	n/a	n/a	n/a
4	23-Jan-14	D- Q-	D- Q-	D- Q-	D- Q-	D+ Q+	D- Q-
5	08-Apr-14	D- Q-	D- Q-	D- Q-	D+ Q-	D+ Q+	D- Q-
6	23-Apr-14	D+ Q-	D+ Q+	D+ Q-	D+ Q-	D+ Q+	D- Q-
	<b>Overall result</b>	<b>D- Q-</b>	<b>D- Q-</b>	<b>D- Q-</b>	<b>D+ Q-</b>	<b>D+ Q+</b>	<b>D- Q-</b>

Table 11-17. TOPORS x PTGDS interactions.

Key: D+ = growth on DDO/X/A; D- = no growth on DDO/X/A; Q+ = growth on QDO/X/A; Q- = no growth on QDO/X/A.

#	Experiment date	Results of tested interactions				+ve	-ve
		pBD- TOPORS	pGBKT7-N	pGBKT7- M	pGBKT7- C	pBD- p53	pBD- Lam
			pAD_PTGDS			pGADT7- T	pGADT7- T
1	28-Oct-13	D- Q-	D+ Q+	D+ Q+	D+ Q+	D+ Q+	n/a
2	06-Nov-13	D+ Q-	D+ Q+	D+ Q+	D+ Q+	D+ Q+	n/a
3	12-Nov-13	D+ Q+	D+ Q-	D+ Q+	D+ Q-	D+ Q+	n/a
4	23-Jan-14	D+ Q-	D+ Q+	D+ Q-	D+ Q-	D+ Q+	D- Q-
5	08-Apr-14	D+ Q-	D+ Q+	D+ Q-	D+ Q+	D+ Q+	D- Q-
6	23-Apr-14	D+ Q+	D+ Q+	D- Q-	D+ Q-	D+ Q+	D- Q-
	<b>Overall result</b>	<b>D+ Q-</b>	<b>D+ Q+</b>	<b>D+ Q-</b>	<b>D+ Q-</b>	<b>D+ Q+</b>	<b>D- Q-</b>

Table 11-18. TOPORS x PSMC1 interactions.

Key: D+ = growth on DDO/X/A; D- = no growth on DDO/X/A; Q+ = growth on QDO/X/A; Q- = no growth on QDO/X/A.

#	Experiment date	Results of tested interactions				+ve	-ve
		pBD- TOPORS	pGBKT7-N	pGBKT7- M	pGBKT7- C	pBD- p53	pBD- Lam
		pAD_PSMC1				pGADT7- T	pGADT7- T
1	28-Oct-13	D+ Q-	D+ Q-	D+ Q+	D+ Q+	D+ Q+	n/a
2	06-Nov-13	D+ Q-	D+ Q-	D+ Q+	D+ Q+	D+ Q+	n/a
3	12-Nov-13	D+ Q+	D+ Q-	D+ Q+	D+ Q+	D+ Q+	n/a
4	23-Jan-14	D+ Q+	D- Q-	D- Q+	D- Q+	D+ Q+	D- Q-
5	08-Apr-14	D- Q-	D+ Q-	D+ Q-	D- Q-	D+ Q+	D- Q-
6	23-Apr-14	D+ Q-	D+ Q+	D+ Q-	D+ Q-	D+ Q+	D- Q-
<b>Overall result</b>		<b>D+ Q-</b>	<b>D+ Q-</b>	<b>D+ Q+</b>	<b>D+ Q+</b>	<b>D+ Q+</b>	<b>D- Q-</b>

### 11.10 ALIGNMENT OF PROTEIN-CODING *PTGDS* ISOFORMS

The sequence of the immunogen, used to generate the antibody against PTGDS (sc-30067, Santa Cruz Biotechnology), corresponds to the *PTGDS* isoform 001 (Figure 11-50). Alignments with isoforms *PTGDS*-004 and *PTGDS*-005, found to be expressed in human retina, were given in section 5.3.1.2 of Chapter 5. Alignments with isoform *PTGDS*-001, pulled out from the Y2H screen, and found to be expressed in the retina, as well as alignments with isoforms *PTGDS*-003 and *PTGDS*-008, found to not be expressed in human retina, are shown below.

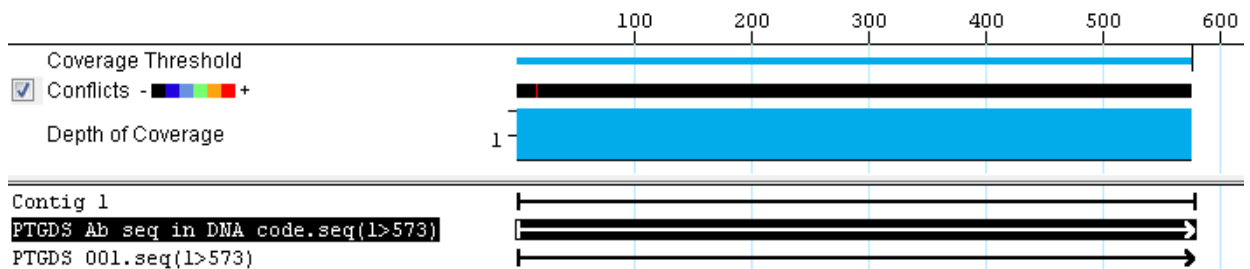


Figure 11-50. The sequence of the immunogen, used to generate the antibody against PTGDS (sc-30067, Santa Cruz Biotechnology), corresponds to the *PTGDS* isoform 001. The highlighted conflict corresponds to a silent change in a codon for threonine.

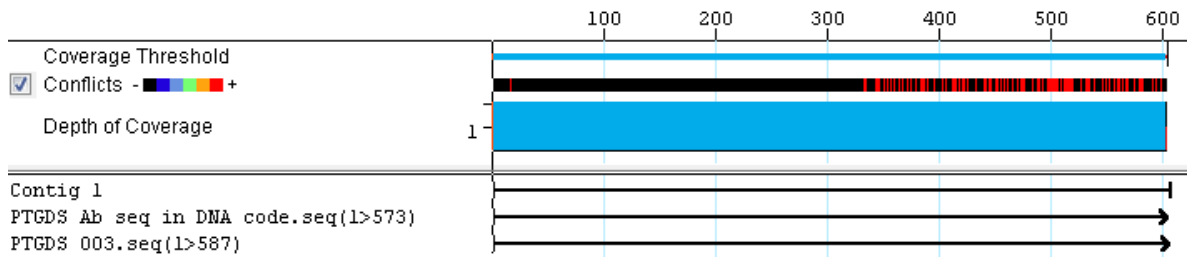


Figure 11-51. The sequence of the immunogen, used to generate the antibody against PTGDS (sc-30067, Santa Cruz Biotechnology), aligns approximately with the N-terminal half of *PTGDS* isoform 003. The red highlighted conflicts represent dissimilarities between the sequence corresponding to the PTGDS immunogen, and the the sequence of isoform 003.

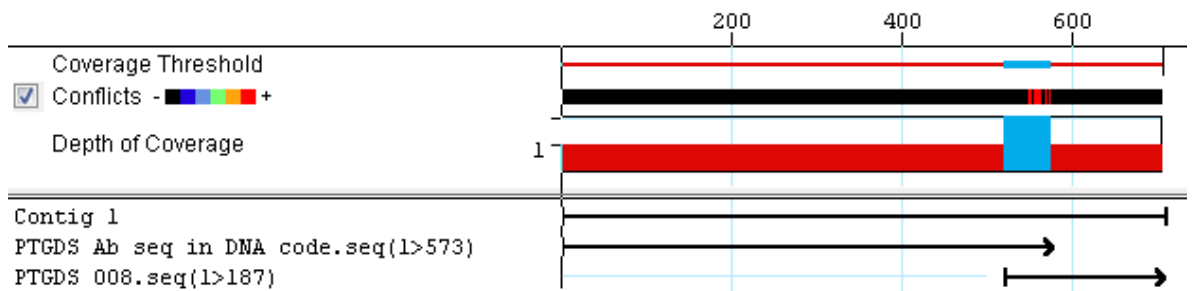


Figure 11-52. The sequence of the immunogen, used to generate the antibody against PTGDS (sc-30067, Santa Cruz Biotechnology), shows virtually no alignment with *PTGDS* isoform 008. The red highlighted conflicts represent dissimilarities between the sequence corresponding to the PTGDS immunogen, and the the sequence of isoform 008.

### 11.11 POSTERS PRESENTED AT SCIENCE CONFERENCES

Abstracts and size-reduced copies of the four posters, listed on page 4 (Publications), are presented on the following pages.

**Title: Identification of Interacting Protein Partners of TOPORS in the Retina**

Authors: Barbara Czub<sup>1</sup>, Amna Shah<sup>1</sup>, Giovanna Alfano<sup>1</sup>, Lourdes Valdes Sanchez<sup>2</sup>, Christina Chakarova<sup>1</sup> and Shomi S. Bhattacharya<sup>1,2</sup>

<sup>1</sup>Institute of Ophthalmology, UCL, London EC1V 9EL, UK

<sup>2</sup> Department of Cell Therapy and Regenerative Medicine, Andalusian Molecular Biology and Regenerative Medicine Centre (CABIMER), Avda. Americo Vespucio, Seville 41092, Spain

**Purpose:** Retinitis pigmentosa (RP) is a clinically and genetically heterogeneous disease characterised by loss of rod photoreceptors. Historically genes linked to RP were associated with rod-specific functions. Recently a novel class of ubiquitously expressed causative genes emerged including splicing factor genes and *TOPORS*. To date studies show *TOPORS* is expressed in all tested human tissues including retina and localises to several compartments of the cell. However, mutations in *TOPORS* only cause RP (no systemic symptoms); this may be due to retina-specific protein interactions, which are perturbed as a result of mutations. This work aims to understand why mutations in this ubiquitously expressed gene cause a retina-only disease by identifying interacting partners of *TOPORS* from human retina.

**Methods:** Human retinal cDNA library was constructed from total retinal cDNA directly in Y187 *S.cerevisiae* yeast strain by homologous recombination in-frame with GAL4 AD. Retina-specificity was validated by sequencing. Bait plasmids (full-length *TOPORS* and deletion constructs) were cloned in-frame with GAL4 BD. The library was screened for protein interacting partners of *TOPORS* using Matchmaker™ Gold Yeast Two-Hybrid (Y2H) System.

**Results:** Library validation identified several retina-specific genes including *RHO* (NM\_000539). Over 10<sup>7</sup> cDNA clones were subsequently screened, leading to isolation of 53 potential interactions. The identified peptides were prioritised for further evaluation and re-tested in yeast leading to identification of three candidates: A brain prostaglandinD2 synthase (*PTGDS*; NM\_000954) highly expressed in the retina, previously suggested to play a role in retinal homeostasis; regulatory subunit 4 of the 26 S protease (*PSMC1*; NM\_002802) conferring substrate specificity to the proteasome complex during degradation of ubiquitinated proteins; and a soluble fragment of integral membrane protein 2B (*ITM2B*; NM\_021999) previously linked to neurodegenerative disorders.

**Conclusions:** The Y2H screen identified potential interacting partners of *TOPORS* and, following validation experiments, three distinct proteins were selected for further studies. Defining their roles will help elucidate the functions of *TOPORS* as well as better understand the photoreceptor cell biology. The outcomes could help explain how mutations in *TOPORS* result only in RP despite its ubiquitous expression and multifunctional character.





**Title: Characterisation of associations between TOPORS and selected interacting protein partners**

Authors: Barbara Czub<sup>1</sup>, Amna Shah<sup>1</sup>, Giovanna Alfano<sup>1</sup>, Lourdes Valdes Sanchez<sup>2</sup>, Berta De La Cerda Haynes<sup>2</sup>, Christina Chakarova<sup>1</sup> and Shomi S. Bhattacharya<sup>1,2</sup>

<sup>1</sup>Institute of Ophthalmology, UCL, London EC1V 9EL, UK

<sup>2</sup> Department of Cell Therapy and Regenerative Medicine, Andalusian Molecular Biology and Regenerative Medicine Centre (CABIMER), Avda. Americo Vespucio, Seville 41092, Spain

**Purpose:** A novel class of genes implicated in Retinitis Pigmentosa (RP) has recently emerged including splicing factor genes and *TOPORS*. To date studies show mutations in *TOPORS* only cause RP despite ubiquitous expression; this may be due to retina-specific protein interactions, which are perturbed as a result of mutations. We previously identified several protein interacting partners of *TOPORS*, one of which has also recently been shown to be implicated in autosomal dominant inherited retinal dystrophy. This work aims to elucidate which protein domains of *TOPORS* mediate these interactions.

**Methods:** *TOPORS* deletion constructs (Figure 1) were cloned in-frame with *GAL4 BD*. Genes of interest were amplified from human retinal cDNA (from human retina total RNA, Clontech) and cloned in-frame with *GAL4 AD*. Direct interactions between each identified interacting partner and individual fragments of *TOPORS*, corresponding to each of the deletion constructs, were tested in yeast.

**Results:** *TOPORS* interacting partners identified by yeast two-hybrid screen include: prostaglandinD2 synthase highly expressed in the retina (*PTGDS*); regulatory subunit 4 of the 26 S protease (*PSMC1*); soluble fragment of integral membrane protein2B (*ITM2B*) originally linked to neurodegenerative disorders and recently associated with inherited retinal dystrophy. Co-immunoprecipitation experiments for each interactant validated association with full-length *TOPORS*. Preliminary experiments in yeast with short *TOPORS* fragments were performed with p53, a known interactant of *TOPORS*, which showed strongest interaction with the *TOPORS* middle fragment, as opposed to either the N- or C-terminus fragments. The domains involved may reflect the role(s) of the interacting proteins.

**Conclusions:** The Y2H study helped identify domains of *TOPORS*, which may be involved in mediating interactions between *TOPORS* and the identified interacting partners. Results contribute towards understanding the relationship between the interactants and *TOPORS* in the retina. Characterising these interactions in more detail will help elucidate their putative function(s) in the retina. The outcomes could help explain how mutations in *TOPORS* result only in RP despite its ubiquitous expression and multifunctional character.



**Title: ITM2B, implicated in familial dementias and retinal dystrophy, associates with ciliary-centrosomal protein, TOPORS**

Authors: Barbara Czub<sup>1</sup>, Amna Shah<sup>1</sup>, Przemysław Kruczek<sup>1</sup>, Giovanna Alfano<sup>1</sup>, Christina Chakarova<sup>1</sup> and Shomi S. Bhattacharya<sup>1</sup>

<sup>1</sup>Institute of Ophthalmology, UCL, London EC1V 9EL, UK

**Purpose:** *TOPORS* (MIM 609507) is a ubiquitously expressed gene implicated in autosomal dominant retinitis pigmentosa (RP [MIM 268000]); mutations are known to cause only RP with no systemic symptoms. We performed yeast two-hybrid (Y2H) screens of human retinal cDNA libraries to identify proteins interacting with TOPORS, which could explain the restricted phenotype. This led to the isolation of a soluble fragment of integral membrane protein 2B (*ITM2B* [MIM 603904]), mutations in which are associated with inherited forms of dementia and, most recently, a dominant form of retinal dystrophy.

**Methods:** Matchmaker™ Gold Y2H System (Clontech) was used for library screening and testing direct protein-protein interactions (PPIs). Results were validated in HeLa and hTERT-RPE1 (RPE1) cell extracts by co-immunoprecipitation. Immunofluorescence methods were used for co-localisation studies in RPE1 cells and mouse retina cryo-sections. ProteoExtract® Subcellular Proteome Extraction Kit (Merck) was used to prepare cellular fractions (HeLa).

**Results:** The TOPORS-ITM2B PPI, identified by screening, was selected for further study due to the role of *ITM2B* in retinopathy. It was detected in complexes with TOPORS precipitated from HeLa and RPE1 extracts, and both proteins co-localised at the centrosome in RPE1 cells. In mouse retina sections the strongest ITM2B signal was observed in rod photoreceptor inner segment, with a weaker signal in the ganglion cell layer. Direct PPI experiments in yeast with artificial TOPORS fragments (corresponding to different protein domains) implied that its mutation hotspot region may be required for association with ITM2B. Interaction with the TOPORS' RING finger region was also consistently observed, suggesting ITM2B could be modified by ubiquitination. Preliminary Western blot results suggest differential expression of proteolytically cleaved ITM2B peptides in cellular fractions.

**Conclusions:** ITM2B is a novel interacting partner of TOPORS; defining the cellular processes in which they both associate could explain their roles and the phenotypes resulting from their mutations. Furthermore, evaluation of their relationship could lead to a better understanding of neurodegeneration mechanisms overall. Subsequent work will aim to delineate the roles of the various ITM2B peptides, generated by physiological proteolytic cleavage of the membrane-bound precursor protein, which could clarify the centrosomal co-localisation with TOPORS.

# ITM2B, implicated in familial dementias and retinal dystrophy, associates with ciliary-centrosomal protein, TOPORS.

Barbara Czub\*, Amna Z. Shah, Przemyslaw M. Kruczek, Giovanna Alfano, Christina F. Chakarova and Shomi S. Bhattacharya\*  
 Institute of Ophthalmology, UCL, London EC1V 9EL, UK



## Purpose

TOPORS (MIM 609507), implicated in autosomal dominant retinitis pigmentosa (RP [MIM 268000]; Chakarova *et al.*, 2007), is a ubiquitously expressed gene encoding a multifunctional protein. TOPORS has been shown to localise to the nucleus and centrosome in mitotic cells, and to the base of primary cilium in non-dividing cells, including the base of the connecting cilium (CC) of rod photoreceptor cells (Chakarova *et al.*, 2011). Mutations in TOPORS are known to cause only RP with no systemic symptoms despite its wide expression pattern.

We performed yeast two-hybrid (Y2H) screens of human retinal cDNA libraries to identify proteins interacting with TOPORS, which could explain the restricted phenotype. This led to the isolation of a soluble fragment of integral membrane protein 2B (ITM2B [MIM 603904]), mutations in which are associated with inherited forms of dementia (Vidal *et al.*, 1999; Vidal *et al.*, 2000) and, most recently, a dominant form of retinal dystrophy (Audo *et al.*, 2013). ITM2B is known to have inhibitory roles in APP processing and A $\beta$  aggregation; however, its functional significance in the retina requires further investigation.

## Methods

Matchmaker™ Gold Y2H System (Clontech) was used for library screening and testing direct protein-protein interactions (PPIs). Results were validated in HeLa and hTERT-RPE1 (RPE1) cell extracts by co-immunoprecipitation (coIP). Immunofluorescence (IF) methods were used for co-localisation studies in RPE1 cells and mouse retina cryosections. Cells were fixed with 4% PFA and permeabilised with 0.3% Triton-X100. ProteoExtract® Subcellular Proteome Extraction Kit (Merck) was used to prepare cellular fractions (HeLa) for analysis by Western Blotting (WB). Primary antibodies were purchased from Abgent and Sigma (both raised in rabbit against ITM2B C-term and middle regions, respectively) and Abnova (raised in mouse against TOPORS).

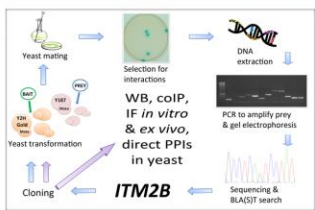


Figure 1. Methods outline. Workflow of the screening process is indicated by blue arrows: Y2H Gold yeast strain was transformed with TOPORS-bait construct; the human retinal cDNA library was expressed in the Y187 strain of the opposite mating type; cultures were mated in liquid Y2H media, followed by spreading on selective agar plates; plasmids were isolated from blue colonies, library inserts were amplified by PCR and sequenced. Full-length cDNA sequences encoding genes of interest were cloned into relevant vectors for further characterisation (black arrows).

## Results

### Human proteins TOPORS and ITM2B interact in yeast

Y2H screening led to identification of 53 putative interacting partners of TOPORS including ITM2B. The TOPORS-ITM2B PPI was selected for further study due to the role of ITM2B in retinopathy. The interaction was validated by direct Y2H PPI and subsequent characterisation experiments in yeast (Figure 2) with artificial TOPORS fragments (corresponding to different protein domains; Figure 3) implied that the mutation hotspot region of TOPORS may be required for its association with ITM2B (Figure 2a). Interaction with the TOPORS' RING domain was also consistently observed (Figure 2a), suggesting ITM2B could be modified by ubiquitination. The direct PPI was also validated with a non-membrane-bound ITM2B fragment (ITM2B90), inclusive of the ITM2B region pulled out from the original Y2H screen (Figure 2b).

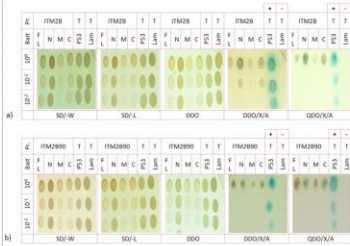


Figure 2. Direct TOPORS-ITM2B PPI in yeast. a) ITM2B interacts with TOPORS and all its fragments. b) Soluble ITM2B90 interacts with TOPORS and all its fragments. Key: P: prey (full-length ITM2B in a) and ITM2B90 in b); Bait: FL: TOPORS and its fragments; 107, 107', 107'': dilutions of the mated cultures; ITM2B: FL: ITM2B; ITM2B90: Soluble, non-membrane-bound ITM2B fragment; FL: FL: TOPORS; N: TOPORS residues 1-380; M: TOPORS residues 373-781; C: TOPORS residues 705-1045; T: 9402 T Antigen; P53: tumour protein 53; Lam: Lamin C. Positive (+) PPI control (T x p53). Negative (-) PPI control (T x Lam). SD/-W: media selective for bait. SD/+L: media selective for bait and prey together. DDO/-A: media selective for PPI (two reporter genes). QDO/+A: media selective for PPI (four reporter genes).

## Results

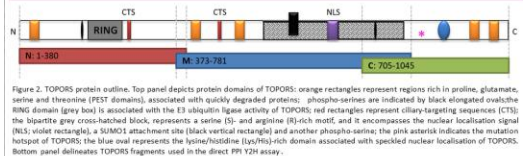


Figure 2. TOPORS protein outline. Top panel depicts protein domains of TOPORS: orange rectangles represent regions rich in proline, glutamate, serine and threonine (PST domains), associated with rapidly degraded proteins; phosphate-binding sites are indicated by black elongated ovals. RING domain (grey box) is associated with the E3 ubiquitin ligase activity of TOPORS; red rectangles represent ciliary-targeting sequences (CTS); the bipartite grey cross-hatched block, represents a serine (S)- and arginine (R)-rich motif, and it encompasses the nuclear localisation signal (NLS; violet rectangle); a SUMO1 attachment site (black vertical rectangle) and another phosphate-binding site; the pink asterisk indicates the mutation hotspot of TOPORS; the blue oval represents the lysine/histidine (LYS/HIS)-rich domain associated with speckled nuclear localisation of TOPORS. Bottom panel delineates TOPORS fragments used in the direct Y2H assay.

### Endogenous TOPORS and ITM2B interact in human cell lines

ITM2B was detected in protein complexes with TOPORS precipitated from HeLa (Figure 5) and RPE1 (data not shown) extracts, and both proteins co-localised at the centrosome in RPE1 cells (Figures 4a), as demonstrated by co-localisation with PCM1 (Figure 4b), PLK4 and Centrin2 (data not shown). In mouse retina sections the strongest ITM2B signal was observed in rod photoreceptor inner segment, with a weaker signal in the ganglion cell layer (Figure 7).

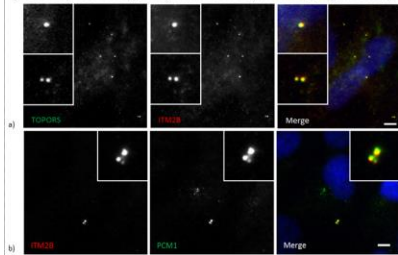


Figure 4. Untransfected RPE1 cells. a) Punctate co-localisation of TOPORS and ITM2B is observed at both centrosomes. b) ITM2B co-localised with PCM1 at the centrosome and centrioles. Insets show a magnification of co-localisation signals. Scale bar: 10 µm.

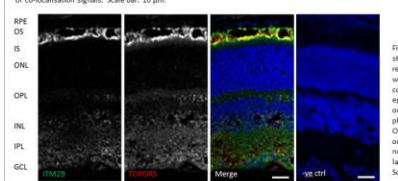


Figure 5. ITM2B (Abgent) is detected in complexes precipitated from HeLa cell extracts with antibody against TOPORS. Input: total cell extract; antibody-negative beads control is indicated by a minus (-); complexes precipitated with mouse anti-TOPORS antibody-conjugated beads are indicated with a plus (+). Two bands are detected in the positive coIP lane.

### WB on extracts from cellular fractions validate ITM2B is post-translationally processed

Preliminary Western blot results demonstrate expression of differentially processed ITM2B peptides in cellular fractions.

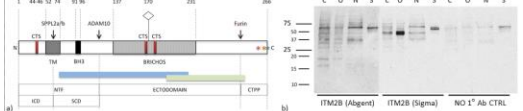


Figure 6. a) Top panel ITM2B protein structure and processing. Amino acids (aa) residues are indicated above the figure. Ciliary-targeting sequences (CTS; aa: 44-46, 166-168 and 174-176) are indicated by red boxes. Transmembrane domain (TM; aa: 52-75); Bcl 2 homology 3 (BH3; aa: 93-96) domain; BRICHOS domain (aa: 117-211) with an N-glycosylation site at aa: 175, denoted by a diamond. ITM2B is subject to proteolytic cleavage by proteases: SPPL2a/b, ADAM10, and Furin. Asterisks indicate mutations identified in ITM2B to date. Bottom panel: Peptide-microarray. Furin-mediated cleavage results in the release of a 23 aa C-terminal pro-peptide (CTPP); a large part of the remaining ectodomain (BRICHOS domain) is shed extracellularly by ADAM10, leaving the membrane-bound N-terminal fragment (NT). The NT undergoes intramembrane proteolysis by SPPL2a or SPPL2b, generating the intracellular domain (ICD) and the secreted C-term domain (SCD). Regions (and hence peptides) potentially recognised by antibodies are indicated in blue (residues 78-224) - Sigma, and green (residues 218-247) - Abgent. b) Several ITM2B species were detected in cellular fractions: C, cytosol; O, organelles; N, nucleus; S, cytoskeleton. Size markers are in kDa (Daltons).

## Conclusions

ITM2B is a novel interacting partner of TOPORS, defining the cellular processes in which they both associate could explain their roles and the phenotypes resulting from their mutations. Furthermore, evaluation of their relationship could lead to a better understanding of neurodegeneration mechanisms overall. Subsequent work will aim to delineate the roles of the various ITM2B peptides, generated by physiological proteolytic cleavage of the membrane-bound precursor protein, which could clarify the centrosomal co-localisation with TOPORS.

## Acknowledgements:

This work has been approved by Fight for Sight, Phoenix Trust, Beaufort Trust, Moorfields Eye Hospital, Moorfields Eye Hospital NHS Foundation Trust and UCL Institute of Ophthalmology and UCL School of Ophthalmology and Visual Science.

Correspondence: Barbara Czub, Institute of Ophthalmology, UCL, London EC1V 9EL, UK. Email: b.czub@ucl.ac.uk

Research Fund Fight for Sight Moorfields Eye Hospital NHS National Institute for Health Research

## References:

Audo I, et al. 2013. The familial dementia gene encodes a membrane protein involved in APP processing and Aβ aggregation. *J Biol Chem* 288: 11000-11007.  
 Chakarova CF, et al. 2007. Mutations in TOPORS cause autosomal dominant retinitis pigmentosa. *Invest Ophthalmol Vis Sci* 48: 1010-1017.  
 Chakarova CF, et al. 2011. Mutations in TOPORS cause autosomal dominant retinitis pigmentosa. *Invest Ophthalmol Vis Sci* 52: 1010-1017.  
 Vidal M, et al. 1999. Mutations in the human gene encoding the protein p53 cause a form of dementia. *Nature* 397: 127-131.  
 Vidal M, et al. 2000. Mutations in the human gene encoding the protein p53 cause a form of dementia. *Nature* 397: 127-131.

**Title: Prostaglandin-D2 synthase localises to centrioles and primary cilium, and interacts with TOPORS, implicated in retinal ciliopathy**

Authors: Barbara Czub<sup>1</sup>, Amna Shah<sup>1</sup>, Przemysław Kruczek<sup>1</sup>, Giovanna Alfano<sup>1</sup>, Christina Chakarova<sup>1</sup> and Shomi S. Bhattacharya<sup>1</sup>

<sup>1</sup>Institute of Ophthalmology, UCL, London EC1V 9EL, UK

**Objective:** Prostaglandin-D2 synthase (*PTGDS*; MIM#176803) is a novel protein-partner of TOPORS (*TOPORS*; MIM#609507), a ubiquitously expressed nuclear and ciliary protein, implicated in retinitis pigmentosa. This study investigated the localisation of *PTGDS* and its potential mechanism-of-association with TOPORS.

**Methods:** Yeast two-hybrid screens, using TOPORS as bait, were performed against human retinal cDNA libraries. Validation and interaction-characterisation were performed in yeast, and by co-immunoprecipitation (co-IP) from HeLa cell extracts. Co-localisation studies were performed in hTERT-RPE1 cell line, and in murine retina cryo-sections. *PTGDS* expression was validated by RT-PCR.

**Results:** Co-IP demonstrated *PTGDS* was found in endogenous protein complexes with TOPORS, whereas in yeast *PTGDS* interacted most strongly with TOPORS' residues 1-380, comprising the RING-domain conferring its E3-ubiquitin-ligase activity. *PTGDS* co-localised with TOPORS, and centriolar markers in dividing cells, and was observed at basal body and along ciliary axoneme in ciliated cells. In mouse retina *PTGDS* was observed in several cell layers, partly overlapping with TOPORS in the photoreceptor layer. In human retina, RT-PCR studies demonstrated expression of several *PTGDS* isoforms.

**Conclusions:** *PTGDS*, a novel component of the primary cilium, could be involved in centriolar-ciliary homeostasis. This putative role of prostaglandin synthases, is additionally supported by independent findings on the role of prostaglandin-E2 in ciliogenesis. Results suggest TOPORS could regulate *PTGDS* levels at the cilium by marking it for degradation by the ubiquitin-proteasome system, providing a basis for understanding the retinal ciliopathy associated with *TOPORS* mutations.

